THE
PHYSICAL REVIEW

A journal of experimental and theoretical physics established by E. L. Nichols in 1893

SECOND SERIES, VOL. 98, NO. 1 APRIL 1, 1955

Isotope Shift in the X-Ray Spectra of Heavy Elements*

M. S. WERTHEIM AND G. IGO†
Sloane Physics Laboratory, Yale University, New Haven, Connecticut
(Received November 22, 1954)

Isotope shifts in the x-ray levels due to the nuclear volume effect have been calculated for three different nuclear potentials by using first-order perturbation theory with the relativistic wave functions in a Coulomb field. In order to correct for the error made in using first-order perturbation theory, the exact relativistic wave function was obtained for one of the potentials. The screening effects of the atomic electrons are taken into account by comparing the value of the wave function at the nuclear radius in a Fermi-Thomas field with that in a Coulomb field. An upper limit is obtained on contributions to the isotope shift due to the change in screening of the other atomic electrons when a K or L shell electron is removed or replaced. The results for isotope shift in Mo and U are one-half and one-twentieth, respectively, of the experimental resolution of Rogosa and Schwarz.

I. INTRODUCTION

COMPARISON of ratios of spin hyperfine structure to isotope shift as given by the volume effect theory[1] in atomic spectra with a calculation[2] on spin hyperfine structure of x-ray terms has indicated[3] the likelihood of an isotope shift in the x-ray terms of the same order of magnitude as the experimental resolution. A recent attempt[4] to detect the isotope shift in x-ray spectra gave negative results. For these reasons, as well as the added interest provided by investigations concerning nuclear radii,[5–7] it seemed desirable to calculate by the theory of the nuclear volume effect[1] the expected shifts for the lines measured by Rogosa and Schwarz.[4] These workers were able to excite a transition $1s(2p_{\frac{1}{2}})^4 \rightarrow (1s)^2(2p_{\frac{1}{2}})^3$ in Mo and a transition $2p_{\frac{1}{2}}(3d_{\frac{1}{2}})^4 \rightarrow (2p_{\frac{1}{2}})^2(3d_{\frac{1}{2}})^3$ in U. Their resolution was 0.2 ev for Mo and 0.4 ev for U. Within their resolution no isotope shift was found in either case. The purpose of the present work has been to calculate the expected shift to 20 percent accuracy or better, in order to compare the displacement with the measurements of Rogosa and Schwarz. First the problem of a nucleus plus one electron is treated in the section on the valence electron. The screening and contributions to the isotope shift due to the effect of the electron transition on the other electrons are then considered in an approximate manner in the section on screening of the nonvalence electrons.

II. THE VALENCE ELECTRON

The calculations have been carried out for the $1s_{\frac{1}{2}}$, $2s_{\frac{1}{2}}$, and $2p_{\frac{1}{2}}$ electrons. The simplest calculation is a first-order perturbation treatment. The change in term value due to the cutoff of the Coulomb field at the nuclear radius is given by

$$\delta E = \int_0^a (F^2+G^2)\delta V dr, \tag{1}$$

where $a=1.5\times10^{-13}A^{\frac{1}{3}}$ cm, A is mass number, and E is energy (unit mc^2). F and G are the small and large components, respectively, of the normalized relativistic radial functions multiplied by r. F and G are identical with the F and G of reference 8, and the φ_1 and φ_2 of reference 1. The potential assumed inside the nucleus is a horizontal line continuation of the value of the Coulomb potential at the nuclear radius. Thus δV is given by

$$\delta V = \gamma/r - \gamma/a, \tag{2}$$

* This research was supported by the U. S. Air Force, through the Office of Scientific Research of the Air Research and Development Command.
† Now at Brookhaven National Laboratory, Upton, New York.
[1] J. E. Rosenthal and G. Breit, Phys. Rev. 41, 459 (1932); G. Breit, Phys. Rev. 42, 348 (1932).
[2] G. Breit, Phys. Rev. 35, 1447 (1930).
[3] G. Breit (private communication).
[4] G. L. Rogosa and G. Schwarz, Phys. Rev. 92, 1434 (1953).
[5] C. H. Townes, Phys. Rev. 94, 773 (1954).
[6] I. Rainwater, Phys. Rev. 94, 773 (1954).
[7] R. Hofstadter, Phys. Rev. 94, 773 (1954).

TABLE I. Isotope shift $\Delta(\delta E)/\Delta A$ (electron volts).

Electronic state \ Element and atomic number	$_{92}$U	$_{82}$Pb	$_{42}$Mo
$1s_{\frac{1}{2}}$	1.2	0.50	0.012
$2s_{\frac{1}{2}}$	0.24	0.088	0.0016
$2p_{\frac{1}{2}}$	0.028	0.0068	0.00003

where r=radial distance (unit $\hbar/mc$) and $\gamma=Z\alpha$. Z is atomic number and α is the fine structure constant.

In computing numerical answers for (1) the exponential factor in the wave function may be replaced by 1 with error less than 1 percent (a is of order 10^{-2} in the units used). Similarly the contributions from all but the constant term of the polynomial can be neglected with error of about 1 percent. The energy level displacement δE is given by

$$\delta E=[F^2(a)+G^2(a)]\frac{\gamma}{2\rho(2\rho+1)}, \tag{3}$$

where $\rho=(1-\gamma^2)^{\frac{1}{2}}$.

The isotope shift $\Delta(\delta E)$ is the difference between the energy level displacements of two isotopes; it is obtained by differentiating (3) with respect to a, the nuclear radius:

$$\Delta(\delta E)=\tfrac{2}{3}\rho(\Delta A/A)\delta E. \tag{4}$$

Table I summarizes shifts obtained by first-order perturbation theory, in the manner just mentioned.

The relativistic effects are very large. Table II gives values of the ratio of the values in Table I to the corresponding values obtained by using nonrelativistic wave functions.

For U^{235} and U^{238} the transition is from $2p_{\frac{1}{2}}(3d_{\frac{1}{2}})^4$ to $(2p_{\frac{1}{2}})^2(3d_{\frac{1}{2}})^3$ with $\Delta A=3$. Therefore the isotope shift is 0.084 ev. For Mo^{92} and Mo^{100} the transition is from $1s(2p_{\frac{1}{2}})^4$ to $(1s)^2(2p_{\frac{1}{2}})^3$ with $\Delta A=8$. The isotope shift is 0.096 ev. The shift ascribed to the configuration in each case is that of the missing electron. Therefore the final level makes a negligible contribution to the isotope shift of the spectral line in both cases. In the case of U the calculated shift is smaller than the resolution by a factor of 5; in the case of Mo by a factor of 2.

The preceding calculations have been made with the "top-slice" potential, which represents the special case, $n=\infty$, of the more general potential[1]

$$V=(-\gamma/na)[-(r/a)^n+n+1] \tag{5}$$

TABLE II. Ratio $\Delta(\delta E)_{\text{rel}}/\Delta(\delta E)_{\text{nonrel}}$.

Electronic state \ Element and atomic number	$_{92}$U	$_{82}$Pb	$_{42}$Mo
$1s_{\frac{1}{2}}$	11.0	6.8	1.7
$2s_{\frac{1}{2}}$	16.7	9.8	1.8

with adjustable n. $n=\infty$ corresponds to having all of the nuclear charge concentrated on the nuclear surface. The case $n=2$ is a uniform charge density inside the nucleus; for $n=1.5$ the charge density peaks toward the center of the nucleus. One finds[1]

$$[\Delta(\delta E)]_n/[\Delta(\delta E)]_\infty=(n+1)/(2\rho+n+1). \tag{6}$$

Values of this factor are given in Table III.

The isotope shift is smaller than for the top slice potential. This result will be referred to later.

Since the perturbation $\delta V(r)$ is singular at $r=0$, it might be expected that the first-order results are not too accurate. To investigate their accuracy one finds the exact wave functions in a Coulomb potential for $r>a$ and a top slice potential for $r<a$. The exact δE is given by

$$\delta E=(\psi_0,\delta V\psi)/(\psi_0,\psi), \tag{7}$$

where $\psi_0=\begin{pmatrix}F_0\\G_0\end{pmatrix}$ is the wave function in a pure Coulomb field and $\psi=\begin{pmatrix}F\\G\end{pmatrix}$ is the exact wave function. The scalar product $(\psi_0,\delta V\psi)$ is defined to be equal to $\int_0^\infty(F_0\delta VF+G_0\delta VG)dr$.

TABLE III. Correction factor for shape of nuclear potential.

	$_{92}$U	$_{82}$Pb	$_{42}$Mo
$n=2$	0.67	0.65	0.61
$n=1.5$	0.63	0.61	0.57

For the case of the top slice potential the functions F and G inside the nucleus may be represented as follows:

$$\begin{aligned} s_{\frac{1}{2}}&\begin{cases}F=-(E^*-1)^{\frac{1}{2}}(\sin Kr/Kr-\cos Kr),\\ G=(E^*+1)^{\frac{1}{2}}\sin Kr,\end{cases}\\ p_{\frac{1}{2}}&\begin{cases}F=(E^*-1)^{\frac{1}{2}}\sin Kr,\\ G=(E^*+1)^{\frac{1}{2}}(\sin Kr/Kr-\cos Kr),\end{cases}\end{aligned} \tag{8}$$

where $E^*=E+\gamma/a$, and $K=(E^{*2}-1)^{\frac{1}{2}}$.

The quantity γ/a is large, ranging from 17 in Mo to 28 in U, while $E<1$; therefore functions of the same k are nearly independent of the principal quantum number except for a normalization factor. (Here k is Dirac's relativistic angular momentum quantum number; it is -1 for an s electron and $+1$ for a $p_{\frac{1}{2}}$ electron.)

It remains to continue these functions from the nuclear radius to infinity. For $r>a$ the perturbed functions satisfy the same differential equations as the unperturbed ones with a slightly different energy $E=E_0+\delta E$. This fact is used in the following calculation employing the phase amplitude method.[8] One substitutes $F=A\sin\varphi$ and $G=A\cos\varphi$ and similarly, with subscript 0, for the unperturbed functions. The results,

[8] G. Breit and G. E. Brown, Phys. Rev. 76, 1307 (1949).

which are consequences of Eqs. (5.1) and (6.1) in reference 8, are

$$\delta\varphi(r)\cong(\delta E)A_0^{-2}(r)\int_r^\infty A_0^2(r)dr, \tag{9a}$$

$$\delta E\cong A_0^2(a)\delta\varphi(a), \tag{9b}$$

$$A(r)=A(a)\exp\left(\int_a^r(-kr^{-1}\cos2\varphi_0+\sin2\varphi_0)dr\right). \tag{9c}$$

Figure 1 shows $\delta\varphi(r)$ for Pb as a function of r.

Taking advantage of the fact that A will turn out to be close to A_0 in the region of interest and that A does not change sign, A may be expressed conveniently in terms of A_0 as follows:

$$A(r)/A_0(r)=[A(a)/A_0(a)]$$
$$\times\exp\left\{2\int_a^r(kr^{-1}\sin2\varphi_0+\cos2\varphi_0)\delta\varphi dr, \right. \tag{10}$$

where $\delta\varphi=\varphi-\varphi_0$. The fact that $\delta\varphi$ is small has been used in arriving at (10); $\delta\varphi(a)$ is of order 0.1 and $\delta\varphi$ decreases initially as r^{-2}. The integral in (10) was evaluated numerically, and is shown in Fig. 2 for the $2s_{\frac{1}{2}}$ electron in Pb. Because of the initial rapid decrease of $\delta\varphi$ this integral increases only slowly beyond a distance of several nuclear radii. For the $2s_{\frac{1}{2}}$ electron in Pb, which has $\gamma a/E=0.0145$, the value of the integral is found to be 0.034 for $\gamma r/E=x=0.03$. It is 0.049 for $x=0.12$, but has increased only to 0.054 at $x=1.2$. For large r, $\delta\varphi$ approaches $\delta E/(1-E^2)^{\frac{1}{2}}$, and $\cos2\varphi$ approaches E. Therefore the exponential factor in A will be $\exp\{-r[(1-E^2)^{\frac{1}{2}}-2E\delta E/(1-E^2)^{\frac{1}{2}}]\}$ while that in A_0 is $\exp\{-r(1-E^2)^{\frac{1}{2}}\}$. Since $2E\delta E\ll(1-E^2)$ the exponential increase of $A(r)/A_0(r)$ at large r can be disregarded as far as the area under $A^2(r)$ is concerned; and it is only this area that matters when one normalizes $A(r)$. Through the region of non-negligible contribution to the area under $A^2(r)$ the value of $\exp\{2\int_a^r(kr^{-1}\sin2\varphi_0+\cos2\varphi_0)\delta\varphi dr\}$ increases by only one percent. Therefore, $A(r)$ is normalized by setting it equal to $A_0(r)$ in this region.

One now evaluates $(\psi_0,\delta V\psi)/(\psi_0,\psi)$. The denominator is $\int_0^\infty A(r)A_0(r)\cos\delta\varphi(r)dr$ which, considering what has been said about the normalization of $A(r)$, is seen to be 1.

The $s_{\frac{1}{2}}$ electrons will now be discussed. The statements made will apply also to the $p_{\frac{1}{2}}$ case provided the symbols F and G as well as F_0 and G_0 are interchanged. In the numerator contributions from F and higher terms than the first of G (expanded in powers of r) are individually of order 1 percent (in Mo) to 3 percent (Pb and U), but they tend to cancel. The answer taking only the leading term in G is

$$\delta E=G_0(a)G(a)(\gamma/\sin\gamma)\int_0^r(r/a)^{1+\rho}(\gamma/r-\gamma/a)dr, \tag{11}$$

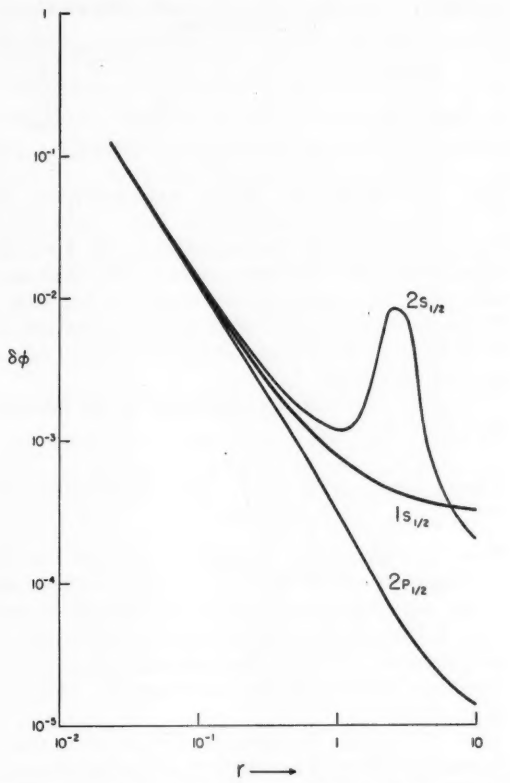

FIG. 1. Change in phase of wave function due to nuclear potential, $\delta\varphi$, for $1s_{\frac{1}{2}}$, $2s_{\frac{1}{2}}$, and $2p_{\frac{1}{2}}$ electrons in Pb ($Z=82$).

which when evaluated, using $G_0^2(a)/A_0^2(a)=(1+\rho)/2$, becomes

$$E=A_0^2(a)[G(a)/G_0(a)]\frac{\gamma}{\sin\gamma}\frac{\gamma}{2(\rho+2)}. \tag{12}$$

The error made in taking only the first term in G is at most 2 percent for Pb and U, less for Mo.

The correction factor over the first-order result is seen to be

$$\left\{[G(a)/G_0(a)]\frac{\gamma}{\sin\gamma}\right\}\frac{\rho(2\rho+1)}{(\rho+2)}. \tag{13}$$

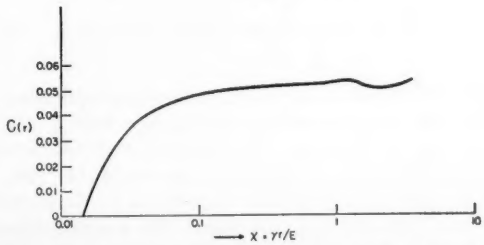

FIG. 2. Value of $C(r)=\int_a^r(kr^{-1}\sin2\varphi_0+\cos2\varphi_0)\delta\varphi dr$ for the $2s_{\frac{1}{2}}$ electron in Pb. This quantity is related in the text to the change in amplitude of the wave function due to the nuclear potential.

TABLE IV. Correction factor to first-order result for wave function distortion.

Element	Mo	Pb	U
Z	42	82	92
$\rho(2\rho+1)/(\rho+2)$	0.93	0.75	0.67

Here $G(a)/G_0(a)$ is given approximately by $\{1-[\tan\varphi_0(a)]\delta\varphi(a)\}A(a)/A_0(a)$, with $A(a)/A_0(a)$ known from (10) and the normalization of $A(r)$. The term in braces in (13) turns out to be very close to 1, within 1 percent, since the two factors deviate from 1 in opposite directions by amounts roughly proportional to γ^2. Table IV gives values of $\rho(2\rho+1)/(\rho+2)$ for the elements considered.

Equation (9a) is an approximation to the following exact relation:

$$\sin\delta\varphi(r)=\delta E A_0^{-1}(r)A^{-1}(r)\int_r^\infty A_0(r')A(r')\cos\delta\varphi(r')dr'.$$

Thus an alternative expression for δE is $\delta E=A(a)A_0(a)\sin\delta\varphi(a)$.[9] It is exact except for the completely negligible error made in letting the integral equal 1. Numerical values obtained for Pb using the above formula check within 1 percent with those obtained by correcting the first-order result by a factor of $\rho(2\rho+1)/(\rho+2)$.

The potential in the presence of the other atomic electrons is taken to be the Fermi-Thomas potential. The effect of screening on the wave function is calculated by the phase-amplitude method,[8] starting from the wave function in the Coulomb field as the unperturbed case. Then

$$\delta\varphi_{\rm scr}(r)=A_{\rm Coul}^{-2}(r)\int_0^r[\delta E-\delta V(r)]A_{\rm Coul}^2(r)dr, \quad (14)$$

where

$$\delta E=\int_0^\infty \delta V(r)A_{\rm Coul}^2(r)dr, \quad (14a)$$

and $\delta V(r)$ is the difference between the Fermi-Thomas potential and the Coulomb potential. The amplitude function in the Fermi-Thomas field is then given by

$$A_{FT}(r)=NA_{\rm Coul}(r)$$
$$\times\exp\left\{2\int_0^r(\cos2\varphi_{\rm Coul}+kr^{-1}\sin2\varphi_{\rm Coul})\delta\varphi_{\rm scr}dr\right\}, \quad (15)$$

where N is determined by the normalization requirement.

The screening correction to the isotope shift is taken to be $A_{FT}^2(a)/A_{\rm Coul}^2(a)$. The calculation of this factor was carried out by numerical integration of (14), (14a), and (15) for the $2s_{\frac{1}{2}}$ and $2p_{\frac{1}{2}}$ electrons in U. Correction factors of 0.90 and 0.76 were found. The wave functions for the $1s_{\frac{1}{2}}$ and $2s_{\frac{1}{2}}$ electrons in a Fermi-Thomas field for $Z=92$ and $Z=49$ have been obtained by direct numerical integration of the radial equations.[10] The correction factor for $2s_{\frac{1}{2}}$ in U is 0.88 in reasonable agreement with the results by the phase-amplitude method. The function given for the $1s_{\frac{1}{2}}$ electron with $Z=49$ yields a correction factor of 0.98. From this one infers a correction factor of 0.98 for Mo, since the atomic numbers differ by only 7.

[9] E. K. Broch, Arch. Math. Naturvidenskab. 48, 25 (1945).

III. SCREENING OF THE NONVALENCE ELECTRONS

When an electron in an atom makes a transition, the other electrons also contribute to the isotope shift[11] because of the change in screening. Upper limits on these contributions have been obtained for the cases of removal (or replacement) of a $1s_{\frac{1}{2}}$ electron in Mo and of a $2s_{\frac{1}{2}}$ or $2p_{\frac{1}{2}}$ electron in U.

In the case of the removal of a $1s_{\frac{1}{2}}$ electron, the contributions by the outer electrons may be estimated by considering the $1s_{\frac{1}{2}}$ electron concentrated at the nucleus. For a $2s_{\frac{1}{2}}$ electron one has, neglecting a factor of $(\rho+E)/[\rho(\rho+1)\Gamma(2\rho+2)]$ with slowly varying Z dependence,

$$\Delta(\delta E)\propto(\gamma a/E)^{2\rho}\gamma, \quad (16)$$

and for the change $\Delta[\Delta(\delta E)]$ in the isotope shift of the $2s_{\frac{1}{2}}$ electron,

$$\frac{\Delta[\Delta(\delta E)]}{\Delta(\delta E)}=\left[\frac{2\rho+1}{Z}-\frac{2\gamma}{\rho}\frac{\ln(\gamma a/E)}{137}\right]\Delta Z. \quad (17)$$

The second term is due to the relativistic dependence of the shape of the wave function on the nuclear charge. Since the actual change of the wave function near the nucleus is almost entirely due to a change of normalization caused by the effect of the screening charge on the wave function far out, while the shape of the wave function near the nucleus is unaffected, this term, which depends on a, leads to an overestimate.

The contribution by the remaining $1s_{\frac{1}{2}}$ electron when a $1s_{\frac{1}{2}}$ electron is removed is obtained by noting that screening by all other electrons has the effect of a change of 2 percent in $A_{1s}^2(0)$ in the case of Mo. Overestimating the effect of the $1s_{\frac{1}{2}}$ electron by ascribing all the screening to it leads to a maximum contribution of 2 percent.

TABLE V. Contributions to the isotope shift of the valence electron by the nonvalence electrons.

Upper limit of contribution by electrons indicated in percent	Electron making transition and element		
	$1s_{\frac{1}{2}}$(Mo)	$2s_{\frac{1}{2}}$(U)	$2p_{\frac{1}{2}}$(U)
$1s_{\frac{1}{2}}$	2	4	23
$2s_{\frac{1}{2}}$	2	2	33
$2p_{\frac{1}{2}}$	negligible	<0.5	3
total	4	6	59

[10] John R. Reitz, Phys. Rev. 77, 10 (1950).

[11] G. Breit, Phys. Rev. 42, 348 (1932). (See pages 352–353 and end of abstract.)

Contributions by the $1s_{\frac{1}{2}}$ electrons to the shifts occurring when a $2s_{\frac{1}{2}}$ or $2p_{\frac{1}{2}}$ electron is removed are estimated by the method of Eqs. (16) and (17) with $2\gamma a$ taking the place of $\gamma a/E$. Here ΔZ is taken to be $\int_0^{r_0} A^2(r)dr$, where r_0 is the radius of the sphere containing one half the charge of the $1s_{\frac{1}{2}}$ electron.

Contributions by $2s_{\frac{1}{2}}$ and $2p_{\frac{1}{2}}$ electrons when a $2s_{\frac{1}{2}}$ or $2p_{\frac{1}{2}}$ electron is removed are estimated by using the known effect of screening due to all other electrons on $A_{2s}{}^2(0)$ and $A_{2p(1/2)}{}^2(0)$. By setting an upper limit on the fraction of screening charge removed one obtains an upper limit on the change of $A^2(0)$ and on the contribution to the isotope shift. Roughly speaking a $2s_{\frac{1}{2}}$ or $2p_{\frac{1}{2}}$ electron is screened by at least 4 charges, if one counts each $1s_{\frac{1}{2}}$ electron as one, each $2s_{\frac{1}{2}}$ and $2p_{\frac{1}{2}}$ as one-half, and allows half a charge for all other electrons. Removal of a $2s_{\frac{1}{2}}$ or $2p_{\frac{1}{2}}$ electron reduces the screening charge by about half an electron charge, which amounts to one-eighth of the total screening charge. This leads to a 1.5 percent effect on $A_{2s}{}^2(0)$ and a 3 percent effect on $A_{2p(1/2)}{}^2(0)$ in the case of U.

Table V summarizes the percentage contributions by the $1s_{\frac{1}{2}}$, $2s_{\frac{1}{2}}$ and $2p_{\frac{1}{2}}$ electrons in the cases considered.

IV. SUMMARY

X-ray isotope shift has been calculated by first-order perturbation theory. Corrections have been made for the effect of the potential inside the nucleus on the wave function, the effect of screening on the wave function, and the contributions from the other atomic electrons. Values of the isotope shift by first-order perturbation theory and corrections are listed in several tables in the text. Combining all results, the predicted isotope shifts for three x-ray levels, including the two measured by Rogosa and Schwarz, are as in Table VI.

TABLE VI. Expected isotope shift $\Delta(\delta E)$ for three x-ray levels.

Level	Element	ΔA	$\Delta(\delta E)$ in ev
$1s_{\frac{1}{2}}$	Mo	8	0.084
$2s_{\frac{1}{2}}$	U	3	0.40
$2p_{\frac{1}{2}}$	U	3	0.018

Comparing the predicted values in Table V with the resolution available in the work of Rogosa and Schwarz, it is understandable that the isotope shift was not detected. It should also be borne in mind that a nuclear potential which assumes the nuclear charge to be distributed through the volume of the nucleus will lead to smaller isotope shifts than the top-slice potential.

The authors wish to thank Professor G. Breit for much help and encouragement, and for suggesting the problem.

Hyperfine Structure of He^{3+} and He^3†

A. M. SESSLER* AND H. M. FOLEY
Columbia University, New York, New York
(Received July 26, 1954)

The ratio of the hfs of He^{3+} to H^1 is calculated by taking into account all effects other than the radiative mass corrections, $\alpha m/M$ (hfs), which contribute a relative correction to hfs greater than 10^{-6}. This includes the effect of nuclear structure and internal motion, and also of interaction currents calculated according to various models. Following A. Bohr, structure effects are calculated in the adiabatic approximation, and corrections for nonadiabaticity are included. Nuclear orbital hfs is evaluated by a perturbation theory which proceeds from a nonadiabatic approximation, and a rather simple general expression is obtained for the evaluation of the effect of interaction currents. Corrections are obtained to the hfs of the He^3 ^3S atomic state, as calculated with a nonrelativistic wave function for a point nucleus of infinite mass. These corrections include both the nuclear structure effects for which the analysis of He^{3+} applies, and the relativistic and reduced mass effects characteristic of the two-electron atom.

INTRODUCTION

THE hyperfine structure of the $^3S_1$ state of He^3 has recently been measured by Weinreich and Hughes[1] with an accuracy of 6 parts in 10^6. It is probable that a radiofrequency measurement of the hfs of the ground state of singly ionized He^3 will be made in the near future. Since the magnetic moment of He^3 and the hfs of H^1 are known to this accuracy, one is in a position, for both of the above experiments, to calculate the hyperfine splitting with the nucleus represented as a point magnetic dipole. The discrepancy between this calculated hfs and the experimental value can be ascribed to the spatial distribution of nuclear currents and magnetic moments. Such an analysis in the case of the H^2 hfs has been made by Bohr[2] and Low[3] and for H^3 by Adams.[4]

The information about the distribution of magnetism in the He^3 nucleus can be compared with the predictions of various nuclear models and wave functions, and furnishes a new datum which nuclear wave functions must satisfy. An analysis of the contribution of "interaction" currents to the hfs anomaly can make possible a choice among various possible forms of these currents.[5]

In the neighborhood of the nucleus the motions of the two electrons in atomic helium are independent and are almost completely governed by the nuclear field. Thus the study of the electron wave functions in and near the nucleus is a single electron problem. The effects of nuclear structure on the hfs for both He atoms and ions is considered in Part A. The complete treatment of the hfs anomaly for He^+ with the exception of the mass correction of order $\alpha m/M$ is given in this section. The additional relativistic and other hfs corrections which must be made for the two electron case are considered in Part B.

The starting point of the calculation of nuclear structure effects, following Low,[3] is the adiabatic approximation for the electron motion in the neighborhood of the nucleus. The electron moves much faster than the nucleons in this region, and thus takes up an orbit with respect to the instantaneous positions of the two protons in He^3. The electron wave function in the region of adiabatic motion can be obtained by taking advantage of the separability of the two center of force problem. We are able to obtain a simple analytic expression for the electron wave function in this region which can be "matched," at large distances to the solution which describes motion about the center of mass of the nucleus. The amplitude of the wave function in the nuclear region can be expressed in terms of $\psi(0)$, the value, at the center of mass, of the wave function for a point nucleus. Corrections to the adiabatic treatment are made in which the "slip" of the electron with respect to the nucleus at large distances is taken into account. The "slip radius" at which the electron motion becomes nonadiabatic is found to be about 25 times the nuclear dimensions in contrast to the small radii given by Adams,[4] but in agreement with the earlier result of Bohr.[2]

The evaluation of the hfs anomaly requires the use of a wave function for the nuclear particles. The Pease-Feshbach[6] function is employed for this purpose as are simple functions constructed by Hughes.[7] The predicted hfs anomaly is a rather sensitive measurement of an average internucleon distance.

The nuclear spin hfs interaction constitutes the major part of the hfs anomaly in He^3 and it is calculated in the adiabatic approximation as indicated above. The contributions of nuclear orbital moments and of certain kinds of interaction currents vanish in this approximation, so that for these cases another approach is employed. The vector potential of the electron current

† Supported in part by a grant from the National Science Foundation.
* National Science Foundation Postdoctoral Fellow now at Cornell University.
[1] G. Weinreich and V. Hughes, Phys. Rev. **95**, 1451 (1954).
[2] A. Bohr, Phys. Rev. **73**, 1109 (1948).
[3] F. Low, Phys. Rev. **77**, 361 (1950).
[4] E. N. Adams II, Phys. Rev. **81**, 1 (1951).
[5] A. M. Sessler and H. M. Foley, Phys. Rev. **94**, 761 (1954).
[6] R. L. Pease and M. Feshbach, Phys. Rev. **88**, 945 (1952).
[7] V. W. Hughes and G. Weinreich, Phys. Rev. **91**, 196 (1953).

is expanded about the nuclear center of mass in nonadiabatic approximation and corrections are made to this expansion by taking into account the adiabatic effects. The small contribution for the D-state nuclear orbital motion is obtained in this way.

The discussion of the effects of interaction currents is limited to working out the hfs anomaly contribution of two rather different forms of these currents. The magnitude of the hfs anomaly is sensitive to the form of these currents.

In Part B are considered all those hfs effects which arise because of the presence of two electrons in He^3 (atom). We anticipate that the nonrelativistic helium problem for a point nucleus of infinite mass will be solved to a high accuracy. The contribution to the hfs from a nuclear structure effect is just that derived in Part A for a single electron. In addition, we must determine all hfs contributions, for atomic He^3 with a point nucleus, which are not given directly by the accurate nonrelativistic wave functions. This wave function is corrected to order α^2 and the hfs for a point nucleus is then obtained to a relative accuracy of order α^2. These corrections include the reduced mass effects, magnetic interaction (Breit operator) effects, and the modification of the nonrelativistic wave function due to the terms neglected in the reduction of the Dirac equation to the Schrödinger form. As in the case of the He^+ ion, radiative mass corrections are not included.

A summary of our results is given in Part C. Atomic units, $\hbar=m=c=1$ are employed throughout.

PART A. HYPERFINE ANOMALY FOR He^3 ION

The discussion of the hfs anomaly for the He^3 ion in this section is complete except for the omission of radiative mass terms. The theory of the structure effects given here applies also to the He^3 atom.

For a single electron He^3 ion, the ratio of the hfs level separation to that of hydrogen is given by[8,9]

$$\frac{\Delta\nu_{He^{3+}}}{\Delta\nu_{H^1}}=\frac{\mu(He^3)}{\mu_P}\left(\frac{M_{He^3}}{M_H}\right)^3 8[1+\tfrac{3}{2}\alpha^2\cdot 3+\bar{\Delta}_{\alpha m/M}+\Delta_{ED}+\Delta_{ss}+\Delta_D+\Delta_{IC}+\Delta_{nad}], \quad (1)$$

$$\Delta_{ED}=-[5/2-\log 2]\alpha^2,$$

where Δ_{ss} = neutron-spin S-state hfs anomaly in adiabatic approximation, Δ_{nad} = nonadiabatic correction to to Δ_{ss} and Δ_D, Δ_D = nucleon spin hfs anomaly in adiabatic approximation from the nuclear D-state, $\bar{\Delta}_{\alpha m/M}$ = relativistic reduced mass effects of order $\alpha m/M$ which has been given by Newcomb and Salpeter[9] for H^1, but has not yet been calculated for He^{3+} or He^3, and Δ_{IC} = contribution to hfs from interaction currents.

[8] N. M. Kroll and F. Pollock, Phys. Rev. 86, 876 (1952); R. Karplus and A. Klein, Phys. Rev. 85, 972 (1952).
[9] E. E. Salpeter and W. A. Newcomb, Phys. Rev. 87, 150 (1952).

I. The Magnetic Hyperfine Interaction Operator

The magnetic interaction may be introduced into the Dirac equation for the electron as $-e\boldsymbol{\alpha}\cdot\mathbf{A}$, in which $\mathbf{A}$ is the vector potential due to nuclear currents and moments. The expectation value of this operator is $-(16/3)\pi\mu_N\mu_e\int(FG/r^2)dr$ for a spherical distribution of electron charge density about the nucleus. An expansion of F and G as nonrelativistic function plus terms of order α^2 shows that the contribution to the α^2 correction to the nonrelativistic hfs value comes from the region of the whole atom. The effect of nuclear structure in the relativistic correction is consequently of order $c\alpha^2$, in which c is a characteristic nuclear dimension. The relativistic correction may thus be obtained using a point nucleus, with sufficient accuracy.

The two-component reduction of the interaction $-e\boldsymbol{\alpha}\cdot\mathbf{A}$, in nonrelativistic approximation, to the general magnetic hyperfine operator between electron spin moments and nuclear spin moments is

$$W_{ss}=-(8/3)\pi\boldsymbol{\mu}_0\cdot\boldsymbol{\mu}_N\delta(\mathbf{r}_e-\mathbf{r}_N)+\frac{1}{r^3}\left[\boldsymbol{\mu}_0\cdot\boldsymbol{\mu}_N-\frac{3(\boldsymbol{\mu}_0\cdot\mathbf{r})(\boldsymbol{\mu}_N\cdot\mathbf{r})}{r^2}\right]. \quad (2)$$

It is clear that both of these terms may be derived from the classical interaction of two moment densities.

II. The Effect of Nuclear Structure on Electron Motion in Adiabatic Approximation

From Eq. (2), it is clear that the nonrelativistic wave function at the position of the nucleons must be determined with some accuracy. The electron wave function in the presence of the two protons must take into account the fact that in and near the nucleus the characteristic electron frequencies are so much higher than the nuclear frequencies that the electron orbits adjust to the instantaneous nucleon positions.[2,3,10] We determine the electron wave function in this region in adiabatic approximation. The effect, on the spin hfs, of corrections to this adiabatic approximation are considered in Sec. IV.

The procedure is to solve the two-center problem for small distances from the nucleus, and to match this wave function to the point nucleus nonrelativistic function, at a distance where structure effects are small. The separability of the hydrogen nolecule ion in prolate spheroidal coordinates,[11] combined with the fact that we need only the solution near the nucleus, and that the proton separation is small compared to the Bohr radius, allows us to obtain the electronic function in this region analytically. Introduction of the coordinates indicated in Fig. 1 gives for the Schrödinger equation:

$$\nabla^2\psi+\frac{2m}{\hbar^2}\left[E+\frac{e^2}{r_1}+\frac{e^2}{r_2}\right]\psi=0. \quad (3)$$

[10] S. Bludman and P. B. Daitch, Phys. Rev. 95, 823 (1954).
[11] V. O. Burrau, Kgl. Danske Videnskab. Selskab, Mat.-fys. Medd. 7, 1 (1927).

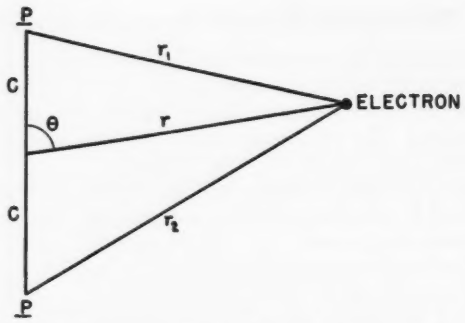

FIG. 1. Electron coordinates in a two-center problem.

Transforming to prolate spheroidal coordinates,

$$\lambda=(r_1+r_2)/2c, \quad \mu=(r_1-r_2)/2c,$$

where m=reduced electron mass for He^3 and φ=azimuthal angle, separates the Schrödinger equation into three equations. The φ solutions are $e^{\pm im\varphi}$, and one sets $m=0$ for the lowest state. There remains:

$$\begin{aligned}(\lambda^2-1)\frac{\partial^2\psi_\lambda}{\partial\lambda^2}+2\lambda\frac{\partial\psi_\lambda}{\partial\lambda}+(\tfrac{1}{3}\gamma+4c\lambda-\gamma\lambda^2)\psi_\lambda=0,\\ (\mu^2-1)\frac{\partial^2\psi_\mu}{\partial\mu^2}+2\mu\frac{\partial\psi_\mu}{\partial\mu}+(\tfrac{1}{3}\gamma-\gamma\mu^2)\psi_\mu=0.\end{aligned} \tag{4}$$

The separation constant is determined as $\frac{1}{3}\gamma+(2/135)\gamma^2+\cdots$, and since $\gamma=2c^2|E|\sim10^{-9}$, all terms but $\frac{1}{3}\gamma$ have been ignored. The μ equation can be solved as a power series in γ and again we need keep only the first term, which is a constant.

For the solution of the λ equation we shall employ a double expansion in c and in a new variable $y=(\lambda-1)c$. When the variable y is used, the λ equation becomes:

$$\begin{aligned}(y^2+2cy)\psi''+2(y+c)\psi'\\ +[\tfrac{2}{3}c^2\epsilon+4(y+c)-2\epsilon(y+c)^2]\psi=0.\end{aligned} \tag{5}$$

This equation has the property that as $c\to0$, $y\to r$, $\psi(\lambda)\to\psi(r)$.

Thus, it is valid to attempt a solution of (5) in powers of c. Let

$$\psi=g_0+cg_1+c^2g_2;$$

we insert this in (5) and separate powers of c.

$$\begin{aligned}c^0:&\quad y^2g_0''+2yg_0'+4yg_0-2\epsilon y^2g_0=0,\\ c':&\quad y^2g_0''+2yg_0''+2yg_1'+2g_0+4yg_1+4g_0\\ &\qquad -2\epsilon y^2g_1-2\epsilon yg_0=0,\end{aligned} \tag{6}$$

etc. Considering the first equation, and that in the region of interest $y\ll1$, we obtain the approximate solution:

$$g_0=a(1-2y+\tfrac{1}{3}(\epsilon+4)y^2+\cdots).$$

The same procedure may be used for g_1, giving:

$$\begin{aligned}\psi=a\{&[1-2y+\tfrac{1}{3}(\epsilon+4)y^2+\cdots]\\ &-c[\tfrac{1}{3}(\epsilon+2)y+\tfrac{2}{3}\epsilon y^2+\cdots]+c^2[\cdots]+\cdots\}.\end{aligned} \tag{7}$$

This analytic wave function is sufficient for our purpose. For large y this becomes:

$$\psi\to a[1-2r+\tfrac{1}{3}(\epsilon+4)r^2+\cdots],$$

which is a hydrogenic function about the center of the two protons. The nonrelativistic machine function is normalized, and we must determine the constant a in terms of the value of the nonrelativistic function at the nucleus. For small r:

$$\psi_{\text{nonrel}}=\psi(0)[1-2r+\tfrac{1}{3}(\epsilon+4)r^2+\cdots].$$

For $y\gg c$, $y=r+c+4(c^2/2r)\sin^2\theta+\cdots$,

$$\psi(\lambda)=a[1-2y+\tfrac{1}{3}(\epsilon+4)y^2],$$

$$\psi(y)\to a(1+2c)[1-2r+\tfrac{1}{3}(\epsilon+4)r^2].$$

Hence, $a(1+2c)=\psi(0)$, and

$$\psi(\lambda)=\psi(0)(1-2c)[1-2y+\tfrac{1}{3}(\epsilon+4)y^2+\cdots]. \tag{8}$$

The change in the normalization of ψ_{nonrel} due to nuclear structure effects is clearly negligible. The function $\psi(\lambda)$ is valid in the region near the nucleus to 1 part in 10^6.

III. Expectation Value of Spin hfs in Adiabatic Approximation

a. Nuclear S State

The evaluation of the spin hfs requires the use of an explicit nuclear wave function. The state of knowledge of this function is quite uncertain and values for the hfs anomaly will be given here for two simple functions given by Hughes,[7] and for the Pease-Feshbach function.[6]

We first assume for the nuclear function[7]:

$$\psi_N(t)=N\exp[-\tfrac{1}{2}\lambda(t+1)2c], \quad N^2=16\lambda^6/7\pi^2, \tag{9}$$

which is a simple, yet very reasonable form. t is defined in Fig. 2, and is determined by two criteria: (1) a crude variational principle; (2) agreement with the "Coulomb energy" difference between He^3 and H^3. Criteria 1 and 2 give:

$$\lambda_1=0.93\times10^{13}\ \text{cm}^{-1}, \quad \lambda_2=0.74\times10^{13}\ \text{cm}^{-1}, \tag{10}$$

respectively.

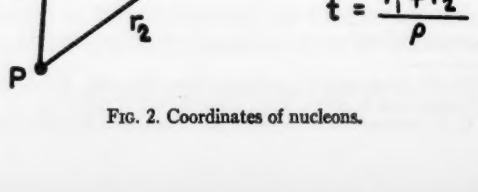

FIG. 2. Coordinates of nucleons.

The Pease and Feshbach[6] function, where coordinates are defined in Fig. 2, is:

$$\psi_N(r)=A_1\exp(-\tfrac{1}{2}\lambda_a(l+1)\rho)+A_2\exp(-\tfrac{1}{2}\lambda_b(l+1)\rho),$$
$$A_1=1.08,\quad A_2=3.01, \tag{11}$$
$$r_c\lambda_a=0.9,\quad r_c\lambda_b=1.8,\quad r_c=1.184\times10^{-13}\text{ cm}.$$

This function must be normalized to one. It is significant that the Pease function is very much in error in attempting to satisfy 2. We consider this a serious objection to the Pease function.

The expectation value of Eq. (2) is obtained in a decoupled representation of electronic and nuclear spins, in which the spin axes are parallel. The electron moment density distribution is not spherical about the nucleus but is constant on ellipsoids with respect to the proton-proton axis as described in Sec. II. In a nuclear S state, however, the proton axis is uncorrelated with the electron spin direction and the hfs interaction is given by just the δ function term of Eq. (2). Hence the quantity

$$H_s'=-(8/3)\pi\mu_0\mu_N\int\psi_e^2(r)\psi_N^2(r)dv \tag{12}$$

represents the spin hfs energy. This integral may be performed analytically with the electron wave function

TABLE I. Spin hfs for nuclear S-state in adiabatic approximation.

Nuclear functions	λ_1	λ_2	Pease-Feshbach
δ	-1.63×10^{-4}	-2.04×10^{-4}	-1.72×10^{-4}
$\Delta_{ss}=(\mu_N/\mu_{He})\delta$	-1.46×10^{-4}	-1.83×10^{-4}	-1.53×10^{-4}

of Sec. II, and the nucleon wave function described above. In Table I is given the value of δ defined by

$$H_s'=-(8/3)\pi\mu_0\mu_N\psi^2(0)[1+\delta]. \tag{13}$$

The contribution to the hfs anomaly from the spin interaction in a nuclear S state (normalized to 1) is also given in Table I.

b. Nuclear D State

There are no $S-D$ cross terms in the hfs interactions, thus the contribution of the nuclear D state is proportional to the small ($\sim$3 percent) probability of the D state. We shall calculate only the δ function part [Eq. (2)] of the D state contribution in Russell-Sanders approximation. This neglects the small additional term corresponding to the nonspherical part of the magnetic spin interaction. Thus for the D state with $J=\frac{1}{2}$, $M_J=\frac{1}{2}$, we obtain for the expectation value of the nucleon spin component $(S_N)_Z=(S_P)_Z=-3/10$, whereas in an S state $(S_N)_Z=+\frac{1}{2}$. With the same radial dependence of the nuclear function as in the Pease-Feshbach S state, we have for the neutron D state contribution:

$$\Delta_{DN}=(\%\ D\text{ state})(-6/10)(\Delta_{ss})=2.9\times10^{-6}. \tag{14}$$

The proton contribution to the hfs anomaly arises from the factor $(1-2c)^2$ in the electron charge density at the proton [Eq. (8)]. Thus the proton contribution is

$$\Delta_{DP}=(\%\ D\text{ state})(-6/10)(4c/a_0)(2\text{ proton})\mu_P/\mu_{He}$$
$$=-4.2\times10^{-6}. \tag{15}$$

IV. Nonadiabatic Correction to Spin Hfs

The correction to the expectation value, in adiabatic approximation, of an operator H' is given in second-order perturbation approximation by:

$$E^{(2)}=\sum_{\substack{i,j\\ i\neq0,j\neq0}}\frac{\langle\Psi_{ij}^0|H'|\Psi_{00}^0\rangle\langle\Psi_{00}^0|[\phi_j^0,u_j^0]\rangle+\langle\Psi_{ij}^0|[\phi_0^0,u_0^0]\rangle\langle\Psi_{00}^0|H'|\Psi_{ij}^0\rangle}{E_{ij}^0-E_{00}^0}, \tag{16}$$

where

$$\langle\Psi_{ij}^0|[\phi_m^0u_n^0]\rangle=\frac{\hbar^2}{2m}\int\int d\mathbf{V}_N d\mathbf{V}_e\phi_j^0(\mathbf{r}_e,\mathbf{R}_\alpha)u_i^0(\mathbf{R}_\alpha)$$
$$\times[(\nabla_{R\alpha}{}^2\phi_m^0)u_n^0+2(\boldsymbol{\nabla}_{R\alpha}\phi_n^0)\cdot(\boldsymbol{\nabla}_{R\alpha}u_n^0)]. \tag{17}$$

Here

$$\Psi_{ij}^0=u_i^0(\mathbf{R}_\alpha)\cdot\phi_j^0(\mathbf{r}_e,\mathbf{R}_\alpha),$$

where u_i^0 is the nucleon wave function and $\phi_j^0(\mathbf{r}_e,\mathbf{R}_\alpha)$ is the adiabatic electron wave function, and depends on nucleon coordinates. The analysis which leads to Eq. (16) is based on the Born-Oppenheimer treatment of the molecular problem.[12–14] From Eq. (16) it is clear that the expression Eq. (17) plays the role of an operator in the perturbation theory calculation. After a transformation to coordinates in terms of the center of mass of the two protons and their separation, Eq. (17) is in the form of a Hermitian operator η_0 which give the nonadiabatic effects due to the motion of the center of mass of the protons and an additional negligible term which gives effects due to the relative motion of the protons.

$$\eta_0=(-\hbar^2/4M_p)[2(\boldsymbol{\nabla}_R u)\cdot(\boldsymbol{\nabla}_R\phi)+(\nabla_R{}^2\phi)u], \tag{18}$$

when R is the coordinate of the center of mass of the protons and M_p is the proton mass. For the correction to the hfs anomaly, this is equivalent to the nonadiabatic operator:

$$(1/2M)\mathbf{p}_e\cdot\mathbf{P}_R, \tag{19}$$

where p_e is the electron momentum and P_R is the nucleon momentum canonically conjugate to R. This operator is just the expression, except for a factor of two, employed by Low[3] to make nonadiabatic corrections to the spin hfs anomaly. Our evaluation of the corrections, following Low and employing the Pease-Feshbach function, yields

$$\Delta_{\text{nad}}=1.17\times10^{-5}. \tag{20}$$

[12] M. Born, and J. R. Oppenheimer, Ann. Physik **84**, 457 (1927).
[13] L. I. Schiff, *Quantum Mechanics* (McGraw-Hill Book Company, Inc., New York, 1949), p. 291.
[14] For a complete derivation see A. M. Sessler, dissertation, Columbia University, 1953 (unpublished).

V. Nuclear Orbital Contribution to hfs Anomaly

a. General Theory

We will calculate the orbital terms starting from a nonadiabatic approximation. In view of the fact that there is no orbital hyperfine structure in the adiabatic approximation, and thus one must obtain a large term in perturbation theory, starting from the nonadiabatic approximation would seem to be a more reasonable procedure. In zero order, ignoring nuclear structure and internal motion, we have a hydrogenic function for the electron, centered on the center of mass of the nucleus. The resulting vector potential of the electrons is, in first approximation:

$$\mathbf{A}_0(\mathbf{r})=-(8/3)\pi\mu_0\psi^2(0)\boldsymbol{\sigma}_e\times\mathbf{r}/2, \tag{21}$$

where $\mathbf{r}$ is measured from the center of mass. This is the first term in a multipole expansion of $\mathbf{A}$. The higher terms would be used in calculating the effect of nuclear structure on hfs. We now allow for the effects of nuclear structure and motion, and calculate the change in $\mathbf{A}$. The first term in the multipole expansion of $\mathbf{A}$ is affected in first order only by the nuclear excited states. It is a term dependent on nuclear motion, and thus is the term in which we are here interested. The second and higher terms in the multipole expansion are modified in first order by contributions involving only electron excitation. Taking into account only electron excitation would lead to the Bohr-Weisskopf effect. Inclusion of nuclear excitations would eventually lead to the results given previously. We have calculated the effect in Sec. III, of the higher multipoles in the adiabatic approximation. The effects of nuclear motion were taken into account then as a nonadiabatic correction.

According to the picture given by Bohr,[2] one expects a region of adiabatic motion extending to a "slip radius" D, with the electron centered on the center of mass outside D, and on the protons inside D. Thus we might expect for the form of $\mathbf{A}$, with Adams,[4]

$$\mathbf{A}_1(\mathbf{r})=-(8/3)\pi\mu_0\psi^2(0)\boldsymbol{\sigma}_e\times\tfrac{1}{2}\mathbf{r}(1-4D/a_0),$$

$$\mathbf{A}_2(\mathbf{r})=-(8/3)\pi u_0\psi^2(0)\times\left[\frac{\boldsymbol{\sigma}_e\times(\mathbf{r}-\mathbf{R}_1)}{2}+\frac{\boldsymbol{\sigma}_e\times(\mathbf{r}-\mathbf{R}_2)}{2}\right]\left(\frac{2D}{a_0}\right), \tag{22}$$

where $\mathbf{R}_1$ and $\mathbf{R}_2$ locate protons 1 and 2, or

$$\mathbf{A}_0=-(8/3)\pi\mu_0\psi^2(0)\boldsymbol{\sigma}_e\times\mathbf{r}/2,$$

$$\mathbf{A}_{\text{pert}}=-(8/3)\pi\mu_0\psi^2(0)[\boldsymbol{\sigma}_e\times\mathbf{R}_1+\boldsymbol{\sigma}_e\times\mathbf{R}_2](D/a_0). \tag{23}$$

We will use perturbation theory to evaluate A_{pert}, and will show that it is of this form, in the appropriate limit, thus evaluating D. We will then be in a position to calculate orbital hfs due to any nuclear currents.

$$\mathbf{A}(r)=-e\langle|\boldsymbol{\alpha}_e/|\mathbf{r}-\mathbf{r}_e||\rangle, \tag{24}$$

where the average is over $\mathbf{r}_e$. Let

$$\Psi(\mathbf{R}_1,\mathbf{R}_2,\mathbf{r}_e)=\phi_0(\mathbf{R}_1,\mathbf{R}_2,\mathbf{r}_e)\psi_0(\mathbf{r}_e)+\sum_{m,n}c_{mn}\phi_m\psi_n, \tag{25}$$

where $E_{mn}=E_m+E_n$, and

$$c_{mn}=\frac{\left\langle\phi_m(\mathbf{R}_1,\mathbf{R}_2)\psi_n(\mathbf{r}_e)\left|\dfrac{e^2}{(\mathbf{r}_e-\mathbf{R}_1)}+\dfrac{e^2}{(\mathbf{r}_e-\mathbf{R}_2)}-\dfrac{2e^2}{r_e}\right|\phi_0(\mathbf{R}_1,\mathbf{R}_2)\psi_0(\mathbf{r}_e)\right\rangle}{E_{mn}-E_{00}}, \tag{26}$$

$$\mathbf{A}_{\text{pert}}(\mathbf{r},\mathbf{R}_i)=-2e\sum_{mn}\phi_0(\mathbf{R}_i)\langle\psi_0(\mathbf{r}_e)|\boldsymbol{\alpha}_e/|\mathbf{r}-\mathbf{r}_e||\psi_n(\mathbf{r}_e)\rangle\varphi_n(\mathbf{R}_i)c_{mn}. \tag{27}$$

The sum is over all nuclear and electronic levels except $m=n=0$, and one must take the real part of the right-hand side. We shall use plane waves for the intermediate electronic states, since most of the contribution comes from momenta of the order of mc. We may also replace $\psi(r_e)$ with $\psi(0)$ and only make an error of order α^2. Let

$$\mathbf{d}_n(\mathbf{r})=\langle\psi_0(\mathbf{r}_e)|\boldsymbol{\alpha}_e/|\mathbf{r}-\mathbf{r}_e||\psi_n(\mathbf{r}_e)\rangle. \tag{28}$$

Then

$$\mathbf{A}_{\text{pert}}(\mathbf{r},\mathbf{R}_i)=-2e\sum_{nm}\mathbf{d}_nc_{mn}\varphi_0(\mathbf{R}_i)\varphi_m(\mathbf{R}_i). \tag{29}$$

First we must evaluate d_n and c_{mn}. Let

$$\psi_n(\mathbf{r}_e)=\exp(i\mathbf{p}\cdot\mathbf{r}_e/\hbar)\mu(\mathbf{p}),$$

where $\mu(\mathbf{p})$ = spinor. Let

$$x=\left\langle\varphi_n(\mathbf{R}_i)\psi_n(\mathbf{r}_e)\left|\frac{e^2}{|\mathbf{r}_e-\mathbf{R}_1|}+\frac{e^2}{|\mathbf{r}_e-\mathbf{R}_2|}-\frac{2e^2}{r_e}\right|\times\varphi_0(\mathbf{R}_i)\psi_0(\mathbf{r}_e)\right\rangle,$$

$$x=x_1+x_2-2x_3.$$

Then

$$x_3=\delta_{m0}\langle\psi_n(\mathbf{r}_e)|e^2/r_e|\psi_0(\mathbf{r}_e)\rangle=\delta_{m0}\psi(0)\frac{4\pi\hbar^2e^2}{p^2}[\mu(\mathbf{p}),\mu(0)],$$

$$x_1=\langle\varphi_m(\mathbf{R}_i)|\exp(i\mathbf{p}\cdot\mathbf{R}_1/\hbar)|\varphi_0(\mathbf{R}_i)\rangle\times\langle\psi_n(\mathbf{r}_e)|e^2/\mathbf{r}_e|\psi_0(\mathbf{r}_e)\rangle,$$

$$x_2=\cdots\exp(i\mathbf{p}\cdot\mathbf{R}_1/\hbar)\cdots,$$

$$\mathbf{d}n=\langle\psi_0(\mathbf{r}_e)|\boldsymbol{\alpha}_e/|\mathbf{r}-\mathbf{r}_e||\psi_n(\mathbf{r}_e)\rangle\simeq\psi(0)(4\pi\hbar^2/p^2)[\mu(0)\boldsymbol{\alpha}_e\mu(\mathbf{p})], \tag{30}$$

$$\mathbf{A}_{\text{pert}}=-2e\psi^2(0)(4\pi\hbar^2)^2e^2\times\sum_m\int_{\text{posit}}\frac{d\mathbf{p}\varphi_0\varphi_m\{\cdots\}\times\{\cdots\}}{(2\pi\hbar)^3p^4(W_m+E(p)-E_0-W_0)}+\int_{\text{neg}}\cdots\{\cdots\}\times\{\cdots\}$$

$$\{\cdots\}\times\{\cdots\}=\{\exp(i\mathbf{p}\cdot\mathbf{R}_1/\hbar)+\exp(i\mathbf{p}\cdot\mathbf{R}_2/\hbar)-\delta_{m0}\}\times\{\mu(0),\boldsymbol{\alpha}_e\Lambda^+(\mathbf{p})\mu(0)\}$$

and

$$\Lambda^+(\mathbf{p})=\frac{1}{2E(p)}[c\mathbf{p}\cdot\boldsymbol{\alpha}+\beta mc^2+|E(p)|].$$

Let

$$\mathbf{B}=\{\mu(0),\alpha_e\Lambda^+\mu(0)\},$$

$$\mathbf{B}=\frac{c}{2E(p)}[i\sigma\times\mathbf{p}+\mathbf{p}].$$

$$\mathbf{A}=\psi^2(0)\frac{4\hbar e^3}{\pi}\sum_m\int\frac{dpc(i\sigma\times\mathbf{p}+\mathbf{p})\{\exp(i\mathbf{p}\cdot\mathbf{R}_1)+\exp(i\mathbf{p}\cdot\mathbf{R}_2)-\delta_{m0}\}}{p^4(W_n-E_0+E(p))E(p)}\varphi_0\varphi_m. \tag{31}$$

We are interested in spin-dependent terms only, so we may drop the term in $\mathbf{p}$. Also note that the $\sum_m$ is over all m, including $m=0$, and that W_0 really belongs in the denominator, so that at $m=0$ the denominator does not become zero. Actually W_0 is negligible except for $m=0$, and then the contribution is zero. Let

$$\mathbf{I}=\int d\mathbf{p}f(p)i\sigma\times\mathbf{p}\exp(i\mathbf{p}\cdot\mathbf{R}/\hbar).$$

Then

$$\mathbf{I}=4\pi\hbar^4\frac{\sigma\times\mathbf{R}}{R^5}\int_0^\infty f\left(\frac{\hbar x}{R}\right)x^2dx\left(\cos x-\frac{\sin x}{x}\right),$$

$$\mathbf{A}=-\psi^2(0)\frac{4}{\pi}\hbar e^3c\sum_n\int x^2dxf\left(\frac{\hbar x}{R}\right)\left(\cos x-\frac{\sin x}{x}\right)\times 4\pi\hbar^4\frac{\sigma\times\mathbf{R}}{R^5}\varphi_0\varphi_m, \tag{32}$$

where

$$f(p)=\frac{1}{E(p)p^4[E(p)+W_m-W_0]},\quad \mathbf{R}=\mathbf{R}_1+\mathbf{R}_2.$$

Let

$$\Delta=W_m-W_0,\quad \delta=R\Delta/\hbar c.$$

Then

$$\mathbf{A}=-(8/3)\pi\mu_0\psi^2(0)\sum_m\frac{\sigma\times\mathbf{R}}{R}\frac{12}{\pi}e^2\varphi_0\varphi_n\left(\frac{R}{\hbar c}\right)\times\int_0^\infty\frac{dx(\cos x-\sin x/x)}{x^2(x+\delta)[1+\epsilon^2x^2]^{\frac{1}{2}}},$$

where $\epsilon^2=\hbar^2/m^2R^2c^2$ and $\delta=\Delta R/\hbar c$, and we can replace $[m^2c^4+\hbar^2x^2c^2/R^2]^{\frac{1}{2}}$ by $\hbar xc/R$ with small error, giving

$$\mathbf{A}=-(8/3)\pi\mu_0\psi^2(0)\frac{12\alpha}{\pi}\sum_m(\sigma\times\mathbf{R})K(\Delta,R)\varphi_0\varphi_m. \tag{33}$$

Now

$$W=-(1/c)\mathbf{j}\cdot\mathbf{A}=-(8/3)\pi\mu_0\psi^2(0)(-1/c)\frac{12\alpha}{\pi}\times\sum_m[\sigma\times\mathbf{R}K(\Delta,R)]_{0m}\cdot\mathbf{j}_{m0}, \tag{34}$$

$$W=-(8/3)\pi\mu_0\psi^2(0)(-1/c)\frac{12\alpha}{\pi}\sum_{n,t}^{\infty}(\sigma\times\mathbf{R})_{mt}\times K(\Delta R)_{t0}\cdot\mathbf{j}_{m0}.$$

$K(\Delta,R)$ is weakly dependent on $\mathbf{R}$. We may not ignore the weak logarithmic dependence on Δ, since this procedure would give zero in the calculation of D state orbital hfs. We can ignore the dependence on R, since no order of magnitude cancellation occurs. Thus we use $\bar{R}$. Then

$$K(\Delta,R)_{t0}=0\quad\text{unless}\quad t=0, \tag{35}$$

$$W=(8/3)\pi\mu_0\psi^2(0)(1/c)\frac{12\alpha}{\pi}\sum_{m=1}^{\infty}(\sigma\times\mathbf{R})_{0m}\cdot\mathbf{j}_{m0}K(\Delta R)_{00},$$

where

$$K(\Delta,R)_{00}=\int_0^\infty dx\frac{(\cos x-\sin x/x)}{x^2[1+\epsilon^2x^2]^{\frac{1}{2}}(x+\delta)},$$

$$\epsilon=\frac{\hbar}{mc}\frac{1}{R},\quad \delta=\frac{W_m-W_0}{mc^2}\frac{mc}{\hbar}R=\frac{\Delta}{mc^2\epsilon}. \tag{36}$$

Fortunately most of the contribution to K comes from momenta between (1/10) mc and 10 mc. There is a correction of less than 10 percent from momenta >50 mc.

Using $R_1=3.54\times10^{-5}$ and $\epsilon=206$, we obtain

$$K(\Delta,R)\approx-\tfrac{1}{3}\int_0^{\frac{1}{3}}\frac{dx}{[1+\epsilon^2x^2]^{\frac{1}{2}}(x+\delta)}.$$

Let $y=\epsilon x$, $f=\epsilon\delta=\Delta/mc^2$, and

$$K(\Delta,R)=-\tfrac{1}{3}\int_0^{\epsilon/2}\frac{dy}{(1+y^2)^{\frac{1}{2}}(y+f)}.$$

This form clearly indicates the weak dependence of $K(\Delta,R)$ on ϵ or $\mathbf{R}$. The integral may be performed exactly, and then expanded in powers of δ. The result, ignoring terms in δ compared to the first term, is

$$K(\Delta,R)=-\frac{1}{3f}\log 2f=-\frac{mc^2}{3\Delta}\log\left(\frac{2\Delta}{mc^2}\right). \tag{37}$$

This corresponds to setting $\epsilon=\infty$. Continuing with the evaluation of A,

$$\mathbf{A}=(8/3)\pi\mu_0\psi^2(0)\frac{4\alpha}{\pi}mc^2\sum_m(\sigma\times\mathbf{R})_{0m}\frac{1}{\Delta}\times\log(2\Delta/mc^2)\varphi_0(R)\varphi_m(R). \tag{38}$$

We replace the excited nuclear levels by free particle

states, in order to make an evaluation possible. Since we wish to use $\mathbf{A}$ to evaluate the hfs due to nuclear currents we are primarily interested in nuclear S-states and shall in this case use

$$\varphi_0(R)=(\gamma^3/\pi)^{\frac{1}{2}}e^{-\gamma R},\quad \gamma=1/R_0,\quad \mathbf{R}_0=\mathbf{R}_1+\mathbf{R}_2.$$

For the excited state, we use

$$\varphi_{lm}(R)=N j_l(\beta R)P_l^m(\cos\theta)\exp(im\varphi),\quad \beta=p/\hbar,$$

where N is a normalizing factor $=3i/(2\pi)^{\frac{1}{2}}$. Let

$$\boldsymbol{\sigma}=\sigma_0\mathbf{k}.$$

Then

$$\boldsymbol{\sigma}\times\mathbf{R}=-Y\mathbf{i}+X\mathbf{j}.$$

We need only calculate the $\mathbf{j}$ component of $\mathbf{A}$. Let

$$\mathbf{A}=-(8/3)\pi\mu_0\psi^2(0)(4\alpha/\pi)mc^2\mathbf{J},$$

with

$$\mathbf{J}=\sum_m(\boldsymbol{\sigma}\times\mathbf{R})_{0m}\log\left(\frac{2\Delta}{mc^2}\right)\frac{\varphi_0(R)\varphi_m(R)}{W_m-W_0}.$$

Then

$$J_j=\varphi_0(R)(1/\pi^2)N^2\alpha\hbar^2(\gamma^3/\pi)^{\frac{1}{2}}2\sin\Theta\times\cos\Phi 4M_pK\frac{4\pi}{3}\left(\frac{16\pi}{3}\right)\frac{1}{8},$$

$$K=K_1+K_2,$$

$$K_1=\frac{\hbar^2}{R^2}\int_0^\infty\frac{pdp}{(p^2+\gamma^2\hbar^2)^3}\sin\left(\frac{pR}{\hbar}\right)\left[\frac{1}{p^2-4M_pW_0}\right]\times\left[\log\frac{p^2-4M_pW_0}{4M_pW_0}+\log\frac{2|W_0|}{mc^2}\right],$$

$$K_2=-\frac{\hbar}{R}\int_0^\infty\frac{p^2dp}{(p^2+\gamma^2\hbar^2)^3}\cos\left(\frac{pR}{\hbar}\right)\left[\frac{1}{p^2-4M_pW_0}\right]\times\left[\log\frac{p^2-4M_pW_0}{4M_pW_0}+\log\frac{2|W_0|}{mc^2}\right].$$

Let

$$x=pR/\hbar,\quad a=R\gamma,\quad b^2=4M_P|W_0|R^2/\hbar^2.$$

Then

$$K=\frac{R^4}{t^4}\int_0^\infty dx\frac{(x\sin x-x^2\cos x)\left[\log\dfrac{x^2+b^2}{b^2}+\log\dfrac{2|W_0|}{mc^2}\right]}{(x^2+a^2)^3(x^2+b^2)}.$$

Since $a=b$, we may approximate and simplify our work by setting $a=b$. $\mathbf{A}$ is now of the correct form [Eq. (23)] as a goes to zero. We may observe that the integral gets its principal contribution for W_m around $+W_0$.

We examine K in the limit that $\gamma\to 0$. In this way we may evaluate an effective D. For an accurate evaluation of the hfs due to a nuclear current, however, one would have to use the correct expression. In view of the great uncertainty about the form of the interaction currents, it appears that Adam's form is sufficient for the present discussion.

Most of the contribution to K comes from values of x around a. As $a\to 0$, we may replace K with

$$K=-\frac{1}{3}\frac{R^4}{\hbar^4}\int_0^\infty dx\left[\log\frac{x^2+b^2}{b^2}+\log\frac{2|W_0|}{mc^2}\right]\frac{x^4}{(x^2+a^2)^4}. \tag{39}$$

Then

$$D=\frac{64}{3\pi}\alpha\cdot\frac{mc^2}{|W_0|}\frac{\hbar^4 3a^3}{R^4}K. \tag{40}$$

Numerical evaluation gives:

$$D=(mc^2/|W_0|)\alpha\times(1.84). \tag{41}$$

In the case of He^3 this yield $D=0.12\alpha$, which is about twenty five times the nuclear dimensions. If the D-state orbital hfs had been used to define an effective D, as was done by Adams,[4] then one would have obtained a value of D about 2.5 times the nuclear dimension.

b. D-State Terms

The previous discussion gives as the D-state proton orbital contribution to the hfs abomaly:

$$W=(8/3)\pi\mu_0\psi^2(0)\frac{12\alpha}{mc}\sum_m(\boldsymbol{\sigma}\times\mathbf{R})_{0m}\cdot\mathbf{j}_{m0}[K(\Delta,R)]_{00},$$

$$\mathbf{j}=(e/Mc)(\mathbf{p}_1+\mathbf{p}_2),\quad \mathbf{R}=\mathbf{R}_1+\mathbf{R}_2,\quad \mathbf{P}=\mathbf{P}_1+\mathbf{P}_2, \tag{42}$$

$$\mathbf{j}=(e/Mc)\mathbf{p},$$

$$W=(8/3)\pi\mu_0\psi^2(0)\frac{12\alpha}{\pi c}S\left(\frac{e}{M}\right)\left(-\frac{mc^2}{3}\right),$$

$$S=\sum_m(\boldsymbol{\sigma}\times\mathbf{R})_{0m}\mathbf{P}_{m0}\frac{1}{\Delta}\left[\log\frac{2\Delta}{mc^2}\right],$$

$$\mathbf{p}_{m0}=(iM/\hbar)\mathbf{R}_{m0}(W_m-W_0),$$

$$S=\frac{2M}{\hbar}\sum_m\mathbf{X}_{0m}\mathbf{Y}_{0m}\left[\log\frac{\Delta}{|W_0|}+\log\frac{2|W_0|}{mc^2}\right]. \tag{43}$$

The constant term gives no contribution, and thus we see that we would have obtained a zero result if we had ignored the dependence of K on Δ. This can be seen because the sum can be done exactly to give $(XY)_0$, which vanishes. Thus we arrive at the same expression as did Low,[3] starting from the adiabatic approximation. Because of the small result we may use his evaluation

of S. We obtain

$$W=-(8/3)\pi\mu_0\psi^2(0)\frac{12\alpha}{\pi c}\frac{e}{M}\frac{\hbar mc^2}{3}\frac{(0.09)\sin^2\omega}{2|W_0|},$$

$$\sin^2\omega\sim 0.03=\%\ D \text{ state},$$

$$W=-(8/3)\pi\mu_0\mu_N\psi^2(0)\frac{mc^2}{|W_0|}\frac{4\alpha}{\pi}(0.09)\sin^2\omega. \quad (44)$$

For He^3, we get a negligible relative correction to hfs:

$$R=0.78\times 10^{-6}. \quad (45)$$

VI. Interaction Current Contribution to hfs

In view of the present state of knowledge of the "interaction currents" which presumably contribute to the nuclear moment, it is not worthwhile to make detailed calculations with all the possible forms for these currents. It is clear that the various forms give rather different contributions to the hfs anomaly. We will content ourselves with two examples here.

One particularly simple choice of interaction currents is that which changes the intrinsic moments of the nucleons, as a function of their relative separation:

$$M=\frac{e\hbar}{2Mc}\sum_{\pi\nu}(\boldsymbol{\sigma}_\pi-\boldsymbol{\sigma}_\nu)J(\mathbf{r}_\pi-\mathbf{r}_\nu), \quad (46)$$

choosing $J(r_\pi-r_\nu)=A\exp(-Kr_{ij})$, and normalizing M to $0.27\mu_0/M$,[15] we obtain for the contribution to the hfs:

$$\Delta_{IC}=\frac{0.27}{M_{\mathrm{He}}}\frac{2}{\Delta(\Delta+1)}\frac{48\Delta^3+43\Delta^2+18\Delta+3}{8\Delta^2+5\Delta+1}, \quad (47)$$

where $\Delta=1+K/\lambda$, and λ depends on the nuclear wave function and is given in Eq. (10).

For a reasonable choice of $K=2\lambda$, we express the resulting hfs anomaly as the fraction of the anomaly obtained by ascribing all of the interaction moment to the neutron as an additional true intrinsic moment ($K=0$). We obtain for the fraction $F=0.41$.

A velocity-dependent nucleon interaction,[16]

$$H=J(|\mathbf{r}_j-\mathbf{r}_k|)[(\mathbf{r}_j-\mathbf{r}_k)\times(\mathbf{p}_j-\mathbf{p}_k)]\times(\boldsymbol{\sigma}_j-\boldsymbol{\sigma}_k)\tfrac{1}{2}(\tau_{j3}-\tau_{k3}), \quad (48)$$

yields a moment density operator,

$$E_{(5)}=e/c\sum J_{\pi\nu}(\boldsymbol{\sigma}_{\pi\nu}\times\mathbf{r}_{\pi\nu}\cdot\mathbf{A}_\pi), \quad (49)$$

which yields for the hfs anomaly:

$$\Delta_5=-0.27\frac{\mu_0}{\mu_{\mathrm{He}^3}}\left(\frac{2D}{a_0}\right). \quad (50)$$

The rather large value of D which we obtain predicts a value of

$$\Delta_5=-2.3\times 10^{-4}. \quad (51)$$

An anomaly of this magnitude can be excluded in the case of H^3.[5] Thus it is unlikely that this form of interaction current contributes a major part of the interaction moment.

PART B. THE HYPERFINE STRUCTURE OF THE He^3 ATOM

The analysis proceeds on the assumption that an accurate solution of the following Hamiltonian exists.

$$H_0=\frac{p_1^2}{2\mu}+\frac{p_2^2}{2\mu}+\frac{e^2}{r_{12}}-\frac{e^2}{r_1}-\frac{e^2}{r_2}, \quad (52)$$

where $\mu=mM_{\mathrm{He}^3}/(m+M_{\mathrm{He}^3})$. The hfs of He^3 in the ^3S state is given in a decoupled high-field representation by

$$W=-2a\mathbf{I}\cdot\mathbf{J},\quad |I|=\tfrac{1}{2},\quad |J|=\tfrac{1}{2},$$

where

$$a=(8/3)\pi\mu_0\mu_{\mathrm{He}^3}\rho(0)\{1+\Delta_{ss}+\Delta_{\mathrm{nad}}+\Delta_D+\Delta_{\alpha m/M}+\bar{\Delta}_{ED}+\Delta_{dm}+\Delta_{IC}+\Delta_{\mathrm{rel}}\}, \quad (53)$$

where

$$\rho(0)=2\int|\psi(\mathbf{r}_1,\mathbf{r}_2)|^2_{r_1=0}d\mathbf{r}_2,$$

$$\bar{\Delta}_{ED}=\left(\frac{\alpha}{2\pi}-2.973\frac{\alpha^2}{\pi^2}\right)-(5/2-\log 2)2\alpha^2,^8$$

Δ_{rel} = contribution to the hfs due to the relativistic correction of $\psi(r_1,r_2)$,

Δ_{dm} = correction to hfs from diamagnetic shielding of one electron by the other.

The other Δ quantities are defined in Eq. (1).

The above effects are all treated in this paper, with the exception of $\Delta_{\alpha m/M}$.

The probability of both electrons occupying the region near the nucleus, where nuclear structure is important, is given by

$$V_{\text{region}}/V_{\text{Bohr radius}}=(D/a_0)^3<10^{-6}.$$

Thus the problem of the effect of nuclear structure on hfs may be treated as in Part A. Part B will be devoted to a study of the corrections to hfs due to the use of H_0, instead of the Dirac equation and Breit operator.

VII. Hamiltonian for He Atom

The Hamiltonian for two electrons in an external field is[17]

$$H=c\boldsymbol{\alpha}_1\cdot[\mathbf{p}_1-(e/c)\mathbf{A}_1]+\beta_1mc^2+c\boldsymbol{\alpha}_2\cdot[\mathbf{p}_2-(e/c)\mathbf{A}_2]+\beta_2mc^2+e\varphi_1+e\varphi_2+e^2/r_{12}+\text{B.O.}, \quad (54)$$

$$\text{B.O.}=(e^2/2r_{12})\boldsymbol{\alpha}_1\cdot\boldsymbol{\alpha}_2+(e^2/2r_{12}^3)(\boldsymbol{\alpha}_1\cdot\mathbf{r}_{12})(\boldsymbol{\alpha}_2\cdot\mathbf{r}_{12}).$$

[15] R. Avery and R. G. Sachs, Phys. Rev. 74, 1320 (1948).
[16] Blanchard, Avery, and Sachs, Phys. Rev. 78, 292 (1950).
[17] H. A. Bethe, *Handbuch der Physik* (Verlag Julius Springer, Berlin, Germany, 1933), Vol. 24, Part 1, p. 377.

A two-component reduction, or use of the Foldy-Wouthuysen transformation, yields[18]

$$H_0=\frac{1}{2\mu}(p_1^2+p_2^2)+e\varphi_1+e\varphi_2+\frac{e^2}{r_{12}}=\frac{1}{2\mu}(p_1^2+p_2^2)+U,$$

$$H_{12}=-\frac{1}{4m^2c^2}\left[\mathbf{p}_1\cdot f\mathbf{p}_1+\mathbf{p}_2\cdot f\mathbf{p}_2-\frac{p_1^2p_2^2}{m}\right],\quad f=E-U,$$

$$H_3=-\frac{\mu_0\sigma_1}{mc}\left[2e\frac{\mathbf{r}_{12}+\mathbf{p}_2}{r_{12}^3}-2\mathbf{E}_1\times\mathbf{p}_1\right]$$
$$-\frac{\mu_0\sigma_2}{mc}\left[2e\frac{\mathbf{r}_{12}\times\mathbf{p}_2}{r_{12}^3}-2\mathbf{E}_2\times\mathbf{p}_2\right],\qquad(55)$$

$$H_4=4\mu_0^2\frac{[\sigma_1\cdot\sigma_2r_{12}^2-3(\sigma_1\cdot\mathbf{r}_{12})(\sigma_2\cdot\mathbf{r}_{12})]}{r_{12}^5}$$
$$-\frac{32}{3}\pi\mu_0^2(\sigma_1\cdot\sigma_2)\delta(r_{12}),$$

$$H_5=-\frac{e^2}{2m^2c^2}\left\{\frac{1}{r_{12}}(\mathbf{p}_1\cdot\mathbf{p}_2)+\frac{1}{r_{12}^3}(\mathbf{r}_{12}\cdot\mathbf{p}_1)(\mathbf{r}_{12}\cdot\mathbf{p}_2)\right\},$$

$$H_6=2\mu_0[\mathbf{H}_1\cdot\sigma_1+\mathbf{H}_2\cdot\sigma_2],$$

$$H_7=(1/M)\mathbf{p}_1\cdot\mathbf{p}_2.$$

$(\mathbf{A},\varphi)$ is the external field produced by the nucleons, $\mu=mM_N/(M_N+m)$, $\mathbf{p}_i=\mathbf{P}_i-(e/c)\mathbf{A}_i$, $\mathbf{P}_i=$momentum, and E_1 is the total field at 1 including that of 2.

H_0 with $\mathbf{p}_i$ replaced by $\mathbf{P}_i$ and $\varphi_i=Ze/r_i$ is the nonrelativistic electrostatic problem which must be solved numerically. We assume the appropriate calculation has been made, and now proceed to calculate the effect of all other terms on the hfs.

H_{12} is the relativistic correction to the motion of the electron, and its effect on the hfs is evaluated in Sec. VIII.

H_3 is a spin orbit and cross-spin orbit term. H_4 is the magnetic electron spin interaction. H_5 is the retarded Coulomb and orbital magnetic interaction. If p_i is replaced by P_i none of these terms contribute (see Sec. X*d*) for the following reasons. The hfs operator is the sum of two one-electron operators, and H_3, H_4, H_5 involve double electron excitations to states such as (p,p), which have very small associated Coulomb operator matrix elements. The same argument holds for H_7.

H_6 gives the hyperfine structure.

H_7 is the Hughes-Eckart[19] Hamiltonian which includes the effect of electron correlation on the reduced mass. The two-component reduction does not yield this term. It gives a diagonal contribution to the hfs, with $\mathbf{p}_i$ replaced by $\mathbf{P}_i$, and is treated in Sec. (X*a*).

[18] J. Sucher and H. M. Foley, Phys. Rev. **95**, 966 (1954).
[19] D. S. Hughes and C. Eckart, Phys. Rev. **36**, 694 (1930).

VIII. Dirac Equation Relativistic Corrections

As explained in Sec. I, it is sufficient to calculate relativistic corrections assuming a point nucleus.

We may carry out the calculation in Hartree approximation, as an examination by perturbation theory, starting from hydrogenic states, shows that the neglected terms in this approximation involve double electron excitations. One of the leading terms contributes a relative correction to hfs:

$$R\sim\frac{\langle 1s\,2s|H_c|2s\,3s\rangle\langle 2s\,3s|H_{12}|1s\,3s\rangle\psi_3(0)\psi_2(0)}{(E_3-E_1)(E_3-E_2)},$$
$$\sim 10^{-7},$$

where $H_c=e^2/r_{12}$. The terms drop off rapidly, and R is probably less than 10^{-6}.

As is well known, the two-component reduction is valid only in regions where $V\ll mc^2$. If $V=Ze^2/r$, then to order α^2, $r\approx a_0$. This unfavorable situation can be circumvented by noting that $V_{\text{actual}}=-Ze^2/r+\varphi(r)$, where $\varphi(r)\to$constant as $r\to 0$. We shall separate out the singularity in the wave function, and show that the remaining function can be expanded in powers of α^2. The two-component reduction is an expansion of the total wave function in powers of α^2, so it is not valid near the nucleus. By this method we can separate out all terms and so calculate them to 1 percent while only knowing the nonrelativistic function to the same accuracy.

The following derivation of the relativistic correction to the electron wave function treats the case of one electron in an applied effective field. This procedure must be modified to take into account the exclusion principle. The appropriate correction is made following Eq. (61), omitting what is a length derivation. Let

$$\Psi=\begin{bmatrix}-i\cos\theta F/r\\ -i\sin\theta e^{-i\varphi}F/r\\ G/r\\ 0\end{bmatrix}.$$

Then a simple reduction of the Dirac equation leads to

$$(\epsilon-V+2mc^2)F-\hbar cG'+(\hbar c/r)G=0,$$
$$(\epsilon-V)G+\hbar cF'+(\hbar c/r)F=0.\qquad(56)$$

The normalization for the radial functions is:

$$\int_0^\infty(G^2+F^2)dr=1.$$

Let $\lambda(r)=\epsilon-V(r)$, solve the first equation for F, and insert it in the second equation, giving the exact equation:

$$\lambda G+\frac{\hbar^2c^2}{(\lambda+2mc^2)}G''-\frac{\hbar^2c^2\lambda'}{(\lambda+2mc^2)^2}(G'-G/r)=0.\quad(57)$$

We introduce atomic units:

$$\lambda=\epsilon-V=mc^2\alpha^2\delta+(e^2/a_0)\varphi,$$

$\lambda/2mc^2=\frac{1}{2}\alpha^2(\delta+\varphi)\ll 1$ for most values of r,

$$\delta,\ \varphi\sim 1,\quad \beta=\delta+\varphi,$$

yielding

$$mc^2\alpha^2\beta G-\frac{\hbar^2c^2mc^2\alpha^2\varphi'}{[2mc^2+mc^2\alpha^2\beta^2]}[G'-G/r]+\frac{\hbar^2c^2G''}{mc^2(2+\alpha^2\beta)}=0. \tag{58}$$

Expand Eq. (58) and keep the first two terms:

$$mc^2\alpha^2\beta G+\frac{\hbar^2}{2m}\left(1-\frac{\alpha^2\beta}{2}\right)G''-\frac{\hbar^2}{4m}\alpha^2\beta(1-\alpha^2\beta)(G'-G/r)=0.$$

Let $\rho=r/a_0$:

$$\beta G+\tfrac{1}{2}(1-\tfrac{1}{2}\alpha^2\beta)G''-\tfrac{1}{4}\alpha^2\beta'(1-\alpha^2\beta)(G'-G/\rho)=0. \tag{59}$$

Now let

$$G=G_0+\alpha^2G_1,\quad \beta=\beta_0+\alpha^2\beta_1. \tag{60}$$

It is clear that β_1 is a constant since it is just the change in the eigenvalue of order α^2. We thus obtain:

$$(\beta_0+\alpha^2\beta_1)(G_0+\alpha^2G_1)+\tfrac{1}{2}(1-\tfrac{1}{2}\alpha^2\beta_0-\tfrac{1}{2}\alpha^4\beta_1)(G_0''+\alpha^2G_1)-\tfrac{1}{4}\alpha^2(\beta_0'+\alpha^2\beta_1')(1-\alpha^2\beta_0+\alpha^4\beta_1)\times(G_0'+\alpha^2G_1'-G_0/\rho-\alpha^2G_1/\rho)=0.$$

Separating orders of α^2:

$$\begin{aligned}&G_0''+2\beta_0G_0=0,\\ &G_1''+2\beta_0G_1=\tfrac{1}{2}\beta_0G_0''-2\beta_1G_0+\tfrac{1}{2}\beta_0'(G_0'-G_0/\rho).\end{aligned} \tag{61}$$

G_0 is the Hartree solution; hence we can calculate the right hand side of the second equation, and then obtain G_1 by numerical integration. To do this we need β_1 and the boundary condition on G_1, since the above is only valid for $\rho\geq 1/10$. The term β_0' contains the total field including that of the other electron. However an examination of H_{12} for a triplet state indicates that β_0' should not contain the field of the other electron. A careful derivation yields the obvious result that β_0' is replaced by $\bar{\beta}_0'=-(a_0/e^2)V_{\text{nuc}}'(\rho)$. β_1 is given by:

$$\beta_1=\tfrac{1}{8}Z[G_0'(0)]^2-\tfrac{1}{8}\int_0^\infty[G_0''(\rho)]^2d\rho. \tag{62}$$

Numerical evaluation was facilitated by using

$$\beta_0=Z/\rho+\delta+c+d\rho,$$

$$G_0(\rho)=A\rho[1-Z\rho+e_0\rho^2+D_0\rho^3+\cdots],$$

where

$$e_0=[Z^2-(\delta+c)]/3\quad\text{and}\quad D_0=[Z(\delta+c)-d-Ze_0]/6.$$

For He, using Hartree functions[20]:

$$\beta_1^{(1s)}=1.89,\quad \beta_1^{(2s)}=0.118.$$

[20] W. S. Wilson and R. B. Lindsay, Phys. Rev. 47, 682 (1935).

To get the solution for $\rho\leq\frac{1}{10}$, we must start from the exact equation:

$$\beta(2+\alpha^2\beta)^2G+(2+\alpha^2\beta)G''-\alpha^2\bar{\beta}_0'(G'-G/\rho)=0. \tag{63}$$

Let $G=\rho^pg$, where $p^2=1-\alpha^2Z^2$. Let

$$g=g_0+\alpha^2g_1,\quad \beta=\beta_0+\alpha^2\beta_1,\quad h=g_0\rho,\quad h_1=g_1\rho. \tag{64}$$

On separating Eq. (63) in power of α^2, we obtain

$$\begin{aligned}&h_0''+2\beta_0h_0=0,\\ &h_1''+2\beta_0h_1=-\frac{\beta_0}{2}h_0''+h_0'\left(\frac{Z^2}{\rho}+\frac{\bar{\beta}_0'}{\beta}\right)-h_0\left(\frac{Z^2}{2\rho^2}+2\beta_0^2+\frac{\bar{\beta}_0'}{2\rho}+2\beta_1\right).\end{aligned} \tag{65}$$

Note that $G_0=h_0$. The connection formulas between G and h are

$$\begin{aligned}&G_0=h_0,\quad G_1=h_1-\tfrac{1}{2}Z^2h_0\log\rho,\\ &G_0'=h_0',\quad G_1'=h_1'-\tfrac{1}{2}Z^2h_0'\log\rho-\tfrac{1}{2}Z^2h_0/\rho.\end{aligned}$$

We match at the point $\rho=\frac{1}{10}$. In order to avoid integrating the h equation, we find a power series solution for small ρ. The result is

$$h_1=B\rho^2+e_1\rho^3+\cdots,$$

where

$$\begin{aligned}&B=-(5/6)A[2(\delta+c)+4],\\ &e_1=(A/6)[(68/3)+(34/3)(\delta+c)-(\delta+c)^2-(7/2)d-2\beta_1].\end{aligned}$$

For large ρ, an integration of Eq. (61) was performed using a modified Euler method and a very small interval. It is estimated that our results are good to one part in 100.

The numerical work gives us G_0 and G_1. To normalize the wave function we need the small component F:

$$F=\alpha[G'-G/\rho]/[2+\alpha^2\beta]. \tag{66}$$

Let $F=F_0+\alpha^2F_1$. Then, for $\rho\geq\frac{1}{10}$,

$$\begin{aligned}&F_0=\tfrac{1}{2}\alpha(G_0'-G_0/\rho),\\ &F_1=\tfrac{1}{2}\alpha(G_1'-G_1/\rho-\tfrac{1}{2}G_0'\beta_0+\tfrac{1}{2}G_0\beta_0/\rho).\end{aligned} \tag{67}$$

For $\rho\leq\frac{1}{10}$:

$$G=\rho^pg,\quad G=\rho^p[g_0+\alpha^2g_1].$$

Using the coupled equations:

$$(\lambda+2mc^2)F-\hbar cG'+\frac{\hbar c}{r}G=0,$$

$$\lambda G+\hbar cF'+\frac{\hbar c}{r}F=0,$$

and letting

$$F=\frac{\alpha\rho^p}{1+p}[j_0+\alpha^2 j_1],$$

and remembering

$$g_0=A[1-Z\rho+e_0\rho^2+D_0\rho^3+\cdots], \quad g_1=B\rho+e_1\rho^2,$$

we may solve and obtain

$$j_0=A[-Z+2e_0\rho+3D_0\rho^2+\cdots], \quad j_1=A[B_1+\rho B_2],$$

where

$$B_1=\tfrac{3}{4}Z^3+\tfrac{1}{2}Z(\delta+c)-e_0Z-\tfrac{5}{6}[Z^4+Z(\delta+c)],$$

$$B_2=\tfrac{1}{2}dZ-Z^2e_0-\tfrac{1}{2}ZD_0-e_0(\delta+c)+\tfrac{1}{3}[(17/12)Z^4+(17/6)Z^2(\delta+c)-(\delta+c)^2-(9/4)Z\delta-2\beta_1].$$

We must normalize our relativistic wave function.

$$\int_0^\infty (G^2+F^2)d\rho=1,$$

$$\int_0^{1/10}(G^2+F^2)d\rho+\int_{1/10}^\infty (G^2+F^2)d\rho=1.$$

The first term is negligible, giving

$$\int_0^\infty G_0^2 d\rho+2\alpha^2\int_0^\infty G_1G_1d\rho+\int_0^\infty F_0^2d\rho=1. \quad (68)$$

Let Γ multiply the function, and let us determine Γ.

$$\Gamma^2=\left\{1+\alpha^2\left[2\int G_0G_1d\rho+\frac{1}{\alpha^2}\int F_0^2d\rho\right]\right\}^{-1}.$$

Since G_0 is normalized,

$$\Gamma=1-\frac{\alpha^2}{2}\left[2\int_0^\infty G_0G_1d\rho+\int_0^\infty\frac{F_0^2}{\alpha^2}d\rho\right]. \quad (69)$$

But we know that

$$\int_0^\infty\frac{F_0^2}{\alpha^2}d\rho=\tfrac{1}{4}\langle|p^2|\rangle=\tfrac{1}{2}\langle|T|\rangle=\tfrac{1}{2}|E|,$$

by the Virial theorem. We then have

$$\Gamma=1-\alpha^2\left[\int_0^\infty G_0G_1d\rho+\tfrac{1}{4}|E|\right]. \quad (70)$$

This was calculated for each electron, leaving us with a wave function which is normalized and sufficient to calculate relativistic effects to 1 percent.

The total hfs interaction for a point nucleus, taking into account the relativistic correction to the wave function given above, is

$$\bar{H}'=-\frac{16}{3}\pi\mu_N\mu_e\int_0^\infty\frac{FG}{r^2}dr. \quad (71)$$

For $\rho\geq\frac{1}{10}$:

$$G=G_0+\alpha^2G_1, \quad F=F_0+\alpha^2F_1.$$

For $\rho\leq\frac{1}{10}$:

$$G=\rho^{p-1}(h_0+\alpha^2h_1), \quad F=[\alpha/(1+p)]\rho^p(j_0+\alpha^2j_1).$$

For $\rho\leq\frac{1}{10}$, F and G can be calculated analytically, and beyond that numerically. Thus:

$$\bar{H}'=-\frac{16}{3}\pi\mu_N\mu_e\left\{\int_0^{1/10}\frac{FG}{r^2}dr+\int_{1/10}^\infty\frac{(F_0+\alpha^2F_1)(G_0+\alpha^2G_1)}{r^2}dr\right\},$$

$$\bar{H}'=-\frac{16}{3}\pi\mu_N\mu_e\left\{\int_{1/10}^\infty\frac{F_0G_0}{r^2}dr+\alpha^2\int_{1/10}^\infty\frac{(F_1G_0+F_0G_1)}{r^2}dr+\int_0^{1/10}\frac{FG}{r^2}dr\right\}.$$

The last can be broken up into a zero order, and α^2 correction term. Finally, then,

$$\bar{H}'=(8/3)\pi\mu_0\mu_N\psi_{\text{nonrel}}{}^2(0)[1+\alpha^2\delta]. \quad (72)$$

Numerical evaluation yields

$$\delta_{1s}=6.06, \quad \delta_{2s}=2.83.$$

IX. Reduced Mass Effects

The problem of separating the motion of the nucleus in an n-electron atomic problem has been considered by Hughes and Eckart.[19] They show that if one solves the problem for a fixed nucleus with electronic mass $=m/(M+m)$ (M=mass of the nucleus), then there is an additional term in the Hamiltonian, namely H_7, still to be taken into account. We assume that the non-relativistic wave function has been calculated for a reduced electronic mass. (If not, the function can be simply scaled.) We shall show that the effect of H_7 on the hyperfine structure is negligible, i.e., less than a part in 10^6. We shall isolate those terms which contribute to hfs, in a perturbation theory calculation of the change in a hydrogenic function due to H_7 and $H_c=e^2/r_{12}$. Both H_7 and H_c commute with the total and orbital angular momentum, and hence only ^3S states will appear in the perturbation theory. Only terms of the form (ns,ms) give a cross term with the hfs operator.

The largest term giving a relative correction to hfs is:

$$R=\frac{4}{18}\left(\frac{32}{27}\right)^3\frac{\langle 1s,3s|H_7|2p,3p\rangle\langle 2p,3p|H_c|2s,2s\rangle}{(E_s-E_2)^2}.$$

By the use of closure and the virial theorem one estimates

$$\left\langle 2p,3p\left|\frac{\mathbf{p}_1\cdot\mathbf{p}_2}{M}\right|1s,3s\right\rangle \leq\left[\frac{4}{3}E_{1s}E_{3s}\right]^{\frac{1}{2}}\frac{1}{M}\leq\frac{0.77}{M},$$

giving $R<10^{-6}$. The terms contributing to R decrease rapidly and it seems reasonable that $R\sim 1\times 10^{-6}$.

The diagonal term obtained by replacing $\mathbf{p}$ with $\mathbf{p}-(e/c)\mathbf{A}$, is zero.

X. The Breit Retarded Interaction

The Breit operator H_3, H_4, H_5, may be used to calculate changes in wave functions as long as one ignores terms in the Breit operator taken twice. This is valid to order α^2.[21,22] There are two possible contributions to hfs from this operator; namely the diagonal value obtained by replacing $\mathbf{p}$ by $\mathbf{p}-(e/c)\mathbf{A}$, and an off-diagonal cross term with the hyperfine operator. We shall first calculate the diagonal terms, and then show that the off diagonal elements make no relative correction to hfs to 1 part in 10^6. Clearly part of H_3 does not come from the Breit operator, but is considered here for convenience.

a. Diagonal Terms

The only diagonal term comes from H_3:

$$W=\frac{e}{mc}\mu_0\frac{1}{r_{12}^3}[\boldsymbol{\sigma}_1\cdot(\mathbf{r}_{12}\times\mathbf{A}_2)-\boldsymbol{\sigma}_2\cdot(\mathbf{r}_{12}\times\mathbf{A}_1)]. \quad (73)$$

Perl[22] has shown that this is a completely classical term, and Lamb[23] has evaluated the term in the classical limit, for an external constant field. For an external dipole field his expression becomes

$$W'=+\tfrac{2}{3}\mu_0\mu_N\alpha^2\int_0^\infty r^2dr\rho_2(r)\int_r^\infty r'^2dr'\frac{\rho_1(r')}{r'^4}. \quad (74)$$

Using

$$\Psi=\frac{1}{\sqrt{2}}[\psi_1(r_1)\psi_2(r_2)-\psi_2(r_1)\psi_1(r_2)],$$

$$\left\langle\left|\frac{1}{r_{12}}\right|\right\rangle=\tfrac{1}{2}\Big\langle\psi_1(r_1)\psi_2(r_2)-\psi_2(r_1)\psi_1(r_2)\times\left|\sum\frac{r_1^n}{r_2^{n+1}}P_n+\frac{r_2^n}{r_1^{n+1}}P_n\right|\times\psi_1(r_1)\psi_2(r_2)-\psi_2(r_1)\psi_1(r_2)\Big\rangle,$$

where $r_1<r_2$ in the first term and $r_2<r_1$ in the second term.

$$\left\langle\left|\frac{1}{r_{12}}\right|\right\rangle=\int_0^\infty d\tau_2\frac{1}{r_2^2}\psi_2^2(r_2)\int_0^{r_1}d\tau_1\psi_1^2(r_1)+\int_0^\infty d\tau_2\frac{1}{r_2}\psi_1^2(r_2)\int_0^{r_2}d\tau_1\psi_2^2(r_1)-2\int_0^\infty d\tau_2\frac{1}{r_2}\psi_2(r_2)\psi_1(r_2)\int_0^{r_2}d\tau_1\psi_1(r_1)\psi_2(r_1). \quad (75)$$

We obtain for W:

$$W=+\tfrac{2}{3}\mu_0\mu_N\alpha^2\left\{\int_0^\infty r^2dr\psi_2^2(r)\int_r^\infty\frac{r'^2dr'\psi_1^2(r')}{r'^4}+\int_0^\infty r^2dr\psi_1^2(r)\int_r^\infty\frac{r'^2dr'\psi_2^2(r')}{r'^4}-2\int_0^\infty r^2dr\psi_2(r)\psi_1(r)\int_r^\infty\frac{r'^2dr'\psi_1(r')\psi_2(r')}{r'^4}\right\}, \quad (76)$$

$$W=+\tfrac{2}{3}\mu_0\mu_N\alpha^2[I_1+I_2-2E_x].$$

We now evaluate these integrals using hydrogenic functions, and because our result is small the error involved is negligible.

$$I_1=128\int_0^\infty\frac{e^{-4x}}{x^2}dx\int_0^x r^2(1-r)^2e^{-2r}dr,$$

$$I_2=128\int_0^\infty\frac{e^{-2x}}{x^2}(1-x^2)dx\int_0^x r^2e^{-4r}dr,$$

$$E_x=128\int_0^\infty\frac{e^{-3x}}{x^2}(1-x)dx\int_0^x r^2dr(1-r)e^{-3r}.$$

The evaluation of these integrals has been facilitated by reversing the order of integration, and then proceeds by expressing them in terms of logarithmic integrals, which all cancel. One obtains:

$$W=-(8/3)\pi\mu_0\mu_N[\psi_1^2(0)+\psi_2^2(0)]\Delta_{dm}, \quad (77)$$

giving a relative correction to hfs, Δ_{dm}:

$$\Delta_{dm}=\frac{-\alpha^3}{(4\pi)(36)}[I_1+I_2-2E_x]. \quad (78)$$

We notice that the exchange integral dominates, and hence we obtain

$$\Delta_{dm}=4.3\times 10^{-6}. \quad (79)$$

[21] G. E. Brown and D. G. Ravenhall, Proc. Roy. Soc. (London) **A208**, 552 (1951).
[22] W. Perl, Phys. Rev. **91**, 852 (1953).
[23] W. E. Lamb, Jr., Phys. Rev. **60**, 817 (1941).

DETROIT PUBLIC LIBRARY

b. Ordinary and Cross Spin-Orbit Interaction[24]

H_3 is of the form $\mathbf{A}_1\cdot\mathbf{s}_1+\mathbf{A}_2\cdot\mathbf{s}_2$. Because $\mathbf{A}_i$ is a vector it must connect a $^3S_1$ state with a P_1 state. Two particles in a $^3S_1$ state have even parity; and since $\mathbf{A}\cdot\mathbf{s}$ has even parity it must connect $(1s,2s)$ to (pp) or (sd) or (ss). Combining these two statements we see that only (pp) states are mixed in to the ground state by this perturbation. However this state gives no hfs. All other terms, including those with the interelectron Coulomb operator are negligible.

c. Interelectron Spin-Spin Interaction

In the triplet S state there is no contact interaction from H_4. Thus we have

$$W\approx-(2\mu_0^2/r_{12}^3)P_2(\cos\theta).$$

This perturbation is a two-electron excitation operator which takes the $(1s,2s)$ ground state to (d,d). It gives no cross term hfs since the hyperfine operator is a one electron operator. All other terms are negligible.

d. Retarded Coulomb and Orbital Magnetic Interaction

We evaluate the correction to hfs resulting from an off-diagonal cross term between H_5 and the hyperfine operator. We shall show that there is no correction to the required accuracy (1 in 10^6).

Consider the ground state of the triplet system in Hartree approximation, i.e., as the product of two s-functions. We will show that H_5 has no matrix elements from this state to any other (ns,ms) state. Thus it gives no change in hfs to this order. The cross terms with the Coulomb operator are negligible.

$$H_5=(1/r_{12})[\mathbf{p}_1\cdot\mathbf{p}_2+(\mathbf{n}\cdot\mathbf{p}_1)(\mathbf{n}\cdot\mathbf{p}_2)], \tag{80}$$

where $\mathbf{n}$ is a unit vector in the $\mathbf{r}_{12}$ direction. Acting on S-states, $\mathbf{p}_i=p_i\mathbf{r}_i$, where $p_i=\partial/\partial r_i$ and $\mathbf{r}_i=$unit vector, we obtain

$$H_5=(p_1p_2/r_{12})[(\mathbf{r}_1\cdot\mathbf{r}_2)+(\mathbf{n}\times\mathbf{r}_2)\cdot(\mathbf{r}_1\times\mathbf{n})+(\mathbf{n}\cdot\mathbf{n})(\mathbf{r}_2\cdot\mathbf{r}_2)].$$

Using a vector identity, remembering that p_1, p_2 belong on the right, and letting θ be the angle between $\mathbf{r}_1$ and $\mathbf{r}_2$, we get

$$H_5=\frac{p_1p_2}{r_{12}}\left[2\cos\theta-\frac{r_1r_2}{r_{12}^2}\sin\theta\right], \tag{81}$$

where $r_{12}^2=r_1^2+r_2^2-2r_1r_2\cos\theta$. If the states are of the form of product functions (antisymmetrized), then the angle θ will not appear in the wave function, and we may perform the integral on θ first. Direct evaluation of this gives zero.

PART C

The ratio of the hfs splitting in He^{3+} and H^1 is given by Eq. (1). Numerical values are as follows:

$$\begin{aligned}&\Delta_{ss}\text{ is given in Table I, for various nuclear functions,}\\&\Delta_D=\Delta_{DN}+\Delta_{DP}-(0.03)\Delta_{ss},\\&\Delta_D=3.3\times10^{-6}\text{ for Pease function,}\\&\Delta_{\text{nad}}=11.7\times10^{-6},\\&\Delta_{IC}=\begin{cases}-2.0\times10^{-6}\text{ for spin modification }(K=2\lambda),\\-230\times10^{-6}\text{ for }E_5.\end{cases}\end{aligned} \tag{82}$$

The hfs of the He^3 atom is given by Eq. (53), where, in addition to the quantities given, we have

$$\begin{aligned}&\Delta_{dm}=4.3\times10^{-6},\\&\Delta_{\text{rel}}=[6.06\alpha^2\psi_{1s}^2(0)+2.83\alpha^2\psi_{2s}^2(0)]/\rho(0),\\&\Delta_{\text{rel}}=5.91\alpha^2=315\times10^{-6}.\end{aligned} \tag{83}$$

We wish to thank Professor N. M. Kroll for several helpful discussions.

[24] G. Breit and E. Teller, Astrophys. J. 91, 215 (1940).

Gamma Rays of 100^{254}†

FRANK ASARO, FRANK S. STEPHENS, JR., S. G. THOMPSON, AND I. PERLMAN
Radiation Laboratory and Department of Chemistry, University of California, Berkeley, California
(Received December 27, 1954)

Gamma rays of 42±4 (2×10^{-2} percent) and 94±2 kev (2.8×10^{-2} percent) were found in coincidence with alpha particles of 100^{254}. The L x-rays (from the internal conversion of the 42-kev gamma ray) were measured and from the intensity the population of the first excited state was calculated to be 15±2 percent. The gamma rays are interpreted as cascading transitions resulting from the de-excitation of Bohr-Mottelson rotational states having spins of 2 and 4, even parity.

The abundances of the alpha transitions to the spin 4 states of even-even nuclides in this region (after normalizing for differences in energy separation from the ground state) exhibit a pronounced minimum for curium emitters and progressively increase for emitters of higher and lower atomic number.

INTRODUCTION

THE alpha-decay properties of even-even nuclei in the heavy-element region present a remarkably uniform picture in several aspects. The energy levels of the product nuclei as defined by analysis of the alpha spectra have spacings which correlate well with the Bohr and Mottelson[1-3] formulation for collective rotational motion in highly deformed nuclei. Other regularities observed are concerned with the degree of population of the several states and these, of course, must receive explanation through alpha-decay theory. As an example, Rasmussen[4] has obtained semiquantitative explanation for the population of the second rotational states in terms of nuclear quadrupole interaction with the emerging alpha particle wave. The interaction is such that a large intrinsic quadrupole moment can suppress the population of the second rotational state ($l=4$ transition) as compared to the $l=2$ and $l=0$ transitions to the first rotational state and the base state of the band, respectively.

In observing the trends of these properties, it is of interest to obtain data over as broad a range of mass numbers and atomic numbers as possible. The present communication is on 100^{254},[5-8] which is the heaviest nuclear species yet available for such studies.[9] The amount of this isotope which has been prepared is too small for measurement of the alpha spectrum with a high resolution spectrograph, but the gamma rays can be measured by α-γ coincidence counting and bear such close resemblance to those of other even-even nuclei which have been examined carefully that the decay scheme can be deduced with some confidence.

The isotope 100^{254} is prepared by the intensive neutron irradiation of lower elements, ultimately uranium.[5,10] Of interest here is the fact that californium isotopes, arising from β^- decay of lower elements, capture neutrons successively until the 20-day β^- emitter, Cf^{253}, is reached. This decays to 99^{253} which is an alpha emitter of 20 days half-life which captures a neutron to give the 36-hour β^- emitter 99^{254}. The 3-hour α emitter 100^{254} soon grows into equilibrium with its parent. In order to take advantage of the longer half-life of 99^{254} in working on 100^{254}, chemical isolation of the 99 fraction was effected. Such preparations therefore contained:

(1) 99^{253}: 20-day half-life, 6.64-Mev α;

(2) 99^{254}: 36-hr half-life, β^-;

(3) 100^{254}: 3.2-hr half-life, 7.22-Mev α.

EXPERIMENTAL RESULTS AND DISCUSSION

For the present measurements two preparations were employed. One of these was of low intensity and consisted of 7000 disintegrations per minute (dis/min) of 99^{253} and 300 dis/min of 36-hour 99^{254} in equilibrium with its daughter, 3.2-hour 100^{254}. The sample was mounted on an aluminum plate 0.5-mil thick. The second sample was more intense and the 100^{254} had been separated chemically from element 99 and was essentially isotopically pure. At the start of measurements it contained 30 000 dis/min.

The weak source (containing mixed radioactivities) was the first one available and was used to establish the population of alpha transitions to the first excited state (see Fig. 1). On the assumption that the decay

† This work was done under the auspices of the U. S. Atomic Energy Commission.

[1] F. Asaro and I. Perlman, Phys. Rev. **87**, 393 (1952); **91**, 763 (1953).

[2] A. Bohr and B. R. Mottelson, Phys. Rev. **89**, 316 (1953); **90**, 717 (1953); Kgl. Danske Videnskab Selskab, Mat.-fys. Medd. **27**, No. 16 (1953).

[3] A. Bohr, *Rotational States of Atomic Nuclei* (Ejnar Munksgaard, Copenhagen, 1954).

[4] J. O. Rasmussen, Jr., University of California Radiation Laboratory Unclassified Document UCRL-2431, December, 1953 (unpublished).

[5] Harvey, Thompson, Ghiorso, and Choppin, Phys. Rev. **93**, 1129 (1954).

[6] Fields, Studier, Mech, Diamond, Friedman, Magnusson, and Huizenga, Phys. Rev. **94**, 209 (1954).

[7] Studier, Fields, Diamond, Mech, Friedman, Sellers, Pyle, Stevens, Magnusson, and Huizenga, Phys. Rev. **93**, 1428 (1954).

[8] Ghiorso, Thompson, Higgins, Harvey, and Seaborg, Phys. Rev. **95**, 293 (1954).

[9] We are greatly indebted to B. G. Harvey, A. Ghiorso, and G. R. Choppin for making available to us the preparations of 100^{254} used in the present study.

[10] Thompson, Ghiorso, Harvey, and Choppin, Phys. Rev. **93**, 908 (1954).

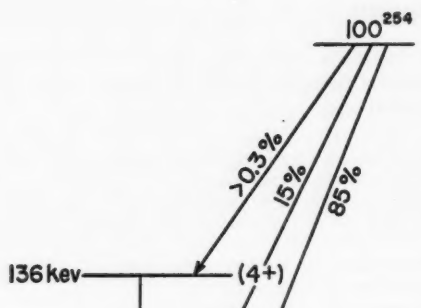

FIG. 1. Decay scheme of 100^{254}.

scheme of 100^{254} is not unlike that of other even-even nuclei such as Cf^{246},[11] Cm^{242},[12] and Pu^{238},[13] this transition should lead to a 2+ state some 40 kev above the ground state and this state would be de-excited by a highly converted gamma-transition. The measurement of the L x-ray intensity would therefore form the basis for calculating the population of the 2+ state.

The alpha-particle—L x-ray coincidence rate was determined in a manner to be explained presently. The geometry of the arrangement was calibrated using the well-known 60-kev γ ray of Am^{241}. The absorption and fluorescence yield[14] corrections were made as second-order corrections by comparison in the same apparatus with the somewhat softer L x-rays from the decay of Cm^{242}. The final corrected intensity of the transition to the 2+ state was 15±2 percent. This is significantly lower than is the case for some lighter elements as will be explained below.

The coincidence counting mentioned above was done with a sodium-iodide crystal and 50-channel pulse height analyzer for the photon side and a thallium-activated potassium iodide crystal ($\frac{1}{32}$ in.×$\frac{1}{4}$ in. ×$\frac{1}{4}$ in.) with a single-channel pulse height selector for the alpha-particle side. The α-γ coincidence counting *per se* discriminated against the gamma rays from 99^{254} decay. To eliminate coincidences with the alpha particles of 99^{253}, the pulses from the potassium-iodide crystal were fed into the single-channel pulse height selector and those within a chosen energy band were used to gate the 50-channel pulse analyzer. (The potassium-iodide crystal could give an alpha-particle energy resolution of 5 percent without difficulty at low geometry but was 7.6 percent in the manner used here.)

[11] Hummel, Stephens, Asaro, Chetham-Strode, and Perlman, Phys. Rev. **97**, 22 (1955).
[12] Asaro, Thompson, and Perlman, Phys. Rev. **92**, 694 (1953).
[13] F. Asaro and I. Perlman, Phys. Rev. **94**, 381 (1954).
[14] B. B. Kinsey, Can J. Research **26A**, 404 (1948).

The second preparation which contained no 99^{253} was used for an examination of the gamma-ray spectrum. It had been mounted on a 0.5-mil platinum plate. Coincidence counting was again employed in order to decrease background effects, but since alpha-energy discrimination was not necessary, a zinc sulfide screen on the face of a photomultiplier tube could serve as a high-geometry alpha-particle detector.

The composite data from three measurements of the alpha-gamma coincidence spectrum is shown in Fig. 2.‡ In addition to the prominent L x-ray peak, two gamma rays of 42±4 kev and 94±2 kev were seen. The decay period of the L x-rays and the 94-kev gamma ray could be measured with some accuracy and both showed half lives of about 3 hours. The peak at 66 kev is seen when any emitter of gamma rays of sufficient energy is counted on platinum and is due principally to K x-rays of platinum produced by fluorescence excitation. There may be small contributions at this energy from the escape peak of the 94-kev gamma ray and also from the backscattered radiation. The line showing the "maximum contribution from spontaneous fission" was determined in the following manner. The isotope Cf^{252} which has a high ratio of spontaneous fission to alpha disintegration[15,16] had been used to determine the gamma-ray spectrum in coincidence with the fission process as it registers in the detection system employed here. The gamma-ray intensity as a function of energy in the range of interest here was flat. It was assumed that this distribution would be the same for 100^{254} and the calculated intensity is shown in Fig. 2 as a maximum value since all of the spontaneous fission fragments may not have been counted by the zinc sulfide detector. In calculating the intensities of the gamma

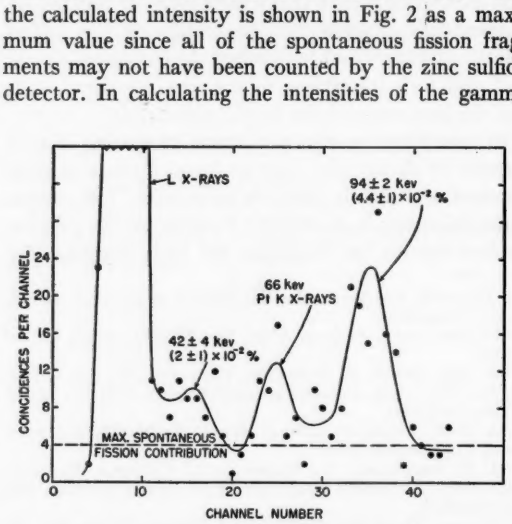

FIG. 2. Alpha-particle—gamma-ray coincidence spectrum of 100^{254}.

‡ *Note added in proof.*—Improved data has shown the abundance of the 94-kev gamma ray to be 2.8×10^{-2} percent. The alpha group to the 136-kev state then has an abundance >0.2 percent.
[15] Ghiorso, Thompson, Choppin, and Harvey, Phys. Rev. **94**, 1081 (1954).
[16] Diamond, Magnusson, Mech, Stevens, Friedman, Studier, Fields, and Huizenga, Phys. Rev. **94**, 1083 (1954).

rays from the alpha decay process, we assumed a spontaneous fission gamma-ray background of one-half the maximum value shown in Fig. 2. This assumption could introduce a 10 percent error in the intensity of the 94-kev gamma ray and a correspondingly larger error for the 42-kev peak.

The 42±4 kev gamma ray did not give a sufficient number of events to determine its energy with accuracy, hence the large limits of error. Its intensity was 2×10^{-2} percent (of the alpha disintegrations), and under the very likely assumption that the gamma ray is from the transition giving rise to the L x-rays, the conversion coefficient can be calculated. It will be recalled that L x-ray measurements indicated 15 percent population of the first excited state; therefore the conversion coefficient is 750. Within the accuracy of our information this is in good agreement with an $E2$ transition similar to that found for all other even-even nuclei in this region.

The 94-kev transition also has its analogy in the alpha decay of other heavy even-even nuclei and has been placed accordingly in the decay scheme (Fig. 1‡) defining a state at 136 kev. The energy spacing agrees with the assignment to a 4+ state as part of a rotational band according to the Bohr-Mottelson theory.[2,3]

The intensities of alpha transitions to the second even-spin states of even-even nuclei have been discussed in previous publications[4,17] and are of interest because they are not explained by previous alpha-decay theory. It is found that the intensities of alpha transitions to these states are much lower than would be calculated from simple alpha-decay theory and follow a trend illustrated by Fig. 3. Here the ratio of expected alpha intensity to measured intensity is plotted as the "hindrance factor" on the ordinate scale.

The point for 100^{254} was determined according to the following reasoning: it is assumed that the 94-kev transition is analogous to the 103-kev transition[12] of Cm^{242} and has the same conversion coefficient. From the measured gamma-ray intensity, 4.4×10^{-2} percent,

[17] F. Asaro and I. Perlman, Phys. Rev. 91, 763 (1953).

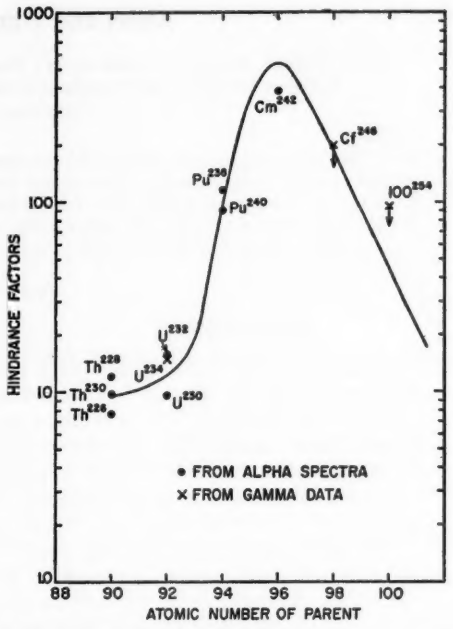

FIG. 3. Hindrance factors for alpha groups to the second even-spin state of even-even nuclei.

the calculated intensity of the alpha group populating this state turns out to be at least 0.3 percent. From this the hindrance factor can be calculated as indicated in Fig. 3.

Rasmussen[4] has obtained semiquantitative explanation of this phenomenon by taking into account the interaction between the outgoing alpha-particle wave and the intrinsic nuclear quadrupole moment. He finds that the population of the 4+ state should be depressed depending upon the magnitude of the quadrupole distortion. It is also of interest that the coupling should cause alpha-particle waves of each angular momentum value to go through a node which may explain the maximum effect in the region of curium alpha emitters.

Alpha and Gamma Spectra of Cf^{246}†

J. P. Hummel, Frank S. Stephens, Jr., Frank Asaro, A. Chetham-Strode, Jr., and I. Perlman
Radiation Laboratory and Department of Chemistry, University of California, Berkeley, California

(Received December 27, 1954)

The alpha and gamma spectra of Cf^{246} have been studied with an alpha-particle spectrograph and gamma-ray scintillation spectrometer. Alpha groups of 6.753 Mev (78 percent) and 6.711 Mev (22 percent) were observed. L x-rays and gamma rays of ~100 kev (1.4×10^{-2} percent) and ~44 kev were assigned to Cf^{246}. These results are evaluated with respect to the developing theory and systematics of complex alpha spectra and excited states of even-even nuclei.

INTRODUCTION

THE preparation of Cf^{246} in a state of high radioactive purity can be effected by irradiating a mixture of curium isotopes (Cm^{242-6}) with alpha particles of about 40-Mev energy.[1] (The mixture of curium isotopes is obtained by prolonged neutron irradiation of Pu^{239}.[2]) Of the californium isotopes produced, Cf^{246} has a half-life of 35.7 hr,[1] while Cf^{247}, Cf^{244}, and presumably Cf^{245} have half-lives sufficiently short[1,3] to allow their complete decay during a period in which the Cf^{246} is not greatly reduced. No appreciable contribution to the radioactivity comes from Cf^{248} because of its relatively long half-life (250 days[4]) and low yield since there were only small amounts of Cm^{246} and Cm^{245} in the bombarded curium. Curium-242 would be present as the daughter product of Cf^{246} decay.

The interest in examining the alpha spectrum of Cf^{246} lies largely in extending the range of even-even alpha emitters for which accurate information can be obtained on the nature of the spectroscopic states and the degree of population of these states. The regularities observed in alpha spectra of heavy nuclei and their implications on nuclear structure and alpha-decay theory have been reviewed recently.[5-7]

The sample of Cf^{246} made available for the present study contained initially 2.9×10^5 alpha disintegrations per minute. Since the transmission of the alpha-particle spectrograph is about 4×10^{-5}, it was necessary to make as long an exposure as possible in order to obtain a reasonable number of alpha tracks. The ratio of peak height to background was about 50 for the main group which makes it impossible to measure alpha groups of abundance lower than several percent. From other spectra of even-even alpha emitters in the region, it was obvious that the transition to the ground state (0+) and first excited state (2+) should be discernible but no others. The sensitivity of gamma-ray detection, however, is such that some information could reasonably be expected from this source on the expected transition to the second excited state (4+). At the time of the first measurements the Cm^{242} activity was small relative to the Cf^{246}. There was some Cf^{250} and Cf^{252} in the sample due to their incomplete removal from the target curium before bombardment. The Cf^{250} and Cf^{252} contribute spontaneous fission-gamma ray coincidences. With our detection system the intensity of these coincidences is nearly constant over the energy range under consideration.

EXPERIMENTAL

The Cf^{246} source was prepared by vacuum sublimation and exposed in the alpha-particle spectrograph according to methods already described.[8] The spectrum so obtained showed, as expected, only two alpha groups characteristic of transitions to the ground state and first excited state of an even-even alpha emitter (see the decay scheme, Fig. 1).

The abundance of the transition to the first excited state could be obtained directly from the alpha spectrum and indirectly by determining the coincidence rate between alpha particles and L x-rays. This indirect determination comes about from the fact that the first excited state drops to the ground state by an $E2$ transition which is highly converted in the L shell. The method of making the coincidence measurement and the corrections necessary to transfer these data into the degree of population of the first excited state are discussed elsewhere.[9]

The gamma-ray spectrum was measured with a scintillation spectrometer and besides the L x-rays, peaks at ~100 kev, ~60 kev, and ~44 kev showed up. The 100-kev photon is interpreted as a gamma ray leading from the sparsely populated second excited state to the first excited state. The 44-kev photon is the gamma ray from the first excited state. The 60-kev peak is probably due to Am^{241} impurity. Because of the high intensity of the Am^{241} 60-kev gamma ray and

† This work was performed under the auspices of the U. S. Atomic Energy Commission.

[1] Hulet, Thompson, Ghiorso, and Street, Phys. Rev. 84, 366 (1951).

[2] We wish to thank Dr. S. G. Thompson and Dr. B. G. Harvey for their part in making this sample available.

[3] Ghiorso, Rossi, Harvey, and Thompson, Phys. Rev. 93, 257 (1954).

[4] Hulet, Thompson, and Ghiorso, Phys. Rev. 95, 1703 (1954).

[5] A. Bohr, *Rotational States of Atomic Nuclei* (Ejnar Munksgaard, Copenhagen, 1954).

[6] I. Perlman and F. Asaro, Ann. Rev. Nuc. Sci. 4 (to be published).

[7] Bohr, Fröman, and Mottelson, Kgl. Danske Videnskab. Selskab, Mat.-fys. Medd (to be published).

[8] Asaro, Reynolds, and Perlman, Phys. Rev. 87, 277 (1952).

[9] Asaro, Stephens, Thompson, and Perlman, University of California Radiation Laboratory Unclassified Document UCRL-2766, October, 1954; Phys. Rev. 98, 19 (1954).

the low intensities of the Cf^{246} photons, an extremely small amount of Am^{241} (80 disintegrations per minute) would give the observed intensity. The gamma-ray spectrum is measured most effectively by α-γ coincidence counting, the details of which are described elsewhere.[9] The coincidence spectrum for Cf^{246} is shown in Fig. 2.

RESULTS AND DISCUSSION

Alpha Spectrum

Two exposures (22.6-hr and 33-hr, respectively) were made on the alpha-particle spectrograph before the sample became too weak. In the first, 5137 tracks were registered: 78 percent in the main group and 22 percent in the group leading to the first excited state. Also by the α-*L* x-ray coincidence method, the abundance of population of the 2+ (first excited) state was found to be 22 percent.

The energy difference between the two groups was found to be 42.0 kev. When correction is made for the differences in recoil energy, the corresponding gamma-ray transition becomes 42.7 kev. The appearance of the first excited state of Cm^{242} is also prominent in the β decay of Am^{242m}. The transition energy has been measured as 42.3±0.2 kev with a bent crystal photon spectrometer (Jaffe[10]), and from the conversion electron spectrum, the value 42.2±0.3 kev was obtained (Church[11]). This photon is also seen in the α-γ coincidence spectrum of Cf^{246} (see Fig. 2), but the energy determination is not as accurate as the three values cited here.

In the second alpha spectrum taken, the photographic plate was also exposed to a source containing the U^{230} series. The Em^{218} line at 7.127 Mev[12] was taken as the energy standard and from this the main group of Cf^{246} was found to be 6.753 Mev. When the recoil energy correction is made, the decay energy for Cf^{246} becomes 6.865 Mev.

Alpha-Gamma Coincidence Spectrum

The photon spectrum in coincidence with Cf^{246} alpha particles is shown in Fig. 2.

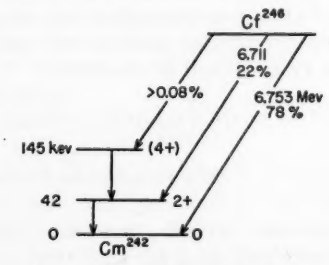

FIG. 1. Decay scheme for Cf^{246}.

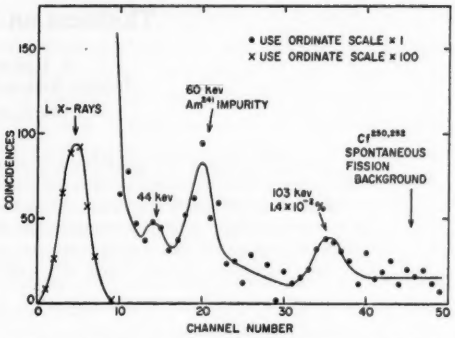

FIG. 2. Alpha-gamma coincidence spectrum of Cf^{246}.

42-kev Transition

The conversion coefficient for this transition was determined by the ratio of the abundance of the 42-kev gamma ray to the previously discussed population of the 42-kev state (22 percent). Two determinations gave the *L*-shell conversion coefficient as 800 and 1200. These values are in the expected range for an *E*2 transition on the basis of extrapolations from the data of Gellman, Griffith, and Stanley.[13]

100-kev Transition

Four determinations gave an average intensity of 1.4×10^{-4} photon per alpha disintegration. Since the energy of this photon corresponds well with the expected transition from the 4+ state to the 2+ state, we can assume that it is an *E*2 transition. Then if we assume that the conversion coefficient is the same as that measured for the corresponding transition in the decay of Cm^{242},[14] the minimum intensity of population of the 4+ state becomes approximately 8×10^{-4} as indicated in Fig. 1.

One of the current points of interest in alpha-decay theory is to explain the variation in population of 4+ states by different even-even alpha emitters. A convenient reference for comparisons is the "hindrance factor," which expresses the ratio of the observed partial half-life for the alpha transition to that calculated on the basis of the theory which gives good agreement with the observed half-lives for the ground-state transitions. For the Cf^{246} transition to the 4+ state the minimum experimental intensity, as mentioned above, is 8×10^{-4}, and this can be shown to correspond with a hindrance factor of 220. This factor is probably somewhat too large because the approximations used in estimating the population of the 4+ state are expected to produce a value which is too low. The relation between this hindrance factor and those of corresponding alpha groups of other alpha emitters is shown in Fig. 3 of another publication.[9] A brief statement on the possible implications of these trends will also be found there.

[10] H. Jaffe, Ph.D. thesis, University of California Radiation Laboratory Unclassified Document UCRL-2537, April, 1954 (unpublished).
[11] E. Church (private communication, February, 1954).
[12] Asaro, Slater, and Perlman (unpublished data, 1953).
[13] Gellman, Griffith, and Stanley, Phys. Rev. 85, 944 (1952).
[14] Asaro, Thompson, and Perlman, Phys. Rev. 92, 694 (1953).

Theorem on Angular Correlation*

S. RABOY AND V. E. KROHN
Argonne National Laboratory, Lemont, Illinois
(Received December 3, 1954)

In a multiple cascade, the angular correlations between a gamma ray and each of two following or preceding gamma rays are shown to be equal for the following conditions: (1) The two observed gamma rays not common to both pairs must have the same multipolarity and must result from basic transitions. (2) If the two observed gamma rays not common to both pairs have unobserved gamma rays between them, these unobserved gamma rays must come from basic transitions. (3) The transitions subject to the first two conditions must take place between levels with spins in monotonic sequence.

IT is the purpose of this note to point out a useful theorem concerning the angular correlation of pairs of gamma rays in multiple cascades. Consider, for example, the case of the triple cascade,

$$j_0 \overset{L_1}{\rightarrow} j_1 \overset{L_2}{\rightarrow} j_2 \overset{L_2}{\rightarrow} j_3,$$

where the spins form a monotonic sequence and each transition is basic.[1]

Then by the theorem of Weneser and Hamilton[2] we have

$$A_k[1,2]=A_k[1,3], \tag{1}$$

where $A_k[n,m]$ is the coefficient of the kth Legendre polynomial in the angular correlation function of the nth and mth gamma rays of the cascade.

The treatment of the angular-correlation problem by Coester[3] is very convenient and is used here. In Coester's notation,[3,4] the following holds for any cascade:

$$\begin{aligned} A_k[1,2]&=A_k(j_0j_1)A_k(j_2j_1),\\ A_k[1,3]&=A_k(j_0j_1)\bar{A}_k(j_2j_1)A_k(j_3j_2), \end{aligned} \tag{2}$$

where

$$\begin{aligned} A_k(j_0j_1)&=F_k(L_1L_1j_0j_1)+\delta_1^2F_k(L_1+1\ L_1+1\ j_0j_1)\\ &\quad+2\delta_1F_k(L_1\ L_1+1\ j_0j_1),\\ \bar{A}_k(j_2j_1)&=(2j_2+1)^{\frac{1}{2}}(2j_1+1)^{\frac{1}{2}}[W(j_2L_2kj_1;j_1j_2)\\ &\quad+\delta_2^2W(j_2\ L_2+1\ kj_1;j_1j_2)]. \end{aligned} \tag{2a}$$

The W's are Racah coefficients and

$$\begin{aligned} F_k(LL'j_aj_b)&=(-)^{j_a-j_b-1}C_{1\ -1}{}^{LL'k}(2j_b+1)^{\frac{1}{2}}\\ &\quad\times(2L+1)^{\frac{1}{2}}(2L'+1)^{\frac{1}{2}}W(j_bj_bLL';kj_a), \end{aligned} \tag{2b}$$

where the C's are the Clebsch-Gordan coefficients. Coester's F's are similar to the F and G coefficients of Biedenharn and Rose.[5]

Equations (1) and (2) can be combined to give:

$$A_k(j_2j_1)=\bar{A}_k(j_2j_1)A_k(j_3j_2), \tag{3}$$

which holds when the second and third transitions are basic. The multipolarity and mixing of the first gamma ray of the cascade and the spin of the first state, j_0, do not affect the terms of Eq. (3). Since Eq. (3) does not depend upon properties of the first gamma ray, it can be combined with Eq. (2) to yield Eq. (1) free of the requirements that first gamma ray must be basic and that of the spin of the first state, j_0, must be part of the monotonic sequence.

We now consider cascades of more than three gamma rays:

$$j_0 \overset{L_1}{\rightarrow} j_1 \overset{L_2}{\rightarrow} j_2 \rightarrow\cdots j_{m-1} \overset{L_m=L}{\rightarrow} j_m \rightarrow\cdots j_{n-1} \overset{L_n=L}{\rightarrow} j_n \rightarrow\cdots j_f,$$

where the spins form a monotonic sequence, all transitions are basic, and $L_m=L_n$. From the theorem of Weneser and Hamilton, we have

$$A_k[m,p]=A_k[n,p], \tag{4}$$

and Coester's formulas (with or without mixing) are:

$$\begin{aligned} A_k[m,p]&=A_k(j_{m-1}j_m)\bar{A}_k(j_{m+1}j_m)\cdots\bar{A}_k(j_nj_{n-1})\cdots\\ &\quad\bar{A}_k(j_{p-1}j_{p-2})A_k(j_pj_{p-1}),\\ A_k[n,p]&=A_k(j_{n-1}j_n)\bar{A}_k(j_{n+1}j_n)\cdots\\ &\quad\bar{A}_k(j_{p-1}j_{p-2})A_k(j_pj_{p-1}). \end{aligned} \tag{5}$$

Equations (5) apply where the pth transition follows the mth and nth but similar expressions can be written where the pth transition precedes the mth and nth transitions. From (4) and (5) we obtain

$$\begin{aligned} A_k(j_{n-1}j_n)&=A_k(j_{m-1}j_m)\bar{A}_k(j_{m+1}j_m)\cdots\bar{A}_k(j_nj_{n-1})\\ &=A_k(j_{m-1}j_m)\prod_{s=m}^{n-1}\bar{A}_k(j_{s+1}j_s), \end{aligned} \tag{6}$$

which holds when the mth, $(m+1)$th, $\cdots n$th transitions are basic and j_{m-1}, j_m, j_{m+1}, $\cdots j_{n-1}$, j_n are in monotonic sequence. Equation (6) is not affected by mixing of the pth gamma ray or any unobserved gamma rays which are common to both cascades. Also, any spin which does not appear as an argument of a factor in Eq. (6) need not be part of the monotonic sequence.

* Work performed under the auspices of the U. S. Atomic Energy Commission.

[1] S. P. Lloyd, Phys. Rev. **83**, 716 (1951). A basic transition between two levels with spins j_1 and j_2, respectively, is defined as the emission of unmixed radiation with multipolarity 2^L, where $L=|j_1-j_2|$.

[2] J. Weneser and D. R. Hamilton, Phys. Rev. **92**, 321 (1953).

[3] F. Coester, Argonne National Laboratory Report ANL-5316 (unpublished).

[4] V. E. Krohn and S. Raboy, Phys. Rev. **97**, 1017 (1955).

[5] L. C. Biedenharn and M. E. Rose, Revs. Modern Phys. **25**, 729 (1953).

We now combine Eqs. (5) and (6) to obtain Eq. (4) subject only to the conditions which remain on Eq. (6). The results are readily extended to the case where the pth gamma ray is not common to both pairs but the n-p and m-q pairs are considered and $L_p=L_q$; $L_n=L_m$.

We have, thus, demonstrated the following theorem: In a multiple cascade the angular correlations between a gamma ray and each of two following or preceding gamma rays are equal when the following conditions are satisfied: (1) The two observed gamma rays not common to both pairs must have the same multipolarity and must result from basic transitions. (2) If the two observed gamma rays not common to both pairs have unobserved gamma rays between them, these unobserved gamma rays must come from basic transitions. (3) The transitions subject to the first two conditions must take place between levels with spins in monotonic sequence.

There are no restrictions on the multipolarity and mixing of unobserved gamma rays which are between the observed members of both pairs or of a gamma ray observed as a common member of each pair. Also, there are no restrictions on the spins of levels which are involved only in these unrestricted transitions.

The application of the theorem to the three-gamma-ray cascade of Pb^{204m} is of interest. The last two gamma rays of the cascade have been identified as $E2$ transitions. The obvious 4–2–0 spin assignment for the lower levels of the cascade will then result in identical angular correlation functions for the first two and the first and third gamma rays if both $E2$ transitions are unmixed. As the observed anisotropies are significantly different[4] and the transition to the ground (spin 0) state cannot be mixed, the second gamma ray must be a mixed ($E2+M3$) transition, or an alternate spin scheme is required.

We wish to thank Professor F. Coester for the use of his notes and for helpful suggestions.

PHYSICAL REVIEW VOLUME 98, NUMBER 1 APRIL 1, 1955

Excitation Functions for Some Proton-Induced Reactions of Thorium*

HOWARD A. TEWES†
Livermore Research Laboratory, California Research and Development Company, Livermore, California
(Received May 3, 1954)

The excitation functions for the (p,f), (p,n), and $(p,3n)$ reactions on thorium have been determined for proton energies up to 32 Mev.

INTRODUCTION

PREVIOUS work on the (p,f), (p,n), and $(p,3n)$ reactions on thorium has indicated that the (p,xn) processes account for much of the total proton cross section at all energies up to 20 Mev.[1]

However, as yet, no absolute cross sections have been published for these reactions, although some theoretical predictions have been made.

The work reported here was undertaken to ascertain the absolute cross sections of the (p,n) and $(p,3n)$ reactions at various energies up to 32 Mev and to allow estimates of the (p,f) cross section to be made over this energy range.

PROCEDURE

A single bombardment of a stack of 2-mil thorium foils was made on the University of California Radiation Laboratory linear accelerator. The energy of the protons as a function of depth in the stack was calculated from previously determined range-energy relationships. The irradiation was carried out over a twelve-hour period with a proton current averaging 10^{-2} microampere. The beam was integrated with a standard electrometer assembly available for routine use with the linear accelerator.

The thorium foils were dissolved in a mixture of hydrochloric and hydrofluoric acids; a few hundred counts of Pa^{231} tracer were added to each sample, as were 10 mg of zirconium carrier. The chemistry used to separate and purify the zirconium and protactinium fractions has been outlined in the appendix.

The proton-induced fission cross sections were calculated from the yields of Zr^{97}, since the fission yields of Zr^{97} have previously been determined for thorium which has been irradiated with protons up to 20-Mev energy.[1]

The ZrO_2 counting samples were slurried into one-inch-diameter aluminum "hats" and counted, using a standard Geiger tube (a thin-window, argon-filled, chlorine-quenched Amperex 100 C tube) and scaling circuit. Since the self-scattering, self-absorption corrections for the Zr^{97}-Nb^{97} combination are known,[2] the absolute counting rates were determined for the Zr^{97}

* This work was performed under the auspices of the U. S. Atomic Energy Commission.
† Present address: University of California Radiation Laboratory, Livermore, California.
[1] H. A. Tewes and R. A. James, Phys. Rev. 88, 860 (1952).
[2] R. E. Batzel (private communication).

TABLE I. Measured cross sections for proton-induced reactions of thorium.

E_p (Mev)	Fission yield of Zr^{97} [a] (percent)	$\sigma(p,f)$ (mb)	$\sigma(p,n)$ (mb)	$\sigma(p,3n)$ (mb)
31.3±0.4	3.5±0.2	1080 ±70	28.6 ±3	106 ± 5
26.1±0.4	3.5±0.2	910 ±60	21.4 ±2.5	402 ±38
20.8±0.5	3.6±0.1	680 ±40	19.5 ±1.5	324 ±12
18.0±0.5	4.1±0.1$_5$	375 ±20	19.9 ±2.0	47 ± 5
14.9±0.6	4.2±0.1	130 ± 8	13.1 ±1.5	5.0± 1
12.1±0.7	4.3±0.2	26 ± 2	6.4 ±0.7	
9.6±0.9	4.1±0.2	9.2± 0.5	0.85±0.07	
7.7±1.0			0.30±0.04	
5.3±1.2			0.39±0.05	

[a] Zr^{97} fission yields for proton energies below 21 Mev are given in reference 1; those yields above 21 Mev are estimated.

samples mounted on one-inch-diameter platinum disks; the beta decay of Pa^{232} was followed on the same counter used for the Zr^{97} counting. The scattering and geometry corrections were made by preparing a weightless Pa^{232} sample on a thin zapon backing, and comparing its counting rate in a proportional counter having 4π geometry with its counting rate as determined (with platinum backing) on the Geiger tube used in this work.

The absolute alpha-decay rates of the protactinium samples were found by counting them in an ionization chamber with a known (52 percent) geometry; a 50-channel pulse analyzer was then used to determine the energy spectrum of the alpha particles, and hence, the fractions of the alpha particles having energies characteristic of different protactinium and uranium isotopes. The amount of Pa^{230} present was calculated from the decay rate of its daughter (U^{230}) which emits 5.85-Mev alpha particles; the chemical yield of Pa^{231} was calculated from the counting rate found for its ~5.0-Mev alpha particles.

RESULTS

The cross sections for the (p,f), (p,n), and $(p,3n)$ reactions at various proton energies are given in Table I; the fission yields for Zr^{97} which were used in the calculation of the (p,f) cross sections are also noted. The excitation functions for the three reactions under investigation are shown in Fig. 1.

Because the reactions $(p,2n)$, (p,pn), and $(p,p2n)$ were not studied, the total proton absorption cross section for thorium could not be calculated.

DISCUSSION

The excitation functions for the reactions which have been studied in this work do not check too closely the results which have been previously reported[1] (see Fig. 2); however, this may be due to the fact that in the earlier work, the incidence of (p,pn) and $(p,p2n)$ reactions were neglected in the calculations of the reported cross sections.

It is believed that the fission cross sections reported here for the lower proton energies may be too high; the large neutron flux present in the region of the thorium stack from which the "low-energy" foils were taken could well have produced an appreciable number of fissions. This conclusion is supported by the observation of appreciable amounts of the 27-day Pa^{233} [from the process $Th^{232}(n,\gamma)Th^{233}(\beta^-/23\text{ min})Pa^{233}$] in the protactinium fractions separated from several of the "low-energy" foils.

Batzel[3] has shown that for any heavy isotope, a correlation may be made between the (a,xn) cross sections and the (a,f) cross section, where a is some initiating particle. The relation can be expressed as

$$\Gamma_f/\Gamma_n = C,$$

where Γ_f/Γ_n may be defined (ignoring charged-particle

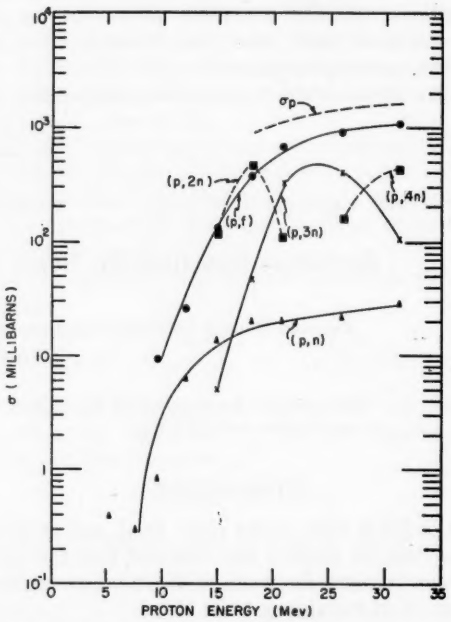

FIG. 1. Excitation functions for proton-induced reactions of Th^{232}.

emission) by the equation:

$$\frac{\Gamma_f}{\Gamma_n} = \frac{\sigma_f}{\sigma_n + 2\sigma_{2n} + 3\sigma_{3n} + \cdots + X\sigma_{xn}} = \frac{\sigma_f}{\sum_x X\sigma_{xn}}.$$

It has been found that this ratio of the probability of fission to the probability of neutron emission is not dependent on the energy of the initiating particle, where this energy is great enough so that resonances in the compound nucleus are not important. However, the value of the ratio does vary for different isotopes, and is apparently a function of Z^2/A.

Since neither the σ_{2n} nor the σ_{4n} for protons on Th^{232} were determined in this work, an attempt was made to predict these cross sections from theoretical considerations.

[3] R. E. Batzel (private communication).

The total absorption cross section for Th^{232} was calculated from relations given by Blatt and Weiskopf,[4] using a radius for Th^{232} given by the relation, $R=1.5\times10^{-13}A^{\frac{1}{3}}$.

The total cross sections thus obtained are given in Table II; the calculations were not made for proton energies below 18 Mev since the values below this energy are extremely energy sensitive, and hence may be quantitatively misleading.

In determining the values of σ_{4n}, it was assumed that only (p,f), $(p,3n)$, and $(p,4n)$ processes were important above 25 Mev; between 18 and 25 Mev, only the (p,f), $(p,2n)$, and $(p,3n)$ processes were considered in finding σ_{2n}.

In order to calculate a value of σ_{2n} for $E_p=14.9$ Mev, the ratio σ_{2n}/σ_n was found by using the treatment of Blatt and Weisskopf;[5] σ_{2n} was then obtained from the known value of σ_n. The calculated values for σ_{2n} and σ_{4n} are given in Table II and are plotted in Fig. 1.

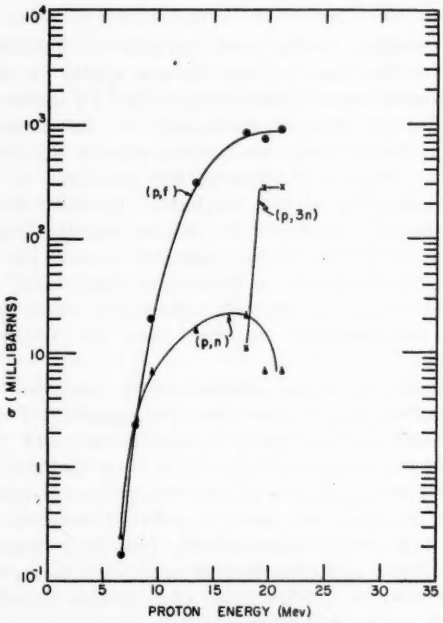

FIG. 2. Semitheoretical excitation functions for proton-induced reactions of Th^{232} (see reference 1, Fig. 9).

The calculated threshold for the $(p,3n)$ reaction is ~17.5 Mev; from neutron binding energies,[6] the threshold for the $(p,2n)$ reaction should be ~12 Mev. Consequently, at and below this energy, only the (p,f) and (p,n) reactions should occur.

[4] J. M. Blatt and V. F. Weisskopf, *Theoretical Nuclear Physics* (John Wiley and Sons, Inc., New York, 1952), p. 352.
[5] See reference 4, p. 379.
[6] G. T. Seaborg, "Nuclear Thermodynamics of the Heaviest Elements," Third Annual Phi Lambda Epsilon Lecture, Ohio State University, 1952 (unpublished).

TABLE II. Calculated cross sections for proton-induced reactions of thorium.

E_p (Mev)	σ_p (total) (mb)	$\sigma(p,2n)$ (mb)	$\sigma(p,4n)$ (mb)
31.3±0.4	1650		430
26.1±0.4	1500		160
20.8±0.5	1130	110	
18.0±0.5	910	470	
14.9±0.6		117	

TABLE III. Calculated values of the ratio Γ_f/Γ_n (probability of fission/probability of neutron emission).

E_p	Γ_f/Γ_n
31.3±0.4	0.52
26.1±0.4	0.49
20.8±0.5	0.56
18.0±0.5	0.34
14.9±0.6	0.49
12.1±0.7	4.3
9.6±0.9	9

On the basis of the foregoing treatment, the values for Γ_f/Γ_n were calculated; Table III is a tabulation of this ratio at different energies. It can be seen that Γ_f/Γ_n remains relatively constant at 0.5 for all energies above 14.9 Mev; the low value at 18 Mev may be attributed to the uncertainty of the total proton absorption cross section as calculated for this energy.

I wish to thank Dr. R. E. Batzel for many helpful discussions regarding the interpretation of the results obtained in this investigation. I should like to express my appreciation to Mr. G. H. Coleman for his help in making the chemical separations; also the cooperation of Mr. W. W. Olson and the linear accelerator operating staff is gratefully acknowledged.

APPENDIX

The chemical procedures used in the separation and purification of the zirconium and protactinium fractions have been slightly modified from those reported by Meinke.[7]

The thorium foils were dissolved in an HCl-HF mixture; the Pa was extracted into diisopropyl ketone (DIPK) from 6*M* HCl solution. The aqueous phase in this procedure was saved for Zr chemistry; the Pa was extracted into 2*M* $HClO_4$ from the DIPK, and subsequently re-extracted into 0.4*M* trifluorothenoylacetone (TTA) in benzene. It was then back extracted into 6*M* HCl (containing 0.1*M* HF) and plated on platinum.

The aqueous phase containing the Zr was made 3*M* in HCl and the Zr was extracted into 0.4*M* TTA in benzene. The TTA-benzene phase was washed and the organic phase was evaporated and ignited to give ZrO_2.

[7] W. W. Meinke, Atomic Energy Commission Report, AECD-2738 (UCRL-432) (unpublished).

Elastic Scattering of 20.6-Mev Protons by Deuterons*†

DAVID O. CALDWELL‡ AND J. REGINALD RICHARDSON
Department of Physics, University of California, Los Angeles, California
(Received August 23, 1954; revised manuscript received November 17, 1954)

The absolute differential cross section for the elastic scattering of 20.6-Mev protons by deuterons was measured by using the external beam of the U.C.L.A. synchrocyclotron. A triple-coincidence proportional counter telescope, with variable absorbers between the second and third counters and differential pulse-height discriminators (set by a new method) on the first two counters, was used to select the desired particle by range and specific ionization. Deuterium gas at atmospheric pressure provided the target for the proton beam, which was collimated to $\frac{1}{8}$ in. diameter, with a maximum angular divergence of $\frac{1}{4}°$. An interchangeable slit system gave angular resolutions of 0.9° or 1.8°. Absolute measurements were made at 22 angles from 12° to 164° (center-of-mass) with an accuracy varying approximately from 1 percent to 3 percent, depending upon the angle. The cross section shows the familiar deep minimum (near 130° in the present case), but in addition a shallower minimum near 18°, due to Coulomb-nuclear interference. This latter minimum should allow fitting the data with a unique set of phase shifts, unlike previous nucleon-deuteron scattering experiments, and thus provide a more stringent test for theories.

I. INTRODUCTION

THE study of the scattering of nucleons by deuterons could be expected to yield information on (1) the character of the force between neutrons, as compared with that between protons; (2) the exchange properties of nuclear forces; and (3) the existence and nature of three-body forces.

Because of the importance of these subjects, a considerable amount of work already has been done in this field. Differential cross sections for *p-d* and *n-d* elastic scattering[1] have been measured over a wide range of energies. While the inelastic scattering has received much less attention, a little information is available on the $d(p,2p)n$ and $d(n,2n)p$ reactions.

A large quantity of theoretical work has also been done. In the intermediate energy region some theoretical work is available on *n-d*[2–6] and *p-d*[7–14] (often with *n-d* included) elastic and inelastic[15–17] scattering. Phase shifts from *p-d* experiments appear to differ from those obtained from corresponding *n-d* scatterings only by an amount attributable to the Coulomb barrier. This evidence for charge symmetry is not very decisive, however, because of the inaccuracy of the experiments. It seems worthwhile to make better experimental comparisons in this intermediate energy region, where the charge symmetry assumption can be tested for several angular momentum states, and where the most accurate *n-d* experiments can be done, using monoenergetic neutrons from the $T(d,n)He^4$ reaction.

Indeed, the recent calculations of Christian and Gammel[14] seem to show that a comparison of only quite accurate *n-d* and *p-d* experiments could yield much information on the *n-n* force. They find that the *n-n* and *p-p* forces are relatively unimportant compared with the triplet even parity *n-p* force. However, this result may stem at least partially from their choice of slow-neutron scattering lengths on which to base phase shifts, whereas a different set of scattering lengths is also allowed by experiments.[18]

It is an important characteristic of the nucleon-deuteron scattering work published so far that each experiment could be fitted by two sets of phase shifts, corresponding to the ambiguity in the scattering lengths. While such an indeterminateness is inherent in *n-d* scattering (unless the experiment could be performed with polarized neutrons) a unique set of phase shifts would be obtainable from *p-d* scattering, if the region of interference between Coulomb and nuclear forces were accurately observed. So far, *p-d* experiments have either not been extended to low enough angles, or have been too inaccurate at low angles to provide the needed additional condition which would remove this ambiguity.

* This work was supported in part by the joint program of the Office of Naval Research and the U. S. Atomic Energy Commission.

† A more complete account of this work is given by D. O. Caldwell and J. R. Richardson, University of California, Los Angeles, Technical Report No. 22, 1954 (unpublished).

‡ Assisted by U. S. Atomic Energy Commission Predoctoral Fellowships and a National Science Foundation Postdoctoral Fellowship. Present address: Physics Department, Massachusetts Institute of Technology, Cambridge, Massachusetts.

[1] A complete bibliography of theoretical and experimental papers is given by D. O. Caldwell and J. R. Richardson, University of California, Los Angeles, Technical Report No. UCLA-22 1954 (unpublished).

[2] R. A. Buckingham and H. S. W. Massey, Proc. Roy. Soc. (London) **A179**, 123 (1941).

[3] H. S. W. Massey and R. A. Buckingham, Phys. Rev. **71**, 558 (1947).

[4] M. Verde, Helv. Phys. Acta **22**, 339 (1949).

[5] M. M. Gordon and W. D. Barfield, Phys. Rev. **86**, 679 (1952).

[6] A. H. de Borde and H. S. W. Massey, as quoted in *Progress in Nuclear Physics* (Pergamon Press, Ltd., London, 1953), Vol. 3, pp. 267–268.

[7] C. L. Critchfield, Phys. Rev. **73**, 1 (1948).

[8] H. S. W. Massey and R. A. Buckingham, Phys. Rev. **73**, 260 (1948).

[9] R. Thomas, Phys. Rev. **76**, 1002 (1949).

[10] J. L. Gamel, Phys. Rev. **78**, 321(A) (1950), and Ph.D. thesis, Cornell University, 1950 (unpublished).

[11] G. Breit, Phys. Rev. **80**, 1110 (1950).

[12] Buckingham, Hubbard, and Massey, Proc. Roy. Soc. (London) **A211**, 183 (1952).

[13] A. L. Latter and R. Latter, Phys. Rev. **86**, 727 (1952).

[14] R. S. Christian and J. L. Gammel, Phys. Rev. **91**, 100 (1953).

[15] H. Höcker, Physik. Z. **43**, 236 (1942).

[16] B. H. Bransden and E. H. S. Burhop, Proc. Phys. Soc. (London) **A63**, 1337 (1950).

[17] R. M. Frank and J. L. Gammel, Phys. Rev. **93**, 463 (1954).

[18] Wollan, Shull, and Koehler, Phys. Rev. **83**, 700 (1951).

Thus it would seem that *p-d* and *n-d* experiments more adequate than those heretofore compared are needed to provide a test of the charge symmetry hypothesis, or even to establish which set of phase shifts is the correct one. A similar conclusion can be reached for the aim of determining the exchange character of nuclear forces. Since the deuteron provides a relatively big target, even fairly low-energy nucleons are scattered in states of angular momentum greater than zero, and hence the existence of exchange forces has been fairly well established by low-energy nucleon-deuteron scattering. However, the more difficult distinction among types of exchange forces requires more complete experimental and theoretical work.

At present, three main theoretical approaches are available for attempting to distinguish among force types by comparison with intermediate energy nucleon-deuteron scatterings, those of (1) Massey and his co-workers,[2,3,6,8,12] (2) Verde[4] and Gammel,[10] and (3) Christian and Gammel.[14] While the present experiment will provide the first comparison with all three methods, it is too much to expect from the theories that a comparison with any of them will provide a definite answer as to the type of exchange force present. The present difficult calculations are incomplete and use potentials which do not give satisfactory answers for intermediate energy nucleon-nucleon scattering, but a more serious trouble may be the omission of a three-body force.

The recent work of Drell and Huang[19] raises the hope that calculations can be carried out soon which will make feasible the obtaining of information about three-body forces from nucleon-deuteron scattering. Generalizing the Lévy[20] two-body potential for many-body forces, they calculated the total energy per nucleon as a function of nuclear density, and found an energy minimum of about the right value at a reasonable nuclear density. Since they find the repulsive three-body force to be almost entirely responsible for nuclear saturation, it would seem likely that such a force would show up in nucleon-deuteron scattering, if the calculations have any relation to reality. At intermediate energies the effects of a possible three-body force may have been masked by employing so many parameters to fit inadequate data. Comparing the predictions of a theory which includes a three-body force with the present experiment could be particularly interesting, since the kinetic energy involved is much like that within a nucleus.

II. EXPERIMENTAL APPARATUS

A. General Considerations

The necessity for carrying the *p-d* scattering measurements down to low enough angles to include the Coulomb-nuclear interference region is evident from the preceding discussion. Since the maximum angle at which Coulomb scattering is important, as given roughly by the square root of the ratio of the barrier to the kinetic energy, is 9° in the laboratory system for 20 Mev, the apparatus was designed to work down to 8°. This minimum angle corresponds to a center-of-mass angle of 12° for protons and 164° for deuterons. For center-of-mass angles larger than 120°, it was desirable to count the recoil deuterons to avoid the multiple scattering losses which could result from counting low-energy protons.

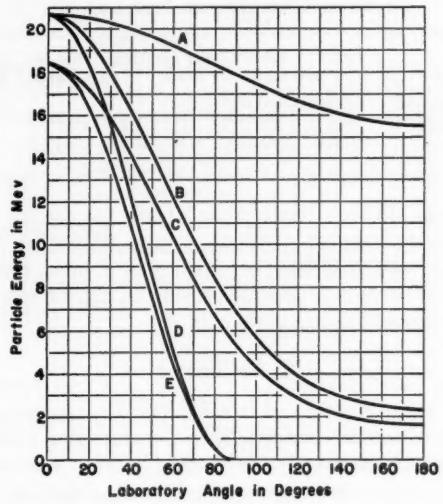

FIG. 1. Particle energy *vs* laboratory angle: (A) protons scattered from nitrogen, (B) protons scattered from deuterons, (C) maximum energy of protons from $d(p,2p)n$, (D) protons scattered from protons, and (E) recoil deuterons from *p-d* scattering.

As can be seen from Fig. 1, at any angle the desired particle had to be separated from four other particle groups. To do this, a triple-coincidence proportional counter telescope was used with absorbers between the second and third counters. A particle separation by range was provided by choosing the absorbers so that the desired particle was near the end of its range in the third counter; the resulting large pulse was then distinguished with an integral discriminator. Differential discriminators were used on the first two counters, in order to provide a separation on the basis of the specific ionization of the particles. While a simpler separation of particles would have been provided by counting both the scattered proton and recoil deuteron in coincidence, reliable low-angle data could not have been obtained in that way.

B. Scattering Chamber Arrangement

The electrostatically-deflected, 21-Mev proton beam of the 41-inch U.C.L.A. synchrocyclotron was made approximately parallel by a double-focusing wedge magnet in the cyclotron field. The external beam, which came in 20-μsec bursts, 1000 times a second, was brought out

[19] S. D. Drell and K. Huang, Phys. Rev. 91, 1527 (1953).
[20] M. M. Lévy, Phys. Rev. 88, 725 (1952).

TABLE I. Analyzing slit dimensions.

Slit	Width in inches	Std.dev.	No. of meas.	Height in inches	Std.dev.	No. of meas.
Front narrow	0.051552	±0.000059	112			
Rear narrow	0.052269	±0.000075	119	0.59234	±0.00016	51
Front wide	0.101023	±0.000041	56			
Rear wide	0.101879	±0.000044	60	0.59249	±0.00010	51

between 18-inch water walls about ten feet to the scattering chamber.

The scattering chamber itself was a brass casting appropriately machined to provide an axis of rotation perpendicular to the beam axis.

C. Collimator

In the collimator all nondefining diaphragms were made of carbon to reduce both the scattering and the neutron background. To further reduce scattering, these diaphragm edges were beveled. Most of the unused external beam was stopped by a carbon insert in the flange which joined the collimator to the cyclotron, and most of the rest on an insert just ahead of the first defining hole. The first defining hole was 0.1248 in. in diameter and the second, 0.1236 in. Their $\frac{1}{32}$-in. thick brass defining edges were 14.22 inches apart, giving a maximum angular divergence of the beam in the chamber of ±0.50°. However, the part of the beam selected by the collimator was so nearly parallel that beam pictures showed essentially all the beam to be contained within an angular divergence of ±0.2°. Between the two defining holes were three nondefining holes spaced by aluminum sleeves so as to fulfill the criteria necessary to make the collimator effectively wall-less. A final 0.170-inch diameter antiscattering hole was added 1.790 in. beyond the second defining hole to limit the spray of protons off the last defining diaphragm to a cone of half-angle 4.7°.

The collimator extended as far as possible into the chamber, the second defining hole being 2.841 in. from the chamber center, in order to make small angle measurements possible, permit a small Faraday cup opening, and reduce the penetration of the first counter slit by low-angle protons.

To keep small the loss of beam from multiple scattering, 0.0005 in. Mylar was used for the foil (just ahead of the first defining hole) which separated the cyclotron vacuum from the chamber.

After preliminary mechanical and optical alignment the final check on the adjustment of the second defining hole was made by exposing photographic paper, placed directly behind a centering needle, to the proton beam.

TABLE II. Constants of the slit geometry.

Slits	r_1 in.	Std.dev. in.	r_2 in.	Std.dev. in.	HD_FD_R/r_1r_2 cm/sterad	Std.dev.
Narrow	3.2289	±0.0011	4.3895	±0.0004	0.28604×10^{-3}	±0.19 percent
Wide	3.2284	±0.0011	4.3885	±0.0004	1.09325×10^{-3}	±0.047 percent

By measuring with a traveling microscope the position of the needle shadow with respect to the beam circle, the beam-centering could be checked to within 0.002 in. Similar beam pictures provided also the final alignment of the whole chamber.

D. Analyzing Slits

To keep corrections for finite angular resolution small at small angles and to maintain reasonable counting rates at larger angles, two interchangeable sets of analyzing, or counter, slits were used, of angular resolution ±0.921° and ±1.800°. It was necessary to resort to the unusual expedient of putting the rear slit of either set between the second and third counters, in order to have simultaneously a practical slit geometry, a small minimum angle, a good angular resolution, a large solid angle, a triple-coincidence counting system, and a small chamber.

The slits were made of commercial bronze (90 percent Cu and 10 percent Zn), since the relatively high density and low Z of copper are desirable for reducing slit penetration. Such penetration was further diminished by milling down each slit plate around the opening to 0.030 in., a stopping thickness for 20-Mev protons.

The results of measurements on the analyzing slits are given in Table I, along with the number of final measurements of each dimension.

The distance between the slits (r_1) and the distance from the scattering center to the last slit (r_2) were measured in the Standards Laboratory of the U.C.L.A. Engineering Department with a Pratt and Whitney Electrolimit Gage, which read directly to 0.00005 in., and Johansson Precision Gage Blocks. A weighted average of the various determinations appears in Table II, along with the constant part of the solid-angle-scattering-length factor, $HD_FD_R/r_1r_2=1/G$, where D_F=front slit width, D_R=rear slit width, and H=rear slit height.

The accuracy of the alignment of the slits was checked for the following slit characteristics: height, left-right positioning, lengthwise and sidewise tilting, rotation, and slit edge nonuniformity. The total errors these introduced into G amounted to 0.004 percent for the narrow slits and 0.002 percent for the wide. The left-right positioning, rotation, and slit nonuniformity contributed also to errors in the scattering angle of 0.036° for the narrow and 0.042° for the wide slits. The amount by which the slit axis did not quite pass through the chamber center was measured and allowed for in setting the counter angle zero. When the error for setting the zero is added quadratically to those for setting the counters at any desired angle and for the slit alignment, the resulting error in angle is 0.063° for the narrow and 0.066° for the wide slits.

The antiscattering baffle (B in Fig. 2) attached by dowel pins to each front slit plate was aligned and checked in the same way as the slits. The baffle de-

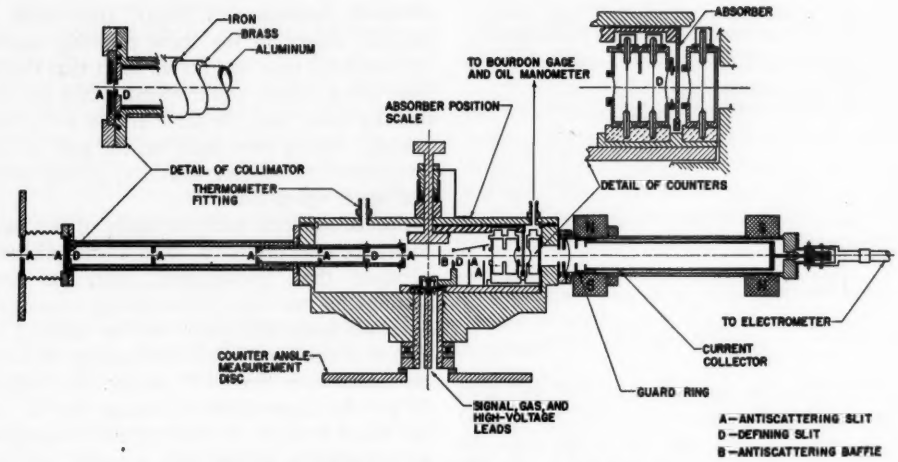

FIG. 2. Sectional view of the scattering chamber and details of the triple coincidence proportional counter telescope.

creased slit-edge penetration by cutting off low-angle protons and also helped prevent protons scattered off the last defining slit of the collimator from getting into the analyzing slit system. At counter angles of 15° and larger, the last antiscattering hole on the collimator also prevented direct slit-slit scattering, but between 15° and 10° the baffle alone was effective. At 8° direct slit-scattered protons could get through the front analyzing slit, but not past further antiscattering slits between the front analyzing slit and the first counter window.

E. Absorbers

The absorbers between the second and third counters, used to provide particle selection by range, were mounted on the rim of a sector, as shown in Fig. 2. The set of absorbers desired could be turned into position by means of a Wilson seal, and all parts determining this position were held in place by dowel pins. Photographic checks with the beam showed that the 10° wide foils were positioned to an accuracy of better than 0.5°, whereas the third counter window was 5° wide.

The 99.4 percent pure aluminum foils were weighed and measured with sufficient accuracy so that variations in surface density for foils of the same nominal thickness could be taken as a measure of the variations in foil thickness. A safety factor of three standard deviations of this foil thickness variation was allowed in determining the thickness of absorber to be used. Much larger allowances had to be made for the angular resolution of the counters (see Fig. 1) and for straggling. For the latter, an integral range distribution was obtained,[21] permitting one to find the number of mg/cm² of Al which have to be subtracted from the mean range in order that not more than 0.1 percent of the particles of the desired energy are lost by straggling. Since the mean range used at a given angle was that corresponding to the largest angle (or lowest energy) the counter slit system could see, the particle loss in the absorbers due to straggling was negligible.

Loss of particles in the absorber because of multiple scattering was also negligible, mainly because the third counter window was quite large compared with the analyzing slits, the absorber was close to the window, and the window was made very thick (about 50 mg/cm²), so that the largest part of the multiple scattering took place in the window itself. Calculations of multiple scattering with energy loss were made using a power law for $-dE/dx$ in the Rossi-Greisen[22] formulation to give $\langle\phi^2\rangle=0.045(E_f^{-0.22}-E_i^{-0.22})$, where ϕ is the rms projected scattering angle in radians and E_i is the proton energy in Mev before, and E_f after, passing through the Al. Even though this gives an overestimate of ϕ, the loss was still found to be negligible.

F. Counters

Because the second slit was placed between the second and third counters (see Sec. IID), the multiple scattering loss between the slits had to be considered carefully. Loss was due mainly to the first counter window and to a lesser extent to the counter gas; the contributions of the deuterium and the second counter window, which was right next to the second slit, were quite small. From multiple scattering[23] calculations it was found that the loss could be made negligible if (1) the first counter window was 0.00025-in. duraluminum, (2) the counter gas was at ½ atmosphere, (3) the narrow slits were not used for particles of energy less

[21] D. O. Caldwell, Phys. Rev. 88, 131 (1952) and in more detail D. O. Caldwell, University of California, Los Angeles, Technical Report No. 9, 1952 (unpublished).

[22] B. Rossi and K. Greisen, Revs. Modern Phys. 13, 267 (1941).

[23] W. T. Scott, Phys. Rev. 85, 245 (1952).

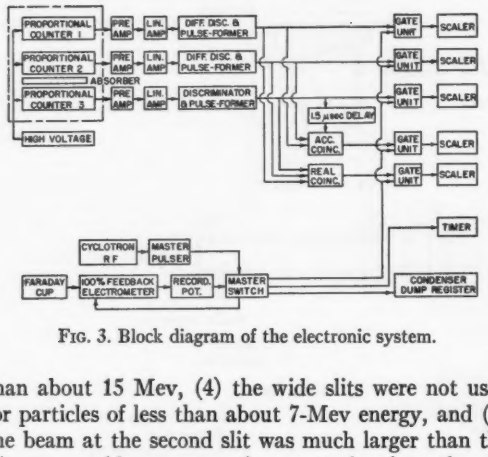

FIG. 3. Block diagram of the electronic system.

than about 15 Mev, (4) the wide slits were not used for particles of less than about 7-Mev energy, and (5) the beam at the second slit was much larger than the slit, to provide compensating scattering into the slit opening.

Since there was no window between the first and second counters, it was necessary to be sure that one did not affect the other. When a source was placed so that several thousand alpha particles a second traversed the first counter but did not quite enter the second, the counter rate in the second was just background, and none of these few counts were in double coincidence. On the other hand, when the source was moved closer, essentially all the counts from the second counter were in coincidence with those from the first.

G. Electronics

A general idea of the electronics system[24] may be obtained from Fig. 3. The speed of the counting system was limited by the Bell-Jordan amplifiers, and was set by the length of shorted delay lines chosen in the discriminators to form the uniform pulses used in the rest of the system. In normal operation, then, both the real and accidental coincidence units had resolving times of 0.71 ± 0.04 μsec. A 1.5-μsec delay line in the third channel of the latter thus assured that all accidental coincidences recorded resulted from real coincident events in the first two counters and a random event in the third (see Sec. IVA).

Two forms of gating were employed: (1) all scalers could be gated on at the beginning of a selected charging cycle of the beam-integrating condenser and off at the end of the same or another cycle, and (2) the scalers could be made to count only during cyclotron beam on-times. This latter gate[25] reduced the chances of getting spurious counts not initiated by the beam by a factor of roughly 60/1000.

The usual checks were made to be sure that the electronic system was linear, that there were not unequal delays in the three counting channels, that the resolving time was not so short that desired counts were being missed, and frequently that the 1–3 and 2–3 doubles rates were the same as the 1–2–3 triples rate. Nightly checks were made on the gain of the system, amplifier-discriminator linearity, gating pulse setting, and scaler operation.

Special mention must be made of the method used to set the discriminators, since it was quicker and more accurate than conventional methods. Approximate settings for the first two counting channels could be obtained from any prior run by using a curve like Fig. 4 of the energy loss distribution in a counter, as calculated from Symon's[26] theory. After making a run to get the approximate counting rate at that angle, the lower level of the first channel discriminator was set arbitrarily higher, and another run was made. Suppose we were counting 16-Mev protons and raising the discriminator to a setting of 200 had decreased the counting rate by 30 percent. Figure 4 shows that this discriminator setting of 200 must have corresponded to a 20-kev energy loss in the counter. Since the energy loss distribution essentially begins (0.1 percent curve) at 14 kev and ends (99.9 percent curve) at 52 kev, the lower level discriminator had to be set below $200(14/20) = 140$ and the upper level had to be set above $200(52/20) = 520$. The second channel was set in the same way, but the third channel, because of the wide range of energies in the third counter due to straggling, had to be set by taking a conventional bias curve. However, by using the energy loss distribution together

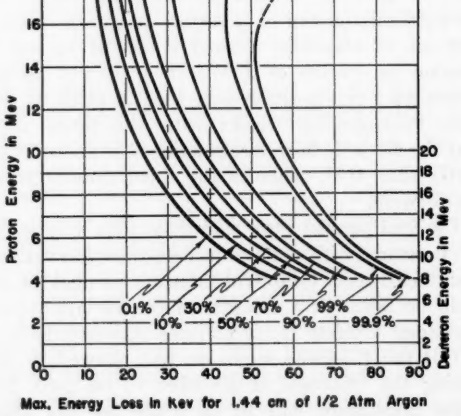

FIG. 4. Energy loss distribution in a counter *vs* proton and deuteron energy. For a given percentage of monoenergetic particles, each curve represents the maximum energy loss *vs* particle energy.

[24] The authors wish to thank C. Wilkin Johnstone and Richard J. Watts of the Los Alamos Scientific Laboratory for generously supplying circuits, information, and advice.

[25] We are indebted to Louis K. Jensen for designing, building, and maintaining this unit, as well as an excellent pulse generator that received continual use.

[26] K. R. Symon, Ph.D. thesis, Harvard University, 1948 (unpublished), as quoted by B. Rossi, *High-Energy Particles* (Prentice-Hall Inc., New York, 1952), pp. 32–35.

with the straggling calculations,[21] plots of minimum energy loss *vs* counter angle for protons and deuterons could be obtained. It was then easy to set the third channel discriminator initially and to pick a minimum of settings to determine the counting rate plateau. The whole procedure, as well as the stability of the electronics, was frequently checked by predicting a first or second channel discriminator setting for a certain percentage particle loss and then making a run to see if that loss was obtained.

H. Current Integration

Considering the collection of the beam, its integration, and the calibration of the integrator, we shall first be concerned with difficulties which can occur in beam collection. Such errors can be caused by (1) ionization in the region of the Faraday cup, (2) leakage in the cup or connecting cable, (3) acquisition or (4) loss of secondary electrons, (5) pickup and rectification of ac, (6) collection of ions by the electrical leads outside of the cup, (7) loss of electrons from the exterior of the cup by gamma ejection, (8) loss of part of the beam, and (9) having a low-energy component of the beam which does not produce countable scattering events.

The probability of a 20-Mev proton forming an ion pair in passing through the 9-in. long Faraday cup, kept at a pressure of less than 1×10^{-5} mm Hg, is only 0.03 percent, which is then an upper limit on the error due to ionization.

The electrometer used to integrate the beam was the 100 percent feedback type, which maintained the Faraday cup near ground potential and thus minimized leakage which was indeed found to be negligible.

The acquisition by the cup of secondary electrons produced by protons going through the 0.002-in. duraluminum foil at the chamber exit was eliminated by having between the foil and cup entrance a field of 1250 gauss (produced by a magnetron magnet outside the cup housing), and a grounded guard ring. Yntema and White,[27] in extensive tests on a similar system, found no effect of secondary electrons on the charge collected for cup potentials several thousand times as large as any encountered in the present experiment.

To prevent the escape from the cup of secondary electrons produced by the stopping of the proton beam (a) a magnetic field was present at the cup entrance; (b) another field (produced by a 1900-gauss magnetron magnet outside the cup housing) was placed at the end of the cup, where the beam stopped; (c) the cup was made unusually long; and (d) the entrance to the cup was partially enclosed. The latter two features decreased the solid angle for escape and minimized the influence of any slight potential difference between the cup and the region outside of it.

That pickup and rectification of ac were not a source of error was borne out by the agreement between calibrations made with and without the cyclotron rf on. To achieve this result, however, it was necessary to use *L-C* filters at both ends of the cable.

Similarly, calibrations made with the cyclotron beam on and off showed that ion collection by the cable and other radiation effects were not sources of error. The beam scattering loss at the Faraday cup entrance was found to be negligible, and indeed essentially all of the beam reached the back of the cup.

The last error considered is that of having a part of the beam penetrate a portion of the collimating diaphragms and lose so much energy that the scattering events it produced not be counted. This low-energy component was largely eliminated by the last collimator antiscattering hole and the chamber exit hole, which was made as small as it could safely be. Slit penetration was decreased by using brass (see Sec. IID) slits of just a stopping thickness and by precollimating the beam. Although the integral range curves taken to measure the beam energy (see Sec. IVC) showed no evidence for such a harmful low-energy component, the total error assigned to the beam collection, 0.3 percent (0.5 percent at a few angles), is mainly to allow for such an effect.

Since the details of the calibrations of the current integrator will be published elsewhere,[28] it is necessary to mention here only that a current-time method was used which provided accurate calibrations over the range of charging currents from 10^{-10} to 10^{-11} amp. Only the 8° data were taken with smaller currents. Three independent checks on the absolute values of the calibration constants and the consistency of over three hundred calibrations made during the course of the experiment led to the assignment of standard errors for the calibrations of from 0.2 percent for currents around 10^{-10} amp to 1 percent for currents smaller than 10^{-11} amp.

I. Vacuum System

While separate mechanical pumps were used for the deuterium and counter filling systems, the main mechanical and diffusion pumps were used on both the scattering chamber and Faraday cup, or either one separately. The whole main system could reach 3×10^{-5} and the Faraday cup alone, 9×10^{-6} mm Hg. With liquid nitrogen, the whole system could get down to 9×10^{-6}, and the cup alone, 2×10^{-6}. For the first few hours after shutting the chamber off from the pumps, the pressure increased 3×10^{-4} mm/min, while for longer periods the rate of rise was slower.

J. Deuterium System

To eliminate all impurities initially except normal hydrogen, the deuterium gas was forced to diffuse through the walls of a heated tube of palladium.

[27] J. L. Yntema and M. G. White, U. S. Atomic Energy Commission Report NYO-3478, 1952 (unpublished).

[28] H. N. Royden and D. O. Caldwell, Rev. Sci. Instr. (to be published).

The two tanks of deuterium from the Stuart Oxygen Company which were used for nearly all of the data were later analyzed mass-spectrographically by the Consolidated Engineering Corporation. The more impure of the two was found to contain only 0.04 percent air and 0.02 percent water, so the *Pd* tube was almost superfluous. The H,D analysis, which had a limit of error of less than 0.05 mole percent, showed one tank contained 99.20 mole percent D and the other 99.25 percent.

After the chamber was filled, the gas pressure was determined relative to the atmospheric pressure by means of a small *U*-tube manometer containing Octoil-*S* diffusion pump oil.

The temperature of the gas at the time the pressure was measured was determined to an accuracy of about ± 0.03 percent, where the large error results from the uncertainty that temperature equilibrium was established to better than 0.1°.

Temperature and pressure readings were made at the beginning and end of the period during which a gas filling was used, and the resulting difference in T/P values, along with the measured chamber leak rate, were used to assign T/P values for each run, according to the time elapsed since the chamber was filled. Since T/P changed by about 0.006 percent per hour and the fillings were used for one and sometimes two nights, the T/P value for most runs was known to at least 0.1 percent.

III. EXPERIMENTAL CHECKS

Of the many experimental checks which were made, the most important was that on the reproducibility of the data afforded by having taken a number of short runs at each angle, and also, for the majority of angles, by having taken data at the same angle on different nights, sometimes weeks apart. For each angle, then, two statistical errors in the data could be computed: a Poissonian one based on the total number of counts, and a Gaussian one based on the reproducibility of the data. These two errors were compared by a chi-square test, and with very few exceptions it was found that the data reproducibility depended only upon the number of counts. The few exceptions were mainly runs during which a faulty relay erratically threw extra counts into the scalers. While a good average background was found to correct for this, the individual runs showed too much variation and have been assigned appropriately larger errors.

Another check on data reproducibility was provided by counting both scattered protons and recoil deuterons at nearly the same center-of-mass angle, since there were important differences in the two types of measurements. For instance, a background subtraction was necessary when counting deuterons. Because of the broadness of the energy loss distribution (see Fig. 4), not all the inelastic protons having a range equal to or longer than that for the deuterons could be excluded by their energy loss in the first two counters. Therefore, a background was measured by using absorbers just thick enough to stop the deuterons. Since the group of protons from deuteron breakup being counted had a slightly higher energy than the group which actually constituted the background, it was necessary to reset the discriminators a little. These new settings were obtained easily using the energy loss distribution and third counter minimum energy loss curves discussed in IIG.

The agreement of the two deuteron check points with the proton data is an especially good test of the background measurement, since these points lie near the main minimum in the cross-section curve, where the inelastic scattering is relatively large compared with the elastic. Indeed, the main group of deuteron points join smoothly onto the proton points right in the minimum, and the point at 130° had a much larger background than did any other deuteron measurement. The deuteron check point at 89.9°, which is close to a proton point at 91.9°, lies on a smooth curve drawn through the proton data.

A further difference in the proton and deuteron measurements at the two check points is that in one case the proton had a considerably higher energy than the corresponding deuteron, and in the other case the deuteron had over twice as much energy as the corresponding proton. In fact, these were, respectively, the lowest deuteron and proton energies used in the experiment. Since the root mean square multiple scattering angle varies approximately inversely as the particle energy, if there were any appreciable multiple scattering loss at any angle, it should have showed up in these two cases.

Since at a fixed energy the multiple scattering loss would have been greater with the narrow slits than with the wide, both the proton and deuteron measurements at a laboratory angle of 20° were made with narrow and wide slits as a further check. For the deuterons, the narrow slit result (4.7 percent statistical error) was 1.2 percent higher than the wide (1.6 percent), while for the protons, the narrow slit cross section (1.4 percent) was 0.87 percent lower than the wide (0.63 percent).

Some check on multiple scattering loss in the gas was provided by a run made with the chamber filled to only half an atmosphere and using narrow slits at 20°, at which angle the proton energy was the lowest used with those slits. Since scattering from the collimating slits to the analyzing slits also would have made the half-atmosphere result larger, an upper limit on both effects is given by the fact that the full-atmosphere cross section (1.4 percent statistical error) was 0.22 percent lower than that obtained with half an atmosphere (1.0 percent).

Another good check on slit-slit scattering was accidentally provided by a shift in the direction of the external beam, which caused a large increase in the

number of protons striking the edges of the last collimator defining hole. Some of these protons, scattering off various metal surfaces, found their way into the first and second counters. However, these protons either could not get through the second analyzing slit, or they had lost too much energy to get through the absorber, for measurements made after the chamber was realigned to the new beam direction agreed within statistical error with those made before realignment. Despite the fact that the first and second counter singles rates decreased by a factor of over two after realigning, the cross section for 12.5° deuterons obtained before (1.3 percent statistical error) agreed to within 1.4 percent with that obtained after (1.1 percent) realignment, and similarly the 10° proton cross sections agreed within 0.82 percent for statistical errors of 1.9 percent and 1.4 percent.

Thus slit-slit scattering was not a source of error in the cross-section measurements, except for deuterons at 8° where direct slit-scattered protons could get through the first analyzing slit (see IID). When counting protons at this angle, the only effect was to increase the singles rates in the first two counters, but with deuterons the absorber was thin enough to admit some of these slit-scattered protons. Since the ratio of background to total counts was six times as large at 8° as at 10°, this high background increased the statistical error. Furthermore, since it was found that the slit-scattered proton background decreased rapidly with energy, a correction had to be made by filling the chamber with ordinary hydrogen and making runs with the same absorbers and discriminator settings as were used when taking deuteron and background counts. A rather large error was assigned for this correction.

While background measurements were made for all deuteron runs, only a few were taken for proton runs. The proton backgrounds were nearly always found to be negligible, indicating the absence of (1) slit-slit scattering, (2) scattering from heavy contaminants, (3) false triple coincidences from neutron recoil background, and (4) electrical noise counts. The only exceptions found were obviously due to the last of these causes.

These proton background measurements served also as a check on the method of determining accidental coincidences, since with stopping, or background, absorber in place the triple coincidence and accidental coincidence counts were about equal.

However, the accidental coincidence correction was quite small even at the lowest angles, because the beam current had to be reduced (by reducing the hydrogen supply for the cyclotron arc) to prevent counting losses. Runs were made of cross section *versus* beam current to determine the maximum singles counting rate which could be tolerated before losses occurred.

Runs at any angle which were made with different beam currents served as a test of the current integrator calibration, since each run was assigned its calibration constant on the basis of the charging time of the integrating condenser. A further check was provided by making runs with two different (0.1 μf and 0.01 μf) condensers. Regardless of having different currents or condensers, the cross-section values always agreed within statistical errors.

The cross section at a given angle was measured also as a function of time to check on amplifier gain changes, counter gas contamination, and scattering from air. As mentioned above, the last of these was also tested by background measurements. Still another check was made by using an appropriate absorber to measure scattering from air at 25° periodically during a night of data taking. By measuring also the cross section for scattering at that angle with only air in the chamber, the increase in air concentration could be determined directly and checked with the measured leak rate of the chamber. In general, the effects of air scattering were found always to be very small.

Two conventional checks are to measure a cross section at the same angle on both sides of the beam, and to measure a cross section someone else has already determined. The former was done at 45°, and the agreement of the two determinations within 0.15 percent is better than the statistical accuracy warrants. The latter was done by determining the p-p scattering cross section at a laboratory angle of 20° to compare with some small angle measurements being made at this laboratory by H. N. Royden. For the present, the result, 24.0 mb/sterad in the center-of-mass system, can be compared with a value of 23.9, obtained by interpolating between the 18.3-Mev and 32-Mev measurements, as fitted[29] by a Lévy potential. The agreement is much better than the uncertainty in the interpolated value.

IV. RESULTS

A. Corrections to the Data

Two corrections to the data have been discussed sufficiently already. These are the background subtraction made (see III) for all deuteron and a few proton runs, and the deuterium temperature/pressure ratio assignment (see IIJ) for each run. A 0.07 percent van der Waals' correction was also made to all the pressures.

The same rate of change of temperature/pressure was used to determine the rate of increase in scattering from air contamination. Corrections had to be made only for proton runs at angles of 17.5° or less, and the largest correction was only 0.34 percent (at 8°). The experimentally confirmed (see III) smallness of this effect was due, at small angles, to using deuterium fillings for only a short time, and at larger angles, to discriminating against the higher energy air-scattered protons.

[29] A. Martin and L. Verlet, Phys. Rev. 89, 519 (1953).

A similar small (0.45 percent in the worst case) correction had to be made at proton angles of 20° or less for scattering from the 0.8 percent ordinary hydrogen impurity in the deuterium (see IIJ). To obtain a good correction, the p-p scattering cross sections were taken from an interpolation between the curves given by Martin and Verlet[29] (see III), and the percentage of p-p protons excluded by the absorbers at each angle was determined by folding the nearly gaussian distribution in range due to straggling[21] with the trapezoidal distribution due to the angular resolution of the analyzing system (see IVC).

Still another source of unwanted counts was the extra particles obtained because the analyzing slits could not be perfectly absorbing. The correction was small, varying from 0.41 percent for 8° protons to 0.17 percent for 45° deuterons, primarily because of the excellent energy resolution of the absorber system (see also IIC and D).

An opposite correction to the preceding three was that for the loss of particles in the absorbers due to single scattering and absorption. However, only the absorption was important in the total corrections, which varied from 1.02 percent for 8° protons to 0.08 percent for 90° protons.

All the data also were corrected for electrometer zero drift, the final value of the drift being read on the Brown Recording Potentiometer (see Fig. 3) immediately after each run. Because the runs were kept short, the drift correction rarely was as large as 1 percent.

All data were corrected for accidental coincidences by means of a coincidence circuit like that used for real triples, but which registered whenever pulses from the first two counters occurred simultaneously with a delayed pulse from the third counter. This method was necessary because $\frac{1}{5}$ to $\frac{1}{2}$ (depending on the angle) of the pulses from the first two counters were in double coincidence, since (1) these counters had a much larger solid angle than the second analyzing slit (see IID), and (2) only they received metal-scattered protons (see III). Since the number of accidental counts for n counters of resolving time τ having N_n counts in a time t when used with a square-pulsed beam of period p and on-time δp is $A_n=nN_1N_2\cdots N_n(\tau/t)^{n-1}\times[\delta^{1-n}-(n-1)\tau/(np\delta^n)]$, it was readily shown, using measured singles and doubles counts, that $A_2\gg A_3$. The value for A_2 calculated from this formula, which was derived following a method used by Feather,[30] gave good agreement with the electronic result when the latter was corrected by the factor $\delta p/(\delta p-d)$ to account for the probability that counts were missed because the delay line kept the accidental system dead for a time d during the first part of the beam pulse.

The final correction to the data was for the finite width and height of the incident and scattered beams. A second-order geometry analysis was kindly supplied by C. L. Critchfield, and some fourth-order terms in the rear slit height were added to it for this particular geometry. The corrections ranged in magnitude from 3.83 percent for 8° protons to 0.03 percent for 85° protons.

B. Summary of Errors

Summarizing the errors in the differential cross section, $\sigma_0(\theta_0)=TC\sin\theta_0/KGPFIQ$, we can first dispose of K, which includes the gas constant, Avogadro's number, and the electronic charge, all contributing essentially no error here.

The ratio of gas temperature to pressure, T/P usually was known with a standard error of 0.1 percent, while the fraction, F, of the gas which was deuterium was determined with a limit of error of 0.05 percent (see IIJ).

Two errors (see IIH) have been assigned in the number of incident particles: (1) an allowance of 0.3 percent (0.5 percent in a few cases) for possible errors in beam collection, and (2) errors varying from 0.2 percent to 1 percent in the determination of the charge per cycle (of which there were I), Q.

Four sources of error must be considered in using $\sin\theta_0/G$ to determine the portion of the scattered beam seen by the counting system. First, the combined errors in the measurement of the geometrical constants of which G is comprised and in the alignment of the counter slit system amount to only 0.047 percent for the wide slits and 0.19 percent for the narrow (see IID). However, the uncertainties in θ_0, the laboratory angle, while only 0.063° for the narrow slits and 0.066° for the wide, give errors in the cross section varying from 0.13 percent to 0.079 percent, as computed from $\Delta\sigma/\sigma=2\Delta\theta_0/\sin2\theta_0$ for deuterons and $[(\cot\theta_0)+\sin\theta(3.5+\cos\theta)/(2+\cos\theta)^2]\Delta\theta_0$ for protons (where θ is the center-of-mass angle). The third error arises from the uncertainty in the centering of the incident beam (see IIC), which amounted to 0.064 percent/$\sin\theta_0$, except for runs made with a shifted beam (see III), for which the error has been doubled. The fourth error comes from the correction for finite beam size (see IVA) and varies from 0.36 percent to 0.003 percent. It stems largely from taking derivatives of the imperfectly known cross section, but also an error of 6 percent of the correction was assigned for the effects of neglected higher order terms and of the approximate treatment of the incident beam.

There were several small contributors to the error in C, the number of properly scattered protons counted. One was the background correction (see III) made for a few proton runs, for which an error of $\frac{1}{3}$ the correction has been assigned, and for all deuteron runs, for which an error of about 5 percent of the correction has been included to allow for possible effects of the small energy difference between the actual and measured back-

[30] N. Feather, Proc. Cambridge Phil. Soc. 45, 648 (1949).

grounds. A larger error was assumed for the unusual 8° deuteron background.

Since the correction for accidental coincidences was usually much less than 1 percent and approached 2 percent at only one angle, the error assigned to it of 10 percent for $\theta_0 \leqslant 25°$ and 20 percent for $\theta_0 > 25°$ was not important. Also small were the errors due to the corrections for scattering from air contamination, taken to be $\frac{1}{3}$ of the correction and amounting to 0.11 percent in the worst case, and for scattering from ordinary hydrogen, which yielded a maximum error in the cross section of 0.06 percent. An error of 0.3 percent in the worst case resulted from assuming a 30 percent uncertainty in the correction for particle loss in the absorbers, mainly to allow for possible inaccuracies in the absolute values of the theoretical absorption cross sections.

Two errors must be considered in regard to slit-edge penetration. First, an error of $\frac{1}{2}$ the correction for penetration of the analyzing slit edges has been assigned because there is a lack of good experimental verification of the treatment, and this gives a 0.2 percent error in the worst case. Secondly, by a calculation similar to that for the analyzing slits, it was found that only 0.11 percent of the scatterings counted could have been produced by lower energy protons which had partially penetrated the collimating slit edges, and these events could not have caused an error in the cross section greater than 0.006 percent. Note that an error has already been assigned in the beam collection (see IIH) to account for protons which could have lost so much energy that their scattering events would not have been counted.

It was not necessary to assign any error for the small and accurate electrometer zero drift correction, for counting losses (see III), nor for multiple scattering losses (see IIE, IIF, and III).

The main source of error in C and in the whole cross section determination was the Poissonian nature of the number of counts, the relative error in the most complicated case being given by

$$\frac{[(C_g+A_g)/I_g^2+(C_b+A_b)/I_b^2)]^{\frac{1}{2}}}{(C_g-A_g)/I_g-(C_b-A_b)/I_b},$$

where the subscript g refers to the measurement of the gross counts and b to the measurement of background alone, and C designates total counts (of which A were accidentals) in I condenser cycles. A tabulation of this statistical error and the relative standard deviation in the cross section at each angle resulting from quadratically combining all the errors considered above may be found in Table III. These errors apply to the absolute values of the cross sections, since each determination was an absolute measurement. The cross sections and angles have been transformed to the center-of-mass system relativistically, but these differ little from the classical values.

TABLE III. Experimental data. The following data for the angular distribution of protons elastically scattered from deuterons is for a proton laboratory energy of 20.57±0.11 Mev. The errors, as well as the differential cross-section values, are absolute, and are expressed as percentage standard deviations.

Lab angle (degrees)	C.m. angle (degrees)	C.m. cross section (mb/sterad)	Percent statistics	Std. error (percent)
8.0-p	12.07	93.92	2.7	3.1
10.0-p	15.03	72.93	1.2[a]	1.8
12.5-p	18.80	69.56	1.4	1.7
15.0-p	22.53	72.37	0.93[a]	1.2
17.5-p	26.26	75.22	0.83[a]	1.1
20.0-p	29.97	77.27	0.53	0.83
25.0-p	37.37	70.77	0.89	1.1
35.0-p	51.87	52.19	0.90	1.0
45.0-p	65.95	36.11	0.83[a]	0.96
55.0-p	79.44	23.27	1.3	1.4
45.0-d	89.86	16.70	1.4	1.7
65.0-p	92.20	15.49	1.8	1.9
75.0-p	104.17	9.66	1.8	1.9
85.0-p	115.16	5.62	2.8	2.9
90.0-p	120.20	4.51	2.1	2.2
25.0-d	129.90	2.64	2.8	3.1
20.0-d	139.91	6.62	1.5	1.9
17.5-d	144.92	11.44	1.2	1.4
15.0-d	149.93	16.97	1.5	1.9
12.5-d	154.94	24.28	0.84	1.3
10.0-d	159.95	33.94	1.9	2.5
8.0-d	163.95	38.65	4.1[a]	4.3
Proton-proton scattering check run:				
20.0	40.20	24.00	0.75	1.1

[a] An additional error due to the background had to be included in the statistical error because of the method of combining sets of data.

C. Beam Energy Determination

In order to check the use and calibration of the absorbers as well as to determine the beam energy, three energy measurements were made during the course of the experiment by taking integral range curves with the absorbers in front of third counter, while counting protons from p-p scattering at 20° and 25°.

There are three uncertainties in the energy: (1) the error in the mean energy determination, (2) the energy spread in the beam at any particular time, and (3) changes in the mean energy with time.

Considering the first of these, there are three errors in the determination of the mean energy, uncertainties of (a) 1.5 mg/cm² in the absorber thickness, (b) 1.5 mg/cm² in the mean-range determination, and (c) 2.3 mg/cm² in the range-energy relation, giving a total error of 0.08 Mev. The range-energy relation for aluminum was computed for a ionization potential[31] of 164±3 ev and was corrected for multiple scattering.

An upper limit of about 0.1 Mev can be placed on the energy spread in the beam, since the integral range curves could be fitted quite well by considering just straggling and angular resolution. This analysis also showed that the absorbers for p-d scattering were being chosen properly (see IIE).

[31] D. O. Caldwell and J. R. Richardson, Phys. Rev. 94, 79 (1954).

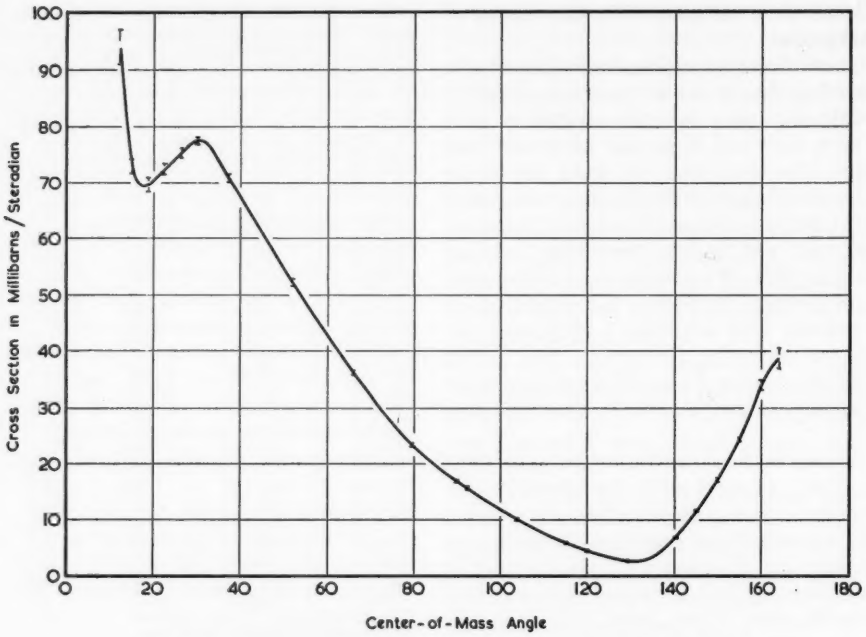

FIG. 5. Center-of-mass differential cross section for the elastic scattering of 20.6-Mev protons by deuterons.

An indication of the constancy of the beam energy under normal conditions is given by the agreement between measurements taken at the beginning 20.56 (Mev) and end (20.57 Mev) of the *p-d* data taking period. An upper limit on the energy change can be set by the third measurement (20.68 Mev), which was made after a beam shift (see III) caused the collimator to select a different part of the beam. Since none of the *p-d* data taken just before this measurement were used, the maximum change in mean energy for any accepted data can be taken as about 0.08 Mev.

Adding quadratically uncertainties (1) and (3) above gives 0.11 Mev as the standard deviation in the mean energy, and the energy spread in the beam at any time, (2) above, is thought not to have exceeded that same value. We have then as the beam energy, 20.57 ± 0.11 Mev.

V. CONCLUSIONS

The results of this experiment, which are given in Table III and Fig. 5 seem a reasonable interpolation between the experimental work at 9.7 Mev[32] and 31 Mev,[33] except for the appearance of the Coulomb-nuclear interference minimum. While it should soon be possible to compare this experiment with the theoretical work of Massey and Gammel,[34] at the moment the only comparison that can be made is with the 20-Mev *n-d* calculation of Verde. Although a phase shift analysis ought to be made, the phase shifts converted to equivalent *n-d* ones, and these compared with Verde's phase shifts for each angular momentum, by just comparing cross-section curves it is hard to see how the present data could give any agreement with Verde's theory. For either his symmetric or neutral potential, the main cross-section minimum comes at too small an angle (about 90°, instead of 130°) and is not deep enough by an order of magnitude. Also, the theoretical backward peaks are four to six times too high. The theoretical forward peak at about 30°, where Coulomb effects are not important, is a factor of two too low for the symmetric potential and a factor of one and one-half too high for the neutral potential.

Except for checking various theoretical approaches, these data probably cannot yet be used for achieving some of the aims outlined in the Introduction. It can only be hoped that this experiment may provide some spur for the necessary theoretical work. The data can perhaps give an answer to the long-standing question as to which set of nucleon-deuteron scattering lengths is the correct one, because of the clear appearance for the first time of a Coulomb-nuclear interference minimum. This minimum should give the added condition needed to make unique the phase shifts used to fit the data. In general, this experiment should provide a more stringent test for present or future theories than do previous low or intermediate energy nucleon-deuteron scattering measurements.

[32] Armstrong, Allred, Bondelid, and Rosen, Phys. Rev. 88, 433 (1952).
[33] V. J. Ashby, University of California Radiation Laboratory Report 2091, 1953 (unpublished).
[34] H. S. W. Massey and J. L. Gammel (private communications).

VI. ACKNOWLEDGMENTS

Beneficial discussions were had with Professor G. Breit, Professor E. Bretscher, Professor K. R. MacKenzie, Professor H. S. W. Massey, and Professor B. T. Wright; and Professor C. L. Critchfield generously supplied the second-order geometry correction. George Jones and Harry E. Handler furnished considerable aid with the electronics, as did Steve Plunkett in the design and construction of the other apparatus. Help in this construction was also given by the Physics Department Shop, under the supervision of E. M. Griffiths. Herbert N. Royden's work on the electrometer and its calibration is gratefully acknowledged, as is the extensive assistance given by Miriam Caldwell in the mathematical and computational tasks. One of us (D.O.C.) wishes also to thank Professor P. Scherrer for the hospitality of the Physics Institute of the Swiss Federal Institute of Technology during the writing of this paper.

PHYSICAL REVIEW VOLUME 98, NUMBER 1 APRIL 1, 1955

Decay of the 3.5-min Metastable State of Sb^{122}

J. M. LeBlanc, J. M. Cork,* and S. B. Burson
Argonne National Laboratory, Lemont, Illinois

(Received November 4, 1954)

The radiations associated with the 3.5-min activity of Sb^{122} have been studied with 180° magnetic photographic spectrometers and a ten-channel coincidence scintillation spectrometer. Two gamma rays with energies of 60.7 and 75.3 kev were detected by means of internal conversion electrons and also by means of the scintillation spectrometer. The 75.3-kev transition is the more strongly converted of the two, and it is concluded that it is the isomeric transition. The two gamma rays are emitted in cascade.

An isomeric state in Sb^{122} was first reported by der Mateosian *et al.*[1] in 1947. They measured its half-life to be 3.5 min. The gamma rays associated with the 3.5-min decay have been investigated by two groups, one employing a scintillation spectrometer[2] and the other an ionization chamber.[3] The results of the scintillation spectrometer study indicated the presence of one gamma ray with an energy of 68 kev, whereas

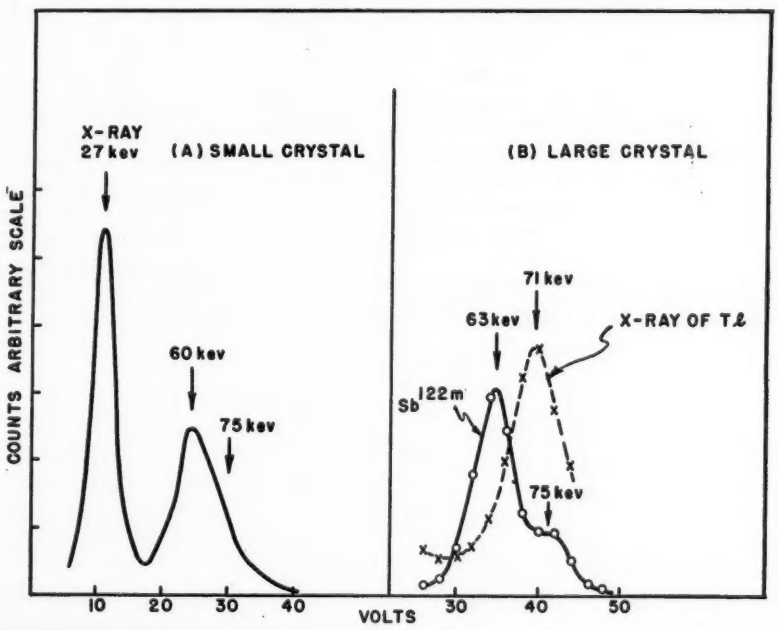

FIG. 1. NaI(Tl) pulse-height distributions of gamma rays from Sb^{122m}.

* University of Michigan, Ann Arbor, Michigan.

[1] der Mateosian, Goldhaber, Muehlhause, and McKeown, Phys. Rev. 72, 1271 (1947).

[2] E. der Mateosian and M. Goldhaber, Phys. Rev. 82, 115 (1951).

[3] J. H. Kahn, Oak Ridge National Laboratory Unclassified Report ORNL-1089, Nov. 1951 (unpublished).

TABLE I. Internal conversion electrons associated with the decay of Sb^{122m}.

Electron line energy (in kev)	Interpretation	Energy sum (in kev)
30.2	K^1	60.7
45.1	K^2	75.6
70.2	L_I^2	74.9
70.9	L_{III}^2	75.0

the results of the ionization chamber study indicated the presence of two gamma rays with energies of 59 and 74 kev.

The Sb^{122m} sources which were used in the present investigation were obtained by the irradiation of enriched Sb^{121} in the Argonne Heavy Water Reactor (CP-3'). They were examined with both 180° magnetic photographic spectrometers[4] and a ten-channel coincidence scintillation spectrometer.[5] Four internal conversion electron lines were detected with the 180° spectrographs. They are listed in the first column of Table I. They are interpreted as internal conversion electrons from gamma rays with energies of 60.7 and 75.3 kev. The electron lines for the 75.3-kev gamma ray are much stronger than the K line of the 60.7-kev transition.

The NaI pulse-height distribution produced by the gamma rays from Sb^{122m} is shown in Fig. 1(a). The peaks decayed with a half-life of about 3.3 min. The low-energy peak, at about 27 kev, is due to the x-rays of Sb. The other peak is quite broad and is distorted on the high-energy side, indicating that it is due to more than one gamma ray. This peak was examined with better resolution and the resulting distribution is shown in Fig. 1(b). The strong component of this peak occurs at about 63 kev, and the distortion of the high-energy side indicates the presence of a gamma ray with an energy in the neighborhood of 75 kev. This agrees with the internal conversion data.

The photopeak of the 75-kev gamma ray is considerably weaker than that of the 60-kev transition. Since the internal conversion electron lines of the 75-kev transition were stronger than those of the 60-kev gamma ray, one concludes that the 75-kev radiation is the more strongly converted of the two. The 75-kev gamma ray is therefore identified as the isomeric transition. From the energy lifetime relations for gamma rays, it is concluded that the 75-kev radiation has a multipolarity of 3.

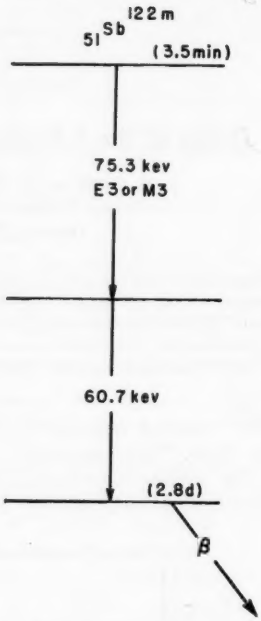

FIG. 2. The decay scheme of $_{51}Sb^{122m}$ (3.5-min).

Coincidences were observed between the x-ray and the 60–75-kev peak. Since the x-rays are produced as a consequence of the internal conversion of one of the gamma rays, one should not observe x-ray gamma-ray coincidence unless the two gamma rays are in cascade.

It is concluded from these experiments that the 3.5-min metastable state decays by means of a 75-kev isomeric transition which is followed by a 60-kev transition as shown in Fig. 2.

[4] H. Keller, and J. M. Cork, Phys. Rev. 84, 1079 (1951); Rutledge, Cork, and Burson, Phys. Rev. 86, 775 (1952).
[5] S. B. Burson and W. C. Jordan, Phys. Rev. 91, 498 (1953).

Excitation Function of $O^{16}(t,n)F^{18}$†

NELSON JARMIE
University of California, Los Alamos Scientific Laboratory, Los Alamos, New Mexico
(Received December 9, 1954)

The excitation function of the reaction $O^{16}(t,n)F^{18}$ has been measured for triton bombarding energies of 0.680 to 2.130 Mev. The half-life of the F^{18} beta decay has been measured to be 111±1 min.

INTRODUCTION

INTEREST has been growing in this and other laboratories[1] in the use of mass-3 nuclides as bombarding projectiles in nuclear reactions. Use of these particles, tritons and He^3 nuclei, has a number of advantages: The large mass defect is of advantage in producing high excitations; new positions on the isotope chart can be reached; and the known energy levels of nuclei can be reached by new routes and with new isobaric spin configurations. Of course, the systematics of reactions with projectiles made up of three nucleons should be studied for its own sake. In line with these thoughts, it was decided to measure the excitation function of $O^{16}(t,n)F^{18}$ for bombarding energies of 0.680 Mev to 2.130 Mev.

EXPERIMENTAL PROCEDURE

Thin mica targets were irradiated by various energy triton beams from one of the 2.5-Mev Los Alamos electrostatic generators. Both HT^+ and T^+ beams were used. The resulting F^{18} was identified by following the well known 111-min decay with a 4π scintillation counter. The target holder acted as a Faraday cup for beam current measurements and a 300-volt "barrier" was used to isolate the Faraday cup from electron currents due to secondary electron emission. The HT^+ beam was used also to avoid uncertainty due to the H_3^+ in the mass-3 beam. The integrator was calibrated with a precision current source. The energy spread of the beam was held automatically to about 2 kev. Individual irradiations lasted not longer than 4 min.

The O^{16} targets used for the different runs were cut out of a single sheet of 0.70 mg/cm² muscovite mica. No crystal plane edges were visible on close inspection, and the targets were assumed to be of uniform thickness. The beam level had to be kept to less than $\frac{1}{10}$ microampere through a $\frac{1}{8}$-in. aperture in order to prevent the targets from disintegrating. Kahn's values of dE/dx for mica were used.[2] The decay was followed in each case for at least eight half-lives and usually more.

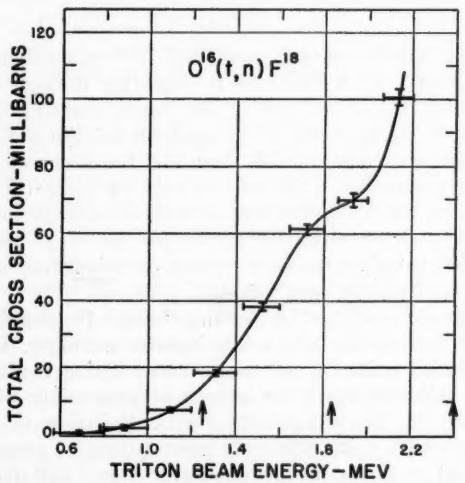

FIG. 1. Excitation function for $O^{16}(t,n)F^{18}$. See text (Results) for discussions of errors. Arrows indicate positions of energy levels of compound nucleus (reference 3). Note suppressed zero. Horizontal bars are not errors but indicate energy spread due to target thickness.

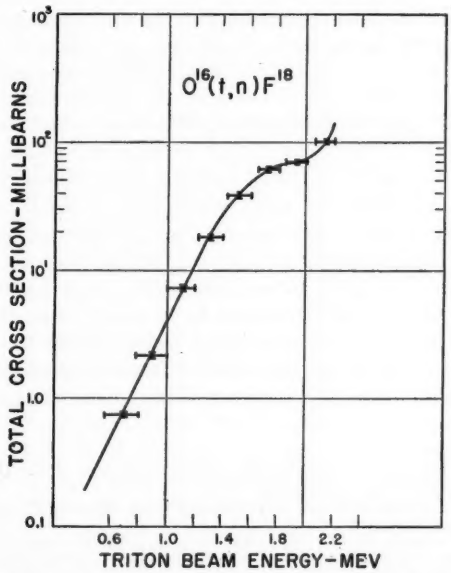

FIG. 2. Excitation function for $O^{16}(t,n)F^{18}$ on a semilog scale. See caption of Fig. 1 for discussion.

† Work performed under the auspices of the U. S. Atomic Energy Commission.

[1] M. L. Pool and D. N. Kundu, Phys. Rev. **82**, 305 (1951); Moak, Kunz, Good, and Kundu, Phys. Rev. **91**, 462 (1953); Almqvist, Allen, Dewan, and Pepper, Phys. Rev. **91**, 1022 (1953); Symposium on H^3 and He^3 Reactions, Phys. Rev. **91**, 488 (1953); C. D. Moak, Phys. Rev. **92**, 383(T) (1953).

[2] D. Kahn, Phys. Rev. **90**, 503 (1953).

RESULTS

The results are shown graphically in Figs. 1 and 2. The relative error between points (indicated by the vertical bars) is about 2 or 3 percent. The horizontal bars on the figures are not errors but indicate the energy spread due to target thickness. The values of the absolute cross section are only good to about 20 percent due to the difficulty of obtaining a reliable absolute measurement. Because of this difficulty the vertical scale should be considered only as a rough indication of the absolute value.

The knee in the curve at about 1.8 Mev was verified by a second run and is consistent with data on the known levels of F^{19}, the intermediate nucleus involved.[3] (See Fig. 1.) The lower energy levels are probably overwhelmed by the effect of barrier penetration. The roughly exponential form of barrier penetration at low bombarding energies is apparent in Fig. 2, where the curve is approximately a straight line up to about 1.2 Mev.

Data from this experiment gave a half-life for the F^{18} beta decay of 111±1 min, in good agreement with published values.[4]

ACKNOWLEDGMENTS

I wish to thank L. H. Treiman for the excellent samples of mica and H. C. Martin for his advice and details of his preliminary work on this reaction. I also wish to acknowledge the help of H. R. Lewis in checking calculations.

[3] Blaser, Boehm, Marmier, and Sherrer, Helv. Phys. Acta 24, 465 (1951).

[4] Blaser, Boehm, and Marmier, Phys. Rev. 75, 1953 (1949).

PHYSICAL REVIEW VOLUME 98, NUMBER 1 APRIL 1, 1955

Half-Life of Rb^{86}†

JAMES B. NIDAY
University of California Radiation Laboratory, Livermore, California
(Received November 19, 1954)

A number of very pure samples of Rb^{86} obtained by a new radiochemical procedure were found to have a half-life of 18.64±0.04 days.

THE accepted value[1] of 19.5 days for the half-life of Rb^{86} was determined by Helmholz *et al.*,[2] on a somewhat impure sample. It has been possible to redetermine the half-life of this nuclide in connection with the separation of a number of very pure samples of Rb^{86} from an intense source of fission-product radioactivities by an improved radiochemical procedure.

The chemical procedure used was based primarily on alternate $Fe(OH)_3$ scavengings from NH_4OH and $NaOH$-Na_2CO_3 solutions, an Sb_2S_3 scavenging from 0.2*N* HCl solution, and several precipitations of the alkali metal perchlorates from ethyl acetate solution. The Rb was separated from Cs by elution with 0.3*N* HCl from the cation exchange resin, Duolite C-3. A column 0.85 cm^2×6 cm of 200–325 mesh resin operated at room temperature gave a very satisfactory separation.

The activities of eight samples of Rb^{86} were followed for from 7 to 9 half-lives by counting through an absorber (110.7 mg/cm^2 of Al) which removed the natural activity of Rb^{87}. The apparent half-life of each sample was constant with time, and the final counts, with no absorber, indicated that only the natural Rb^{87} activity remained. The lack of residual activity indicates a decontamination factor for Cs of at least 5×10^4, based on the Cs^{137} content of cesium fractions isolated from the same samples.

The data obtained by counting through the absorber were analyzed for λ by a least-squares technique. The statistical reliability of counts taken during the last few half-lives was lower because of uncertainty with regard to the background counts. Rejection of all counts with a probable error greater than 1.4 percent left 20 to 24 counts (obtained over 6 or 7 half-lives) for each sample. The following values for the half-life (in days) were obtained: 18.700, 18.565, 18.628, 18.690, 18.547, 18.660, 18.639, and 18.682.

This leads to a mean value for the half-life of Rb^{86} of 18.64 days with a probable error of ±0.04 day.

† This work was performed under the auspices of the U. S. Atomic Energy Commission.

[1] Hollander, Perlman, and Seaborg, Revs. Modern Phys. 25, 513 (1953).

[2] Helmholz, Pecher, and Stout, Phys. Rev. 59, 902 (1941).

Gamma Rays from the Deuteron Bombardment of Carbon-13†

R. J. MACKIN, JR.,* W. B. MIMS,‡ AND W. R. MILLS, JR.
Kellogg Radiation Laboratory, California Institute of Technology, Pasadena, California
(Received December 30, 1954)

A magnetic lens spectrometer was used to investigate the gamma radiation produced by the deuteron bombardment of C^{13} enriched carbon targets. A study of the Compton electron spectra from a thin Al converter at $E_d=1.42$ Mev revealed the following gamma lines (energies in kev, not corrected for possible Doppler shift): 4930±40, 5130±30, 5730±30, 6120±25. A weak line at 3910±50 kev was established with the spectrum from a thick Al converter. At $E_d=1.9$ Mev, additional lines appeared at 6450±50, 6730±40, and 811±3 kev. The last-named was identified by photoelectrons from a thorium converter. No new lines were discovered at $E_d=2.7$ Mev. The well-known 6.12-Mev line is from C^{14*}, as are probably the 6.73- and 0.811-Mev lines. All others correspond to known levels of N^{14}.

I. INTRODUCTION

INFORMATION about the levels of N^{14} below 7 Mev has been derived principally from investigations of neutron groups[1] and gamma rays[2] from $C^{13}+D^2$, and more recently from measurements on gamma rays[3] from $C^{13}+H^1$. In view of difficulties which have attended attempts to infer a consistent level scheme, it appeared worthwhile to re-examine certain controversial portions of the gamma-ray spectrum from the former reaction. Additional measurements were made at bombarding energies up to 2.7 Mev in a search for new gamma lines.

II. EXPERIMENTAL PROCEDURE

A magnetic lens spectrometer[2,4] was used to study Compton electron spectra produced by gamma rays from $C^{13}+D^2$. A C^{13} enriched, compressed soot target at the spectrometer focal point was bombarded by magnetically analyzed deuterons from a 3-Mev electrostatic accelerator. Because several closely-spaced gamma lines were anticipated, a 20-mg/cm² target was backed with an aluminum converter of minimum thickness consistent with adequate counting statistics, 21 mg/cm². Additional runs were made with a 125-mg/cm² converter to detect any weak lines.

The spectrometer was operated with 1.9 percent resolution (Gaussian window) and an effective solid angle of 2.3 percent of a sphere. The momentum calibration for the Compton spectra was based on the ThD X-line at 9988.4 gauss-cm.[5] A helical baffle permitted separation of electrons and positrons. The detector of focused electrons was a magnetically compensated *trans*-stilbene scintillation counter[6] which made possible energy discrimination against scattered electrons. The customary beam currents (0.5–1.5 μa) provoked copious emission from the soot of thermal electrons or positive ions, depending on the target potential. In view of this difficulty, no attempt was made to measure beam current, and the detector count readings were normalized by means of a gamma-ray monitor. The monitor consisted of two thin-wall Geiger counters in coincidence, set along a line from the target perpendicular to the incident beam and separated from one another by $\frac{1}{32}$-inch Al so as to record only radiation above 1 Mev. The system was thus insensitive to the delayed (annihilation) radiation from N^{13}, produced by $C^{12}(d,n)N^{13}$. Tests with natural sources confirmed that monitor and detector sensitivity were independent of the magnetic field. Measurements were made at bombarding energies of 1.42, 1.90, and 2.7 Mev.

A special search was made for gamma lines in the region 0.5 to 1.0 Mev with a carbon foil target[7] (about 0.3 mg/cm²), backed with a 20.2-mg/cm² thorium photoelectric converter.

III. RESULTS AND ANALYSIS

Because internal conversion pairs contributed a significant background to the Compton electron spectrum, it was necessary to measure the positron spectrum. It is expected for light nuclei (and has been roughly verified in work at this laboratory)[8] that the electron and positron internal pair spectra will be practically identical. Accordingly, the difference of electron and positron curves was regarded as consisting entirely of Compton electrons. This spectrum is shown in Fig. 1, along with the positron data.

The spectrum above 20.5 kilogauss-centimeters (at $E_d=1.42$ Mev) was analyzed by comparison with a theoretical Compton spectrum[2] which was derived from the Klein-Nishina formula. The theoretical curve included the effects of Doppler line broadening, electron energy losses in the converter, and the spectrometer

† Assisted by the joint program of the Office of Naval Research and the U. S. Atomic Energy Commission.
* National Science Foundation Fellow, now at the Office of Naval Research, Washington 25, D. C.
‡ Commonwealth Fund Fellow, now at the Clarendon Laboratory, Oxford, England.
[1] R. E. Benenson, Phys. Rev. **90**, 420 (1953).
[2] R. G. Thomas and T. Lauritsen, Phys. Rev. **88**, 969 (1952).
[3] Woodbury, Day, and Tollestrup, Phys. Rev. **92**, 1199 (1953).
[4] Hornyak, Lauritsen, and Rasmussen, Phys. Rev. **76**, 731 (1949).
[5] W. Brown, Phys. Rev. **83**, 271 (1951).
[6] C. Wong, Phys. Rev. **95**, 761 (1954).
[7] J. D. Seagrave, Phys. Rev. **85**, 197 (1952); E. A. Milne, Phys. Rev. **93**, 762 (1954).
[8] Dougherty, Hornyak, Lauritsen, and Rasmussen, Phys. Rev. **74**, 712 (1948).

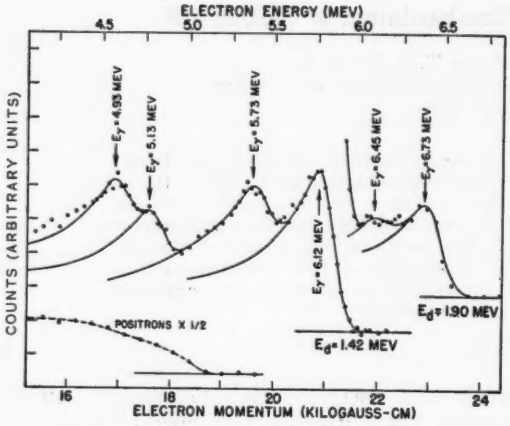

FIG. 1. Compton electrons from 20-mg/cm² C plus 21-mg/cm² Al converter.

resolution window.[9] In addition to the gamma-ray energy and yield determination, the theoretical line shape permitted extrapolation to lower momenta and made possible separation of the contributions from succeeding gamma lines. The solid curves in Fig. 1 were produced in this way and resulted in the line energies and relative yields given in Table I.

The discrepancy between points and curve below 16 kilogauss cm may reflect the presence of a gamma line at 4.5 Mev reported by the Rice Institute group[10] and assigned by them to the reaction $C^{13}(d,\alpha)B^{11*}$. It was not found possible to accentuate this line with a thicker converter.

Analysis of the data taken at $E_d=1.9$ Mev, also shown in Fig. 1, involved the same procedure. The spectrum shows clearly the existence of a line at 6.73 Mev; the deviation from the calculated line shape below 22.5 kilogauss cm is taken to indicate the presence of a line whose energy is 6.45 Mev. The establishment of the 6.45-Mev line was dependent upon certainty that it was not a part of the 6.1-Mev line spectrum; the end point of the latter was carefully determined at $E_d=1.4$ Mev.

Figure 2 shows a 3.91-Mev line (suspected earlier[2]) whose presence was confirmed by measurements with a 125-mg/cm² Al converter. The end point of the 3.4-Mev line immediately below was fixed by comparison with a theoretical line shape.

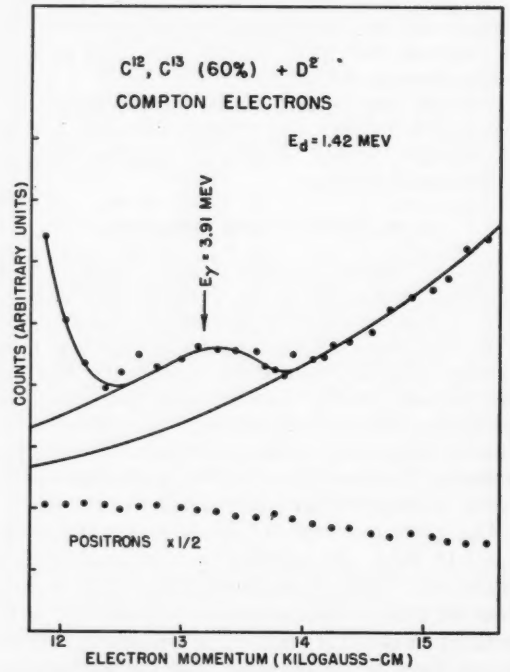

FIG. 2. Compton electrons from 20-mg/cm² C plus 125-mg/cm² Al converter.

TABLE I. Summary of results.

Gamma-ray energy (kev)	Maximum Doppler shift (kev)	Relative yield (E_d=1.42 Mev)	Assigned level (kev)	Reaction and reference
3910±50	19	0.14	N^{14} 3945±15	$N^{14}(p,p')N^{14*}$[a]
4930±40	24	0.37	N^{14} 4910±10	$N^{14}(p,p')N^{14*}$[a]
5130±30	25	0.34	N^{14} 5104±10	$N^{14}(p,p')N^{14*}$[a]
5730±30	28	0.45	N^{14} 5687±20	$C^{13}(d,n\gamma)N^{14}$ (cascade)[b]
6120±25	30	1.00	C^{14} 6095±15	$C^{13}(d,p)C^{14*}$[c]
6450±50	36		N^{14} 6440±20	$C^{13}(p,\gamma)N^{14d}$
6730±40	38		C^{14} 6723±15	$C^{13}(d,p)C^{14*}$[e]
729± 3	4		N^{14} 5810±20	$C^{13}(p,\gamma)N^{14d}$
811± 3	4.5		C^{14} 6894±15	$C^{13}(d,p)C^{14*}$[e]
869± 3	5		O^{17} 870.5± 2	$O^{16}(d,p)O^{17*}$[b]

[a] Bockelman, Browne, Buechner, and Sperduto, Phys. Rev. **92**, 665 (1953).
[b] See reference 2.
[c] Sperduto, Holland, Van Patter, and Buechner, Phys. Rev. **80**, 769 (1950).
[d] See reference 3.
[e] Sperduto, Buechner, Bockelman, and Browne, Phys. Rev. **96**, 1316 (1954).

The photoelectron spectrum between 0.5 and 1.0 Mev (taken at $E_d=2.6$ Mev) appears in Fig. 3. Three gamma lines at 729, 811, and 869 kev are indicated therein by their K-photopeaks. The expected L-peak of the 729-kev line is shown as a dashed curve. Correction for electron energy loss in the thorium converter[4] was checked by study of the Cs^{137} gamma rays at 661.60±0.14 kev[11] with the same converter. The 811-kev line was found to have an apparent threshold near $E_d=1.9$ Mev.

All of the line energies are given in Table I, where also appear the relative yields (at $E_d=1.45$ Mev) and the maximum possible Doppler shifts produced by center-of-mass motion. The actual line-shifts may differ

[9] W. R. Mills, Jr., and R. J. Mackin, Jr., Phys. Rev. **95**, 1206 (1954).

[10] Bent, Bonner, and Sippel, Phys. Rev. **95**, 649(A) (1954).
[11] Muller, Hoyt, Klein, and Du Mond, Phys. Rev. **88**, 775 (1952).

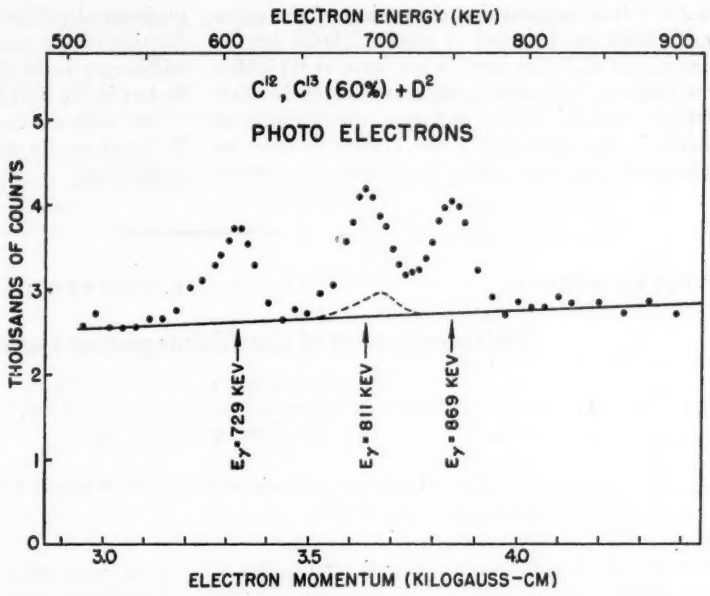

FIG. 3. Spectrum of photolines from 20.2-mg/cm² Th converter.

from these if the distribution of the motion of the emitting nuclei in the center-of-mass system is asymmetric about 90°, as in a stripping reaction, or if the mean life for emission is comparable with the nuclear stopping time. Other columns in the table suggest the most likely source of each line and give current values for the excitation energies of the assigned levels as reported by other investigators.

Measurements made at $E_d=2.7$ Mev revealed no further lines above 16 kilogauss-cm, although such lines are reported at $E_d=4$ Mev.[10]

IV. DISCUSSION

The 869-kev line at the end of Table I is attributed to the reaction $O^{16}(dp)O^{17*}$, presumably produced by bombardment of oxygen in the surface of the thorium converter. The line did not appear when a copper foil was interposed between target and converter. The line energy confirms the value given by Thomas and Lauritsen.[2]

The other assignments in the table are based on energy agreement with known levels together with threshold considerations. In particular, the yield of the 6.73-Mev line at $E_d=1.9$ Mev is believed to be too great to permit assignment to the 6.76-Mev level of B^{11}, since the bombarding energy is less than a hundred kev above threshold for the production of this level.

The assignment of the 3.91-Mev line to the 3.95-Mev level of N^{14} is consistent with the value given by Woodbury, *et al.*[3] for the branching ratio of that level. The assignment of the line as a cascade from the 6.23-Mev level to the 2.31-Mev level would appear to be excluded on the basis of the observation[3] that the former level decays only to the ground state.

The existence of a 5.82-Mev level in N^{14} is manifested only in the (p,γ) data[3] and in the assignment of the 729-kev line. For this assignment, a best level excitation value is $5.104+0.729=5.833\pm0.013$ Mev. Our failure to observe a line of this energy sets its intensity as less than 0.2 that of the 5.73-Mev line and suggests a cascade branching ratio greater than earlier supposed.[3]

From observations on the gamma rays[3] in $C^{13}(p,\gamma)N^{14}$ and elastically scattered protons[12] in $C^{13}(p,p)C^{13}$, it has been reasonably well established that the 8.06, 8.70, and 9.17-Mev levels in N^{14} have spins and parities 1^-, 0^-, and 2^-, respectively. Because of the large γ-width for the ground-state radiation from the 8.06-Mev level, and the absence of a transition to the 2.3-Mev level ($J=0^+$, $T=1$), it has been suggested[13] that the 8.06-Mev state has $T=1$. Similarly, the 8.70-Mev level has been assigned $T=1$ on the basis of the large ground-state γ-ray width.[14]

Calculation shows that the analog states of the 6.1-, 6.7-, and 6.9-Mev levels in C^{14} should lie near 8.4, 9.0, and 9.2 Mev in N^{14}. It has been suggested, on the basis of the internal pair spectrum,[2] that the radiation from the 6.1-Mev level in C^{14} to the ground state is $E1$ ($M1$ and $E2$ are not excluded), implying $J=1^-$ for this state. This assignment is borne out by the stripping analysis of the proton group from $C^{13}(dp)C^{14*}$ (1). Thus, one might identify the 6.1-Mev level in C^{14} as the analog of the 8.06-Mev level in N^{14}. The absence of a ground-state transition from the 6.9-Mev state in C^{14} suggests $J=0$ for it, and a correspondence with the 8.70-Mev level in N^{14}. The apparent absence of levels between 8.06 and 8.70 Mev in N^{14} (except one

[12] E. A. Milne, Phys. Rev. **93**, 762 (1954).
[13] A. B. Clegg and D. H. Wilkinson, Phil. Mag. **44**, 1269 (1953).
[14] D. H. Wilkinson, Phil. Mag. **44**, 450 (1953).

with $J=0$) then suggests that the analogs of the upper two C^{14} levels are inverted. A possible choice for the analog of the 6.73-Mev level is the level at 9.17 Mev whose large ground-state gamma-ray width is characteristic of electric dipole radiation, which would be inhibited if that level had $T=0$. Finally, it must be remembered that the analog level may thus far be unobserved. If its reduced proton width is a large fraction of the so-called sum rule limit, the observed width may be of the order of Mev, and the level may be lost in the background.

The authors are indebted to C. C. Lauritsen and T. Lauritsen for enlightening discussions and valuable suggestions.

PHYSICAL REVIEW VOLUME 98, NUMBER 1 APRIL 1, 1955

Redetermination of the Disintegration Constant of U^{238}

A. F. KOVARIK AND N. I. ADAMS, JR.
Sloane Physics Laboratory, Yale University, New Haven, Connecticut
(Received December 30, 1954)

A recount of alpha particles from previously used specimens of natural uranium gives 1.538×10^{-10} yr^{-1} for the disintegration constant of U^{238}.

IN 1932, the authors[1] made a new determination of the disintegration constant of uranium I(U^{238}). Alpha particles from a thin layer of natural uranium in the form of the oxide U_3O_8 were allowed to pass through a grid of known geometry into an ionization chamber. The electrical impulses there produced were amplified and applied to an electromechanical recording system. By this means the specific alpha activity of natural uranium was observed to be 1486 disintegrations per minute per milligram. In 1938, the apparatus was improved to give a better resolution of close counts, in connection with determination of thorium constants.[2] A subsequent recount made on some of the original uranium specimens gave the value 1501 disintegrations per minute per milligram.[3] Recently Fleming, Ghiorso, and Cunningham[4] have measured the specific alpha-activities of U^{234}, U^{235}, and U^{236}. In their excellent paper these investigators discussed and evaluated previous work, not only on the isotopes in question, but on U^{238} as well. They also adopted "best values" for the various physical constants involved. Shortly before this, in connection with other work, the writers had constructed a new apparatus capable of much more rapid counting than the apparatus previously employed. It seemed of some interest, therefore, to make a fast recount on three of the original specimens, which were still intact. In all, approximately 3×10^6 alpha particles were recorded, giving for the specific alpha-activity 1503 disintegrations per minute per milligram. This agrees substantially with our 1941 value and with the recent "best value."[4]

Since the present accepted values of the isotopic atomic weights and of the other pertinent constants differ slightly from the values used in the earlier work, we must recalculate λ^{238}, the disintegration constant of U^{238}. The isotopic atomic weights are taken from Segrè's book[5]; the other constants from Fleming *et al.*,[4] in whose paper references to the original sources may be found. It must be remembered that the atomic weights are based on the physical scale, on which the atomic weight of O^{16} is 16.0000 and that of O (natural oxygen) is 16.0043. Using isotopic atomic weights and relative atomic abundances from the sources indicated above, we find that the atomic weight of U (natural uranium) is 238.103 and that the relative *mass* abundances of U^{238}, U^{235}, and U^{234} are 0.99285, 0.00710, and 0.00005, respectively. Hence, since the alpha activities of the isotopes are in the ratios 1:0.046:1, the specific alpha activity of U^{238} is 739.9 disintegrations per minute per milligram. This corresponds to a number of U^{238} atoms equal to $6.02501\times10^{20}/238.125=2.53019\times10^{18}$, since 6.02501×10^{23} is Avogadro's number (on the physical scale). Thus, finally,

$$\lambda^{238}=1.538\times10^{-10}\ \text{yr}^{-1},$$

with an estimated probable error of 0.2 percent. The corresponding half-life is 4.507×10^9 years. It will be noted that these values differ from the earlier values[1] by only 0.4 percent, the effect of the increased value of the natural alpha activity being largely offset by the effect of the other small changes.

[1] A. F. Kovarik and N. I. Adams, Jr., Phys. Rev. **40**, 718 (1932).
[2] A. F. Kovarik and N. I. Adams, Jr., Phys. Rev. **54**, 413 (1938).
[3] A. F. Kovarik and N. I. Adams, Jr., J. Appl. Phys. **12**, 296 (1941).
[4] Fleming, Ghiorso, and Cunningham, Phys. Rev. **88**, 642 (1952).
[5] E. Segrè, *Experimental Nuclear Physics* (McGraw-Hill Book Company, Inc., New York, 1953), Vol. 1, Part 5.

$(n,2n)$ Cross Section of Na^{23} at 14.1 Mev*

R. J. PRESTWOOD
University of California, Los Alamos Scientific Laboratory, Los Alamos, New Mexico
(Received December 6, 1954)

An experimental determination of this cross section was made on six individual samples and involved the use of 4π counting, low background counting, neutron monitoring, and sample thickness corrections. The value obtained is 13.8 ± 2.2 millibarns and the error quoted is twice the standard deviation obtained from the six samples. The experimental work is described in detail and a discussion of the possible errors is given.

I. INTRODUCTION

THIS investigation describes the determination of the absolute cross section for the reaction $Na^{23}(n,2n)Na^{22}$ for neutrons at 14.1 Mev and supplements previous work[1,2] on activation cross sections for 14-Mev neutrons. The number of $(n,2n)$ events was measured by counting the positrons from Na^{22}(2.6-yr half-life; β^+ 0.542 Mev; γ 1.272 Mev). The measurement is limited in accuracy by the low value of the cross section and the long half-life of Na^{22}.

The 14-Mev neutron flux from a Cockcroft-Walton machine was monitored by Al foils which undergo the reaction $Al^{27}(n,\alpha)Na^{24}$. Absolute positron counting involved the counting of weightless Na^{22} samples in a 4π counter to establish the effective geometry of a second low background counter; and the experimental measurement of a self-absorption correction for the thick sodium chloride samples actually prepared from fast-neutron-irradiated targets.

II. EXPERIMENTAL

(a) Neutron Source

Neutrons were obtained from the Los Alamos Cockcroft-Walton machine by bombarding a thick tritium target[3] with 240-kev monatomic deuterium ions. The intensity of the neutron source was determined by counting α particles from the d-T reaction. The neutrons emitted at 90° with respect to the incident beam were used in the present investigation and have an energy of 14.1 Mev. However, because of the finite size of the Na foils which were irradiated, the incident neutron energy had a total spread of 13.9 to 14.3 Mev, most of the incident neutrons being 14.1 Mev. The foils consisted of NaF mixed with polythene and rolled into sheets approximately 15 mils thick.[4] Sample foils of area 1.3 cm^2 were punched from these sheets by means of a special punch.

(b) Irradiations

The NaF foils were sandwiched between two 5-mil Al monitor foils of identical area and were placed 2 cm from the tritium target. Al foils were also placed at 10- and 20-cm positions from the target in the same alignment. The Al foils undergo the $Al^{27}(n,\alpha)Na^{24}$ reaction with high-energy neutrons. Since at distances of 10 and 20 cm the inverse square law is found to hold, it is possible to calculate the flux (neutrons per cm^2) at these distances. By comparing the counting rates of Na^{24} made in these two distant foils with that of the foils sandwiching the NaF, the flux irradiating the NaF is found.

(c) Preparation of Na^{22} Samples for Counting

After the Na foils were irradiated, they were ignited at 600°C to remove the polythene. The remaining NaF was dissolved in water and converted to $NaClO_4$ by fuming to dryness with concentrated $HClO_4$. The $NaClO_4$ was then dissolved in n-butanol and the solution heated. NaCl was precipitated by the addition of n-butanol which had been saturated with HCl gas.[5] The NaCl precipitate was filtered onto a tared No. 50 Whatman Filter circle ($\frac{7}{8}$-in. diameter) on a ground-off Hirsch funnel attached to a filter chimney. (This technique gives a sample of uniform thickness and well-defined area of 2.9 cm^2.) The sample was dried at 110°C, weighed, mounted, and counted.

(d) The Counter

The instrument used for counting the Na^{22} samples is a very low background methane proportional counter. The background of this counter during this investigation was 3.8 counts per minute. This counter was calibrated for the absolute counting of Na^{22} in the following manner. Samples from a high specific activity Na^{22} solution (<4 μg total solids per μC) obtained from Oak Ridge were accurately measured out and evaporated to dryness on thin Zapon films suitable for 4π counting. The technique for mounting these samples and the reliability of the 4π counter had been checked previously.[6] From the 4π count of the samples the

* This work performed under the auspices of the U. S. Atomic Energy Commission.
[1] E. B. Paul and R. L. Clarke, Can. J. Phys. 31, 267 (1953).
[2] Stuart G. Forbes, Phys. Rev. 88, 1309 (1952).
[3] Graves, Rodriguez, Goldblatt, and Meyer, Rev. Sci. Instr. 20, 579 (1949).
[4] These foils were prepared by Pierre Hartshorne and Marvin R. Murphy of the Chemistry and Metallurgy Division of the Los Alamos Scientific Laboratory.
[5] H. H. Willard and G. F. Smith, J. Am. Chem. Soc. 44, 2816 (1922).
[6] The author acknowledges his indebtedness to J. P. Balagna who developed the mounting technique and spent much time in establishing the reliability of the 4π counter.

TABLE I. Summary of data.

Sample	Wt. of NaCl mg	I neutron/cm²	Net counts/min at counting time	Net counts/min corrected to irradiation time		Disintegrations/min, per mg Na $-dN/dt$	$\sigma_{n,2n}$ millibarns
1	57.4	1.865×10^{12}	1.60	2.04	1.83	0.331	13.35
			1.29	1.66			
			1.35	1.78			
2	81.0	4.078×10^{12}	3.92	4.79	4.70	0.693	12.79
			3.75	4.62			
			3.71	4.69			
3	75.9	4.247×10^{12}	4.39	4.70	4.97	0.761	13.48
			4.59	4.96			
			4.73	5.24			
4	34.2	7.816×10^{12}	4.91	5.13	5.00	1.305	12.56
			4.73	4.98			
			4.52	4.89			
5	36.2	3.111×10^{12}	2.54	2.67	2.51	0.630	15.24
			2.18	2.31			
			2.35	2.56			
6	51.9	3.805×10^{12}	3.65	3.93	3.98	0.771	15.25
			3.53	3.83			
			3.76	4.19			
						Average	13.78
						Total spread	19.5%
						Standard deviation	7.9%

disintegrations per minute per ml were determined. One ml of the Na^{22} solution was then added to 12.0 ml of a standardized NaCl solution containing 10.0 mg of Na per ml. The resulting solution was made up to 25 ml and thoroughly mixed. Six aliquots of varying size were than taken, evaporated to dryness, and, as described under Sec. II(c), filtered, weighed, and mounted. The samples were then counted on the low background counter, and from the weight of NaCl in each sample the number of disintegrations of Na^{22} were calculated. A curve was obtained giving the weight of NaCl *vs* ratio of counts/min to disintegrations/min.

III. RESULTS

For the calculations of the cross section of the $Na^{23}(n,2n)Na^{22}$ reaction, the following fundamental equations are required:

$$-dN/dt=\lambda N, \tag{1}$$

$$N=I\sigma n, \tag{2}$$

where $-dN/dt$=disintegrations per minute per mg of irradiated Na; λ=decay constant of Na^{22}(=5.076×10^{-7} min^{-1});[7] N=atoms of Na^{22} per mg of irradiated Na; I (flux)=neutrons per cm^2; σ=cross section in millibarns (10^{-27} cm^2); n=atoms of Na^{23} per mg of irradiated Na(=2.619×10^{19}). By combining Eqs. (1) and (2), one obtains

$$-dN/dt=\lambda I\sigma n. \tag{3}$$

Separate irradiations were made on six different NaF foils. After allowing the Na^{24} formed by the (n,γ) reaction to decay, the foils were treated and mounted as previously described. The samples were then counted on the low background counter over a period of 3 months. Alternate one-hour sample and background counts were made until each sample had been counted a total of 10 hours. The counting process was repeated twice, thus giving a total of 30 hours of counting for each sample. A chi-square analysis[8] of all the backgrounds during this period indicated that the counter was behaving properly. By means of the curve obtained giving the weight of NaCl *vs* ratio of counts/min to dis/min, each sample count was converted to disintegrations per minute. The value of n and λ are known. I was calculated for each sample from the α-monitor count and the Al foil measurements. Then by substitution in Eq. (3) of the appropriate numbers, six values for the cross section were obtained.

A summary of the data is shown in Table I.

IV. DISCUSSION

The errors in this measurement may come from the following sources: (1) contamination of samples; (2) calibration of low background counter with 4π counting; (3) the α monitor of the Cockcroft-Walton machine; (4) counting statistics of the samples; (5) using the $Al^{27}(n,\alpha)Na^{24}$ reaction to monitor an $(n,2n)$ reaction.

(1) Every precaution was taken to avoid any contamination, but one cannot say definitely that any sample is not contaminated. The internal consistency of the counting over a 3-months period at least eliminates the possibility of short-lived contamination. The chemistry performed and the fact that fast neutrons were used lead to a low probability for contamination.

(2) The 4π counter was checked carefully against our own standards as well as standards furnished by the Bureau of Standards and was shown to be accurate to ±1 percent on both P^{32} and Na^{22} standards.

(3) The α monitor of the Cockcroft-Walton machine is believed to be accurate to ±4 percent. During this investigation the α monitor was changed and recalibrated. The results obtained after this change showed no consistent variation in the cross-section value.

(4) The standard deviation of each 10-hour count for these samples ranged from approximately $\pm3\frac{1}{2}$ percent for the higher counting samples to ±8 percent for the lowest. The cross section calculated in Table I is based on an average of three such counts for each sample.

(5) The plot of energy of the neutrons from the Cockcroft-Walton machine *versus* laboratory angle is very linear in the region used in this investigation. Also in this region the $Al^{27}(n,\alpha)Na^{24}$ excitation function was found to be quite linear. Several $(n,2n)$ excitation functions on elements with high thresholds (10 to 12 Mev) have shown linearity in the 14-Mev region. The threshold for the $Na^{23}(n,2n)Na^{22}$ reaction is 12.57 ± 0.21 Mev.[9] One can conclude that the use of the $Al^{27}(n,\alpha)Na^{24}$ reaction to monitor the $Na^{23}(n,2n)Na^{22}$ reaction would not lead to a very large error.

[7] L. J. Laslett, Phys. Rev. **76**, 858 (1949).

[8] A. G. Worthing and J. Geffner, *Treatment of Experimental Data* (John Wiley and Sons, Inc., New York, 1943), pp. 183–187.

[9] Sherr, Halpern, and Mann, Phys. Rev. **84**, 387 (1951).

In view of the discussion above, the error quoted for the cross section is twice the standard deviation obtained for the six measurements, namely 13.8±2.2 millibarns.

The author wishes to express his thanks to R. W. Davis for operating the Cockcroft-Walton machine and to many members of the Cockcroft-Walton group for assistance and suggestions.

PHYSICAL REVIEW VOLUME 98, NUMBER 1 APRIL 1, 1955

Angular Distributions and Yields of Neutrons from (p,n) Reactions

BERNARD L. COHEN
Oak Ridge National Laboratory, Oak Ridge, Tennessee
(Received December 8, 1954)

Angular distributions of neutrons from (p,n) reactions on Mg, Al, Cu, Mo, Ag, Ta, Au, Th, and U were measured for 23-Mev protons incident on thick targets. All angular distributions show peaks in the forward direction; except for Mg and Al, the 0°/180° intensity ratios vary from 5 to 15 for ~13-Mev neutrons, and from 1.3 to 5 for ~8-Mev neutrons. The Mg and Al high-energy data show minima and secondary maxima. Yield determinations indicate that the number of neutrons per nuclear reaction increases with atomic number from about 0.25 for Mg and Al to about 2.0 for most heavy elements and more than 4 for Th and U (probably due to fission). Temperatures of the neutron energy distributions are estimated; for the heavy elements at the backward angles, they are about 0.85 Mev at 3-Mev neutron energy, and about 1.9 Mev at 10-Mev neutron energy. It is concluded that direct interactions are of considerable importance in these reactions.

IT has generally been assumed that nuclear reactions induced by neutrons and protons in the 10- to 25-Mev energy region proceed by a compound nucleus interaction.[1,2] This assumption was originally based on theoretical predictions of very short mean free paths in nuclear matter for nucleons of this energy, but experimental supporting evidence was soon forthcoming. Measurements of energy spectra of emitted neutrons[3] and protons[4] showed them to be approximately Maxwellian. Excitation functions for $(n,2n)$ and $(\alpha,2n)$ reactions confirmed this.[5] Excitation functions for proton-induced reactions on Cu^{63} and alpha-induced reactions on Ni^{60} were found[6] to be remarkably similar when plotted against the excitation energy of the compound nucleus, which is the same in the two cases. All of these facts were considered to be more or less complete confirmation of the compound nucleus hypothesis.

Recently, however, accumulated evidence indicates that mean free paths in nuclear matter are considerably longer than had previously been suspected.[7] It has been pointed out that the deviations from Maxwellian shape in the energy distributions of emitted particles are in the opposite direction from what is demanded by even very general considerations from compound nucleus theory.[8] It was found that (n,p) reaction cross sections in heavy elements are considerably larger than expected from compound nucleus interactions[9]; this was tentatively explained[10] by assuming that a small fraction of the reactions (~10 percent) take place by a direct interaction. Very convincing evidence for direct interactions was obtained by Eisberg and Igo[11] in their measurements of angular distributions and energy distributions from inelastic scattering of 32-Mev protons by various heavy elements.

In this paper these matters are further studied by measurement of angular distributions of neutrons from (p,n) reactions induced by ~20-Mev protons. In the process, data on neutron yields were automatically obtained, so that they are also presented.

EXPERIMENTAL

Angular distributions of neutrons from (p,n) reactions were measured by means of the internal, circulating, 23-Mev proton beam of the ORNL 86-inch cyclotron. The most feasible method of detecting neutrons in an experiment of this type is by activation detectors (sometimes called "threshold detectors"). This method has frequently been criticized as being potentially subject to large errors, but a rather extensive study indicated that, in these particular experiments at

[1] N. Bohr, Nature **137**, 344 (1936).
[2] J. M. Blatt and V. F. Weisskopf, *Theoretical Nuclear Physics* (John Wiley and Sons, Inc., New York, 1952).
[3] P. C. Gugelot, Phys. Rev. **81**, 51 (1951); P. H. Stetson and C. Goodman, Phys. Rev. **82**, 69 (1951); B. G. Whitmore and G. E. Dennis, Phys. Rev. **84**, 296 (1951); E. R. Graves and L. Rosen, Phys. Rev. **89**, 343 (1953).
[4] P. C. Gugelot, Phys. Rev. **93**, 425 (1954).
[5] Brolley, Fowler, and Schlacks, Phys. Rev. **88**, 618 (1953); H. C. Martin and B. C. Diven, Phys. Rev. **86**, 565 (1952); D. J. Tendam and H. L. Bradt, Phys. Rev. **72**, 1118 (1947); Bleuler, Stebbins, and Tendam, Phys. Rev. **90**, 460 (1953).
[6] S. N. Ghoshal, Phys. Rev. **80**, 939 (1950).
[7] Feshbach, Porter, and Weisskopf, Phys. Rev. **90**, 166 (1953).
[8] B. L. Cohen, Phys. Rev. **92**, 1245 (1953).
[9] E. B. Paul and R. L. Clarke, Can. J. Phys. **31**, 267 (1953).
[10] H. McManus and W. T. Sharp, Phys. Rev. **87**, 188 (1952).
[11] R. M. Eisberg and G. Igo, Phys. Rev. **93**, 1039 (1954).

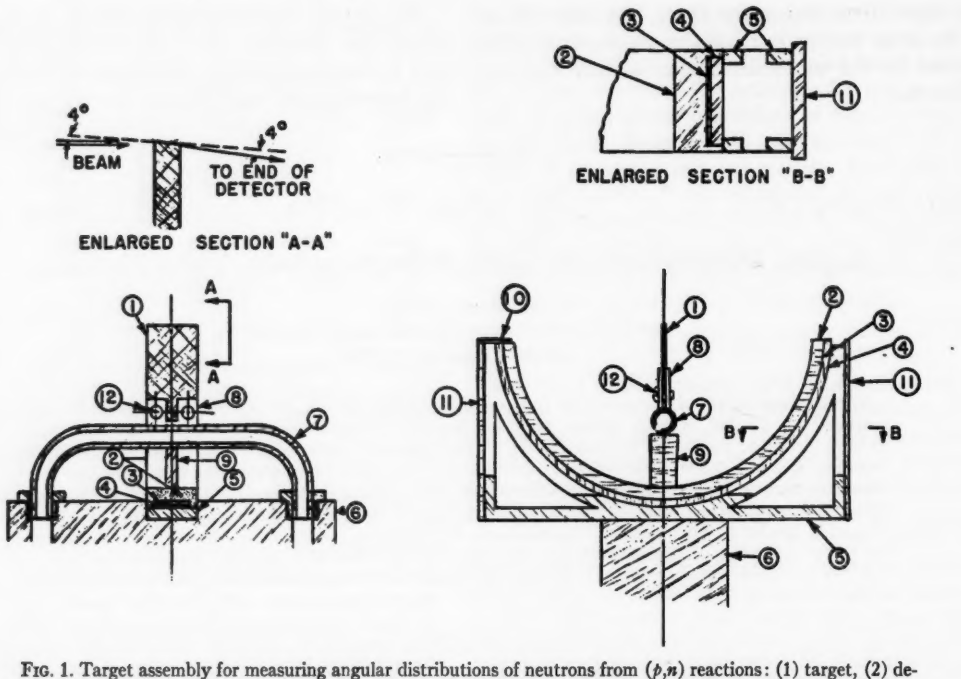

FIG. 1. Target assembly for measuring angular distributions of neutrons from (p,n) reactions: (1) target, (2) detector cover (carbon), (3) detector foils (Al and Ag), (4) detector backing (carbon), (5) assembly body (brass), (6) header for cooling water (brass), (7) water cooling tube (copper), (8) target holder (brass, soldered to cooling tube), (9) wedge (carbon) for holding the detector cover, foils, and backing against the assembly body, (10) detector positioner (carbon), (11) shields (carbon), (12) target clamping screws. Principle sections are through center of assembly. Distance from target tip to detectors is $3\frac{3}{8}$ in. Nearest material, not shown, (dees) is $4\frac{1}{4}$ in. from closest part of assembly.

least, errors which could materially affect the conclusions are highly improbable.

The neutrons were detected by silver and aluminum threshold detectors, the reactions being

$$Ag^{107}(n,2n)Ag^{106}\rightarrow Pd^{106}+\beta^{+}\ (24\ \text{min}),$$
$$Al^{27}(n,p)Mg^{27}\rightarrow Al^{27}+\beta^{-}\ (9.6\ \text{min}).$$

The silver reaction has an energetic threshold at 9.6 Mev, and is theoretically expected to rise quite rapidly to a maximum within a few Mev. Since the energy distributions of the neutrons are Maxwellian, the average energy of the neutrons it detects is about 13 Mev. The aluminum reaction has an energetic threshold at about 2.0 Mev, but theoretically the cross section should remain quite small until the energy available to the emitted proton approaches the Coulomb barrier, which is about 4.5 Mev. Since the neutron energy distributions are Maxwellian, the average energy of the neutrons it detects is about 8 Mev.

The target assembly is shown in Fig. 1. The explanation for its various features will become evident in the discussion to follow. In its simplest form it consists of a target of the element to be studied at the center of a semicircle, with an aluminum and silver foil lying along the circumference of the semicircle and covered by an absorber sufficiently thick to remove all charged particles. The principle difficulty was in the determination and elimination of background.

The most obvious way of being certain that the detected neutrons originate in the target is to stop the entire beam there. In the ORNL 86-inch cyclotron this cannot be done because the beam is 6 inches wide, while the largest practicable radius for the detector semicircle is $3\frac{3}{8}$ inches; this would give very poor angular resolutions and, in addition, there would be no way of measuring backgrounds. These problems were solved by inserting a carbon probe in the cyclotron 180 deg from the target assembly. Narrow targets can then be used, with the remainder of the beam being stopped by the probe. Since the probe is twenty times further from the detectors than the target, and since carbon gives very low neutron production,[12] the probe does not produce an appreciable background. Furthermore, stopping the major portion of the beam on the probe allows determinations of background. This is done by making consecutive runs with and without the target, but with the same current striking the probe. With the exception of the very small and very large angles, which will be discussed below, the background measured in this way was less than 10 percent. In fact, about 80 percent of

[12] Carbon-12 has a (p,n) threshold near 20 Mev, so that the principle neutron production is from carbon-13 (a 1.1 percent isotope) and impurities.

all neutrons, as measured by an energy-insensitive neutron counter at a large distance from the cyclotron, originate in the target even though more than 80 percent of the current strikes the probe.

In the runs made with the target removed, a high activity is produced in the small angle detector foils; it falls off very rapidly with increasing angle. By using proton detectors it was found that this was due to stray beam striking the detector covers, thus producing neutrons very close to the detectors. The best way to eliminate this difficulty, it was found, was to make the targets thick, so as to act as a shield against this stray beam. Use of thick targets somewhat obscures the detailed results of the measurements by making the protons which produce the neutrons by (p,n) reactions nonmonoenergetic. Since only the general form rather than the detailed shape of the angular distributions is used in the theoretical interpretation, this is not a major difficulty. Moreover, the use of thick targets alleviates many other experimental problems.

There still remains the difficulty of measuring the background at small angles. One approach was to make bombardments with a carbon target. These runs gave small angle intensities about 10 percent of those with other target elements, but there were strong indications that a large fraction of that was due to neutrons from the carbon target.[12] Backgrounds at the forward angles were therefore assumed to be the same as those at 45 degrees, which were generally about 5 percent. Part of this background is undoubtedly due to the above-mentioned stray beam, but no large error is possible by this procedure.

In the backward direction there is considerable background in the silver-detector data, presumably due to stray beam striking the back of the detector holder. At 165 deg this is frequently larger than foreground. It drops off rapidly with decreasing angle, averaging about 40 percent at 150 deg. Since this correction is probably uncertain by 25 percent, it introduces an error of more than 10 percent at angles greater than

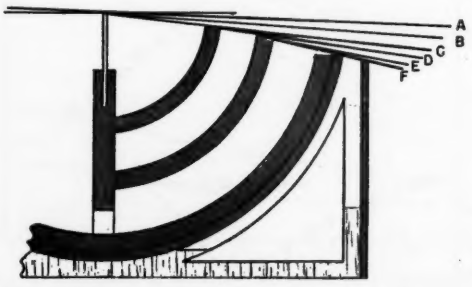

FIG. 2. Target modification to test effect of elastically scattered protons. Except for effects of transparencies and imperfections, beam particles scattered from the target cannot get below line B; if they could, they would not get below line C unless scattered from inner carbon piece; if they were scattered from it, they could not get below line D; etc. This should eliminate any maximum in the forward direction due to (p,n) reactions induced in the detector cover by elastically scattered protons.

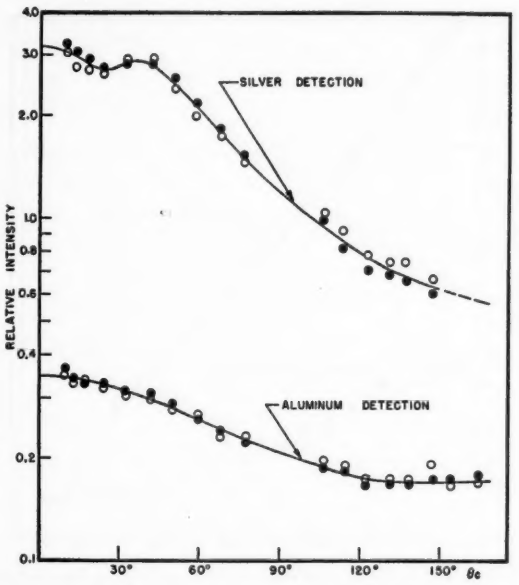

FIG. 3. Angular distribution of neutrons from Al(p,n). Energy of incident protons was 23 Mev, and target was thick. Each set of points represents an average of two or three runs. Silver and aluminum detect only neutrons above 9.5 Mev and 2.0 Mev, respectively; the average energy of the neutrons they detect is about 13 Mev and 8 Mev. Data are corrected for center-of-mass angle and solid angle, and background has been subtracted.

150 deg. In the figures, the data at these angles are therefore indicated only by a dashed line showing its general trend, although even this is uncertain. In the aluminum-detector data, this background is not nearly as large; even at 165 deg it was never larger than 20 percent.

In addition to these backgrounds which are present when the target is removed, there are still two possible sources of background that are inherently due to the target itself:

(1) Protons, elastically scattered from the target, could produce neutrons in the detector covers. Since thick targets were used, it was possible to bevel the tops of the targets so that protons would require several scatterings in the target before they could reach the detector covers (see Sec. A–A, Fig. 1). The effect was then studied by constructing the target assembly shown in Fig. 2. Protons scattered from the target would have to undergo several scatterings in order to reach the detector cover, so that these effects should be greatly reduced. Aside from causing a uniform decrease in intensity relative to backward angles (due to absorption), it did not change the observed angular distributions; the effect of scattered protons was thus considered to be negligible.

(2) Neutrons originating in the target could be scattered into the detectors. Every effort was made to reduce this by keeping the amount of extraneous material to the bare minimum. The geometry was such

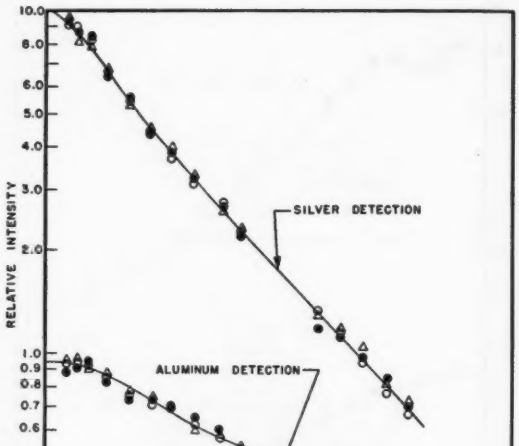

FIG. 4. Angular distribution of neutrons from Cu(p,n). See caption for Fig. 3. Ordinate scale is same as in Fig. 3.

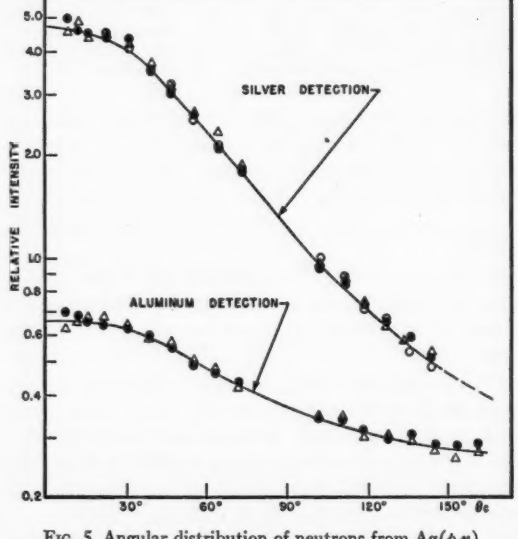

FIG. 5. Angular distribution of neutrons from Ag(p,n). See captions for Figs. 3–4.

that all detectors were closer to the target than to any part of the cyclotron dees. Calculations indicate that under these conditions effects due to scattered neutrons are quite small. To test this, thick pieces of carbon were added to the back and each side of the detector semicircle at the backward angles. Neither the intensities relative to those at the forward angles, nor the shape of the angular distributions was noticeably changed; thus this effect can be assumed to be negligible. As an added precaution, with a few trivial exceptions, everything in the experimental setup was maintained symmetric about 90 deg; this assures that scattered neutrons cannot have an important effect.

The expected errors in these measurements due to well-known effects, such as counting statistics, beta counting errors, and decay corrections, are about 6 percent at each point; this could have very little effect on the general shape of the angular distributions. Inaccuracies in target and detector alignment should not produce errors greater than about 4 percent in the asymmetry about 90 deg. Angles are known to within about 2 degrees.

RESULTS

Angular distributions were measured for Mg, Al, Cu, Mo, Ag, Ta, Au, Th, and U. Some typical data are shown in Figs. 3–6, and the lines through the data for all elements are shown in Figs. 7 and 8. Backgrounds have been subtracted, and corrections have been applied for center-of-mass motion. If it is assumed that the neutrons are emitted with a Maxwellian energy distribution characterized by temperature T, this can be corrected for quite accurately even though there is considerable uncertainty in the excitation functions for the detecting reactions. For example, these corrections are the same whether the excitation functions rise sharply to a plateau, rise gradually and monotonically, or consist of one or more resonances, either very wide or very narrow, providing these effects occur at about the same energy; and even the dependence on energy is relatively slight. These corrections are shown by the dashed lines in Figs. 7 and 8, as calculated for $T=2.5$ Mev for Mg and

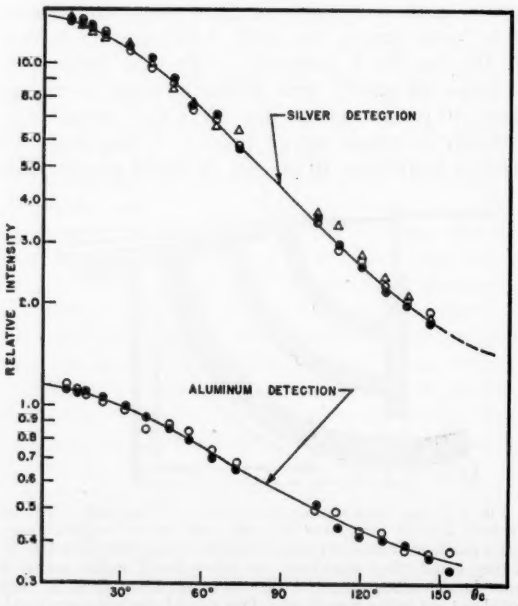

FIG. 6. Angular distribution of neutrons from Ta(p,n). See captions for Figs. 3–4.

Al, and for $T=2.0$ Mev for the other elements. There is some evidence for these values, as will be mentioned below, but the correction for other values of T can easily be estimated by assuming the percentage corrections to be inversely proportional to T.

The data in Figs. 3–6 are normalized to the same current striking the 180-deg probe; this is roughly equivalent to normalizing them to the same current striking the targets. The relative average cross sections for neutron production in the various target elements can thus be easily computed by correcting for the range of protons in the various materials. This is shown in Fig. 9 for neutrons detected by aluminum and by silver, and for all neutrons as detected by an energy-insensitive counter.

By making use of the theoretical total reaction cross sections given by Blatt and Weisskopf,[2] the data for all neutrons from Fig. 9 can be corrected for the relative number of nuclear reactions to be expected, to give the relative number of neutrons per nuclear reaction; this is illustrated in Fig. 10. The excitation functions for the principle neutron-producing reactions in copper have been measured by activation experiments,[6,13] so that the absolute number of neutrons per reaction can be closely estimated for that element. This was used to normalize the data in Fig. 10. A point on the curve at $Z=83$ can be obtained from Kelly's excitation functions on bismuth.[14]

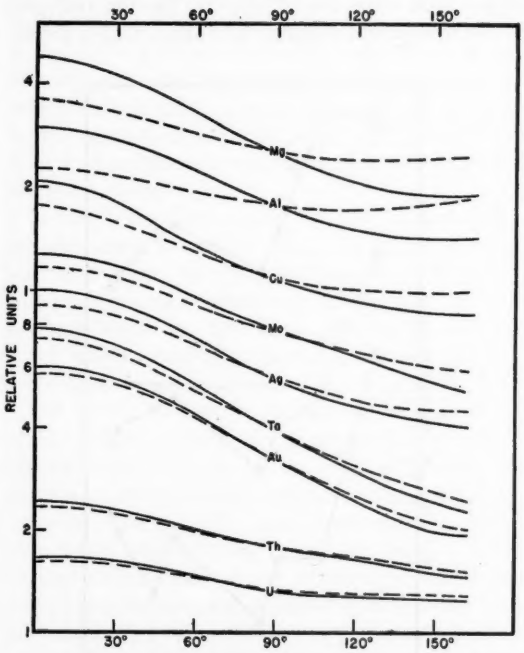

FIG. 7. Composite of aluminum detection data. Dashed lines show corrections for variation of energy with angle due to center-of-mass effects. They were calculated by assuming temperatures of 2.5 Mev for Mg and Al, and 2.0 Mev for the other elements. Corrections are approximately inversely proportional to the temperature.

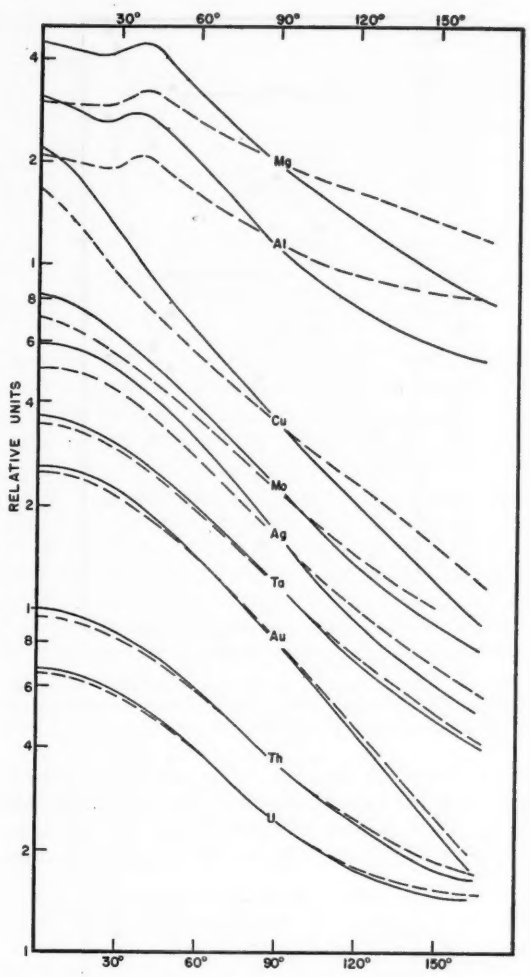

FIG. 8. Composite of silver detection data. See caption for Fig. 7.

Figures 11 and 12 show the relative fraction of all neutrons that are detected by aluminum and silver, respectively, at 0, 90, and 150 deg for the various elements. These were obtained by dividing the detector activities by the neutron counter readings.

DISCUSSION AND CONCLUSIONS

The principle conclusion from this work is that, contrary to what is expected from compound nucleus theory and in agreement with expectations from direct interactions,[15] the angular distributions are not nearly sym-

[13] Cohen, Newman, Charpie, and Handley, Phys. Rev. 94, 620 (1954).

[14] E. Kelly, University of California Radiation Laboratory Report UCRL-1044 (unpublished).

[15] The term "direct interaction" is used here to mean not only interactions consisting of a single, direct collision between the incident and emerging particles, but any interaction in which

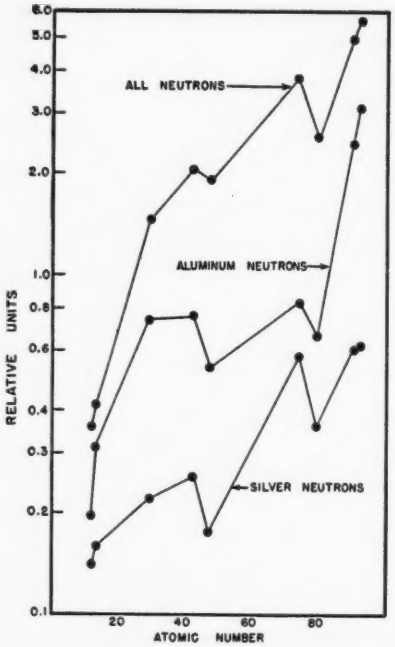

FIG. 9. Cross section for production of neutrons *vs* atomic number. This data was obtained from yields by correcting for stopping cross sections of the materials.

metric about 90 deg, but rather are quite strongly peaked in the forward direction. The large magnitude of the effect is especially interesting. For the high-energy neutrons, the 0-deg intensity is in many cases

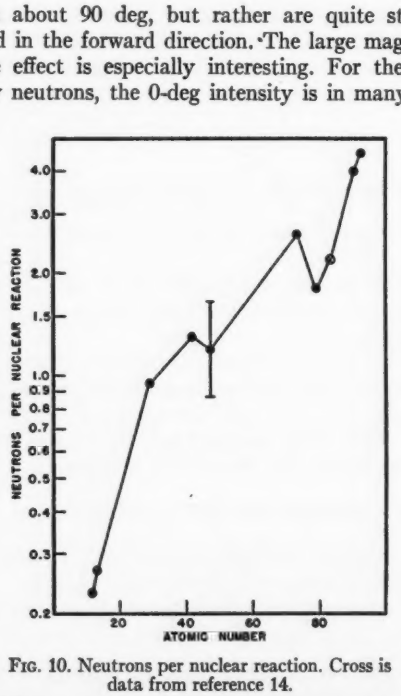

FIG. 10. Neutrons per nuclear reaction. Cross is data from reference 14.

the outgoing particle is emitted before the energy has been shared with more than a small fraction of the nucleons in the nucleus. See R. M. Eisberg, Phys. Rev. 94, 739 (1954).

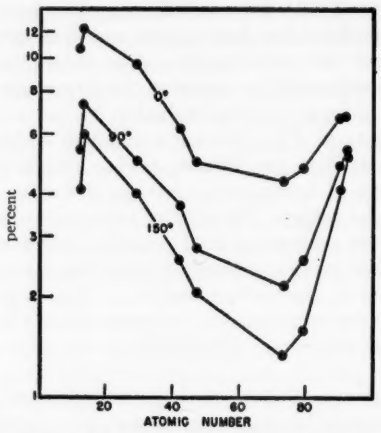

FIG. 11. Percent of all neutrons that are detected by aluminum. Ordinate was calibrated as described in final paragraph of this paper neglecting anisotropy of "all neutrons."

higher than the 180-deg intensity by an order of magnitude. This implies that almost none of these neutrons are produced in compound nucleus reactions.[16] The minima at about 25 deg and the subsequent maxima at about 40 deg in the magnesium and aluminum data suggest that some sort of resonant process analogous to that in deuteron stripping is in effect. Such a process

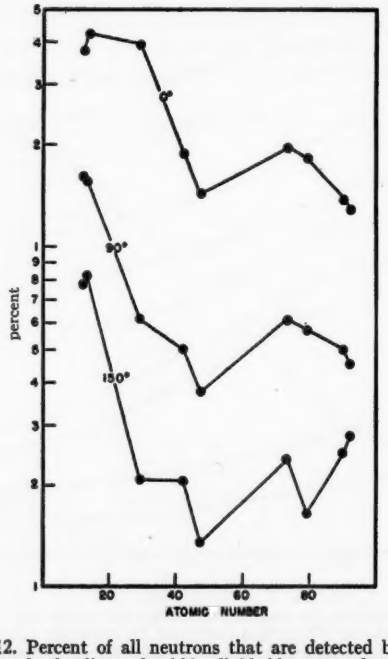

FIG. 12. Percent of all neutrons that are detected by silver. Lower decade of ordinate should be divided by ten so that ordinate scale covers 0.1 to 5.0 percent. See caption for Fig. 11.

[16] L. Wolfenstein, Phys. Rev. 82, 690 (1951); W. Hauser and H. Feshbach, Phys. Rev. 87, 366 (1952).

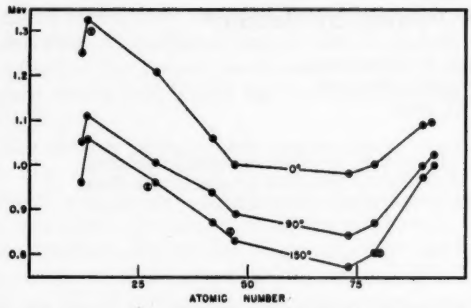

FIG. 13. Temperatures of neutron energy spectra at about 3-Mev neutron energy. Crosses are from reference 3.

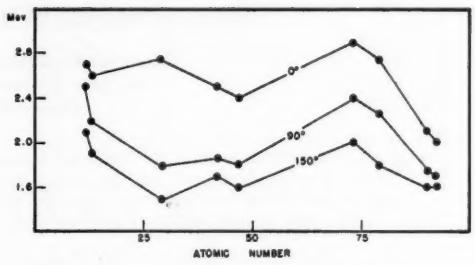

FIG. 14. Temperatures of neutron energy spectra at about 10-Mev neutron energy.

has been suggested by Austern *et al.*[17] On the other hand, the general similarity between angular distributions from elements in the same mass region is almost suggestive of some sort of nonresonant process (e.g., charge exchange, diffraction). In the aluminum-detector data, the 0°/180° ratio is never larger than five, and in the light elements is generally less than two. This may indicate that an appreciable fraction of these neutrons are from compound nucleus interactions, although even from direct interactions lower energy angular distributions would be more isotropic. The rather small anisotropies in thorium and uranium are probably due to the fact that fission occurs with higher probability in these elements, and fission neutrons are emitted approximately isotropically. The smaller anisotropies in the lighter elements may be due to the fact that most noncompound nucleus interactions in these elements result in proton emission.[18]

Several interesting conclusions may be drawn from the yield data, in spite of the fact that it is generally somewhat rough. The very low neutron production in aluminum and magnesium is quite surprising, although it complements the data on $(p,pn)+(p,2n)$ cross sections[19] where essentially the same effect is found to be quite common on elements up to about mass 60.

The very high neutron production in thorium and uranium is undoubtedly due to fission. However, those elements also have the highest cross section for production of silver-detected neutrons. Since these neutrons exhibit a markedly forward angular distribution, they cannot originate from fission. The nearly isotropic angular distributions of the aluminum-detected neutrons from thorium and uranium indicate that these are principally fission neutrons. The ratio of "aluminum neutrons" to total neutrons is quite sensitive to the temperature[20] with which the neutrons are emitted, so that if the fission temperature is assumed to be 1.0 Mev, all other temperatures may be readily estimated. These estimates are shown in Fig. 13, and may be considered to be the average temperature at a neutron energy of about 3 Mev. Figure 13 also shows the temperatures found by Gugelot[3] at these neutron energies from 16-Mev proton-induced reactions. The agreement is excellent. It is important to note that, as has been pointed out in another paper,[18] the spectra at these energies are largely determined by "second" neutrons from (p,pn) and $(p,2n)$ reactions, and therefore are not too meaningful.

Of somewhat more interest is the temperature at higher neutron energies. A simple calculation reveals that the ratio of activities between the silver and aluminum should be very sensitive to the temperature of the neutron energy spectrum. This ratio has been measured for $T=2.5$ Mev with neutrons from the Be(d,n) reaction[21]; from that ratio, the values of T required to explain the ratios of silver to aluminum activities in this experiment were obtained and are shown in Fig. 14. These values are the temperatures of that portion of the spectrum between the energies detected by aluminum and silver, or roughly about 10 Mev. It is interesting to note that these temperatures agree with those obtained from Gugelot's inelastic proton scattering data at 10-Mev outgoing proton energy.

By use of Figs. 13 and 14, the energy spectrum may be roughly approximated, so that the absolute fraction of all neutrons detected by aluminum and silver may be estimated. This calculation was used to obtain the ordinates in Figs. 11 and 12. The relatively small fraction of all neutrons detected in these experiments indicates that compound nucleus formation may still be the principle interaction.

The author is greatly indebted to Mrs. M. K. Hullings for her invaluable assistance in parts of the counting and calculating.

[17] Austern, Butler, McManus, and Sharp, Phys. Rev. **91**, 453 (1953).
[18] B. L. Cohen and E. Newman (to be published).
[19] Cohen, Newman, and Handley (to be published).
[20] The term "temperature" is used here in a purely experimental sense, referring to the reciprocal of $\partial/\partial E[\log(N(E)/E]$ where $N(E)$ is the energy distribution of the emitted neutrons.
[21] B. L. Cohen, Phys. Rev. **81**, 184 (1951).

Elastic Scattering of 9.76-Mev Protons by Helium*

JOHN H. WILLIAMS AND STANLEY W. RASMUSSEN
University of Minnesota, Minneapolis, Minnesota

(Received December 13, 1954)

The differential cross section for elastic scattering of 9.76-Mev protons by helium has been investigated over the range of center-of-mass angles from 43° to 174°. The results are in essential agreement with those of Putnam at 9.48 Mev, differ from those by Freemantle *et al.* at 9.55 Mev by a constant factor, but do not confirm those of Cork and Hartsough at 9.7 Mev.

I. INTRODUCTION

INVESTIGATIONS of the differential cross section for the elastic scattering of protons in the energy region 1 to 10 Mev have been carried out by several groups of experimenters.[1–3] These data have been analyzed in terms of phase shifts by Critchfield and Dodder[4] and by Dodder and Gammel[5] and served to establish the nature of the inverted doublet $P_{\frac{1}{2}}$, $P_{\frac{3}{2}}$ of the compound nucleus Li^5.

Recent work by Cork and Hartsough[6] with 9.7-Mev protons was in marked disagreement with Putnam's[3] observations on the scattering of 9.48-Mev protons by He^4. Since the theoretical analysis[5] in this higher-energy region was based largely on Putnam's results and because an accurate understanding of the upper, $P_{\frac{1}{2}}$, state of Li^5 was essential in order to utilize resonant scattering of protons by He^4 as a proton-polarization analyzer,[7] it was considered desirable to repeat Putnam's observations. An independent research by the Birmingham group employing 9.55-Mev protons has just been published.[8]

II. APPARATUS

The first section of the University of Minnesota proton linear accelerator provides a well collimated and highly monoenergetic beam of 9.89-Mev protons. This beam was passed through a thin beryllium foil[9] which served to dissociate the 5-Mev molecular hydrogen ions which constitute a small percentage contamination of the total beam emitted from the accelerator. Subsequent magnetic deflection removed the resulting 2.5-Mev protons from the desired higher energy beam. After passing through a 0.0005-inch aluminum window into the helium gas region, the protons had been degraded in energy to 9.76 Mev.

Differential scattering cross-section measurements were made with the Los Alamos nuclear emulsion multiple-plate camera.[10] The reliability of this method has been established by comparing results[10] on (p,p) scattering with 3.04-Mev protons and (p,α) scattering with 2.63-Mev protons with earlier data[1,11] taken under carefully controlled conditions with proportional counter detectors.

III. EXPERIMENTAL

The purpose of the present experiment was to eliminate as many possible uncertainties in Putnam's[3] observations as was feasible. The availability of highly monoenergetic protons and low background radiation provided such an opportunity. In addition we chose to make a single exposure at laboratory scattering angles from 22½° to 172½° and helium gas pressure 9.92 cm of Hg, so that errors due to current integrator, gas pressure, and temperature calibrations would not influence the form of the cross section *vs* angle experimental curve. We also circulated helium gas, purified by passing over activated charcoal at liquid air temperatures, through the scattering region by means of differential pumping in order to reduce the amount of undesirable contamination gas scattering. The single-exposure compromise limited the least scattering angle at which proton tracks could be counted reliably to 35° and reduced the number of tracks observed at 90° and backward angles to such an extent that it was not feasible to obtain statistical accuracy greater than five percent.

The scattering angles were defined by the divergence of the incident proton beam, less than $\pm\frac{1}{4}°$ as a property of the proton linear accelerator, and the angular definition of the slits between the scattering volume and the photographic emulsion, $\pm\frac{3}{4}°$. The over-all angular definition was thus approximately $\pm 1°$.

Preliminary range analyses were made on the proton tracks in several emulsions to establish that our selection criteria (range, angle, and entry at the surface of the emulsion) were adequate to exclude the relatively few protons scattered by slit edges and contaminant gases as well as recoil protons in the

* Work supported by the U. S. Atomic Energy Commission.

[1] Freier, Lampi, Sleator, and Williams, Phys. Rev. **75**, 1345 (1949).

[2] Kreger, Kerman, and Jentschke, Phys. Rev. **86**, 593 (1952).

[3] T. M. Putnam, Phys. Rev. **87**, 932 (1952).

[4] C. L. Critchfield and D. C. Dodder, Phys. Rev. **76**, 602 (1949).

[5] D. C. Dodder and J. L. Gammel, Phys. Rev. **88**, 520 (1952).

[6] B. Cork and W. Hartsough, Phys. Rev. **96**, 859 (1954).

[7] M. Heusinkveld and G. Freier, Phys. Rev. **85**, 80 (1952).

[8] Freemantle, Grotdal, Gibson, McKeague, Prowse, and Rotblat, Phil. Mag. **45**, 1090 (1954).

[9] Be foils of approximately 3×10^{-5} inch were made available through the courtesy of Dr. Hugh Bradner, University of California Radiation Laboratory.

[10] Allred, Rosen, Tallmadge, and Williams, Rev. Sci. Instr. **22**, 191 (1951).

[11] Blair, Freier, Lampi, Sleator, and Williams, Phys. Rev. **75**, 1345 (1949).

emulsion arising from neutrons. A set of plates exposed under identical conditions, except that no helium was admitted to the camera, were examined and no background tracks were found that satisfied the selection criteria.

The number of acceptable proton tracks scattered per unit width of swath on the exposed plates was counted with a Leitz Ortholux microscope. Similarly, we determined the number of helium recoil nuclei that were incident, during the single exposure described above, on the plates placed at laboratory angles from $22\frac{1}{2}°$ to 35°. Helium recoils at angles greater than 35° did not have an energy sufficient to produce tracks long enough to be identified reliably.

IV. RESULTS

The differential scattering cross section as a function of the angle of scattering of the proton in the center-of-mass system of coordinate can be obtained from the observations of either the scattered protons or recoil alpha particles from the dynamics of the elastic collision process. Agreement between the cross sections for a given proton angle obtained by these two methods is particularly satisfying and convincing.

The numerical results are given in Table I and are presented graphically by the solid and open circles in Fig. 1. The solid circles are data obtained from measurements on scattered protons, the open circles from recoil alpha particles. Only at the minimum of the curve do they differ by slightly more than the statistical accuracy, ±5 percent. The full curve drawn through these circles represents the present measurements of the (p,α) elastic scattering cross section for 9.76-Mev (laboratory energy) protons.

Also shown in Fig. 1, by means of the dotted curve, are the results of Putnam[3] with 9.48-Mev protons in the angular region where they are not in essential agreement with the full line. Elsewhere the data agree throughout the limited common angular range. The

TABLE I. Observed differential cross sections in millibarns per steradian for elastic scattering of 9.74-Mev protons by helium as a function of proton scattering angle in the center-of-mass system. At angles marked by an asterisk, results were obtained by observing the recoil helium nuclei.

$\theta_{c.m.}$	$d\sigma/d\Omega$	$\theta_{c.m.}$	$d\sigma/d\Omega$
43°15′	236 ±10		
49°15′	232 ±9	*135	41.9±2.1
52°13′	220 ±11	141° 3′	51.4±2.6
63°56′	153 ± 7	143° 7′	53.3±2.7
75°19′	105 ±5	149°15′	64.8±3.2
86°18′	66.7±3.3	150°18′	65.4±3.3
96°51′	37.0±1.8	157°11′	76.3±3.8
106°58′	25.6±1.5	159°18′	72.5±3.6
*110°	20.7±0.8	161°4′	78.0±3.9
*115°	19.7±1.0	162°55′	76.0±3.0
116°39′	22.3±1.3	164°54′	75.3±3.8
*120°	20.2±1.0	166°49′	81.3±4.1
*125°	27.0±1.3	168°43′	85.7±2.2
125°51′	27.9±1.4	170°36′	81.7±4.1
*130°	30.0±1.5	172°29′	86.9±4.3
134°40′	39.7±2.0	174°22′	84.4±4.2

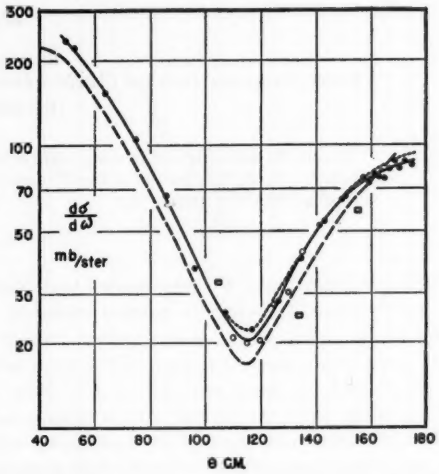

FIG. 1. Differential cross section for elastic scattering of 9.74-Mev protons by helium as a function of proton scattering angle in the center-of-mass system. The full circles represent results from observing scattered protons, the open circles from observing recoil helium nuclei. The dotted curve shows Putnam's (reference 3) results where they differ from the present. The dashed curve is that of Freemantle *et al.* (reference 8). The squares are the higher-angle results of Cork and Hartsough (reference 6).

difference between the dotted and full curves may result from the difference in proton energy, 9.48 Mev and 9.76 Mev, for the two experiments. Detailed calculations of phase shifts must be made before such an explanation can be certain.

The more recent results of the Birmingham[8] group with 9.55-Mev protons are shown by the dashed line in Fig. 1. Over the angular region 40° to 155°, the forms of the full and dashed curves are very nearly the same but the latter is only 85 percent of the former in magnitude of cross section. The explanation for this difference may lie in errors of measuring one or several factors such as current or gas pressure. The relatively rapid rise of the dashed curve at angles greater than 155° can probably be accounted for by a recently discovered error[12] in a geometry factor of the Birmingham experiment.

The results of Cork and Hartsough[6] agree with those of Putnam[3] and the present report in the angular range up to 90° (c.m.). The observations of Cork and Hartsough at angles greater than 90° (c.m.) are shown by the squares in Fig. 1. No attempt is made to draw a curve through these points, but the lack of agreement with the present results lies well outside their statistical accuracy, approximately 2 percent.

ACKNOWLEDGMENTS

We wish to express our sincere thanks to the Los Alamos Scientific Laboratory and particularly to Dr. Louis Rosen for making the multiplate camera available for these experiments.

[12] J. Rotblat (private communication).

Decay of Y^{91}

B. KAHN AND W. S. LYON
Health Physics and Analytical Chemistry Division, Oak Ridge National Laboratory, Oak Ridge, Tennessee
(Received December 6, 1954)

Yttrium-91 was observed to decay with a half-life of 57.5±0.5 days. In addition to the 1.55-Mev beta transitions, 0.22±0.01 percent of the Y^{91} decay consists of a 0.36±0.02-Mev beta group in coincidence with a 1.190±0.005-Mev gamma ray.

THE disintegration of Y^{91} was studied to determine the fraction decaying by gamma emission. According to the most recent investigation[1] (which appeared since this work was begun), Y^{91} decays with a half-life of 58.5±1 days, emitting a 1.55-Mev beta group in more than 99 percent of its decay, and a 0.330±0.010-Mev beta particle in coincidence with a 1.22±0.01-Mev gamma ray in 0.30±0.05 percent of its decay. The presence of this gamma ray had previously been doubted,[2] and the presence of another, weaker gamma ray has been reported[3] and disputed.[1] Values of half-life, gamma energy, and gamma intensity differing somewhat from those cited have also been reported.[4]

PROCEDURE

A one-year-old sample of Y^{91} was received from the Operations Division of the Oak Ridge National Laboratory as the nitrate in dilute nitric acid. The Y^{91} had been separated from other fission products on a cation exchange column. Part of the solution was evaporated to dryness, after which the Y^{91} was taken up in 5-ml concentrated HNO_3 and extracted into 1-ml 60 percent tributyl phosphate in hexone. The organic phase was washed twice with conc. HNO_3, after which the Y^{91} was extracted into 1 ml water. This method[5] was tested with Y^{91} and Pm^{147} tracer, and it was shown that 86 percent of Y^{91} and 6.8 percent of Pm^{147} were recovered. Hence, a separation factor of at least 12 can be expected from the rare earths formed in fission, which are the only expected contaminants.

To determine the beta activity of the extracted Y^{91}, aliquots made slightly acid with HNO_3 were evaporated on polystyrene and counted in 4-pi counters, and also with end-window counters, using the absolute beta counting method. To determine the gamma activity, other aliquots were counted in a calibrated high-pressure ion chamber; correction for the relatively large amount of bremsstrahlung detected by the ion chamber was made by subtracting from the total reading the bremsstrahlung from a source of P^{32} of equal beta activity. The energy and intensity of the gamma rays were compared with the 1.1715-Mev gamma rays of a Co^{60} source of known activity, using a scintillation spectrometer with a 3-in. diameter×3-in. thick NaI(Tl) detector. In order to detect any gamma rays of less than 0.5-Mev energy that may be obscured by the large amount of bremsstrahlung which Fig. 1 indicates is present, Lazar and Bell utilized a scintillation spectrometer having a scintillating absorber in anticoincidence with the NaI(Tl) crystal.[6] By this procedure, the amount of external bremsstrahlung counted is greatly reduced. To characterize the antecedent of the gamma ray, the beta-gamma coincidence rate of Y^{91} as a function of the thickness of aluminum absorber placed before the beta detector of a coincidence counter was observed. The coincidence counter consisted of an argon-methane proportional tube as the beta detector, and the NaI(Tl) spectrometer, adjusted to detect only the 1.190-Mev photoelectric peak, as the gamma detector.

The decay of Y^{91} was observed for five half-lives in a beta proportional counter and in the high-pressure ion chamber, and the decay of the 1.190-Mev photoelectric peak was followed on the NaI(Tl) spectrometer.

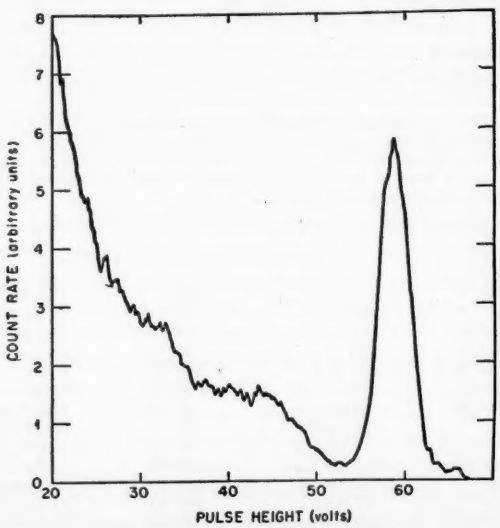

FIG. 1. Gamma-ray spectrum of Y^{91}.

[1] Bunker, Mize, and Starner, Phys. Rev. 94, 1694 (1954).
[2] F. I. Boley and D. S. Dunavan, Phys. Rev. 90, 158 (1953).
[3] L. M. Langer and H. C. Price, Jr., Phys. Rev. 76, 641 (1949).
[4] Hollander, Perlman, and Seaborg, Revs. Modern Phys. 25, 469 (1953).
[5] C. W. Stanley, Los Alamos Report La-1566, 1953 (unpublished).
[6] N. H. Lazar and P. R. Bell, Phys. Rev. 95, 612 (1954).

RESULTS AND DISCUSSION

No significant difference in the decay characteristics of the extracted and the original Y^{91} was observed; hence, the Y^{91} supplied by the Operations Division may be considered to be uncontaminated by any rare earth fission products. The two methods of determining the beta activity of the Y^{91} give results which are in agreement, as do the two methods for determining the gamma activity; the ratio of gamma to beta activity is 0.22 $\pm$0.01 percent. Only one gamma ray having an energy of 1.190 Mev was observed. Coincidence counting indicated that weak beta particles are in coincidence with the 1.190-Mev gamma rays. In coincidence counting,

$$C_\beta = e_{\beta-1} fN + e_{\beta-2}(1-f)N, \quad (1)$$

$$C_\gamma = e_\gamma fN, \quad (2)$$

$$C_{\text{coincidence}} = e_{\beta-1} e_\gamma fN, \quad (3)$$

where e is the counting efficiency, C the observed count rate, f the fraction decaying to excited state, N the disintegration rate, $\beta-1$ the beta particle in coincidence with the gamma rays, and $\beta-2$ the beta particles not in coincidence. Hence,

$$C_{\text{coincidence}}/C_\gamma = e_{\beta-1}, \quad (4)$$

and by varying the absorber thickness before the beta detector, an "absorption curve," shown in Fig. 2, for the beta particles in coincidence with the gamma ray was obtained. The maximum energy of this beta group, determined by comparing the slope of the curve shown in Fig. 2 with slopes of beta groups of known energy, is given in Table I. Since f is very small, Eqs. (1), (2), and (3) can be combined so that

$$N = \frac{C_\beta C_\gamma}{C_{\text{coincidence}}} \cdot \frac{e_{\beta-1}}{e_{\beta-2}}. \quad (5)$$

TABLE I. Decay characteristics of Y^{91}.

Half-life—β	57.5 $\pm$0.05 days
Half-life—γ	58.0 $\pm$1 days
Beta-1	0.36 $\pm$0.02 Mev
Beta-2	1.55 Mev[a]
Gamma	1.190$\pm$0.005 Mev, 0.22$\pm$0.01%
Other gammas	0.1 to 2.0 Mev, <0.01%

[a] See reference 4.

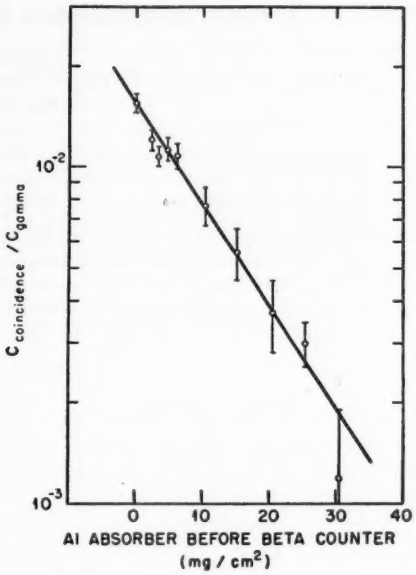

FIG. 2. Variation of β-γ coincidence count per gamma count with aluminum thickness before β counter.

Thus, using $e_{\beta-1}$ from Fig. 2, and $e_{\beta-2}$ found by absolute beta counting, N can be determined. This value of N agrees with the values obtained by 4 pi and absolute beta counting.

No impurity in the Y^{91} was found by following its decay for ten months; the half-life values determined by both beta and gamma counting agreed within the experimental error.

CONCLUSION

Y^{91} has been found to decay mainly with a strong beta group, reported to have a maximum beta energy of 1.55 Mev,[4] while 0.22 percent decays by the emission of a 0.36-Mev group in coincidence with 1.190-Mev gamma rays. The gamma spectrum between 0.1 and 2.0 Mev shows only a strong bremsstrahlung continuum and the 1.190-Mev gamma ray. The gamma-beta ratio, determined by several methods, and the gamma energy, found by comparison with the Co^{60} gamma rays, are in fair agreement with the ratio and gamma energy arrived at by comparison with Na^{22}.[1]

Isotopic Spin Selection Rule for Electric Dipole Transitions

WILLIAM M. MACDONALD*
Princeton University, Princeton, New Jersey
(Received December 24, 1954)

The validity of the isotopic spin quantum number in nuclei provides a selection rule on electric dipole transitions. The extent to which this selection rule is violated provides a means of experimentally determining the isotopic spin impurity of nuclear states providing that the radiation widths for uninhibited $E1$ radiation can be predicted. The sources of possible variations of $E1$ matrix elements are discussed with reference to the reliability of predicted $E1$ radiation widths in nuclei for $A \leq 20$ and excitation energy ~ 15 Mev. Higher order corrections to the $E1$ selection rules are determined and found to be negligible compared to the effects of isotopic spin impurity. It is concluded that the isotopic spin selection rule on $E1$ transitions provides a sensitive test of charge independence. Isotopic spin impurity determined in this way can be attributed solely to the Coulomb potential.

INTRODUCTION

THE most striking evidence for the validity of isotopic spin in light nuclei is the existence of the selection rules on electric dipole transitions. These selection rules were first derived on the basis of supermultiplet theory by Trainor,[1] but it was pointed out by Radicati[2] and Christy[3] that these restrictions on electric dipole radiation actually follow more generally from properties of the interaction of the electromagnetic field with a system of nucleons and from the hypothesis of charge-independent nuclear forces. A more complete statement of the isotopic spin selection rules was then given by Gell-Mann and Telegdi[4] who also discussed the effect of these selection rules on the absorption cross section for γ rays.

The experimental investigation of the validity of the isotopic spin quantum number was undertaken by Wilkinson[5–7] with various collaborators. Although the operation of the selection rule was verified in several cases by the complete absence of $E1$ transitions which should have been detectable, in a number of cases the forbidden $E1$ transitions were actually found to have small but measurable radiative widths. Knowledge of the radiative width to be expected for $E1$ transitions if uninhibited by any isotopic spin selection rule should then enable the experimentalist to estimate the admixture of other isotopic spin eigenstates to the nuclear states involved in the transition.

In order to determine the extent to which the isotopic spin selection rules are operating, therefore, we must know whether there are likely to be any other causes for variation in a particular $E1$ transition. Actually, as Kinsey and Bartholomew[8] have pointed out, very little has been known about $E1$ transitions until quite recently. For this reason we shall discuss in some detail the magnitude of $E1$ transitions and the several inhibiting factors such as the isotopic spin selection rules, correlation of neutron and proton distributions, and complex coupling of single particle states.

The results of Wilkinson on isotopic spin impurity in light nuclei have been thrown into doubt, however, by the observation of Gell-Mann and Telegdi that higher order terms in the $E1$ matrix elements are perhaps sufficient to promote "forbidden" $E1$ transitions to an even greater extent than the isotopic spin impurity would provide. To investigate this question we shall derive the exact electromagnetic multipole moments for nonrelativistic quantum mechanics and with these proceed to estimate the higher order corrections to the isotopic spin selection rules on $E1$ radiation. We shall find that these higher order corrections are ~ 1000 times less effective than isotopic spin impurity in producing violations of the isotopic spin selection rules. The estimates of isotopic spin impurity by Wilkinson still stand, subject only to the uncertainty in $E1$ radiative widths. The investigation of $E1$ radiation provides in fact a sensitive test of the hypothesis of charge independence of nuclear forces.

INHIBITION OF $E1$ TRANSITIONS

The nonrelativistic Schrödinger Hamiltonian for the interaction of a system of nucleons with an electromagnetic field can be written in the isotopic spin formalism correct to first order in the vector potential $\mathbf{A}$

$$H_I = -\sum_{i=1}^{A} \left\{ \frac{e}{Mc} \mathbf{p}_i \cdot \mathbf{A}(\mathbf{r}_i)(\tfrac{1}{2} - t_{fi}) + [\mu_P(\tfrac{1}{2} - t_{fi}) + \mu_N(\tfrac{1}{2} + t_{fi})] \boldsymbol{\sigma}_i \cdot [\nabla \times \mathbf{A}(\mathbf{r}_i)] \right\}, \quad (1)$$

where the isotopic spin operator t_f has the eigenvalue

* Present address, Radiation Laboratory, University of California, Berkeley, California.
[1] L. E. H. Trainor, Phys. Rev. **85**, 962 (1952).
[2] L. A. Radicati, Phys. Rev. **87**, 521(L) (1952).
[3] R. F. Christy, Pittsburgh Conference on Medium Energy Nuclear Physics, 1952 (unpublished).
[4] M. Gell-Mann and V. L. Telegdi, Phys. Rev. **91**, 169 (1952).
[5] D. H. Wilkinson, Phil. Mag. **44**, 547, 1019 (1953).
[6] D. H. Wilkinson and A. B. Clegg, Phil. Mag. **44**, 1269, 1322 (1953).
[7] G. A. Jones and D. H. Wilkinson, Phys. Rev. **90**, 722 (1953).
[8] G. A. Bartholomew and B. B. Kinsey, Phys. Rev. **93**, 1260 (1954).

$+\frac{1}{2}$ for a neutron and $-\frac{1}{2}$ for a proton. The neutron-proton mass difference has been neglected as is certainly justified in first approximation. This equation differs from that of Radicati[2] and Gell-Mann and Telegdi[4] by a sign because our e is positive for protons and negative for electrons. The H_I in (1) is the sum of a part H_0 which is a scalar in isotopic spin space and a part H_1 which is ζ component of an isotopic spin vector.

$$H_0=-\sum_{i=1}^{A}\left\{\frac{e}{2Mc}\mathbf{p}_i\cdot\mathbf{A}(\mathbf{r}_i)+\tfrac{1}{2}(\mu_P+\mu_N)\boldsymbol{\sigma}_i\cdot[\nabla\times\mathbf{A}(\mathbf{r}_i)]\right\}, \quad (2)$$

$$H_1=\sum_{i=1}^{A}\left\{\frac{e}{Mc}\mathbf{p}_i\cdot\mathbf{A}(\mathbf{r}_i)+(\mu_P-\mu_N)\boldsymbol{\sigma}_i\cdot[\nabla\times\mathbf{A}(\mathbf{r}_i)]\right\}t_{\zeta i}. \quad (3)$$

If one makes the assumption $(kR)\ll 1$, one can demonstrate that the electric dipole transitions induced by H_0 are proportional to the square of the electric dipole moment Q_{1m} between the initial and final nuclear states, $\varphi_i(1,\cdots,A)$ and $\varphi_f(1,\cdots,A)$, which depend on the relative coordinates of A nucleons.

$$Q_{1m}{}^{(0)}=\tfrac{1}{2}\sum_{k=1}^{A}e\int r_kY_{1m}{}^*(\vartheta_k,\varphi_k)\times\varphi_f{}^*(1,\cdots,A)\varphi_i(1,\cdots,A). \quad (4)$$

Correspondingly, $E1$ transitions induced by H_1 have transition probabilities proportional to the square of

$$Q_{1m}{}^{(1)}=\sum_{k=1}^{A}el_{\zeta k}\int r_kY_{1m}{}^*(\vartheta_k,\varphi_k)\times\varphi_f{}^*(1,\cdots,A)\varphi_i(1,\cdots,A). \quad (5)$$

If we now neglect nuclear recoil on emission of a γ ray, the center of mass of the nucleus can be taken as the origin and $\sum_{k=1}^{A}\mathbf{r}_k=0$. Since (4) vanishes only H_1 can produce $E1$ transitions.

From the fact that H_1 is the ζ component of a vector in isotopic spin space, the following selection rules on $E1$ radiation follow immediately[9]:

$$\begin{aligned}&\Delta T=0,\pm1, \quad T_\zeta\neq0;\\ &\Delta T=\pm1, \quad T_\zeta=0.\end{aligned} \quad (6)$$

The selection rule for $T_\zeta=0$ $(N=Z)$ nuclei is a generalization of Radicati's requirement of no $T=0\rightarrow T=0$ transitions. The absolute validity of (6) for $T_\zeta=0$ nuclei can be impaired either by the impurity of isotopic spin states or by certain higher order terms in the multipole matrix elements.

In addition to the inhibition of $E1$ transitions by the isotopic spin selection rules, there exists the possibility of inhibition of $E1$ matrix elements by the correlation of the neutrons and protons in the nucleus. This effect upon the matrix elements of H_1 follows immediately from (5) where we note that the terms of $\sum_{k=1}^{A}l_{\zeta k}\mathbf{r}_k$ referring to neutrons will have opposite signs from those referring to protons. This diminution of $E1$ matrix elements was pointed out by Delbruck and Gamow,[10] and was later derived by Bethe[11] in a more general form to explain the anomalously small $E1$ transition probabilities thought to occur in heavy nuclei. The evidence for small $E1$ transition probabilities at that time was of several kinds: (1) anomalously long lifetimes for low-lying states in heavy nuclei (10^{-12} sec *versus* theoretical estimated 10^{-16} for $E1$), (2) radiative widths for (n,γ) reactions, (3) $Li^7(p,\gamma)Be^8$, 17.63 Mev γ ray, and (4) radiative widths observed in (p,γ) capture in F^{19}.

Since considerably more experimental information has recently been obtained on isomeric transitions, we shall discuss this evidence for a neutron-proton correlation effect on $E1$ matrix elements. We shall be interested particularly in the implications for inhibition of $E1$ transitions in light nuclei $(A\leq20)$ for moderate excitation energies $(E\sim15$ Mev).

As remarked by Bartholomew and Kinsey,[8] the evidence in (1) has lost most of its significance since more accurate tables of internal conversion coefficients have shown that these $E1$ transitions in heavy nuclei are really $E2$ transitions. Although several true $E1$ transitions in heavy nuclei have been detected recently[12,13] and these have low-transition probabilities, it has been suggested that the emitting state is formed by a complex coupling of several nucleons with a consequent reduction of the extreme single-particle matrix element. That complex coupling can reduce transition probabilities by factors of ~100 has been demonstrated by Lane and Radicati.[14] In particular their results show that a variation by a factor of 50 depending on the coupling is possible for the $E1$ matrix element from the 7.48-Mev state of B^{10} to the ground state. The reason for the small number of $E1$ transitions in heavy nuclei and consequent long lifetimes for the low-lying states may be simply the absence of low-lying states of the proper spin and parity.

As stated in (2) we find that the radiative widths derived from (n,γ) reactions in heavy nuclei are rather narrower than one should expect on the basis of simple theory. Yet from the existence of a sum rule for $E1$ transitions it is clear that the widths of $E1$ resonances for high-energy γ rays cannot be given by the simple theory.[15] Blatt and Weisskopf[16] have suggested in fact that the radiation width for a single level should be inversely proportional to the level density at the posi-

[9] E. P. Wigner, *Gruppentheorie* (Edwards Brothers, Inc., Ann Arbor, Michigan, 1944).

[10] M. Delbruck and G. Gamow, Z. Physik **72**, 492 (1931).
[11] H. Bethe, Revs. Modern Phys. **9**, 222 (1937).
[12] Beling, Newton, and Rose, Phys. Rev. **87**, 670 (1952).
[13] A. W. Sunyar, Phys. Rev. **90**, 387 (1953).
[14] A. M. Lane and L. A. Radicati, Proc. Phys. Soc. (London) **A67**, 167 (1954).
[15] V. Weisskopf, Phys. Rev. **83**, 1073 (1951).
[16] J. M. Blatt and V. Weisskopf, *Theoretical Nuclear Physics* (John Wiley and Sons, Inc., New York, 1952).

tion of the emitting state. Such a dependence of level widths on level spacing does produce a reduction of $E1$ matrix elements which is in agreement with experiment.[8] This reduction of level width cannot be interpreted as a neutron-proton correlation effect, however, since the ratio both of $E2$ to $E1$ level widths and of $M1$ to $E1$ level widths seem to be correctly predicted by the Weisskopf formulas.[8]

In any case, for light nuclei and excitation energies less than ~15 Mev, the dependence of matrix elements on level density should cause no appreciable reduction of widths of $E1$ emission.[6]

The evidence in (3) is that the 17.63-Mev state in Be^8 displays a width for radiative decay which is several hundred times smaller than one should expect for an $E1$ transition. More recent experimental results suggest, however, that the 17.63-Mev state is (1+) in spin and parity. Since the ground state of such an even-even nucleus is expected to be (0+), the radiative decay of the 17.63-Mev state to the ground state must be magnetic dipole or electric quadrupole. This is in agreement with experiment.[17]

The experimental evidence mentioned in (4) has been clarified quite recently with the separation of the 6-Mev background from $F^{19}(p,\gamma)O^{16*}$ and identification of the spins and parities of the states in Ne^{20} lying just above the threshold for proton capture.[18] The only capture radiation which has been observed in $F^{19}(p,\gamma)Ne^{20}$ up to 1 Mev above the proton capture threshold is from the 13.51-Mev state, which emits a γ ray of ~12 Mev. Since the 1.63-Mev level is now known to be (2+), $E1$ emission by the (2−) levels at 13.70 and 13.44 Mev to this level should be observed also. The reduced widths for alpha-particle emission of both these levels, however, strongly imply that these are $T=0$ states. The isotopic spin selection rule should operate therefore to inhibit $E1$ transitions to any of the low-lying $T=0$ states. This explanation of the $E1$ inhibition has been suggested by Wilkinson[6] and used by him as the basis of a determination for the upper limit of 3 percent intensity of isotopic spin impurity in the 13.70-Mev state. The absence of $E1$ radiation by any of the other states lying just above the proton capture threshold in Ne^{20} is explained by the absence of lower levels in Ne^{20} with the proper spin and parity.

Some evidence for the existence of an effect on $E1$ transitions arising from the collective motion of neutrons and protons can be drawn from the existence of the giant resonances in photoemission cross sections[19–25] which occur at 15–25 Mev excitation of the product nucleus. These resonances have been interpreted by Goldhaber and Teller[26] as due to the relative vibration of two interpenetrating spheres containing separately the neutrons and protons. Levinger and Bethe[27] have shown, however, that many of the results of Goldhaber and Teller follow directly from the sum rules. The principal success of Goldhaber and Teller's model is that of predicting nearly correctly the position in energy of the maximum in the photoemission cross sections as a function of atomic number. Whether a model not embodying the concept of collective motion of the neutrons and protons can also predict this dependence remains to be seen.

The conclusion from this discussion of the $E1$ transitions is that at moderate energies (~15 Mev) there is slight evidence for some inhibition of $E1$ transitions in light nuclei,[5] but that this inhibition is not nearly so pronounced as one thought previously. It is not even certain that this remaining apparent diminution of $E1$ matrix elements is not due to overestimates inherent in the approximate nature of the Weisskopf[15] formulas.

EXPERIMENTAL RESULTS ON ISOTOPIC SPIN SELECTION RULES

The experimental investigation of the selection rules undertaken by Wilkinson[5–7] began with the determination of a semi-empirical method for predicting uninhibited (by isotopic spin selection rules) $E1$ radiation widths. This formula was then used to check for the allowed γ rays expected in nuclei belonging to isobaric triads in which the selection rule should operate. Finding these allowed γ rays Wilkinson and collaborators then proceeded to examine the $E1$ transitions in $T_<=0$ nuclei between states of the same isotopic spin T. Transitions which were inhibited so strongly that they could not be observed provided upper limits on isotopic spin impurity. Transitions which were observed with greatly reduced radiative widths provided lower limits on isotopic spin impurity. These limits are given in Table I.

As is evident from the necessarily tentative analysis of the experiments, considerable doubt should be attached to the exact values of the impurity and, in some cases, to the order of magnitude. Perhaps the most reliable value is that for N^{14} where the forbidden

TABLE I. Experimental estimates of isotopic spin impurity.

Nucleus	Level	Energy (Mev)	Limits on isotopic spin impurity
B^{10}	(2−)	5.11	$<3\times10^{-2}$
N^{14}	$1^-\rightarrow0^+$	8.06 → 2.31	$<2\times10^{-2}$
O^{16}	$1^-\rightarrow0^+$	7.116 → ground	$>4\times10^{-6}$
	$2^+\rightarrow3^-$	6.913 → 6.137	$<10^{-3}$
	$1^-\rightarrow0^+$	12.09 → ground	$>3\times10^{-2}$
Ne^{20}	$2^-\rightarrow2^+$	13.70 → 1.63	$<3\times10^{-2}$

[17] F. Ajzenberg and T. Lauritsen, Revs. Modern Phys. **24**, 321 (1954).
[18] The second article of reference 6 contains a brief discussion of the experimental data on the relevant levels of Ne^{20}.
[19] W. Bothe and W. Gentner, Z. Physik **112**, 45 (1939).
[20] G. C. Baldwin and G. S. Klaiber, Phys. Rev. **73**, 1156 (1948).
[21] J. L. Lawson and M. L. Perlman, Phys. Rev. **74**, 1190 (1948).
[22] M. L. Perlman and G. Friedlander, Phys. Rev. **74**, 442 (1948).
[23] J. McElhinney *et al.*, Phys. Rev. **75**, 542 (1948).
[24] K. Strauch, Phys. Rev. **81**, 973 (1951).
[25] Montalbetti, Katz, and Goldemberg, Phys. Rev. **91**, 659 (1953).
[26] M. Goldhaber and E. Teller, Phys. Rev. **74**, 1046 (1948).
[27] J. S. Levinger and H. Bethe, Phys. Rev. **78**, 115 (1950).

8.06 → 2.31-Mev $E1$ transition is compared with the allowed $E1$ transition to the ground state. The impurities obtained for the levels of O^{16} are obtained from the $E1$ and $E2$ branching ratio from a level. Among isomeric transitions, however, the $E2$ have been known for some time to be unusual because of their large matrix elements which equal or exceed the Weisskopf estimates. The $E1$ transitions, on the other hand, were found by Wilkinson to have transition probabilities only $\frac{1}{5}$ of those predicted by the Weisskopf formulas.[5] It is therefore quite possible that the upper limit of 10^{-3} quoted for isotopic spin impurity for the low-lying levels (~7 Mev) in O^{16} is too small.

All these experimental results are in agreement with the theoretical estimates of isotopic spin impurity introduced by Coulomb forces.[28,29] Indeed we shall show that the higher order corrections to the electric dipole selection rule are negligible compared to the effect of isotopic spin impurity. The experimental values given by Wilkinson must be interpreted therefore as the isotopic spin impurity.

HIGHER ORDER CORRECTIONS TO THE ISOTOPIC SPIN SELECTION RULES

The selection rules on isotopic spin changes for $E1$ transitions are based on the vanishing of the H_0 matrix element [Eqs. (2), (4)] in the lowest order approximation. There are three higher order effects to be considered: (1) neutron-proton mass difference, (2) lowest order electric dipole matrix element of the spin dependent part of H_0, and (3) higher order terms in the expressions for the electric dipole moment.

The first of these effects is easily dismissed by noting that the dipole moment of the nucleus involves $\sum_{k=1}^{A}\mathbf{r}_k$. Taking the center of mass as the origin,

$$m_p\sum_{k=1}^{s}\mathbf{r}_k+m_n\sum_{k=s+1}^{A}\mathbf{r}_k=(m_p-m_n)\sum_{k=1}^{s}\mathbf{r}_k+m_n\sum_{k=1}^{A}\mathbf{r}_k=0, \quad (7)$$

where m_p is the proton mass, m_n the neutron mass. Therefore,

$$\sum_{k=1}^{A}\mathbf{r}_k=\left(\frac{m_p-m_n}{m_n}\right)\sum_{k=1}^{s}\mathbf{r}_k, \quad (8)$$

so that the effect of the center of mass and the center of charge nearly coinciding is to reduce the single-particle transition probability by

$$\left(\frac{m_p-m_n}{m_n}\right)^2\approx 2\times 10^{-6}.$$

Since the isotopic spin impurity produces $E1$ widths which are at least 10^{-3} times the single-particle widths, the neutron-proton mass difference can be neglected in considering the violation of the isotopic spin selection rules.

In order to treat the corrections (2) and (3), we shall need expressions for the electromagnetic transition probabilities in terms of the exact multipole moments. The usual expressions for the transition probabilities are derived in the long-wavelength approximation $(kR)\ll 1$, where k is the propagation vector for the emitted photon and R is the nuclear radius. Higher order terms in (kR) will therefore enter the exact electric dipole matrix elements of H_0 and will produce transitions which violate the selection rules.

EXACT NONRELATIVISTIC MULTIPOLE TRANSITION PROBABILITIES

We shall derive the quantum mechanical transition probabilities for emission of electric and magnetic multipole radiation of all orders correct to all orders of (kR). We begin directly with the Schrödinger equation for a charged particle in an electromagnetic field so that our results can be compared directly with the usual formulas. The transition probabilities for the interaction of nucleons with an electromagnetic field as given by Eq. (1) then can be written down immediately if desired. To first order in the vector potential $\mathbf{A}$, the interaction Hamiltonian for a charged particle in a radiation field is

$$H_I=-(e/mc)(\mathbf{A}\cdot\mathbf{p})-\mu\boldsymbol{\sigma}\cdot(\nabla\times\mathbf{A}), \quad (9)$$

where $\mathbf{A}$ satisfies the gauge condition $\nabla\cdot\mathbf{A}=0$. The transition probability per unit time for emission of radiation is given by

$$T_{a\to b}=(2\pi/\hbar)|H_{ab}|^2\rho(E), \quad (10)$$

where a and b are indices denoting the initial and final states, φ_a and φ_b, respectively of the nucleus and $\rho(E)$ is the density of final states per unit energy. H_{ab} is not the matrix element of H_I but of the part of H_I arising from the positive frequency component of $\mathbf{A}$, i.e., from $\mathbf{A}(\mathbf{r})$ defined in

$$\mathbf{A}=\mathbf{A}(\mathbf{r})e^{-i\omega t}+\mathbf{A}^*(\mathbf{r})e^{i\omega t}. \quad (11)$$

The vector potential is now expanded into a series by use of the vector spherical harmonics $Y_{JL1}{}^M(\vartheta,\varphi)$ which are eigenfunctions of the angular momentum operator L^2, J^2, and J_z, where

$$\mathbf{L}=(\hbar/i)\mathbf{r}\times\nabla \quad \mathbf{J}=\mathbf{L}+\mathbf{S} \quad \mathbf{S}=i\hbar\mathbf{e}_k\times, \quad (12)$$

and $\mathbf{e}_k$ is a unit vector along the x_k axis. For representing the Maxwell fields it is well known that one can use $X_{JM}(\vartheta,\varphi)=Y_{JJ1}{}^M$ and $\nabla\times\mathbf{X}_{JM}$ to expand $\mathbf{A}(\mathbf{r},t)$. The part of A represented by terms in X_{JM} provides a magnetic field of parity $(-1)^J$ and is called the electric multipole field $\mathbf{A}_E(\mathbf{r},t)$. The sum of terms in $\mathbf{A}(\mathbf{r},t)$ which contain $\nabla\times\mathbf{X}_{JM}$ is called the magnetic

[28] L. A. Radicati, Proc. Phys. Soc. (London) A66, 139 (1953).
[29] W. M. MacDonald, Princeton thesis, 1954 (unpublished).

multipole field $\mathbf{A}_M(\mathbf{r},t)$ and has an associated magnetic field of parity $(-1)^{l+1}$.

We now normalize $\mathbf{A}_M(\mathbf{r},t)$ and $\mathbf{A}_E(\mathbf{r},t)$ to energy (hck) inside a sphere of radius a and volume V on the boundary of which A vanishes. The resulting expressions for the vector potentials for the electric and magnetic multipole fields are

$$\mathbf{A}_E(l,m)=i\left(\frac{\hbar ck}{a}\right)^{\frac{1}{2}}\frac{\mathbf{L}}{[l(l+1)\hbar^2]^{\frac{1}{2}}}j_l(kr)Y_{lm}(\vartheta,\varphi), \quad (13)$$

$$\mathbf{A}_M(l,m)=\frac{1}{k}\left(\frac{\hbar ck}{a}\right)^{\frac{1}{2}}\frac{\nabla\times\mathbf{L}}{[l(l+1)\hbar^2]^{\frac{1}{2}}}j_l(kr)Y_{lm}(\vartheta,\varphi), \quad (14)$$

where

$$\begin{aligned}L^2\mathbf{A}_{E,M}(l,m)&=l(l+1)\hbar^2\mathbf{A}_{E,M}(l,m),\\ J^2\mathbf{A}_{E,M}(l,m)&=l(l+1)\hbar^2\mathbf{A}_{E,M}(l,m),\\ J_Z\mathbf{A}_{E,M}(l,m)&=mh\mathbf{A}_{E,M}(l,m).\end{aligned} \quad (15)$$

From the boundary condition that $\mathbf{A}(a)=0$ the density of final states per unit energy $\rho(E)$ follows immediately as

$$\rho(E)=a/(hc\pi). \quad (16)$$

The matrix element H_{ab} which appears in (10) can be written as

$$H_{ab}=-\frac{1}{c}\int\mathbf{J}_{ab}\cdot\mathbf{A}-\mu\int\varphi_a^*\boldsymbol{\sigma}\cdot(\nabla\times\mathbf{A})\varphi_b, \quad (17)$$

where

$$\mathbf{J}_{ab}=(e/2mc)[\varphi_a^*(\mathbf{p}\varphi_b)+(\mathbf{p}\varphi_a)^*\varphi_b]$$

is the quantum-mechanical transition current.

By combining Eqs. (14), (16), and (17), we find the magnetic multipole transition probability per unit time and per unit solid angle for the direction of the emitted photon to be

$$T_{ab}{}^M=\frac{2}{\hbar}\frac{k}{l(l+1)\hbar^2}\left|-\frac{i}{c}\int\mathbf{J}_{ab}\cdot\mathbf{L}j_lY_{lm}-i\mu\int\varphi_a^*\boldsymbol{\sigma}\cdot(\nabla\times\mathbf{L})j_lY_{lm}\varphi_b\right|^2. \quad (18)$$

Similarly, one finds for the electric transition probability per unit time and per unit solid angle:

$$T_{ab}{}^E=\frac{2}{\hbar}\frac{k}{l(l+1)\hbar^2}\left|-\frac{1}{kc}\int\mathbf{J}_{ab}\cdot(\nabla\times\mathbf{L})j_lY_{lm}-\mu k\int\varphi_a^*\boldsymbol{\sigma}\cdot\mathbf{L}j_lY_{lm}\varphi_b\right|^2. \quad (19)$$

We have transformed the second term of $T_{ab}{}^E$ by means of the relation $\nabla\times\mathbf{A}_E(l,m)=-ik\mathbf{A}_M(l,m)$. We now transform the integrals appearing in $T_{ab}{}^M$ and $T_{ab}{}^E$ by integration by parts and the operator identity

$$\nabla\times\mathbf{L}=i\left[\nabla\left(\frac{\partial}{\partial r}r\right)-\mathbf{r}\nabla^2\right].$$

Define the generalized multipole moments:

Magnetic.—

$$\mathfrak{M}_{lm}=-\frac{(2l+1)!!}{(l+1)k^l}2\mu\int j_l(kr)Y_{lm}(\vartheta,\varphi)\,\mathrm{div}(\varphi_a\mathbf{L}\varphi_b),$$

$$\mathfrak{M}_{lm}'=-\frac{(2l+1)!!}{(l+1)k^l}\mu\left\{\int\frac{\partial}{\partial r}rj_l(kr)Y_{lm}(\vartheta,\varphi)\,\mathrm{div}(\varphi_a^*\boldsymbol{\sigma}\varphi_b)-k^2\int j_l(kr)Y_{lm}(\vartheta,\varphi)(\varphi_a^*\boldsymbol{\sigma}\cdot\mathbf{r}\varphi_b)\right\}. \quad (20)$$

Electric.—

$$\mathfrak{Q}_{lm}=\frac{(2l+1)!!}{(l+1)k^l}\left\{e\int\left[\frac{\partial}{\partial r}rj_l(kr)Y_{lm}(\vartheta,\varphi)\right]\varphi_a^*\varphi_b+\frac{ik}{c}\int j_l(kr)Y_{lm}(\vartheta,\varphi)\mathbf{r}\cdot\mathbf{J}_{ab}\right\},$$

$$\mathfrak{Q}_{lm}'=\frac{(2l+1)!!}{(l+1)k^l}\left(-i\mu k\int j_l(kr)\times Y_{lm}(\vartheta,\varphi)\,\mathrm{div}(\varphi_a^*\mathbf{r}\times\boldsymbol{\sigma}\varphi_b)\right), \quad (21)$$

where $(2l+1)!!=(2l+1)(2l-1)\cdots2$, or 1. The transition probabilities per unit time (integrated over solid angle) are

$$T_{ab}{}^M=\frac{8\pi(l+1)}{l[(2l+1)!!]^2}\frac{k^{2l+1}}{\hbar}|\mathfrak{M}_{lm}+\mathfrak{M}_{lm}'|^2, \quad (22)$$

$$T_{ab}{}^E=\frac{8\pi(l+1)}{l[(2l+1)!!]^2}\frac{k^{2l+1}}{\hbar}|\mathfrak{Q}_{lm}+\mathfrak{Q}_{lm}'|^2. \quad (23)$$

The formulas are exact so far in that no assumption about the magnitude of (kR) has been made. If we make the "long-wavelength approximation" $kR\ll1$, we put $j_l(kr)\sim(kr)^l/(2l+1)!!$. Since $\nabla^2(r^lY_{lm})=0$, the multipole moments defined in (20) and (21) become

$$M_{lm}{}^{(0)}=-\frac{1}{l+1}2\mu\int r^lY_{lm}\,\mathrm{div}(\varphi_a^*\mathbf{L}\varphi_b),$$

$$M_{lm}{}^{(0)\prime}=-\mu\int r^lY_{lm}\,\mathrm{div}(\varphi_a^*\boldsymbol{\sigma}\varphi_b), \quad (24)$$

$$Q_{lm}{}^{(0)}=e\int r^lY_{lm}\varphi_a^*\varphi_b,$$

$$Q_{lm}{}^{(0)\prime}=\frac{-ik}{l+1}\mu\int r^lY_{lm}\,\mathrm{div}(\varphi_a^*\mathbf{r}\times\boldsymbol{\sigma}\varphi_b). \quad (25)$$

These are precisely the single-particle moments of Blatt and Weisskopf.

Although no derivation of the exact multipole moments for nonrelativistic quantum mechanics has been given, the exact multipole moments for the classical Maxwell field have been given by Wallace[30] and by French and Shimamoto.[31] Quite recently a derivation of the exact multipole moments for the Dirac equation has been given by Stech[32] using a treatment similar to the preceding development. Brennan and Sachs[33] also have discussed higher order corrections to the $E1$ matrix element from a different point of view, and have formally defined the exact multipole moments.

EFFECT OF ELECTRIC DIPOLE CORRECTIONS

Two types of higher order terms in H_0 exist to produce contributions to $E1$ radiation which therefore violate the selection rules in $T_\zeta=0$ nuclei. We estimate first the contribution of the spin-dependent part of H_0 to the $E1$ radiation. This contribution appears as $Q_{1m}{}^{(0)\prime}$ in (25) and is of course neglected in the Weisskopf formulas. We calculate $Q_{1m}{}^{(0)\prime}$ for H_0, noticing first by comparing (2) and (9) that we should use $\mu=\frac{1}{2}(\mu_p+\mu_n)$, $e/mc=e/2Mc$. In using $Q_{1m}{}^{(0)}$ and $Q_{1m}{}^{(0)\prime}$, we are of course using the extreme single-particle picture, but this approximation gives the proper orders of magnitude. To evaluate $Q_{1m}{}^{(0)}$ and $Q_{1m}{}^{(0)\prime}$, assume that ϕ_a and ϕ_b are constant over a sphere of radius R, the radius of the nucleus, and that Y_{lm} is of order unity. In $Q_{lm}{}^{(0)\prime}$ we also take σ of order unity and $\frac{1}{2}(\mu_p+\mu_n)\sim 0.5eh/2Mc$. The divergence in $Q_m{}^{(0)\prime}$ is approximated by $(1/R)$. We then obtain

$$|Q_{1m}{}^{(0)\prime}/Q_{1m}{}^{(0)}|^2\sim(1/25)(\hbar\omega/Mc^2)^2.$$

For gamma rays of $\sim$10 Mev, $|Q_{1m}{}^{(0)\prime}/Q_{1m}{}^{(0)}|^2\sim 4\times10^{-6}$. The contribution of the magnetic moment in H_0 to $E1$ transitions therefore provides a rate 4×10^{-6} times an uninhibited $E1$ matrix element. This is negligible compared to the effect of isotopic spin impurities.

The higher order term in $\mathfrak{Q}_{lm}{}'$ arising from the second term of $j_l(kr)$ can be found by using

$$j_l(kr)=\frac{(kr)^l}{(2l+1)!!}-\frac{(kr)^{l+2}}{(2l+3)!!2}.$$

The second term in an expansion of $\mathfrak{Q}_{lm}$,

$$\mathfrak{Q}_{lm}=Q_{lm}{}^{(0)}+Q_{lm}{}^{(1)}+\cdots,$$

found from successive terms in $j_l(kr)$, is

$$Q_{lm}{}^{(1)}=-\frac{(2l+1)!!}{(2l+3)!!}\frac{k^{l+2}}{2k^l}\left\{\int(l+3)r^{l+2}Y_{lm}\varphi_a{}^*\varphi_b \right.$$
$$\left.+\frac{ik}{c}\int r^{l+2}Y_{lm}\mathbf{r}\cdot\mathbf{J}_{ab}\right\},$$

or

$$Q_{1m}{}^{(1)}=-\frac{k^2}{5}\left\{4\int r^3Y_{1m}\varphi_a{}^*\varphi_b+\frac{ik}{c}\int r^3Y_{1m}\mathbf{r}\cdot\mathbf{J}_{ab}\right\}.$$

By the same approximations as before, we obtain the result:

$$|Q_{1m}{}^{(1)}/Q_{1m}{}^{(0)}|^2\sim(2/15)^2(kR)^4.$$

From $(kR)\approx\hbar\omega/137$, we find that for 10-Mev photons,

$$|Q_{1m}{}^{(1)}/Q_{1m}{}^{(0)}|^2\sim10^{-6}.$$

We can conclude that all the higher order terms in H_0 give rise to Γ_λ widths for $E1$ emission which are of order 10^{-6} times the uninhibited widths. The Γ_λ widths produced by isotopic spin impurities are proportional to the impurity p and are at least 10^{-3} times a "normal" $E1$ width.[28,29]

I am indebted to Professor E. P. Wigner for suggesting this topic and for stimulating conversations during the investigation.

[30] P. R. Wallace, Can. J. Phys. **29**, 393 (1951).
[31] J. B. French and Y. Shimamoto, Phys. Rev. **91**, 898 (1953).
[32] B. Stech, Z. Naturforsch. **A7**, 401 (1952).
[33] J. G. Brennan and R. G. Sachs, Phys. Rev. **88**, 824 (1952).

Radioactivity of Co^{57}

BERND CRASEMANN AND D. L. MANLEY*
Department of Physics, University of Oregon, Eugene, Oregon
(Received December 24, 1954)

Co^{57}(270-day) has been prepared by the reactions $Mn^{55}(\alpha,2n)$ and $Ni^{58}(p,2p)$, separated chemically, and its disintegration studied with a magnetic lens and a scintillation spectrometer. Co^{57} decays by electron capture; an upper limit of 2×10^{-5} positron per disintegration has been set. Positron groups previously assigned to Co^{57} presumably belong to one of the neighboring isotopes of cobalt. Gamma rays of 0.137 and 0.123 Mev have a relative abundance of 7 and 93 percent, and presumably are $E2$ and $M1$ transitions, respectively. A decay scheme is outlined.

I. INTRODUCTION

COBALT-57 (270-day) was first reported by Livingood and Seaborg,[1] who measured a positron energy of 0.26 Mev by absorption. Plesset[2] found highly converted gamma rays of 0.130 and 0.117 Mev in the decay of this isotope. The energy of these gamma rays was found to be 0.131 and 0.119 Mev by Elliot and Deutsch[3] and 0.138 and 0.123 Mev by Alburger and Grace,[4] who also measured their conversion coefficients. Deutsch and Wright[5] reported a 0.014-Mev excited state, of half-life 1.1×10^{-7} sec, of the Fe^{57} daughter of Co^{57}. Cheng, Dick, and Kurbatov[6] assigned a 0.320-Mev positron transition to the disintegration of Co^{57}.

In order to establish a decay scheme for Co^{57}, it seemed desirable to re-examine the positron spectrum of this isotope and to search for possible branching. For this reason, the present work was undertaken.

II. APPARATUS

The thick magnetic lens beta-ray spectrometer used in the present work is of the Siegbahn type[7] and has a resolution of 3.1 percent. A helical baffle of aluminum allows transmission of only positrons or only electrons, depending on the direction of the current in the magnet coils. By this device, a positron spectrum can be studied without interference from conversion electrons. The magnet current is electronically controlled to one part in 10 000. The current regulator, designed by K. D. Jenkins of the University of California, consists of a comparison network, dc chopper, push-pull ac amplifier with a gain of 200 000, and a full-wave power phase detector whose output is directly applied to the field of a dc generator. The magnet current is measured by determining the voltage drop across a 0.01 ohm standard resistor with a Leeds and Northrup 7552 potentiometer.

The detector consisted, for some runs, of a laboratory made Geiger tube with a 0.67 mg/cm² window of DuPont Mylar, and for the remaining runs, of a Victoreen 1B67 tube with a 2.1-mg/cm² mica window. In the latter case, corrections for window absorption were applied to the data. The correction factors were taken from the curves of Saxon,[8] which had been supplemented with experimental points derived from a Fermi plot of the electron spectrum of S^{35}.

The spectrometer was calibrated by means of the 0.6242-Mev conversion electrons[9] from Cs^{137} and the 0.0620-Mev conversion line[10] from Cd^{109}. Hysteresis effects, amounting to 7.3 gauss-cm, were taken into account.

III. PREPARATION OF SOURCES

Two methods were used for preparing Co^{57}. "Sample I" was obtained in the following manner: Manganese, electrolytically deposited on a copper probe, was bombarded with approximately 100 μa-hr of 32-Mev alpha particles in the University of California's Crocker Laboratory cyclotron, in order to produce Co^{57} by the reaction $Mn^{55}(\alpha,2n)$. The manganese layer was dissolved in 8N HCl containing Co carrier, and Ga and Fe were extracted with β,β'-dichlorodiethylether. The solution was boiled to dryness, the residue redissolved in water and made slightly acidic in HCl. The cobalt was precipitated with hot α-nitroso-β-naphthol in 50 percent acetic acid. The precipitate was washed, and the organic molecule destroyed by boiling with a mixture of nitric and perchloric acids. The precipitation and destruction of cobalti-nitroso-β-naphthol was repeated. The cobaltous perchlorate was finally dissolved in a small quantity of water and the solution evaporated onto 20–30 μg/cm² Tygon films held by Lucite sleeves, for mounting in the spectrometer. Through two independent chemical separations, three spectrometer sources were prepared from sample I, ranging in thickness from 50 to 300 μg/cm².

"Sample II" consisted of 1 millicurie of Co^{57} obtained from the Radioisotopes Sales Department of the Oak Ridge National Laboratory. It had been produced by

* Present address: Department of Radiological Physics, University of Rochester, Rochester, New York.
[1] J. J. Livingood and G. T. Seaborg, Phys. Rev. **60**, 913 (1941).
[2] E. H. Plesset, Phys. Rev. **62**, 181 (1942).
[3] L. G. Elliot and M. Deutsch, Phys. Rev. **64**, 321 (1943).
[4] D. E. Alburger and M. A. Grace, Proc. Phys. Soc. (London) **A67**, 280 (1954).
[5] M. Deutsch and W. E. Wright, Phys. Rev. **77**, 139 (1950).
[6] Cheng, Dick, and Kurbatov, Phys. Rev. **88**, 887 (1952).
[7] K. Siegbahn, Phil. Mag. **37**, 163 (1946).
[8] D. Saxon, Phys. Rev. **81**, 639 (1951).
[9] Muller, Hoyt, Klein, and DuMond, Phys. Rev. **88**, 775 (1952).
[10] Cork, Rutledge, Stoddard, Branyan, and LeBlanc, Phys. Rev. **79**, 938 (1950).

the bombardment of nickel with 22-Mev protons. Spectrometer sources of varying strengths were prepared from this sample in the same manner as described above.

IV. GAMMA-RAY SPECTRUM

The gamma rays of Co^{57} were studied by investigating the distribution of internal conversion electrons, using the spectrometer baffle to discriminate against positrons. A detail of the conversion electron spectrum is reproduced in Fig. 1. It yields energies of 0.137 ± 0.002 Mev, for γ_1, and 0.123 ± 0.002 Mev, for γ_2. These energy values agree, within the limits of error, with the values determined by Alburger and Grace.[4] The energy of γ_3, reported by Deutsch and Wright[5] as 0.014 Mev, was not redetermined directly. A survey with a scintillation spectrometer revealed no other gamma rays in the range from 0.05 to 0.6 Mev.

The areas under the conversion electron peaks were planimetered on a plot of N/η *vs* i. The ratio of the number of conversion electrons of γ_2 to that of γ_1 was thus found to be 1.0 ± 0.2. This corresponds to a value of 13 ± 5 for the intensity branching ratio $I(\gamma_2)/I(\gamma_1)$, computed with Alburger and Grace's values[4] for the conversion coefficients.

V. POSITRONS

The positron spectrum of the cobalt samples was measured in the magnetic lens spectrometer, with conversion electrons eliminated by the helical baffle. Figure 2 shows a Fermi plot of the data from sample I. Admixtures of Co^{56} and Co^{58}, from the $Mn^{55}(\alpha,3n)$ and $Mn^{55}(\alpha,n)$ reactions, produce components with end points of 1.50 and 0.47 Mev, respectively, that have been previously reported by other investigators.[11] A positron component with maximum energy of 0.312 ± 0.020 Mev is presumably identical with a 0.320-Mev group observed by the Ohio State workers.[6] The

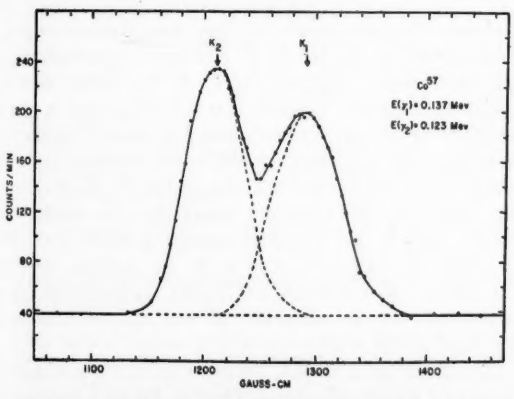

FIG. 1. Internal conversion electron spectrum of Co^{57}.

[11] Way, Fano, Scott, and Thew, *Nuclear Data*, National Bureau of Standards Circular 499 (U. S. Government Printing Office, Washington, D. C., 1950) and supplements.

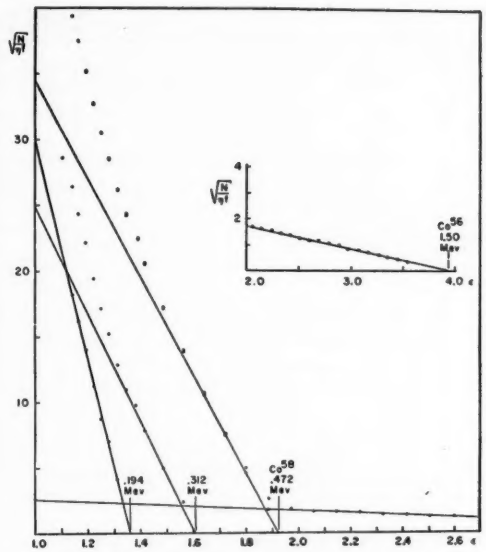

FIG. 2. Fermi plot of the positron spectrum from cobalt isotopes in sample I.

existence of a low-energy group, of 0.194-Mev maximum energy, cannot be considered certain, due to the compounding of errors by multiple subtractions in the Fermi plot, the magnitude of the window correction at low energies, and the possibility of source thickness effects. The 0.312- and 0.194-Mev positron groups were tentatively assigned to Co^{57},[12] following previous work in the literature, but this assignment was proved erroneous by further investigation with sample II, which contained only traces of Co^{56} and Co^{58}. Figure 3 shows the gamma-ray spectrum of Co^{57} from sample II, obtained with a scintillation spectrometer. No annihilation peak is observed. In the magnetic lens spectrometer, no positron group of end-point energy below 0.4 Mev could be found from sample II. Through the use of two sources varying in strength by a factor of 8, an upper limit of 6×10^{-4} positrons of less than 0.4 Mev maximum energy per Co^{57} conversion electron could be set, which corresponds to an upper limit of, approximately, 2×10^{-5} positron per disintegration. If the 0.312-Mev positron transition occurred in the decay of Co^{57}, a ratio of electron capture to positron emission of about 2.2×10^{2} would be expected from theory.[13] It must be concluded, therefore, that the 0.312-Mev positrons and a possible low-energy group belong to one of the neighboring isotopes of cobalt. Work towards their assignment is now in progress in this laboratory.†

[12] The printed abstract of a paper by B. Crasemann and D. L. Manley at the Berkeley Meeting of the American Physical Society, December, 1954 [Bull. Am. Phys. Soc. **27**, No. 8, 31 (1954)] makes use of this assignment. The paper actually read was based on the later results.

[13] E. Feenberg and G. Trigg, Revs. Modern Phys. **22**, 399 (1950).

† *Note added in proof.*—The absence of positrons in the decay of Co^{57} has also recently been observed at The Clarendon Labora-

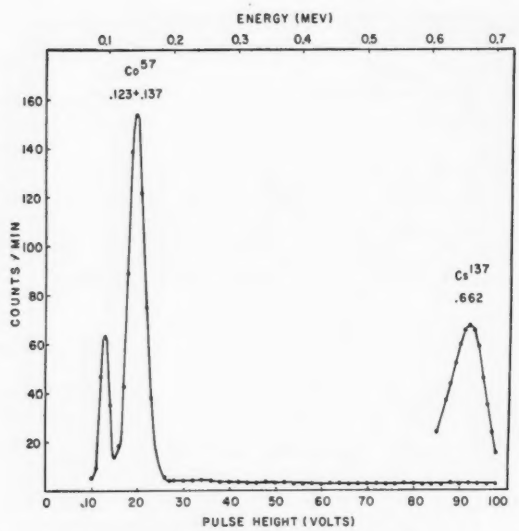

FIG. 3. Gamma spectrum of Co^{57}, sample II. No annihilation peak is observed.

VI. DISCUSSION

The shell model predicts the ground-state proton configuration $(f_{7/2})^7$ for Co^{57}.[14] The spin of this isotope has been measured to be 7/2 by the method of paramagnetic resonance, and its magnetic moment has been determined as 4.6,[15] which is consistent with the shell assignment.[16]

The ground state of Fe^{57}, according to the shell model, should be $p_{\frac{1}{2}}$. This is born out by the angular distribution[17] of the protons from the Fe(d,p) reactions which show that the ground-state group corresponds to the transfer of one unit of orbital angular momentum, so that the ground state of Fe^{57} must have a spin of 1/2 or 3/2 and odd parity. The 0.137-Mev level of Fe^{57} has been reached by Coulomb excitation[18] with 3-Mev alpha particles, with a cross section indicating that this state is most probably reached by an electric quadrupole transition.

The 0.137- and 0.123-Mev gamma transitions in Fe^{57}, linking the second excited state with the 0.014-Mev level and the ground state, respectively, have been identified as either $E2$ and $M1$ or $M2$ and $E1$ by Alburger and Grace[4] on the basis of their determination of the conversion coefficients. The results of reference 18 show that the first of these choices is correct, as indicated in Fig. 4.

The first excited state of Fe^{57}, at 0.014 Mev, has a half-life of 1.1×10^{-7} sec, measured by Deutsch and Wright.[5] On this basis, Goldhaber and Sunyar[19] identified the 0.014 Mev transition as magnetic dipole. It follows that the first excited state of Fe^{57} must have the same (odd) parity as the ground state.

The decay scheme shown in Fig. 4 contains two sets of spin assignments for Fe^{57}. While the 3/2–5/2–7/2 set is more likely on the basis of shell-model considerations, the 1/2–3/2–5/2 possibility cannot be excluded with the experimental evidence now available.

VII. ACKNOWLEDGMENTS

The authors wish to express their sincere appreciation to Professor E. G. Ebbighausen, for turning over his spectrometer to them, and to Professor A. C. Helmholz, of the University of California, for obtaining the cyclotron bombardment of the manganese target. Professor Helmholz, Dr. D. E. Alburger, of Brookhaven National Laboratory, and Dr. C. L. McGinnis, of the National Research Council, have kindly read a preliminary report on this work and contributed valuable comments and criticism, for which the authors wish to thank them. Thanks are also due to Dr. H. G. Richter, for advice on the chemical separation of cobalt, to H. D. Osborn, for technical assistance with the construction of equipment, and to K. D. Jenkins, of the University of California's Crocker Laboratory, for advice on the construction of the magnet current regulator of his design.

One of the authors (B.C.) is indebted to the Graduate School of the University of Oregon for two Research Grants that made this work possible.

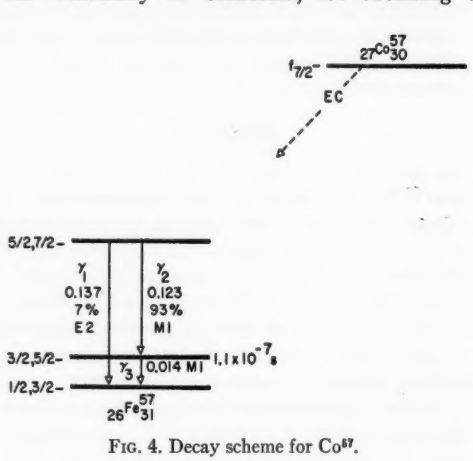

FIG. 4. Decay scheme for Co^{57}.

tory, Oxford, by M. A. Grace, H. R. Lemmer, and O. J. A. Segaert, who obtained an upper limit of 1/1500 positron per disintegration. (Private communication by M. A. Grace.)

[14] P. F. A. Klinkenberg, Revs. Modern Phys. **24**, 63 (1952).

[15] Baker, Bleaney, Bowers, Shaw, and Trenam, Proc. Phys. Soc. (London) **A66**, 305 (1953).

[16] The authors are indebted to Dr. C. L. McGinnis of the National Research Council, Nuclear Data Group, for calling their attention to this work and to that mentioned in the following paragraph.

[17] C. F. Black, Phys. Rev. **90**, 381(A) (1953).

[18] N. P. Heydenburg and G. M. Temmer, Phys. Rev. **95**, 629(A) (1954); Phys. Rev. **93**, 351 (1954), and Phys. Rev. **96**, 426 (1954).

[19] M. Goldhaber and A. W. Sunyar, Phys. Rev. **83**, 906 (1951).

Photodisintegration of the Deuteron

Y. YAMAGUCHI AND Y. YAMAGUCHI
Department of Physics, University of Illinois, Urbana, Illinois
(Received November 26, 1954)

The electric dipole cross section for $\gamma(d,p)n$ is examined, assuming no forces in ^3P states. The nonvanishing D-state probability P_D of deuteron gives rise to the isotropic part a_e in angular distribution of the photoproton: $d\sigma/d\omega = a_e + b_e \sin^2\theta$. It turns out, however, that the resulting value for a_e is still small to explain the experimental cross section, even if P_D is as large as 8 percent.

THE photodisintegration of the deuteron at high energies has now been observed extensively.[1] One of the most striking features has been the large isotropic component in the cross section at high-photon energies. Theoretical calculations to date have been unable to explain the magnitude of this component which is experimentally rather insensitive to the photon energy over a considerable energy range (20–160 Mev). There are at least three separate areas in which the previous theoretical work may have been deficient:

(a) The D-wave in the deuteron function, important because $^3D \rightarrow {}^3P$ transition gives an isotropic part (see reference 2, cited hereafter as II).

(b) The very singular forces acting in the final neutron-proton system, presumably in the ^3P-states as discussed by Austern.[3]

(c) The interaction or mesonic effects.[4]

About (b) we have nothing to say. In a forthcoming paper we shall discuss (c) but since machinery for discussing (a) has already been developed,[2] we wish to present now some special results on this point. If we adopt the deuteron function proposed in II,

$$\frac{(\text{const})}{\alpha^2+p^2}\left\{\frac{1}{\beta^2+p^2}-\frac{1}{\sqrt{8}}\left[(\sigma_p\mathbf{p})(\sigma_n\mathbf{p})\frac{3}{p^2}-(\sigma_p\sigma_n)\right]\frac{tp^2}{(\gamma^2+p^2)^2}\right\},$$

TABLE I. Three sets of parameters, β, γ, and t are given below.[a]

β/α	6.255	5.759	5.337
γ/α	···	6.771	9.175
t	0	1.748	6.013
D-state probability in %	0	4.000	8.000
Quadrupole moment in 10^{-27} cm	0	2.74	2.72
Triplet n-p scattering length in 10^{-13} cm	5.378	5.378	5.378
Triplet n-p effective range in 10^{-13} cm	1.716	1.704	1.697
Shape dependent factor	−0.0242	1.82×10^{-5}	0.0146

[a] For details, see reference 2.

[1] Schriever, Whalin, and Hanson, Phys. Rev. **94**, 763(A), (1954); T. Yamagata *et al.*, Phys. Rev. **95**, 574 (1954); L. Allen and A. O. Hanson, Phys. Rev. **95**, 629(A), (1954); E. A. Whalin, Phys. Rev. **95**, 1362 (1954). Other references will be found in II.
[2] Y. Yamaguchi and Y. Yamaguchi, Phys. Rev. **95**, 1635 (1954).
[3] N. Austern, Phys. Rev. **85**, 283 (1952).
[4] N. Austern, and R. G. Sachs, Phys. Rev. **81**, 710 (1951); A. Sugie and S. Yoshida, Progr. Theoret. Phys. (Japan) **10**, 236 (1953).

α^2/M = binding energy of the deuteron. As was described in II, it is possible to choose parameters β, γ, and t so as to fit the D-state probability and the quadrupole moment of the deuteron, as well as the effective range in ^3S n-p scattering. Best fit values are listed in Table I. If we assume no forces in ^3P-states, the Siegert theorem tells us that the electric dipole cross section can be evaluated completely from our deuteron function. The

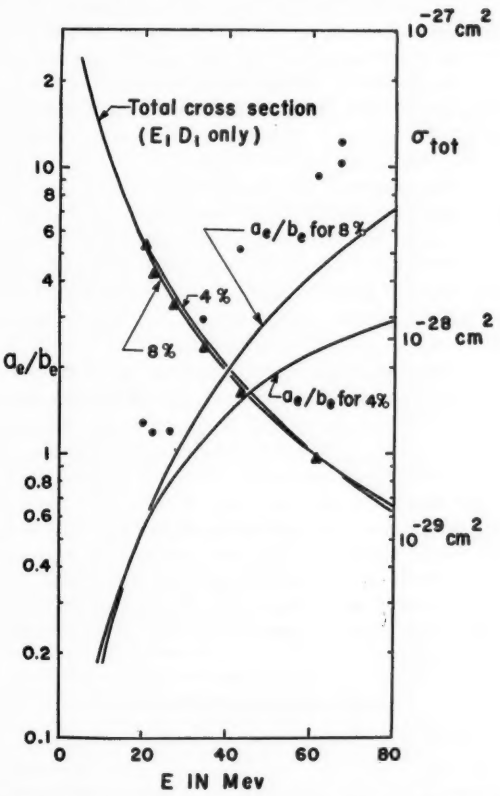

FIG. 1. The electric dipole cross section for $d(\gamma,p)n$ takes the form

$$d\sigma/d\omega = a_e + b_e \sin^2\theta, \quad \sigma_{\text{tot}} = 4\pi(a_e + \tfrac{2}{3}b_e).$$

Calculated values σ_{tot} and a_e/b_e are illustrated in this figure, choosing two different values (8 percent and 4 percent) for the D-state probability of the deuteron. Experimental results are shown by ▲: total cross section, and ●: a/b (see reference 2). E = available energy in c.m. system = (photon energy ν) + (kinetic energy of the deuteron $\nu^2/4M$).

results are shown in Fig. 1 and do not drastically depend upon the change of the D-state probability P_D. In other words, the isotropic part of the cross section is still insufficient even if P_D were as large as 8 percent. Thus we may conclude that the possibility (a) is not satisfactory by itself.

PHYSICAL REVIEW VOLUME 98, NUMBER 1 APRIL 1, 1955

Reaction D$(t,\alpha)n$ at 1.5 Mev*†

A. HEMMENDINGER AND H. V. ARGO
University of California, Los Alamos Scientific Laboratory, Los Alamos, New Mexico
(Received December 6, 1954)

The differential cross section for the reaction D$(t,\alpha)n$ has been measured at 10° intervals from 10° to 140° in the laboratory system for a triton energy of 1.5 Mev. The total cross section is 280±8 mb.

INTRODUCTION

THE D-T reaction has been used so extensively as a source of monoergic neutrons[1] that the knowledge of precise values of differential cross sections has become a practical problem. For this reason and also because of general theoretical interest in the reaction constants of light elements a study of the reaction was undertaken at this laboratory, the results of which, at one energy, are here reported.

A beam of 2-Mev HT^+ ions from the new Los Alamos 2.5-megavolt electrostatic accelerator traversed a deuterium-filled scattering chamber. The HT^+ beam was more suitable than T^+ because the relatively great admixture of HHH^+ ions in the ion beam would have melted the entrance foil at much lower triton currents. The obvious problems associated with the acceleration of tritons and collection of tritium at the forevacuum will be discussed elsewhere and it need only be stated that it is a routine operation to accelerate tritons in this machine. There are distinct advantages in accelerating the triton rather than the deuteron: The target gas is not so costly that it cannot be discarded when it becomes contaminated; if a beam window into the target breaks, the gas lost need not be recovered; the inside of the chamber does not become so radioactive as to make it hazardous to handle; and small leaks of target gas into a counter do not produce counter background.

EXPERIMENTAL PROCEDURE

The scattering chamber, 14 inches in diameter and 4 inches high, was provided with two proportional counters for the observation of the alpha particles from D(t,α); one was fixed at −15° and the other could be rotated about the chamber center. Details of the chamber appear elsewhere,[2] but the geometry used in this experiment is shown schematically in Fig. 1.

Entrance Window

The ion beam entered the scattering chamber through a thin Pyrex foil. The thickness of this foil was measured by removing the exit foil, inserting in the Faraday cage a thick Zr-T target, and measuring the threshold voltage for the reaction T(p,n). Deuterium gas at a pressure of 0.5 mm Hg was kept in the chamber to cool the entrance window and the energy loss in the gas was computed. The thickness t measured in this way is the energy loss of a proton which has an energy of 1.019 Mev after traversing the foil; usual values were between 8 and 30 kev. The entrance foil was thin enough that only a few percent of the beam was lost due to scattering. The glass foil appears to be uniquely suitable for this experiment[3]; counting rates would have been prohibitively small with any of the usual metal foils.

The energy loss for 1.5-Mev tritons in the entrance foil was found by assuming Pyrex (Corning No. 774) to have an energy loss nearly the same as Al and

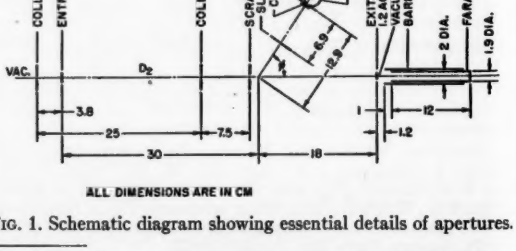

FIG. 1. Schematic diagram showing essential details of apertures.

* Work performed under the auspices of the U. S. Atomic Energy Commission.
† A preliminary report on this work was given by H. V. Argo and A. Hemmendinger, Phys. Rev. **96**, 851 (1954).
[1] Hanson, Taschek, and Williams, Revs. Modern Phys. **21**, 635 (1949).
[2] M. E. Ennis and A. Hemmendinger, Phys. Rev. **95**, 772 (1954).
[3] Some notes on the preparation and use of these foils will appear in the Review of Scientific Instruments.

referring to the stopping power curves of Allison and Warshaw.[4] From these data we find that the value of dE/dx for 0.5-Mev protons is 240 kev cm^2 mg^{-1} and for 1-Mev protons it is 183 kev cm^2 mg^{-1}. Inasmuch as the value of dE/dx is the same for 0.5-Mev protons and 1.5-Mev tritons, we find the window thickness for tritons to be $240t/183$. Even if the assumption concerning the similarity of Pyrex and Al is off by 50 percent, the error in the ratio will not be excessive. The triton beam energy was adjusted to exceed 1.5 Mev by the sum of the losses in the entrance window and deuterium path to the chamber center.

Exit Window

With a beam of 2-Mev HT^+ ions incident on the entrance foil, there emerged from this foil 0.5-Mev H^+ and 1.5-Mev T^+ ions. The H^+ beam had a greater divergence due to multiple scattering. Collimation of this beam by the second defining aperture increased the T^+ to H^+ ratio, so the only way to measure the T^+ ion current in a Faraday cage was first to stop all of the H^+. This separation was accomplished by using an exit window of 0.35-mil Al.

Faraday Cage

The Faraday cage was isolated from space electron currents by a cylindrical barrier electrode surrounding the cage and overhanging for 1 cm at the front end. The barrier electrode potential was -300 volts. The cage remained close to ground potential. At first some of the triton current fell on the barrier, but the solid angle subtended by the cage was increased until the current to the barrier vanished. Furthermore, we used the method outlined by Dickinson and Dodder[5] for evaluation of particle loss due to multiple scattering in foils to compute the error in current collection. We found the rms scattering angle to be 3.5°. Assuming that the beam is uniformly distributed over the exit foil, the particle loss is 0.08 percent. Actually the beam is concentrated near the center of this foil so the particle loss will be even smaller.

Proportional Counters

The angular distribution of the alpha particles was measured at 10° intervals from 10° to 140° for a fixed number of alpha counts in the monitor. In the relative distribution this eliminated errors due to changes in target pressure, temperature, composition, and current integrator calibration. Although the alpha pulses in the monitor were much larger than those due to scattering, counting rates due to scattering were so high as to cause pileup. For this reason the monitor counter window was made of 0.65-mil Al, which was thick enough to stop all of the scattered particles. There were similar effects in the movable counter at small angles, but the solid angle subtended by the movable counter was smaller than that subtended by the monitor, and with a window of 0.25-mil Al, alpha counts were well resolved from scattered particle counts for angles up to 40°. For angles greater than 40° the window was 0.05-mil Ni, except at the largest angle of 140°; here the alpha counting rate was less than that due to neutron recoils. This situation was improved by using a glass counter window about half as thick as the 0.05-mil Ni, and this foil could have been used for all angles greater than 30°. At every angle the background, measured by moving a magnetic shutter over the counter slit, was subtracted from the observed alpha count.

Both counter fillings were argon at 40-cm pressure. Counter geometry was the same as described earlier,[2] but a redetermination was made of some of the constants, particularly A, the area of the counter hole.

Pressure Measurement

The target gas pressure was indicated by a manometer made of 0.5-inch i.d. tubing filled with Octoil-S. A density determination gave the value $0.9103[1-(t-25)0.000659]$ g cm^{-3}, where t is the centigrade temperature. The oil was partially outgassed by vacuum boiling in the manometer, but outgassing never stopped and continual pumping on the vacuum side was required.

Composition of Gas

The target gas, taken from a Stuart Oxygen Company bottle and marked 99.4 percent deuterium, was checked mass-spectrometrically and found to contain 0.38 percent hydrogen and essentially no other contaminants.

Sources of Error

The dimensions of the collimator and of the counter assembly, indicated in Fig. 1, determine an angular spread of $\pm 2°$ for each measurement. Since the angular distribution does not have a large second derivative, the error due to poor angular resolution is insignificant.

Upper limits for the errors, systematic and otherwise, in the several measurements required to determine a cross section are estimated as follows:

Current integral	0.3 percent
Pressure	0.1 percent
Counter slit and hole geometry	1.0 percent
Composition of gas	0.1 percent.

To these errors, which amount to 1.5 percent or less, we must add errors due to counting, which for most points do not exceed 1 percent; the extreme statistical error is 2.2 percent at 130°. Allowing for possible

[4] S. K. Allison and S. D. Warshaw, Revs. Modern Phys. 25, 779 (1953).
[5] W. C. Dickinson and D. C. Dodder, Rev. Sci. Instr. 24, 428 (1953).

TABLE I. The values of D(t,α) differential cross section in both lab and c.m. systems. The column ϵ is the percent statistical probable error.

Lab system		C.m. system		P.E.
ϕ deg	$\sigma(\phi)$ mb/sterad	θ deg	$\sigma(\theta)$ mb/sterad	ϵ %
10	50.28	14.415	24.4	0.5
20	48.12	28.716	24.1	0.9
30	45.83	42.801	24.2	0.7
40	42.18	56.547	24.0	0.7
50	37.84	69.834	23.7	0.7
60	32.80	82.568	23.1	1.2
70	28.22	94.634	22.8	1.0
80	23.22	105.877	21.9	1.0
90	19.36	116.302	21.6	1.0
100	15.43	125.874	20.5	1.1
110	12.50	134.607	19.8	1.5
120	10.24	142.566	19.2	1.6
130	8.60	149.844	18.8	2.2
140	7.60	156.549	19.0	1.8

unknown errors, we arrive at 3 percent as a maximum probable error for the differential cross section.

RESULTS

A relative angular distribution was determined by making runs at various angles, always for 10^4 counts in the monitor. Frequently the pulses from the monitor counter were displayed on the 18-channel pulse-height analyzer to determine where to set the bias on the monitor scaler, the important point being that the bias was always set at a readily identified minimum in the distribution. Pulses from the movable counter were recorded on the 18-channel analyzer. After subtraction of the background due to neutron recoils the alphas always fell in a well resolved peak.

The determination of an absolute cross-section scale was accomplished by measurements of chamber temperature and pressure, and of the current integral for 10^4 monitor counts. The cross section at the angle ϕ is

$$\sigma(\phi)=Y\sin\phi/(NnG),$$

where Y is the number of α counts per microcoulomb, $N=6.242\times10^{12}$ tritons per microcoulomb, n=the volume density of deuterons, and $G(=4.082\times10^{-5}$ cm) is the usual geometry factor.[1] In terms of measured quantities,

$$\sigma(\phi)=0.20331(10)^{-27}TP^{-1}C^{-1}Y\sin\phi \text{ cm}^2/\text{sterad},$$

where T is the absolute temperature, C is the concentration of deuterium in the target gas, and P is the pressure in mm of Hg.

The results, both in the laboratory and center-of-mass systems, are presented in Table I. The value of Q used for the c.m. transformation is 17.577 Mev. The table contains also a column for ϵ, the percent probable error due only to statistics. The total cross section is

$$\sigma=2\pi\int_0^\pi\sigma(\theta)\sin\theta d\theta.$$

Figure 2 shows how the data of Table I are plotted and extrapolated to 0 and 180°. Integration by Simpson's rule gives $\sigma=280\pm8$ mb.

There is a measurement of the d-T total cross section for $15<E_T<160$ kev,[6] one in the range $30<E_T<210$ kev,[7] another for $75<E_T<1200$ kev,[8] and a measurement of the 90° differential cross section

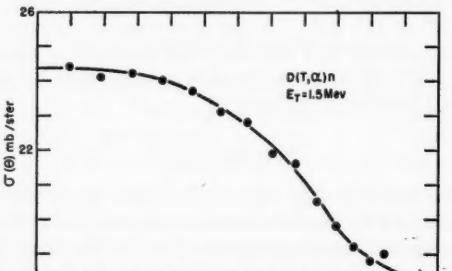

FIG. 2. Differential cross section extrapolated to 0 and 180°. Note that the scale of ordinates has a suppressed zero.

(made on the neutron yield) for $200<E_T<1450$ kev,[7] all of which measurements are mutually compatible. There is also a differential cross section measurement at 3.31 Mev[9] done by essentially the same technique (except that the deuteron was accelerated) as the present experiment. The total cross-section curve[8] is very flat at $E_T=1.2$ Mev, and extrapolation to 1.5 Mev gives good agreement with the present 280-mb measurement.

[6] Arnold, Phillips, Sawyer, Stovall, and Tuck, Phys. Rev. 93, 483 (1954).
[7] Conner, Bonner, and Smith, Phys. Rev. 88, 468 (1952).
[8] Argo, Taschek, Agnew, Hemmendinger, and Leland, Phys. Rev. 87, 612 (1952).
[9] T. F. Stratton and G. D. Freier, Phys. Rev. 88, 261 (1952).

Absolute Cross Section for the Reaction $C^{12}(\gamma,n)C^{11}$†

W. C. Barber, W. D. George, and D. D. Reagan
High-Energy Physics Laboratory, Stanford University, Stanford, California
(Received December 13, 1954)

The activation curve for the reaction $C^{12}(\gamma,n)C^{11}$ was obtained with the use of both the Mark II (38-Mev) and Mark III (630-Mev) linear accelerators, covering the energy range 18–260 Mev. Stacked foils of polystyrene detectors and tantalum and copper radiators were exposed to the direct electron beam and the resulting C^{11} activity was measured with a 4π scintillation counter. The photon flux was obtained from the measured electron flux by means of the Bethe-Heitler theory of bremsstrahlung, and the photon-difference method was applied to obtain the cross-section curve. This curve was found to be similar to some previous results, but with the addition of a high-energy tail extending beyond 38 Mev. The experimental accuracy does not permit a precise determination of the shape of this tail, but it cannot be accounted for by mesonic effects alone. The cross section has a peak value of about 8.3 millibarns at 22.5 Mev, and integrated values of 0.056 ± 0.003 and about 0.080 ± 0.01 Mev-barns when the integrals are carried up to 38 and 250 Mev, respectively. These numerical values were obtained from the data obtained by using a copper radiator. The corresponding results with a tantalum radiator are about 7 percent lower, indicating a possible failure of the bremsstrahlung formula for high atomic numbers.

INTRODUCTION

THE energy dependence of the x-radiation yield for the $C^{12}(\gamma,n)C^{11}$ reaction has been investigated extensively by using radiation from internal targets in circular machines.[1–7] A linear machine, while giving a relatively broad electron energy spectrum, makes it simple to use a Faraday-cup electron collector to measure the bombardment-flux directly. Two such monitors have been constructed and tested, and have been used in conjunction with a residual-activity technique to evaluate the yield of $C^{12}(\gamma,n)C^{11}$ over the energy range from threshold to 260 Mev. Previous results relied upon the calibration of ionization chambers.

The experimental method was basically the same as that described by Berman and Brown.[8] Pairs of closely matched polystyrene foils were used as detectors, while a tantalum or copper radiator foil placed between the detector foils produced the bremsstrahlung photons. The stack of foils was thin so that all of the electrons passed through them into the Faraday cup. Also, the area of the foils was large enough to intercept all of the bremsstrahlung produced by the electrons. The use of two detector foils enables one to correct for the undesired background reactions induced by electrons, neutrons, and gamma radiation. The corrected net difference in the reaction yield between the two foils is then due to the bremsstrahlung production in the effective radiator.

The Bethe-Heitler theory,[9] including screening effects, was used to calculate the number of photons in each quantum-energy interval. The degradation of the electrons and photons in passing through a thick target was calculated and corrected for by the method of Wilson.[10]

EXPERIMENTAL

The Mark II (38-Mev) and Mark III (630-Mev) accelerators were the sources of electrons. The Faraday-cup electron collector used in conjunction with Mark II has been described in a previous paper.[8] It has an absolute accuracy better than 2 percent. An evaluation of the performance of the high-energy Faraday cup has been made by Tautfest.[11] The absolute accuracy is better than $\frac{1}{2}$ percent. In each case the Faraday cup was used with an electronic integrating system which accumulated the total charge on a condenser having high leakage resistance. The voltage on the condenser was measured with a potentiometer. The capacity was determined with an accuracy of $\frac{1}{2}$ percent by feeding a known current into the system for a definite time and then measuring the voltage in the usual way. To compensate for the radioactivity lost during the bombardment, resistances were placed across the integrating capacitors to give an RC value close to the mean life of C^{11}. (The decay of the activity in the polystyrene was observed to be exponential over a period of 78 minutes, with a half-life of 20.26 ± 0.1 minutes. This is in agreement with other recent determinations of the half-life of the C^{11} decay.) These resistances varied slightly with time and temperature; hence the time constant was measured periodically, and small corrections were made to each value of the integrated voltage from the electron collector. There

† The research reported here was supported by the joint program of the Office of Naval Research and the U. S. Atomic Energy Commission.

[1] L. Katz and A. G. W. Cameron, Can. J. Phys. **29**, 518 (1951).
[2] L. W. Jones and K. M. Terwilliger, Phys. Rev. **91**, 699 (1953).
[3] R. Sagane, Phys. Rev. **84**, 587 (1951).
[4] Montalbetti, Katz, and Goldemberg, Phys. Rev. **91**, 659(1953).
[5] R. Nathans and J. Halpern, Phys. Rev. **93**, 437 (1954).
[6] K. Strauch, Phys. Rev. **81**, 973 (1951).
[7] L. Marshall, Phys. Rev. **83**, 345 (1951).
[8] A. I. Berman and K. L. Brown, Phys. Rev. **96**, 83 (1954).
[9] H. A. Bethe and W. Heitler, Proc. Roy. Soc. (London) **A146**, 83 (1934).
[10] R. Wilson, Proc. Phys. Soc. (London) **A66**, 638 (1953).
[11] G. Tautfest (private communication).

was no *RC* network available on the high-energy electron collector, so the values of the integrated voltage were read periodically during the bombardment and the correction for decay was calculated.

The presence of the foils and a vacuum-tight window in front of the mouth of the Faraday cup introduced an error due to secondary electrons being knocked out of the foils into the cup. The effect of the foil stack was determined experimentally by employing an ionization chamber in the beam ahead of the foils as a monitor. The test showed that the foil stack increased the Faraday-cup current by a constant amount of (1.5±0.2) percent over the energy range 18–38 Mev. The effect of the vacuum window was calculated to increase the current by an additional constant amount of (2.0±1.0) percent.

A 4π scintillation counter using two anthracene crystals[8] measured the positron activity from C^{11}. The counter background was approximately 80 counts per minute at the operating discriminator setting.

It was necessary to know the electron energy, and thereby the maximum photon energy incident on the foils. This was accomplished by an energy calibration done on the Mark II deflecting-magnet system, which has a relative accuracy of 0.2 percent and an absolute accuracy of 2 percent.[8] The Mark III calibration employed a floating-wire method with an absolute accuracy of ½ percent.[11]

ACTIVATION CURVES

The yield, as a function of the maximum electron energy E_0, is given by

$$Y(E_0)=N_C\left(N_{eff}\cdot\frac{Z+1}{Z}\right)\int_0^{E_0}\phi(E_0,k,t)\sigma(k)dk, \quad (1)$$

where $Y(E_0)$ is the number of radioactive atoms produced per electron; N_C is the number of C^{12} atoms per cm²; N_{eff} is the number of atoms per cm² in the effective radiator; $(Z+1)/Z$ is an approximate correction for the radiation produced in the field of the atomic electrons; $\phi(E_0,k,t)$ is the thick-target bremsstrahlung cross section (except for the region near the end point, the thick-target formula was accurate to ½ percent as used in this experiment); $\sigma(k)$ is the reaction cross section; and k is the photon energy.

This yield was obtained from the observed activity in the foils after the data were corrected. The raw data were first corrected for: (a) any residual activity; (b) dead time of the 4π counter; (c) background; (d) C^{11} decay; (e) difference in thickness of the two detector foils; and (f) variations in the effective radiator thickness (the tantalum radiator plus the mean thickness of the front foil was 2.855×10^{-2} radiation length). The net difference activity of each individual run was then corrected for: (a) multiple scattering of the electrons in passing through the foils, thus giving more activity in the rear foil (½ percent); (b) the fact that the electron-induced activity is not the same in the two foils due to electron-energy degradation in the effective radiator (2.8±1.3 percent); (c) the setting of the discriminator of the 4π counter. A curve of discriminator setting *vs* counting rate was made in order to extrapolate to zero discriminator setting (4.5±1.0 percent); (d) the self-absorption of the C^{11} beta rays in the foil. For the absolute result, thin (8×10^{-3} g/cm²) polystyrene foils were used (6.0±2.5 percent).

The yield was investigated in some detail in the region from 18 to 38 Mev using the Mark II accelerator. Data were taken at 1- and 2-Mev intervals for both tantalum and copper radiators. The two radiators gave similarly shaped activation curves, but the absolute values at the high-energy limit were not consistent with the *Z*-dependence of the bremsstrahlung formula, corrected for screening.[12] The tantalum result was 7 percent lower than copper, indicating a possible failure of the formula for high-*Z* elements.[13]

From the reproducibility of the results at a given energy, the relative accuracy of the points was calculated to be ½ percent. Figure 1 shows the corrected yield curves from these Mark II data, using the tantalum radiator of 169.77 mg/cm².

The points taken on the Mark III accelerator covering the range 35–260 Mev, were taken at different times, some with the same tantalum radiator as was used in obtaining the data of Fig. 1, and some with a 0.1-radiation-length copper radiator. Those taken with the copper radiator were marked with a subscript *C*, and have been arbitrarily normalized to fit the tantalum points. There were few runs on Mark III using both tantalum and copper radiators at the same energy and conditions. This corrected activation curve is shown in Fig. 2. The density of points and their statistical

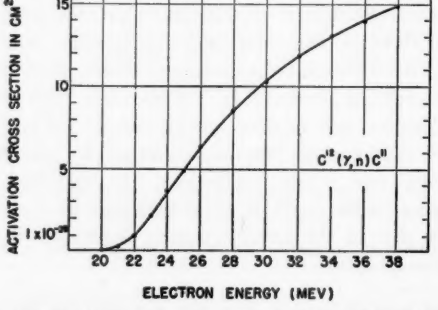

FIG. 1. Yield curve for the reaction $C^{12}(\gamma,n)C^{11}$. The data shown as dots were taken with a tantalum radiator of 169.77 mg/cm². However, the yield as expressed by Eq. (1) has been divided by N_C and by the thickness of the radiator in radiation lengths so that the ordinate scale represents the cross section for the reaction induced by the bremsstrahlung of one electron in a unit radiator.

[12] Further experiments to measure the *Z*-dependence of bremsstrahlung are in progress in this laboratory.
[13] C. D. Curtiss, Phys. Rev. 89, 123 (1953).

accuracy were limited by the running time available on the large accelerator, and by the difficulty of getting high beam intensities in the low-energy region.

CROSS SECTION AS A FUNCTION OF PHOTON ENERGY

The cross-section curve in Fig. 3 was obtained from the corrected activation curve of Fig. 1 by the photon-difference method.[1] The photon spectrum was calculated for the tantalum radiator, but the absolute value of the cross section was everywhere increased by 7 percent to give agreement with the results obtained with the copper radiator. The copper result is thought to be more accurate because errors due to the Born approximation used in deriving the bremsstrahlung formula are expected to be proportional to Z^2. The oscillations characteristic of the photon-difference method are quite evident by 38 Mev, and application of the method to still higher energies would require an activation curve of considerably greater accuracy than we have achieved. This cross-section curve is similar to those of previous experimenters in many respects. It has the usual sharply-peaked resonance; this one centered at 22.5 Mev with a peak of 8.3 millibarns, but with the addition of a high-energy tail extending at least to 38 Mev.

In order to get information about the shape of the cross-section curve above 38 Mev, different high-energy tails were fitted to the curve of Fig. 3 and the corresponding activation curves were computed by numerical integration of Eq. (1). The results are shown in Fig. 2. Referring to this figure: (1) Circled E is the contribution that comes from the cross-section curve of Fig. 3 cut off at 36 Mev. It is far outside of experimental error, proving that a considerable part of the cross-section curve is beyond 36 Mev. (2) Circled A is the same as E, but with a symmetrical bump added to the cross-section curve, centered at 50 Mev, and of

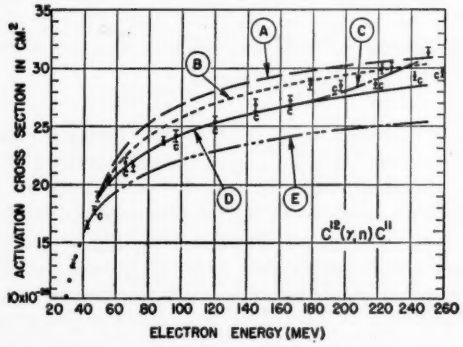

FIG. 2. Yield curve for the reaction $C^{12}(\gamma,n)C^{11}$ extended to high energies. Absolute points taken with the tantalum radiator are shown as plain dots, while the points labeled with a subscript C, taken with a thick copper radiator, have been arbitrarily normalized. The ordinate scale is the same as for Fig. 1. The curves A to E are computed yield curves assuming various cross-section curves described in the text.

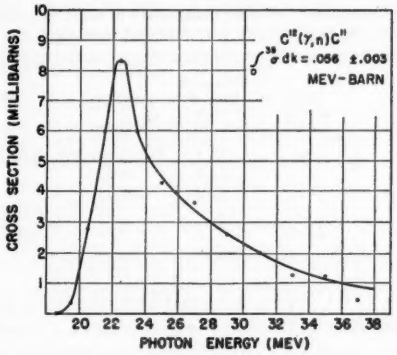

FIG. 3. Cross-section curve for the reaction $C^{12}(\gamma,n)C^{11}$. The shape of the curve was determined by the photon-difference analysis of the yield curve of Fig. 1, but the absolute value of the ordinate scale was determined from the data with a copper radiator. The smooth curve shown is consistent with the data, but because of the insensitivity of the method the detailed shape of the high-energy portion is uncertain.

base-width 12 Mev. The shape of the bump was chosen arbitrarily, but the magnitude gives the correct contribution to the yield at 250 Mev. The curve A is definitely too high in the region from 60 to 200 Mev, indicating that the cross section is finite at energies beyond 56 Mev. (3) B is the contribution from Fig. 3 with a tail inversely proportional to the cube of the photon energy beginning at 44 Mev with a value of 1.27 millibarns. A flat portion closes the gap between 34 and 44 Mev. (4) D is the contribution from Fig. 3 with the addition of a k^{-3} tail fitted at 34 Mev, again with the value of 1.27 millibarns. B and D enclose most of the experimental points between them and any cross-section curve of gross shape between those assumed in deriving B and D would be compatible with the data. (5) C contains a contribution, additional to D, of a possible meson rise in the cross section. The rise was calculated from particle kinematics and experimental data on the production of π^0-mesons from low-Z elements. The calculation is expected to be correct only to an order of magnitude because it is not known how often the production of a π-meson is accompanied by the emission of only a single neutron. For this reason, the production of C^{11} by other processes such as $(\gamma,\pi^- p)$ was not included in the calculation.

The result for the expected activation cross section can be expressed as

$$\frac{Y'(E_0)}{N_C\cdot(t/t_0)}=2.2\times10^{-28}\frac{\int_{150}^{E_0}(k_{eff}^2-\pi^2)^{\frac{1}{2}}(dk/k)}{\int_{150}^{320}(k_{eff}^2-\pi^2)^{\frac{1}{2}}(dk/k)}\text{cm}^2, \quad (2)$$

where (t/t_0) is the thickness of the radiator in radiation lengths, and $k_{eff}^2=k^2[1-(2k/M)+(M_\pi^2/Mk)]$. The plotted values, curve C, are three times those obtained

TABLE I. Comparison of some parameters of the $C^{12}(\gamma,n)C^{11}$ cross section as determined by different investigators.

Reference	Mean energy (Mev)	Energy at peak of cross section (Mev)	$\int_0^{\sim 25}\sigma(k)dk$ (Mev-barns)	$\int_0^{>50}\sigma(k)dk$ (Mev-barns)
This paper	34	22.5	0.032±0.003	0.080±0.01
4	...	21.3	0.029	...
5	...	22.0	0.027	...
6	27	...	...	0.090±0.022
7	23–32	...	...	0.086±0.02

from Eq. (2). Curve C is a good fit to the data, but this fact alone does not prove the existence of a meson rise. The data would rule out a meson rise greater than ten times the increase calculated by Eq. (2).

Gell-Mann *et al.*[14] derive the sum-rule result in a general form which makes no restrictive assumptions as to multipolarity of the transitions or the nature of nuclear forces and wave functions. By making use of experimental data on photomeson production, they obtain

$$\int_0^{M_\pi}\sigma_T(k)dk = \frac{2\pi^2e^2\hbar}{Mc}\frac{NZ}{A}\left(1.0+0.1\frac{A^2}{NZ}\right)\text{ Mev-barns} \quad (3)$$

for the integral up to the meson threshold. In Eq. (3), $\sigma_T(k)$ is the total cross section for gamma absorption, and the constant 0.1 on the right-hand side is evaluated from experimental data with a stated accuracy of about 30 percent.

From the present experiment the value of the integrated cross section to 38 Mev was found to be 0.056±0.003 Mev-barns. The value up to 250 Mev depends on the shape of the high-energy tail and is therefore more uncertain. Using cross sections proportional to k^{-3} fitted at energies 34 and 44 Mev corresponding with yield curves D and B, respectively, one finds integrated cross sections to 250 Mev of 0.073 and 0.091 Mev-barns. The value predicted by Eq. (3) for C^{12} is 0.25±0.03 Mev-barns, and therefore the totality of other reactions must contribute about twice as much as the (γ,n) reaction alone. This is not improbable because the (γ,p) and (γ,pn) reactions are likely comparable with the (γ,n) while a host of less probable reactions, such as (γ,α), (γ,γ), and $(\gamma,2n)$, are each expected to make some contribution.

A comparison of the results of this paper with those of some other investigators is shown in Table I. The comparison reveals how some of the large discrepancies in the reported values of the integrated cross section are accounted for by the existence of the tail on the cross-section curve. This relative prominence of the tail is not a general feature of the (γ,n) reactions. For example, Berman and Brown,[8] using basically the same technique as described herein, found no contribution to the cross section beyond 30 Mev in the case of Cu^{63}. However, Sagane[3] has pointed out the existence of a high-energy tail in the case of (γ,n) reactions on C^{12} and O^{16}, and its occurrence may be relatively common in reactions on the light elements.

ACKNOWLEDGMENT

The authors wish to express their appreciation to those who helped in the completion of this experiment; especially A. Berman, K. Brown, and G. Tautfest, for their help with the instrumentation, and to Professor W. K. H. Panofsky for his advice and encouragement.

[14] Gell-Mann, Goldberger, and Thirring, Phys. Rev. **95**, 1612 (1954).

Correction to the Exponential Dependence of Neutron Transmissions*

R. G. THOMAS
University of California, Los Alamos Scientific Laboratory, Los Alamos, New Mexico
(Received December 3, 1954)

If the energy spread of the neutron source used in a transmission type of measurement of total neutron cross sections is large compared with the mean spacing of the resonance levels of the sample, these levels may effect a deviation from the simple exponential dependence on sample thickness. The correction to this dependence is derived in the case where capture, inelastic scattering, and Doppler broadening may be neglected. The derivation does not depend upon any special assumption regarding the distributions of the widths and spacings of the levels other than that they have suitable averages, and the correction is found to be proportional to the ratio of these averages, as one would expect. It is noted that by measurement of this ratio for certain elements, it may be possible to distinguish between the predictions of the strong-coupling and complex square-well representations of the neutron-nucleus interaction.

IF the energy spread of the neutron source used in a transmission type of measurement of total neutron cross sections[1] is large compared with the mean spacing D of the resonance levels of the sample, these levels will effect a deviation from the simple exponential dependence on sample thickness t.[2] Thus, the transmission

$$T=\int f(E)\exp[-\sigma(E)Nt]dE, \tag{1}$$

where the normalized function $f(E)$ represents the source spectrum in terms of the neutron energy E, will deviate from $\bar{T}=\exp(-\bar{\sigma}Nt)$, where $\bar{\sigma}=\int f(E)\sigma(E)dE$ is the average of the total cross section $\sigma(E)$, by a factor such as $(1+\alpha)$:

$$T=\bar{T}(1+\alpha); \tag{2}$$

$\alpha=\alpha(T)$ and N is the atomic density. This correction may be large at low energies where elastic scattering is the dominant process, the cross section of which varies from 0 to $4\pi\lambda^2$ through resonances and thus may depart considerably from the average.

At low energies where only the s-wave interaction is effective and in the case of a monoisotopic sample of zero spin, the total cross section may be expressed in terms of a single collision function $U(E)$ according to[3]

$$\sigma(E)=\pi\lambda^2[2-U(E)-U(E)^*]. \tag{3}$$

The correction term $\alpha(T)$ may be expressed theoretically in terms of the average $\bar{U}$ of $U(E)$ by substitution of (3) into (1) and evaluation of the averages of the individual terms arising in a power series expansion of the exponential. It is assumed that the neutron energies are low enough so that inelastic scattering and reactions do not occur and high enough so that capture is negligible, in which case $|U(E)|=1$. It is also assumed that

$$\int f(E)U(E)^n=\bar{U}^n \tag{4}$$

for positive integers n. It has been shown that $\bar{U}$ is obtained by substitution of the Stieltjes transform of the strength function $s(E_\lambda)=\langle\gamma_{\lambda n}^2\rangle_{Av}/D$ for the R function in the theoretical expression for $U(E)$.[3] Equation (4) constitutes a generalization of Eq. (43) of reference 3, and the arguments given in connection with the latter equation may also be used to justify (4). It is also convenient to use the expansion $a^n+b^n=\sum_q C_q{}^n \times(a+b)^{n-2q}(ab)^q$, in which the q sum extends from 0 to $\frac{1}{2}n$ if n is even and to $\frac{1}{2}(n-1)$ if n is odd, with the coefficients $C_q{}^n=(-1)^q n(n-q-1)!/q!(n-2q)!$. The result is that

$$\alpha(T)=Qc^2\exp(-c\bar{F})\times\sum_{n=2}^{\infty}\xi_n, \tag{5}$$

where

$$c=\pi\lambda^2Nt,\quad Q=1-|\bar{U}|^2,$$

$$\bar{F}=\bar{U}+\bar{U}^*=2-(\bar{\sigma}/\pi\lambda^2),$$

$$\xi_n=\frac{c^{n-2}}{n!}\Big[\sum_{r=1}\binom{n}{r}P_r(Q)\times\sum_{q=0}C_q{}^{n-2r}\bar{F}^{n-2(r+q)}(1-Q)^q$$

$$+\binom{n}{\frac{1}{2}n}P_{\frac{1}{2}n}(Q)\cdot\frac{1+(-1)^n}{2}\Big],$$

$$P_r(Q)=r+\sum_{t=1}^{r-1}(-1)^t\binom{r}{t+1}Q^t.$$

The upper limit of the r sum of ξ_n is $\frac{1}{2}n-1$ if n is even and $\frac{1}{2}(n-1)$ if n is odd, and that of the q sum is $\frac{1}{2}(n-2r)$ if n is even and $\frac{1}{2}(n-2r-1)$ if n is odd. The quantity $Q(\leq 1)$ is significant as the cross section for compound nucleus formation divided by $\pi\lambda^2$; if the average of the neutron widths $\Gamma_{\lambda n}$ is small compared with D, Q is equal to $2\pi\langle\Gamma_{\lambda n}\rangle_{Av}/D$. Since the first term $\xi_2=1$, it is evident that $\alpha(T)$ is proportional to t^2, to Q, and inversely to E, for small values of t, as one would expect.

* Work performed under auspices of the U. S. Atomic Energy Commission.

[1] H. H. Barschall, Am. J. Phys. **18**, 535 (1950).
[2] Darden, Okazaki, and Becker, Bull. Am. Phys. Soc. **30**, No. 1 (1955).
[3] R. G. Thomas, Phys. Rev. **97**, 224 (1955).

In general there will be contributions $\sigma_i(E)$ to $\sigma(E)$ from various partial waves, channel spin states, and isotopes of atomic densities N_i, so that $T=\int f(E)\prod_i \times\exp[-\sigma_i(E)N_i]dE$ where $\sigma_i(E)=\pi\lambda^2\omega_i[2-U_i(E) -U_i(E)^*]$, ω_i being the statistical factor for the ith interaction. Since the resonance levels associated with the various interactions i are presumably uncorrelated, it is reasonable to assume that[4] $T=\prod_i T_i$, where $T_i=\int f(E)\exp[-\sigma_i(E)N_i]dE$, in which case $T =\bar{T}(1+\alpha)$, where $\bar{T}=\prod_i \bar{T}_i$ and $1+\alpha=\prod_i(1+\alpha_i)$. In view of the proportionality for small i, of α_i to $N_i^2\omega_i^2$ and α to $\sum_i\alpha_i$, $\alpha(T)$ will be smaller the larger the number of participating isotopes and spin states.

The effect of capture and inelastic scattering, which was not considered in the derivation, is to broaden the resonances and to reduce their effective maxima, thus diminishing the α_i. In fact at high energies where the total level widths are much larger than the spacings, the $U_i(E)$ and their associated $\sigma_i(E)$ are essentially constant. The α_i will also be reduced by the Doppler effect. For this effect to be negligible it is necessary that the $\Gamma_{\lambda n}$ be much greater than the Doppler width $\Delta=2(EkT/A)^{\frac{1}{2}}$ of the sample element of mass number A.

The complex square well (c.s.w.) has been found to provide an accurate representation of certain aspects of the neutron-nuclei interactions at low energies.[5] The Stieltjes transform of the strength function corresponding to this model is simply the reciprocal of the product of the nuclear radius with the logarithmic derivative at the radius of the radial part of the c.s.w. wave function.[3] A prediction of this model is that the strength $s(E_\lambda)$ of the s-wave resonances, and hence the Q_i, are considerably larger at the "giant resonances" of the c.s.w. than the strong-coupling theory (s.c.t.) value and considerably smaller between these resonances.[3,5] With a 42-Mev well depth, the c.s.w. resonances for s neutrons are predicted to appear at atomic weights 11, 55, and 150.[5] Indeed, by surveying individual resonance levels of elements with $A>100$, some indication of the predicted maxima of $s(E_\lambda)$ is found in the neighborhood of $A=160$.[6] It would be desirable to verify this indication by the alternative procedure of determining the Q_i, and thus $s(E_\lambda)$, from the measurement of α for these elements. Unfortunately, as also indicated by the survey, $\Gamma_{\lambda n}\lesssim\Delta$ for the elements in this neighborhood, and therefore the α_i would be subject to an appreciable Doppler reduction unless the sample were cooled to extremely low temperatures. However, in the vicinity of the predicted giant s resonance at $A=55$, the individual resonance level spacings are much larger,[7] indicating that $\Gamma_{\lambda n}\gg\Delta$. With a 42-Mev well depth and $\zeta=0.03$ as the imaginary-part parameter, it is predicted that for (monoisotopic) Mn, $\alpha(\frac{1}{4})=0.27$ [compared with $\alpha(\frac{3}{4})=0.012$], which may be distinguishable from the predictions of the s.c.t. of $\alpha(\frac{1}{4})=0.22$ [compared with $\alpha(\frac{3}{4})=0.014$]. Bismuth, being magic, may have a level spacing considerably larger than that of the normal isotopes of the heavy elements,[8] and it is therefore likely that $\Gamma_{\lambda n}\gg\Delta$. It would be of interest to determine its Q by a transmission measurement because Bi falls between the s resonances of the c.s.w. and is therefore predicted to have a small Q and associated α: $\alpha(\frac{1}{4})=0.019$ [compared with $\alpha(\frac{3}{4})=4\times10^{-4}$]; while the correction predicted by the s.c.t. is relatively larger: $\alpha(\frac{1}{4})=0.085$ [compared with $\alpha(\frac{3}{4})=2\times10^{-3}$].

The possible existence of the resonance transmission correction was suggested by H. H. Barschall; the writer is also grateful to him for valuable suggestions and discussions on this subject.

[4] We have not succeeded in proving this assumption, and therefore the results may not be entirely correct.

[5] Feshbach, Porter, and Weisskopf, Phys. Rev. **96**, 448 (1954).

[6] Carter, Harvey, Hughes, and Pilcher, Phys. Rev. **96**, 113 (1954).

[7] *Neutron Cross Sections*, Atomic Energy Commission Report AECU-2040 (Technical Information Division, Department of Commerce, Washington, D. C. 1952), and supplements thereto.

[8] Hughes, Garth, and Levin, Phys. Rev. **91**, 1423 (1953); J. H. Gibbons and Henry W. Newson, Phys. Rev. **91**, 209(A) (1953).

Radiations of Mo^{90} and the Isomeric States of Nb^{90}†

HIRDAYA B. MATHUR‡ AND EARL K. HYDE
Radiation Laboratory and Department of Chemistry, University of California, Berkeley, California
(Received October 15, 1954; revised manuscript received December 14, 1954)

Gamma-gamma coincidence measurements of the radiations of 5.7-hour Mo^{90} showed that the 120- and 250-kev gamma rays previously reported by Diamond were delayed. Further experiments showed the existence of a 24-second isomer of Nb^{90} emitting 120-kev gamma rays and a 10 to 20 millisecond isomer emitting 250-kev gamma rays. The transition types were not assigned unambiguously but the 24-second isomer is probably $E2$ and the 10 to 20 millisecond isomer $E3$ or $M3$ in nature.

The radiations of the 14.6-hour ground state of Nb^{90} were also studied. The 140-kev and 1.14-Mev gamma rays are in coincidence with each other and with annihilation radiation. A prominent 2.2-Mev gamma ray is not in coincidence with annihilation radiation or x-rays. Hence, it must be a delayed transition with $\Delta I \geq 3$. This is of interest because of the rarity of such transitions in even-even nuclei.

I. INTRODUCTION

THIS paper deals with a study of the radiations of Mo^{90} and of the niobium isomers Nb^{90}, Nb^{90m_1}, and Nb^{90m_2} formed in its decay. Molybdenum-90 has been studied previously by Diamond[1] who prepared it by proton bombardment of niobium in the Harvard cyclotron. Diamond reported Mo^{90} to be a positron emitter with a half-life of 5.7±0.2 hours. The mass assignment was made by identification of the 14.6-hour Nb^{90} daughter. He reported positrons of maximum energy of 1.4 Mev and gamma rays with energies of 1.0, 0.24 to 0.26, and 0.1 to 0.13 Mev.

At Diamond's suggestion we extended the study of Mo^{90} and also carried out a detailed study of the gamma rays of 14.6-hour Nb^{90} previously reported by Boyd.[2] During the course of our work we found evidence for nuclear isomerism in Nb^{90} and also in the even-even isotope Zr^{90}.

II. MOLYBDENUM-90

In our experiments with Mo^{90} produced by the bombardment of Nb^{93} with 80-Mev protons in the 184-inch cyclotron, we found Mo^{90} to have positrons of maximum energy 1.15±0.1 Mev. Figure 1 shows the positron end point as determined by an anthracene crystal spectrometer.

Figure 2 shows the gamma spectrum of Mo^{90} as determined by a sodium iodide crystal-photomultiplier assembly coupled to a 50-channel differential-pulse analyzer. There are two gamma rays of 120- and 250-kev energy in addition to the annihilation radiation. The small peak at 65 kev is due to the platinum x-rays produced by the platinum backing on which the sample was mounted. Correcting for counting efficiency according to the values given by Kahn and Lyon[3] the abundance of the two gamma rays was about equal. We were not able to detect the presence of 1-Mev gamma rays in a freshly prepared sample of Mo^{90} although a gamma ray of 1.14 Mev did appear later as Mo^{90} decayed to Nb^{90}.

Conversion electrons of the 120- and 250-kev gamma rays were measured by a magnetic double-focusing spectrometer. Figure 3 shows the spectrum thus obtained. The K/L conversion ratios of 120- and 250-kev gamma rays were determined to be 3.6±0.2 and 5.2 ±0.2, respectively. We are indebted to Dr. T. O. Passell for substantial help in these measurements.

With the help of Dr. F. Asaro and Mr. F. S. Stephens we carried out gamma-gamma coincidence studies and found that 120- and 250-kev gamma rays were not in coincidence with each other, with 510-kev annihilation radiation, or with 16.5-kev x-radiation.

III. 24-SECOND ISOMER, Nb^{90m_1}

The gamma-gamma coincidence studies suggested the existence of isomeric states of Nb^{90} in addition to the ground state of Nb^{90}, the 14.6-hour activity previously studied by Boyd,[2,4] Kundu and Pool,[5] and Jacobson

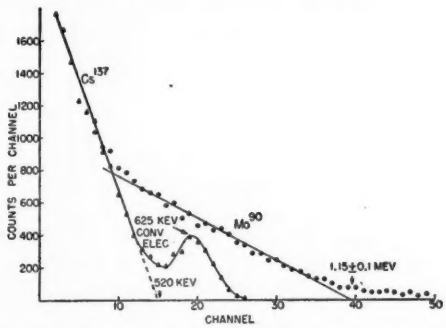

FIG. 1. Positron end point of Mo^{90} as determined on an anthracene crystal spectrometer. Cs^{137} was used as a standard. The data were taken on a 50-channel pulse-height analyzer.

† This research was performed under the auspices of the U. S. Atomic Energy Commission.

‡ On leave of absence, Department of Chemistry, University of Delhi, Delhi, India. Present address: Institute for Nuclear Studies, University of Chicago, Chicago 37, Illinois.

[1] R. M. Diamond, Phys. Rev. 89, 1149 (1953).

[2] G. E. Boyd, Oak Ridge National Laboratory Report ORNL-229, February 1949 (unpublished) as reported by Hollander, Perlman, and Seaborg, Revs. Modern Phys. 25, 469 (1953).

[3] B. Kahn and W. S. Lyon, Nucleonics 11, 61 (1953).

[4] G. E. Boyd and B. H. Ketelle, unpublished data (1951) as reported by Hollander, Perlman, and Seaborg, Revs. Modern Phys. 25, 469 (1953).

[5] D. N. Kundu and M. L. Pool, Phys. Rev. 76, 183 (1949).

FIG. 2. Gamma spectrum of Mo^{90} as determined with a sodium iodide crystal-photomultiplier combination coupled to a 50-channel pulse-height analyzer.

and Overstreet.[6] Experiment soon showed that one of these isomers had a half-life of 24±3 seconds. To do this an intense carrier-free sample of Mo^{90} was placed on shelf one of our scintillation counter for a one-minute growth period. The aluminum front cover on the sodium iodide crystal was not grounded and in our equipment carried a potential of 500 volts negative with respect to the sample. The sample was then quickly withdrawn and the recoil daughter atoms of Nb^{90} collected from the molybdenum source during the growth period were counted. The gamma spectrum was determined by a 50-channel differential-pulse analyzer. Figure 4 shows the gamma spectrum of the recoil activity immediately after the growth period. A pure gamma ray of 120 kev was observed. The gamma spectrum of Mo^{90} is also shown in the same figure for comparison. The 120-kev gamma-ray peak for the recoil activity decayed with a half-life of 24±3 seconds. This activity will henceforth be designated as Nb^{90m_1}.

The fact that this 24-second activity is the product of the decay of Mo^{90} was further confirmed by plotting the yield of the recoil activity in a one-minute growth period as a function of time at which the recoil collection was done. From the data of 6 recoil daughter collections spaced over a 20-hour period, a half-life of 5±1 hours was obtained for the molybdenum parent, confirming the genetic relationship.

The 24-second isomer was proved to be a niobium activity by chemical separation. From the work of Huffman *et al.*,[7] Kraus and Moore,[8] and Hicks, Stevenson, and Gilbert[9] it was known that niobium and molybdenum form complexes in strong hydrochloric acid which are strongly adsorbed on anion exchange resins. On reinvestigation we found that a mixture of molybdenum and niobium in 6*M* HCl is adsorbed by Dowex-1, a strong-base quaternary-amine polymer. Niobium can be eluted with 5*M* HCl but molybdenum is strongly held at this hydrochloric acid concentration. Molybdenum-90 activity in 6*M* HCl solution was run through a 4-cm×0.5-cm column of Dowex-1 previously equilibrated with 12*M* HCl. The molybdenum on the column was washed free of niobium activity with 5*M* HCl and after a growth period of one minute, niobium formed by decay during this period was quickly stripped from the column by 5*M* HCl and studied in a scintillation counter. The gamma spectrum showed the presence of 120-kev gamma rays decaying with a half-life of 24±3 seconds, thereby further establishing that the 24-second activity was a niobium activity.

An experimental measurement of the conversion coefficient of the 120-kev gamma ray was carried out in this manner. A sodium iodide crystal covered with a beryllium window was substituted for the usual aluminum-covered crystal in the gamma-ray spectrometer. By means of this crystal, a sample of Mo^{90} was examined

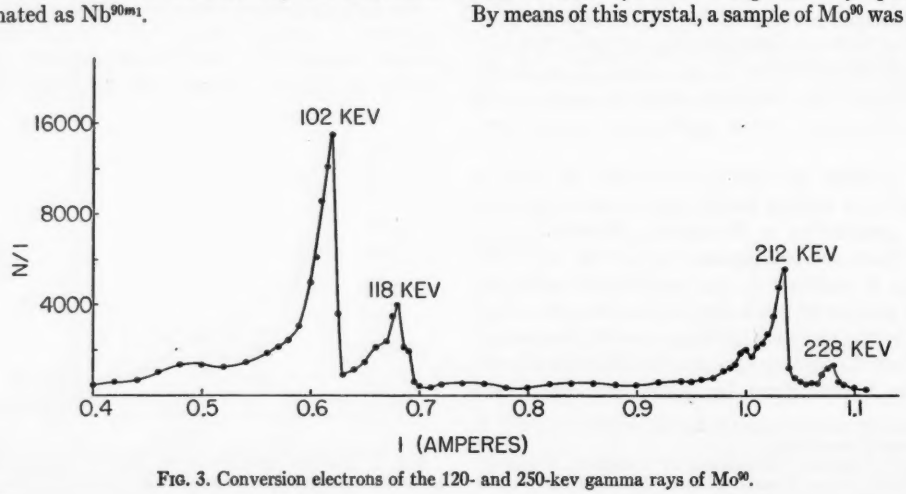

FIG. 3. Conversion electrons of the 120- and 250-kev gamma rays of Mo^{90}.

[6] L. Jacobson and R. Overstreet, *Radiochemical Series: The Fission Products* (McGraw Hill Book Company, Inc., New York, 1951), Paper No. 91, National Nuclear Energy Series, Plutonium Project Record, Vol. 9, Div. IV.
[7] Huffman, Iddings, and Lilly, J. Am. Chem. Soc. **73**, 4474 (1951).
[8] K. A. Kraus and G. E. Moore, J. Am. Chem. Soc. **73**, 9 (1951).
[9] Hicks, Stevenson, and Gilbert (private communication).

and the intensity of the 16.5-kev K x-rays was compared with the intensity of the 120-kev gamma-ray peak.

This comparison required a correction of the observed x-ray counts for absorption losses in the beryllium window plus magnesium oxide reflector around the crystal and also for fluorescence yield. The absorption loss was estimated by using the same counter to determine the ratio of the L x-ray peak from a pure sample of Am^{241} to the 60-kev gamma-ray peak from the same sample. The area under the unresolved 17.3- and 13.5-kev L x-ray peaks was compared with the area to be expected from the abundance figures reported by Beling, Newton, and Rose.[10] We determined that the absorption loss was about 25 percent for this particular L x-ray mixture. It was assumed that the absorption loss of the 16.5-kev x-rays of niobium was the same. This is not strictly correct but the error cannot be more than 50 percent and is probably considerably less. The fluorescence yield was estimated as 0.73 from the tables of Broyles, Thomas, and Haynes.[11] Absorption of x-rays in the sample itself was negligible as the sample was carrier free.

With these corrections and assumptions the ratio of K-shell vacancies to 120-kev quanta was calculated to be 1.5. This is only an upper limit to the K-conversion coefficient of the 120-kev gamma transition because some of the K vacancies may be accounted for by K capture or by conversion of the 250-kev gamma ray. A more significant measurement was made by collecting some of the 24-second activity by recoil on the cover of the beryllium-window sodium iodide crystal in the manner discussed above and then measuring the low-energy spectrum of this activity. The x-ray and 120-kev gamma spectrum of the recoil activity showed that only $\frac{1}{3}$ of the x-ray peak observed in the Mo^{90} sample can be assigned to conversion of the 120-kev gamma ray of Nb^{90m_1} and that the true K-shell conversion coefficient is about 0.5.

The tables and curves of Rose *et al.*[12] do not provide values of conversion coefficients for gamma rays below 150 kev. An extrapolation of their curves for $Z=40$, however, indicates that the K-shell conversion coefficient for an $E3$ transition of 120 kev in niobium is of the order of 2 to 4 and somewhat higher for an $M3$ transition. The value expected for $E2$ is of the order of 0.4 to 0.8 and for $M2$ a factor of 2 higher. Hence the observed value of ~ 0.5 is in best agreement with an $E2$ assignment and quite out of line with either an $E3$ or $M3$ assignment. The K/L ratio of 3.6 is reasonable for this assignment according to the rough empirical curves of Goldhaber and Sunyar.[13]

The half-life of 24 seconds is unusually long for an

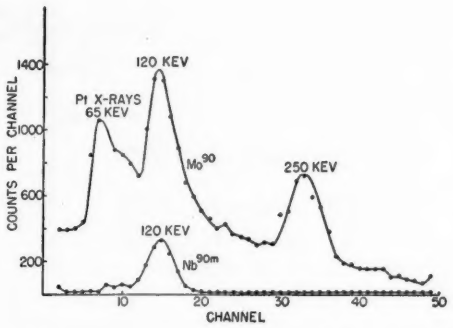

FIG. 4. Gamma spectrum of 24-second Nb^{90m} as determined with a sodium iodide crystal-photomultiplier combination coupled to a 50-channel pulse-height analyzer. The gamma spectrum of Mo^{90} is shown for comparison.

$E2$ transition. If the Montalbetti[14] nomogram of the Weisskopf[15,16] formula for the mean lives of gamma transitions is applied in this case, a mean life of $\sim 10^{-6}$ second is predicted. For other transition types the predictions are as follows: $\sim 2\times 10^{-4}$ second for $M2$, 2 seconds for $E3$, 200 seconds for $M3$.

Goldhaber and Sunyar[13] have shown that half-lives of transitions with $\Delta I=2$ or 3 are frequently much slower than predicted by the Weisskopf formula. The discrepancy in some cases is as high as 10^4 or 10^5.

If the $E2$ assignment in Nb^{90m} is correct the delay is a factor of approximately 10^8, much higher than any listed by Goldhaber and Sunyar.

IV. 10 TO 20 MILLISECOND ISOMER, Nb^{90m_2}

The gamma-gamma coincidence studies mentioned above showed that the half-life of the 250-kev gamma ray was greater than 5×10^{-6} second, the resolving time of the coincidence circuit. Study of the radioactivity in niobium fractions isolated very rapidly from Mo^{90} sources placed an upper limit of a few seconds to the half-life. An electronic delayed-coincidence technique was used to determine whether the half-life was in the millisecond region, and a half-life of 10 to 20 milliseconds was determined as described in the following paragraphs. The instrumentation for this determination was carried out by Almon E. Larsh.

A weak sample of Mo^{90} with a count rate of a few tens per minute and mounted on a 3-mil aluminum backing was placed between two sodium iodide crystals. The output from the photomultiplier tube of the gate crystal was fed to a single-channel pulse-height analyzer and pulses corresponding to annihilation radiation were selected and applied to the trigger input of a Tektronix-514D oscilloscope to start a trace across the oscilloscope face. The second sodium iodide crystal was simultaneously detecting gamma radiation from the Mo^{90}

[10] Beling, Newton, and Rose, Phys. Rev. **86**, 797 (1952); erratum: **87**, 1144 (1952).
[11] Broyles, Thomas, and Haynes, Phys. Rev. **89**, 715 (1953).
[12] Rose, Goertzel, Spinrad, Harr, and Strong, Phys. Rev. **83**, 79 (1951).
[13] M. Goldhaber and A. W. Sunyar, Phys. Rev. **83**, 906 (1951).
[14] R. Montalbetti, Can. J. Phys. **30**, 660 (1952).
[15] V. F. Weisskopf and J. M. Blatt, *Theoretical Nuclear Physics* (John Wiley and Sons, Inc., New York, 1952).
[16] V. F. Weisskopf, Phys. Rev. **83**, 1073 (1951).

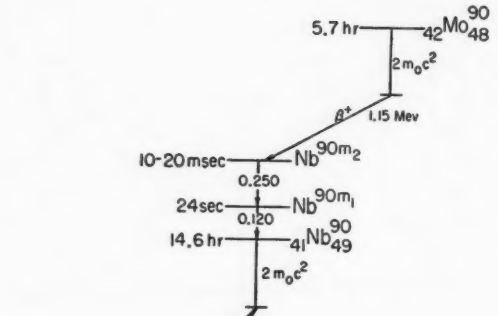

FIG. 5. Decay scheme of Mo^{90}.

sample. These signals after amplification were fed to the vertical deflecting system of the oscilloscope. Signal pulses arriving in prompt coincidence with the annihilation trigger pulses were displayed as dots at the start of the trace. The energy of the gamma radiation was proportional to the amount of vertical deflection on the face of the cathode-ray tube. Any delayed gamma-ray signal pulses or randomly occurring chance pulses which arrived during the sweep appeared as dots at a corresponding distance from the start of the trace.

A Polaroid Land camera was used to take 20-minute exposures of the scope face. A finished photograph showed 3 bands of dots. The density of dots corresponding to chance pulses of 120- and 510-kev radiation was small and did not decrease across the trace. The density of dots corresponding to 250-kev radiation showed a real decrease to a chance background of 25 to 35 percent of the initial density when the trace sweep speed was set at 1 cm per 4.5 milliseconds.

The density of dots in the 250-kev band was plotted *versus* the distance (time) from the beginning of the traces and the chance background was subtracted to show the true decay curve. Analysis of many photographs gave a value of 10 to 20 milliseconds for the half-life of the 250-kev radiation.

In initial trials of this method halatron from the base line made the recording of the desired data almost impossible. Hence, some changes from the normal operation of the Tektronix instrument were required. The normal unblanking circuit was not used. Instead, when the positive signal pulse was fed to the vertical deflection system as mentioned above, it was simultaneously fed to an inverter circuit which inverted and amplified the pulse. The resulting negative pulse was fed to the cathode input post on the oscilloscope to unblank the trace at the instant a signal appeared on the vertical deflector.

This identical instrumental method of half-life measurement has been applied to the determination of the half-life of a 0.37-millisecond decay in Y^{88m}.[17]

Mean-life predictions of the Weisskopf formula for Nb^{90m_2} are as follows: $E2$, $\sim 10^{-8}$ second; $M2$, 10^{-6} second; $E3$, 10^{-2} second; and $M3$, 1 second. The observed value of 15 to 30 milliseconds corresponds to an undelayed $E3$ or to a highly delayed $E2$ or $M2$ transition. The tables of Rose *et al.*[12] give precise K-conversion coefficients of the following magnitude in this case: $E2$, 0.034; $M2$, 0.075; $E3$, 0.14; and $M3$, 0.33. The only information we have on the conversion coefficient is the fact that the number of conversion electrons of the 250-kev gamma ray of Nb^{90m_2} is within a factor of 2 or 3 of the number of conversion electrons of the 120-kev gamma ray of Nb^{90m_1}. This would favor a choice of $E3$ or $M3$ rather than $E2$ or $M2$.

A decay scheme summarizing some of our information of the decay of Mo^{90} is shown in Fig. 5.

V. RADIATIONS OF 14.6-HOUR Nb^{90} AND AN ISOMERIC STATE IN THE EVEN-EVEN ISOTOPE Zr^{90}

The 14.6-hour ground state of Nb^{90} produced as the end product of the decay of Mo^{90} has been studied previously by several workers. Boyd[2] reported Nb^{90} to be a positron emitter with a maximum energy of approximately 1.7 Mev while Diamond,[1] and Kundu and Pool[5] have reported the positrons to have a maximum energy of 1.2 Mev. Boyd and Ketelle[4] reported three gamma rays of energies 140 kev, 1.14 Mev, and 2.23 Mev in Nb^{90}.

In our determination of the positron end point of Nb^{90} by means of an anthracene crystal spectrometer coupled to a 50-channel differential-pulse analyzer, we obtained a value of 1.7 ± 0.1 Mev for the positron end point as shown in Fig. 6. The gamma spectrum of Nb^{90} is shown in Fig. 7. There are three gamma rays of energies 140 kev, 1.14 Mev, and 2.20 Mev in addition to the annihilation radiation. After taking into account

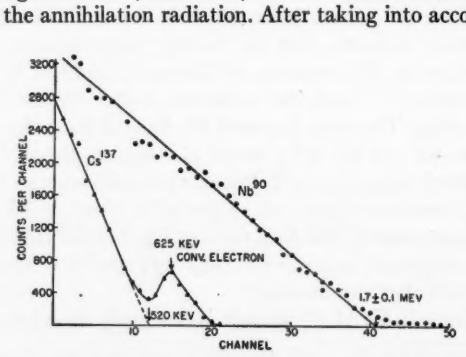

FIG. 6. Positron end point of Nb^{90} as determined on an anthracene crystal spectrometer. Cs^{137} was used as a standard. The data were taken on a 50-channel pulse-height analyzer.

[17] Hyde, Florence, and Larsh, Phys. Rev. 97, 1255 (1955).

the counting efficiency of the sodium iodide crystal for the 3 energies, the ratios of their abundances are 1:2.8:1.7.

Coincidence measurements made on the gamma rays of Nb^{90} showed that the 140-kev and 1.14-Mev gamma rays are in coincidence with each other and with the annihilation radiation. From the fact that the 1.14-Mev gamma ray is more abundant, the 140-kev transition must lie above the 1.14-Mev gamma ray. This is in keeping with the expectations from the systematics of the first excited state of even-even nuclei, inasmuch as in Zr^{90} one would expect the first excited state to be high.[18]

The 2.20-Mev gamma ray showed no coincidences with 140-kev or 1.14-Mev gamma rays, or with the annihilation radiation. This result suggested the possibility of a delayed transition involving the 2.20-Mev level in Zr^{90}, although the possibility existed that this level was reached by K-capture decay rather than by positron emission. This possibility was eliminated by showing that the intensity of K x-rays relative to the 140-kev peak was only about 80 percent and hence too low by a factor of 2 to account for the 2.2-Mev radiation. The x-ray measurements were made with the sodium iodide crystal with beryllium casing described above. Furthermore, a coincidence experiment in which K x-rays were applied to the gate showed no evidence of an x-ray—2.2-Mev gamma-ray coincidence.

Zirconium was precipitated as barium fluozirconate from a Nb^{90} sample and was examined for gamma radiation of 2.20 Mev with negative results. By performing this separation rapidly and counting the resulting barium fluozirconate precipitate in a scintillation counter we could fix the delay to be less than one minute.

Considerable thought was given to the problem of determining the half-life by some instrumental method but no feasible way could be devised with the equipment available. The low counting efficiency of the 2.2-Mev radiation in any sodium iodide crystal available to us was a serious disadvantage.

Because of the high energy the spin change in this transition must be quite high, i.e., ≥ 3. This transition is especially interesting because of the rarity of delayed transitions in even-even isotopes.§

VI. EXPERIMENTAL PART

Cyclotron bombardments.—During the course of this work Mo^{90} was produced by $Nb^{93}(p,4n)Mo^{90}$ reaction by bombarding Nb^{93} (100 percent abundance) in the form of 5-mil foil. Protons of 80-Mev energy from the 184-inch cyclotron were used for bombardment.

[18] G. Scharff-Goldhaber, Phys. Rev. **90**, 587 (1953).

§ *Note added in proof.*—A new isomer of Zr^{90} with a half-life of 0.83 second and a gamma energy of 2.30±0.02 Mev has been prepared by pile neutron bombardment of enriched Zr^{90} by Campbell, Peele, Maienschein, and Stelson [Bull. Am. Phys. Soc. **30**, No. 1, 33 (1955)]. This isomer may or may not be identical with the delayed 2.3-Mev transition in the decay of Nb^{90} but preliminary experiments indicate that it is not. We are indebted to E. C. Campbell for calling our attention to this work.

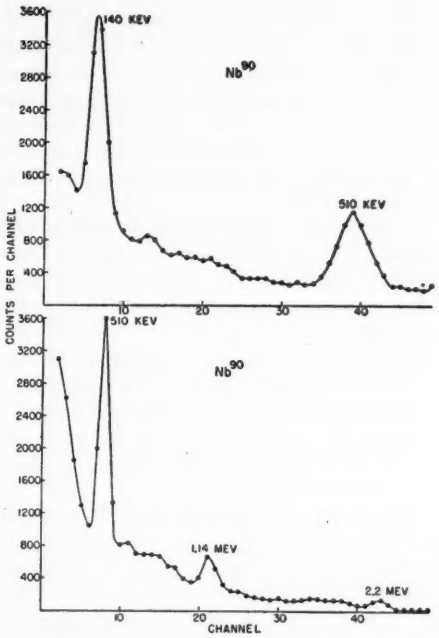

FIG. 7. Gamma spectrum of 14.6-hour Nb^{90} as determined with a sodium iodide crystal-photomultiplier combination coupled to a 50-channel pulse-height analyzer.

In addition to the reaction mentioned previously, Mo^{90} was also prepared in a novel way by the bombardment of bromine with accelerated nitrogen ions. This was done in the 60-inch cyclotron using a beam of hextuplicately charged nitrogen ions.[19] The nitrogen ions have a continuous spread of energy with a maximum of 140 Mev. Sodium bromide wrapped in a thin tantalum foil was bombarded to carry out the following reactions:

$$_7N^{14}+{}_{35}Br^{81}\rightarrow{}_{42}Mo^{91}+4_0n^1,$$
$$_7N^{14}+{}_{35}Br^{81}\rightarrow{}_{42}Mo^{90}+5_0n^1.$$

At the end of the bombardment the activity in the molybdenum fraction was about 9/10 Mo^{91} and 1/10 Mo^{90}.

In some cases Nb^{90} was produced by the bombardment of 5-mil zirconium foils with 20-Mev protons in the Berkeley linear accelerator. In addition, Nb^{90} was also produced by bombarding silver foils with 340-Mev protons in the 184-inch cyclotron.

Radiochemical procedures.—For the isolation of molybdenum, the niobium foils were dissolved in a mixture of concentrated HNO_3+HF and the solution was evaporated to dryness. The residue was then taken up in 6M HCl, centrifuged to remove Nb_2O_5, and molybdenum was extracted from the supernatant with an equal volume of diethyl ether. The extraction was repeated thrice. Ether from the three extractions was

[19] Rossi, Jones, Hollander, and Hamilton, Phys. Rev. **93**, 256 (1954).

evaporated over 5 ml of distilled water which was then saturated with hydrogen chloride gas and the resulting solution was run through a 4 cm×0.5 cm column of Dowex-1 anion-exchange resin previously equilibrated with concentrated hydrochloric acid. The resin column was then washed free of niobium with 5*M* HCl following which the molybdenum activity was eluted from the column with 1*M* HCl.

In the nitrogen-ion bombardment, sodium bromide was dissolved in 6*M* HCl and molybdenum was extracted with diethyl ether. Thereafter the chemical procedure was the same as that described in the preceding paragraph.

For the extraction of niobium from zirconium targets, the foils were dissolved in hydrofluoric acid and all the zirconium was precipitated from the solution as barium fluozirconate by adding Ba^{++}. The resulting solution was saturated with hydrochloric acid and niobium was extracted into di-isopropyl ketone.

The silver targets were dissolved in 10*M* HNO_3 and niobium was coprecipitated on MnO_2 by adding a few drops of a dilute solution of potassium permanganate and heating the solution in a water bath. The precipitate of MnO_2 was dissolved in concentrated hydrochloric acid, and niobium was extracted into di-isopropyl ketone. Part of the manganese was extracted by the ketone.

Alternatively, to the solution of silver in 10*M* HNO_3, a few drops of $La(NO_3)_3$ were added and the solution was saturated with ammonia gas to precipitate $La(OH)_3$. After removal of the precipitate by centrifugation it was washed with distilled water, dissolved in hydrochloric acid and then saturated with hydrogen chloride gas. The resulting solution was run through a column of the anion-exchange resin Dowex-1, the column was washed with concentrated hydrochloric acid a few times and finally niobium was desorbed from the column with 5*M* HCl.

Beta-ray spectrometer.—The spectrometer used was a double-focusing type of 25-cm radius. It is after the design of Svartholm and Siegbahn,[20] and by Shull and Dennison.[21] A detailed description of this instrument has been given by O'Kelley.[22]

Scintillation spectrometer.—The gamma-ray scintillation spectrometer used in this work was assembled by A. Ghiorso and A. E. Larsh of this Laboratory. The photomultiplier was a Dumont-6292 tube coupled to a sodium iodide (thallium activated) crystal, 1.5 inches in diameter and 1 inch thick. The output from the photomultiplier after being amplified in a preamplifier was fed into a linear amplifier. The final pulse was then analyzed by a 50-channel differential pulse-height analyzer designed by Ghiorso and Larsh. Details of this equipment will be given in a forthcoming publication of Ghiorso and Larsh.

For gamma-gamma coincidence studies, a second sodium iodide-photomultiplier assembly in combination with a single-channel pulse analyzer was incorporated into the above instrument.

VII. ACKNOWLEDGMENTS

The authors wish to express their thanks to James T. Vale and Lloyd Houser and members of the 184-inch cyclotron crew for the numerous 184-inch cyclotron bombardments. Similarly, acknowledgement is made to G. B. Rossi, W. B. Jones, A. Ghiorso, and members of the 60-inch cyclotron crew for the nitrogen-ion bombardments. The linear accelerator bombardments were carried out through the courtesy of W. W. Olson, R. D. Watt, and the accelerator crew.

We also wish to acknowledge the indispensable assistance of Dr. T. O. Passell for beta-ray spectroscopy and to Dr. F. Asaro and Mr. F. S. Stephens for coincidence studies.

---

[20] N. Svartholm and K. Siegbahn, Arkiv. Mat. Astron. Fysik **33A**, No. 21 (1946); see also Hedgran, Siegbahn, and Svartholm, Proc. Phys. Soc. (London) **A63** (1950).

[21] F. Shull and D. Dennison, Phys. Rev. **71**, 681 (1947); **72**, 256 (1947).

[22] G. D. O'Kelley, Ph.D. thesis, University of California Radiation Laboratory report UCRL-1243, March 15, 1951 (unpublished).

Angular Distribution of Disintegration Products from the $O^{16}(d,p)O^{17}$, $Be^{9}(d,p)Be^{10}$, and $Be^{9}(d,t)Be^{8}$ Reactions

MIRA K. JURIĆ
Institute of Nuclear Sciences "Boris Kidrich," Belgrade, Yugoslavia
(Received October 18, 1954)

The angular distributions of disintegration products from the reactions $O^{16}(d,p)O^{17}$, $Be^{9}(d,p)Be^{10}$, and $Be^{9}(d,t)Be^{8}$ were examined, with deuteron energies from 0.60 to 1.45 Mev. Pronounced asymmetry is found with respect to 90°. The results are analyzed to determine the relative contributions of stripping and compound nucleus formation.

IT would be desirable to be able to make more definite statements about the question as to whether stripping or compound nucleus formation predominates in the reactions with deuterons of energies insufficient to overcome the Coulomb barrier. Therefore, the angular distributions of disintegration products from the reactions $O^{16}(d,p)O^{17}$, $Be^{9}(d,p)Be^{10}$, and $Be^{9}(d,t)Be^{8}$ with deuteron energies from 0.60 to 1.45 Mev were examined in order to determine the extent to which these two processes contribute to these reactions.

The angular distribution of protons from the $O^{16}(d,p)O^{17}$ reaction, produced by deuterons of lower energies, has not yet been published except for 1.07-Mev deuterons on a slightly thick oxide target; the $Be^{9}(d,p)Be^{10}$ angular distribution has been more investigated, but the $Be^{9}(d,t)B^{8}$ angular distribution was measured only for deuterons of 1.3 Mev and below 0.62 Mev.[1-5]

We examined the angular distribution of long-range protons and tritons at bombarding energies of deuterons of E_d=0.60, 0.80, 0.90, 1.00, 1.10, 1.20, 1.30, and 1.45 Mev. The bombarding deuterons were produced in the Cockcroft-Walton accelerator of the Institute of Nuclear Sciences "Boris Kidrich" in Belgrade, whose ion source is of relatively high intensity.[6]

The targets were MoO_3 and metallic Be evaporated in vacuum onto a 0.005-mm copper foil. The weight of the targets was 0.136–0.260 mg/cm². The target plates were placed at an angle of 45° to the bombarding beam. The angular distributions were measured from 0° to 170° at 10° intervals. The solid angles of 1.87×10^{-3} steradian for each interval were defined by square holes in a ring (150-mm diameter) which surrounded the target.

The reaction products were detected by means of photonuclear emulsions placed around the target in such a way that each plate covered one of the solid angles. The average angle of incidence of particles on the surface of the emulsions was 10°. The plates used were Ilford C_2, 100 μ thick. In order to prevent the blackening of the plates by elastically scattered particles and to reduce the ranges of their tracks, the plates were shielded by 0.005–0.022 mm Al foils, covering the square holes of the collimating ring.

The scanning of the emulsions was performed by means of Leitz immersion microscopes, using the standard methods. The tracks were divided according to length into different groups, and all the tracks of one group were counted in every angle covered by one plate. The total number of tracks per plate varied from 400 to 12 500, according to the energy of deuterons and the position of the plate.

The protons from the $O(d,p)$ reaction, produced from the oxygen layer formed on the target can represent a considerable source of error in the angular distribution from the $Be(d,t)$ reaction. In the region of the energy of the bombarding deuterons (E_d=0.60–1.45 Mev), the lengths of the proton tracks from the $O(d,p)$ reaction in photonuclear emulsions at some angles of incidence are equal to the lengths of the triton tracks from the $Be(d,t)$ reactions. However, since at some angles the two groups of tracks were of different length, it was possible to subtract the proton tracks at all angles, because the angular distribution from $O(d,p)$ reaction was already determined (see Fig. 1).

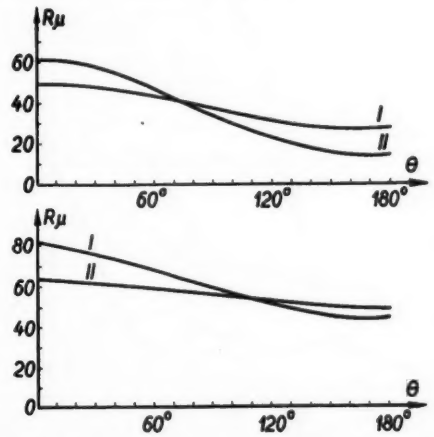

FIG. 1. Abscissa—angles; ordinate—ranges of particles in photonuclear emulsions. I—tritons from $Be(d,t)$ at E_d=0.8 and 1.2 Mev; II—protons from $O(d,p)$ reaction at E_d=0.8 and 1.2 Mev.

[1] N. P. Heydenburg and D. N. Inglis, Phys. Rev. **73**, 230 (1948).
[2] J. Resnick and S. S. Hanna, Phys. Rev. **82**, 462 (1952).
[3] F. L. Canavan, Phys. Rev. **87**, 136 (1952).
[4] D. Jong and P. M. Endt, Physica **18**, 679 (1952).
[5] P. Cuer and J. Jung, Phys. Rev. **89**, 1151 (1953).
[6] B. Nikolić and M. Crnilović, Bull. Inst. Nuclear Sci., Belgrade **3**, 29 (1953).

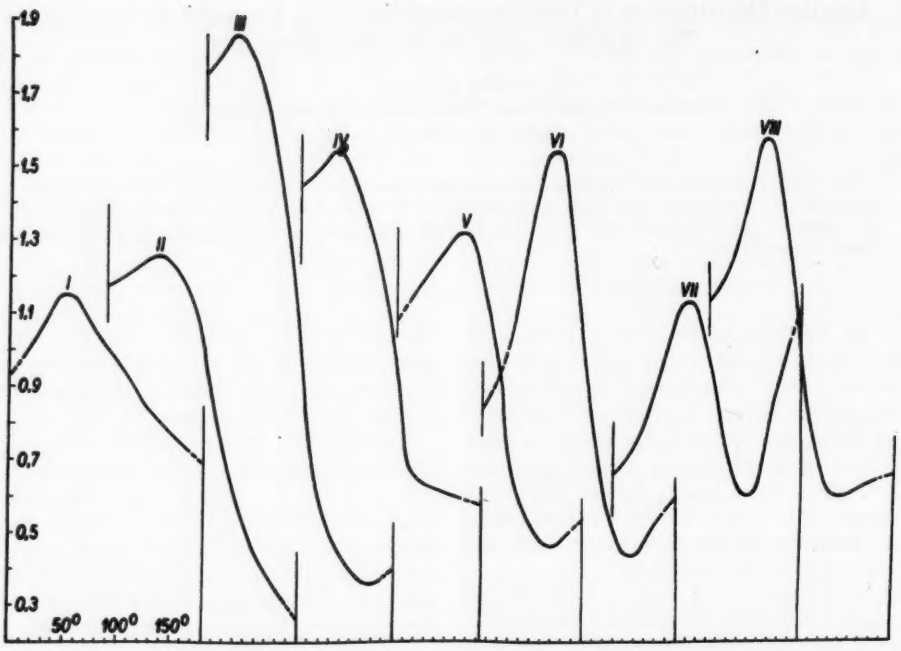

FIG. 2. The angular distribution of protons from the $O(d,p)$ reaction. The curves have been plotted according to the equation:

$$\frac{\sigma(\theta)}{\sigma(90°)} = \sum_{n=0}^{5} A_n P_n.$$

The effective deuteron energy obtained by substracting half the target thickness in kev from the bombarding energy is, in Mev, 0.58 for curve I, 0.76 for curve II, 0.84 for III, 0.98 for IV, 1.05 for V, 1.14 for VI, 1.26 for VII, and 1.40 for VIII.

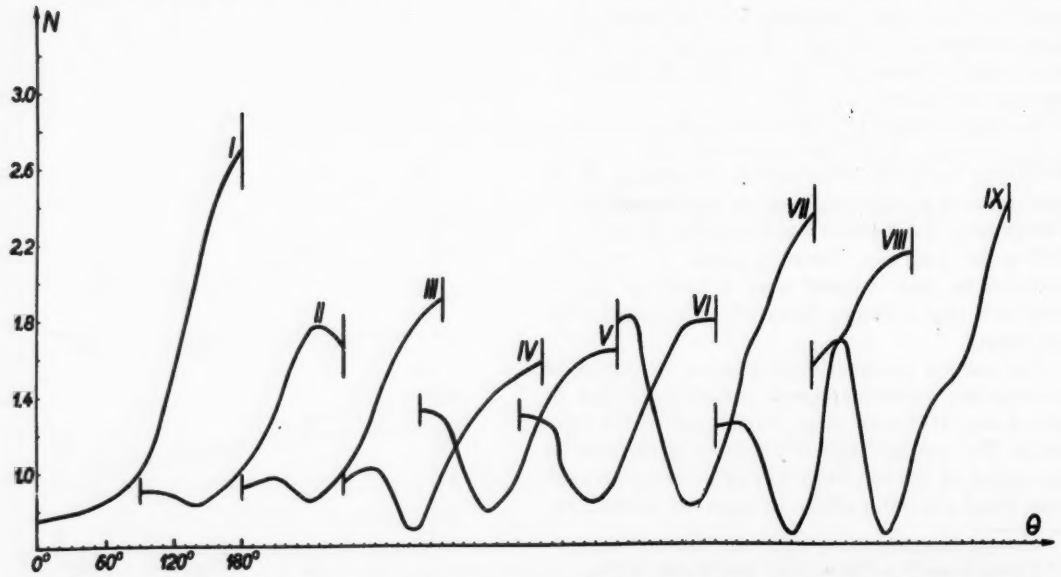

FIG. 3. The angular distribution of protons from the $Be(d,p)$ reaction. The curves have been plotted according to the equation:

$$\frac{\sigma(\theta)}{\sigma(90°)} = \sum_{n=0}^{5} A_n P_n.$$

The effective deuteron energy, obtained by subtracting half the target thickness in kev from the bombarding energy, is, in Mev, 0.62 for curve I, 0.81 for II, 0.90 for III, 0.94 for IV, 1.03 for V, 1.06 for VI, 1.19 for VII, 1.28 for VIII, and 1.403 for IX.

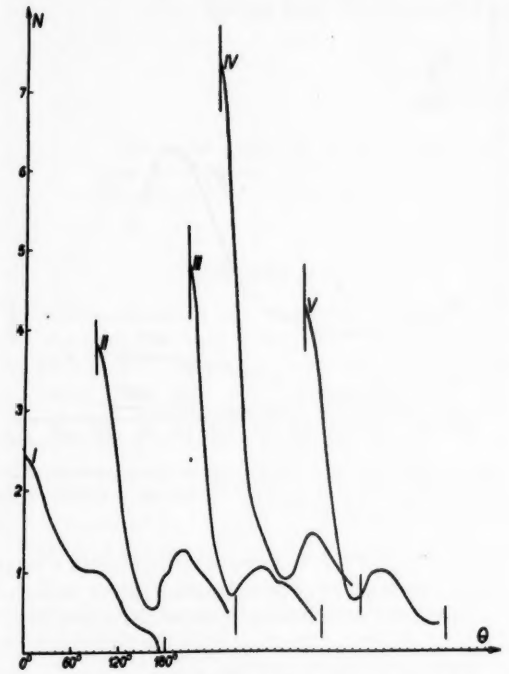

FIG. 4. The angular distribution of tritons from the Be(d,t) reaction. The curves have been plotted according to the equation:

$$\frac{\sigma(\theta)}{\sigma(90^\circ)}=\sum_{n=0}^{7} A_n P_n.$$

The effective deuteron energy, obtained by substracting half the target thickness in kev from the bombarding energy, is, in Mev, 0.58 for curve I, 1.03 for II, 1.19 for III, 1.28 for IV, and 1.40 for V.

The angular distribution of reaction products has been determined by measuring the yields at 18 various angles, and the results have been converted to the center-of-mass coordinate system. The angular distribution obtained in this way is given in Figs. 2, 3, and 4.

These angular distributions have been analyzed in terms of Legendre polynomials:

$$\frac{\sigma(\theta)}{\sigma(90^\circ)}=\sum_{n=0} A_n P_n$$

TABLE I. The coefficients A_n of the angular distribution for $O^{16}(d,p)O^{17}$.

E_d Mev	A_0	A_1	A_2	A_3	A_4	A_5	A_6
0.58	0.98	0.195	−0.10	−0.06	−0.04	—	—
0.76	0.93	0.53	−0.19	−0.10	0.02	—	—
0.84	1.08	0.94	0.03	−0.25	−0.03	—	—
0.98	1.05	0.60	0.17	−0.16	−0.03	—	—
1.05	0.95	0.53	−0.23	−0.25	0.04	0.03	—
1.14	0.98	0.61	−0.16	−0.49	−0.04	+0.03	—
1.26	0.90	0.15	−0.16	−0.37	0.16	0.00	—
1.40	1.06	0.59	−0.10	−0.43	−0.09	0.09	0.03

TABLE II. The coefficients A_n of the angular distribution for $Be^9(d,p)Be^{10}$.

E_d Mev	A_0	A_1	A_2	A_3	A_4	A_5	A_6	A_7
0.62	1.21	−0.79	0.48	−0.16	0.00	—	—	—
0.81	1.11	−0.48	0.28	0.00	0.02	—	—	—
0.90	1.11	−0.45	0.33	0.00	0.03	—	—	—
0.94	1.10	−0.40	0.26	0.15	0.00	—	—	—
1.03	1.14	−0.35	0.38	0.25	0.00	—	—	—
1.06	1.14	−0.35	0.45	0.20	0.00	—	—	—
1.19	1.13	−0.46	0.74	0.27	0.05	−0.02	—	—
1.28	1.28	−0.65	0.64	0.32	−0.16	−0.16	0.00	—
1.403	1.26	−0.31	0.70	0.27	0.07	−0.36	0.04	—

TABLE III. The coefficients A_n of the angular distribution $Be^9(d,t)Be^8$.

E_d Mev	A_0	A_1	A_2	A_3	A_4	A_5	A_6	A_7	A_8	A_9
0.62	0.97	0.73	0.09	0.34	0.32	0.05	0.03	—	—	—
1.03	1.09	0.44	0.68	1.12	0.25	0.06	0.03	—	—	—
1.19	1.16	0.85	0.95	1.29	0.68	0.36	0.02	—	—	—
1.28	1.45	0.90	1.31	1.5	0.50	0.64	0.59	0.53	0.00	—
1.403	1.03	0.79	0.65	1.08	0.62	0.83	0.01	0.00	—	—

(P_n=Legendre polynomial). The coefficients A_n of the Legendre polynomials were computed by using an analog computer machine of the Institute "Boris Kidrich," with a total error of approximately ±0.04 (Tables I, II, III). The coefficients A_n in the function for the deuteron energy are shown in Figs. 5, 6, and 7.

The most remarkable characteristics of the observed angular distributions is their strong asymmetry with respect to the 90° plane which is perpendicular to the incoming deuteron beam. It appears from these results that the reactions produced by deuterons contain contributions from two processes: stripping and com-

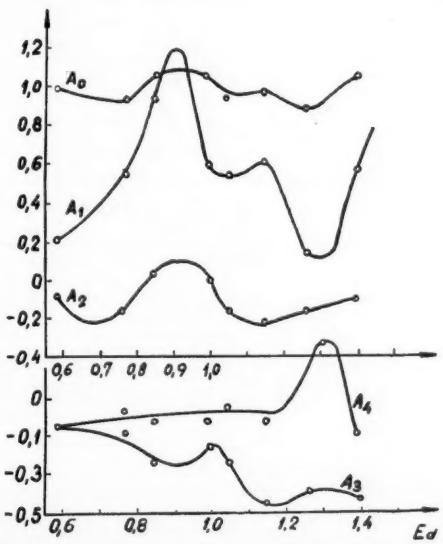

FIG. 5. The coefficients A_n as functions of the deuteron energy E_d for the O(d,p) reaction

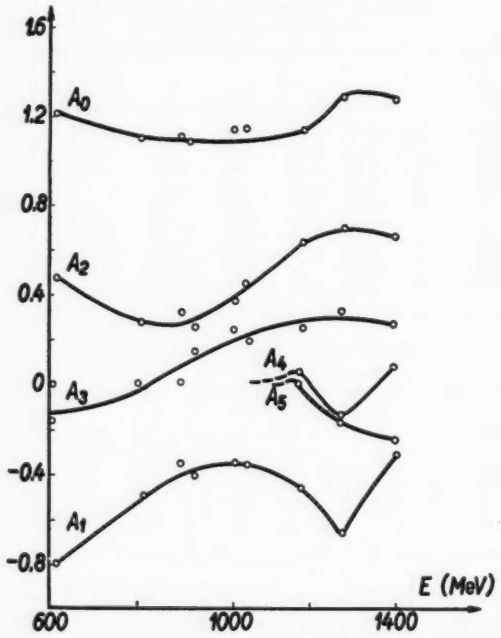

FIG. 6. The coefficients A_n as functions of the deuteron energy E_d for the Be(d,p) reaction.

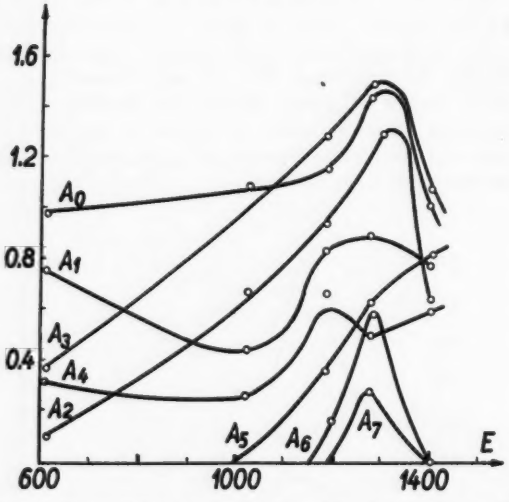

FIG. 7. The coefficients A_n as functions of the deuteron energy E_d for the Be(d,t) reaction.

pound-nucleus formation. All the shapes of the angular distribution curves for stripping are very similar, showing a strong peak for the forward direction with a maximum at small angles. These peaks, as shown in Figs. 1 and 2, increase with bombarding energy, which means that the relative contribution from the stripping effect increases with deuteron energy.

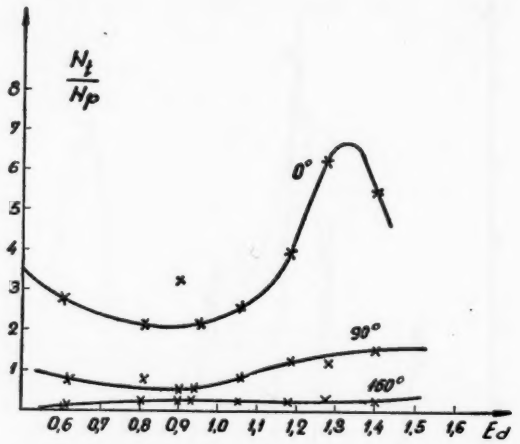

FIG. 8. Abscissa—bombarding energy of the deuteron; ordinate—ratio of the number of tritons to the number of protons in the reactions Be(d,p) and Be(d,t).

In addition to the structure which can be attributed directly to the stripping effect, the angular distribution also shows a contribution of the compound-nucleus formation. This contribution will be especially accentuated for the resonance bombarding energies, and the characteristics of the energy levels of the compound nucleus will influence the angular distribution. This may be the case for $E_d=0.84$ Mev and $E_d=1.26$ Mev in the O(d,p) reaction, and for $E_d=1.28$ Mev in the Be(d,p) and Be(d,t) reactions (curves No. III and No. VII, Fig. 2; No. VIII, Fig. 3 and No. IV, Fig. 4). It is of interest to note that the state produced by deuteron energy of $E_d=1.28$ Mev, prefers the Be(d,t) disintegration to the Be(d,p). Figure 8 shows that the yield of the Be(d,t) reaction is higher than that of the Be(d,p) at $E_d=1.28$ Mev, but only for those particles having a forward direction. This resonance could therefore be due to that of the pickup effect.

If we assume that the resonances result only from the effect of the compound-nucleus formation, then the compound nucleus F^{18} has energy levels at about $E_{ex}=8.38$ Mev and $E_{ex}=8.76$ Mev, and B^{11} at about $E_{ex}=16.77$ Mev.

Further work on these subjects is in progress.

Spins and Parities of Excited States of Ce^{140} and Sr^{88}

G. R. Bishop* and J. P. Perez Y Jorba
Clarendon Laboratory, Oxford, England
(Received December 17, 1954)

The angular correlations and the direction-polarization correlations of γ rays of Ce^{140} and Sr^{88} have been measured. Spins and parities have been assigned to the excited states of these nuclei as follows. Ce^{140}: 2.42 Mev, 3^-; 2.09 Mev, 4^+; 1.60 Mev, 2^+. Sr^{88}: 2.78 Mev, 3^-; 1.87 Mev, 2^+.

1. INTRODUCTION

THE measurement of the angular correlation and direction-polarization correlation of γ rays emitted in cascade leads to the assignment of angular momentum and parity.[1] We have made measurements of these types on the γ rays emitted from excited states of Sr^{88} and Ce^{140} using a γ-ray polarimeter similar to the instruments already described.[1] Gamma rays are scattered preferentially in a direction perpendicular to the electric vector in the incident beam. It is thus possible to distinguish between electric and magnetic radiations.

2. PRINCIPLES OF METHOD FOR DETERMINING DIRECTION-POLARIZATION CORRELATIONS

The degree of polarization to be expected for direction-polarization measurements on cascade γ rays has been calculated by several authors.[2]

The calculated correlations are expressed as functions of θ and ϕ, where θ is the angle between the directions of emission of the cascade γ rays, and ϕ the angle between the direction of the electric vector and the normal to the plane of the γ rays. The expected experimental direction-polarization correlation for a cascade is given by

$$W(\theta,\phi)=\eta_1(\phi)W_1(\theta,\phi)+\eta_2(\phi)W_2(\theta,\phi),$$

where $W_1(\theta,\phi)$ is the theoretical correlation when the polarization of one γ ray and the direction of the other are measured, and η_1 is the over-all efficiency of this measurement. $W_2(\theta,\phi)$ and η_2 are the corresponding quantities for the reverse measurement.

The γ-ray incident on the polarimeter is scattered preferentially in the plane perpendicular to its polarization. From the theoretical direction-polarization correlations, we calculate the ratio $N_\perp/N_\parallel$, where $N_\parallel$ is the number of γ rays scattered in the plane containing the γ rays of the cascade, and $N_\perp$ the number of γ rays scattered in the perpendicular plane.

The simplest case is presented by a cascade of only two γ rays. If, then, one γ ray is registered by the direction detector and the other enters the polarimeter, all the necessary information about the polarization of the other γ ray may be expressed by stating the intensities $W(\pi/2,\pi/2)$ and $W(\pi/2,0)$ in the linear polarizations parallel and perpendicular respectively to the plane containing the cascade γ rays.

$$N_\parallel=W(\pi/2,\pi/2)\times d\sigma_{\psi=0}+W(\pi/2,0)\times d\sigma_{\psi=\pi/2},$$
$$N_\perp=W(\pi/2,\pi/2)\times d\sigma_{\psi=\pi/2}+W(\pi/2,0)\times d\sigma_{\psi=0},$$

where $d\sigma_\psi$ is the differential cross section given by the Klein-Nishina formula for scattering of an incident quantum of energy k_0 through an angle δ, with an angle ψ between the direction of polarization of the incident γ ray and the plane of scattering.

$$d\sigma=\frac{e^4}{2m^2c^4}d\Omega\frac{k^2}{k_0^2}\left[\frac{k}{k_0}+\frac{k_0}{k}-2\sin^2\delta\cos^2\psi\right],$$

where k is the energy of the secondary quantum:

$$k=\frac{k_0}{1+(k_0/mc^2)(1-\cos\delta)}.$$

The ratio $R=d\sigma_{\psi=\pi/2}/d\sigma_{\psi=0}$ is a measure of the analyzing efficiency. Then, combining these expressions,

$$\frac{N_\parallel}{N_\perp}=\frac{p+R}{1+pR},\quad p=\frac{W(\pi/2,\pi/2)}{W(\pi/2,0)}.$$

Thus p is determined by the theoretical direction-polarization correlation for the decay-scheme investigated and R is determined by the geometry of the polarimeter and the energy of the γ ray. Measurements with polarized γ rays from oriented Mn^{54} nuclei[3] have given one experimental value of $R=1.9$ for γ rays of 0.85 Mev.

An average scattering angle of $\delta=80°$ has been chosen which gives R its maximum value, when the incident γ-ray energy is about 1 Mev.

In the case of several γ rays of the same or of different cascades entering the polarimeter, one has to work out completely the values of $N_\parallel$ and $N_\perp$ from the known values of the differential Compton cross sections for each energy and from the values of $W(\theta,\phi)$ for each correlation involved.

* This work was performed during the tenure of an I.C.I. Research Fellowship. Now at the Ecole Normale Supérieure, Paris, France.

[1] F. Metzger and M. Deutsch, Phys. Rev. **78**, 551 (1950).

[2] D. L. Falkoff, Phys. Rev. **73**, 518 (1948); D. R. Hamilton, Phys. Rev. **74**, 782 (1948); S. P. Lloyd, Phys. Rev. **88**, 906 (1952). L. C. Biedenharn and M. E. Rose, Revs. Modern Phys. **25**, 729 (1953).

[3] Bishop, Daniels, Durand, Johnson, and Perez, Phil. Mag. **45**, 1197 (1954).

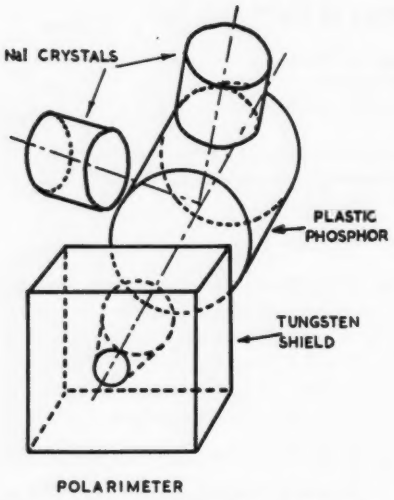

FIG. 1. Schematic diagram of the polarimeter.

APPARATUS

The instrument consists of a direction detector and a polarimeter. The polarimeter is composed of three scintillating phosphors and photomultiplier tubes situated behind a 5-cm thick tungsten collimator (Fig. 1). The center phosphor (channel 3) into which the γ-ray beam is collimated is a cylinder of polystyrene activated with diphenyl tetrabutadiene. The dimensions are varied according to γ-ray energy since double scattering within this phosphor must be minimized. For γ rays of 100-kev energy or less, the diameter was $1\frac{1}{4}$ inches and the height $1\frac{1}{2}$ inches. For higher energies, a diameter of 2 inches and height of 2 inches were adopted. With these dimensions, not more than 15 percent of the scattered γ rays will undergo secondary scattering before escaping to the side counters (channels 1 and 2). The side phosphors are 1-inch cubes of NaI (Tl activated). One is situated in the plane containing the γ rays of the cascade, the other is situated in the perpendicular plane.

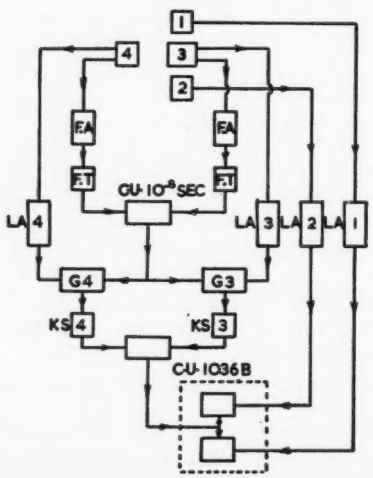

FIG. 2. Block diagram of the electronic apparatus. *F.A.*—fast amplifier. *F.T.*—fast sensitive trigger. *C.U.*—coincidence unit. *L.A.*—linear amplifier Harwell type 201. *G.*—gate. *K.S.*—kick-sorter. For simplicity the scalers and E.H.T. supplies are not shown.

All phosphors are surrounded with a diffusely reflecting shield of TiO_2 paint. The direction counter (channel 4) consisted of a cylinder of NaI (Tl activated) $1\frac{1}{2}$ inches in diameter and $1\frac{1}{2}$ inches in length. The direction of one γ ray in a cascade was determined with this detector and the polarization of the other in the polarimeter.

The over-all efficiency of direction-polarization measurements is small and if reasonable counting rates are to be maintained, strong sources of γ rays must be used. In this case, the average counting rates of channels 3 and 4 are large, and a short resolving time must be introduced to reduce the number of random coincidences. Figure 2 is a block diagram of the apparatus.

Channels 3 and 4 were made of E.M.I. (6262) 14 stage photomultipliers with a fast saturated signal taken from each collector and mixed in a short resolving time coincidence circuit. Proportional signals were taken from the ninth dynodes of the photomultipliers in channel 3 and channel 4. They were amplified linearly and fed through gates opened by the output of the coincidence circuit. Once through the gate, these pulses are fed into single-channel kick-sorters. The two pulses thus obtained are coincident within the resolving time and each corresponds to a chosen γ ray.

For the annihilation quanta emitted by a source of Na^{22}, a resolving time of 5×10^{-9} sec was obtained with NaI crystals on both channels. A resolution of 7 percent was found given by the width of the photoelectric peak at half the maximum counting rate on the peak.

The output pulses corresponding to the desired events in channels 3 and 4 were then fed to a modified Harwell 1036 *B* type coincidence unit, where the number of coincidences of channels 3 and 4 with either channel 1 or channel 2 was measured simultaneously (3×10^{-7} sec resolving time).

The experimental selection of the γ ray which is measured in the polarimeter can be achieved by making use of the fact that the polarimeter is a crude Compton spectrometer. As an example, we show in Fig. 3 that the differential pulse height spectrum in channel 3 due to recoil Compton electrons in the plastic phosphor for the γ rays of Sr^{88} shows two Compton edges. Each recoil Compton electron is accompanied by a scattered γ ray. Those recoil Compton electrons which are accompanied by a scattered γ ray detected in channel 1 or 2 have a reasonably well-defined energy. This is shown (Fig. 4) by the differential pulse height spectrum of those pulses in channel 3 which are in coincidence with pulses in channel 1 or 2.

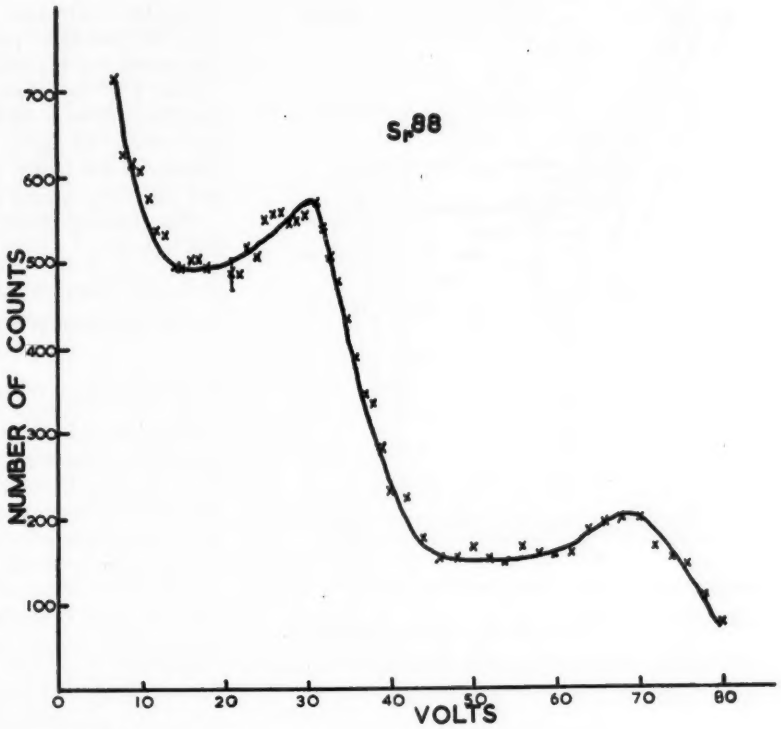

FIG. 3. The differential pulse height spectrum due to recoil electrons in the plastic phosphor from the γ rays of Sr^{88}.

EXPERIMENTAL RESULTS

Ce^{140}

One of the nuclei studied was Ce^{140}. La^{140} decays by complex β^- spectrum to various excited states of Ce^{140}. The γ-ray energies as determined by several authors[4–6] are in good agreement. They do not allow however a final conclusion as to the decay scheme. We have made measurements of noncoincident and coincident spectra and also of the angular correlations of those γ rays to which we could hope to assign parities by direction-polarization correlation measurements. They are the γ rays of 0.328, 0.485, 0.815, 1.60 Mev energy traced in heavy lines on Fig. 5. We found they fitted well into the scheme proposed by Peacock *et al.*[4] (Fig. 5).

Different spin and parity assignments have been given for the first excited states. Robinson and Madansky[7] gave a spin 2 for the 1.60-Mev level, a spin 4 for the 2.41 Mev level. Roggenkamp *et al.*, as quoted in Hollander, Perlman, and Seaborg,[8] gave a 1^+ assignment to the 1.60 Mev level, a 3^+ assignment to the 2.41-Mev level.

[4] Peacock, Quinn, and Oser, Phys. Rev. **94**, 372 (1954).
[5] Cork, Stoddard, LeBlanc, Branyan, Martin, and Childs, Phys. Rev. **83**, 856 (1951).
[6] Beach, Peacock, and Wilkinson, Phys. Rev. **76**, 1624 (1949).
[7] B. L. Robinson and L. Madansky, Phys. Rev. **84**, 1067 (1951).
[8] Hollander, Perlman, and Seaborg, Revs. Modern Phys. **25**, 469 (1953).

(*a*) *Angular Correlations*

The angular correlations were first measured. In order to measure the correlation between the 0.815-Mev and 1.60-Mev γ rays, the γ rays of lower energy were biased off. One inch cube NaI crystals were used at a distance of 15 cm from the source. Corrections were applied for the finite solid angles of the detectors and the data were reduced by a least squares analysis. This

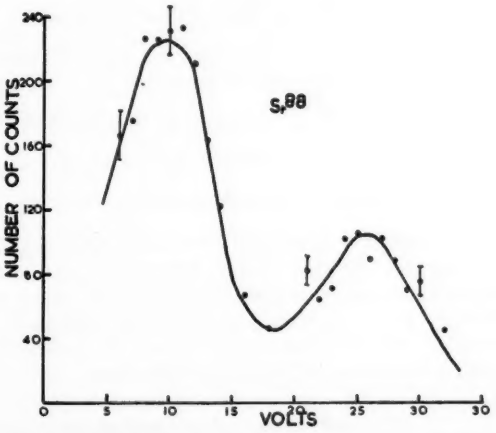

FIG. 4. The differential pulse height spectrum due to recoil electrons which are in coincidence with scattered γ rays detected in the side channels of the polarimeter.

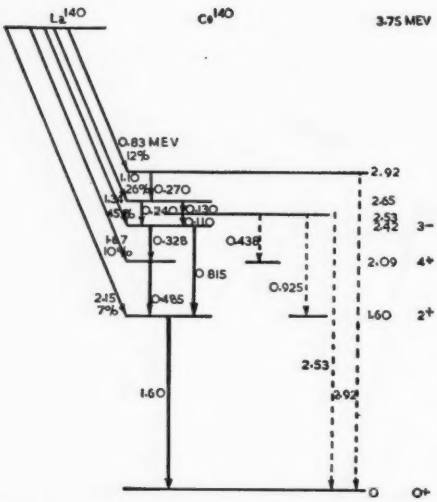

FIG. 5. The decay scheme of La^{140}. The γ rays studied in the present experiments are indicated by heavy lines.

measurement, corrected for geometry, gave:

$$W(\theta)=1-(0.0745\pm0.019)P_2+(0.013\pm0.024)P_4.$$

The result is consistent with either a 3, 1, 0 or a 3, 2, 0 scheme for which the correlation is:

$$W(\theta)=1-0.0714P_2.$$

Next, the angular correlation between the 0.485-Mev and 1.6-Mev γ rays was measured. The 0.485-Mev γ ray was selected by placing the kicksorter channel on the corresponding photoelectric peak in the coincidence spectrum. The observed correlation was than corrected for the fraction of the 0.815 Mev–1.6 Mev cascade also accepted, since the channel includes part of the Compton spectrum of the 0.815-Mev γ ray.

The uncorrected correlation was found to be

$$W(\theta)=1+(0.050\pm0.012)P_2+(0.016\pm0.015)P_4.$$

This becomes, after correction for the 0.815-Mev Compton distribution and for geometry,

$$W(\theta)=1+(0.083\pm0.015)P_2+(0.021\pm0.019)P_4.$$

This result is consistent with a 4, 2, 0 scheme for which

$$W(\theta)=1+0.102P_2+0.009P_4.$$

Combining the results for the two measured angular correlations, we have a spin scheme 3, 4, 2, 0. The angular correlation between the 0.328-Mev and 1.60-Mev γ rays (without observing the intermediate radiation of 0.485 Mev) could be used to confirm the result but this was not measured separately.

(b) *Direction-Polarization Correlations*

The direction-polarization correlations were then measured. Biases were set to accept the 0.328-Mev, 0.485-Mev, 0.815-Mev γ rays in the polarimeter and only the 1.60-Mev γ ray in the directional counter. The reason for this choice is the following.

Since Ce^{140} is an even-even nucleus, it is probable that the parities of the levels with spin 4 and spin 2 are both even. The parity of the level with spin 3 is less certain. If the parity were odd, both the 0.328-Mev and 0.815-Mev γ rays would be $E1$.

The expected direction-polarization correlations in this case, are

$$(0.815\text{–}1.60)\text{Mev}: W(\theta,\phi)=1-0.0714(P_2+\tfrac{1}{2}\cos2\phi P_2^2),$$

$$(0.485\text{–}1.60)\text{Mev}: W(\theta,\phi)=1+0.102(P_2-\tfrac{1}{2}\cos2\phi P_2^2)+0.009[P_4+\tfrac{1}{12}\cos2\phi P_4^2],$$

$$(0.328\text{–}1.60)\text{Mev}: W(\theta,\phi)=1-0.1403(P_2+\tfrac{1}{2}P_2^2\cos2\phi).$$

With the odd parity for the third excited level, the polarization-dependence for each of these cascades is of the same sign. If, however, the parity of the third excited state is even, then the coefficients of P_2^2 for the first and third cascades change sign, and thus the polarization dependence of these cascades is opposite in sign to that of the second cascade.

In the latter case, the direction-polarization correlation would be smaller than in the first case.

In order to calculate the expected ratios $N_\perp/N_\parallel$, it was necessary to know the relative intensities of the γ rays. They were investigated by several authors[4,9–11] with quite different results, as shown in Table I.

The relative intensities obtained from the pulse height spectra and the coincidence experiments which we made agreed well with the results of Bannerman *et al.*[9]

The various possibilities are given in Table II. If the other values quoted for the relative intensities of the γ rays are used, the calculated values for the last six schemes are less than unity. The calculated value for the first two schemes is not altered very much.

The experimental result found was

$$N_\perp/N_\parallel=1.077\pm0.022.$$

This is consistent with either 3^-, 4^+, 2^+, 0^+ or 3^+, 4^-, 2^-, 0^+. From the Goldhaber-Sunyar rule which would give 2^+ for the first excited state, and 4^+ for the second

TABLE I.

	0.328 Mev	0.485 Mev	0.815 Mev	1.60 Mev
Bannerman *et al.*[a]	5	39	29	100
Rall *et al.*[b]	3	6	13	100
Miller *et al.*[c]	1	10	20	100
Peacock *et al.*[d]	10	10	10	100

[a] See reference 9.
[b] See reference 10.
[c] See reference 11.
[d] See reference 4.

[9] Bannerman, Lewis, and Curran, Phil. Mag. 42, 1097 (1951).
[10] W. Rall and R. G. Wilkinson, Phys. Rev. 71, 321 (1947).
[11] L. C. Miller and L. F. Curtiss, Phys. Rev. 70, 983 (1946).

excited state, we can expect that the first possibility is the correct one.

Support for this scheme is found by calculating the *ft* values for the β^- transitions from the ground state of La^{140} using the relative intensity measurements (Fig. 5). The parity of the ground state of La^{140} is likely to be odd according to the shell model. Thus a change of parity is necessary for those transitions leading to the 4^+ and 2^+ levels and no change for that leading to the 3^- level. The *ft* values from Moszkowski's tables are 9.7(2.15 Mev), 8.6(1.67 Mev), and 7.5(1.34 Mev). Thus the transition to the 3^- level seems to be more favored.

Sr^{88}

The second nucleus studied was Sr^{88}. The decay scheme[12,13] (Fig. 6) shows that two γ rays are emitted in cascade following K-capture and β^+ emission of Y^{88}. A cross-over γ ray occurs in 2 percent of the transitions. The source of Y^{88} was prepared by the reaction $Sr^{88}(d,2n)Y^{88}$ on the cyclotron of Birmingham University.

(*a*) *Angular Correlations*

The angular correlation of the γ rays was first measured in order to confirm the spin assignments given to the levels by Steffen.[14] The results were consistent with either a 3, 2, 0 or 3, 1, 0 decay scheme. This leads to 8 possible schemes differing in assignments of spin or parity. From the results of the direction-polarization correlation experiment, which is discussed below, all but 2 could be eliminated.

(*b*) *Direction-Polarization Correlations*

Then, the direction-polarization correlations of the γ rays were measured.

The values of the coefficients η_1 and η_2 could be varied by altering the biases on both counters. Two measurements were made, firstly with $\eta_2=0$ by biasing channel 4 above the 0.91-Mev γ ray and secondly with both channels 3 and 4 at zero bias. However, for the latter conditions, η_1 and η_2 are still different since the over-all efficiency is a function of γ-ray energy.

TABLE II.

Schemes	Calculated effects for a point geometry	Calculated effects for our geometry
$3^-, 4^+, 2^+$ / $3^+, 4^-, 2^-$	$N_\perp/N_{\parallel}=1.21$	$N_\perp/N_{\parallel}=1.09$
$3^+, 4^+, 2^+$ / $3^-, 4^-, 2^-$	$N_\perp/N_{\parallel}=1.05$	$N_\perp/N_{\parallel}=1.02$
$3^-, 4^-, 2^+$ / $3^+, 4^+, 2^-$	$N_\perp/N_{\parallel}=0.90$	$N_\perp/N_{\parallel}=0.95$
$3^+, 4^-, 2^+$ / $3^-, 4^+, 2^-$	$N_\perp/N_{\parallel}=0.88$	$N_\perp/N_{\parallel}=0.95$

[12] W. C. Peacock and J. W. Jones, U. S. Atomic Energy Commission Declassified Document AECD 1812, March 1948 (unpublished).

[13] R. T. Overman, U. S. Atomic Energy Commission Report AECD 354 (unpublished).

[14] R. M. Steffen, Phys. Rev. **90**, 321 (1953).

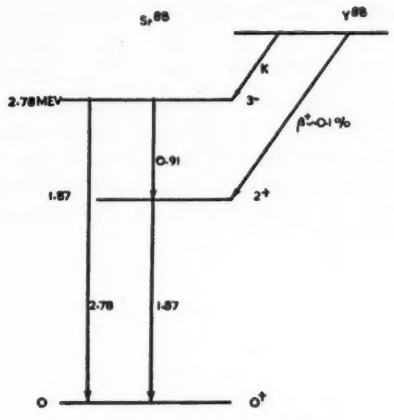

FIG. 6. The decay scheme of Y^{88}.

W_1 and W_2 are given by:

$$W(\theta,\phi)=1-0.0714[P_2(\cos\theta)\pm\tfrac{1}{2}\cos 2\phi P_2^2(\cos\theta)],$$

with the plus sign for W_1, and the minus sign for W_2.

With no energy discrimination, the observed normalized ratio was

$$N_\perp/N_{\parallel}=1.033\pm0.016.$$

Various possibilities for the decay scheme would give the following values of $N_\perp/N_{\parallel}$ (0^+ is assumed for the ground state of the even-even nucleus Sr^{88}):

$3^-\,1^+\,0^+$, $3^-\,2^+\,0^+$: 1.04

$3^-\,1^-\,0^+$, $3^-\,2^-\,0^+$: 0.96

$3^+\,1^+\,0^+$, $3^+\,2^+\,0^+$: 0.91

$3^+\,1^-\,0^+$, $3^+\,2^-\,0^+$: 1.09.

The result is thus most consistent with the 3^-, 2^+, 0^+ or 3^-, 1^+, 0^+ scheme.

With $\eta_2=0$, the normalized value for the observed ratio was

$$N_\perp/N_{\parallel}=1.083\pm0.024.$$

The expected ratios would be:

0.91 Mev being an $E1$ or $M2$: 1.07

0.91 Mev being an $M1$ or $E2$: 0.94.

Thus the 0.91-Mev γ ray must be $E1$ or $M2$, the 1.87-Mev γ ray $E2$ or $M1$, and the decay scheme of Sr^{88} must be 3^-, 2^+, 0^+ or 3^-, 1^+, 0^+.

The internal conversion coefficient for the 0.91-Mev transition has been determined by Peacock and Jones[12] ($\alpha_K=27\times10^{-5}$) and Metzger and Amacher[15] [α_K

[15] F. R. Metzger and H. C. Amacher, Phys. Rev. 88, 147 (1952).

$=(34\pm7)\times10^{-5}$]. The theoretical values are:

	$E1$	$E2$	$M1$	$M2$
$\alpha_K\times10^{+5}=$	28	68	66	165.

Both results are nearest to the coefficient of $E1$. The direction-polarization correlation measurements exclude $E2$ and $M1$. With these latter results, one is only left with a choice between $E1$ and $M2$ which puts the decision for $E1$ beyond any doubt. The decay scheme of Sr^{88} is then 3^-, 2^+, 0^+.

The authors wish to thank Professor H. Halban for his continued encouragement and advice, and Miss Goldschmidt for her assistance in the construction of the apparatus and in the early stages of the measurements.

We are also indebted to the Birmingham cyclotron group for providing us with the yttrium source. We are very grateful to Professor Lord Cherwell for allowing us to use the facilities of his laboratory.

PHYSICAL REVIEW VOLUME 98, NUMBER 1 APRIL 1, 1955

Iridium-194†

C. E. MANDEVILLE, JAGDISH VARMA,* AND BABULAL SARAF‡
Bartol Research Foundation of The Franklin Institute, Swarthmore, Pennsylvania

(Received December 14, 1954)

Electromagnetically enriched quantities of Ir^{193} were exposed for time intervals ranging from 0.5 to 2.0 hr on five successive occasions in the Brookhaven pile. The 19-hour Ir^{194} was found to emit gamma rays of energies 0.295, 0.325, 0.635, 0.640, 0.93, 1.14, 1.28, 1.45, 1.58, 1.77, and ~2.00 Mev. By coincidence studies, cascade relationships were established between ten pairs of gamma rays. The first and second excited states of the residual nucleus were located at 325 and 620 kev. The angular correlation function of the 0.295 Mev—0.325 Mev cascade was measured and found to correspond to a $2\rightarrow2\rightarrow0$ distribution, thus giving the spins of the first two excited states of Pt^{194}.

INTRODUCTION

THE 19-hour Ir^{194} has been shown on several previous occasions[1–10] to emit hard beta rays and gamma rays. It has been generally agreed that all but a few percent of the beta rays are contained in a very hard spectrum of maximum energy ~2.2 Mev. Beta-gamma coincidences have been detected,[6] showing the presence of at least one inner beta spectrum which is followed by gamma rays. Until recently,[10] only three gamma rays had been shown to be definitely related to the 19-hour period, a relatively hard one of energy ~1.4 Mev[6] and softer gamma rays at 0.3275 Mev[5–8] and 0.290 Mev.[9] Gamma rays at energies of 1.7 Mev and more have been suggested by the photodisintegration of beryllium and deuterium.[7] A far more complex gamma spectrum has been of late indicated in scintillation counter studies[10] wherein quantum energies of 0.32, 0.61, 1.18, 1.45, and ~1.8 Mev with relative intensities of 100, 22, 10, 5, and 1.2 were reported.

To investigate further the radiation characteristics and decay scheme of Ir^{194}, samples of metallic iridium of weight about 10 mg, isotopically concentrated[11] in Ir^{193}, were exposed on five successive occasions in the Brookhaven pile. The times of irradiation varied from 0.5 hour to 2 hours, and measurements were commenced at a time not exceeding twenty hours after removal of the exposed target material from the reactor and were continued in each case for a period of about three days. The gamma-ray spectrum of Ir^{194} was observed in sodium iodide scintillation spectrometers, and gamma-gamma coincidence data were obtained with two such spectrometers in coincidence. One sodium iodide detector was replaced by an anthracene counter to measure the beta spectra and observe beta-gamma coincidences.§

† Assisted by the joint program of the Office of Naval Research and the U. S. Atomic Energy Commission.

* Research Fellow, Bartol; at present at the University of Glasgow, Scotland.

‡ Research Fellow, Bartol; at present at the Nobel Institute of Physics, Stockholm, Sweden.

[1] Alichanian, Alichanow, and Dzelepow, Physik Z. Sowjetunion **10**, 78 (1936).

[2] McMillan, Kamen, and Ruben, Phys. Rev. **52**, 375 (1937).

[3] C. M. Witcher, Phys. Rev. **60**, 32 (1941).

[4] C. E. Mandeville and H. W. Fulbright, Phys. Rev. **64**, 265 (1943).

[5] L. J. Goodman and M. L. Pool, Phys. Rev. **71**, 288 (1947).

[6] C. E. Mandeville and M. V. Scherb, Phys. Rev. **73**, 1434 (1948).

[7] Richard Wilson, Phys. Rev. **79**, 1004 (1950).

[8] Cork, LeBlanc, Stoddard, Childs, Banyan, and Martin, Phys. Rev. **82**, 258 (1951).

[9] Baker, Bleuler, and Steffen, Purdue University Progress Report. II, June, 1952, quoted by Hollander, Perlman, and Seaborg, Revs. Modern Phys. **25**, 469 (1953).

[10] F. D. S. Butement and A. J. Poe, Phil. Mag. **45**, 31 (1954).

[11] On comparing the ratio of the activity of Ir^{194} to that of Ir^{193} in an isotopic target with the same ratio for a sample of normal elemental iridium, it was possible to conclude that the concentration of Ir^{193} was greater than 90 percent.

§ *Note added in proof.*—Since this article was submitted for publication, a paper by Johns and Nablo, Phys. Rev. **96**, 1599 (1954), has appeared. They report sixteen gamma rays from Ir^{194}, having resolved several additional quanta at high energies.

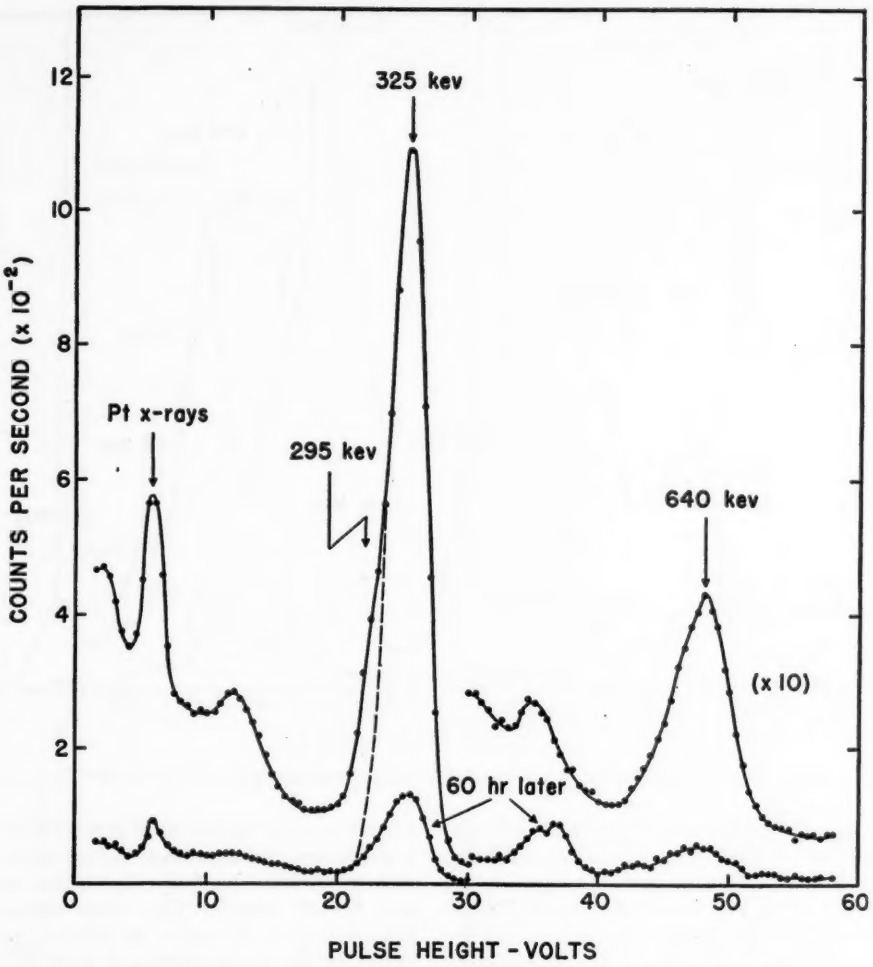

FIG. 1. Pulse height distribution in NaI(Tl) of the softer gamma rays of the 19-hour Ir^{194}.

GAMMA-RAY SPECTRA

The region of relatively low quantum energies was explored by placing before a scintillation counter a source of Ir^{194} with an intervening absorber equivalent to about 1.2 g/cm² of aluminum. The gamma-ray spectrum thus obtained is shown in Fig. 1. To examine the nature of the spectrum at higher energies, absorbers of 14 g/cm² of lead and 1.35 g/cm² of cadmium were interposed. The resulting data are shown in Fig. 2. From the two sets of curves and the indicated rate of decay of the ordinate values, it may be concluded that the observed gamma rays can be attributed to the nineteen hour Ir^{194}. Gamma-ray peaks are clearly present with quantum energies of 0.325, 0.640, 0.930, 1.14, 1.45, 1.77, and ~2.0 Mev. It is furthermore to be noted that deformations appear in the spectrum in the vicinity of 1.28 and 1.58 Mev. It will be later shown that the possibility of the presence of quanta of these energies is indicated by the proposed disintegration scheme. Another distortion appears at 295 kev. Coincidence studies to follow show that a gamma ray of that energy is also present in the decay of Ir^{194}. It should be pointed out that the 640-kev peak is sufficiently wide to suggest complexity. The quantum energies and relative intensities of the gamma rays of Ir^{194} are summarized in Table I.

COINCIDENCE MEASUREMENTS

A series of coincidence studies were carried out to determine the cascade relationships between the various gamma rays. In Fig. 3A are shown the curve of the single counting rate near 325 kev and the coincidence rate in that region with one detector set at the 640-kev peak. A similar set of curves is shown in Fig. 3B. To obtain this curve of coincidences, one detector was set on the high-energy side of the 325-kev peak while the other was moved through the region of lower energies

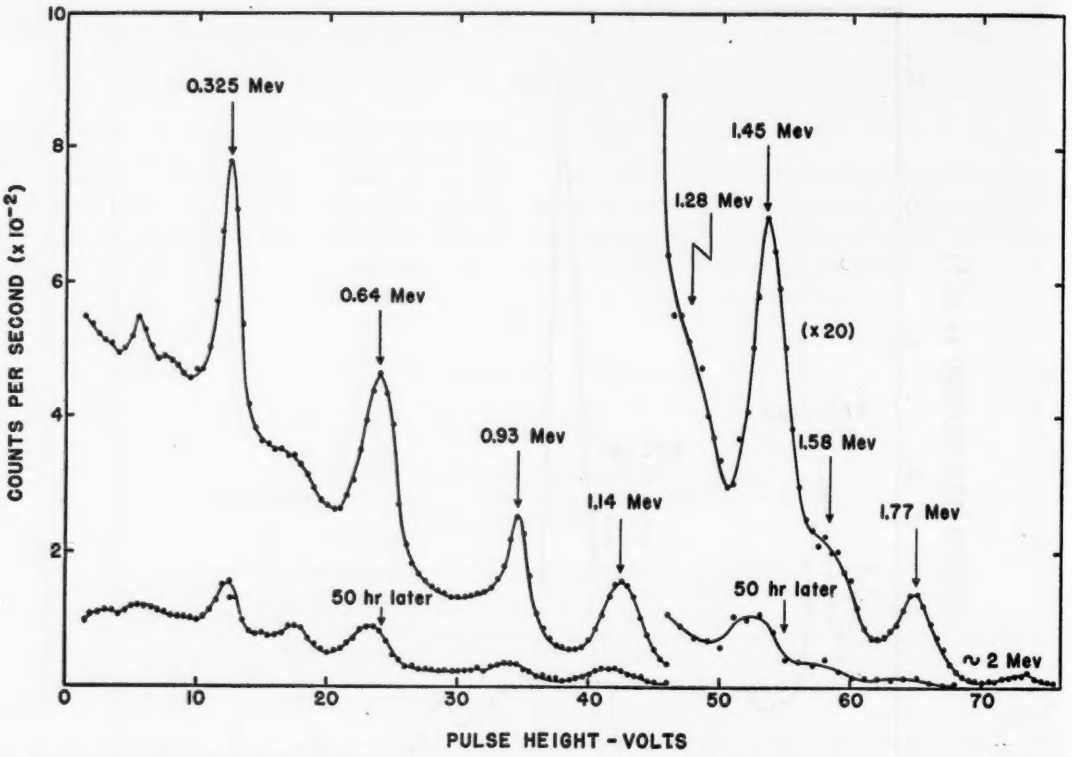

FIG. 2. Pulse height distribution of the gamma rays of Ir^{194} as observed through pre-absorption of 14 g/cm² of Pb and 1.35 g/cm² of Cd.

to locate a second gamma ray at precisely 295 kev. Returning to Fig. 3A, it is now clear that both a 295-kev gamma ray and a 325-kev gamma ray, which are themselves in cascade, are coincident with the 640-kev radiation. In Fig. 4A and 4B are plotted, along with the curves of single counts, coincidences in the neighborhood of 325 kev with one detector fixed at 1.14 Mev and 0.930 Mev, respectively. On comparing the widths of the coincidence peaks with those of the curves of single counts, it is clear that the 295-kev radiation is non-coincident with the two hard gamma rays. In Fig. 5A is shown the coincidence rate in the vicinity of 640 kev with one channel fixed to count pulses from the 295- and 325-kev quanta. This curve indicates that all gamma rays in the region of 640 kev are coincident with the two above-mentioned gammas. In Fig. 5B are shown coincidences in the region of 640 kev with one channel fixed on the high-energy side of the photo-peak of single counts. It will be noted that the observations of coincidences lie upon the curve of single counts, denoting little difference in the energies of the two or more gamma rays of energy ~640 kev which give rise to the coincidence rate.

TABLE I. Energies and relative intensities of the gamma rays of the 19-hour Ir^{194}.*

Quantum energies (Mev)	Relative intensities
0.295	...
0.325	100
0.635, 0.640	10
0.93	7.6
1.14	8.5
1.28	...
1.45	1.8
1.58	...
1.77	0.9
2.00	0.2

* The estimates of relative intensities are those obtainable from the data of Figs. 1 and 2. Earlier investigations (see reference 9) have shown the 0.295-Mev gamma ray to have an intensity one-fifth as great as that of the 0.325-Mev radiation.

DISINTEGRATION SCHEME

Returning to the spectrum of Fig. 1, it can be shown that no other gamma ray present has an intensity approaching that of the 325-kev line. This fact remains true though the intensity of any one of the other gamma rays might be increased by an amount sufficient to take into account the presence of all the x-radiation if it is assumed produced by internal conversion of the particular gamma ray. Thus, for reasons of intensity, the 325-kev transition must originate at the first excited state of Pt^{194}. The 295-kev gamma ray has been previously shown to have an intensity one-fifth[9] as great as that of the 325-kev quantum. Since the

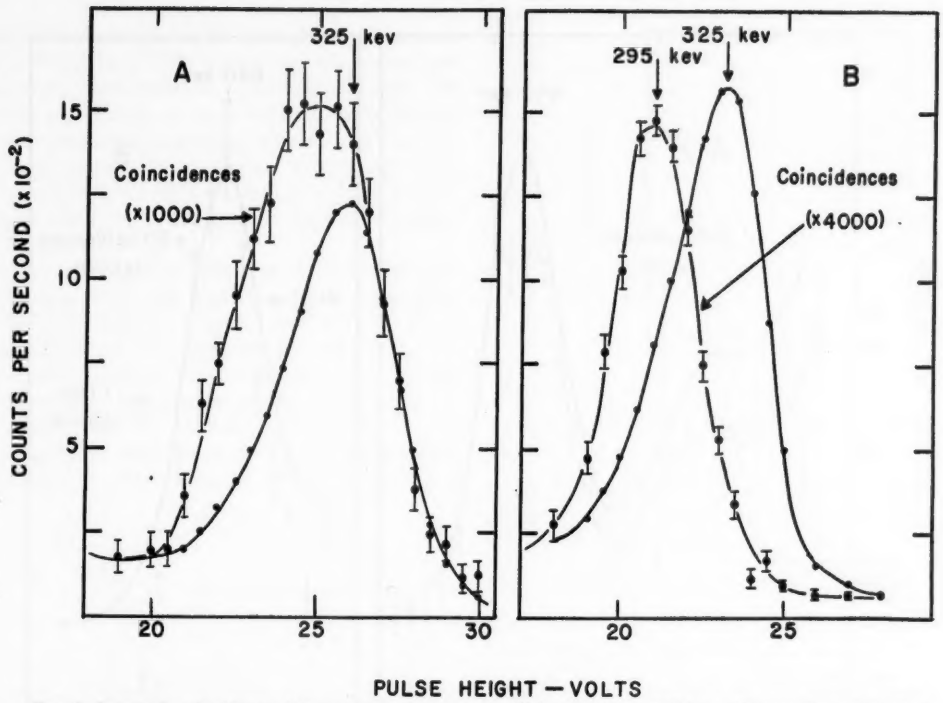

FIG. 3. Curves A, coincidences between gamma rays at ~640 kev and at ~325 kev with one channel fixed at ~640 kev. Curves B, coincidences between 325-kev and 295-kev gamma rays with one channel fixed on high-energy side of 325-kev peak.

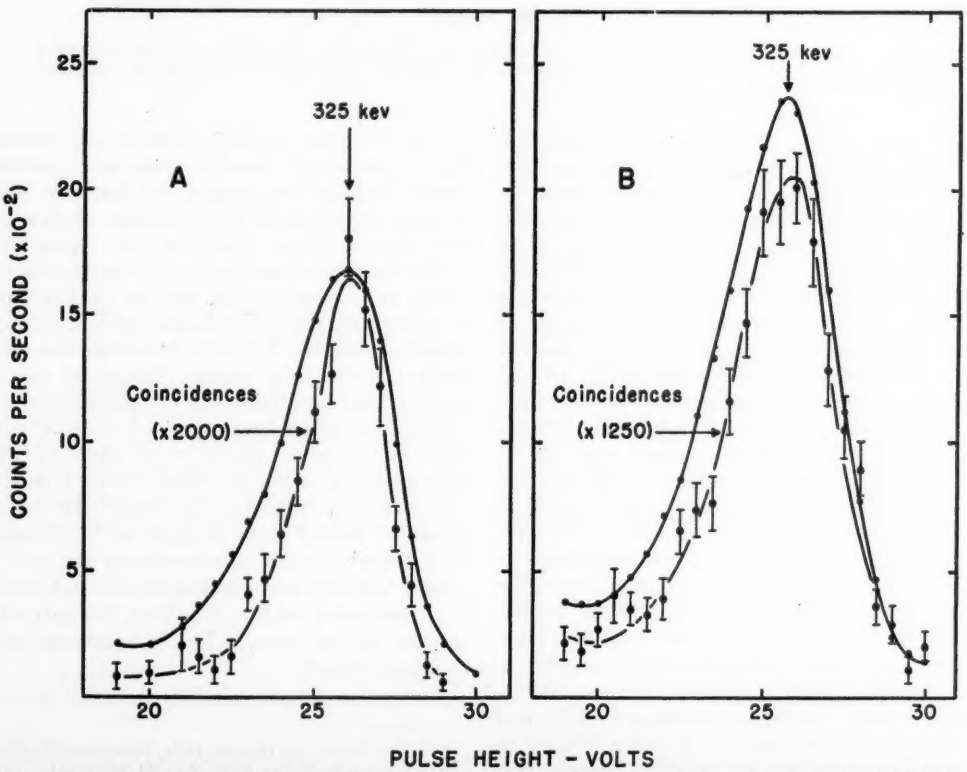

FIG. 4. Curves A, coincidences between 325-kev radiation and the 1.14-Mev line with one channel fixed at 1.14 Mev. Curves B, coincidences between 325-kev radiation and the 0.93-Mev gamma ray with one channel fixed at 0.93 Mev.

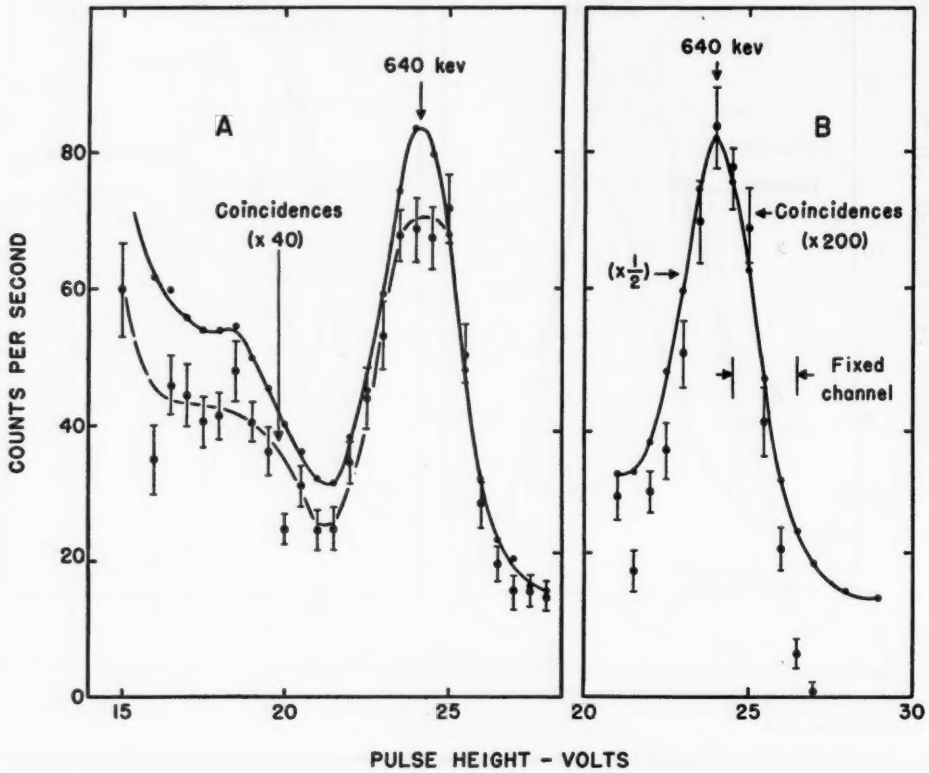

FIG. 5. Curves A, coincidences between 325-kev radiation and 640-kev peak with one channel fixed at 325 kev. Curves B, coincidences between gamma rays in the region of 640 kev with one channel fixed on the high-energy side of the 640-kev peak.

composite peak at 640 kev has one-tenth of that intensity (see Table I), it must be assumed that the level from which the 295-kev line is emitted must be fed by more beta rays than any level other than the first excited state. Thus, the 295-kev radiation is emitted from the second excited state. The 635-kev→295-kev→325-kev cascade was established from the data of Fig. 3A. Figure 4B indicates the 935-kev→325-kev cascade; so the third excited state is located at about 1.25 Mev. The coincidences of Fig. 4A and the absence of coincidences between the 1.14-Mev gamma ray and any quanta other than the 325-kev radiation show that the fourth excited state lies at ~1.465 Mev above the ground state. Though the data have not been depicted in any figure, it was found that the 1.45-Mev radiation is coincident only with 325-kev quanta. Thus the fifth excited state must lie at ~1.775 Mev. By observation of coincidences between the 640-kev radiation and the 930-kev quanta, the sixth excited state was placed at 1.895 Mev. Moreover, the 640-kev→635-kev cascade studied in Fig. 5B is consistent with a 640-kev→930-kev cascade. Specific full-energy peaks corresponding to 1.58- and 1.28-Mev gamma rays were not detected because of their low intensities relative to other gamma rays present. However, the single counting-rate spectrum of Fig. 2, the general trend of coincidence curves, and energy considerations suggest the indicated positions in the decay scheme of Fig. 6. Because of these various uncertainties, these transitions are represented by broken lines. No coincidences between gamma rays of energy more than 1.6 Mev and the 325-kev quantum were detected. From this observation and from energy considerations, the 1.77-Mev transition was given its position in the decay scheme. Though no coincidence studies could be carried out in relation to the weak 2.0-Mev radiation, energy considerations evolving about the maximum energy of the hardest beta spectrum suggest it to proceed directly to the ground state.

Gamma rays of energies 328 and 291 kev have been reported[12] emitted in the decay of Au^{194}. The measured K/L ratios[12] for the two transitions are such as to suggest that both are of multipole order $E2$. Since Pt^{194} is an even-even nucleus ($I_g=0+$), the spin value of the first excited state is $2+$, in agreement with the Goldhaber rule.[13]

Earlier beta-gamma coincidence studies[6] have shown

[12] Steffen, Huber, and Humbel, Helv. Phys. Acta 22, 167 (1949).
[13] G. Scharff-Goldhaber, Phys. Rev. 90, 587 (1953).

that most of the beta rays of Ir^{194} proceed to the ground state of Pt^{194} in the 2.2-Mev spectrum whereas a few are coincident with gamma radiation. Though the results are not shown in any figures, beta-gamma coincidence measurements were carried out in the present investigation which showed three inner beta spectra of end points 1.88, 0.94, and 0.74 Mev, coincident respectively with the gamma rays of energies 0.325, 0.930, and 1.14 Mev.

To obtain information with regard to the second excited state of Pt^{194}, the spatial correlation function of the 295-kev→325-kev cascade has been studied. The channels of the two pulse-height analyzers were set at the photopeaks of the two gamma rays, one at the 325-kev peak, the other on the low-energy side of the same peak (see Fig. 1), and adjusted to give the maximum genuine coincidence rate. A two-volt width was employed in either channel. With one detector

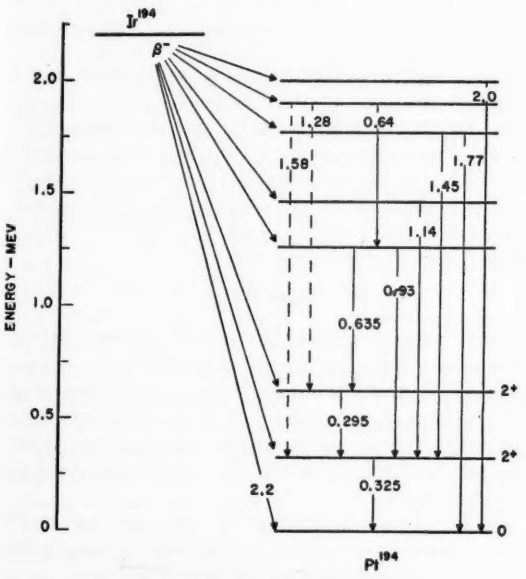

FIG. 6. Disintegration scheme of Ir^{194}.

fixed, the coincidence rates with the other at angles of 112.5°, 135.0°, 157.5°, and 180° with the axis of source and fixed detector were compared with the coincidence rate at 90° to measure any asymmetry. At least ten to twelve thousand true coincidences were obtained at each of the above listed angles. The experimentally

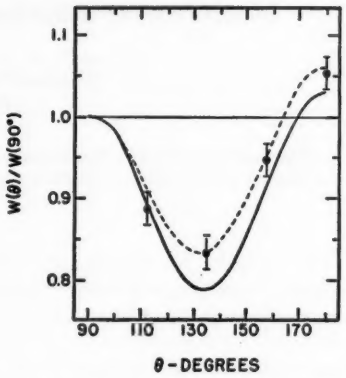

FIG. 7. Angular correlation function of the 295-kev—325-kev cascade.

determined asymmetries for the several angles of observation are shown in Fig. 7 along with a "least squares fit" (broken line) of quadratic form,

$$W(\theta)=1-0.725\cos^2\theta+0.787\cos^4\theta.$$

The theoretically expected correlation function for a 2→2→0, quadrupole-quadrupole transition is also shown, modified for the finite angular resolution of the detectors (half-angle 9.25°). The actual polynomial series, corrected for angular resolution, gives a correlation function of the form

$$W(\theta)=1-1.05\cos^2\theta+1.16\cos^4\theta.$$

The probable errors in the coefficients of the cosine terms are about five percent. The absolute values of the coefficients are not inconsistent with a pure quadrupole-quadrupole cascade. Because of the probable errors in the coefficients, the possibility of an $E2-M1$ mixture cannot be excluded. The deviation from the theoretically expected curve shown in Fig. 7 might also be explained by the presence of Ir^{192} and by coincidences between Compton recoils of high-energy gamma rays and photoelectrons of the quanta at 325 kev and 295 kev.

ACKNOWLEDGMENT

The writers wish to acknowledge the kind interest of Dr. W. F. G. Swann, Director of the Bartol Research Foundation. Two of them (J.V. and B.S.) wish to express appreciation for research fellowships granted them by the Bartol Research Foundation.

Measurement of the Scattering Constant in Nuclear Emulsion*

LYLE W. SMITH
Brookhaven National Laboratory, Upton, New York
(Received October 19, 1954)

The general solution to the diffusion equation is used to show that a measurement of track-to-track scattering of identical particles yields a value of the scattering constant in an unambiguous manner.

SINCE the operation of high-energy particle accelerators has made available well-collimated monokinetic beams of charged particles, several investigators[1–5] have reported measurements on the multiple Coulomb scattering of such particles. These measurements afford a calibration of the scattering constant in nuclear emulsion and allow a comparison with the predictions of the theory[6–8] as to the magnitude of the scattering constant and its variation with energy, cell length, etc. It is the purpose of this note to point out that such calibration experiments do not necessitate the use of an elaborate ultralinear microscope stage. Exposures may be made with suitable track densities so that the scattering of one track with respect to another of the same energy instead of with respect to a straight line gives the required information in an unambiguous manner.

We consider the form of the theory as developed by Scott and Snyder.[6] They show that the 3-point distribution in scattering-induced curvature is equivalent to the distribution in lateral displacement along a track, and we take their exact solution to the diffusion equation, subject only to the small angle approximation,

$$p(c|z)=\frac{z}{4\pi}\int_{-\infty}^{\infty}du\exp\left\{i\tfrac{1}{2}zcu-\frac{zh(u)}{\lambda u}\right\}, \qquad (1)$$

where $p(c|z)$ is the probability distribution of curvature c observed on a track of length z,λ is the mean free path for scattering and the exact form of the elementary scattering law is contained in $h(u)$. If we now denote by $P(c|z)$ the distribution in curvature deduced by the differences in lateral displacement between two identical tracks, then

$$P(c|z)=\int_{-\infty}^{\infty}dc_1p(c-c_1|z)p(c_1|z), \qquad (2)$$

and performing the indicated integrations, obtain

$$P(c|z)=\tfrac{1}{2}p(\tfrac{1}{2}c|2z). \qquad (3)$$

Averaging over c to determine the mean curvature, we have

$$\bar{C}(z)=2\bar{c}(2z), \qquad (4)$$

where $\bar{c}$ refers to curvature of a single track and $\bar{C}$ refers to relative curvature between two tracks. The quantity usually measured is the second difference, δ in lateral displacement y where $\delta=y_1+y_3-2y_2$ and the y_i are the lateral displacements at three equally separated points. Then $c=4\delta/X^2$, X being the separation between points or "cell length." Using this relation (with X respectively $2z$ and $4z$), we obtain

$$\bar{\Delta}(z)=\tfrac{1}{2}\bar{\delta}(2z), \qquad (5)$$

i.e., the average second difference $\bar{\Delta}$ as measured between two identical tracks is one-half the average second difference $\bar{\delta}$ of one track, twice as long, measured with respect to a straight line. It is to be noted that this result is independent of the exact form of the elementary scattering law and the initial angle between the two tracks.

Track to track scattering has been used previously for rough energy estimates[9] but the method is applicable to a good measurement of the scattering constant. In addition to the advantage of not requiring a precision microscope stage, noise due to emulsion distortion is essentially eliminated and the remaining noise due to reading errors is independent of cell length and is easily subtracted.

I am indebted to Dr. H. S. Snyder for some helpful conversations.

* This work was performed under the auspices of the U. S. Atomic Energy Commission.

[1] D. R. Corson, Phys. Rev. **84**, 605 (1951).
[2] L. Voyvodic and E. Pickup, Phys. Rev. **85**, 91 (1952).
[3] M. J. Berger, Phys. Rev. **88**, 59 (1952).
[4] K. Gottstein *et al.*, Phil. Mag. **42**, 708 (1951).
[5] Backus, Lord, and Schein, Phys. Rev. **88**, 1431 (1952).
[6] W. T. Scott and H. S. Snyder, Phys. Rev. **78**, 223 (1950).
[7] W. T. Scott, Phys. Rev. **85**, 245 (1952).
[8] G. Molière, Z. Naturforsch. **3a**, 78 (1948).

[9] See, e.g., Lord, Fainberg, and Schein, Phys. Rev. **80**, 970 (1950). *Note added in proof.*—M. Koshiba and M. F. Kaplon, Phys. Rev. **97**, 193 (1955), have also pointed out the advantages of track to track scattering and have used the method for energy measurements by assuming a Gaussian scattering distribution.

Example of τ^+-Decay in Flight*

J. R. BURWELL, R. W. HUGGETT, AND R. W. THOMPSON
Department of Physics, Indiana University, Bloomington, Indiana
(Received December 2, 1954)

A τ^+-meson, of 0.83 Bev/c, is observed to undergo normal decay in flight with $Q(3\pi)=73.9\pm5.8$ Mev. The center-of-mass kinetic energies are found to be $T'=24.3\pm1.8$ and 28.7 ± 1.8 Mev for the two positive pions and $T'=20.9\pm4.3$ Mev for the negative pion.

THE fact that the masses of the τ meson[1,2] ($965.5\pm0.7\ m_e$)[3] and of the θ^0 meson[4] ($966\pm10\ m_e$) are almost identical led to the conjecture[4] that the θ^0 meson might be a neutral counterpart of the $\tau^\pm$ meson. Preliminary evidence against this identification has appeared in the analysis of τ-decay data by Dalitz,[5] in which the theoretical dependence of the distribution of decay configurations on the τ-meson spin j and parity w is calculated and compared with experiment. The preliminary results rather suggest even j and odd w for the τ meson. On the other hand, the fact that the θ^0 meson probably undergoes 2π decay[6,7] requires $w=(-1)^j$, which is incompatible with $\theta^0\equiv\tau^0$. Thus there is preliminary evidence that the θ meson and the τ meson represent different K-particle families with almost identical masses.

However, as pointed out by Dalitz,[5,8] such conclusions cannot be more than tentative at the present time, in view of possible experimental bias in the nuclear emulsion where the majority of τ decays are recorded. The effects of such bias are rather prominent in the work on V^0-decay in the emulsions,[9] hence it is to be expected that bias will also be present in the τ-decay data, although to a lesser extent. Estimates of the bias might be made from geometrical considerations. An alternate procedure would be to make comparison between τ-decay data from emulsion and from magnetic cloud chamber, since the latter would be expected to be relatively unbiased.

In view of the limited number of τ decays which have been observed in the magnetic cloud chamber, it may therefore be worthwhile to publish an example of τ^+ decay in flight, observed in the large rectangular chamber,[4] which can be analyzed in detail. A photograph of the event, film *R*-366, is shown in Fig. 1. The τ^+, track 0, enters from the rear at an angle of 3.5° with the plane of the chamber. After traversing about $\frac{2}{3}$ of the illuminated height, it decays into two

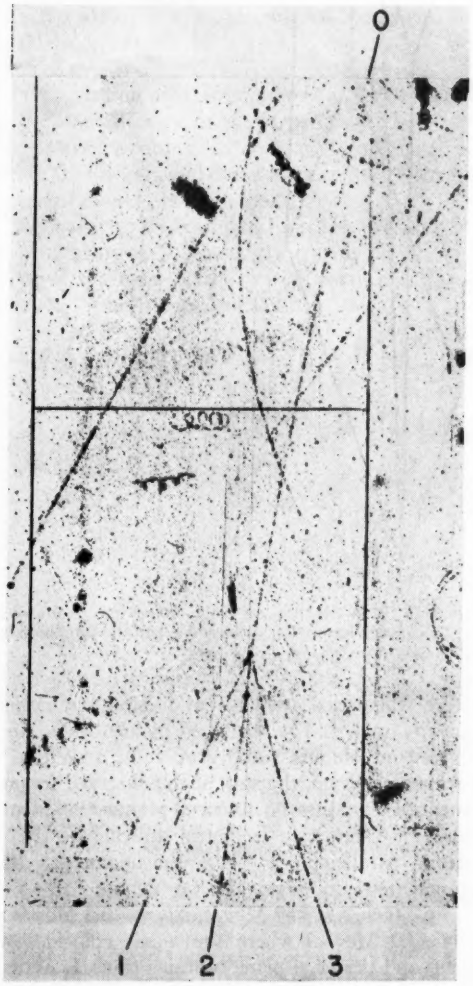

FIG. 1. Right eye view of film *R*-366, showing a τ^+ meson (track 0) disintegrating in flight into 3 pions (tracks 1, 2, and 3). Track 2 is that of the negative pion.

* Assisted by the U. S. Office of Ordnance Research and by grant of the Frederick Gardner Cottrell Fund of the Research Corporation.

[1] Brown, Camerini, Fowler, Muirhead, Powell, and Ritson, Nature **163**, 82 (1949).
[2] Amaldi, Baroni, Castagnoli, Cortini, and Manfredini, Nuovo cimento, **10**, 937 (1953).
[3] Proceedings of the Padua Conference, to be published in *Nuovo cimento*.
[4] Thompson, Buskirk, Etter, Karzmark, and Rediker, Phys. Rev. **90**, 329 (1953).
[5] R. H. Dalitz, Phys. Rev. **94**, 1046 (1954).
[6] Thompson, Burwell, Huggett, and Karzmark, Phys. Rev. **95**, 1576 (1954).
[7] Burwell, Huggett, and Thompson, Bull. Am. Phys. Soc. **29**, No. 7, 32 (1954).
[8] R. H. Dalitz (private communication).
[9] R. W. Thompson in *Progress in Cosmic-Ray Physics*. (North-Holland Publishing Company, Amsterdam, to be published), Vol. 3, Chap. 5.

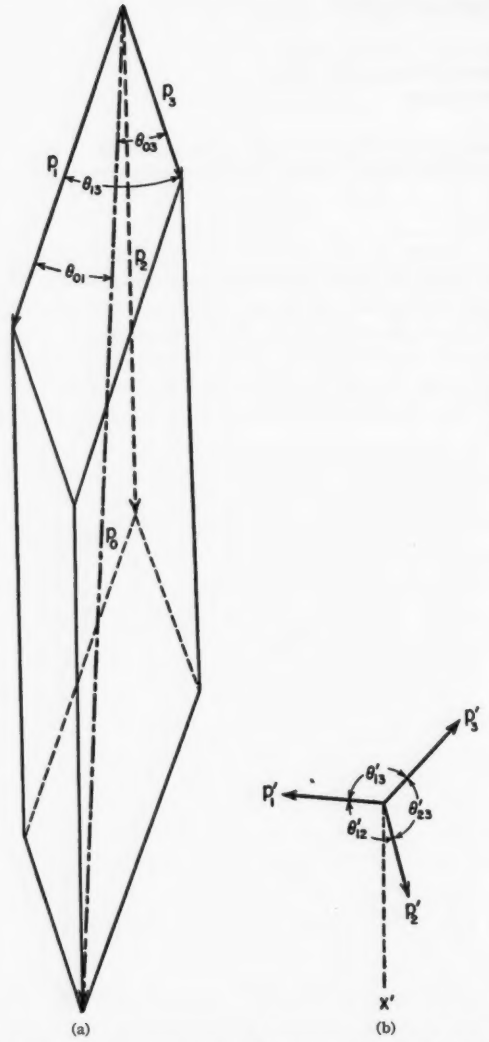

FIG. 2. (a) Isometric drawing of the momentum parallelopiped in the laboratory frame. (b) τ-decay configuration in the center-of-mass system.

positive fragments, tracks 1 and 3, and a negative fragment, track 2. The measured momenta and angles are given in columns 1 and 2 of Table I. Within the experimental errors, the sum of the observed fragment momenta is equal to the observed primary momentum. Figure 2(a) shows an isometric drawing of the momentum parallelopiped, with the momenta drawn approximately to scale. If we denote $\Delta\mathbf{p}=\mathbf{p}_1+\mathbf{p}_2+\mathbf{p}_3-\mathbf{p}_0$, then $\Delta p_x=69$ Mev/c, $\Delta p_y=-0.3$ Mev/c and $\Delta p_z=-3.0$ Mev/c; where the x-axis coincides with track 0 and the (x,y)-plane contains track 1. Actually, the measurements on track 2 are not altogether satisfactory from the point of view of scatter in the comparator plots and of agreement between the three stereoscopic views. Thus, uncertainty in track 2 may easily account for the residual momentum in the x-direction (about 8 percent of the total). For this reason, the remaining analysis is based on the six measured quantities relative to the other tracks: p_0, p_1, p_3, θ_{01}, θ_{03}, and θ_{13}, as given in column 1 of Table I; and assumption of momentum conservation. Column 3 of Table I gives the momentum and direction of track 2 as calculated from the data in column 1. Comparison with the corresponding directly measured quantities in column 2 indicates agreement, again within the estimated errors.

The $Q(3\pi)$ value computed from the data and errors in column 1 is 73.9±5.8 Mev. The agreement with the well-established Q-value[3] of 74.7±0.3 Mev gives assurance that the event is correctly interpreted as normal τ decay.

The center-of-mass kinetic energies, momenta, and angles computed from the data and errors in column 1 of Table I are given in Table II. The center-of-mass decay configuration is shown in Fig. 2(b). The equation of the unit normal to the decay plane (in the direction of $\mathbf{p}_1'\times\mathbf{p}_3'$) is

$$\mathbf{n}'=-0.0998\mathbf{i}'+0.0042\mathbf{j}'-0.9950\mathbf{k}'.$$

The direction of motion of the τ makes an angle $\theta'=84.3°$ with $\mathbf{n}'$; thus the event is almost planar in the laboratory system. For isotropic decay this is a probable configuration, since the element of available solid angle goes as $\sin\theta' d\theta'$. As to the orientation of the fragment momenta in the decay plane, $\mathbf{p}_1'$ makes an angle of 2.1°, in the backward direction, with the y'-axis.

TABLE I. Basic data.

Momenta-Bev/c angles-degrees	1 Measured data used in analysis	2 Measured data for track 2	3 Calculated data for track 2
p_0	0.83±0.03		
p_1	0.28±0.01		
p_2		0.49±0.06	0.42±0.03
p_3	0.154±0.005		
θ_{01}	17.7±0.1°		
θ_{02}		3.3±0.5°	3.8±1.1°
θ_{03}	22.9±0.3°		
θ_{12}		20.8±0.5°	21.3±0.8°
θ_{23}		19.8±0.5°	19.5±1.2°
θ_{13}	40.4±0.3°		

TABLE II. Decay parameters in center-of-mass system.

Fragment	Sign	Kinetic energy Mev	Momentum Mev/c	Angle opposite
1	+	24.3±1.8	86±3	58.7±5.0°
2	−	20.9±4.3	79±9	52.0±5.5°
3	+	28.7±1.8	94±3	69.3±1.4°

Pion-Pair Production in a Nuclear Emulsion

HERMAN YAGODA
National Institutes of Health, Bethesda, Maryland

(Received August 23, 1954; revised manuscript received December 10, 1954)

A positive and a negative π-meson pair of tracks with energies of 17.94 and 18.65 Mev, respectively, are observed to originate in an emulsion without any other associated ionizing particles. It is shown that the event probably did not originate from a nuclear collision. Among the mechanisms considered are materialization from a photon, the decay of a theta-meson, and decay of a (previously postulated) zeta meson. The Q-value of the event, computed as a 2-body decay is 27.9 Mev. If it is a two-body decay the mass of the parent particle is about 600 m_e. This event is also consistent with the decay of a neutral tau meson into a neutral pion and two charged pions for which the total kinetic energy of the charged mesons could vary between 0 and about 80 Mev.

IN our studies on the emission of slow mesons from nuclear disruptions produced by cosmic radiation,[1] one event has been observed in which only the tracks of a positive and a negative meson diverge from a common point in the recording medium. Both particles terminate their range within the confines of a single 1500-micron layer of Ilford G5 emulsion. One of the particles is captured near the end of its range and produces a 2-pronged star, the other exhibits the typical π-μ-e decay processes characteristic of a π^+ meson. Examination of the common point of origin shows complete absence of any associated recoil or delta-ray tracks (Fig. 1). The preparation was sensitive to fast singly charged particles at the minimum of ionization (15 developed blobs per 100 microns). Had any relativistic particles of this character been associated with the event their tracks would be clearly evident, as the origin is located 271 microns below the air interface of the processed gelatin and is accessible to examination by oil immersion objectives of 1.3 numerical aperture.

The event might have originated in a collision of a high-energy neutron ($\geq$700 Mev) with a surface neutron producing the pion-pair and ejecting the uncharged target nucleon. The residual nucleus may then have only a small excitation, of the order of 5 Mev, and may reach stability by either γ ray or neutron emission. While it is possible for the proposed collision to produce two slow π mesons and an absence of recoil, it is to be expected that in the c.m. system of the colliding neutrons that both mesons would have to be projected almost backward and with a velocity closely related to the c.m. velocity of the neutrons. This circumstance might occur with a probability, estimated by Dalitz,[2] of about 1 in 10^4 in a process whose total cross section is at the most about 10^{-27} cm^2.

An alternative mechanism is the simple creation of a positive and negative meson pair by materialization of a photon near the Coulomb field of a nucleus. One difficulty with this novel process is that the difference between the momentum of the photon ($\gtrsim$350 Mev/c) and the total momentum of the π mesons (148 Mev/c) would have to be absorbed by the nucleus. Assuming that the latter escaped distruption in absorbing more than 200 Mev/c momentum, its resulting recoil energy would be about 0.3 Mev even if the nucleus was as massive as silver, yet no recoil is observed. At best, the cross section for this hypothetical process would be $\lesssim 10^{-32}$ cm^2. Because of the large momentum transfer, the process would have to occur very close to or within the nucleus, and direct nuclear meson-production processes should predominate.[3]

The event could originate from the two-body decay of an uncharged K-meson. By employing the data in Table I, the mass of the parent particle X has been estimated from the relationship:

$$X^2=2m^2+2p_1p_2\left[\left\{1+\left(\frac{m}{p_1}\right)^2\right\}^{\frac{1}{2}}\left\{1+\left(\frac{m}{p_2}\right)^2\right\}^{\frac{1}{2}}-\cos\varphi\right],$$

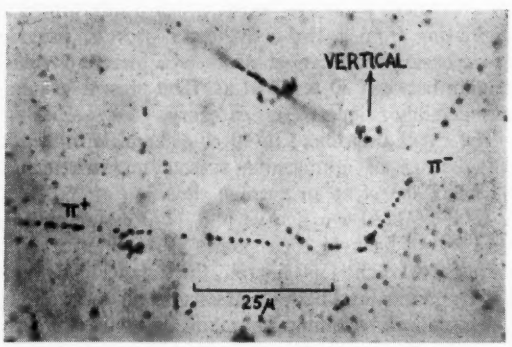

FIG. 1. Photomicrograph showing the origin of the pion pair. The angle between the tracks is 120°. Both tracks terminate in a 1500-micron emulsion layer, and can be identified as positive and negative π mesons by phenomenological behavior at the end of their range.

[1] H. Yagoda, Phys. Rev. 87, 753 (1950); 85, 891 (1952); 95, 648 (1954).
[2] R. H. Dalitz (private communication).
[3] In this connection our observations on the emission of two or more slow mesons per nuclear evaporation are of interest. Among 18 stars, only 2 exhibit a positive and a negative π-meson track, and in one event both mesons are positive. In the 15 other examples both mesons are of negative sign. These stars invariably exhibit a large number of black and gray prongs indicative of the disruption of heavy nuclei. The slow mesons are, with but one exception, wide-angle members of a large shower of relativistic particles.

TABLE I. Properties of the pion-pair.

Meson track	π^-	π^+
Range in microns	6890±300	6440±300
Kinetic energy, Mev[a]	18.65±0.67	17.94±0.65
Momentum, Mev/c	73.0 ±1.4	74.5 ±1.4
Initial dip, tan β	0.133	~0
Angle between tracks in emulsion plane	120±1°	
Spatial angle	119.8±1°	
Q-value for 2-body decay[b]	27.85±0.76 Mev	

[a] Based on range-energy tables for nuclear emulsions by Fay, Gottstein, and Hain, Nuovo cimento 12, Suppl. No. 2, 234 (1954). Errors in energy were estimated by combining as root mean squares the errors in range measurement and those introduced by straggling (2.5 percent of E_π).
[b] The error in the Q-value was estimated by the method described by Leighton, Wanlass, and Anderson, Phys. Rev. 89, 148 (1953).

where m refers to the average pion mass, taken as 273 m_e, and p_1 and p_2 are the momenta of the meson particles. The mass of the K-meson is thus estimated at 600 m_e and the Q-value of the decay process at 27.9±0.8 Mev. These values are not reconcilable with either the θ^0-meson ($M\sim1000\ m_e$, $Q=214$ Mev) or the once postulated[4] neutral zeta meson with a Q-value of about 2 Mev.

The pion pair may have originated from a three-body decay of a neutral K-meson, $K^0\to\pi^+ + \pi^- +$neutral particle. Then, as shown in the appendix, the kinetic energy Q of the charged pions (measured in their c.m. system) may be between zero and $M_{K^0}-m_+-m_- -m_0$, where m_0 is the mass of the neutral particle. In a τ^0-decay, for example, where the third particle is a neutral pion, Q must lie between 0 and 80 Mev, assuming a τ^0 mass equal to that of the charged tau meson. This event is therefore not incompatible with interpretation as a τ^0-decay. Several cloud-chamber pictures of "anomalous θ^0-decays" exist, which if interpreted as originating from a two-body decay process, provide, on the basis of the charged members, apparent Q-values ranging between 30 to 55 Mev.[5] The present example may possibly belong to this category.

The event was found in 60 cc of emulsion flown in the absence of appreciable surrounding matter for 8.2 hr at λ55°N at an average elevation of 95 000 ft. A total of 1180 π-μ decays and 1740 σ-star endings were traced back to their points of origin within the confines of each 1500-micron thick layer. Of these 102 π^+-mesons and 320 π^--mesons originated in stars. The feedback scanning mechanism resulted in the detection of one coplanar tau-meson decay, a mesonic-decay of an excited triton,[6] and a small group of π^- mesons originating from one-prong stars.[7]

[4] Danysz, Lock, and Yekutieli, Nature 169, 364 (1952).
[5] Unpublished observations by the California and Princeton University cloud chamber groups. See V. A. J. van Lint, Duke University Natural Science Foundation Cosmic Ray Conference, Durham, North Carolina, 1954 (unpublished), p. II-40.
[6] H. Yagoda, Phys. Rev. (to be published).
[7] When these events are analyzed on the assumption that they originated from the decay of a Λ^0-particle, one event yields a Q-value of 35.7 Mev, and six events have $16<Q<24$ Mev. Results on a transverse momentum analysis of the latter will be described elsewhere.

Pion-pair production may be more frequent than these observations would indicate as recognition is dependent on both particles terminating their range. This is particularly true, if as in the present example, both mesons emerge with equal velocity. The gain densities about the point of origin are then identical, and in following back one of the meson tracks, the origin of the pair would be interpreted as a large-angle scatter, unless a sufficient length of the second member recorded to indicate a pronounced increase in gain density.

Opportunity is taken to thank the members of the Office of Naval Research Skyhook Project for the high-altitude balloon exposure. Appreciation is expressed to Howard Smith for assistance in the development and scanning of the emulsion ensemble. The writer is particularly indebted to R. H. Dalitz for a discussion of potential mechanisms for the origin of the pion pair.

APPENDIX A. THREE-PARTICLE DECAY OF A NEUTRAL PARTICLE[8]

Consider the disintegration of a neutral particle of mass M into two charged particles of masses m_+, m_- and a neutral particle of mass m_0. In the system in which the particle M is initially at rest, suppose that the disintegration products have momenta p_+, p_-, p_0, and total energies E_+, E_-, E_0. Then conservation of momentum and energy are expressed by the equations (taking $c=1$)

$$p_+ + p_- + p_0 = 0, \tag{1}$$

$$E_+ + E_- + E_0 = M. \tag{2}$$

Consider now the quantity $(E_+ + E_-)^2 - (p_+ + p_-)^2$, which has the same value in all reference systems. Its value in the rest system of particle M is

$$(E_+ + E_-)^2 - (p_+ + p_-)^2 = (M - E_0)^2 - p_0^2,$$
$$= M^2 + m_0^2 - 2ME_0. \tag{3}$$

In the c.m. system of the two charged particles, their total momentum is zero. If one designates their total energies by ϵ_+ and ϵ_-, then $\epsilon_+ + \epsilon_- = m_+ + m_- + Q$. In this expression, Q represents the sum of the kinetic energies of the two charged particles in their c.m. system and is identical with the apparent Q-value computed on the assumption of a two-particle decay. In this system, (3) has the value $(\epsilon_+ + \epsilon_-)^2$, and

$$Q = (M^2 + m_0^2 - 2ME_0)^{\frac{1}{2}} - m_+ - m_-. \tag{4}$$

The value of Q therefore depends only on the kinetic energy in the M-rest system acquired by the neutral decay particle. Its maximum value, $Q_{\max} = M - m_+ - m_- - m_0$, is assumed when $E_0 = m_0$, and the minimum value $Q=0$ corresponds to the maximum value of E_0,

$$(E_0)_{\max} = [M^2 + m_0^2 - (m_+ + m_-)^2]/2M. \tag{5}$$

Latitude Effect of Cosmic Radiation at Low Altitudes*

MARTIN A. POMERANTZ†
Bartol Research Foundation of The Franklin Institute, Swarthmore, Pennsylvania
(Received December 17, 1954)

The latitude effect, $L=1-[N(\lambda_2)/N(\lambda_1)]$, where $N(\lambda_1)$ is the intensity at $\lambda_1>40°$ and $N(\lambda_2)$ is the intensity at low latitude λ_2, has been determined on the basis of absolute flux measurements at two ground stations in India. Near sea level, $L=8.8\pm0.6$ percent ($\lambda_2=18°$ N). At an atmospheric depth of 770 g cm^{-2}, $L=13.1\pm0.6$ percent ($\lambda_2=23°$ N). At low altitudes (up to 30 000 ft) the latitude effect with respect to the geomagnetic equator in Peru is equal to that with reference to 18° N in India as expected on account of the eccentricity of the terrestrial dipole.

RECENT measurements[1] have revealed an anomalously large variation of the primary cosmic-ray intensity between geomagnetic latitudes 18° N and 3° N in India, compared with the over-all change between 52° N and 3° N. The data recorded within the equatorial region (cutoff rigidities for vertical incidence 13.8 Bv and 15.4 Bv) require a higher value of the exponent in the magnetic rigidity distribution than the average determined on the basis of the observed fluxes at high and low latitudes (cutoff rigidities 2.1 Bv and 15.4 Bv, respectively).

Although a systematic investigation of the latitude effect at low altitudes was not specifically undertaken, extensive data were accumulated during the ground runs of the balloon-borne instruments. In view of the fact that the primary flux at 18° N in India is higher than would be expected on the basis of the customary assumptions, it is of interest to ascertain whether the intensity near sea level at that station reflects this condition.

Table I is a summary of a series of measurements at Aligarh, Uttar Pradesh ($\lambda=18°$ N) and Swarthmore, Pennsylvania ($\lambda=52°$ N), respectively, obtained with coincidence counter trains containing no interposed absorber operated under a concrete roof. The instruments have been described in detail previously.[2] Two experimentally-determined corrections for differences in altitude and in thickness of material overhead are required in order to normalize the counting rate at Swarthmore to permit direct comparison with that at Aligarh. The latitude effect near sea level (atmospheric

TABLE I. Summary of data recorded on the ground at Swarthmore, Pennsylvania, and Aligarh, Uttar Pradesh. All of the uncertainties indicated are statistical standard deviations.

Station	Swarthmore, geomagnetic latitude 52° N			Aligarh, geomagnetic latitude 18° N			
Average atmospheric pressure	756 mm of Hg			745 mm of Hg			
Absorber overhead	35 g cm^{-2} concrete			67 g cm^{-2} concrete			
Instrument number	Total counts	Total time, min	Counting rate, counts per min	Instrument number	Total counts	Total time, min	Counting rate, counts per min
1	9595	11 500	0.834±0.008	1	3062	4133	0.741±0.013
2	5865	6919	0.849±0.011	2	5812	8050	0.723±0.010
3	3333	3864	0.862+0.015	3	5157	6932	0.745±0.012
4	3910	4568	0.855±0.013	4	2707	3572	0.758±0.015
5	3645	4258	0.855±0.014	5	3103	4132	0.752±0.014
6	3296	3907	0.844±0.014	6	8294	11 578	0.718±0.008
7	4471	5465	0.820±0.012	7	1805	2409	0.749±0.017
8	4925	6001	0.820±0.012	8	2884	3887	0.741±0.013
9	2023	2413	0.839±0.018	9	3312	4618	0.716±0.012
10	1604	1894	0.847±0.020	10	3489	4693	0.744±0.013
				11	4271	5839	0.732±0.011
Totals	42 658	50 789	0.840±0.004	Totals	43 896	59 843	0.734±0.004
Corrected to absorber thickness and atmospheric pressure at Aligarh							
	$N(52°)=0.805\pm0.004$						$N(18°)=0.734\pm0.004$
Latitude effect, $L(52°-18°)=8.8\pm0.6$ percent							

* Supported by the joint program of the Office of Naval Research and the U. S. Atomic Energy Commission. Field expedition sponsored by National Geographic Society.
† Fulbright Professor, Muslim University, Aligarh, U. P., India, during the year 1952–1953.
[1] M. A. Pomerantz, Phys. Rev. 95, 531 (1954).
[2] Geometrical factors for converting counting rates to absolute particle flux values are listed in Table II, reference 1.

TABLE II. Summary of data recorded at Gulmarg, Kashmir, and Echo Lake and Mt. Evans, Colorado. The measurements obtained at each location with two separate instruments of each type have been combined.

Station	Average atmospheric pressure, mm of Hg	Instrument	Interposed absorber,[a] g cm^{-2} Pb	Total counts	Total time, minutes	Counting rate, counts per minute	Counting rate reduced to atmospheric pressure at Gulmarg	Observed counting rate at Gulmarg	Latitude effect, $L(49°-23°)$, percent
Gulmarg,—	567	*A*	0.0	9568	5935	1.61±0.02			
geomagnetic latitude			47.2	7507	7190	1.04±0.01			
23° N, altitude			85.0	6310	6425	0.98±0.01			
9000 ft		*B*	0.0	32 135	11 490	2.80±0.02			
Echo Lake,—	515	*A*	0.0	874	365	2.39±0.08	1.91	1.61	15.7
geomagnetic latitude			70.8	711	514	1.38±0.05	1.16	1.01[b]	12.9
49° N, altitude									
10 700 ft									
Mt. Evans,—	453	*A*	0.0	3560	1090	3.27±0.05	1.83	1.61	12.6
geomagnetic latitude			47.2	4608	2499	1.84±0.03	1.20	1.04	13.3
49° N, altitude			85.0	2690	1645	1.64±0.03	1.10	0.98	10.9
14 150 ft		*B*	0.0	7479	1392	5.37±0.06	3.24[c]	2.80	13.6

[a] Not including counter walls.
[b] By interpolation.
[c] Adjusted on basis of direct calibration at Swarthmore for slight geometrical change.

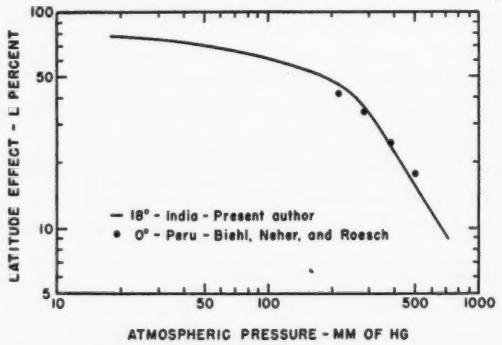

FIG. 1. Altitude dependence of the latitude effect between 52° N and 18° N. The extrapolated values of the flux at the "top of the atmosphere" (see reference 1 and previous publications cited therein) correspond to a latitude effect $L(52°-18°)=81$ percent.

depth = 1010 g cm^{-2}) with respect to 18° in India is then

$$L(52°-18°)=1-\frac{N(18°)}{N(52°)}=8.8\pm0.6 \text{ percent.}$$

This is in good accord with the observations at sea level of Millikan and Neher[3] with shielded electroscopes, although somewhat lower than is indicated by the ionization chamber measurements of Compton *et al.*[4] According to the data of the latter, the latitude effect with respect to 21° N in India amounts to 16.9 percent at the same altitude.

The present result also agrees with that of Winckler *et al.*[5] with respect to 18° N in the Pacific Ocean, as is expected on the basis of the approximately equal threshold magnetic rigidities. However, as has already been pointed out,[1] the corresponding observed value of the total primary flux is higher in India.

It is also possible to deduce the latitude effect at an atmospheric depth of 770 g cm^{-2} from measurements recorded during a limited period of operation in the Himalayas at Gulmarg, Kashmir ($\lambda=23°$ N), and at Mt. Evans and Echo Lake, Colorado ($\lambda=49°$ N). Empirical corrections for differences in altitude and absorber thickness are applied to the data to obtain the results tabulated in Table II. The average value of the latitude effect at 770 g cm^{-2} is $L(49°-23°)=13.1\pm0.6$ percent.

Figure 1 indicates the altitude dependence of the latitude effect between 52° N and 18° N on the basis of the present measurements and those obtained in balloon flights with identical instruments containing small thicknesses of interposed absorber (4.0–7.5 cm of Pb). At low altitudes, the latitude effect with respect to the geomagnetic equator in Peru, as determined in airplane flights by Biehl, Neher, and Roesch,[6] is equal to that with reference to 18° N in India as measured by the present author. This would be compatible with the equality of the threshold magnetic rigidities at the two locations, which prevails when the eccentricity of the terrestrial dipole is taken into account.

A complete discussion of these experiments will be published in the *Transactions of the Bose Institute.*

[3] R. A. Millikan and H. V. Neher, Phys. Rev. **50**, 15 (1936).
[4] A. H. Compton, Phys. Rev. **43**, 387 (933).
[5] Winckler, Stix, Dwight, and Sabin, Phys. Rev. **73**, 656 (1950).
[6] Biehl, Neher, and Roesch, Phys. Rev. **76**, 914 (1949).

High-Energy Proton Spallation-Fission of Uranium

R. L. FOLGER,* P. C. STEVENSON, AND G. T. SEABORG
Radiation Laboratory and Department of Chemistry, University of California, Berkeley, California
(Received November 12, 1954)

The fission and spallation reactions produced in uranium by bombardment with high-energy protons (340 to 350 Mev) were investigated. The reaction products were separated from the target by chemical processes and identified by their radioactive properties. The relative yields of the observed fission products are calculated, and the results plotted as a function of mass number. Several of the spallation products are identified and their yields estimated.

An attempt is made to determine the most probable atomic number for a nuclide of given mass formed directly from fission. Studies are made of the relative yields along several isobaric chains as a function of atomic number. From these data, estimates of the mass and charge of the fissioning nucleus are made.

By using the reaction $Al^{27}(p,3pn)Na^{24}$ of known cross section to monitor the bombarding beam, the absolute formation cross sections for several fission product nuclides were measured. Values for these reference nuclides are used to transform all of the relative yields into formation cross sections. Summation integration over the range of mass numbers of the area under the plot of formation cross sections as a function of mass number leads to a value of 2.0 barns for the total fission cross section for uranium bombarded with high-energy protons, if one assumes binary fission.

I. INTRODUCTION

IN recent years there has been considerable interest in the mechanism of fission induced by high-energy particles (greater than a few Mev) as compared to that of low-excitation fission. This work has been reviewed by Spence and Ford.[1] In the case of the heavy elements, work has been done with the target elements bismuth,[2–4] thorium,[4–8] and uranium.[4,9–11] High-energy fission of tantalum[12] and other heavy elements[2] from $Z=73$ to $Z=82$ has been observed. Batzel and Seaborg[13] have announced the high-energy fission of a number of medium weight elements. The yield distribution of fission products has been studied by chemical separation techniques followed by identification of the nuclides through radioactivity measurements, and also by measurement of the kinetic energies of the fission fragments.

The predominant characteristics of very high-energy fission which appear from these studies are:

(1) A single peak is found in the yield *versus* mass distribution curve, as opposed to the double peak found in low-energy fission.

(2) Prefission evaporation of nucleons is suggested. The mass number of the peak of the yield distribution is substantially less than one-half the mass number of the target nucleus.

(3) The kinetic energies of the fission fragments seem to be practically independent of the initial target-nucleus excitation.[4,14]

Predominantly symmetric fission caused by very high-energy particles has been reported by Goeckermann and Perlman[2] (bismuth plus 190-Mev deuterons), Biller and Perlman[3] (bismuth plus 340-Mev protons), O'Connor and Seaborg[9] (uranium plus 380-Mev helium ions), and Jungerman and Wright[4] (uranium plus 90-Mev neutrons).[15] At intermediate energies, the contribution of asymmetric fission is shown by the appearance of two peaks with a shallow dip between them with the peak-to-trough ratio increasing as the energy is decreased. This effect has been observed by Newton[5] (thorium plus 38-Mev helium ions), Jungerman and Wright[4] (uranium plus 45-Mev neutrons), Tewes and James[6] (thorium plus 6.7- to 21.1-Mev protons), Fowler, Jones, and Paehler[11] (uranium plus 11- to 18-Mev protons), Turkevich and Niday[7] (thorium plus pile neutrons), Turkevich, Niday, and Tompkins[8] (thorium plus 6- to 11-Mev neutrons) and Spence[16] (U^{235} plus 14, ~1.2, and ~0.4 Mev neutrons). The same effect has been observed in photofission by Schmitt and Sugarman[17] (uranium plus 7 to 300 Mev x-rays), Hiller and Martin[18] (thorium plus 69-Mev

* Now at E. I. du Pont de Nemours Company, Savannah River Plant, Augusta, Georgia.

[1] R. W. Spence and G. P. Ford, Ann. Rev. Nuc. Sci. **2**, 399 (1953).

[2] R. H. Goeckermann and I. Perlman, Phys. Rev. **73**, 1127 (1948); **76**, 628 (1949); Perlman, Goeckermann, Templeton, and Howland, **72**, 352 (1947).

[3] W. F. Biller and I. Perlman (unpublished); W. F. Biller, Ph.D thesis, University of California, Berkeley, California (unpublished).

[4] J. Jungerman and S. C. Wright, Phys. Rev. **76**, 1112 (1949).

[5] A. S. Newton, Phys. Rev. **75**, 17 (1949).

[6] H. A. Tewes and R. A. James, Phys. Rev. **88**, 860 (1952).

[7] A. Turkevich and J. B. Niday, Phys. Rev. **84**, 52 (1951).

[8] Turkevich, Niday, and Tompkins, Phys. Rev. **89**, 552 (1953).

[9] P. R. O'Connor and G. T. Seaborg, Phys. Rev. **74**, 1189 (1948).

[10] M. Lindner and R. Osborne, Phys. Rev. **94**, 1323 (1954).

[11] Fowler, Jones, and Paehler, Phys. Rev. **88**, 7 (1952).

[12] W. Nervik and G. T. Seaborg, Phys. Rev. **97**, 1092 (1955).

[13] R. E. Batzel and G. T. Seaborg, Phys. Rev. **79**, 528 (1950); Phys. Rev. **82**, 607 (1951). See also D. H. Greenberg and J. M. Miller, Phys. Rev. **84**, 845 (1951) and P. K. Kofstad, Ph.D. thesis, University of California Radiation Laboratory Report UCRL-2265, June, 1953 (unpublished).

[14] E. M. Douthett and D. H. Templeton, Phys. Rev. **94**, 128 (1954).

[15] Represents ionization chamber measurement of fragment kinetic energies.

[16] R. W. Spence, Brookhaven National Laboratory BNL-C-9, June, 1949 (unpublished), p. 43.

[17] R. A. Schmitt and N. Sugarman, Phys. Rev. **95**, 1260 (1954).

[18] D. M. Hiller and D. S. Martin, Jr., Phys. Rev. **90**, 581 (1953).

x-rays), Spence[16] (U^{235} plus 12 to 16-Mev x-rays), and Richter and Coryell[19] (uranium plus 9- to 14-Mev x-rays).

Recent results at extremely high energies, 2-Bev protons on lead[20] and bismuth,[21] show mass number distribution curves unlike those observed in the hundred-Mev range, with a monotonic decrease in yield with decreasing atomic numbers of the product throughout the entire range of the products. It appears that more work at these extremely high and at intermediate energies will be necessary before these results can be correlated with results such as those presented here from investigations in the hundred-Mev range.

In the high-energy (190-Mev) deuteron fission of bismuth, Goeckermann and Perlman[2] observed that the mass number at the symmetric peak of the fission-product distribution curve was less than one-half the mass number of the target nucleus. The mass difference indicated the evaporation of 10 to 12 nucleons. The relative yields of the fission-product isobars seemed to indicate that the most probable primary products were those having the same charge-to-mass ratio as the fissioning nucleus. Yamaguchi,[22] in a theoretical treatment of nuclear evaporation, has indicated that for bismuth bombarded with 200-Mev deuterons, the probability for neutron emission may be greater than that for fission until 10 to 11 neutrons have been emitted. In the case of uranium bombarded with 380-Mev helium ions,[9] the mass number at the peak of the distribution curve was not well enough defined to demonstrate corresponding neutron emission although the curve showed a strong possibility that such evaporation had occurred.

Measurements of fission-fragment kinetic energies have been made by Jungerman and Wright,[4] using ionization chamber techniques, and indirectly by Douthett and Templeton,[14] who measured the ranges of the fragments in aluminum. In bombarding uranium with 45- and 90-Mev neutrons, Jungerman and Wright[4] observed the mean kinetic energies to be 79±3 and 80±2 Mev, respectively. Within the limits of experimental error, the ranges of fission fragments obtained by radiochemical separation from absorber foils are equal for the corresponding products formed by slow-neutron fission of U^{235},[23,24] uranium plus 18-Mev deuterons,[14] and uranium plus 335-Mev protons,[14] if one takes account of the changes in mass of the complementary fragments. These results seem to indicate that there is no mechanism for converting excitation energy into recoil energy. The excitation energy goes into the emission of nucleons, mostly neutrons, but the information presently available is not sufficient to allow a decision as to whether the neutrons are emitted before or after the separation of the nucleus into the primary fission fragments. The results are consistent with the picture in which the actual fissioning nucleus in each case is in a relatively unexcited state following the dissipation of the initial excitation energy primarily by the prefission evaporation of nucleons.

[19] H. G. Richter and C. D. Coryell, Phys. Rev. **95**, 1550 (1954).
[20] J. M. Miller and G. Friedlander, Phys. Rev. **91**, 485 (1953).
[21] Sugarman, Duffield, Friedlander, and Miller, Phys. Rev. **95**, 1704 (1954).
[22] Y. Yamaguchi, Progr. Theoret. Phys. (Japan) **5**, 143 (1950).
[23] Finkle, Hoagland, Katcoff, and Sugarman, *Radiochemical Studies: The Fission Products* (McGraw-Hill Book Company, Inc., New York, 1951), paper No. 46, National Nuclear Energy Series, Plutonium Project Record, Vol. 9B.
[24] F. Suzor, Ann. Physik **124**, 269 (1949).

II. EXPERIMENTAL PROCEDURES

Our work has been done by bombarding uranium in the circulating proton beam of the 184-in. Berkeley cyclotron. The proton energy at the radius used is approximately 340 Mev. The fission products so produced were isolated by standard radiochemical means and identified by observation of their half-lives and radiation characteristics. In the early work it was customary to evaporate an aliquot of the final solution on a counting plate for the radioactive sample, then precipitate a suitable compound for the gravimetric analysis from the balance of the solution. In later work it was found desirable to use the final precipitate itself, after weighing, for the radioactive sample (see sections below on scattering and absorption corrections). In these cases the final precipitate, after washing, was slurried with an organic liquid and transferred by pipet to an aluminum dish approximately one inch in diameter and weighing between 70 and 80 mg. The sensitivity of the balance used was of the order of 10^{-2} mg and the sample usually had a net weight between 1 and 10 mg. In contrast to samples dried and weighed on filter paper, samples mounted on aluminum dishes show much greater weight stability since the aluminum does not absorb moisture from the air.

Detecting instruments.—Alpha-emitting samples were measured either in a proportional counter or in an ionization chamber instrument. Alpha energies were determined by means of an alpha pulse analyzer.[25]

Samples emitting beta and gamma radiation were counted by means of end-window Geiger-Müller tubes. When this work was begun, the tubes available were of the argon-alcohol type. For the more recent work, end-window tubes filled with a mixture of argon and chlorine were used. These tubes (Amperex Type 100C, obtainable from Amperex Electronic Company, New York, New York) have a window thickness of 3.5 mg/cm^2.

Backscattering.—Correction factors for the scattering of beta particles into the counter from the backing material on which the sample is mounted have been empirically determined by several workers.[26–28] The

[25] Ghiorso, Jaffey, Robinson, and Weissbourd, *The Transuranium Elements: Research Papers* (McGraw-Hill Book Company, Inc., New York, 1949), paper No. 16.8, National Nuclear Energy Series, Plutonium Project Record, Vol. 14B.
[26] L. R. Zumwalt, U. S. Atomic Energy Commission Declassified Document MDDC-1346, Februrary, 1949 (unpublished).
[27] B. P. Burtt, Nucleonics **5**, No. 2, 28 (1949).

amount of backscatter depends primarily upon the thickness and atomic number of the backing material. The scattering is relatively insensitive to beta energy in the range 0.6 to 3 Mev.[27,28] In most of our work, the samples were mounted on similar backings so that for relative yields the backscattering correction nearly cancelled out for all but soft beta particles.

Self-scattering and self-absorption corrections.—Since the radioactive samples in many cases were of finite mass, it was necessary to determine the loss or gain of apparent activity in passing through the mass of the sample. There is a loss of apparent activity due to absorption in the material of the sample. Scattering of beta particles and electrons by the material of the sample causes an apparent increase in the activity. Some preliminary experiments were performed to determine empirically the combined self-absorption and self-scattering corrections.[29,30] The absorbing power of sample material for particles increases only slowly with the atomic number, but the scattering power increases markedly. In some cases the scattering effects were so great that a net increase in apparent counting rate was obtained even for many milligrams per square centimeter of sample thickness. Uncertainties in the self-scattering corrections are believed to be the major source of error in our measurements.

Air-window absorption.—The loss of activity by absorption in the air between the sample and the counter window, and in the window itself, was determined by extrapolation of aluminum and/or beryllium absorption curves whose initial portions were carefully measured by using thin absorbers.

Counting efficiencies.—In determining yields of various nuclides, it was necessary to make some assumptions regarding relative counting efficiencies. For beta particles and electrons a counting efficiency of 100 percent was assumed. The calculated counting efficiencies for electromagnetic radiation, based on absorption in the gas of the counter tube, were 0.5 percent for energies from 20 kev to 0.5 Mev, and 1 percent per Mev thereafter for argon-filled tubes.[31] The ratio of the over-all efficiency of the argon-chlorine (Amperex) tubes to the argon-alcohol tubes for the same geometrical arrangement was determined to be 45 percent by counting a number of samples having beta and electromagnetic radiations of various energies.[32]

Effective geometry.—The sample holders used for the counting with the Geiger-Müller tubes could be placed in any one of five positions varying from 0.3 to 6.7 cm from the tube window. Attempts were usually made to measure the counting rate with a monitor sample in the same position as the sample of the nuclide whose relative yield was being determined. When such an arrangement was not practical initially because of too great a difference in the counting rates of the samples, the "geometry" ratio was later determined empirically when the counting rates were more nearly equal. This ratio was not a true geometric ratio alone because of increased air absorption at greater distances from the counter window. In cases where the absorption characteristics of a particular beta particle were rather well known, measurements of the true geometric ratios between various positions were made.

III. ACTIVE SPECIES OBSERVED

Sodium.—The isolated sodium fraction from a uranium target, prepared with extreme care to eliminate any light-element surface contamination, showed a beta activity of 15-hour half-life in amount larger than could be accounted for by impurities in the uranium. The decay was followed for four half-lives without any deviation because of radioactive impurities being observed. Aluminum absorption measurements of the beta radiation showed the 1.4-Mev beta particle of Na^{24}.[33–35]

Manganese.—A 5.8-day activity was observed in the manganese fraction separated after an eight-hour bombardment of a uranium target. The absorption characteristics and half-life corresponded to those observed for Mn^{52} formed by spallation of iron with 340-Mev protons. The amount of Mn^{52} produced could be accounted for by the known amounts of iron and nickel impurities in the uranium target. No manganese activity was observed which could unambiguously be attributed to uranium fission.

Iron.—The iron fraction decay showed two major components. One was the expected 46-day Fe^{59}, characterized by half-life and aluminum absorption measurements. The other component had a half-life of approximately 8 hours and very energetic negative beta radiations. This was at first thought to be a new isotope of iron, but is now believed to be caused by gallium contamination, the observed half-life being caused by a mixture of Ga^{72} and Ga^{73}.

Cobalt.—Decay measurements of the cobalt fraction showed a component of 1.7 hours, corresponding to Co^{61}. Aluminum absorption measurements of the 1.7-hour activity showed a beta energy of about 1.3 Mev.

Nickel.—The decay of nickel showed components of 2.6 hours and 56 hours, corresponding to Ni^{65} and Ni^{66}, respectively. Aluminum absorption measurements of the 56-hour Ni^{66} showed the 2.9-Mev beta particle of 4.3-minute Cu^{66} in equilibrium.

---

[28] L. Yaffe and K. M. Justus, J. Chem. Soc. (London) 341 (1949).

[29] L. Malatesta (unpublished).

[30] W. Nervik and P. C. Stevenson, Nucleonics **10**, No. 3, 18 (1952).

[31] M. Studier and R. James (unpublished).

[32] E. Potter and H. P. Robinson (unpublished).

[33] Unless otherwise indicated, values of the half-life and beta-particle energy for the various nuclides were obtained from either the *Table of Isotopes* or the *Chart of the Nuclides*.

[34] Hollander, Perlman, and Seaborg, Revs. Modern Phys. **25**, 469 (1953).

[35] General Electric Chart of the Nuclides, Knolls Atomic Power Laboratory, Fourth Edition, originally prepared by G. Friedlander and M. Perlman, revised by J. R. Stehn.

Copper.—Three isotopes of copper were identified. The 3.4-hour Cu^{61} was observed by following the decay of its positrons with a crude beta ray spectrometer. The 12.9-hour Cu^{64} was also seen in this manner as well as by resolution of the decay curve obtained with a conventional Geiger-Müller counter. Sixty-hour Cu^{67} was clearly seen as a component in the beta decay curve.

Fermi-Kurie plots of the crude beta-spectrometer positron data showed the 1.2-Mev β^+ of Cu^{61} and the 0.66-Mev β^+ of Cu^{64}. Aluminum absorption measurements, taken after the 12.9-hour activity had decayed, showed the 0.6-Mev β^- of Cu^{67}. Careful spectrographic analyses of the uranium revealed that sufficient zinc, copper, and nickel impurities were present to give the observed yields of the neutron-deficient copper isotopes. The correction to the Cu^{67} yield from this source is small.

Zinc.—Observation of the decay of the zinc samples showed a half-life of 49 hours. A growth corresponding to a daughter half-life of 14 hours was observed, indicating the presence of 49-hour Zn^{72} with 14-hour Ga^{72} daughter.

Arsenic.—Decay of the arsenic radiation observed through 350 mg/cm² of aluminum (to block the particulate radiation of As^{77}) showed an activity of 26.8-hour half-life, corresponding to As^{76}. Observations without absorber showed the 40-hour activity of As^{77}.

Selenium.—The predominant activity in the selenium samples was the 59-minute Se^{81m} with the 17-minute Se^{81} in equilibrium. It was possible to detect the 25-minute Se^{83} both by resolution of the decay curve and by observing the 2.4-hour Br^{83} daughter in the decay measurements. Twenty-four hours after bombardment, the decay curve showed essentially no activity other than the 2.4-hour Br^{83}.

Aluminum absorption measurements on the 59-minute activity showed the 1.5-Mev beta particle of Se^{81}.

Bromine.—The bromine decay curves showed mainly 2.4-hour and 35-hour components when measurements were made without absorber. Decay of radiation measured through 490 mg/cm² of aluminum showed components of 4.4-hour and of 34-minute half-lives after subtraction of a 35-hour component due to the penetrating radiation of Br^{82}. Measurements through 750 mg/cm² of aluminum showed a component of 34-minute half-life and a residuum of 4.4-hour and 35-hour activities. The relative counting efficiency for the 4.4-hour activity was considerably reduced by the increased absorber. Aluminum absorption measurements of the 2.4-hour activity showed a 1-Mev beta particle.

From the evidence we conclude that Br^{80m}, Br^{82}, Br^{83}, and Br^{84} are formed as fission products with Br^{83} being produced in highest yield.

Rubidium.—The rubidium sample showed an activity of 19.5-day half-life, corresponding to Rb^{86}. The sample was not isolated soon enough to detect any of the shorter-lived rubidium isotopes. Aluminum absorption measurements on the rubidium activity showed a 1.8-Mev beta particle.

Strontium.—From decay measurements a 9.7-hour strontium activity was observed. A 60-day yttrium activity was chemically separated from the strontium sample, indicating the presence of Sr^{91}. Another strontium sample, from which yttrium had been removed a week after bombardment of the target, showed an activity of 54-day half-life. Aluminum absorption measurements on the 54-day activity showed the presence of the characteristic 1.5-Mev beta particle of Sr^{89}. The background due to electromagnetic radiation was negligible.

Zirconium.—The zirconium decay showed a 17-hour activity from which grew a 69-minute daughter, indicating the presence of Zr^{97} and Nb^{97}. After decay of the Zr^{97}, a decay line of predominantly 65 days half-life (Zr^{95}) was seen.

Niobium.—Four major species were identified in the niobium decay: 68-minute Nb^{97}; an activity of approximately 23 hours, probably Nb^{96}; 90-hour Nb^{95m} as established by analytical treatment of the counting data; and 37-day Nb^{95}.

Molybdenum.—The only activity observed in the molybdenum fraction was the 67-hour Mo^{99}. Activities of less than 30-minute half-life would not have been observed.

Ruthenium.—Decay measurement showed a 4.4-hour activity and longer components. After allowing one year for intermediate activities to die out, decay for a period of one year showed a one-year activity. When the activity due to this component was subtracted from the earlier data, the presence of an activity of approximately 43-day half-life was established. Subtraction of this in turn showed a 37-hour activity, indicating the presence of 4.4-hour Ru^{105} decaying to 37-hour Rh^{105}. The 43-day activity was presumed to be Ru^{103}.

Aluminum absorption measurements on the one-year activity showed the characteristic hard beta particle of the Rh^{106} daughter in equilibrium with 1.0-year Ru^{106}.

Palladium.—Two palladium activities were observed directly, 21-hour Pd^{112} and 14-hour Pd^{109}. The formation of 26-minute Pd^{111} was demonstrated by the separation of 7.5-day Ag^{111} from a portion of the target immediately after bombardment and from a second portion after an interval of three to four hours. The specific activity of Ag^{111} was significantly higher in the second portion than in the first, indicating its formation by the decay of Pd^{111}.

Decay was measured without absorber, through 80 mg/cm² of aluminum (to block the beta particles of Pd^{112}), and through 490 mg/cm² of aluminum (blocking the beta particles of Pd^{112} and Pd^{109}, but allowing the radiation of 3.2-hour Ag^{112} in equilibrium with Pd^{112} to be counted). Growth of the 3.2-hour Ag^{112} was observed.

Silver.—Decay measurements through 1380 mg/cm²

aluminum (to block all particulate radiation from silver isotopes except that of Ag^{112}) showed the 3.2-hour Ag^{112}. Decay measurements without absorber on a sample separated very soon after bombardment (to minimize the effect of the growth of 3.2-hour Ag^{112} from 21-hour Pd^{112}) gave the best data on the 5.3-hour Ag^{113}. The 7.5-day Ag^{111} was clearly seen, and shown to be formed (see above) as a primary fission product, its independent yield being 18–20 percent of the total observed β^- chain. Decay followed over a period of ten months showed an activity of 250–270 days, presumably Ag^{110}.

The formation of 20-minute Ag^{115} was shown by separating 53-hour Cd^{115} from a portion of the target immediately after bombardment and from a second portion after an interval of about four hours. The specific activity of Cd^{115} separated from the second portion was significantly higher than that from the first portion, indicating its formation by decay of Ag^{115}.

A sample of silver was initially separated from cadmium, then allowed to decay. Cadmium separated from this sample after four hours showed a 53-hour half-life with no indication of a 43-day component. This indicates that Ag^{115} decays predominantly to the Cd^{115} ground state rather than to Cd^{115m}.

Aluminum absorption measurements on the 3.2-hour activity showed the presence of the characteristic 3.6-Mev beta particle of Ag^{112}. Measurements on the 7.5-day activity showed the 1-Mev beta energy of Ag^{111}. The background due to electromagnetic radiation was less than 0.05 percent of the initial activity. Correcting for the difference in counting efficiencies, this means that any 8.6-day Ag^{106} must be present in an amount less than 5 percent of that of Ag^{111}.

Cadmium.—Decay measurements through 946 mg/cm² of beryllium (to block all particles of energy less than 1.9 Mev) showed evidence of the 49-minute Cd^{111m} and indicated the possible presence of 6.7-hour Cd^{107}. Decay of the beta radiation showed 2.8-hour Cd^{117}, 53-hour Cd^{115}, and 43-day Cd^{115m}. There was a very long-lived component which suggested the presence of either 470-day Cd^{109} or 5-year Cd^{113m}. Aluminum absorption measurements showed the 1.1-Mev beta particle of the 53-hour Cd^{115}.

Tin.—Decay measurements showed components of about 27-hour and of 9.5-day half-lives and a longer component, presumably of 130-day half-life. These seem to be due to Sn^{121}, Sn^{125}, and Sn^{123}, respectively. The other isomer of each mass number was not observed.

Tellurium.—Of the many components in the tellurium decay curve, it was possible to resolve only the 30-hour Te^{131m} and its 8-day I^{131} granddaughter in the decay curve.

Cesium.—The predominant activity in the cesium fraction was the 13-day Cs^{136}. Aluminum absorption measurements on this activity showed the characteristic 0.3-Mev beta energy of Cs^{136}.

Barium.—Most of the bombardments were interrelated by measuring the amount of 12.8-day Ba^{140} produced and using this as an internal monitor. In most cases the barium was not separated from radium. In these cases, the radiation from the sample was measured through sufficient aluminum absorber to prevent any alpha particles emitted by radium or its daughters from reaching the counter tube. In addition to observing its half-life, we identified Ba^{140} by observing the growth of its 40-hour La^{140} daughter.

A sample of the radioactive barium was analyzed in the mass spectrograph.[36] The emulsion side of the collector plate was placed against the emulsion of a second plate and the radioactive species allowed to decay for a period of about two weeks. Lines on the second or "transfer" plate indicated radioactive barium isotopes of masses 131, 133, 135, and 140 in comparable yields.

An approximately 10-day activity was observed in a cesium sample separated from a purified barium sample some time after bombardment. Although Ba^{131} has approximately the same half-life and may be present in yields of the same order of magnitude as Ba^{140}, the counting rate due to the activity of $Ba^{131}-Cs^{131}$ detected by the Geiger-Müller tube is less than one percent of that of an equal amount of $Ba^{140}-La^{140}$ because of the large difference in counting efficiencies.

Components of 29 to 39 hours with soft particle radiation were observed in the decay curves. These probably represent a mixture of Ba^{133m} and Ba^{135m}. An 85-minute component, corresponding to Ba^{139}, was also observed. In a sample of barium separated from radium with an ion-exchange column, the 85-minute, 29- to 39-hour, and 12.8-day components were observed. The positrons of 2-hour Ba^{129} were not observed during a crude beta-ray spectrometer measurement of the column-separated barium.

Lanthanum.—Decay curves showed essentially a single component, the 40-hour La^{140}, over a period of 8 to 9 half-lives. Decay of the radiation which passed through 946 mg/cm² of beryllium (to block the particles and hence allow other possible electromagnetic radiation to show a more favorable counting efficiency relative to the radiation from La^{140}) showed a curve essentially parallel to the curve taken without absorber. Since the final separation of lanthanum was not accomplished until 56 hours after bombardment, the possibility of formation of nuclides of shorter half-life in comparable yield is not excluded.

Aluminum absorption curves of the 40-hour activity compared closely with known absorption curves of the radiations from the 40-hour negative beta particle emitting daughter of Ba^{140}. Through the use of the absorption curves, the counting rate was corrected for air and window absorption, and for the contribution of the electromagnetic radiation. The disintegration rate was calculated from this corrected counting rate.

[36] Mass spectrographic analysis by F. L. Reynolds of this laboratory.

Calculations based on the relative yields of Ba^{140}, La^{140}, and Nd^{140} (explained in Sec. V) show that approximately 30 percent of the total yield at mass number 140 is initially formed as La^{140}.

Cerium.—Decay curves showed components of approximately 35 hours and approximately 30 days with a component of intermediate half-life. Analysis of the data indicated the presence of Ce^{143} with Pr^{143} daughter, and Ce^{141}. Additional decay over a period of about six months indicated the presence of 275-day Ce^{144}.

Comparison of the number of x-rays emitted by the long-lived activity with the number from Ce^{144} tracer obtained from slow neutron fission of uranium indicated the presence of 140-day Ce^{139} in our sample. Aluminum absorption measurements on the long-lived component showed two beta components which could be attributed to Ce^{144} and the 17-minute Pr^{144} in equilibrium.

Praseodymium.—Observation of the decay through 406 mg/cm^2 of aluminum showed a 19-hour half-life. Observation of the decay without absorber showed two components, one of 13.5-day half-life, the second of half-life 16 to 19 hours. Aluminum absorption measurements on the 19-hour activity showed hard beta radiation of 2.3-Mev energy and indicated a soft component of about 0.6-Mev energy in about 20 percent abundance. After decay of the 19-hour activity, aluminum absorption measurements on the 13.5-day activity showed a particle of 0.92-Mev maximum energy. On the basis of the decay and absorption measurements, it was concluded that Pr^{142} and Pr^{143} were both present in good yield.

The Pr^{142} is a shielded nuclide; consequently, its independent yield was obtained directly. The independent yield of Pr^{143} was obtained as the result of an experiment in which the 33-hour Ce^{143} parent was removed from the rare earth group within two hours after bombardment. From the yield curve (Fig. 1) it is expected that the total yield of products of mass number 143 will be less than the total yield of products of mass number 142. Since in the case of these two isotopes the ratio of the yield of Pr^{143} to that of Pr^{142} was about 1.7, the Pr^{143} represents a greater fraction of the total yield at mass number 143 than the Pr^{142} does of its total mass number yield. This indicates that whereas the most probable primary atomic number for a given mass number corresponds to the neutron excess side for isotopes of the lighter elements, the trend is for the most probable primary product to be much closer to the region of beta stability for the higher mass chains.

Neodymium.—Observation of the decay through 407 mg/cm^2 of beryllium (sufficient to block the beta particles of Nd^{147}) showed two components. After subtraction of the gamma ray activity due to the 11-day Nd^{147}, a 3.3-day decay was found. This corresponds to Nd^{140}. Decay measurements without absorber showed the 11-day half-life of Nd^{147} for over three half-lives. Aluminum absorption curves showed the characteristic beta particle energy of Nd^{147}. Since less than 2 percent of the initial total activity could be attributed to Nd^{140}, this activity did not interfere and was not characterized by absorption measurements. Its counting efficiency was calculated from the data of Wilkinson and Hicks.[37]

Calculations based on the relative yields of Ba^{140}, La^{140}, and Nd^{140} show that approximately 7.4 percent of the total yield at mass number 140 is due to Nd^{140}.

Promethium.—Decay was observed both without absorber and through 485 mg/cm^2 of aluminum. The decay as observed without absorber showed components with half-lives of about 13 hours, about 47 hours and 43 days. The first component is as yet unidentified, although an activity with such a half-life has been reported[38] to be formed by deuteron bombardment of neodymium. The other two components correspond to Pm^{149}, for which several half-lives between 47 and 55 hours have been reported, and to one of the two isomers of Pm^{148}. Crude beta-ray spectrometer measurements on the long-lived species show two resolvable beta components, one of about 600 kev and the other of about 2.4 Mev, the second component being about 5–10 percent as abundant as the first. This leads us to believe that the 43-day species corresponds to the upper state of Pm^{148}, since the 2.4-Mev radiation could arise from an unobserved isomeric transition leading to a small equilibrium amount of 5.3-day Pm^{148} ($\sim$2.5 Mev β^-). Absorption of the electromagnetic radiations of the 43-day component in copper showed no detectable neodymium x-rays.

Decay measurements through absorber showed all three of the above components and, in addition, the 5.3-day Pm^{148}.

Samarium.—The samarium decay showed components of about 10 hours and of 47 hours, the 47-hour component being quite prominent. After decay of this activity, a 15- to 16-day line was observed. Aluminum absorption measurements on the 47-hour activity indicated a beta particle of about 0.8-Mev energy. The 2.4-Mev beta particle of Eu^{156} was also observed in the absorption measurements.

The principal activities found in the samarium fraction were thus the 47-hour Sm^{153} and the 10-hour Sm^{156} with its 15.4-day Eu^{156} daughter. The yield of Sm^{156} relative to Sm^{153} was about 27 percent. The yield of Sm^{153} represents the entire beta decay chain for mass 153 whereas Eu^{156} is expected to be a large contributor to the yield of mass number 156.

Europium.—The principal europium activity was the 15.4-day Eu^{156}. Aluminum absorption measurements showed the characteristic 2.4-Mev beta particle of Eu^{156}.

Terbium.—The terbium decay curve could be resolved roughly into two components, the longer of which had a half-life of 74 days. The shorter component

[37] G. Wilkinson, and H. G. Hicks, Phys. Rev. 75, 1687 (1949).
[38] M. L. Pool and L. L. Quill, Phys. Rev. 53, 437 (1938).

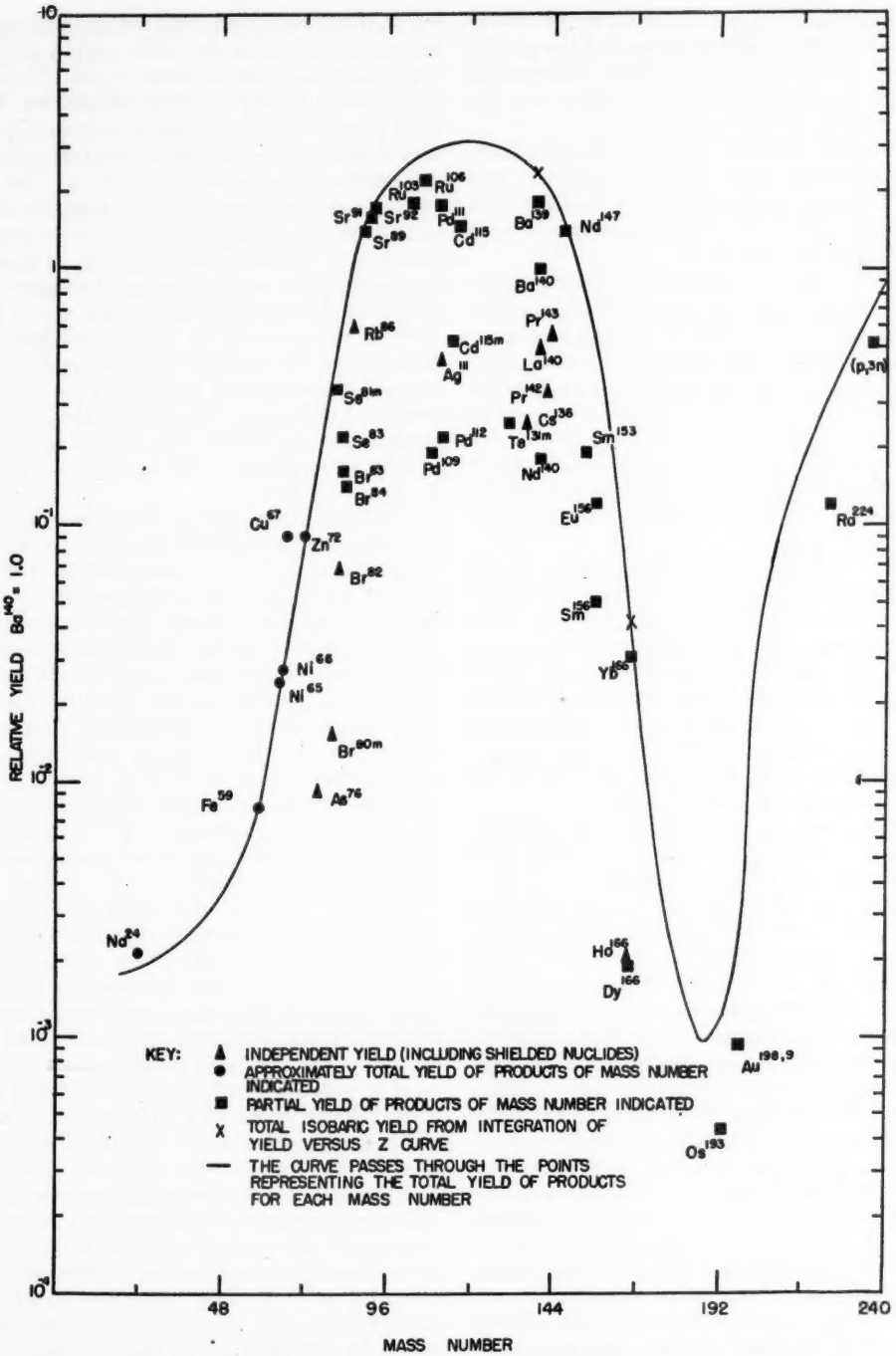

FIG. 1. Yields of the various observed species (relative to Ba^{140}) plotted as a function of mass number.

was due to a mixture of activities with half-lives between 5 and 7 days and a shorter one. Decay was observed without the use of absorber and also through 183 mg/cm² of beryllium (sufficient to block the 0.5-Mev beta particles of Tb^{161}). After subtraction of the activity due to the 74-day residuum, the decay measurement taken through beryllium showed strong indication of a 5.1-day activity. The decay observed without the

use of absorber showed a mixed activity with a 6.8-day activity predominating after subtraction of the activity due to the 74-day component. These observations indicate the formation of Tb^{160} and Tb^{161}, and the probable formation of Tb^{153} and Tb^{156}.

In the terbium fractions separated 12 to 14 hours after bombardment, traces of alpha activity were observed. A sample submitted to Dr. J. O. Rasmussen for alpha pulse analysis showed alpha energy and decay corresponding to 4.1-hour Tb^{149}.

Dysprosium.—The chief component observed in the dysprosium decay was the 80-hour Dy^{166}. A long-lived activity was also observed, but it was not possible to determine its half-life. Aluminum absorption measurements on the equilibrium mixture showed the 0.4-Mev beta particle of Dy^{166} and the 1.9-Mev beta particle of the Ho^{166} daughter.

Calculations based on the relative yields of Dy^{166}, Ho^{166}, and Yb^{166} (see Sec. V) indicate that 2.54 percent of the total yield at mass number 166 is formed as Dy^{166}.

Holmium.—The major component observed in the holmium decay was due to the 27-hour Ho^{166}. The decay was measured through eight half-lives. The activity remaining as a long-lived component corresponded to less than 0.02 percent of the Ho^{166} activity present at the end of the bombardment. Aluminum absorption measurements showed the approximately 1.9-Mev beta energy of Ho^{166}. The 7-day activity presently assigned to Ho^{163} was not observed in our holmium sample in a resolvable amount.

Calculations based on the relative yields of Dy^{166}, Ho^{166}, and Yb^{166} indicate that 4.7 percent of the total yield at mass number 166 is due to Ho^{166}.

Erbium.—Decay of the erbium fraction could be resolved into at least three components, one of which gave rise to a holmium daughter of about 4.5 hours half-life. Half-lives of the three components were 9.4 days (Er^{169}), 72 hours (unknown) and a shorter component with an apparent half-life of 12 to 24 hours. Aluminum absorption measurements showed that the 72-hour component was associated with 1.3-Mev electrons (either positive or negative), while the shortest-lived component decayed primarily by gamma-ray emission. Nervik and Seaborg[12] have identified a 29-hour Er^{160} which decays to a 5.0-hour Ho^{160}, the mass assignment being verified by mass spectrometric separation. Ten-hour Er^{165} is expected to be present also, so it is felt that the short-lived component represents a mixture of Er^{160} and Er^{165}. The 72-hour component represents a previously unreported activity. On the basis of its counting yield relative to Er^{169} we expect it to be a negatron active isotope of erbium with mass number 169 or greater. The possibility of an independently-decaying isomer of Er^{169} is not eliminated. Decay measurements on the erbium fraction taken through 99.7 mg/cm^2 of beryllium (to eliminate the activity of Er^{169}) showed that the initial activity due to the 72-hour component was approximately equal to that of Er^{169} while the initial activity of the short-lived component was ten times as great. This indicates (considering relative counting efficiencies) that the yield of neutron-deficient erbium isotopes is considerably greater than the yield of neutron-rich isotopes.

Thulium.—Decay measurements on the thulium fraction could not be resolved into separate components unambiguously. Strong indications were seen of the presence of 9.6-day Tm^{167} and of a shorter-lived component with possible growth of a daughter activity, which could be 29-hour Tm^{165} giving rise to 10.2-hour Er^{165} as characterized by Nervik and Seaborg,[12] together with 7.7-hour Tm^{166} which is known to be present as the result of the observation of its growth from its Yb^{166} parent. The later portions of the decay curve seemed to indicate the presence of a very long-lived activity, which could be due to Tm^{168}, Tm^{170}, Tm^{171} or a mixture.

Ytterbium.—Decay of the ytterbium sample showed two prominent components, the 32.5-day Yb^{169} and a component of 66-hour apparent half-life. Growth of a 7.7-hour component, chemically identified as thulium, is due to Tm^{166} as mentioned above. The shorter-lived ytterbium activity is therefore presumed to be due to Yb^{166}. Decay measurements taken through 183 mg/cm^2 of beryllium absorber showed the same components, but the half-life of the shorter-lived component was reduced to 60 hours. Nervik and Seaborg[12] have reported the half-life of Yb^{166} to be 53.8 hours. We presume that the discrepancy in half-life indicates the presence of a small amount of Yb^{175} (4.2 days) whose radiations would be discriminated against as a result of the presence of the absorber.

Spallation products.—The work of O'Connor and Seaborg[9] on the bombardment of uranium with 380-Mev helium ions showed that there was apparently a continuous yield of radioactive products for the entire range of elements from the uranium region down to the vicinity of atomic number 25, the lowest atomic number for which they attempted to determine a yield. Above mass number about 120, the yield of fission products decreased with increasing atomic number. In the region above mass number about 200 the yield curve was observed to increase with increasing mass number. This increase was attributed to products formed by high energy spallation of uranium. The yield of products found in the region of the minimum of the curve might be attributed to a combination of fission products and spallation products. That fission can occur in such a manner as to give products of such high mass was shown by the detection of product nuclei of correspondingly low mass.

In the present work it was observed that the primary fission products tend toward the neutron-deficient side of stability with increasing mass number in the region 130 to 170. In the region of mass number 180 to 200, however, several negatron-emitting nuclides were

observed which we have attributed tentatively to spallation reactions.

IV. TABULATION OF OBSERVED YIELDS

The relative yield values, Y_R, (Ba^{140} taken to be 1.00) are given in Table I and are plotted in Fig. 1. These were calculated from the measured counting rates for the listed nuclides, whose identification was described in the previous section, taking into account the various factors described in Sec. II. The curve in Fig. 1 is drawn so as to represent the total isobaric yield at each mass number with this total yield estimated as described in Sec. V.

Since it was thought desirable to establish the relationship between these relative yields and the corresponding absolute yields (cross sections) some of these yields (which include the precursors) were redetermined in experiments where direct comparisons with the known yield of the reaction[39] $Al^{27}(p,n3p)Na^{24}$ could be made. These cross sections are listed in Table II together with the corresponding relative yields (from Table I).

TABLE I. Yields of observed fission and spallation products relative to Ba^{140}.

Mass number	Nuclide measured	Class[a]	Y_R
24	Na^{24}	2	0.0021
59	Fe^{59}	2	0.0078
65	Ni^{65}	2	0.024
66	Ni^{66}	2	0.027
67	Cu^{67}	2	0.091
72	Zn^{72}	2	0.090
76	As^{76}	1	0.0091
80	Br^{80m}	1	0.015
81	Se^{81m}	3	0.32
82	Br^{82}	1	0.067
83	Se^{83}	3	0.22
	Br^{83}	3	0.16
84	Br^{84}	3	0.14
86	Rb^{86}	1	0.59
89	Sr^{89}	3	1.5
91	Sr^{91}	3	1.6
92	Sr^{92}	3	1.7
103	Ru^{103}	3	1.8
106	Ru^{106}	3	2.2
109	Pd^{109}	3	0.19
111	Pd^{111}	3	1.6_5
	Ag^{111}	3	0.4_1
112	Pd^{112}	3	0.22
115	Cd^{115}	3	1.4_6
	Cd^{115m}	3	0.51
131	Te^{131m}	3	0.25
136	Cs^{136}	1	0.25
139	Ba^{139}	3	1.8
140	Ba^{140}	3	1.00
	La^{140}	1	0.48
	Nd^{140}	3	0.18
142	Pr^{142}	1	0.33
143	Pr^{143}	1	0.55
147	Nd^{147}	3	1.4
153	Sm^{153}	3	0.19
156	Sm^{156}	3	0.05
	Eu^{156}	3	0.12
166	Dy^{166}	3	0.0019
	Ho^{166}	1	0.0020
	Yb^{166}	3	0.030
193	Os^{193}	3	0.00043
~198	$Au^{195,199}$	3	0.00094
224	Ra^{224}	3	0.12
236	Np^{236} [b]		0.51

[a] Class 1, independent yield or shielded nuclide; Class 2, approximately total yield of mass number; Class 3, partial yield of mass number.
[b] Meinke, Wick, and Seaborg (unpublished).

TABLE II. Cross sections for formation of certain observed fission products.

Nuclide	σ_f(mb)	Y_R (Ba^{140} = 1.00)
Cu^{67}	2.1	0.09
Se^{81m}	7.5	0.32
Sr^{89}	35	1.5
Ag^{111}	$48._5$	2.1
Cd^{115}	$33._6$	1.4
Cd^{115m}	12	0.51
Ba^{140}	$23._5$	1.0

TABLE III. Yields of nuclides along certain isobaric chains.

Mass number	Nuclide measured	Relative yield (Ba^{140} = 1.00)	Estimated fraction of total chain
83	Se^{83}	0.22	0.45
	Br^{83}	0.16	0.33
111	Pd^{111}	1.6_5	0.5
	Ag^{111}	0.4_1	0.08
140	Ba^{140}	1.00	0.43
	La^{140}	0.48	0.21
	Nd^{140}	0.18	0.075
166	Dy^{166}	0.0019	0.044
	Ho^{166}	0.0020	0.047
	Yb^{166}	0.030	0.72

Integration of the yield *versus* mass number curve (Fig. 1) in terms of the cross sections for the formation of the fission products indicates a total fission cross section of 2.0 barns for uranium irradiated with 340- to 350-Mev protons. A single direct measurement[40] with an ionization chamber for the same reaction yielded a definitely lower value, somewhat less than a barn.

V. ISOBARIC YIELD STUDIES

Identification of the charge of the fissioning nucleus depends on the determination of the primary fission products. Experimentally we have attempted to measure the independent yields of various members of several reference mass number chains. The nuclide whose yield is represented by the maximum of the curve obtained by plotting the independent yield as a function of atomic number for a given mass number is defined to be the "primary" product for that mass number. In practice it is usually quite difficult experimentally to measure directly the independent yields for many of the members of a given mass number chain. Those independent yields which have been measured experimentally are listed in Table III. The yields of the measured members farthest from beta stability for any chain included the yields of their precursors.

In order to interpret the data obtained for independent yields we have assumed that the independent

[39] Stevenson, Hicks, and Folger (to be published).
[40] J. Jungerman, Phys. Rev. 79, 632 (1950).

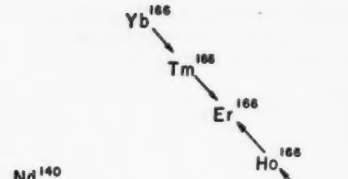

FIG. 2. Genetic relationships of the mass number 140 and mass number 166 decay chains.

yields of the various isobars of a given decay chain are distributed symmetrically about some particular Z in a manner which can be well approximated by the normal curve of error, using suitable parameters to adjust the half-width and peak height of such a distribution curve to the experimental results obtained. A description of the mathematical method of fitting the normal curve of error to such data is given in the Appendix.

It will be seen from the Appendix that three experimental data are sufficient to establish the constants of the curve. One eventually, therefore, could obtain some idea of the validity of our basic assumption by studying the independent yields in chains containing more than three members. Suitable chains are those of mass numbers 166, 141, 111, and 72, each chain containing four measurable members. Initial sets of three experimental data, as shown in Table III, have been obtained for the chains of mass number 140 and mass number 166. The genetic relationship of these chains is shown in Fig. 2.

Figures 3 and 4 show the standard curve of error histograms for the mass number 140 and mass number 166 chains, respectively. The parameters for these curves are tabulated in Table IV.

It is apparent that if we could predict the parameters of these charge-distribution histograms as functions of the chain mass number, we could derive factors for each mass number to give the total chain yield, including stable nuclides, in terms of the yield of any nuclide of the chain. The rough estimates of the fractions of total chain yields given in Table III were made in this manner on the basis of the few data presently available.

VI. DISCUSSION

Examination of the data presented here shows a few marked trends. Almost all of the low atomic number nuclides which were identified are of the neutron-excess type. As higher atomic numbers are approached, neutron-deficient nuclides increase in relative abundance of formation. In the ytterbium fraction, almost all the activity is due to neutron-deficient nuclides. In the spallation region which merges with the heavy fission fragments in the region of mass number 180, however, neutron-excess nuclides again are observed (in the elements osmium, gold, and radium). There seems to be a rather well defined region of fission products in the mass number range of the single hump in Fig. 1, and a region of spallation products in the region of the ascending curve starting around mass number 190, with a pronounced minimum in the yield curve between these two regions, presumably representing products from both fission and spallation reactions.

The yield *versus* mass number curve appears to be roughly symmetrical about mass number 114, indicating a "most probable fissioning nucleus" of mass number about 228. The data on independent yields can also be used to derive information concerning the nature of the fissioning nucleus, or, as it turns out, about the spread in mass number of the fissioning nuclei.

In a test of the possible extension to uranium of the hypothesis of Goeckermann and Perlman[2] that in high-energy fission of bismuth the most probable primary fission products are those with the same charge-to-mass ratio as the fissioning nucleus, we can take our value for Z/A of the "primary" fission products and calculate the mass of the "most probable fissioning nucleus" assuming various reasonable values for its

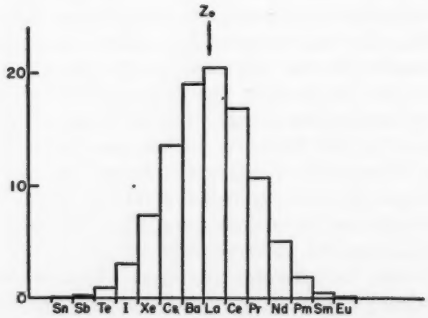

FIG. 3. Relative direct yields of fission products of mass number 140.

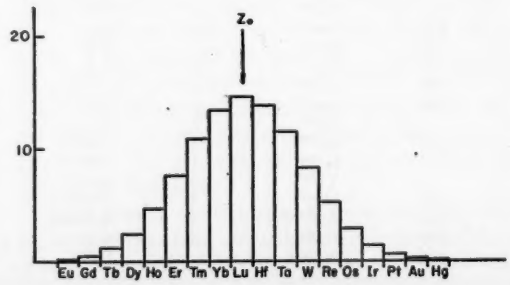

FIG. 4. Relative direct yields of fission products of mass number 166.

Z. The results (based on our best experimental value for Z/A of 0.42 from the mass number 140 and 166 chains) are listed in Table V.

It will be seen that this method leads to a maximum value of 221 for the mass number of the most probable fissioning nucleus, which is not in agreement with the value 228 as deduced above from mass-yield data. The maximum value of 221, moreover, can be attained only by a rather unlikely reaction mechanism. When we consider the probable sources of error in the mass-yield measurements the agreement is worse, since the yields on the heavy-mass side of the curve are most likely to pass unobserved because of direct formation of stable or neutron-deficient nuclides. Consequently we expect the observed location of the peak at mass number 114 to be, if anything, too low.

The different results from the two methods of arriving at a "most probable fissioning nucleus" are apparently due at least in part to the fact that any postulate of the existence of such a nucleus (or small range of nuclei) is not a good approximation in the high energy fission of uranium. It is reasonable to expect that uranium nuclei bombarded with 340-Mev protons will be left in widely different states of internal excitation; further, that even those which are left in roughly the same state of excitation will de-excite before fission by several different modes, leading (among other results) to different numbers of nucleons evaporated. This suggests that the observed fission yield curve is the result, not of a small number of fissioning species, but of a group of fissioning species whose relative importance is distributed in a manner dependent upon the bombarding energy and the bombarding particle, in agreement with the deductions of Douthett and Templeton.[14] The spread in mass number of the nuclei which undergo fission will be much broader than in the case of the high-energy fission of bismuth because in the case of uranium all of the spallation product nuclei formed by the emission of any number of neutrons (and a few protons) have relatively low potential barriers against fission. In the case of bismuth a most probable fissioning nucleus is better defined because the emission of a certain number of neutrons is necessary in order to lower the potential barrier to a point where fission is relatively probable and the emission of any protons leads to nuclei for which fission is relatively improbable. In addition, the greater possibility of fission for nuclei

TABLE IV. Measured constants of the mass number 140 and mass number 166 chains.

	Z_0	Standard deviation	Z_0/A
mass 140	57	2.7	0.41
mass 166	71	3.9	0.43

TABLE V. Nature of the fissioning nucleus deduced from charge-to-mass ratio.

Z	A	$\Delta A = 238 - A$
93	221	17
92	219	19
91	217	21
90	214	24
89	212	26

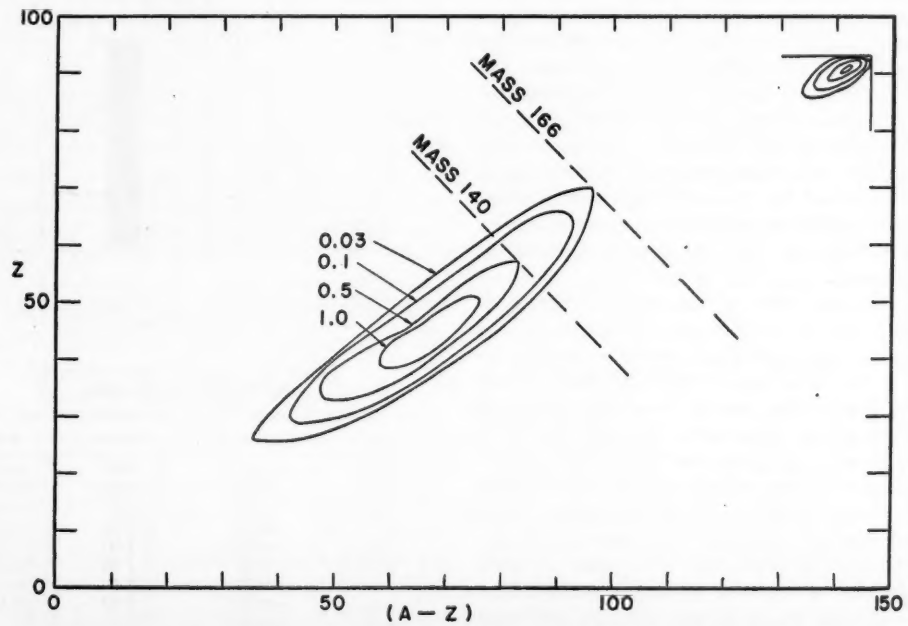

FIG. 5. Distribution of fission events and direct fission products in Z and $A-Z$ (schematic only).

with low excitation in the case of uranium means that a number of these nuclei may have a longer time to undergo the fission reaction which may permit more internal rearrangement of nucleons during fission.

Let us consider a nuclide formed by high-energy spallation of a U^{238} nucleus, this nuclide having an amount of internal energy much in excess of the fission potential barrier. This energy may be dissipated in one of three different ways: it may be used to cause fission; it may be dissipated as radiation or particle emission, the final nuclide descending to a nonfissioning ground state; or it may be carried off, in part or entirely, by an emitted neutron, proton, or composite particle, leading to a different nuclide which again may undergo one of these three changes. If we represent all the possible spallation product nuclides as points on a plane with coordinate axes Z and $A-Z$, then the various spallation and fission products possible from U^{238} bombarded with protons will all fall within the quadrant of this plane having $Z<93$, $A-Z<146$. The relative numbers of fission events occurring in various heavy nuclei lying within the spallation region can be described by a contour map. The contour lines are loci of points of equal numbers of fission events. The fission fragment yield curve may be plotted in the same way on the same chart (see Fig. 5). A dotted line of slope -1 represents an isobaric chain. The independent yield of the members of this chain as a function of Z is given by the value represented by the contour line intersected for each Z.

We may assume that the shape of the fissioning-nucleus contour map is markedly energy-sensitive. Factors influencing this shape will include the abundance of excited nuclei of various A and Z, their degree of excitation (which, presumably, is different for different A and Z and which is, also, probably not unique for any given A and Z) and the probability of fission for a nucleus of each particular A and Z under the given conditions of excitation. Let us further assume that the fission-fragment yield distribution is uniquely determined by the fissioning nucleus distribution. Some qualitative predictions of the behavior of the fission-fragment yield curve with variation of bombarding energy may then be made.

The most obvious effect of increasing the bombardment energy will be to increase the spread of the distribution of the spallation products leading to fission, since Douthett and Templeton[14] have shown that excess bombarding energy does not appear as kinetic energy of the fragments. This will lead to a lower average mass number for the "fissioning nucleus," with its concurrent effect of lowering the mass number of the maximum yield of fission fragments. Also, should neutrons be evaporated from the excited pre-fissioning nuclides in preference to protons or other charged particles in sufficient degree, as seems likely, the charge-to-mass ratio of the average fissioning nucleus, and hence of its fragments, should be increased. We thus expect that at high energies nuclides closer to beta stability, or even on the neutron deficient side, should appear in greater relative abundance, as is actually observed.

VII. ACKNOWLEDGMENTS

We wish to express our gratitude to Professors I. Perlman and L. Malatesta, Drs. H. G. Hicks, J. Miller, B. C. Haldar, G. Higgins, W. Nervik, and G. Rudstam and Major W. Worthington for helpful discussion and experimental assistance. We wish also to thank J. Conway and M. Moore for providing many spectrographic analyses of materials used, J. T. Vale, Lloyd Hauser, and the crew of the 184-in. cyclotron for their cooperation in irradiating our targets, and Mrs. Elinor Potter and Mrs. Roberta Garrett for their valuable assistance in the counting of samples. One of us (P. C. Stevenson) wishes to thank the National Research Council for a U. S. Atomic Energy Commission Postdoctoral Fellowship in the Physical Sciences. This work was performed under the auspices of the U. S. Atomic Energy Commission.

APPENDIX. DERIVATION OF THE CHARGE DISTRIBUTION OF ISOBARIC PRIMARY FISSION FRAGMENTS FROM CHAIN YIELD DATA

1. Let us assume that the independent fission yields of the fission fragments of a given mass are distributed according to a normal curve of error.

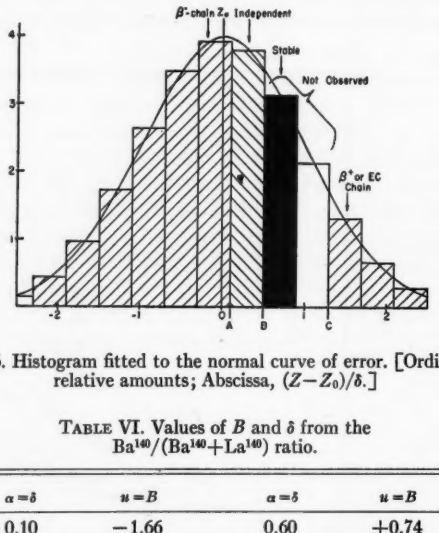

FIG. 6. Histogram fitted to the normal curve of error. [Ordinate, relative amounts; Abscissa, $(Z-Z_0)/\delta$.]

TABLE VI. Values of B and δ from the $Ba^{140}/(Ba^{140}+La^{140})$ ratio.

$\alpha=\delta$	$u=B$	$\alpha=\delta$	$u=B$
0.10	−1.66	0.60	+0.74
0.15	−0.89	0.70	+0.90
0.20	−0.47	0.80	+1.04
0.25	−0.19	0.90	+1.17
0.30	+0.02	1.00	+1.29
0.35	+0.20	1.20	+1.50
0.40	+0.34	1.40	+1.71
0.45	+0.46	1.60	+1.92
0.50	+0.56		

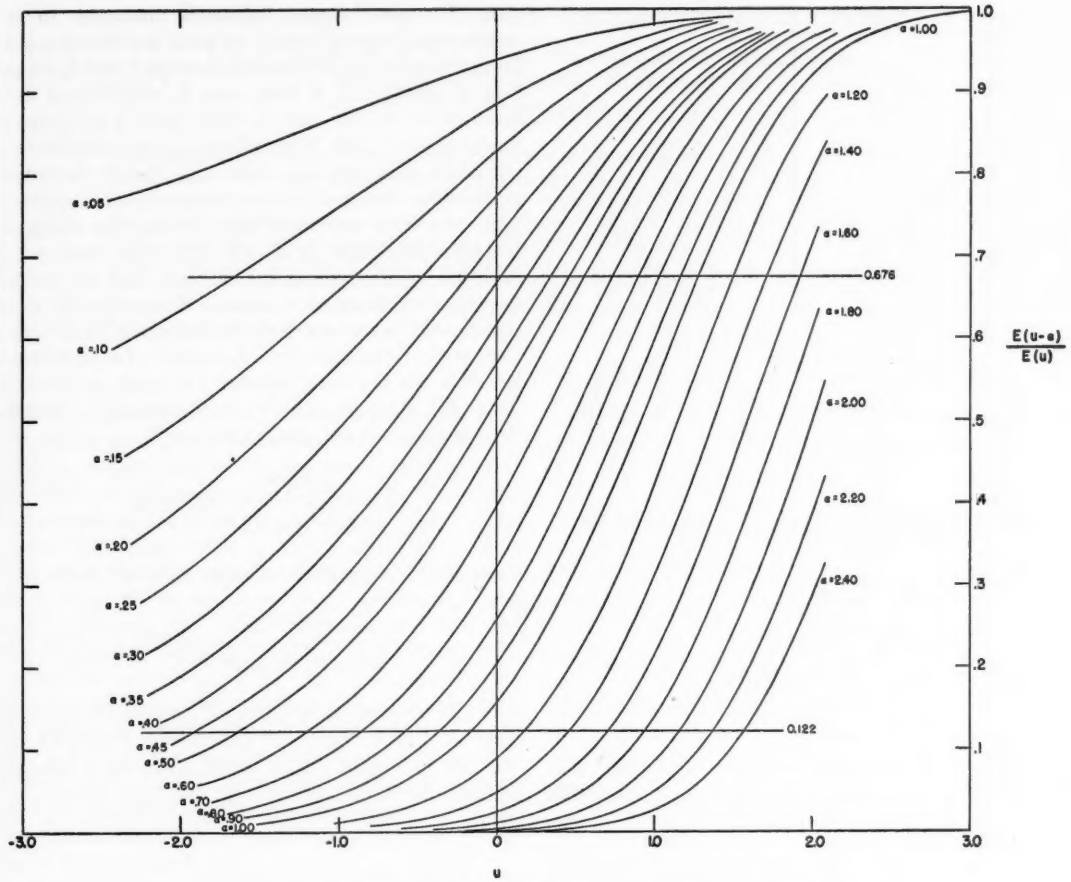

FIG. 7. $[E(u-\alpha)]/[E(u)]$ plotted as a function of u for various α.

2. Let us consider a normal curve of error fitted to a histogram, as shown in Fig. 6. Let the standard deviation of the normal curve of error be unity and the width of each block of the histogram be δ.

3. Let us consider data of the form obtained in our experiments. The yields observed for observable nuclides furthest from stability (on each side of stability) include all the yields from isobars still further from stability. Let species "A" be a β^- active nuclide with precursors too short to separate chemically; let species "B" be the (unstable) decay product of "A"; let species "C" be an isobaric neutron-deficient species which is chemically observable and has short precursors. Let us assume that the independent yield of "B" is measurable.

TABLE VII. Values of B and δ from the $Nd^{140}/(Ba^{140}+La^{140})$ ratio.

α	$u=B$	$\delta=\frac{1}{2}\alpha-u$	α	$u=B$	$\delta=\frac{1}{2}\alpha-u$
0.45	−1.92	+2.15	1.20	+0.17	+0.43
0.50	−1.64	+1.89	1.40	+0.46	+0.25
0.60	−1.21	+1.51	1.60	+0.70	+0.09
0.70	−0.87	+1.21	1.80	+0.93	−0.03
0.80	−0.58	+0.98	2.00	+1.16	−0.16
0.90	−0.32	+0.77	2.20	+1.37	−0.26
1.00	−0.16	+0.66	2.40	+1.57	−0.37

4. Let σ_A be the yield of A, σ_B be the yield of B, and σ_C be the yield of C, and let Σ be the yield of the total isobaric chain.

5. Let

$$E(x)=\int_{-\infty}^{x}\operatorname{erf}(t)dt.$$

Then

$$\sigma_A=E(A)\cdot\Sigma,$$
$$\sigma_A+\sigma_B=E(B)\cdot\Sigma,$$
$$\sigma_C=E(-C)\cdot\Sigma.$$

6. Now if the block width is δ, then $A=B-\delta$ and $C=B+n\delta$, where n is the number of intervening unobservable species (shown as two in the figure).

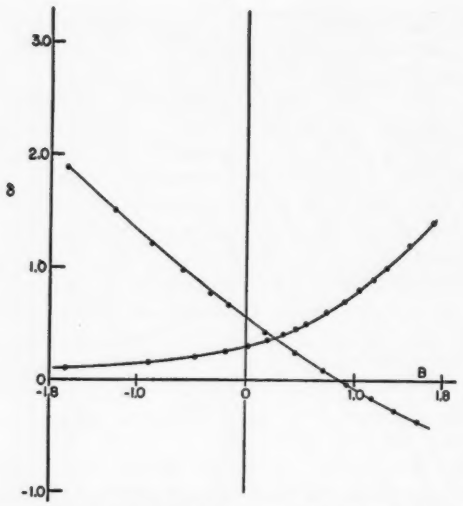

FIG. 8. Graphical solution for δ and B (mass number 140).

Therefore,

7. $$\frac{\sigma_A}{\sigma_A+\sigma_B}=\frac{E(B-\delta)}{E(B)},$$

8. $$\frac{\sigma_C}{\sigma_A+\sigma_B}=\frac{E[B-(2B+n\delta)]}{E(B)}.$$

9. Figure 7 shows a plot of $[E(u-\alpha)]/[E(u)]$ as a function of u for various α. By selecting a particular value for this fraction, which is analogous to the expressions in steps 7 and 8, we get α as a function of u. In the cases of the expressions in steps 7 and 8, we get δ as a function of B from step 7, and $2B+n\delta$ as a function of B from step 8 which gives δ as a second function of B. This is equivalent to two simultaneous equations in δ and B, which can readily be solved graphically. The standard deviation of the histogram in units of atomic number is then $1/\delta$ and the charge Z_0 for maximum yield is $Z_B+\frac{1}{2}-B/\delta$ (the term $+\frac{1}{2}$ is included to compensate for the fact that the atomic number corresponding to species B is presumed to be represented in the center of the histogram block rather than at the righthand edge). Example 1: Let us consider the data for the mass number 140 chain as given in Table III. Here, since Ce^{140} (stable) and Pr^{140} (half-life 3.4 minutes) are not observable, $n=2$.

$$\frac{\sigma(Ba^{140})}{\sigma(Ba^{140})+\sigma(La^{140})}=0.676.$$

From Fig. 7, we get the values in Table VI, and

$$\frac{\sigma(Nd^{140})}{\sigma(Ba^{140})+\sigma(La^{140})}=0.122,$$

which in conjunction with Fig. 7 gives us the values in Table VII. The values of δ and B from Tables VI and VII are plotted in Fig. 8, which gives for a common solution $B=0.265$, $\delta=0.370$; or $Z_0=56.8$, $\delta=2.70$.

Production of Heavy Unstable Particles by 1.37-Bev Pions*

W. B. FOWLER, R. P. SHUTT, A. M. THORNDIKE, AND W. L. WHITTEMORE
Brookhaven National Laboratory, Upton, New York

(Received December 9, 1954)

Five additional events interpreted as the production of heavy unstable particles by 1.37-Bev pions have been observed in a hydrogen-filled diffusion cloud chamber. In each case the observations are most naturally interpreted as due to the associated production of a hyperon and K-meson. These and earlier observations can be made consistent with known hyperon and K-meson masses if the reaction $\pi^-+p\rightarrow\Sigma^0+\theta^0$ is assumed to be a possibility with an immediate γ-decay $\Sigma^0\rightarrow\Lambda^0+\gamma$ as suggested by Gell-Mann and Pais. The total cross section for production of heavy unstable particles is estimated to be about 0.9 millibarn. The five new events confirm the previous indications that the Λ^0's tend to be emitted backwards in the center-of-mass system of the initial collision and to decay in a plane at a small angle to that of the production plane. The orientations of Λ^0's from the wall also support these angular correlations.

IN a previous report[1] we have discussed four interactions of 1.37-Bev pions from the Cosmotron with protons, which resulted in the production of heavy unstable particles. Investigations of the production mechanism of heavy unstable particles (also referred to as V-particles in this article) in collisions between elementary particles are of interest for several reasons. First, one wishes to know the V-production cross section. Second, one hopes to determine whether two V-particles are normally produced simultaneously in elementary collisions. If so, one can reconcile the observed relatively large production cross section with the relatively long lifetimes of the particles.[2] Third, one is interested in finding what kinds of V-particles (classified according to charge, decay schemes, lifetimes, etc.) are produced together. Fourth, observed angular correlations may give information on the spins of some heavy unstable particles.

We now wish to describe five additional examples of the production of heavy unstable particles observed under similar conditions. While the previous four cases were obtained in a 16-in. diameter hydrogen-filled diffusion chamber provided with a magnetic field, the present five were found in a long chamber (six feet by eleven inches) without magnetic field. Although this chamber had no magnetic field, the V-events produced in the gas could be analyzed from the measured angles and estimated densities of ionization of the emergent tracks and the known momentum of the incident pions. The few V-events produced in the walls of the long chamber are not reported since the measured data are insufficient for useful analysis. However, fifteen such events obtained from the walls of the magnet chamber could be analyzed and will also be reported for comparison with the results on V-events produced in the hydrogen. Details on the operation and arrangement of the cloud chambers appear elsewhere.[3,4]

I. ANALYSIS OF EVENTS PRODUCED IN THE GAS OF THE LONG CHAMBER

Detailed information has been given previously[1] on a total of six events identified individually as Cases A to F. (Cases A, B, D, and E showed V-production in hydrogen, Cases C and F referred to V-events originating in the chamber walls.) The present five additional events produced in hydrogen in the long cloud chamber will be called Cases G to K. Three of these, Cases G, H, and I, involve the production of neutral unstable particles. Two more, Cases J and K, involve the production of charged unstable particles.

Since the momenta of the observed decay product particles are not known here, their masses are not known either without further assumptions. Since, however, the point of origin is known for each V-event, we know the angles between the charged decay products and the line of flight of the unstable particle. By assuming values for the masses of the decay products and for the Q-value of the decay process we can now calculate what the momenta of the decay products must be in the laboratory system. To be accepted, these assumed masses and computed momenta must be in agreement with the observed estimated densities of ionization. In this procedure we will not make arbitrary assumptions as to the masses of the decay products and Q-values, but we shall assume values consistent with known V-particle decay modes. The possibilities which we admit are described below in the Bagnères nomenclature.[5] Among hyperons (Y), which are heavier than nucleons, there are: $\Lambda^0\rightarrow p+\pi^-+37$ Mev (mass 1107 Mev), with lifetime $\tau=3.6\times10^{-10}$ sec; $\Sigma^{\pm}\rightarrow$nucleon+pion+115 Mev (mass 1185 Mev), $\tau\approx10^{-10}$ sec (?); and $\Xi^-\rightarrow\Lambda^0+\pi^-+65$ Mev (mass 1312

* Work performed under the auspices of the U. S. Atomic Energy Commission.

[1] Fowler, Shutt, Thorndike, and Whittemore, Phys. Rev. **91**, 1287 (1953), and **93**, 861 (1954). The incident π^- energy of 1.5 Bev then used has had to be revised to the presently used value of 1.37 Bev. This does not substantially change any of the previous conclusions.

[2] M. Gell-Mann, Phys. Rev. **92**, 833 (1953); A. Pais, Phys. Rev. **86**, 663 (1952) and Physica **19**, 869 (1953); M. Gell-Mann and A. Pais, Proceedings of the International Conference on Nuclear Physics, Glasgow, July, 1954 (unpublished).

[3] Fowler, Shutt, Thorndike, and Whittemore, Rev. Sci. Instr. **25**, 996 (1954).

[4] Eisberg, Fowler, Lea, Shephard, Shutt, Thorndike, and Whittemore, Phys. Rev. **97**, 797 (1955).

[5] R. W. Thompson, Science **120**, 585 (1954).

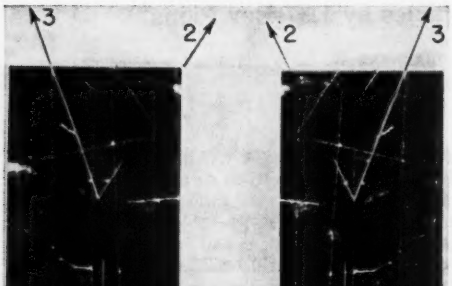

FIG. 1. Case *G*. Photograph of a probable Λ^0 produced in a 1.37-Bev π^--p collision. Track 1 is the incident pion, tracks 2 and 3 are pion and proton, respectively, from Λ^0 decay. Tracks 1, 2, and 3 have been reinforced with white ink for better contrast from other beam and background tracks.

Mev), $\tau \approx 10^{-10}$ sec (?). The symbols $\Sigma^{\pm}$ and Ξ^- have been used by Gell-Mann and Pais.[2] On theoretical grounds Σ^0 and Ξ^0 might be expected, but have not been identified experimentally. Among *K*-mesons (K), which are lighter than nucleons, there are: $\theta^0 \rightarrow \pi^+ + \pi^-$ +214 Mev (mass 494 Mev), $\tau \approx 1.2 \times 10^{-10}$ sec, probably $\theta^+ \rightarrow \pi^+ + \pi^0 + 214$ Mev (mass 494 Mev), τ uncertain;[6] and also tau mesons and kappa mesons (whose presence is nowhere required for the interpretation of our events). On theoretical grounds a θ^- might be expected, but has not been identified experimentally.

We will try to fit the observed *V*-events to one of the decay schemes given in the previous paragraph by using the given decay products and *Q*-values. If one assumed particle is consistent with the observed data,

TABLE I. Data for event *G*.

	(1)	(2)	(3)
1. Estimated ionization density	~Minimum	~Minimum	2 to 4 ×minimum
2. Assumed particle	Pion	Pion	Proton
3. Angle between incident π^- and direction of flight of V (degrees)		12.5±4	
4. Angle between direction of flight and decay products (degrees)		35.5±3	13.5±1
5. Assignment of momenta (Mev/c) consistent with 2, 3, 4, and Q=37 Mev		144	360

[6] Hodson, Ballam, Arnold, Harris, Rau, Reynolds, and Treiman, Phys. Rev. **96**, 1089 (1954). Hill, Salant, and Widgoff, Bull. Am. Phys. Rev. **29**, No. 7, 32 (1954).

while the others are not, we consider the event to be identified as due to this particle even though the *V*-event could not be identified if its point of production were unknown. In all cases, energy and momentum balance requires that at least one particle in addition to the *V*-event must have been produced. The masses of these additional particles are calculated on the assumption that only one is involved in each case.

Case *G*, Interpreted as a Λ^0 Produced in π^--p Collision

Figure 1 shows a photograph of a track of a negative pion (1) disappearing suddenly in hydrogen. The

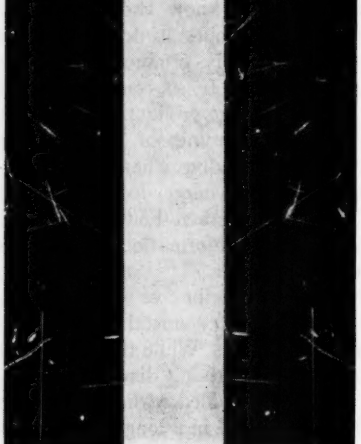

FIG. 2 Case *H*. Photograph of a possible θ^0 produced in a 1.37-Bev π^--p collision. Track 1 is the incident pion, tracks 2 and 3 are pions from θ^0 decay. These tracks have been reinforced with ink for better contrast from other beam and background tracks.

V-event with tracks labeled (2) and (3) lies in a plane which contains the end point of (1) and is consistent with a Λ^0 but not with a θ^0. The information leading to this identification is given in Table I. Although no momenta are measured it seems safe to assume that track (1) is a beam pion with a momentum of 1500±200 Mev/c, as has been determined for this beam.[4] There is no evidence for the nature of the missing neutral particle produced by the incident pion. Assuming an incident pion with momentum of 1500 Mev/c and only

a single neutral particle we find for its mass a value of 670 Mev, consistent with the values found in Cases *A* and *B*. This mass is relatively unaffected by the error in the flight angle of the Λ^0 (12.5±4°), being most sensitive to the assumed momentum of the incident pion. In this beam very few pions have been observed to have momenta as low as 1200 Mev/*c*. With this as the lower limit, the mass for the unobserved neutral particle is computed to be 570 Mev, still larger than 494 Mev, the presently accepted value for the θ^0.[7] Naturally, for an individual event this interpretation is uncertain since it is possible that two or more neutral particles are involved instead of a single K^0.

Case *H*, Interpreted as a Probable θ^0 Produced in a π^--*p* Collision

Figure 2 shows a pion (1) disappearing in the hydrogen with the probable appearance of a θ^0. Table II gives the pertinent data for this event. The plane containing (2) and (3) also contains the end point within an uncertainty of only 2 mm, although the decay takes place quite far from the origin. The interpretation of this event is sensitive to the exact value

TABLE II. Data for event *H*.

	(1)	(2)	(3)
1. Estimated ionization density	Minimum	2 to 4 ×minimum	Minimum
2. Assumed particles	Pion	Pion	Pion
3. Angle between incident π^- and direction of flight of *V* (degrees)		12.5±1.5	
4. Angle between direction of flight and decay products (degrees)		26±2	4±2
5. Momenta (Mev/*c*) consistent with 2, 3, 4, and *Q*=214 Mev		93	1168

taken for the direction of track (3). With the nominal value of 4°, the *V*-event is not consistent with either a Λ^0 or a θ^0 particle, since for either particle the required ionization densities do not agree with the observed values. To be consistent with a Λ^0 decay, track (3) must make an improbably small angle of 1.3° with the line of flight of the Λ^0. Therefore, the observed *V*-event is probably not a Λ^0 particle. For consistency with a θ^0, track (3) must make an angle of 2° with the line of flight of the θ^0, which is more probable. For this assumption the unseen neutral particle has a mass of 1107 Mev for an incident pion of 1600 Mev/*c*. Thus it is not necessary here to postulate an improbable value for the momentum of the incident pion, or a *K*-meson with mass in excess of 494 Mev, but one can obtain a satisfactory solution using only a θ^0 and a Λ^0. (Assuming that the observed decay event is a Λ^0 despite the poorer agreement with the measured angles leads to a mass for the missing particle that is quite consistent with that of a θ^0.)

[7] Thompson, Buskirk, Etter, Karzmark, and Rediker, Phys. Rev. **90**, 1122 (1953).

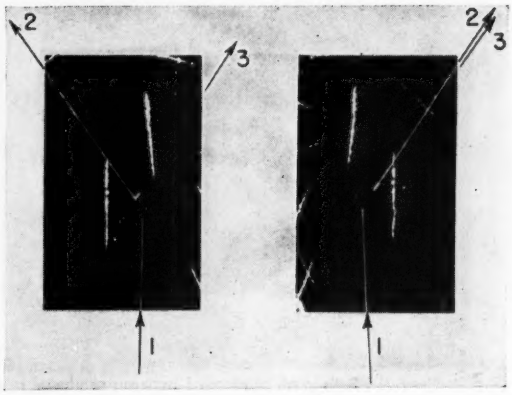

FIG. 3. Case *I*. Photograph of probable θ^0 produced in a 1.37-Bev π^--*p* collision. Track 1 is the incident pion, tracks 2 and 3 are pions from θ^0 decay. These tracks have been reinforced with ink for better contrast from other beam and background tracks.

Case *I*, Interpreted as a θ^0 Produced in a π^--*p* Collision

Figure 3 shows another example of a pion disappearing in hydrogen with the subsequent appearance of a θ^0. Table III gives the measured data on angles and ionization densities. This *V*-event is entirely consistent with a θ^0 particle having a *Q*-value of 214 Mev. The plane containing (2) and (3) also contains the end point of (1). No assignment of momenta is possible to allow this particle to be a Λ^0 since the proton would ionize more than 10 times the minimum rate. If one again assumes a single unseen particle involved in the interaction, its mass is computed to be 1310±140 Mev for an incident pion momentum of 1500±300 Mev/*c*. This is considerably larger than the value of 1107 Mev for a Λ^0, though an improbably low value of the incident pion momentum would yield this mass for the unseen

TABLE III. Data for event *I*.

	(1)	(2)	(3)
1. Estimated ionization density	Minimum	1 to 2 ×minimum	1 to 4 ×minimum (foreshortened)
2. Assumed particles	Pion	Pion	Pion
3. Angle between incident π^- and direction of flight of *V* (degrees)		42±3.5	
4. Angle between direction of flight and decay products (degrees)		50±10	40±10
5. Assignment of momenta (Mev/*c*) consistent with 2, 3, 4, and *Q*=214 Mev		262	313

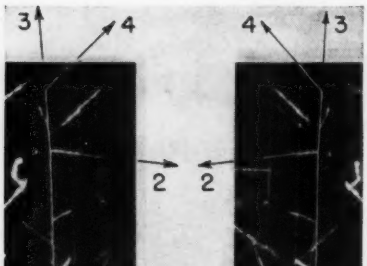

FIG. 4. Case *J*. Photograph of charged hyperon produced in a 1.37-Bev π^--p collision. Track 1 is the incident pion, track 2 is probably a *K*-meson, track 3 is the hyperon, and track 4 is probably a pion from hyperon decay. These tracks have been reinforced with ink for better contrast from other beam and background tracks.

particle. Other possible explanations for the discrepancy are discussed in Sec. IV. On the other hand, if we assume that the mass of the observed particle is 600–650 Mev, then the computed mass of the unseen particle is consistent with a Λ^0 particle for an incident pion with 1500 Mev/c.

Case *J*, Interpreted as a $Y^{\pm}$ and $K^{\mp}$ Produced in π^--p Collision

Figure 4 shows a pion interaction in hydrogen in which two charged particles are emitted. Several features of this event indicate that the outgoing particles can best be identified as heavy unstable particles. Table IV gives the data on the angles and ionization densities. Since track (3) makes a very small angle with track (1), it is rather difficult to determine whether tracks (1) and (3) lie in the plane containing (2). Since tracks (2) and (4) lie in a common plane, all four tracks must lie in a common plane, assuming that no neutral particle is produced in the collision.

Consider first tracks (1), (2), and (3). Conservation of momentum alone determines the momenta of (2) and (3), if we postulate the momentum of (1). If (2) is assumed to be a $K^{\pm}$ with mass of 494 Mev, then (3) has a $\Sigma^{\pm}$ mass of 1185 Mev (Q=115 Mev) for an incident pion with momentum of 1450 Mev/c. Each of these masses is consistent with the observed density of ionization and the computed momentum. The mass of 1185 Mev for (3) would agree with that inferred for Case *E*. To make the mass of (3) consistent with that of a Ξ^- (mass 1312 Mev), without making the mass of (2) substantially less than 494 Mev, the incident pion must have a momentum of 1800 Mev/c which is unlikely.[8]

[8] Case *E*, previously interpreted as production of a Σ^-, could perhaps have been a Ξ^-. Case *F* could not have been a Ξ^-, since the Q-value obtained on this assumption would be too high (~100 Mev).

Consider now the decay of (3) to give a pion (4) plus at least one additional neutral particle. If the mass of the hyperon (3) is 1185 Mev, the neutral particle a neutron (n), and the momentum of the pion is 200 Mev/c, then the decay of (3) according to $\Sigma^{\pm}\rightarrow n+\pi^{\pm}+Q$ yields a value for Q of 115 Mev. On the other hand, if the neutral particle is a Λ^0, and the pion has a momentum of 100 Mev/c, then the decay would be consistent with $\Xi^-\rightarrow\Lambda^0+\pi^-+65$ Mev, except that a pion of 100 Mev/c would ionize 2×minimum instead of minimum.

Further consideration of Case *J* shows that the above interpretation is unique. For example, an elastic pion scattering is not possible on three accounts. First, track (2) is observed at an angle which is very likely greater than 90°, which is impossible if (2) is a proton. Second, if track (1) is a pion with the nominal beam energy, then a decay of the pion subsequent to the collision could not yield a larger decay angle than 1.5°. Since the observed angle is 54°, this possibility is definitely ruled out. Third, if track (2) were a pion, then track (3) would have a mass of 1700±150 Mev for an incident pion with momentum of 1500±300 Mev/c. Such a large mass for (3) would give an ionization density of 1.6×minimum instead of minimum and would be much larger than even that of a Ξ^-. As an alternative explanation of the event one might consider the possibility that track (1) is a *K*-meson produced in the target or in the collimating channel. If track (2) definitely emerges at greater than 90°, the interaction cannot be an elastic *K*-p scattering with the subsequent decay of the *K*. Furthermore, there is a very small chance that a *K*-meson so produced would scatter in the cloud chamber and also decay within a few centimeters. Finally, the possibility that a long-lived (~10^{-8} sec) K^- from the Cosmotron undergoes

TABLE IV. Data for event *J*.

	(1)	(2)	(3)	(4)
1. Estimated ionization density	Minimum	>2.5 × minimum	Minimum	Minimum
2. Assumed particles	Pion	*K*-meson	Hyperon	Pion
3. Angle between incident π^- and direction of flight (degrees)		96±8	3±2	
4. Angle between (3) and its decay product (degrees)			54±4	
5. Momenta (Mev/c), assuming a $\Sigma^{\pm}$ for (3)	1450	76	1460	200
6. Momenta (Mev/c) assuming a $\Xi^{\pm}$ for (3)	1800	95	1810	100

the reaction $K^-+p\rightarrow\pi^\mp+\Sigma^\pm$ with subsequent short-lived ($\sim 3\times 10^{-10}$ sec) decay of the $\Sigma^\pm$ is ruled out by energy conservation.

Case *K*, Interpreted as a $Y^\pm$ and $K^\mp$ Produced in π^--p Collision

Figure 5 shows an event similar to that in Fig. 4, where a π^--p interaction results in two charged particles. The angles show that probably all four tracks lie in a single plane. For reasons similar to those given in Case *J*, this interaction cannot represent the elastic scattering of a pion nor is it likely to be the scattering of a *K*-meson produced in the target of the Cosmotron. Table V gives the data on angles and ionization densities.

The analysis is carried out assuming that tracks (2) and (3) are heavy unstable particles. Track (2) cannot

TABLE V. Data for event *K*.

	(1)	(2)	(3)	(4)
1. Estimated ionization density	Minimum	Minimum	2 to 4 ×minimum	1 to 2 ×minimum
2. Assumed particles	Pion	*K*-meson	Hyperon	Pion
3. Angle between incident π^- and direction of flight (degrees)		32.5±3.5	23±2.5	
4. Angle between (3) and its decay product (degrees)				51±7
5. Momenta (Mev/*c*), assuming $\Sigma^\pm$ for (3)	1350	652	878	235
6. Momenta (Mev/*c*), assuming $\Xi^\pm$ for (3)	1950	940	1265	160

be as heavy as a hyperon because the minimum density of ionization would require so great a momentum for (2) that conservation of energy and momentum would be impossible for a beam pion for track (1). If we assume that track (2) is a *K*-meson with mass of 494 Mev, and track (3) is a hyperon ($\Sigma^\pm$) with mass of 1185 Mev, conservation of energy requires that the incident pion have a momentum of 1350 Mev/*c*. With this identification the measured densities of ionization and computed momenta are consistent. The subsequent decay of (3) into a neutron and pion requires that (4) have a momentum of 235 Mev/*c*, which is possible for the observed ionization density of 1 to 2 times minimum. It is impossible to make track (3) a $\Xi^\pm$ with associated production of a $K^\mp$ without assuming the incident pion has the unreasonably large momentum of 1950 Mev/*c*.

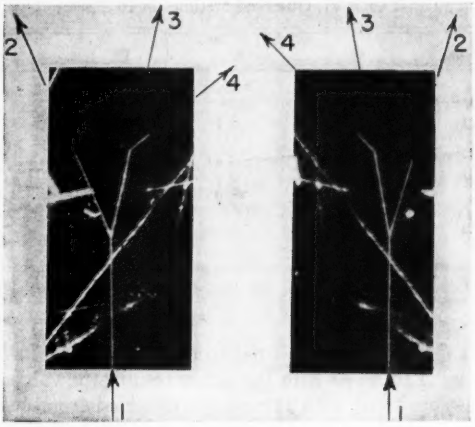

FIG. 5. Case *K*. Photograph of charged hyperon produced in 1.37-Bev π^--p collision. Track 1 is the incident pion, track 2 is a possible *K*-meson, track 3 is the hyperon, and track 4 is probably a pion from hyperon decay. These tracks have been reinforced with ink for better contrast from other beam and background tracks.

Also the Ξ would ionize only 1.5 times the minimum rate. If (2) were a pion (3) could be a Ξ for an incident π^- momentum of 1.2 Bev/*c*.

II. UNSTABLE PARTICLES PRODUCED IN WALLS OF MAGNET CHAMBER

As mentioned above, the few isolated *V*-events produced in the walls of the long chamber and decaying in the gas could not be analyzed usefully, since no momenta could be measured, and their geometrical arrangement with respect to the incident pion was unknown. With the magnet cloud chamber, about twenty-seven possible neutral *V*-events were found for seventeen of which momenta and angles could be measured sufficiently well that *Q*-values could be calculated. Of these, twelve were identified as Λ^0, three as θ^0 (including Case *C*), and two were consistent with either Λ^0 or θ^0. All *Q*-values except one were consistent within the errors with the usual values of 37 and 214 Mev for Λ^0 and θ^0, respectively.

Five possible cases of charged heavy unstable particles originating in the walls were found. One of these could be a K^+ but could just as well be a θ^0, one case may represent a Σ^+ decay, but is very uncertain, and three cases are definite decays of negatively charged particles. One of the latter has been identified as a Σ^- (Case *F*).

III. LIFETIMES, CROSS SECTION, AND ANGULAR RELATIONSHIPS

As in the earlier report,[1] chance still plays a large part in the results on lifetime, cross section, and angular relations. However, some available data will be given for the events occurring in the gas as well as for the events produced in the walls of the cloud chamber.

TABLE VI. Observed lifetimes in 10^{-10} sec.

Event	Λ^0	K^0	$Y^\mp$	$K^\pm$
A	0.4	>4[a]		
B	0.3	>3[a]		
D	9	0.1		
E			2	>0.7
G	2.6	>3.4[a]		
H	>8[a]	8.1		
I	>5[a]	0.7		
J			1.0	>2.9
K			2.1	>2.4

[a] Lower limits for lifetimes, provided decay into neutral particles did not occur.

Table VI gives the data on the lifetimes for the Cases *A* to *K*. As with the earlier results, the values are still consistent with the results obtained from cosmic ray studies[9] which indicate for the Λ^0 a lifetime of $(3.6_{-0.7}{}^{+1.1})\times10^{-10}$ sec and for the θ^0 $(1.2_{-0.3}{}^{+0.8})\times10^{-10}$ sec.

The cross section now computed for production of heavy unstable particles is close to the 1 mb originally estimated.[1] In both chambers 470 interactions were observed (not including 9 resulting in heavy unstable particle production). Making use of Fermi's calculation of statistical weights for different charge states,[10] one can estimate that ~15 percent of the observed interactions leading to meson production should give all neutral prongs and therefore remain undetected in the present experiment. Then about 550 pion interactions may have really occurred in both chambers. A count of the π-μ decays in the long chamber served to give the flux of pions through that chamber. When combined with the interactions observed in that chamber, the cross section for pion interaction was found to be 34.6 ± 2.7 mb.[4,11] One can estimate that, for the given geometry, about 90 percent of the *V*-events are found, assuming a mean lifetime of 3×10^{-10} sec for the hyperons and 1.5×10^{-10} sec for the *K*-particles. Within reasonable limits this estimate does not depend strongly on the angular distributions of the lines of flight of the unstable particles. The 9 cases of unstable-particle production in hydrogen may, therefore, correspond to 11 ± 4 cases. These data lead to a cross section for heavy unstable particle production of ~0.7 millibarn for collisions of 1.4-Bev π^- mesons with protons. (This does not yet take into account the decay of V^0-particles into neutral particles only or possible production of long-lived *K*-particles, the effect of which will be discussed in Sec. IV.)

Tables VII and VIII give the data on angular correlations for all cases considered above. The quantity α is the angle between the production and decay planes, where the production plane is determined by the lines of flight of the incident pion and the heavy unstable particle and the decay plane is determined by the lines of flight of the heavy unstable particle and its decay products. Obviously the concept of decay plane fails for the decay into three products. The quantity β is the angle between the incident pion and the line of flight of the unstable particle in the c.m.s. (center-of-mass system) of the incident pion and the struck proton. The quantity γ is the angle between the incident pion and the positive track in the *V*-event in the rest system of the *V*-particle. For random distribution α should cover the range 0–90° uniformly. For isotropic angular distributions β and γ should occur preferably around 90° (largest solid angle available).

The angle between the production and decay planes (α) still exhibits the rather close correlation shown earlier.[1] For the Λ^0 particles, α is less than 45° for all events produced in the gas. For the events produced in the chamber walls this effect is less pronounced, possibly because it is diluted by the uncertainty in origin of the events. For the θ^0 events, α does not show such an effect, but the data are few. For the charged unstable events, the heavy particle ($Y^\pm$) decays in a plane which is also closely correlated with the production plane. An investigation of several cosmic ray examples[12] has shown a similar effect for the hyperons. Probably this effect indicates that hyperons have spin greater than $\frac{1}{2}$.

TABLE VII. Angular correlations for events produced in gas.[a]

Event	α	β	γ
A Λ^0	5±5	141	107
B Λ^0	30±20	125	19
D Λ^0	27±10	174	151
D θ^0	70±5	6	
E Y^-	7±5	30	77[b]
G Λ^0	38±5	160	115
H θ^0	22±10	28	
I θ^0	58±3	98	
J $K^\pm$	20±20	169	46[b]
J $Y^\mp$		11	
K $K^\pm$	10±10	70	28[b]
K $Y^\mp$		110	

[a] α with its error was measured, where errors were determined directly; all other angles were computed for the assumed decay schemes.
[b] For these cases, γ is the angle between the incident pion and the neutron from the hyperon in the rest system of the hyperon.

For the events produced in the gas, the line of flight of the *V*-event in the c.m.s. with respect to the incident pion (angle β) shows that the Λ^0 prefers to travel backward in the c.m.s.[13] If we make the assumption that two heavy particles and no pions are produced in

[9] D. I. Page, Phil. Mag. **45**, 863 (1954); G. D. Rochester and C. C. Butler, Repts. Progr. in Phys. **16**, 364 (1953). Also see Proceedings of the Duke University Cosmic Ray Conference, 1953, p. II-22 (unpublished).
[10] E. Fermi, Annais da Academia Brasileira de Ciencias **26**, 61 (1954).
[11] This value agrees well with the total cross section, 34 ± 3 mb, of Cool, Madansky, and Piccioni, Phys. Rev. **93**, 249 (1954).
[12] Ballam, Hodson, Martin, Rau, Reynolds, and Treiman, Phys. Rev. **97**, 245 (1955).
[13] One can estimate that, because of the difference in momenta in the laboratory system, the chance of observation of a Λ^0 travelling forward in the c.m.s. is about 30 percent smaller than that of a Λ^0 travelling backward. This bias is far from sufficient to explain the observed distribution.

each interaction, then these cases show the Λ^0 always going backwards except for Case *I* where $\beta=180-98=82°$. The events produced in the cloud chamber wall show the same effect, only three Λ^0 particles being emitted at less than 90° while nine were emitted backwards. In fact, five were emitted at angles greater than 150°, where the solid angle forms only 13 percent of the hemisphere. Reynolds and Treiman[14] have observed a similar effect with cosmic rays. For the charged hyperon cases, on the other hand, two are emitted at small angles and one at 110°.

Several authors[15] have discussed a possible dependence on spin of the *V*-particles for the distribution of γ (here defined as the angle between the incident pion and the positive decay product of a *V*-event in its rest system), which of course would also affect the distribution of the α just discussed. The angle γ is also tabulated in Tables VII and VIII. For four cases where the Λ^0 is produced in the gas the values of γ are 19, 107, 115, and 151 degrees, which shows no obvious preference. For the events coming from the walls, there appears to be a preference for γ near 180° where

TABLE VIII. Angular relations for 15 events produced in walls of magnet chamber, including Case *C*.

Angle interval, degrees	Number of cases in angle interval					
	α		β		γ	
	Λ^0	θ^0	Λ^0	θ^0	Λ^0	θ^0
0–22½	6	0	0	2	0	0
22½–45	1	1	0	0	0	0
45–67½	2	2	1	1	2	1
67½–90	3	0	2	0	1	1
90–120			1	0	3	1
120–150			3	0	2	0
150–180			5	0	4	0

the relative solid angle is small. The distribution of γ may not be isotropic, but there is no evident reason for such a lack of symmetry. We prefer to believe that the effect seen for the *V*-events from the wall is due to an experimental bias. In the three cases where charged hyperons were produced in the gas (Cases *E*, *J*, *K*), the nucleon from the decay of the $Y^{\pm}$ went forward in the rest-system of the $Y^{\pm}$ with $\gamma=28$, 46, and 77 degrees. Much better statistics are needed for the detailed distributions. At this point, however, from the distribution in α alone, there is fair evidence that the spins for some hyperons may be at least as high as $\frac{3}{2}$. At the same time, it is perhaps improbable that the hyperon spin is much larger than this value since then

[14] G. T. Reynolds and S. B. Treiman, Phys. Rev. **94**, 207 and 797 (1954).

Note added in proof.—A production mechanism suggested by M. Goldhaber (Phys. Rev. **92**, 1279 (1953)) consists of simultaneous production of two θ^0's, possibly virtual, which can form compound states with pions or nucleons, resulting in the different observed heavy unstable particles. As pointed out by Goldhaber, strongly nonisotropic angular distributions for the emitted particles may result.

[15] L. Wolfenstein, Phys. Rev. **94**, 786 (1954); Treiman, Reynolds, and Hodson, Phys. Rev. **97**, 244 (1955).

TABLE IX. Masses for all heavy unstable particles produced in the gas.

Case	Hyperon	*K*-Meson
A	1107(Λ^0)	650±70[a]
B	1107(Λ^0)	620±70
D	1107(Λ^0)	517±20
E	1185(Σ^-)	510±50
G	1107(Λ^0)	670±70
H	1023±150	494(θ^0)
I	1310±90	494(θ^0)
J	1217±120	494($K^{\pm}$)
K	1185($\Sigma^{\pm}$)	560±80

[a] Masses with indicated errors were derived from assumed particles, labelled Λ^0, $\Sigma^{\pm}$, θ^0, $K^{\pm}$, for nominal incident π^- momentum of 1500 Mev/*c*. Errors take into account ±200 Mev/*c* uncertainty for π^- momentum and other, mostly less important, uncertainties.

the distribution of γ should be so peaked forward and backward that the experimentally observed angles in the range $60°<\gamma<120°$ (Table VII) become very improbable. The expected distribution in γ, however, depends not only on the hyperon spin but also on the other angular momenta involved in the production mechanism, such as the spin of the *K*-particle and the states of angular momenta in which the two particles were emitted. Therefore the observed distribution of γ might be consistent with a large spin for the hyperon under some conditions.

IV. MASSES AND IDENTITY OF *V*-PARTICLES PRODUCED IN HYDROGEN

Table IX shows a compilation of all the masses found for the 9 events occurring in the gas. It is apparent that all of these events are consistent with associated production of a hyperon together with a *K*-meson.[16]

From the geometry of the cloud chambers, assuming that hyperons and *K*-mesons are usually produced together (associated production) and decay with the lifetimes cited in Sec. III, one infers that in about 10 to 20 percent of all *V*-production events both produced particles should be observed to decay. This fraction of expected double decays becomes smaller if some produced particles have long lifetimes, or if decay into neutral particles only should take place often. In a total of eleven *V*-production events observed in π^--p collisions (nine reported here and two mentioned in footnote 16), two have shown both particles decaying. This is certainly consistent with the fraction expected from associated production.

Further arguments to be reported in detail at a later

[16] Several additional events have been found meanwhile, under somewhat different conditions, which are also consistent with this production mechanism. In particular, one probable Λ^0+K^0 event in a 0.9-Bev π^--p collision, found by W. D. Walker (University of Wisconsin) in photographs obtained with the same equipment as the photographs under discussion, shows both Λ^0 and K^0 decaying. Here the Λ^0 again shows angular correlations similar to those exhibited by the hyperons tabulated in Table VIII. Here γ is less than 90°. Furthermore, one event in a 1.8-Bev π^--p collision, and one event in a 2.7-Bev p-p collision show the same general behavior. (For the latter event see Block, Harth, Fowler, Shutt, Thorndike, and Whittemore, Bull. Am. Phys. Soc. **29**, No. 7, 33 (1954).)

date involve indications of V-production thresholds observed in proton and neutron beams. For instance, in a 1.5-Bev proton beam only one possible case of a heavy unstable particle was observed to originate in the chamber wall. This proton energy is near the threshold for associated production of hyperons with K-mesons. ("Fermi energy" in compound nuclei favors production.) In a neutron beam of average energy of 1.7 Bev, some particles were produced in the wall. In a 2.7-Bev proton beam, heavy unstable particles were again produced in gas as well as wall.[16,17]

Out of 26 photographs showing V-events originating from the chamber wall only one, reported as Case C, showed both a Λ^0 and a θ^0 decaying. Associated production was indicated for this case. Three to five such cases should have been observed if mostly associated production occurred, and if the geometries for V-events from the wall and from the hydrogen were identical. The latter is not strictly true, and discovery of associated V-events from the walls is probably less likely. Furthermore, cosmic ray results on V-events,[18] mostly obtained in plates of heavy metals, have indicated very little associated production. Examples of associated production in cosmic radiation have been discussed in detail by several authors.[12,19]

The possibility of associated production can be used to explain[2] the relatively long lifetimes observed for heavy unstable particles ($\sim 10^{-10}$ sec instead of 10^{-22} sec for an "excited" nucleon or pion) together with their relatively large production cross section ($\sim$1 millibarn, or $\sim$3 percent of the total interaction cross section for 1.4-Bev π^--p collisions).

Inspection of Table IX shows four events (A, B, G, I) where the masses of Y and K cannot easily be reconciled simultaneously with those of Λ^0 (1107 Mev) and θ^0 (494 Mev). For agreement one would have to assume improbably small momenta for the incident π^- for all of these cases. Furthermore, in none of the four cases in question was it possible to ascertain that only two particles were produced since only one neutral particle was seen to decay, and therefore, only one line of flight was established. Event H is similar in the latter respect but is consistent with Λ^0 and θ^0 masses. For the remaining four events (D, E, J, K) both lines of flight could be established, and thus coplanarity could be used as an argument for production of two particles only, and here indeed reconcilable masses were found. There are several possible explanations for the discrepancies from known Λ^0 or θ^0 masses in events A, B, G, I. First, it is not yet certain that there are no K-mesons with masses other than 494 Mev (970 electron masses) although most observed events are consistent with this mass. Second, neutral pions (or perhaps photons) in addition to the K-mesons and hyperons may have been produced. It is unlikely that two pions were produced instead of a K-meson because then in at least some cases the mass inferred for the neutral particle should have been smaller than that of a θ^0. Also the inferred K-masses in question are all too large by similar amounts ($\sim$150 Mev). Third, a possibility worth considering is that the Λ^0's in the events in question were not produced directly but themselves were decay products of a hypothetical Σ^0 decaying into $\Lambda^0+\gamma$ with very short lifetime ($\sim 10^{-22}$ sec).[2] No metastable Σ^0 decaying into $p+\pi^-+115$ Mev has ever been observed. Since $\Sigma^\pm$ and Λ^0 have quite different Q-values, they cannot easily be called members of the same charge triplet (or quartet). For considerations of charge independence[2] in production of heavy unstable particles, the assumption of a Σ^0 with mass nearly equal to that of the $\Sigma^\pm$ is thus desirable. By just assuming that a particle of mass of 1185 Mev (Σ^0) was produced instead of one of 1107 Mev (Λ^0) one can almost reconcile Cases A, B, G, and I with simultaneous production of Σ^0 and θ^0. In addition, however, the postulated almost immediate decay of $\Sigma^0 \rightarrow \Lambda^0+\gamma$ can considerably alter the course of the Λ^0 which is finally observed to decay from that of the original Σ^0, since the γ ray can carry a momentum of ~ 75 Mev/c. Thus the observed angle of the direction of flight of the Λ^0 is not necessarily the same as that of the original Σ^0. Application of this possibility can be used further to obtain consistency with simultaneous Σ^0, θ^0 production in the four cases under discussion. Then we would have the following final production schemes for the nine events. Cases A, B, G, and I: $\pi^-+p \rightarrow \Sigma^0+\theta^0$, $\Sigma^0 \rightarrow \Lambda^0+\gamma$, Cases D, H: $\rightarrow \Lambda^0+\theta^0$ (direct production of Λ^0 thus would not seem to be ruled out), and Cases E, J, and K: $\rightarrow \Sigma^\pm+K^\mp$. The production symmetry for $\Sigma^\pm$ with Σ^0 thus experimentally indicated is an advantage which makes this explanation for the observed apparent discrepancies not improbable.

V. STATISTICAL FACTORS IN PRODUCTION AND DECAY

Having tentatively accepted the possible production of Σ^0, we wish to state some possible further theoretical consequences, specifically making use of Gell-Mann's[2] scheme. There it is assumed that for all production phenomena (strong interaction because of large cross section) isotopic spin T and z-component of isotopic spin T_z are conserved while for the decay phenomena (weak interaction because of long lifetimes) T and T_z change by ΔT and $\Delta T_z = \pm\frac{1}{2}$. Σ is assigned $T=1$, and $T_z=+1$, 0, -1 for Σ^+, Σ^0, and Σ^-, respectively, Λ^0 has $T=0$, $T_z=0$, and θ-mesons $T=\frac{1}{2}$, $T_z=+\frac{1}{2}$, $-\frac{1}{2}$ for θ^+, θ^0, respectively, and $T=\frac{1}{2}$, $T_z=+\frac{1}{2}$, $-\frac{1}{2}$ for $\bar{\theta}^0$, θ^-, respectively, where $\bar{\theta}^0$, θ^- are anti-particles to θ^0, θ^+. (Any K-mesons which are not θ's are omitted from this

[17] This dependence on energy qualitatively confirms the result reported by S. L. Ridgway and G. Collins, Bull. Am. Phys. Soc. 29, No. 7, 32 (1954).

[18] Leighton, Wanlass, and Anderson, Phys. Rev. 89, 148 (1953); Fretter, May, and Nakada, Phys. Rev. 89, 168 (1953); Bridge, Peyrou, Rossi, and Safford, Phys. Rev. 90, 921 (1953); 91, 362 (1953).

[19] Thompson, Burwell, Huggett, and Karzmark, Phys. Rev. 95, 1576 (1954).

discussion, for example tau and kappa-mesons.) For π^--p collisions (total $T_z=-\frac{1}{2}$ to be conserved, if for nucleons $T=\frac{1}{2}$, $T_z=+\frac{1}{2}$, $-\frac{1}{2}$ for proton and neutron, for pions $T=1$, $T_z=+1$, 0, -1 for π^+, π^0, π^-, respectively) the reactions $\rightarrow\Lambda^0+\theta^0$, $\Sigma^0+\theta^0$, $\Sigma^-+\theta^+$ are then possible while the reaction $\rightarrow\Sigma^++\theta^-$ is not possible. Similarly for π^--n collisions ($T_z=-\frac{3}{2}$) the reaction $\rightarrow\Sigma^-+\theta^0$ is possible while $\rightarrow\Lambda^0+\theta^-$, $\Sigma^0+\theta^-$ are not. Thus production of Σ^+ or θ^- in π^--nucleon collisions would not be possible. (In Pais' scheme $\pi^-+n\rightarrow\Sigma^0+\theta^-$ is possible,[2] but $\pi^-+p\rightarrow\Sigma^++\theta^-$ is still not possible.) Within the bad statistics, no identified Σ^+ was observed in the magnet chamber. Only a possible Σ^- produced in the gas (Case *E*) and a Σ^- originating in the wall (Case *F*) were found in addition to two other negative decays not further identified. (Of course, Σ^+ or θ^- could be produced in the walls by collisions of secondary π^+-mesons or nucleons.)

A π^--p reaction can proceed through isotopic spin states $T=\frac{1}{2}$ or $\frac{3}{2}$, with $T_z=-\frac{1}{2}$. The reaction $\pi^-+p\rightarrow\Lambda^0+\theta^0$ is possible only through $T=\frac{1}{2}$ since $T=0$ for Λ^0. For $T=\frac{1}{2}$ the reaction $\rightarrow\Sigma^0+\theta^0$ has statistical weight $\frac{1}{3}$ and $\rightarrow\Sigma^-+\theta^+$ has $\frac{2}{3}$. For $T=\frac{3}{2}$ the relative weights are reversed to $\frac{2}{3}$ and $\frac{1}{3}$, respectively. Whether the reaction proceeds preferably through the initial isotopic spin state of $\frac{1}{2}$ or $\frac{3}{2}$ is not known. We will, however, here also assume their relative statistical weights of $\frac{2}{3}$ and $\frac{1}{3}$. It follows that the relative probabilities of (Σ^0,θ^0) and (Σ^-,θ^+) production are 4/9 and 5/9, respectively. As just stated, we may have observed four (Σ^0,θ^0) and three (Σ^-,θ^+) events, which is not in disagreement with these probabilities. If we believe that two (Λ^0,θ^0) events were observed then the probabilities for (Λ^0,θ^0) and (Σ^0,θ^0) production are of same order of magnitude.

A Λ^0 can decay into (p,π^-) or (n,π^0) with change of isotopic spin from $T=0$ for the Λ^0 to $T=\frac{1}{2}$ for the decay products so that $\Delta T=\frac{1}{2}$, $\Delta T_z=-\frac{1}{2}$. Although isotopic spin is not conserved for the decay mechanism, the interaction between the decay products is usually considered to be charge-independent. If one imagines that the decay products are still in very close proximity after the interaction leading to decay of the heavy unstable particle has ceased, one might still apply the isotopic spin formalism to the final T, T_z state.[20] For $T=\frac{1}{2}$, (p,π^-) has the statistical weight $\frac{2}{3}$, and (n,π^0) has $\frac{1}{3}$. Since we can observe only (p,π^-), four of which were observed to be produced in hydrogen, the true number of Λ^0 produced in the gas and decaying in the chamber (into both combinations) may therefore have been six. The same assumptions can be applied to the θ^0 decay. The two pions from a decaying θ^0 can be in a state $T=0$ or 1, $T_z=0$. The two possibilities for decay (π^+,π^-) or (π^0,π^0) exist. For $T=0$ we have the weights $\frac{2}{3}$ for (π^+,π^-) and $\frac{1}{3}$ for (π^0,π^0). For $T=1$ (π^0,π^0) is not possible.[21] Thus the $3(\pi^+,\pi^-)$ decays observed to be produced in hydrogen imply a total of not more than four θ^0's. Combining these weights for the unseen decays with the previous considerations on lifetimes and geometry, one estimates that a total of nine events resulting in θ^0 and Σ^0 or Λ^0 may have been produced.

All Σ^- and θ^+ can be observed when they decay. It is possible, however, that the θ^+ are long-lived in which case they would have only a small chance to decay inside the chamber. In this case, only the Σ^- are seen to decay in the chamber with a probability of 60 percent as inferred from lifetime and geometry. Then the 3 events observed correspond to five (Σ^-,θ^+) events actually produced. (There is no experimental evidence that the K^+'s involved are really to be identified as θ^+'s.)

The total number of V-production events in the gas for this run may, therefore, have been $9+5=14$, leading to a cross section for production of $\sim$0.9 mb for 1.4-Bev π^--p collisions. This value may represent a somewhat better estimate (disregarding the poor statistics) for the production cross section than the value of $\sim$0.7 mb given in the previous section.

VI. SUMMARY

The five examples given here of the production of hyperons and K-mesons in π^--p collisions, together with those previously reported,[1] indicate that a hyperon and K-meson are normally produced together. None of the nine examples is inconsistent with the reaction $\pi^-+p\rightarrow Y+K$, and in each case the simplest and most natural interpretation of the observed data involves a reaction of that type, which is described by the term "associated production." These observations by themselves do not, however, determine whether associated production occurs because of special selection rules or because of the high spin of the hyperons and K-mesons, since the latter could lead to associated production at these energies.[2] There has been little evidence for associated production in cosmic ray experiments, and the reason for this difference is not clear.

If we use the schemes of Pais and Gell-Mann for the classification of hyperons as a guide to the interpretation of our results, we have the following choices for hyperons: Λ^0, Σ^+, Σ^0, Σ^-, Ξ^-, and Ξ^0. It is then possible to fit the observations with a single species of K-meson, of which the θ^0 is the well-established member: θ^+, θ^0, and θ^-. In most cases, however, our interpretation is to be considered as an hypothesis which fits the observations rather than a demonstrated fact. The events

[20] This procedure is not rigorously justified because the weak decay interaction is not invariant with respect to rotation in isotopic spin space and therefore can be stronger for some charge states than others.

[21] Of course, spin and parity considerations are completely neglected here. Schemes such as those suggested by M. Gell-Mann and A. Pais [Phys. Rev. 97, 1387 (1955)] may lead to a way of estimating more properly probabilities for decay into different combinations.

are interpreted as follows:

$$\pi^- + p \rightarrow \Lambda^0 + \theta^0 \quad \text{Cases } D \text{ and } H,$$
$$\rightarrow \Sigma^0 + \theta^0 \quad \text{Cases } A, B, G, \text{ and } I,$$
$$\rightarrow \Sigma^- + \theta^+ \quad \text{Cases } E, J, \text{ and } K.$$

The positions of observed decay events and the fraction of cases in which both Y and K decays are observed are consistent with previous information on the mean lifetimes of Λ^0 and θ^0.

To determine the total cross section for V-production, it is necessary to estimate the number of V-production cases where the decays were not seen either because they were outside the sensitive region or involved only neutral secondaries. This estimate is very uncertain, but leads to a cross section of $\sim$0.9 millibarn.

Data on angular correlations might be expected to provide some information on the spins of the particles involved. Three effects have been observed: (1) The angle between line of flight of the hyperon and incident π^- in the c.m.s. of the π^--p system (β) shows that the Λ^0 and Σ^0 prefer to travel backward in the c.m.s. The same backwards preference was noted[4] for nucleons from π^--p interactions which lead to emission of pions. (2) For Λ^0 and $Y^\pm$, the angle between production and decay planes (α) is less than 45° in all cases. (3) The angle between incident pion and nucleon from the hyperon decay in the hyperon rest system (γ) has been calculated, but the data are inconclusive because of insufficient statistics. However, the rather striking correlation shown by α may indicate that the spin of the hyperon is at least $\frac{3}{2}$.

We wish to acknowledge the continuing cooperation of the Cosmotron staff and of the other members of the cloud chamber group, without whose support this work would not have been possible.

PHYSICAL REVIEW VOLUME 98, NUMBER 1 APRIL 1, 1955

Recurrence Phenomenon in the 24-Hour Variation of Cosmic-Ray Intensity*

R. P. KANE†
Institute for Nuclear Studies, The University of Chicago, Chicago, Illinois
(Received December 1, 1954)

Changes of cosmic-ray intensity in 24-hour intervals were studied at four neutron monitor stations and for one ionization chamber in the geomagnetic latitude range 0°–52° N. There is evidence that the fluctuations in the 24-hour variation of cosmic-ray intensity have a recurrence tendency of 27–28 days. There does not appear to be, however, any unique relationship between this recurrence and the well-known recurrence in the amplitude of the mean daily intensity. The association of this phenomenon with 27 day recurring disturbances in the geomagnetic field is also investigated.

I. INTRODUCTION

IT is now well established that the amplitude and phase of the daily variation of cosmic-ray intensity are not constant. For example, the amplitude and phase of the 24 hourly variation of the nucleonic component undergo large day-to-day changes.[1] The purpose of the present investigation is to determine whether the amplitude of this variation possesses any recurrence characteristics. Also, since the 27-day daily mean intensity variation has been associated with solar processes and since there is evidence[2] that the amplitude of the daily variation follows roughly the pattern of the solar activity cycle, it is further proposed to investigate whether a 27-day recurrence of the daily variational intensity exists and to explore its association with solar induced geophysical phenomena.

II. NATURE OF THE PROBLEM

The principle difficulty in approaching this question is the measurement of the daily amplitude for a single day. Usually, an harmonic analysis is obtained for 24 hourly values (or 12 bi-hourly values) so as to determine the amplitude and phase of the best fitting sine curve. Such a procedure may, however, be incorrect and unreliable due to both the large statistical errors involved in counting rate and the presence of prominent day-to-day variations, e.g., a large 27-day recurrence in the mean daily cosmic ray intensity. Consider, for example, the arbitrary plot in Fig. 1 of cosmic-ray intensity over a period of 5 consecutive days. A, B, C, and D represent respectively the four 6 hourly intervals, 0000 to 0600, 0600 to 1200, 1200 to 1800, and 1800 to 2400 hours local time. An harmonic analysis for the 24 hourly values of day 1 and 2 would yield an hour of maximum late at night, and, for days 4 and 5, early in the morning. The amplitudes would be greatly affected by the average slopes of the day-to-day variation. Clearly, the essential features of the daily variation

* Assisted by the Office of Scientific Research, Air Research and Development Command, U. S. Air Force.
† Fulbright and U. S. Government scholar from India.
[1] Firor, Fonger, and Simpson, Phys. Rev. 94, 1031 (1954).
[2] V. Sarabhai and R. P. Kane, Phys. Rev. 90, 204 (1953).

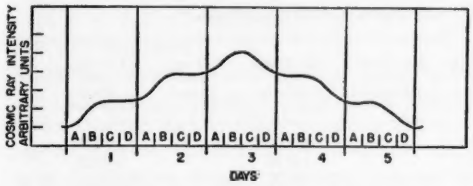

FIG. 1. Arbitrary plot of hourly values of cosmic-ray intensity for five consecutive days.

would thus be greatly distorted by the presence of a prominent systematic variation of the mean daily intensity.

However, for study of the recurrence phenomenon in the amplitude of daily variation in this paper, a precise determination of the hour of maximum intensity is not required. As a first approximation, it is sufficient to know whether the maximum occurred in the daytime or in the night time. This can be determined by taking the difference between the total counting rates of the day hours and night hours. The magnitude and sign of the "day minus night" intensities may be taken as representative of the amplitude and phase, respectively, of the daily variation.

To avoid distortions due to systematic day-to-day variations of mean daily intensity, the following procedure was adopted:

(a) The day intensity was defined as the 12-hour interval $B+C$, i.e., 0600 to 1800 hours local time and designated as D. The night intensity was defined as the sum of the two 6 hour intervals A and D, on either side of the day interval, and designated as N. Thus the difference, $D-N$, would be independent of any straight slope of the day-to-day variation such as for day 1 and 2, or 4 and 5. A dependence on slope would still persist in day 3 which happens to be at the peak of the mean daily variation.

(b) The value of $D-N$ for each day was expressed as a percentage of the $D+N$ value of the same day, for the following reason. The mean daily intensity $D+N$ is known to undergo fluctuations with a 27-day recurrence tendency. If the fractional changes during the day and night are the same at all times, the $D-N$ values would tend to increase for days at the maximum of the mean daily intensity $D+N$. This effect would be reduced by using the percentage $100(D-N)/(D+N)$.

If the $D-N$ values are independent of the $D+N$ variations, this procedure would introduce false recurrence tendencies in the $(D-N)/(D+N)$ values. However, the magnitude of the false recurrences would be about the same as the magnitude of the fluctuations in $D+N$ values, which is about ± 5 percent or less. The percentage amplitude of the 24 hour variation varies in the limits of about $+1$ percent to -1 percent. The maximum errors involved would, therefore, be about ± 0.05 percent. During years of low solar activity, this error will be still reduced, since the fluctuations in $D+N$ values hardly exceed ± 1 percent, as shown later in this paper.

(c) Averages over three consecutive days were evaluated and taken as representative of the middle day. Thus for any day 0, the percentage daily amplitude was represented by

$$\frac{1}{3}\sum_{n=-1}^{n=+1}\left\{\frac{100(D-N)}{D+N}\right\}_n.$$

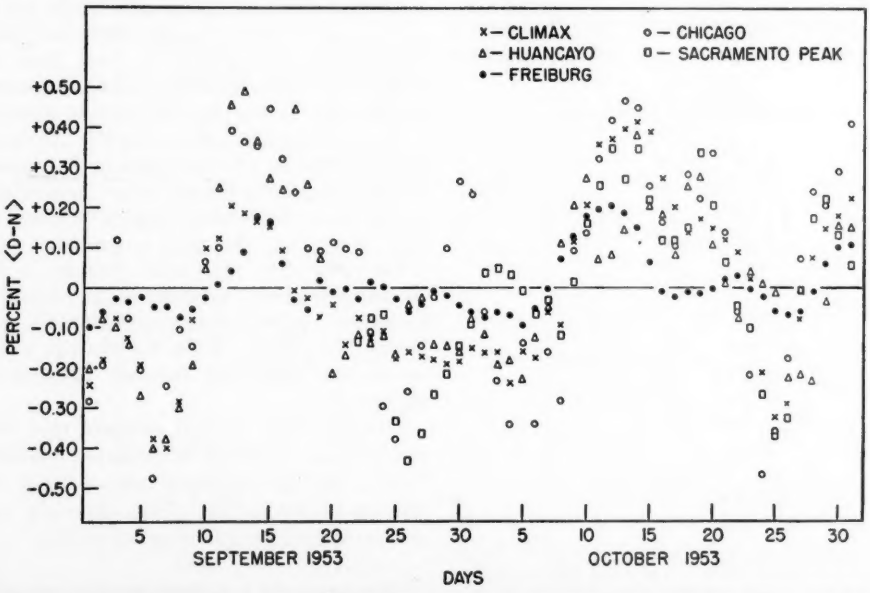

FIG. 2. $\langle D-N\rangle$ values for the neutron piles at Climax, Chicago, Sacramento Peak, and Huancayo, and the ionization chamber intensity at Freiburg, for September and October, 1953.

TABLE I. Correlation coefficients among the $\langle D-N \rangle$ values at various stations.

Year and months	Climax and Sac. Peak	Climax and Chicago	Climax and Huanc.	Climax and Freib.	Sac. Peak and Chicago	Sac. Peak and Huancayo	Sac. Peak and Freiburg	Chicago and Huanc.	Chicago and Freib.	Huanc. and Freib.
1951										
May–Jun.	+0.54	+0.13		+0.54	−0.14		+0.66		−0.09	
Jul. –Aug.	+0.67	+0.33		+0.44	+0.20		+0.36		−0.01	
Sep. –Oct.	+0.24	+0.24		+0.23	+0.11		−0.27		−0.25	
Nov.–Dec.	+0.60	+0.47		+0.33	−0.12		+0.53		+0.12	
1952										
Jan. –Feb.	+0.51	+0.32	+0.62	+0.70	+0.04	+0.33	+0.28	+0.24	+0.41	+0.64
Mar.–Apr.	...	+0.28	+0.41	+0.45	...	...	...	+0.14	+0.27	+0.57
May–Jun.	+0.70	+0.69	+0.46	+0.77	+0.38	+0.33	+0.59	+0.35	+0.57	+0.50
Jul. –Aug.	+0.59	+0.27	+0.68	+0.51	+0.32	+0.38	+0.21	+0.11	+0.32	+0.48
Sep. –Oct.	+0.61	+0.48	+0.49	+0.50	+0.50	+0.61	+0.58	+0.25	+0.43	+0.62
Nov.–Dec.	+0.56	−0.15	+0.37	+0.28	−0.15	+0.31	+0.36	−0.08	0	+0.40
1953										
Jan. –Feb.	−0.32	+0.44	+0.44	+0.50	+0.05	+0.26	+0.14	+0.36	+0.31	+0.52
Mar.–Apr.	+0.56	+0.66	+0.57	+0.60	+0.36	+0.45	+0.28	+0.26	+0.52	+0.33
May–Jun.	+0.31	+0.47	+0.34	+0.54	+0.15	+0.21	+0.60	+0.28	+0.33	+0.65
Jul. –Aug.	...	+0.61	+0.69	+0.79	...	...	...	+0.40	+0.32	+0.48
Sep. –Oct.	+0.92	+0.84	+0.77	+0.83	+0.83	+0.50	+0.58	+0.66	+0.62	+0.60
Nov.–Dec.	+0.56	+0.58	+0.17	+0.50	+0.21	+0.11	−0.04	+0.18	+0.49	−0.08

This reduces statistical errors and reduces distortions in days at the maxima (e.g., day 3 in Fig. 1) or minima of variations in the mean daily intensity.

The quantity

$$\frac{1}{3}\sum_{n=-1}^{n=+1}\left\{\frac{100(D-N)}{D+N}\right\}_n$$

will be designated, hereafter, as $\langle D-N \rangle$ for convenience. $\langle D-N \rangle$ values have been obtained for the neutron detector stations at Climax, Chicago, and Sacramento Peak (for May, 1951 to December, 1953), and Huancayo, Peru (for January, 1952 to December, 1953). To investigate the problem at higher mean primary particle energy, the ionization chamber data[3] from Freiburg, Germany, have also been analyzed in the same way.

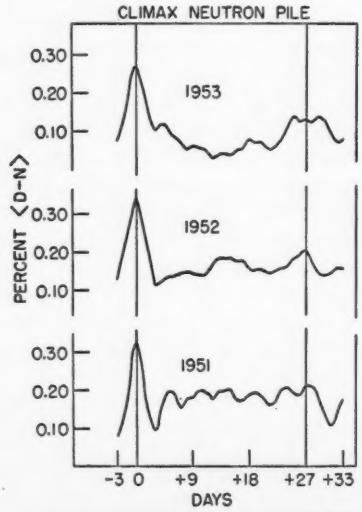

FIG. 3. Chree type diagram for Climax $\langle D-N \rangle$ maxima.

III. EXPERIMENTAL RESULTS

(a) Recurrence Properties of the Amplitude of the 24-Hour Variation

Any recurrence phenomenon in a cosmic-ray intensity variation which is to be attributed to a variation in the total primary cosmic radiation must satisfy the condition that the variation is observed throughout the world. There has been increasing evidence over the past few years that this condition is satisfied for the amplitude changes in the daily intensity variation, provided the observations are compared in local time. Additional evidence will be presented here to demonstrate that the data used in this paper fulfill these requirements.

For example, Fig. 2 shows the $\langle D-N \rangle$ values for the neutron piles at Climax, Chicago, Sacramento Peak, and Huancayo, and the ionization chamber at Freiburg for the period September through October, 1953. This is an interval of rather good agreement.

To investigate this point further, a correlation analysis was carried out between the $\langle D-N \rangle$ values for the different pairs of observing stations using successive bi-monthly periods. Table I gives the values of the correlation coefficients between pairs of observing stations.

Although there is good evidence that the 24-hour variations are worldwide in character, it is obvious from Table I that the tracking between pairs of the various stations is not perfect. This imperfect tracking is associated with the following difficulties:

[3] Data obtained by A. Sittkus of the University of Freiburg are published quarterly in "Sonnen-Zirkular" of the Fraunhofer Institute, Freiburg I.B., Germany.

(1) In 1951, both Chicago and Climax neutron piles had low counting rates.

(2) Since it is well established that the amplitude changes day by day, stations at different geomagnetic longitudes observe slightly different amplitudes due to different local times. The fact that the 24-hour variation is principally due to charged particles enhances these differences for stations at different geomagnetic latitudes.

To investigate the main problem of searching for a recurrence tendency in the $\langle D-N\rangle$ maxima at any station, the Chree type of analysis was adopted.[4] It consists in designating a day of $\langle D-N\rangle$ maximum as day 0, and writing down the $\langle D-N\rangle$ values for days $n=-3$ or less to $n=+33$ or more. All maxima within the period under study are superposed on $n=0$ and the values for each of the other days are added separately. The superposition of data for days -3 to $+33$ gives the Chree diagram where the maximum value is at $n=0$ and the day of any *other* maximum (if any) indicates the recurrence period in days.

Since the correlations among the various stations are not always high, it has not been possible to select individual days on which all the stations simultaneously display $\langle D-N\rangle$ maxima. Hence the selection of $\langle D-N\rangle$ maxima to form the set of $n=0$ days has been carried out independently for each cosmic-ray station. The total number of maxima in any year for each of the stations was about 30.

Figures 3, 4, 5, 6, and 7 show the Chree type diagrams for each of the observing stations for different years.

The principle features of the Chree diagrams for $\langle D-N\rangle$ maxima may be summarized as follows:

(1) The $\langle D-N\rangle$ values show a 27–28 day recurrence tendency at all stations.

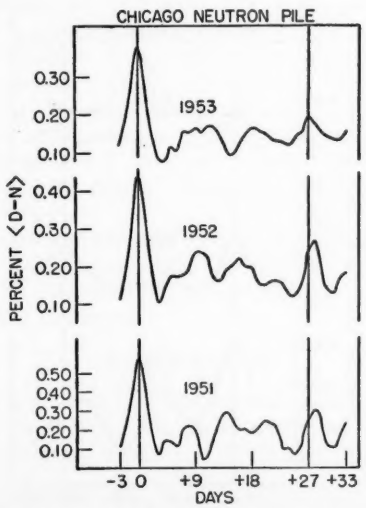

FIG. 4. Chree type diagram for Chicago $\langle D-N\rangle$ maxima.

[4] C. Chree, Trans. Roy. Soc. (London) **A212**, 75 (1913).

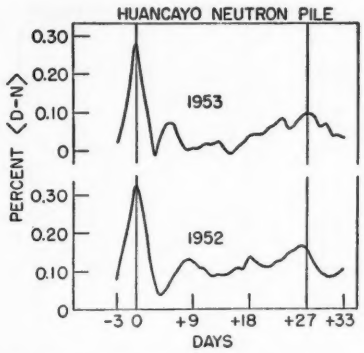

FIG. 5. Chree type diagram for Huancayo $\langle D-N\rangle$ maxima.

(2) The range of the $\langle D-N\rangle$ values, i.e., the difference between the maximum and minimum values of $\langle D-N\rangle$ in the 27-day recurrence, is about the same for 1951, 1952, and 1953. Thus, the magnitude of the changes in $\langle D-N\rangle$ values seems to remain about the same over the three year period.

(3) The maximum values of $\langle D-N\rangle$ at $n=0$ seem to be smallest in absolute magnitude in 1953. Also, the average $\langle D-N\rangle$ value for a 27-day cycle is smaller in 1953 than in 1951 or 1952.[5]

(4) The observed 27-day recurrence in 1953 seems to be more pronounced than in 1951 or 1952.

Whether the *maxima* of $\langle D-N\rangle$ values or the *minima* are more important for a physical interpretation of this 27-day recurrence, depends upon which particular hypothesis is invoked to account for the origin of these variations. To check whether one could give more im-

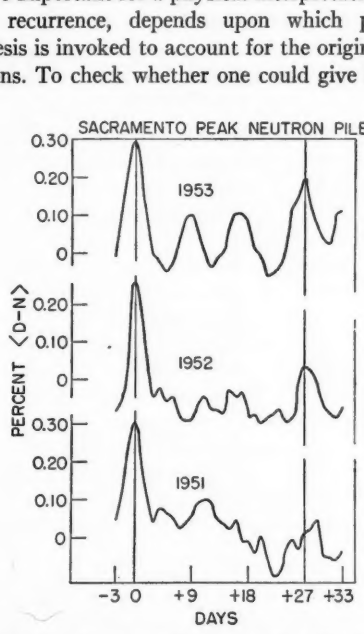

FIG. 6. Chree type diagram for Sacramento Peak $\langle D-N\rangle$ maxima.

[5] This is in agreement with the results of Sarabhai and Kane (see reference 2) who report a tendency of the daily amplitude to be smaller at the time of sunspot minimum.

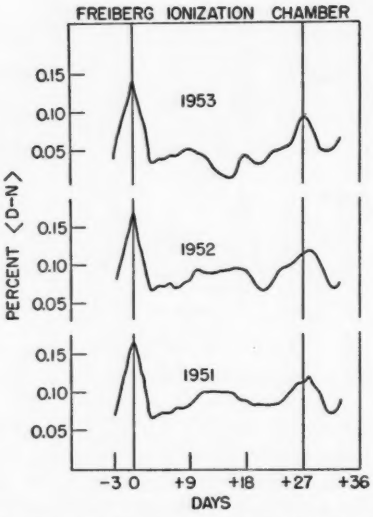

FIG. 7. Chree type diagram for Freiburg $\langle D-N \rangle$ maxima.

portance to the maxima or the minima from the experimental data alone, a Chree analysis was also carried out for the *minima* of $\langle D-N \rangle$ values using data from the Climax neutron pile. Figure 8 shows the Chree diagrams for the Climax neutron pile with $\langle D-N \rangle$ minima as $n=0$ days. Since all minimum values are at $n=0$, the sign of the ordinate scale is reversed.

Clearly, the $\langle D-N \rangle$ minima show similar characteristics to the $\langle D-N \rangle$ maxima.

(b) Association with Geophysical and Solar Phenomena

The daily mean intensity of cosmic rays is known to have a recurrence tendency of about 27 days. This is shown in Fig. 9 for the mean daily intensity of $D+N$ obtained from the data used in this paper. The recurrence tendency decreases in successive years 1951, 1952, 1953. Since the $\langle D-N \rangle$ values also possess a 27-day recurrence, the question arises as to whether the two variations are related in some way. Since, as pointed out in Sec. II above, the $\langle D-N \rangle$ values used in the present analysis are expressed as percentages of the $D+N$ intensity, the 27-day recurrence tendency in $\langle D-N \rangle$ values is not the induced effect of a 27-day recurrence in $D+N$ intensity.

To determine whether there was any meaningful phase relationship between the two variations, a Chree analysis was carried out for the Climax neutron pile. The days for which the mean daily intensity $D+N$ had maximum values were selected as $n=0$ days. The $\langle D-N \rangle$ values were written down for $n=-3$ to $n=+33$ and the superposition was carried out for all the $n=0$ days of $D+N$ maxima in any particular year. These Chree diagrams are shown in Fig. 10.

It is obvious from Fig. 10 that the $\langle D-N \rangle$ values do not show any unique phase relationship with the $D+N$ maxima for any year.

Geomagnetic disturbances are known to possess a pronounced 27-day recurrence as a consequence of their association with solar phenomena. The K_p index of geomagnetic activity has been established to represent the degree of the worldwide disturbance. This recurrence is illustrated for the period 1951 through 1953 in Fig. 11 as a 27-day calendar. Each row represents a period of 27 days between the vertical lines $n=0$ and $n=27$. Starting in January, 1951, successive 27-day intervals are represented by successive rows in Fig. 11. The dates corresponding to days $n=0$ are given at the left of the diagram. The days on which the K_p index

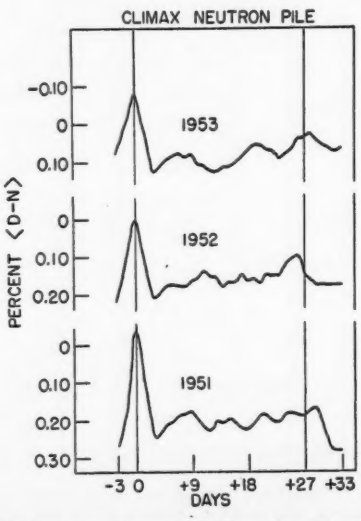

FIG. 8. Chree type diagram for Climax $\langle D-N \rangle$ minima.

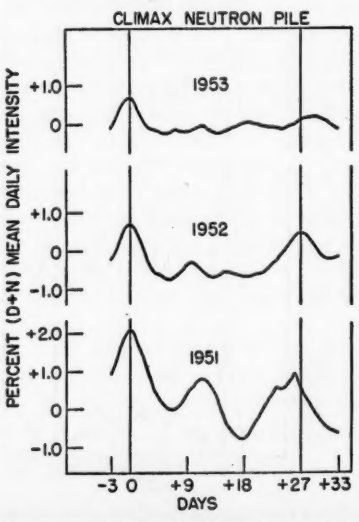

FIG. 9. Chree type diagram for Climax mean daily neutron intensity $D+N$ maxima.

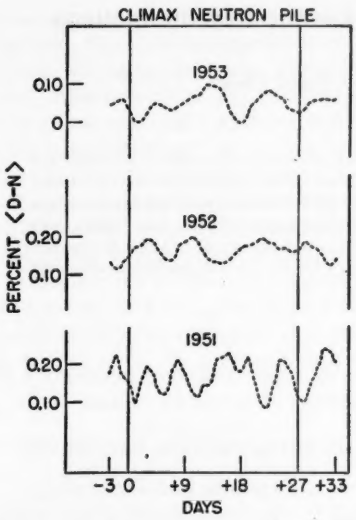

FIG. 10. Chree type diagram for Climax $\langle D-N \rangle$. The "0" day corresponds to Climax mean daily intensity maxima.

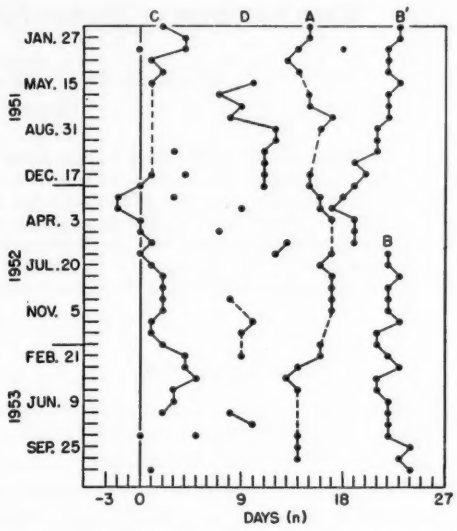

FIG. 11. Location of K_p maxima on a 27-day calendar.

attained maximum values are denoted by circular dots. In general, five 27-day sequences may be identified for the period under consideration. These are indicated as A, B', B, C, and D in Fig. 11. Sequence B may be a continuation of sequence B'.

To study the phase relationship between these 27-day sequences of K_p maxima and the $\langle D-N \rangle$ and $D+N$ values of cosmic-ray intensity, a Chree analysis was carried out separately for $\langle D-N \rangle$ and $D+N$ values, selecting for $n=0$ the days of K_p maxima belonging to one 27-day sequence at a time for 1951, 1952 and 1953 separately.

The results may be summarized as follows:

In general: (1) Not every 27-day sequence of K_p maxima is preceded by $D+N$ maxima. (2) Not every 27-day sequence of K_p maxima is associated with $\langle D-N \rangle$ maxima.

However, for some periods and for some of the sequences of K_p maxima: (1) The K_p maxima are preceded by $D+N$ maxima by about three days. (2) The maxima of $\langle D-N \rangle$ coincide with the maxima of K_p values.

These latter statements are specially borne out for sequence D in 1951, sequence C in 1952, and sequence B in 1953 for data from the neutron monitor stations at Climax and Huancayo.

IV. CONCLUSION

There is evidence that the fluctuations in the amplitude of the 24-hour variation of cosmic-ray intensity have a recurrence tendency of 27–28 days. Recurrence tendencies of the same period are known to exist in the mean daily intensity of cosmic rays. However, at present there does not appear to be any unique relationship between the mean daily intensity and the amplitude of the 24-hour variation.

Phase relationships with the 27-day recurrence phenomenon in the intensity of geomagnetic disturbances, represented by worldwide K_p indices, have also been studied. Though, in general, it is not possible to identify a phase relationship of *all* the K_p maxima with either the daily mean cosmic-ray intensity or the amplitude of the 24-hour variation, it seems to be true for particular 27-day sequences of K_p maxima that the maxima of the daily mean cosmic-ray intensity precede the K_p maxima by about three days whereas the maxima of the amplitude of the 24-hour variation of cosmic-ray intensity coincide with the maxima of K_p values. This latter relation is in agreement with the reports of some observers who find increases in the amplitude of the 24-hour variation of cosmic-ray intensity on magnetically disturbed days.[6,7]

The author is deeply grateful to Professor J. A. Simpson for guidance and helpful discussions during the course of this investigation. Thanks are due to the computation group for computational help. The author is also indebted to the Department of State (U. S. A.), the U. S. Educational Foundation and the Institute of International Education for the grant of a scholarship.

[6] Y. Sekido and S. Yoshida, Rept. Ionospheric Research, Japan **4**, 37 (1950).
[7] H. Elliot and D. W. N. Dolbear, J. Atm. and Terrest. Phys. **1**, 205 (1951).

Mass Spectrum of Shower Particles from Cosmic-Ray Interactions

A. HUSAIN* AND E. PICKUP
Division of Physics, National Research Council, Ottawa, Canada
(Received December 16, 1954)

The masses of particles with an ionization less than about twice the minimum value emitted in cosmic-ray stars in a photographic emulsion have been determined by observations on the grain density and scattering of suitably long tracks. About 100 tracks with an average length of 16.5 mm were analyzed using a single emulsion exposed to cosmic rays in a high-altitude balloon flight of nine hours duration. The results show groups of pions, protons, deuterons, heavy mesons with mass $\sim 925m_e$ and the possibility of a group with mass closer to that of the proton. This latter is uncertain, however, with the present resolution and could be a statistical fluctuation on the edge of the proton distribution.

I. INTRODUCTION

EVIDENCE for the production of heavy mesons with mass ~ 1200–$1300m_e$, obtained by measurements of grain density and scattering of secondary particles emitted in cosmic-ray disintegrations, was submitted by Daniel *et al.*[1] and Daniel and Perkins,[2] although the statistical accuracy of this work was not very good. The present work was started in the hope of improving the resolution between the heavy meson and proton groups by using longer track lengths. An extension of the Bristol work has been made since by Fowler and Perkins,[3,4] using longer track lengths, from which they obtain evidence for a heavy-meson group with mass 900–$1000m_e$ and a possible group with mass intermediate between this and the proton mass. This latter group is considered uncertain yet, however, being close to the edge of the proton distribution. The present measurements, while using shorter track lengths than in the latest work of Fowler and Perkins, gives similar results. In addition, measurements have also been made in the region of the ionization minimum and the results give an indication of the possibility for discrimination in this region and some information about the energy spectrum of the heavy mesons.

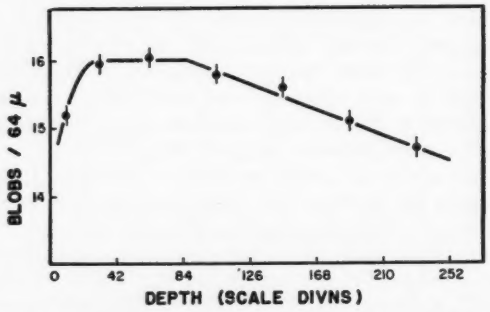

FIG. 1. Variation of plateau blob density with depth in the emulsion. The drop in blob density near the air surface indicates grain corrosion here.

II. EXPERIMENTAL PROCEDURE

1. Exposure and Processing

Ilford *G*5 emulsions, 600μ thick, 4 in.$\times$4 in. and mounted on glass, 2 mm thick for rigidity, were exposed in a "Skyhook" balloon flight for nine hours at about 95 000 feet. The emulsions were developed by the hot-plate method, using acid amidol after which they were kept in a room with controlled temperature and humidity where the measurements were made.

2. Grain Density

Ionization was measured by counting blobs (unresolved groups of grains) along the tracks using a Leitz microscope with 90/1 objective and 15$\times$ Kellner eyepieces, the electron plateau blob density being about 25 blobs per 100μ. Since the star population density was fairly high, it was decided at first to make as many measurements as possible in one emulsion. This obviated the necessity of normalizing results because of possible differences between emulsions. There was a variation of grain density with depth in the emulsion used, and this is shown in Fig. 1. High-energy "plateau" electron pairs were used to obtain this curve and it was also verified by blob counting on long tracks with grain density $\sim 1.5\times$ the plateau value. Blob counts on all shower tracks measured were then normalized to the electron plateau value corresponding to the appropriate depth in the emulsion. It is estimated that any error due to this correction is not more than 1 percent. Blob counting was not made within 50μ from the surface since there was evidence of grain corrosion here, the effect of this being shown in Fig. 1. No correction was made for background grains since the measurements are all relative ones. The standard error for blob counting was taken to be $(70/\sqrt{n})$ percent, where n is the number of blobs.

3. Scattering

Values of $p\beta$ were obtained by the usual multiple-scattering procedure. The cell size was always chosen

* National Research Laboratories Postdoctorate Fellow.
[1] Daniel, Davies, Mulvey, and Perkins, Phil. Mag. **43**, 753 (1952).
[2] R. R. Daniel and D. H. Perkins, Proc. Roy. Soc. (London) A221, 351 (1954).
[3] Proceedings of the Duke University Cosmic-Ray Conference, 1953 (unpublished).
[4] C. F. Powell, Nuovo cimento Suppl. No. 2, 165 (1954).

to be about six times the noise level and overlapping cells were used. Since measurements are relative ones, no correction was made for noise. Any distortion correction was estimated to be $\lesssim 1$ percent. Theoretical values with cutoff were used for the scattering constant[5] and, in assessing the errors, no account was taken of the fact that there is still doubt about the agreement between theory and experimental scattering calibrations for emulsions using protons of several hundred Mev. The standard error was taken as $(75/\sqrt{n})$ percent, where n is the number of independent nonoverlapping cells used for any track.[6] The validity of this relation was checked in the present work by calculating the standard deviation of the measurements for several tracks.

III. RESULTS

1. Track Length and Statistics

The track-length distribution is shown in Fig. 2, the average length being 16.5 mm. For the four groups of particles (pions, K-mesons, protons, and deuterons) the average number of second differences in scattering was 82, 110, 37, and 47, respectively, giving standard errors of 8.3, 7.1, 12.3, and 10.9 percent. Since the standard error for blob counting was $\lesssim 1$ percent, the total experimental standard error used in assessing the accuracy for the four groups was taken as 9, 8, 13, and 11 percent. The doubtful heavy-meson group at mass $\sim 1250m_e$ was considered as belonging to the proton group for this purpose.

2. Mass Spectrum

In Fig. 3, $p\beta$ (the scattering parameter) is plotted against blob density (corresponding to ionization) for the tracks measured, the points above the ionization plateau resolving themselves into a family of curves corresponding to different masses. The best curve was drawn through the proton group of points and the other

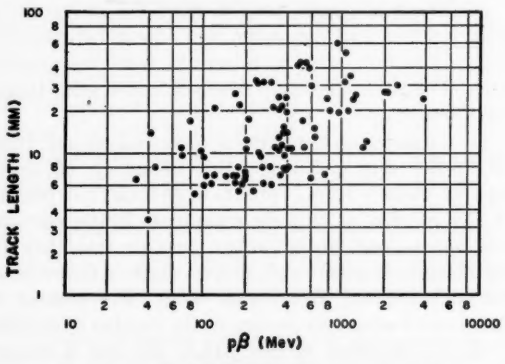

FIG. 2. Length distribution of tracks measured; mean length = 16.5 mm.

[5] L. Voyvodic and E. Pickup, Phys. Rev. 85, 91 (1952).
[6] See Nuovo cimento Suppl. No. 2, 228 (1954).

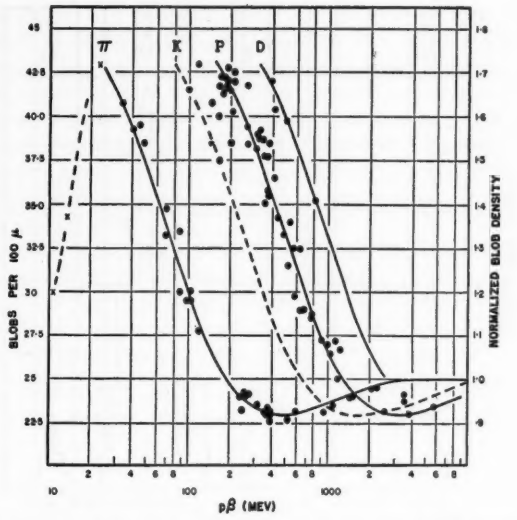

FIG. 3. Variation of blob density with $p\beta$ for all tracks in single G5 emulsion. Above the plateau the best curve is drawn through the proton group of points, and the π and d curves calculated from this. The K curve is drawn parallel to the other curves passing through the point at normalized blob density = 1.5.

full line curves were calculated from this assuming a proton mass, $1837m_e$, pion mass, $273m_e$, and deuteron mass, $3674m_e$. The K-meson curve was drawn parallel to the other curves passing through the point at normalized blob density = 1.5, and corresponds to a mass, $925m_e$. It should be noted that, with the plateau blob density of 25 blobs per 100μ in this emulsion, 1.8 was about the useful upper limit of normalized blob density which could be used since saturation occurred in this region below which the blob density decreased with $p\beta$. This is shown for pions in the dotted part of the curve in Fig. 3. A similar curve, not shown, was measured for protons. Protons are losing energy rapidly here and can be distinguished from K-mesons on this account. The assignment of the lower-energy K-meson in Fig. 3 as such was partly based on comparison with a proton of similar $p\beta$ which came to rest in the emulsion. However, for work in the region above a normalized blob density of about 1.5, it is more desirable to have a plateau blob density <25 blobs per 100μ (e.g., ~ 20 blobs per 100μ, as used in the Bristol work).

Taking the best curve through the proton points in Fig. 3 as the curve representing mass $1837m_e$, the masses corresponding to all points were calculated. The resulting mass spectrum is shown in the histogram in Fig. 4. Superimposed on this histogram are the expected normal distribution curves corresponding to the mean standard errors for each group. Although the number of particles is small, the agreement between the different groups is very reasonable and there is little doubt about the meson group with mass, $925m_e$ ± 8 percent. Fowler and Perkins appear to have another mass group at about $1400m_e$. There could be a group

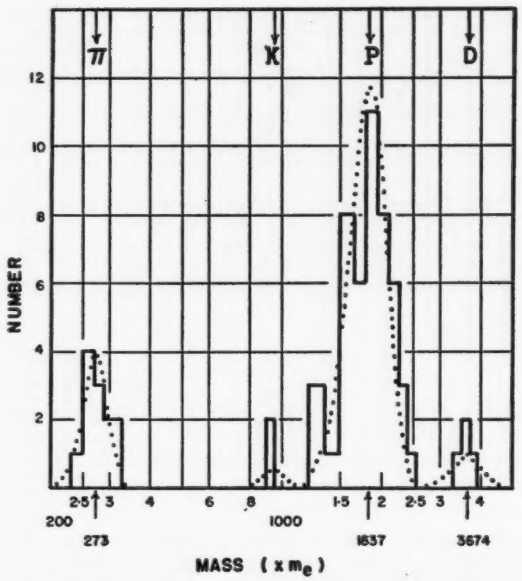

FIG. 4. Histogram showing the mass spectrum calculated from the results in Fig. 3. Mass units (abscissa) for the different groups were taken as $20m_e$ (π); $50m_e$ (K); $150m_e$ (p); $250m_e$ (d). The dotted curves show the normal distribution calculated using the mean experimental standard deviations for each group. The abscissas are plotted on a logarithmic scale for convenience.

with a similar mass ($\sim 1250m_e$) in the present work, but this could also be a statistical fluctuation on the edge of the proton group. It should also be noted that, as in the case of the latest Bristol work,[3,4] the heavy mesons are all of relatively low energies, so far.

3. Measurements Below the Ionization Plateau

Some measurements were also made on particles in the region of minimum ionization. As seen in Fig. 3, there is a well-defined group of pions showing a minimum of ionization at $p\beta \sim 500$ Mev and 8 percent below the plateau. This is in reasonably good agreement with some recent results on the relativistic increase in ionization by Judek and Pickup[7] using artificially produced particles and the same degree of emulsion development and is taken as an indication of the reliability of measurements in this emulsion. It may also be taken to indicate the absence of any fading effects due to events being formed at different times,[7] or perhaps under different conditions of temperature and humidity throughout the balloon flight.

On the high-energy side of the minimum it will be seen that it should be possible to distinguish between the pion, $925m_e$ and proton curves up to $p\beta \simeq 2$ Bev with tracks of lengths suitable for scattering. The present precision of scattering stages is also good enough for this limit. The presence of a group of mesons between $925m_e$ and the proton mass could, of course, lower the limit. Above 2 Bev the heavy meson and proton curves lie so close together that differentiation would be difficult even with very precise measurements, and only a marked change in the depth of the ionization minimum could help here. It may be possible to separate pions from K-mesons and protons up to about 8 Bev.

Referring to Fig. 3 again, it may be noted that there is no definite evidence for any K-mesons about or below the plateau. The two points at $p\beta \sim 3.5$ Bev were put on the graph, although the tracks were rather short, but, in any case, these could be interpreted as due to deuterons. Even allowing for the "loss" of particles of higher $p\beta$ in an emulsion of finite thickness, since longer tracks are needed to give similar statistics as for particles with lower $p\beta$, there does not seem to be a grouping of heavy mesons in the neighborhood of minimum ionization as there is for pions.

4. Nature of Stars Whose Secondary Tracks Were Measured

Defining, for this purpose, the number of shower particles produced in a star, n_s as the number with a normalized blob density $\leqslant 1.5$, six stars were measured with $n_s=0$, 32 with $n_s=1-3$ and for the remainder n_s was $\geqslant 4$. Most of the stars were probably in the 1–50-Bev region and there were no high-energy "jets." The star primaries were protons and a few neutrons, α particles and heavier nuclei. The two K-mesons were produced in stars of type $(7+1p)$ and $(13+1\alpha)$. The present sample thus probably included some stars of lower energy than those used in the Bristol work.

5. Secondary Star Production

Seven secondary stars were observed giving an interaction length $=24\pm 9$ cm or, considering only tracks with a normalized blob density <1.6, the interaction length was 21.7 ± 8 cm.

IV. COMMENTS

(1) There is a small peak in the mass spectrum for mass $\sim 925m_e$ and the presence of a peak between this and the proton mass is uncertain from the present work. The observations are being extended using longer track lengths.

(2) Considering the present observations and those of Fowler and Perkins,[3,4] the frequency of heavy mesons, mass $\sim 925m_e$, appears to be about two percent of the number of protons measured. If the particles with mass closer to the proton mass are real, they are surprisingly frequent and, as yet, there is no evidence for such a group from other work. The number of deuterons is about six percent of the number of protons.

(3) As observed in Sec. III.3, the few K-mesons found are of relatively low energies, as in the work of Fowler and Perkins. Thus, although the statistics are poor, there may be a tendency for the K-mesons to be produced preferentially at low energies when compared

[7] B. Judek and E. Pickup (to be published).

with pions. If so, this could indicate a mode of production for heavy mesons different from that for pions. It may be noted, however, that heavy mesons of greater energy have been observed in cloud chamber work, but little is known about the energy spectrum at present. Powell[4] conjectures that the hyperons and heavy mesons may often originate from secondary interactions of pions (produced in nucleon-nucleon collisions) with other nucleons in the same nucleus. Evidence that hyperons and K-mesons are created in the interaction of pions with hydrogen nuclei has been obtained in work with the Brookhaven Cosmotron.[8] Recent work on a very high-energy nuclear shower by Koshiba and Kaplon[9] gives a production ratio of neutral mesons to charged shower particles of 0.50 ± 0.11 indicating little, if any, production of heavy mesons in such an event as opposed to what might be expected from the statistical theories of multiple-meson production. This apparent lack of an abundant production of heavy mesons at high energies could also be in accordance with a secondary mode of production for the heavy mesons.

(4) We are indebted to the office of Naval Research for enabling our emulsions to be exposed on "Skyhook" balloon flights, to Miss Margaret Stott for some scanning of the emulsion used, and to Miss Jacqueline Dazé for the drawings.

[8] Fowler, Shutt, Thorndike, and Whittemore, Phys. Rev. **91**, 1287 (1953).

[9] M. Koshiba and M. F. Kaplon, Phys. Rev. **97**, 193 (1955).

PHYSICAL REVIEW VOLUME 98, NUMBER 1 APRIL 1, 1955

Spin Polarization of the Deuteron*†

W. Lakin
Carnegie Institute of Technology,‡ Pittsburgh, Pennsylvania
(Received December 2, 1954)

Methods of specifying the state of polarization of a particle of spin 1 are discussed. Selection rules for polarization effects in simple nuclear reactions are derived; in general four parameters are needed to describe the deuteron polarization due to such reactions. Methods of determining these parameters include the use of magnetic deflection. A rough analysis is made of the polarization of deuterons scattered by carbon.

INTRODUCTION

RECENTLY many successful experiments have been done with polarized beams of protons and neutrons. The present paper deals with the theoretical possibilities of extending such experiments to spin 1 particles, in particular, the deuteron. Considerable care must be taken in defining the state of polarization of a spin 1 particle, and this is discussed in Sec. 1. Sections 2 and 3 present general theorems applicable to experiments involving polarized spin 1 particles, whereas Sec. 4 presents a rough analysis of polarization effects for the special case of scattering of deuterons by a nucleus with zero spin and zero isotopic spin, such as carbon. The first three sections apply to any particle of spin 1 and may be of interest in considering the possibility that some of the heavy mesons have spin 1.

1. POLARIZATION STATES OF THE DEUTERON

The spin state of a particle (or nucleus) taking part in a nuclear reaction in general must be described as a statistical mixture of the pure spin states in which the particle may be found. If the description consists of weighting equally all members of any basis set of mutually orthogonal spin functions, the mixture is spatially isotropic and describes *unpolarized particles*. Any different distribution will describe anisotropic states and refers to *polarized particles*.[1] States which may be described by a single wave function will be called *completely polarized*. In the case of particles of spin $\frac{1}{2}$ the most general spin state may be described as a mixture of a completely polarized state with statistical weight P and an unpolarized state with weight $(1-P)$, where P is the percentage polarization. No such simple picture exists for particles of spin greater than $\frac{1}{2}$.

The von Neumann density matrix ρ is a convenient starting point in discussing polarization.[2] It may be expressed as a linear combination of independent Hermitian matrices, whose number equals the square of

* Submitted in partial fulfillment of the requirements for the degree of Doctor of Philosophy at Carnegie Institute of Technology.

† Aided in part by the Office of Naval Research. A brief report of some of this work was given in Phys. Rev. **90**, 365 (1953).

‡ Now at General Electric Research Laboratory, Schenectady, New York.

[1] The term polarization as we use it includes both "polarization" and "alignment" in the sense of Bleaney: B. Bleaney, Proc. Phys. Soc. (London) **A64**, 315 (1951); Simon, Rose, and Jauch, Phys. Rev. **84**, 1155 (1951). *Alignment* may be considered as special cases of the *tensor* type of polarization discussed later, whereas *polarization* corresponds to the *vector* type.

[2] L. Wolfenstein and J. Ashkin, Phys. Rev. **85**, 947 (1952); R. H. Dalitz, Proc. Phys. Soc. (London) **A65**, 175 (1952). Our methods and notation generally follow those of the former paper.

the dimensionality of the spin space, and whose expectation values determine ρ and thus the state of the system. One of these may be the identity matrix, the expectation value of which specifies the normalization; that is, the trace of ρ. The remaining expectation values determine the polarization of the system.

We choose operators which form components of irreducible tensors[3] of rank zero (the identity matrix) one, and two. The operator which transforms under rotations like the spherical harmonic Y_{JM} is denoted by T_{JM}. This set is clearly equivalent to a set of independent Hermitian base matrices, namely that set formed by the Hermitian and anti-Hermitian parts of these operators. The orthogonality and normalization conditions are chosen:

$$\mathrm{Tr}T_{JM}T_{J'M'}{}^{\dagger}=3\delta_{JM,J'M'}. \tag{1.1}$$

The matrix elements of T_{JM} are determined by the tensorial properties and normalization (1.1):

$$(m'|T_{JM}|m)=\sqrt{3}C_{11}(J-M|-m'm), \tag{1.2}$$

where $C_{j_1j_2}(jm|m_1m_2)$ is a Clebsch-Gordan coefficient for combining angular momentum.[4] Explicit forms of the tensor operators in terms of components of the spin operator $\mathbf{S}$ are

$$\begin{aligned}
T_{11}&=-\tfrac{1}{2}\sqrt{3}(S_x+iS_y),\\
T_{10}&=(\tfrac{3}{2})^{\frac{1}{2}}S_z,\\
T_{22}&=\tfrac{1}{2}\sqrt{3}(S_x+iS_y)^2,\\
T_{21}&=-\tfrac{1}{2}\sqrt{3}[(S_x+iS_y)S_z+S_z(S_x+iS_y)],\\
T_{20}&=(\tfrac{1}{2})^{\frac{1}{2}}(3S_z{}^2-2),\\
T_{J,-M}&=(-1)^MT_{JM}{}^{\dagger}.
\end{aligned} \tag{1.3}$$

The density matrix may be written

$$\rho=\tfrac{1}{3}\textstyle\sum_{JM}\langle T_{JM}\rangle T_{JM}{}^{\dagger}, \tag{1.4}$$

where angular brackets denote statistical expectation values. One of the inequalities associated with ρ is that the trace of ρ is less than or equal to unity, or

$$\textstyle\sum_{JM}{}'|\langle T_{JM}\rangle|^2\leq 2, \tag{1.5}$$

where the prime on the summation indicates that $J=0$ (the identity) is omitted. The equality is a necessary and sufficient condition for complete polarization and the left hand side equals zero only for the unpolarized state. Therefore, one may define a percentage polarization

$$P=(\tfrac{1}{2}\textstyle\sum_{JM}{}'|\langle T_{JM}\rangle|^2)^{\frac{1}{2}}. \tag{1.6}$$

The components of $\mathbf{S}$ (if they do not all vanish) define a pseudovector whose direction may be used as the Z-axis so the $\langle T_{1,\pm1}\rangle$ vanish. In Sec. 2 we shall show that in all states produced in the simple reactions of interest to us, the $\langle T_{2,\pm1}\rangle$ vanish too. We now restrict our consideration to this class of states. Geometrically this class of states is characterized by the fact that the direction of the spin is also a principal axis of the symmetrical second-rank tensor formed by $\langle T_{2M}\rangle$. [That this follows from the vanishing of $\langle T_{2,\pm1}\rangle$ may be seen directly from Eqs. (1.3).] Included in this characterization are singular cases in which it is possible but not necessary to choose the spin direction parallel to a principal axis; namely, cases in which the expectation value of the spin vanishes or in which the principal axes of the tensor are not determined uniquely. This class obviously includes the unpolarized state and may be shown to include all completely polarized states.

A useful method of describing the state of polarization is to consider the representation in which ρ is diagonal. Any state then may be described as a statistical mixture of the three pure mutually orthogonal states ψ_n which form the basis of this representation, and the corresponding eigenvalues λ_n of ρ are the weights. Our restricted class of polarization states is a statistical mixture of a restricted set of pure states, which may be shown to be

$$\begin{aligned}
\psi_1&=\chi_0,\\
\psi_2&=A\chi_1+B\chi_{-1},\\
\psi_3&=B^*\chi_1-A^*\chi_{-1}.
\end{aligned} \tag{1.7}$$

Here χ_m is an eigenstate of S_z, where the Z-axis is chosen in the spin direction. If the X- and Y-axes are taken as the other principal axes of the tensor, the constants A and B must be real. [As a matter of fact, since all pure states belong to our restricted class, it follows that any pure state may be represented as one of the forms in (1.7) in a suitable coordinate system. The *set* of pure states (1.7) however is restricted by the condition that the same coordinate system is used for all three states.] Only in special cases will the states ψ_2 and ψ_3 be oriented[5]: (1) when A (or B) vanishes, the states are oriented along the Z-axis; (2) when $A=B$, the three states are χ_0 states oriented along three mutually-perpendicular axes, the principal axes of the tensor. In general states ψ_2 and ψ_3 have average spin equal in magnitude but opposite in direction. They are analogous to two elliptically polarized states of light with opposite senses of rotation and crossed major axes.

A state of the class we are considering is seen to be specified by six parameters; this is in contrast to the four parameters required to specify a pure state and the eight parameters required to specify the most general state. Three of these six parameters define the principal axes, while the other three may be taken as (A/B) and two of the λ_n (the normalization $\mathrm{Tr}\rho$ is not considered as a parameter). In place of the last three, we shall use the three real numbers $\langle T_{20}\rangle$, $\langle T_{10}\rangle$, and

[3] See for example G. Racah, Phys. Rev. **62**, 438 (1942).

[4] See for example J. Blatt and V. F. Weisskopf, *Theoretical Nuclear Physics* (John Wiley and Sons, Inc., New York, 1952), p. 789.

[5] An oriented state is one which is an eigenstate of the operator S_z for some choice of z-axis. E. Majorana, Nuovo cimento **9**, 43 (1932).

$\sqrt{2}\langle T_{22}\rangle$[6] which are given by

$$\begin{aligned}\langle T_{10}\rangle &= (\tfrac{3}{2})^{\frac{1}{2}}(\lambda_2-\lambda_3)(A^2-B^2),\\ \langle T_{20}\rangle &= (\tfrac{1}{2})^{\frac{1}{2}}(1-3\lambda_1),\\ \sqrt{2}\langle T_{22}\rangle &= (6)^{\frac{1}{2}}(\lambda_3-\lambda_2)AB.\end{aligned} \tag{1.8}$$

Equations (1.8) yield

$$\langle T_{10}\rangle^2+[\sqrt{2}\langle T_{22}\rangle]^2\leq\tfrac{1}{3}[\langle T_{20}\rangle+\sqrt{2}]^2. \tag{1.9}$$

Each possible state may be represented by a point in a space whose coordinates are $\langle T_{10}\rangle$, $\sqrt{2}\langle T_{22}\rangle$, and $\langle T_{20}\rangle$ respectively; these points fill the interior of a cone, whose apex is at $\langle T_{20}\rangle=-\sqrt{2}$ on the $\langle T_{20}\rangle$-axis, and whose base has a radius of $\sqrt{\frac{3}{2}}$ and is normal to this axis at $\langle T_{20}\rangle=+\frac{1}{2}\sqrt{2}$. The completely polarized state ψ_1 is at the apex, while the completely polarized states ψ_2 and ψ_3 are on opposite ends of a diameter of the base. The unpolarized state, of course, is at the origin.

2. SELECTION RULES FOR SIMPLE REACTIONS

We consider reactions in which both initial and final states contain only two particles (nuclei). The states are specified by the momenta in the c.m. system (center-of-mass) and the polarization. The polarization state may be specified by a density matrix in the product of the spin spaces of the two particles. Transition amplitudes for the various pure spin states may be written as a matrix M whose rows and columns are characterized by the spin quantum numbers of final and initial states, respectively.[7] We express ρ_i and ρ_f as linear combinations of base matrices R^ν and S^μ in the spin spaces of the initial and final systems, respectively. We find, as in reference 2:

$$I\langle S^\mu\rangle_f=\frac{1}{n_i}\sum_\nu\langle R^\nu\rangle_i\,\mathrm{Tr}(MR^\nu M^\dagger S^\mu). \tag{2.1}$$

Here I is the differential cross section for this reaction, and the basic operators are normalized so that

$$\begin{aligned}\mathrm{Tr}(R^\mu R^{\nu\dagger})&=n_i\delta_{\mu\nu},\\ \mathrm{Tr}(S^\mu S^{\nu\dagger})&=n_f\delta_{\mu\nu},\end{aligned} \tag{2.2}$$

where n_i and n_f are the dimensionalities of initial and final spin spaces. If neither initial particle is polarized and one reaction product is a deuteron and the polarization of the other is not observed, the only $\langle R^\nu\rangle_i$ unequal to zero is the expectation value of the identity, and the only S^μ of interest will be the direct products of the tensor operators T_{JM} in the deuteron spin space with the identity operator in the spin space of the other reaction product. Then (2.1) gives for the polarization of the outgoing deuterons

$$I_0\langle T_{JM}\rangle_f=\frac{1}{n_i}\mathrm{Tr}(MM^\dagger T_{JM}), \tag{2.3}$$

where I_0 denotes the cross section for unpolarized incident particles.

Since M must be invariant under space rotations and reflections $MM^\dagger$ must be similarly invariant. Terms of interest must be contractions of the T_{JM} with tensor quantities formed from $\mathbf{k}_i$ and $\mathbf{k}_f$, the initial and final momenta; to be invariant under space reflection, they must be of even degree in $\mathbf{k}_i$ and $\mathbf{k}_f$. Consequently the most general form of $MM^\dagger$ is

$$\begin{aligned}MM^\dagger=J_0&+J_1\textstyle\sum_M Y_{2M}(\mathbf{k}_i)T_{2M}{}^\dagger+J_2\sum_M Y_{2M}(\mathbf{k}_f)T_{2M}{}^\dagger\\ &+J_3\textstyle\sum_M Y_{2M}(\mathbf{k}_i\mathbf{k}_f)T_{2M}{}^\dagger\\ &+J_4\textstyle\sum_M Y_{1M}(\mathbf{k}_i\times\mathbf{k}_f)T_{1M}{}^\dagger+\cdots.\end{aligned} \tag{2.4}$$

Here the J's depend only on $\mathbf{k}_i\cdot\mathbf{k}_f$, k_i, and k_f, and must be real in order that $MM^\dagger$ be Hermitian. The Y_{JM} are solid spherical harmonics formed from the components of their indicated arguments,[8] and $+\cdots$ indicates quantities depending on operators in the spin space of the second reaction product.

Equation (2.3) shows that $\langle T_{JM}\rangle_f$ equals the coefficient of $T_{JM}{}^\dagger$ in (2.4) divided by I_0; the terms denoted by $+\cdots$ contribute nothing. To study the polarization state of these deuterons, we choose the Z-axis normal to the reaction plane. Then the Z-components of $\mathbf{k}_i$ and $\mathbf{k}_f$ vanish and $\mathbf{k}_i\times\mathbf{k}_f$ is in the Z-direction, hence all harmonics of the type $Y_{J,\pm1}$ in (2.4) vanish, and thus all $\langle T_{J,\pm1}\rangle_f$. This proves the assertion in Sec. 1 that the polarization states produced in simple reactions will have the spin along a principal axis; moreover, we see this preferred direction is normal to the reaction plane.

We have already discussed the general features of these polarization states. However, it is useful to examine the $\langle T_{JM}\rangle_f$ using an axis in the reaction plane as the polar axis, for if we try to detect polarization by a second reaction, it is convenient to choose the direction of incidence of this second reaction as the Z-axis. We single out the normal as the y-axis. In this coordinate system, all nonvanishing second rank harmonics involving $\mathbf{k}_i$ and $\mathbf{k}_f$ in (2.4) are real, while $Y_{1,\pm1}(\mathbf{k}_i\times\mathbf{k}_f)$ is pure imaginary. These determine the relations between the $\langle T_{JM}\rangle_f$:

$$\langle T_{2,-M}\rangle_f=(-1)^M\langle T_{2,M}\rangle_f, \tag{2.5}$$

$$\langle T_{1,-M}\rangle_f=(-1)^{M+1}\langle T_{1M}\rangle_f. \tag{2.6}$$

Equation (2.6) includes the vanishing of $\langle T_{10}\rangle_f$, which we already know, since $\langle\mathbf{S}\rangle_f$ lies on the normal.

A second problem of interest is the angular distribution of the reaction products when the initial state consists of a polarized deuteron and an unpolarized

[6] In the principal axis system $\langle T_{22}\rangle$ is real and equal to $\langle T_{2,-2}\rangle$. If we consider as our base matrices the hermitian and the anti-Hermitian parts of T_{22}, then the expectation value of the former is $\sqrt{2}\langle T_{22}\rangle$ and the expectation value of the latter vanishes.

[7] This matrix and the following equations are a straightforward extension of the corresponding ones in reference 2.

[8] $Y_{2M}(\mathbf{k}_i,\mathbf{k}_f)$ is a second-degree harmonic, bilinear, and symmetrical in $\mathbf{k}_i$ and $\mathbf{k}_f$.

TABLE I. Maximum degree in $\cos\theta$ of the polynomial functions I_0, A, B, C, and D.

Polynomial	Maximum degree in $\cos\theta$
$I_0(\theta)$	$2L_{max}$
$A(\theta)$	$2L_{max}+2$
$B(\theta)$	$2L_{max}+1$
$C(\theta)$	$2L_{max}-1$
$D(\theta)$	$2L_{max}$

target of spin j. The general form of $M^\dagger M$ may now be found by the arguments used in deriving (2.4); substituting this form into (2.1) with S^μ equal to unity, we find a general expression for the differential cross section I:

$$I=I_0+I_2\sum_M Y_{2M}^*(\mathbf{k}_i)\langle T_{2M}\rangle_i+I_1\sum_M Y_{2M}^*(\mathbf{k}_f)\langle T_{2M}\rangle_i +I_3\sum_M Y_{2M}^*(\mathbf{k}_i\mathbf{k}_f)\langle T_{2M}\rangle_i +I_4\sum_M Y_{1M}^*(\mathbf{k}_i\times\mathbf{k}_f)\langle T_{1M}\rangle_i, \quad (2.7)$$

where the I's are real quantities depending on k_i, k_f, and $\mathbf{k}_i\cdot\mathbf{k}_f$.

If the polarized deuterons used as projectiles in a reaction are products of a previous reaction, the $\langle T_{JM}\rangle_i$ in Eq. (2.7) applied to the second reaction must satisfy (2.5) and (2.6), where the Z-axis is the direction of incidence of the second reaction and the y-axis is normal to the plane of the first. Combining terms containing $Y_{JM}^*(\mathbf{k}_f)$ and $Y_{J,-M}^*(\mathbf{k}_f)$, we obtain the dependence of I on $\mathbf{k}_f$, which gives us the angular distribution

$$I(\theta,\phi)=I_0(\theta)+\langle T_{20}\rangle_i A(\theta) +[\langle T_{21}\rangle_i B(\theta)+iC(\theta)\langle T_{11}\rangle_i]\sin\theta\cos\phi +\langle T_{22}\rangle_i D(\theta)\sin^2\theta\cos 2\phi. \quad (2.8)$$

Here θ is the polar angle, ϕ the azimuthal angle measured from the plane of the first reaction, and the functions I_0, A, B, C, D, are polynomials in $\cos\theta$. If L_{max} is the maximum effective incident orbital angular momentum (in the second reaction, the degrees of these polynomials are limited as given in Table I[9]:

In elastic collisions, the polarization produced by scattering unpolarized deuterons is related to the azimuthal asymmetries obtained by scattering polarized deuterons, assuming the Hamiltonian is invariant under time reversal.[10,11] If M' is the time-reverse of M, it may be defined

$$M_{a,b}{}'=M_{-b,-a}, \quad (2.9)$$

where $-b$, $-a$ are the time-reversed states of b and a respectively. The invariance argument becomes

$$M'=M,$$

so that

$$(MM^\dagger)'=M^\dagger M. \quad (2.10)$$

[9] The argument is an extension of that used for unpolarized beams; see e.g., reference 4, page 535. For an extension to polarized beams see A. Simon and T. Welton, Phys. Rev. **90**, 1036 (1953); L. Wolfenstein, Phys. Rev. **92**, 123 (1953).

[10] E. Wigner, Nachr. Ges. Wiss. Göttingen **31**, 546 (1932).

[11] This is an extension of the argument of reference 2.

The operator $\mathbf{S}$ changes sign under time-reversal and $\mathbf{k}_i$ and $\mathbf{k}_f$ are transformed into $-\mathbf{k}_f$ and $-\mathbf{k}_i$ respectively. Comparing the explicit forms for $MM^\dagger$ and $M^\dagger M$, Eq. (2.10) yields the result that J_i in Eq. (2.4) equals I_i in Eq. (2.7). It follows that, if we choose the Z-axis in the direction of the outgoing deuterons and the y-axis as usual normal to the reaction plane, the values of $\langle T_{JM}\rangle$ produced by scattering unpolarized deuterons are related to the coefficients I_0, A, B, C, and D of (2.8) by

$$\begin{aligned} I_0\langle T_{20}\rangle&=A,\\ I_0\langle T_{21}\rangle&=\tfrac{1}{2}B\sin\theta,\\ I_0\langle T_{22}\rangle&=\tfrac{1}{2}D\sin^2\theta,\\ I_0\langle T_{11}\rangle&=-(i/2)C\sin\theta. \end{aligned} \quad (2.11)$$

Then in two successive scatterings of a deuteron by an infinitely heavy nucleus through the same scattering angle θ, the angular distribution is

$$I=I_0[1+\langle T_{20}\rangle^2+2(\langle T_{21}\rangle^2+|\langle T_{11}\rangle|^2)\cos\phi +2\langle T_{22}\rangle^2\cos 2\phi]. \quad (2.12)$$

Thus four parameters are required to describe the result of a double scattering experiment in contrast to the one parameter needed for a spin $\frac{1}{2}$ particle; in Eq. (2.12) these parameters are taken as the expectation values of the tensor operators after the first scattering. Experimentally the value of $\langle T_{20}\rangle^2$ is obtained by comparing the total intensity averaged over ϕ with that produced by scattering unpolarized deuterons; then the value of $\langle T_{22}\rangle^2$ is obtained from the $\cos 2\phi$ term in the azimuthal distribution. But the $\cos\phi$ term contains contributions from both first and second rank tensors so that a simple double scattering does not distinguish $\langle T_{11}\rangle$ from $\langle T_{21}\rangle$. (See Sec. 3.)

It is particularly interesting to examine some of the cases of double scattering where the first scattering produces completely polarized particles. If the pure state is χ_0 oriented along the y-axis or x-axis, the $\cos 2\phi$ asymmetry is a maximum and

$$I=I_0(\tfrac{3}{2}+\tfrac{3}{2}\cos 2\phi). \quad (2.13)$$

If the pure state is $\chi_{\pm 1}$ oriented along the y-axis the $\cos\phi$ asymmetry is a maximum, but this is also true in the more general case when the pure state is any state like Ψ_2 (or Ψ_3) of Eq. (1.7) if the principal axes of the tensor in the X-plane make angles of 45° with the Z-axis. Then I becomes

$$I=I_0(1\tfrac{1}{8}+\tfrac{3}{2}\cos\phi+\tfrac{3}{8}\cos 2\phi). \quad (2.14)$$

It may be noted by comparing (2.12) with (1.6), that in all cases where the first scattering produces completely polarized particles the cross section I for the second scattering at $\phi=0$ is three times the unpolarized cross section.

3. EFFECTS OF MAGNETIC DEFLECTION

In double-collision experiments, the first may take place inside the cyclotron; the magnetic field in general will alter the polarization of the outgoing deuterons. Such effects would have to be considered in interpreting the experiments; moreover, they may be useful in studying nuclear reactions. We treat the case where the interaction of the deuteron and magnetic field may be treated as the interaction of a magnetic dipole with a static field normal to the plane of the first reaction. The spin state rotates about the field with a frequency equal to $\mu\omega$, where μ is the deuteron magnetic moment in nuclear magnetons and ω the proton Larmor frequency. The deuteron's cyclotron frequency is one-half that of the proton and thus equals the Larmor frequency. Therefore the angle of rotation of the spin relative to the direction of motion equals $(\mu-1)$ times the angle of deflection. Since $(\mu-1)$ is about $-1/7$, fairly large deflections are generally required to get appreciable effects on the polarization. Since $\langle\mathbf{S}\rangle$ is in the direction of the field, it remains unchanged. The principal axes of the second rank tensor in the reaction plane are rotated relative to the direction of motion through an angle $(\mu-1)$ times the angle of deflection.

If the deuterons can be deflected through sufficiently large angles, some of the ambiguities in the double scattering experiment discussed in Sec. 2 can be resolved. The effect of the rotation of the principal axes relative to the direction of motion will be to replace the $\langle T_{2M}\rangle$ in (2.8) by $\langle T_{2M}\rangle'$

$$\langle T_{2M}\rangle'=\sum_{M'}C_{MM'}(R)\langle T_{2M}\rangle, \tag{3.1}$$

where the C's are determined by the rotation and are readily calculated. Experiments discussed in Sec. II both with and without magnetic deflection will then determine in principle $|\langle T_{20}\rangle|$, $|\langle T_{20}\rangle'|$, $|\langle T_{22}\rangle|$, $|\langle T_{22}\rangle'|$, and the signs of the primed quantities relative to the unprimed. Then (3.1) will determine all $\langle T_{2M}\rangle$ and $\langle T_{2M}\rangle$ uniquely including all relative signs. Since (3.1) is invariant under change of sign of all $\langle T_{2M}\rangle$ there remains one ambiguity in sign. The value of the $\cos\phi$ asymmetry then provides a determination of $|\langle T_{11}\rangle|$. We may translate the result for the $\langle T_{JM}\rangle$ to the coordinate system used in Sec. 1 and represent it as a point in the space with coordinates $\langle T_{10}\rangle$, $\sqrt{2}\langle T_{22}\rangle$, and $\langle T_{20}\rangle$. Then the ambiguity in the sign of $\langle T_{2M}\rangle$ corresponds to a reflection in the origin of the $\sqrt{2}\langle T_{22}\rangle-\langle T_{22}\rangle$ plane so that if one possible result corresponds to a statistical mixture with a surplus (more than $\frac{1}{3}$) of state ψ_1, the other corresponds to a deficiency. In many cases the effect of the reflection may be to put the point outside of the allowed cone [Eq. (1.9)] so that in these cases there exists no ambiguity in the signs of the $\langle T_{2M}\rangle$. The sign of $\langle T_{11}\rangle$ cannot be determined by any of these experiments.

Magnetic deflection may yield valuable partial information about nuclear reactions under conditions which are not experimentally favorable for the complete set of experiments described above. For example, if the polarized deuterons are produced in the forward direction, the selection rules show that $\langle T_{20}\rangle$ may be the only nonvanishing expectation value. If $\langle T_{20}\rangle$ is large enough, one can produce known relative amounts of the $\langle T_{2M}\rangle$ by magnetic deflection and then obtain the cross section I and the ratios of A, B, and D of (2.9) for a second reaction. This partially calibrated detector could be useful in determining relative values of the $\langle T_{2M}\rangle$ of deuteron beams.

4. ELASTIC SCATTERING OF DEUTERONS BY CARBON

The double scattering of deuterons by carbon has been studied experimentally by Chamberlain *et al.*[12] This experiment is particularly simple because the target has both spin and isotopic spin equal to zero, and the scattering amplitude may be calculated in terms of that for protons by carbon if the impulse approximation is valid.[13] The matrix M may be written

$$M=\int d_3p[f(2\mathbf{p}+\mathbf{k})(\mathbf{k}+\mathbf{p}|t_1+t_2|\mathbf{k}_0+\mathbf{p}) \times f(2\mathbf{p}+\mathbf{k}_0)]. \tag{4.1}$$

Here $\mathbf{k}_0$ and $\mathbf{k}$ are initial and final deuteron momenta respectively, the t's are scattering amplitudes from carbon for the two nucleons inside the deuteron, and f is the deuteron ground-state wave function in momentum space, which may be written[14]

$$f(\mathbf{p})=f_0(p)+f_2(p)S_{12}(\mathbf{p}), \tag{4.2}$$

where

$$S_{12}(\mathbf{p})=3\boldsymbol{\sigma}_1\cdot\mathbf{p}\boldsymbol{\sigma}_2\cdot\mathbf{p}-p^2\boldsymbol{\sigma}_1\cdot\boldsymbol{\sigma}_2.$$

The t_1 and t_2 have the same dependence upon their arguments according to the charge symmetry hypothesis and may be written

$$(\mathbf{k}+\mathbf{p}|t_i|\mathbf{k}_0+\mathbf{p})=g+h\boldsymbol{\sigma}_i\cdot[(\mathbf{k}_0+\mathbf{p})\times(\mathbf{k}+\mathbf{p})], \tag{4.3}$$

where g and h are scalars.

Equation (4.1) simplifies greatly if we assume the deuteron ground state is a pure S-state. We look first at results that are independent of the form of g and h. Since M is linear in the spin operator, it has the form

$$M=G+H\mathbf{S}\cdot\mathbf{n}, \tag{4.4}$$

where $\mathbf{n}$ is a unit vector perpendicular to $\mathbf{k}_0$ and $\mathbf{k}$. Then

$$MM^\dagger=(|G|^2+\tfrac{2}{3}|H|^2) +2(\tfrac{2}{3})^{\frac{1}{2}}\,\mathrm{Re}(G^*H)\sum_M T_{1M}Y_{1M}^*(\mathbf{n}) +\tfrac{1}{3}\sqrt{2}\,|H|^2\sum_M T_{2M}Y_{2M}^*(\mathbf{n}), \tag{4.5}$$

[12] O. Chamberlain *et al.*, Phys. Rev. **95**, 1104 (1954).

[13] G. F. Chew, Phys. Rev. **80**, 196 (1950); G. F. Chew and G. C. Wick, Phys. Rev. **83**, 636 (1952). In the present case in which the proton scattering amplitude is sharply peaked in the forward direction the neglect of multiple collisions may not be justified.

[14] W. Rarita and J. Schwinger, Phys. Rev. **59**, 436 (1941).

where Re means the real part is to be taken. The resulting polarization state is a statistical mixture of the pure states oriented along $\mathbf{n}$ and is unaltered by the magnetic deflection discussed in Sec. 3. If the y-axis is taken along $\mathbf{n}$ the nonvanishing $\langle T_{JM}\rangle$ are given by

$$\begin{aligned} I_0\langle T_{11}\rangle &= -(2i/\sqrt{3})\,\mathrm{Re}(G^*H), \\ I_0\langle T_{22}\rangle &= (\tfrac{3}{2})^{\frac{1}{2}} I_0\langle T_{20}\rangle = -(1/2\sqrt{3})|H|^2, \\ I_0 &= |G|^2+\tfrac{2}{3}|H|^2, \end{aligned} \tag{4.6}$$

and the angular distribution of the double scattering is given by substituting (4.6) into (2.12). A maximum left-right asymmetry of about 17 to 1 in double scattering can occur for $|G|^2$ about equal to $\frac{2}{3}|H|^2$. For $|H|\gg|G|$ we get the maximum $\cos 2\phi$ asymmetry, the angular distribution approaching $(1+\frac{1}{3}\cos 2\phi)$. The ratio of the $\cos\phi$ term to the azimuthally symmetric term in the experiments of Chamberlain *et al.*[12] are consistent with (4.6) if the ratio $\frac{2}{3}|H|^2/|G|^2$ is about 0.09 and G and H have the same phase; also if the phases of G and H differ by 45° and $\frac{2}{3}|H|^2/|G|^2$ is about 0.23. In both cases by choosing $(\frac{2}{3})^{\frac{1}{2}}|H|$ less than $|G|$ we have made sure that the $\cos 2\phi$ term is small enough to be consistent with the experiments. Much larger values of the relative phase are not possible.

If the g and h in (4.3) depend only on the momentum transfer, we may take these quantities out of the integral in (4.1). This would be true if the Born approximation were valid for the scattering of protons by carbon, but is must be noted that the important contributions to the integral come from proton energies about half the deuteron energy and scattering angles about twice the deuteron scattering angle. Continuing to neglect the D-state part of f, we obtain

$$\begin{aligned} M=&[2g(q)+h(q)(\boldsymbol{\sigma}_1+\boldsymbol{\sigma}_2)\cdot(\mathbf{k}_0\times\mathbf{k})] \\ &\times\int f_0(|2\mathbf{p}+\mathbf{k}|)f_0(|2\mathbf{p}+\mathbf{k}_0|)d_3p+h(q)(\boldsymbol{\sigma}_1+\boldsymbol{\sigma}_2) \\ &\cdot\left[(-\mathbf{q})\times\int \mathbf{p}f_0(|2\mathbf{p}+\mathbf{k}|)f_0(|2\mathbf{p}+\mathbf{k}_0|)d_3p\right], \end{aligned} \tag{4.7}$$

where $\mathbf{q}$ is the momentum transfer. The second integral in (4.7) has nonvanishing components only in the direction of $(\mathbf{k}_0+\mathbf{k})$. If we make the approximation that $|\mathbf{k}|$ is large compared to momenta inside the deuteron the product of the f's in the integrand will be peaked in the region where $\mathbf{p}\cdot(\mathbf{k}_0+\mathbf{k})=-\frac{1}{4}(\mathbf{k}_0+\mathbf{k})^2$. Taking this value of $\mathbf{p}\cdot(\mathbf{k}_0+\mathbf{k})$ out of the integral, the second integral just cancels half of the spin term in the first and we have

$$\begin{aligned} M=&[2g(q)+h(q)\mathbf{S}\cdot(\mathbf{k}_0\times\mathbf{k})] \\ &\times\int f_0(|2\mathbf{p}+\mathbf{k}|)f_0(|2\mathbf{p}+\mathbf{k}_0|)d_3p. \end{aligned} \tag{4.8}$$

The spin term involves $h(q)k^2\sin\theta$, which in general is expected to increase relative to $g(q)$ with increasing θ for small angles θ. In the scattering of protons of the same momentum $\mathbf{k}$, the maximum polarization occurs when the magnitudes of $g(q)$ and $h(q)k^2\sin\theta$ are about equal; in deuteron scattering the maximum $|\langle T_{11}\rangle|$ occurs when the magnitude of $2g(q)$ and $(\frac{2}{3})^{\frac{1}{2}}h(q)k^2\sin\theta$ are about equal, or at somewhat larger θ. In order that the $\cos 2\phi$ asymmetry approach its maximum, the magnitude of $(\frac{2}{3})^{\frac{1}{2}}h(q)k^2\sin\theta$ must be large compared to $2g(q)$. This most likely would require still larger angles θ if it occurs at all. We would like to relate the deuteron polarization to that for proton, but it is not possible to predict the deuteron polarization from the proton without knowing the relative phase of g and h. If we take (4.8) literally we may state, however, that for the deuteron double-scattering results[12] to be correct within experimental error the proton polarization at the same momentum and angle should be more than 0.05. Since the proton polarization appears to be somewhat smaller we may say that Eq. (4.8) predicts either a smaller $\cos\phi$ term or a larger $\cos 2\phi$ term than observed. However, experimental data are too limited to show how poor Eq. (4.8) may really be.

Since large momenta are important in (4.1), the D-state part of the deuteron functions may not make a small contribution. Then M in general would contain all terms allowed by symmetry arguments even in the Born approximation. Since I_0 generally would be the sum of five positive terms while the $\langle T_{JM}\rangle$ would be sums of terms which may have different signs, polarization effects, especially the $\langle T_{2M}\rangle$, might be reduced.

ACKNOWLEDGMENT

The author is indebted to Professor L. Wolfenstein for suggesting this problem, for his continued assistance throughout the course of this work, and for suggesting many improvements in the manuscript.

Lower Limit for the Energy Derivative of the Scattering Phase Shift

EUGENE P. WIGNER
Palmer Physical Laboratory, Princeton University, Princeton, New Jersey
(Received December 10, 1954)

It is shown that the derivative of the scattering phase shift with respect to energy, $d\eta/dE$, must exceed a certain limit if the interaction of scattered particle and scatterer vanishes beyond a certain distance. This limitation of $d\eta/dE$ is, fundamentally, a consequence of the principle of causality; it is derived, however, from a property of the derivative matrix R.

I

THE cross section and its angular dependence, as functions of energy, do not seem to determine in general the phase shifts uniquely.[1] It may be useful, therefore, to derive certain general rules about the energy dependence of phase shifts which may facilitate the choice between the apparently equivalent sets of phase shifts. The relations to be derived here are based, fundamentally, on what has come to be called "the principle of causality." It states that the scattered wave cannot leave the scatterer before the incident wave has reached it. However, the calculation to be carried out will make use of a single property of the derivative matrix R which was given already by Eisenbud and the present writer.[2]

Before carrying out the very simple calculation, the general nature of the result will be illustrated by means of Eisenbud's interpretation of the energy derivative of the phase shift as time delay.[3] Let us consider, for sake of simplicity, a scattering center of radius a, i.e., assume that the incident particle behaves like a free particle outside a sphere of this radius. Let us consider then an incident beam which is the superposition of two monoenergetic beams of energy $\hbar(\nu+\nu')$ and $\hbar(\nu-\nu')$, respectively. The corresponding wave numbers will be denoted by $k+k'$ and $k-k'$. Hence,

$$\psi_{\text{inc}}=r^{-1}(e^{-i(k+k')r-i(\nu+\nu')t}+e^{-i(k-k')r-(\nu-\nu')t}). \quad (1)$$

Both k' and ν' are infinitesimally small so that (1) is a substitute for a wave packet,[4] the center of which is at the point where the two spherical waves of (1) are in phase, i.e., where

$$2k'r+2\nu't=0. \quad (1a)$$

Since $\nu'/k'=d\nu/dk$ is the velocity of the particle, the incident particle indeed moves with a velocity v toward the scattering center. If $\eta+\eta'$ and $\eta-\eta'$ are the phase shifts which correspond to the energy values $\hbar(\nu+\nu')$ and $\hbar(\nu-\nu')$, the outgoing wave will be

$$\psi_{\text{out}}=r^{-1}(e^{i(k+k')r-i(\nu+\nu')t+2i(\eta+\eta')}+e^{i(k-k')r-i(\nu-\nu')t+2i(\eta-\eta')}). \quad (1b)$$

The two waves of (1b) are in phase where

$$2k'r-2\nu't+4\eta'=0,$$

i.e., where

$$r=-2\eta'/k'+(\nu'/k')t=-2d\eta/dk+(d\nu/dk)t. \quad (1c)$$

One sees that the outgoing wave is retarded by a stretch $2d\eta/dk$; it arrives at a point $r-2d\eta/dk$ at the time it would have arrived at r without the action of the scattering center. The causality principle as formulated in the first paragraph gives no upper value for the retardation $2d\eta/dk$: if the particle is temporarily captured by the scattering center, there is no reason for it not being retained an arbitrarily long time. However, the "retardation" cannot assume arbitrarily large negative values, in classical theory it could not be less than $-2a$. It will be seen that the wave nature of the particles does permit some infringement of the relation

$$d\eta/dk>-a. \quad (2)$$

It will be shown that, nevertheless, (2) is essentially preserved also in quantum theory. It does hold, in particular, for large k.

The relation (2) gives a simple physical interpretation to the qualitative behavior of the energy dependence of η. Close to resonances, where the incident particle is in fact captured and retained for some time by the scattering center, $d\eta/dk$ will assume large positive values. On the other hand, $d\eta/dk$ will be close to $-a$ at energy values at which the incident particle hardly enters the scatterer. One would expect (on the basis of Liouville's theorem or the completeness relations) that the two effects, on the whole, balance each other, i.e., that the integral of $d\eta/dE$ over the whole energy range is close to zero, at least if the scattering can be described by a nonsingular potential. This is indeed the case: $\eta=0$ at $E=\infty$ and $\eta=b\pi$ for $E=0$, where b is the number of bound states.[5] Hence, if the cross section

[1] See, e.g., the articles of Fermi, Metropolis, and Alei, Phys. Rev. **95**, 1581 (1954); de Hoffmann, Metropolis, Alei, and Bethe, Phys. Rev. **95**, 1586 (1954); and of R. L. Martin, Phys. Rev. **95**, 1606 (1954) for the ambiguities in the case of pion-nucleon scattering.

[2] E. P. Wigner and L. Eisenbud, Phys. Rev. **72**, 29 (1947), see (i) on page 35.

[3] L. Eisenbud, dissertation, Princeton, June 1948 (unpublished).

[4] Instead of the superposition of only two monoenergetic waves, one can use a regular wave packet in this consideration; r in (1a) and (1c) then becomes the coordinate of the center of mass of that wave packet.

[5] I am much indebted to Dr. V. Bargmann for this observation.

shows a resonance behavior, one will expect η to decrease slowly between resonances and increase fast at resonances, increases and decreases almost exactly balancing if considered over the whole energy spectrum.

II

In order to derive a rigorous minimum value for $d\eta/dk$, it will be necessary to assume that there is a radius a outside of which the wave function is that of a free particle. This is a somewhat artificial assumption which will be hardly ever satisfied rigorously. One can, therefore, expect that the condition (4b) to be derived under this assumption will be violated occasionally. However, if a is chosen reasonably large the violations will be uncommon and will extend over narrow energy intervals.

We define as internal region the inside of a sphere of radius a and call the rest of space the external region. The wave function ψ in the external region is then given by

$$r\psi = I(r) - e^{2i\eta} I^*(r), \tag{3}$$

where $I(r)$ is the radial part of an incoming spherical wave (of arbitrary angular momentum), its conjugate complex $I^*(r)$ is the outgoing wave; η is called the phase shift. For $\eta=0$, ψ must be regular at $r=0$, which fixes the phase of I except for I's sign.[6] We shall normalize I so that

$$I(r)I'(r)^* - I(r)^* I'(r) = 2i. \tag{3a}$$

$I(r)$ then represents a wave with flux $m/\hbar$. The prime denotes the derivative with respect to r. Both I and η also depend on the energy; we shall use, instead, the wave vector k as variable and denote differentiation with respect to k by a dot.

The value of the reciprocal logarithmic derivative R of ψ, with respect to r, at $r=a$, becomes

$$R = \frac{I - e^{2i\eta} I^*}{I' - e^{2i\eta} I'^*}. \tag{3b}$$

The I, I', etc., without argument, denote the value of the corresponding expression at $r=a$. Calculation of $e^{2i\eta}$ from (3a) yields

$$e^{2i\eta} = (I - I'R)(I^* - I'^* R)^{-1}. \tag{3c}$$

It may be remarked, parenthetically, that this expression remains valid if, in addition to scattering, transmutations are also possible. The left side has to be replaced then by the collision matrix, R by the derivative matrix, and I, I', etc., by diagonal matrices, the diagonal elements of which are the $I(a)$, $I'(a)$, etc., for the channel to which the row of the collision matrix refers.

[6] It is necessary, in collision theory, to fix also the sign of $I(r)$ in terms of the decomposition of the plane wave into spherical waves. This is not necessary, however, for the derivation of (4b).

III

In the present case, all quantities in (3c) are numbers and logarithmic differentiation of (3c) with respect to k gives

$$\dot\eta = \frac{1}{2i}\left[\frac{\dot I - \dot I' R - I'\dot R}{I - I'R} - \frac{\dot I^* - \dot I'^* R - I'^* \dot R}{I^* - I'^* R}\right]. \tag{4}$$

The term proportional to $\dot R$ in (4) is

$$\frac{-I'(I^* - I'^* R) + I'^*(I - I'R)}{2i|I - I'R|^2}\dot R = \frac{\dot R}{|I - I'R|^2}. \tag{4a}$$

The last part follows from (3a). The partial fraction expansion[2] of R shows directly that $\dot R = (\hbar^2 k/m)dR/dE > 0$ for $k>0$ so that omission of the term containing $\dot R$ will make the left side of (4) larger than the right side. Elimination of R from the resulting inequality by means of (3b) yields

$$d\eta/dk = \dot\eta > \tfrac{1}{2}\,\mathrm{Re}[\dot I' I^* - \dot I I'^* + (\dot I I' - \dot I' I)e^{-2i\eta}]. \tag{4b}$$

$\mathrm{Re}[\cdots]$ denotes the real part of the expression contained in the bracket. The computation leading from (4) to (4b) involves the use of (3a) and the equation obtained from it by differentiation with respect to k.[6]

It remains to point out that the partial fraction expansion of R, though obtained in reference 2 by direct calculation, has been shown[7] to follow also from the causality condition described at the beginning of this note. This establishes the relation between (4b) and the qualitative consideration based on Eisenbud's early work. The connection becomes even clearer if one inserts, into (4b), the expressions for I for $l=0$ or $l=1$:

$$I_0(r) = k^{-1} e^{-ikr}; \quad I_1(r) = k^{-1}[(kr)^{-1} + i]e^{-ikr}. \tag{5}$$

These give, in the former case,

$$\dot\eta_0 > -a + (2k)^{-1}\sin 2(\eta_0 + ka); \tag{5a}$$

while one has, in the latter case,

$$\dot\eta_1 > -a + (k^2 a)^{-1}[1 - \cos 2(\eta_1 + ka)] - (2k)^{-1}\sin 2(\eta_1 + ka). \tag{5b}$$

It will be noted that, as long as $ka \ll 1$, these equations actually entail $\dot\eta > 0$ for a reasonably large interval of η. However, at very low k, (5b) merely expresses the fact that η_0 and η_1 are proportional to k and k^3, respectively, without limiting the proportionality constant.

Naturally, the proper limitation of a constitutes the principal difficulty in using (4b) to select the actual

[7] In addition to Eisenbud's doctoral dissertation, see W. Schutzer and J. Tiomno, Phys. Rev. 83, 249 (1951) and, in particular N. G. Van Kampen, Phys. Rev. 89, 1072 (1953); 91, 1267 (1953). Also J. S. Toll, doctoral dissertation, Princeton University, 1952 (unpublished), and the more recent article of Gell-Mann, Goldberger, and Thirring, Phys. Rev. 95, 1612 (1954). This article also contains references to the early literature.

phase shifts among the sets which reproduce the cross section. An estimate of a can be obtained only from an at least qualitative theory of the nature of the interaction. It is commonly believed, for instance, that the pion-nucleon scattering proceeds via absorption and re-emission of the pion by the nucleon. If this is the case, a will be of the order of the pion Compton wavelength, i.e., $\hbar/\mu c$. However, it would be quite difficult to tell to what extent $a=2\hbar/\mu c$ is a permissible choice or whether it is necessary to assume $a=3\hbar/\mu c$ or an even larger a, giving less and less stringent forms to (4b). An alternative form of applying the relations of this paper, which might be somewhat more free of this ambiguity, would be to plot R, as calculated from (3b), against the energy and to judge whether any possible deviation of the R obtained this way from a regular R function can be blamed on having assumed a too low value for a.

PHYSICAL REVIEW VOLUME 98, NUMBER 1 APRIL 1, 1955

Scattering of Polarized Nucleon Beams*

REINHARD OEHME
Institute for Nuclear Studies, University of Chicago, Chicago, Illinois
(Received December 22, 1954)

The polarization formulas for the general reaction $a+b\rightarrow c+d$ are given in a compact form and specialized for the scattering of polarized nucleon beams at unpolarized targets. These targets may have arbitrary spin, possibly being different before and after collision. An interesting quantity in this problem is the polarization of the scattered nucleon beam. On the basis of general invariance properties of the transition matrix, this polarization is expressed by the polarization of the incoming nucleon beam and the relative momenta before and after collision. The invariant coefficients in this relation are functions of energy and scattering angle only; they are given in terms of the parameters of the transition matrix.

By using these formulas, it is shown that with triple scattering experiments one can obtain two new relations between the parameters of the transition matrix at fixed energy and angle. Quadruple scattering leads to two further relations. These relations represent information in addition to the differential cross section and the polarization resulting from unpolarized beams. The results are specialized for targets of spin zero and spin one-half, where in the latter case also the scattering of identical particles is discussed briefly.

I. INTRODUCTION

A BEAM of identical free particles with equal momentum represents in general a quantum-mechanical mixture, i.e., a classical statistical ensemble of different pure states.[1] We can characterize such an ensemble by the contributing pure states Ψ and their relative abundance $W(\Psi)$, where $\sum_\Psi W(\Psi)=1$. According to the usual rules of probability the expectation value of any operator ω in this beam is given by

$$\langle\omega\rangle_{\text{beam}}=\sum_\Psi W(\Psi)(\Psi,\omega\Psi).$$

Decomposing Ψ with respect to a complete set of orthogonal eigenstates Φ_k, $\Psi=\sum_k a_k(\Psi)\Phi_k$, we can write this expectation value in the form

$$\langle\omega\rangle_{\text{beam}}=\mathrm{Tr}(\rho\omega)=\sum_{ik}\left(\sum_\Psi W(\Psi)a_i(\Psi)a_k^*(\Psi)\right)(\Phi_k,\omega\Phi_i).$$

Here ρ is the density matrix[1] of the beam. If the particles have spin s and differ only by their spin state, then ρ is a Hermitian $2s+1$ by $2s+1$ matrix in spin-space. From the normalization of the state vectors to one follows $\mathrm{Tr}\rho=1$.

It is useful to expand the density matrix in terms of a complete set of $(2s+1)^2$ basic Hermitian matrices ω^μ in spin space,[2] which obey the relation

$$\mathrm{Tr}(\omega^\mu\omega^\nu)=(2s+1)\delta_{\mu\nu}.$$

These ω^μ are related to the irreducible spin tensor moments $T_k^{(q)}$, where q is the rank of the tensor and $k(|k|\leq q\leq 2s)$ indicates its components.[3,4] The tensor moments are not Hermitian operators as the ω^μ, but they transform directly according to the representation $\mathfrak{D}^{(q)}$ of the three dimensional rotation group. Using the Hermitian matrices ω^μ we can express the density matrix by the expectation values of all basic matrices ω^μ in the beam:

$$\rho=\frac{1}{2s+1}\sum_{\mu=1}^{(2s+1)^2}\langle\omega^\mu\rangle_{\text{beam}}\omega^\mu.$$

We say a beam is completely unpolarized if the expectation values of all tensor moments and therefore all operators ω^μ vanish, except the expectation value of the zero rank tensor $T_0^{(0)}=\omega^1=1$.

* Research supported by the U. S. Atomic Energy Commission.

[1] J. von Neumann, *Mathematische Grundlagen der Quantenmechanik* (Springer, Berlin, 1932 and Dover Publications, New York, 1943), p. 174; and H. Weyl, *Theory of Groups and Quantum Mechanics* (Dover Publications, New York, 1931), p. 78.

[2] See, for example, U. Fano, Phys. Rev. **90**, 577 (1953); and F. Coester and J. M. Jauch, Helv. Phys. Acta **26**, 3 (1953); these papers contain further references.

[3] E. Wigner, *Gruppentheorie und ihre Anwendung auf die Quantenmechanik der Atomspektren* (F. Vieweg, Braunschweig, 1953 and Edwards Brothers, Ann Arbor, 1944), p. 263.

[4] G. Racah, Phys. Rev. **62**, 442 (1942).

II. REACTION $a+b\to c+d$ WITH POLARIZED BEAMS[5,6]

In the general reaction $a+b\to c+d$ we can describe the system before collision either by the density matrices $\rho_{\text{in}}^{(a)}$ and $\rho_{\text{in}}^{(b)}$ of the two independent beams of free particles with spin s_a and s_b respectively,[7] or by a density matrix in the combined spin space of the two particle system. In the latter case the expectation value of any operator Ω is

$$\langle\Omega\rangle_{\text{in}}=\text{Tr}(\rho_{\text{in}}\Omega), \tag{1}$$

provided $\text{Tr}\rho_{\text{in}}=1$. Let Ω^μ be a complete set of $(2s_a+1)^2(2s_b+1)^2$ basic Hermitian matrices in this combined spin space with the property

$$\text{Tr}(\Omega^\mu\Omega^\nu)=(2s_a+1)(2s_b+1)\delta_{\mu\nu}. \tag{2}$$

We can expand ρ_{in} in terms of these operators and find with Eqs. (1) and (2):

$$\rho_{\text{in}}=\frac{1}{(2s_a+1)(2s_b+1)}\sum_\mu\langle\Omega^\mu\rangle_{\text{in}}\Omega^\mu. \tag{3}$$

The matrices Ω^μ are the direct products $\Omega^\mu=\omega_a{}^\alpha\times\omega_b{}^\beta$ of the corresponding basic matrices $\omega_a{}^\alpha$ and $\omega_b{}^\beta$ in the spin spaces of the particles a and b respectively. If the expectation values of all basic operators in the incoming beams are known, the density matrix ρ_{in} is completely determined.

The system after collision consists of the two beams of particles c and d, having spin s_c and s_d respectively. These final beams may be completely characterized by a density matrix ρ_{out} in the combined spin space of the particles c and d. If ρ_{in} is known and also the transition matrix $T(a+b\to c+d)$, which transforms every initial pure state contained in the quantum-mechanical mixture described by ρ_{in} into a corresponding final state in the mixture ρ_{out}, we find for the density matrix of the outgoing beams

$$\rho_{\text{out}}=T\rho_{\text{in}}T^\dagger. \tag{4}$$

The matrix ρ_{out} is not normalized to one, but $\text{Tr}\rho_{\text{out}}$ gives the differential cross section of the reaction. The expectation value of any operator Ω' in the combined spin space of the particles c and d after collision is then

$$\langle\Omega'\rangle_{\text{out}}=\text{Tr}(\rho_{\text{out}}\Omega')/\text{Tr}\rho_{\text{out}}. \tag{5}$$

Using the expansion (3) of ρ_{in} with respect to the operators Ω^μ, we find for the differential cross section

$$Q=\frac{1}{(2s_a+1)(2s_b+1)}\sum_\mu\langle\Omega^\mu\rangle_{\text{in}}\,\text{Tr}(T\Omega^\mu T^\dagger); \tag{6}$$

and with Eq. (5) the expectation value of an operator Ω' becomes:

$$\langle\Omega'\rangle_{\text{out}}=\frac{\sum_\mu\langle\Omega^\mu\rangle_{\text{in}}\,\text{Tr}(T\Omega^\mu T^\dagger\Omega')}{\sum_\nu\langle\Omega^\nu\rangle_{\text{in}}\,\text{Tr}(T\Omega^\nu T^\dagger)}. \tag{7}$$

Equation (7) expresses the expectation value of any operator Ω' in the outgoing beams by the expectation values of the complete set of basic matrices Ω^μ in the incoming beams. The relations (6) and (7) give a complete description of all physically measurable quantities for the general reaction $a+b\to c+d$ in terms of the transition matrix; they hold for particles of arbitrary spin and beams with any polarization.

III. NUCLEONS SCATTERED AT UNPOLARIZED TARGETS†

Let us now consider the special case of particles with spin one-half scattered at unpolarized targets with spin I before and spin I' after collision. The basic matrices $\Omega^\mu=\omega^\alpha(\frac{1}{2})\times\omega^\beta(I)$ in the combined spin space of the incoming particles are then of the form $1\times\omega^\beta(I)$ and $\boldsymbol{\sigma}\times\omega^\beta(I)$. Since the targets are initially unpolarized, only the matrices 1×1 and $\boldsymbol{\sigma}\times1$ have nonzero expectation values before collision. If T is the transition matrix, we obtain the cross section for the process $a(\frac{1}{2})+b(I,\text{ unpolarized})\to c(\frac{1}{2})+d(I')$ by specialization of Eq. (6). It is of the form

$$Q^{pu}=\frac{1}{2(2I+1)}\{\text{Tr}(TT^\dagger)+\text{Tr}(T\boldsymbol{\sigma}T^\dagger)\cdot\mathbf{P}^{\text{in}}\}, \tag{8}$$

where we have written $\boldsymbol{\sigma}$ for $\boldsymbol{\sigma}\times1$ and $\mathbf{P}^{\text{in}}$ for the expectation value $\langle\boldsymbol{\sigma}\times1\rangle_{\text{in}}$. The expectation value of $\boldsymbol{\sigma}$ in the out-going nucleon beam becomes according to Eq. (7):

$$\mathbf{P}^{pu}\equiv\langle\boldsymbol{\sigma}\times1\rangle_{\text{out}}=\frac{\text{Tr}(T^\dagger\boldsymbol{\sigma}T)+\text{Tr}(\boldsymbol{\sigma}T\boldsymbol{\sigma}\cdot\mathbf{P}^{\text{in}}T^\dagger)}{\text{Tr}(TT^\dagger)+\text{Tr}(T\boldsymbol{\sigma}T^\dagger)\cdot\mathbf{P}^{\text{in}}}. \tag{9}$$

In the special case of an unpolarized incident nucleon beam the quantities Q^{pu} and $\mathbf{P}^{pu}$ reduce to

$$Q^{uu}=\frac{1}{2(2I+1)}\,\text{Tr}(TT^\dagger),$$

and

$$\mathbf{P}^{uu}=\text{Tr}(T^\dagger\boldsymbol{\sigma}T)/\text{Tr}(TT^\dagger). \tag{10}$$

In Eqs. (8) and (10) the traces containing $\boldsymbol{\sigma}$ are *a priori* different. But Wolfenstein and Ashkin[6] have shown that these traces must be equal as a consequence of the invariance of the transition matrix with respect to inversion of motion as well as to the usual invariance

[5] See A. Simon and T. A. Welton, Phys. Rev. **90**, 1036 (1953), and A. Simon, Phys. Rev. **92**, 1050 (1953) for a treatment in terms of Fano X-functions.

[6] L. Wolfenstein and J. Ashkin, Phys. Rev. **85**, 847 (1952); these authors discuss the special case of particles with spin one-half.

[7] We assume always that incident particle and target particle are incoherent.

† *Note added in proof.*—After having submitted this paper the author was informed about the independent work of L. Wolfenstein [Phys. Rev. **96**, 1654 (1954)], which contains discussions similar to those given in Secs. III, V, and VI. The author is indebted to Professor Wolfenstein for sending him a copy of this paper and for bringing to his attention a surplus term originally contained in Eq. (19) of the present paper.

properties. The consequences derived from inversion of motion are applicable only for pure elastic scattering. Using this we may write Eq. (8) in the form

$$Q^{pu}=Q^{uu}(1+\mathbf{P}^{uu}\cdot\mathbf{P}^{in})=Q^{uu}(1+A), \qquad (11)$$

where $A\equiv\mathbf{P}^{uu}\cdot\mathbf{P}^{in}(|A|\leq 1)$ is the asymmetry of the scattering. Furthermore, the polarization $\mathbf{P}^{pu}$ can be written:

$$\mathbf{P}^{pu}=\mathbf{P}^{uu}+\mathfrak{T}\mathbf{P}^{in}/(1+\mathbf{P}^{uu}\cdot\mathbf{P}^{in}). \qquad (12)$$

The components of the real second rank tensor $\mathfrak{T}$ are

$$\mathfrak{T}_{ik}=\mathrm{Tr}(\sigma_i T\sigma_k T^\dagger)/\mathrm{Tr}(TT^\dagger). \qquad (13)$$

Invariance of the transition matrix under inversion of motion etc., does not imply the symmetry of this tensor.

We also may ask for the expectation values of spin and higher tensor moments in the beam of the recoiling target particles. From Eq. (7) we find

$$\langle\omega^\beta(I')\rangle_{out}=\frac{\mathrm{Tr}(T^\dagger\omega^\beta(I')T)+\mathrm{Tr}(\omega^\beta(I')T\boldsymbol{\sigma}\cdot\mathbf{P}^{in}T^\dagger)}{\mathrm{Tr}(TT^\dagger)+\mathrm{Tr}(T\boldsymbol{\sigma}T^\dagger)\cdot\mathbf{P}^{in}}, \qquad (14)$$

but let us confine our attention to the outgoing Fermion beam.

The polarization $\mathbf{P}^{uu}$ resulting from an unpolarized incident nucleon beam can only be a function of the relative momenta $\mathbf{k}_i$ and $\mathbf{k}_f$ of the particles before and after collision. Because $\mathbf{P}^{uu}$ is an expectation value of a spin operator, it must transform like a pseudovector under rotations and inversions of the observer's coordinate system. Therefore, since the cross product of $\mathbf{k}_i$ and $\mathbf{k}_f$ is the only pseudovector one can form from these vectors, we have

$$\mathbf{P}^{uu}=P^{uu}\mathbf{n},$$

with

$$\mathbf{n}=(\mathbf{k}_i\times\mathbf{k}_f)/|\mathbf{k}_i\times\mathbf{k}_f|. \qquad (15)$$

The invariant quantity P^{uu} is a function of the energy and the scalar product $(\mathbf{k}_i\cdot\mathbf{k}_f)$. Equation (15) expresses the well-known fact that the polarization resulting from the scattering of an unpolarized beam by an unpolarized target is always orthogonal to the plane of scattering.[5,8,9] As a consequence of this, measurements of the asymmetry $A=P^{uu}(\mathbf{n}\cdot P^{in})$ in the scattering of a polarized beam of nucleons from an unpolarized target can only give information about the components of the polarization $\mathbf{P}^{in}$ orthogonal to the direction of propagation of that beam.

IV. GENERAL FORM OF $\mathbf{P}^{pu}$

In the scattering problem considered here the transition matrix depends on $\mathbf{k}_i$ and $\mathbf{k}_f$, the matrix $\boldsymbol{\sigma}$ and the components of the spin matrices $\mathbf{S}(I)$ and $\mathbf{S}(I')$ of the target particles before and after collision. The vectors $\mathbf{k}_i$ and $\mathbf{k}_f$ are taken as unit vectors in the direction of the corresponding relative momenta in the center-of-mass system. The dependence on the energy in the center-of-mass system shall not be indicated explicitly.

[8] L. Wolfenstein, Phys. Rev. **75**, 1664 (1949).
[9] R. J. Blin-Stoyle, Proc. Phys. Soc. (London) **A64**, 700 (1951).

TABLE I. Transformation properties of the matrix coefficients in the transition matrix.

	a	b	c	d
Space inversion	Scalar	Scalar	Pseudo-scalar	Pseudo-scalar
Inversion of motion	+	+	−	+

Because T must be invariant under rotations, it can be written in the form

$$T(\mathbf{k}_i,\mathbf{k}_f;\boldsymbol{\sigma},S_i(I),S_k(I'))=a+\boldsymbol{\sigma}\cdot\mathbf{B}, \qquad (16)$$

where a and $\mathbf{B}$ are nonquadratic matrices for $I\neq I'$. They depend on $\mathbf{k}_i$, $\mathbf{k}_f$, $S_i(I)$, and $S_k(I')$ and have matrix elements connecting spin space I and spin space I'. We can decompose $\mathbf{B}$ with respect to the three orthogonal unit vectors

$$\mathbf{n}=\frac{\mathbf{k}_i\times\mathbf{k}_f}{\sin\vartheta},\quad \mathbf{m}=\frac{\mathbf{k}_i-\mathbf{k}_f}{2\sin(\vartheta/2)},\quad \mathbf{l}=\frac{\mathbf{k}_i+\mathbf{k}_f}{2\cos(\vartheta/2)},$$

where $\cos\vartheta=(\mathbf{k}_i\cdot\mathbf{k}_f)$ and have

$$\mathbf{B}=b\mathbf{n}+c\mathbf{m}+d\mathbf{l}. \qquad (17)$$

The quantities a, b, c, and d are rotation invariant matrices. Considering furthermore the invariance of T under space reflections and with respect to inversion of motion, we find from the known transformation properties of $\boldsymbol{\sigma}$, $\mathbf{n}$, $\mathbf{m}$, and $\mathbf{l}$, that these matrices must transform as indicated in Table I.[10] Note that their behavior under inversion of motion refers only to the case of pure elastic scattering.

If we now express Q^{pu} and $\mathbf{P}^{pu}$ in terms of the matrices a, b, c, and d, there appear only traces of products of two of them. Because these traces are rotation invariant functions of $\mathbf{k}_i$ and $\mathbf{k}_f$, they depend only on $(\mathbf{k}_i\cdot\mathbf{k}_f)$ and therefore must transform as $(S,+)$, i.e., as scalars not changing sign under inversion of motion. As a consequence of this all traces of those matrix products, which do not transform as $(S,+)$, must vanish. The only real coefficients which may appear in observable quantities will be the traces of products of the matrices with their own Hermitian conjugates and the expressions $\mathrm{Tr}(ab^\dagger+ba^\dagger)$ and $i\,\mathrm{Tr}(ab^\dagger-ba^\dagger)$. We find from Eqs. (10) and (13)

$$\begin{aligned}
Q^{uu}&=\frac{1}{2(2I+1)}\mathrm{Tr}(aa^\dagger+bb^\dagger+cc^\dagger+dd^\dagger),\\
Q^{uu}\mathbf{P}^{uu}&=\frac{1}{2(2I+1)}\mathrm{Tr}(ab^\dagger+ba^\dagger)\mathbf{n},\\
Q^{uu}(\mathfrak{T}\mathbf{P}^{in})&=\frac{1}{2(2I+1)}\{\mathrm{Tr}(aa^\dagger-bb^\dagger-cc^\dagger-dd^\dagger)\mathbf{P}^{in}\\
&\quad+2\,\mathrm{Tr}(bb^\dagger)(\mathbf{n}\cdot\mathbf{P}^{in})\mathbf{n}+2\,\mathrm{Tr}(cc^\dagger)(\mathbf{m}\cdot\mathbf{P}^{in})\mathbf{m}\\
&\quad+2\,\mathrm{Tr}(dd^\dagger)(\mathbf{l}\cdot\mathbf{P}^{in})\mathbf{l}+i\,\mathrm{Tr}(ba^\dagger-ab^\dagger)[\mathbf{n}\times\mathbf{P}^{in}]\}.
\end{aligned} \qquad (18)$$

[10] See appendix to reference 6 for similar considerations.

By the use of Eqs. (11), (12), and (18) the quantities Q^{pu} and $\mathbf{P}^{pu}$ can be expressed in terms of the coefficients of the transition matrix.

The last expression in Eq. (18) may be rewritten in the form

$$\mathfrak{T}\mathbf{P}^{in}=V(\mathbf{n}\cdot\mathbf{P}^{in})\mathbf{n}+X\{(\mathbf{k}_i\cdot\mathbf{P}^{in})\mathbf{k}_i+(\mathbf{k}_f\cdot\mathbf{P}^{in})\mathbf{k}_f\}+Y(\mathbf{k}_f\cdot\mathbf{P}^{in})\mathbf{k}_i+Z(\mathbf{k}_i\cdot\mathbf{P}^{in})\mathbf{k}_f. \quad (19)$$

The coefficients in this relation are functions of the energy and of $(\mathbf{k}_i\cdot\mathbf{k}_f)$ and can be easily expressed by the traces mentioned before Eqs. (18). In Eq. (19) the only consequence of the invariance of the transition matrix under inversion of motion is the equality of the coefficients of $(\mathbf{k}_i\cdot\mathbf{P}^{in})\mathbf{k}_i$ and $(\mathbf{k}_f\cdot\mathbf{P}^{in})\mathbf{k}_f$. The azimuthal dependence of $\mathbf{P}^{uu}$ and $\mathbf{P}^{pu}$ is exhibited completely in Eqs. (18) and (19).

In principle it is possible to measure the four coefficients V, X, Y, and Z at any given energy and angle. This would give us, aside from Q^{uu} and P^{uu}, four further relations between the parameters of the transition matrix at fixed energy and angle. In order to see to what extent we may measure these four coefficients, we will discuss in the following section special cases of Eq. (19), which can be realized by performing triple and possibly quadruple scattering experiments with nucleons.

V. TRIPLE AND QUADRUPLE SCATTERING

The information obtainable from triple scattering is reduced by the fact that with the scattering of a primary unpolarized beam at unpolarized targets we can only produce a polarization orthogonal to the direction of motion of the scattered beam. Therefore, in order to study the influence of a longitudinal component of $\mathbf{P}^{in}$ on the polarization $\mathbf{P}^{pu}$ in the outgoing nucleon beam, we must have two previous scatterings to produce such a component. A third scattering then can lead to an additional term in the polarization $\mathbf{P}_3{}^{pu}$, depending on the longitudinal component of $\mathbf{P}^{in}=\mathbf{P}_2{}^{pu}$. A fourth scattering is needed to analyze $\mathbf{P}_3{}^{pu}$ by measuring the asymmetry $A_4=\mathbf{P}_3{}^{pu}\cdot\mathbf{P}_4{}^{uu}$. The production of a nucleon beam with a known longitudinal component of polarization is discussed in Sec. VI. A further restriction in triple scattering experiments is that by measuring the asymmetry in a third scattering we can determine only those components of the polarization $\mathbf{P}_2{}^{pu}$ which are orthogonal to the direction of motion of the scattered beam in the laboratory system.

Let us now assume that the incident nucleon beam is polarized orthogonal to the plane of scattering: $\mathbf{P}^{in}=P_n{}^{in}\mathbf{n}$. One sees from Eqs. (15) and (19) that $\mathbf{P}^{pu}$ must be also proportional to the normal vector $\mathbf{n}$. By use of Eq. (12), the polarization $\mathbf{P}^{pu}$ becomes

$$\mathbf{P}^{pu}=P_n{}^{pu}\mathbf{n}=\frac{P^{uu}+VP_n{}^{in}}{1+P^{uu}P_n{}^{in}}\mathbf{n}. \quad (20)$$

For an incoming nucleon beam which is completely polarized in the direction $\mathbf{n}$, we obtain for the depolarization, which is defined by $D_n\equiv P_n{}^{pu}-P_n{}^{in}$:

$$D_n=\frac{V-1}{1+P^{uu}}.$$

In this expression we have assumed that $P_n{}^{in}=+1$. In terms of the parameters of the transition matrix [Eqs. (16) and (17)] the depolarization can be expressed as

$$D_n=-\frac{2}{1+\mathrm{Tr}\{(a+b)(a+b)^\dagger\}/\mathrm{Tr}(cc^\dagger+dd^\dagger)}. \quad (21)$$

D_n is a function of energy and angle; it varies from zero to minus two, which is guaranteed by the positive definiteness of the traces appearing in Eq. (21). Even if the depolarization D_n vanishes in a special case (e.g., if the target has spin zero; Sec. VI), we get a change of polarization for a partially polarized beam, which according to Eq. (20) becomes

$$P_n{}^{pu}(D_n=0)=\frac{P^{uu}+P_n{}^{in}}{1+P^{uu}P_n{}^{in}}.$$

The polarization is increased or decreased if $P_n{}^{in}$ and P^{uu} have the same or the opposite sign respectively.

If, at a certain energy and angle, P^{uu} is known from a double scattering experiment and $P_n{}^{pu}$ is measured by triple scattering with all three scatterings in the same plane, then we can determine $V(\vartheta)$ and with this the depolarization D_n. Thus we obtain a new relation between the parameters of the transition matrix at this energy and angle. Obviously we do not obtain any new information if the analyzing scattering occurs in a plane orthogonal to the common plane of first and second scattering. In this case $\mathbf{P}_3{}^{uu}$ is orthogonal to $\mathbf{P}_2{}^{pu}$, and the symmetry A_3 vanishes.

If we now assume that the incoming nucleon beam is polarized in the plane of scattering, we see from Eq. (19) that also $\mathfrak{T}\mathbf{P}^{in}$ is a vector in that plane. In this case, according to Eq. (12), the component of $\mathbf{P}^{pu}$ orthogonal to the plane of scattering is independent of the incoming polarization and given by $\mathbf{P}^{uu}$. The asymmetry $(\mathbf{P}^{uu}\cdot\mathbf{P}^{in})$ occurring in the denominator of Eq. (12) vanishes because $(\mathbf{n}\cdot\mathbf{P}^{in})$ is zero. Therefore the triple scattering experiment provides no more information than a double scattering experiment, if the first scattering occurs in a plane which is orthogonal to the common plane of second and third scattering. For this arrangement the asymmetry $A_3=\mathbf{P}_2{}^{pu}\cdot\mathbf{P}_3{}^{uu}$ becomes equal to $\mathbf{P}_2{}^{uu}\cdot\mathbf{P}_3{}^{uu}$.

Of more interest is a triple scattering experiment with producing and analyzing scattering occurring in the same plane, which itself is orthogonal to the plane of the second scattering. Then $\mathbf{P}^{in}$ is orthogonal to $\mathbf{n}$ and $\mathbf{k}_i$ (the indices referring to the second scattering are always omitted) and for positive $P_3{}^{uu}$ the vector $\mathbf{P}_3{}^{uu}$

is parallel to $\mathbf{n}_3=[\mathbf{k}_f(\text{lab})\times\mathbf{n}]/|[\cdots]|$. $\mathbf{n}_3$ is a unit vector orthogonal to $\mathbf{k}_f(\text{lab})$ and in the plane of the second scattering. Thus we find from Eq. (19) for the special case considered here:

$$\mathbf{P}^{pu}=P^{uu}\mathbf{n}+(\mathbf{k}_f\cdot\mathbf{P}^{in})\{X\mathbf{k}_f+Y\mathbf{k}_i\}.$$

The asymmetry in a third analyzing scattering becomes

$$A_3=\mathbf{P}^{pu}\cdot\mathbf{P}_3^{uu}=P^{in}P_3^{uu}\Lambda,$$

where

$$\Lambda=\sin\vartheta\{X(\mathbf{k}_f\cdot\mathbf{n}_3)+Y(\mathbf{k}_i\cdot\mathbf{n}_3)\} \tag{22}$$

and $\mathbf{P}^{in}$ is defined by $\mathbf{P}^{in}=P^{in}[\mathbf{n}\times\mathbf{k}_i]$. In terms of the coefficients of the transition matrix this is

$$\Lambda=\frac{-1}{2(2I+1)Q^{uu}}\Big\{\mathrm{Tr}(aa^\dagger-bb^\dagger)\cos(\vartheta/2+\chi)+i\,\mathrm{Tr}(ba^\dagger-ab^\dagger)\sin(\vartheta/2+\chi)+\mathrm{Tr}(cc^\dagger-dd^\dagger)\cos(\vartheta/2-x)\Big\}. \tag{22a}$$

Here the angle χ is defined by $\cos\chi\equiv\mathbf{n}_3\cdot\mathbf{m}$ and we have $\chi=0$ if the masses of the incident particles and the target particles are equal. This experiment gives further information about the transition matrix. Note that Λ can be different from zero even if D_n vanishes, i.e., if $\mathrm{Tr}(cc^\dagger)$ and $\mathrm{Tr}(dd^\dagger)$ are both zero.

Because $\mathbf{P}^{pu}(1+A)=\mathbf{P}^{uu}+\mathfrak{T}\mathbf{P}^{in}$ is a linear vector function of $\mathbf{P}^{in}$, one can easily see that D_n and Λ are the only independent new relations between the parameters of the transition matrix, which may be obtained by triple scattering experiments with nucleons.

We have yet to discuss the influence of a longitudinal component of the polarization $\mathbf{P}^{in}$ in the incoming nucleon beam on the transverse component of $\mathbf{P}^{pu}$. As mentioned in the beginning of this section, this influence may be determined, at least theoretically, from quadruple scattering experiments. If $\mathbf{P}^{in}$ is proportional to $\mathbf{k}_i$, $\mathbf{P}^{in}=P^{in}\mathbf{k}_i$, we find from Eq. (19)

$$\mathbf{P}^{pu}=P^{uu}\mathbf{n}+P^{in}\{(X+Y\cos\vartheta)\mathbf{k}_i+(X\cos\vartheta+Z)\mathbf{k}_f\}.$$

The asymmetry of a fourth scattering occurring in a plane orthogonal to the plane of the third scattering becomes

$$\frac{A_4}{P^{in}P_4^{uu}}=\frac{1}{2(2I+1)Q^{uu}}\Big\{\mathrm{Tr}(aa^\dagger-bb^\dagger)\sin(\vartheta/2+\chi)-i\,\mathrm{Tr}(ba^\dagger-ab^\dagger)\cos(\vartheta/2+\chi)+\mathrm{Tr}(cc^\dagger-dd^\dagger)\sin(\vartheta/2-\chi)\Big\}. \tag{23}$$

Summing up we see that with single, double, and triple scattering we can obtain the four relations Q^{uu}, P^{uu}, D_n, and Λ between the parameters of the transition matrix at fixed energy and angle. Including quadrupole scattering we gain two more independent relations. We could then determine all four coefficients in Eq. (19). Further information would of course be obtainable from the scattering of polarized nucleon beams at polarized targets.

VI. TARGETS WITH SPIN ZERO AND SPIN ONE-HALF

For the scattering of nucleons at spin zero targets,[11–13] the rotation invariant matrices a, b, c, and d in Eqs. (16) and (17) become complex functions of energy and angle. Therefore the pseudoscalars c and d must vanish, and the transition matrix $T=a+b(\boldsymbol{\sigma}\cdot\mathbf{n})$ at fixed energy and angle is determined by the amounts $|a|=a_0$ and $|b|=b_0$ and the relative phase $\psi=\arg(a^*b)$, aside from an absolute phase factor. If one includes triple scattering experiments, the physically measurable quantities are, in terms of these parameters, in the laboratory system:

$$Q^{uu}=a_0^2+b_0^2,\quad D_n=0,\qquad P^{uu}=\frac{2a_0b_0\cos\psi}{a_0^2+b_0^2},\quad \Lambda=\left\{\frac{a_0^2-b_0^2}{a_0^2+b_0^2}\cos\vartheta-\frac{2a_0b_0\sin\psi}{a_0^2+b_0^2}\sin\vartheta\right\}. \tag{24}$$

Measurements of Q^{uu}, P^{uu}, and Λ at given energy and angle are sufficient to determine the transition matrix for this energy and angle aside from the arbitrary absolute phase. If we have once determined T for a certain process, we can compute $\mathbf{P}^{pu}$ for an incident nucleon beam with any polarization $\mathbf{P}^{in}$. This fact may possibly be used in order to produce a beam with known longitudinal component of polarization. Choosing the polarization $\mathbf{P}^{in}$ orthogonal to $\mathbf{k}_i$ and $\mathbf{n}$ we find by the use of Eq. (18) or (19) for the polarization $\mathbf{P}^{pu}$ in the beam scattered from a spin zero target

$$\mathbf{P}^{pu}=\mathbf{P}^{uu}\mathbf{n}+P^{in}\left\{\frac{a_0^2-b_0^2}{a_0^2+b_0^2}[\mathbf{n}\times\mathbf{k}_i]+\frac{2a_0b_0\sin\psi}{a_0^2+b_0^2}\mathbf{k}_i\right\}.$$

The longitudinal component of $\mathbf{P}^{pu}$ becomes in this case

$$(\mathbf{P}^{pu}\cdot\mathbf{k}_f)=P^{in}\left\{\frac{a_0^2-b_0^2}{a_0^2+b_0^2}\sin\vartheta+\frac{2a_0b_0\sin\psi}{a_0^2+b_0^2}\cos\vartheta\right\}.$$

If, in the special case of targets with spin zero, the incoming nucleon beam is completely polarized in any direction, the scattered beam must also be completely polarized, because the quantum-mechanical mixtures before and after collision reduce to pure states. For any pure state of free fermions the magnitude of the expectation value of $\boldsymbol{\sigma}$ becomes one. The angle between initial and final polarization in this case is given by

$$\cos\Theta=(\mathbf{P}^{pu}\cdot\mathbf{P}^{in})=\frac{a_0^2-b_0^2+2(\mathbf{n}\cdot\mathbf{P}^{in})(a_0\cos\psi+1)b_0}{(a_0^2+b_0^2)\{1+2(\mathbf{n}\cdot\mathbf{P}^{in})a_0b_0\cos\psi\}},$$

[11] J. Schwinger, Phys. Rev. **69**, 681 (1946).
[12] L. Wolfenstein, Phys. Rev. **75**, 1664 (1949).
[13] J. V. Lepore, Phys. Rev. **79**, 137 (1950).

which becomes

$$\cos\Theta=\begin{cases}1 \text{ for } (\mathbf{n}\cdot\mathbf{P}^{in})=1\\ \dfrac{a_0^2-b_0^2}{a_0^2+b_0^2} \text{ for } (\mathbf{n}\cdot\mathbf{P}^{in})=0.\end{cases}$$

For $|\mathbf{P}^{in}|\leq 1$ we obtain for the amount of polarization in the scattered beam

$$|\mathbf{P}^{pu}|^2=1-\frac{1-|\mathbf{P}^{uu}|^2}{(1+\mathbf{P}^{uu}\cdot\mathbf{P}^{in})^2}(1-|\mathbf{P}^{in}|^2),$$

which reduces to one for $|\mathbf{P}^{in}|=1$.

Finally let us consider the case of targets with spin one-half. For the matrix-coefficients in the transition matrix we find from their transformation properties listed in Table I:

$$a=\alpha+\gamma(\boldsymbol{\sigma}_2\cdot\mathbf{n}),\quad c=\delta(\boldsymbol{\sigma}_2\cdot\mathbf{m}),$$
$$b=\gamma'+\beta(\boldsymbol{\sigma}_2\cdot\mathbf{n}),\quad d=\epsilon(\boldsymbol{\sigma}_2\cdot\mathbf{l}).$$

The quantities α, etc., are complex functions of energy and scattering angle in the center-of-mass system. Indicating the spin matrices referring to incoming nucleons and target particles by $\boldsymbol{\sigma}_1$ and $\boldsymbol{\sigma}_2$ respectively, we obtain the transition matrix in the form

$$T=\alpha+\beta(\boldsymbol{\sigma}_1\cdot\mathbf{n})(\boldsymbol{\sigma}_2\cdot\mathbf{n})+(\gamma'\boldsymbol{\sigma}_1+\gamma\boldsymbol{\sigma}_2\cdot\mathbf{n})$$
$$+\delta(\boldsymbol{\sigma}_1\cdot\mathbf{m})(\boldsymbol{\sigma}_2\cdot\mathbf{m})+\epsilon(\boldsymbol{\sigma}_1\cdot\mathbf{l})(\boldsymbol{\sigma}_2\cdot\mathbf{l}).^{6,14}$$

The experimentally measurable quantities in single, double, and triple scattering become in terms of these parameters

$$Q^{uu}=|\alpha|^2+|\beta|^2+|\gamma|^2+|\gamma'|^2+|\delta|^2+|\epsilon|^2,$$
$$Q^{uu}P^{uu}=2\,\mathrm{Re}(\alpha^*\gamma'+\beta^*\gamma),$$
$$D_n=-\frac{2}{1+(|\alpha+\gamma'|^2+|\beta+\gamma|^2)/(|\delta|^2+|\epsilon|^2)},\quad(25)$$
$$Q^{uu}\Lambda=(-|\alpha|^2+|\beta|^2-|\gamma|^2$$
$$+|\gamma'|^2-|\delta|^2+|\epsilon|^2)\cos(\vartheta/2)$$
$$+2\,\mathrm{Im}(\alpha^*\gamma'-\beta^*\gamma)\sin(\vartheta/2).$$

For identical particles the transition matrix must be symmetric under interchange of $\boldsymbol{\sigma}_1$ and $\boldsymbol{\sigma}_2$. Therefore γ must be equal to γ' in this case. If we neglect electromagnetic interactions, the same holds for neutron proton scattering because of charge independence. Thus the transition matrix for nucleon-nucleon scattering depends on five complex functions, i.e., excluding the absolute phase factor, on nine real parameters at every angle and energy. Including triple scattering we can measure only the four relations (25) between these parameters. This lack of information available at present makes it preferable at lower energies to separate the angular dependence of these coefficients by making a phase shift analysis. This is usually done in a representation of T where the total spin operator S^2 of the two nucleon system and its z-component S_z are diagonal. Using a nomenclature similar to that of Swanson[15] we can then write T in the form:

$$(TS'm_s',Sm_s(\lambda,\vartheta,\phi))$$
$$=\frac{\lambda}{4i}\begin{pmatrix}A & -\sqrt{2}Be^{-i\phi} & Ce^{-2i\phi} & 0\\ \sqrt{2}De^{i\phi} & 2E & -\sqrt{2}De^{-i\phi} & 0\\ Ce^{2i\phi} & \sqrt{2}Be^{i\phi} & A & 0\\ 0 & 0 & 0 & S\end{pmatrix},\quad(26)$$

with the additional condition

$$A-C-2E=2\cot\vartheta(D-B).$$

This relation is a consequence of the invariance of T under inversion of motion. The complex functions A, B, $\cdots$, and S in Eq. (26) can be easily expressed in terms of the functions α, β, $\cdots$, and ϵ. The elements S, A, and E are series in $P_l^0(\vartheta)$, B and D in $P_l^1(\vartheta)$, and C is a series in $P_l^2(\vartheta)$. In all of these series the coefficients depend on the corresponding phase shifts. In terms of the matrix elements in Eq. (26) we get for P^{uu} and D_n

$$Q^{uu}P^{uu}=-\frac{\lambda^2}{16}\tfrac{1}{2}\,\mathrm{Im}\{(A-C+2E)(B^*+D^*)\},^{16-19}$$
$$Q^{uu}[1+D_n(1+P^{uu})]=Q^{uu}V$$
$$=\frac{\lambda^2}{16}\tfrac{1}{2}\,\mathrm{Re}\{(A+C)S^*+(A-C)2E^*+4BD^*\}.$$

Also the cross section Q^{pu} and the quantity Λ defined in Eq. (22) may be easily expressed by the elements of the transition matrix (26). The polarization P^{uu} depends, in a direct way only on triplet elements of the transition matrix, whereas D_n and also Λ contain singlet-triplet interference terms aside from pure triplet contributions. Of course there is a dependence on singlet terms through the cross section Q^{uu} for unpolarized beams, but this quantity can be measured independently.

For identical particles the singlet part of T must be symmetrized and the triplet matrix elements correspondingly antisymmetrized. We can write the transition matrix $\bar{T}$ for identical particles in the same form as T in Eq. (26), with the quantities A, B, $\cdots$, and S replaced by the corresponding elements $\bar{A}$, $\bar{B}$, $\cdots$, and $\bar{S}$, where $\bar{A}=A(\vartheta)-A(\tau-\vartheta)$, $\bar{B}=B(\vartheta)+B(\tau-\vartheta)$

[14] R. H. Dalitz, Proc. Phys. Soc. (London) **A65**, 175 (1952).

[15] D. R. Swanson, Phys. Rev. **89**, 740 (1953); this paper contains further references.

[16] L. Wolfenstein, Phys. Rev. **76**, 973 (1949).

[17] L. J. B. Goldfarb and D. Feldman, Phys. Rev. **88**, 1099 (1952).

[18] D. R. Swanson, Phys. Rev. **89**, 749 (1953).

[19] G. Breit and J. B. Ehrman, Phys. Rev. **96**, 805 (1954).

$S(\vartheta)+S(\pi-\vartheta)$, etc. In practice this simply means summing only over odd l for triplet elements and even l for the singlet element and multiplying the results by a factor of two. We note that $\bar{A}$ and $\bar{E}$ are proportional to $\cos\vartheta$ and that $\bar{C}$ is proportional to $\sin^2\vartheta\cos\vartheta$. Whereas these elements become zero at ninety degrees in the center-of-mass system, the quantities $\bar{B}$, $\bar{D}$ and $\bar{S}$ do not vanish identically at this angle. The functions $\bar{B}$ and $\bar{D}$ are proportional to $\sin\vartheta$. Using these properties of the matrix elements we find for *identical* particles that $P_n{}^{pu}(\vartheta=\pi/2)$ becomes

$$P_n{}^{pu}(\pi/2)=P_n{}^{\text{in}}+D_n(\pi/2)P_n{}^{\text{in}}$$

$$=\frac{\lambda^2 P_n{}^{\text{in}}}{8Q^{uu}(\pi/2)}\,\text{Re}\left\{\bar{B}(\pi/2)\bar{D}^*(\pi/2)\right\}.$$

At this angle the depolarization depends only on triplet elements and thus provides a new relation between triplet phase shifts.

If the polarization of the incoming beam is orthogonal to $\mathbf{n}$ and $\mathbf{k}_i$, the polarization $\mathbf{P}^{pu}(\vartheta=\pi/2)$ in the beam scattered at ninety degrees becomes

$$\mathbf{P}^{pu}(\pi/2)=\frac{\lambda^2 P^{\text{in}}}{16Q^{uu}(\pi/2)}[-\,\text{Re}\{\bar{S}(\pi/2)\bar{D}^*(\pi/2)\}\mathbf{k}_i].$$

In this relation P^{in} is defined by

$$\mathbf{P}^{\text{in}}=P^{\text{in}}[\mathbf{n}\times\mathbf{k}_i].$$

According to Eq. (22), the quantity $\Lambda(\vartheta=\pi/2)$ is then

$$\Lambda(\pi/2)=\frac{-\lambda^2}{\sqrt{2}16Q^{uu}(\pi/2)}\,\text{Re}\{\bar{S}(\pi/2)\bar{D}^*(\pi/2)\}$$

and depends only on singlet triplet interference terms.

The author wishes to express his thanks to Dr. S. Cohen, Professor M. L. Goldberger, and Dr. H. Miyazawa for helpful discussions. Thanks are also due to Dr. G. Lüders for a remark about time inversion.

PHYSICAL REVIEW VOLUME 98, NUMBER 1 APRIL 1, 1955

Mesonic Decay of an Ejected Triton

HERMAN YAGODA
National Institutes of Health, Bethesda, Maryland
(Received September 23, 1954)

A heavy fragment is ejected from a star of type $21+5p$ which decays at rest into three charged particles. Gap counts indicate that the ejected fragment is singly charged and heavier than a proton. The mass of the particle, as estimated by constant sagitta scattering along its range of 1330 microns, is 2.93 ± 1.36 proton masses. All three secondary particles terminate their range, and one of them can be identified as a negative pi meson of 26.6 ± 0.9 Mev kinetic energy. Two short recoil tracks, if assumed to be protons, have kinetic energies of 1.43 ± 0.04 and 2.31 ± 0.15 Mev, respectively. Momentum balance applied to several decay schemes suggest that the event probably represents $H^{3*}\rightarrow H^1+H^1+n^0+\pi^-+Q=31.5\pm1$ Mev. The binding energy of the excited triton is found to be 5.4 ± 1 Mev, less than that of the normal triton (8.48 Mev). The time of flight of the excited triton is 4.2×10^{-11} sec.

IN the examination of a unit of Ilford G5 emulsions flown in the stratosphere[1] a star of type $21+5p$ was observed in which two of the gray tracks could be identified as negative pi mesons of 13.5 and 16.6 Mev. In the detailed study of this event it was noted that one of the heavy prongs (F of Fig. 1) had a 3-prong star at the end of its range. As indicated in the photomicrograph of this detail (Fig. 2) track F appears to have come to rest, and the tracks of the disintegration products seem to reside in a single plane approximately perpendicular to the field of view. The recoil tracks A and B terminated in the same emulsion sheet (1500 microns thick) and the third track C could be followed into an adjacent pellicle where it terminated with the formation of a 4-prong sigma star. This identification indicated a mesonic-decay process, occurring under exceptionally favorable circumstances, such that the momenta of the decay products could be evaluated accurately from the measured ranges of the tracks. A study was therefore made on the identification of the several members and the evaluation of the most probable mode of decay of the heavy fragment.

[1] For details of exposure see H. Yagoda, this issue [Phys. Rev. 98, 103 (1955)].

IDENTIFICATION OF THE EXCITED FRAGMENT

The range of track F is 1330 microns and it makes a small angle with the original emulsion plane ($\tan\beta=0.344\pm0.017$). This permits the determination of the charge of the particle by gap counting.[2] These measurements are summarized in Fig. 3 where the solid curves

[2] Our gap-counting procedure yields essentially a gap-length measurement. The gap of minimum discernibility of about 0.4 micron is given a single count. Larger gaps are weighted visually in proportion to their apparent length with the aid of a reticule in the eyepiece scale. This technique is rapid and eliminates the need for a special stage constructed with a micro screw feed.

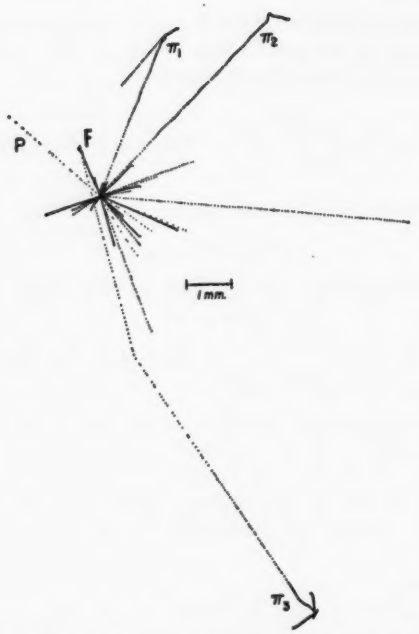

FIG. 1. Projection drawing of a star showing the emission of two slow negative pi mesons and a heavy fragment F. The latter undergoes decay with the emission of three charged particles, one of the disintegration products of which can be identified as a negative pi-meson π_3.

are average functions for pi mesons, protons, and alpha-particle tracks occurring in the same emulsion with approximately the same dip. The gap count indicates that track F is singly charged and more massive than a proton. The measurement does not permit distinction between the possibilities of its being a deuteron or a triton.

Recently, constant sagitta scattering techniques have been described[3] which permit the estimation of the mass of particles that come to rest in the emulsion. This method has been applied to track F, and its mass computed from the relationship: $M_f = M_p(\bar{D}_p/\bar{D}_f)^{2.31}$ where $\bar{D}_p$ is the mean sagitta measured on known proton tracks and M_f is the mass of the fragment in proton mass units. These measurements indicate that the mass of the fragment is 2.93 ± 1.36 proton masses. The error has been evaluated on the basis of $\Delta M/M = 2.31 \Delta D/D$. This can be interpreted that the particle is probably a triton, but that owing to the small number of cells available for measurement, the large statistical uncertainty does not exclude the possibility of its being a deuteron.

DECAY PRODUCTS

The properties of the three disintegration tracks are recorded in Table I. Tracks A and B, while terminating in the emulsion, are too short for identification by quantitative measurements. Visual inspection suggests that track A is probably singly charged. Track B is very steep. By comparing it with steep alpha-particle tracks originating from alpha stars, its charge would appear to be not greater than 2. The third track has a recorded range of 11 000 microns in the emulsion in which it originated and exhibits the rapid change in grain density and scatter typical of an L-meson. It was possible to follow this track into an adjoining emulsion where it came to rest with the production of a sigma

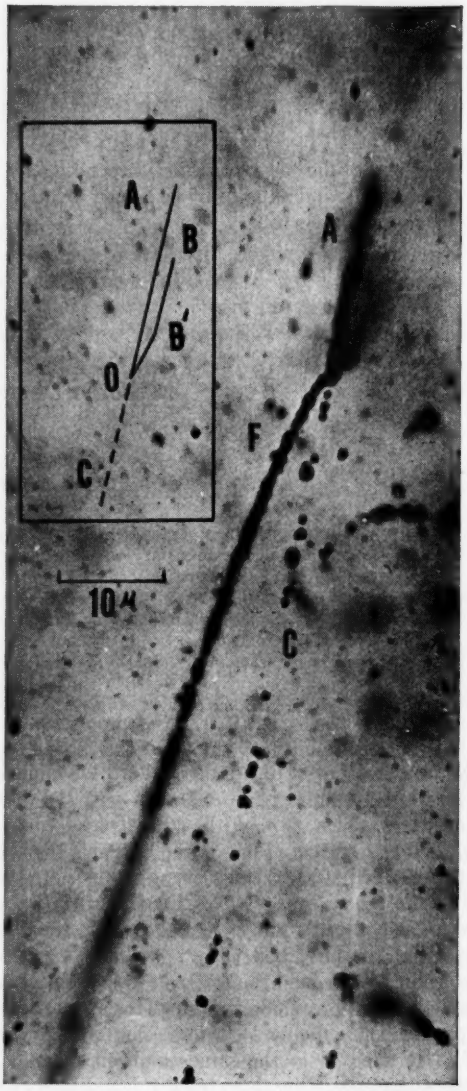

FIG. 2. Photomicrograph showing track F coming to rest and two of its disintegration products. The third track b is not visible in this focal setting, as the plane of coplanarity is perpendicular to the field of view. Track c terminates after traversing 13 000 microns of emulsion and can be identified as a π^- meson of 27-Mev kinetic energy.

[3] Dilworth, Goldsack, and Hirschberg, Nuovo cimento 11, 113 (1954).

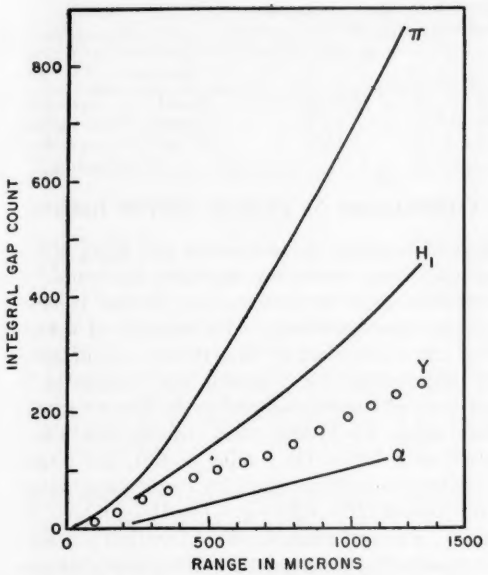

FIG. 3. Range-gap count relationship for pi mesons, protons, and alpha particles. The corresponding function for track F is delineated by the circles.

star (track π_3 of Fig. 1). This identifies the particle as a negative pi meson with a kinetic energy of 26.63±0.9 Mev based on its total range of 12 900±500 microns.

As shown in the photomicrograph of the decay point (Fig. 2), track F exhibits the typical curl of a massive singly charged particle that has come to rest. In the plane of the emulsion (xy plane) the projection of track A is colinear with the meson track C. Owing to the steepness of track B it is difficult to define its initial direction unambiguously. Measurement of the average angle between tracks A and B in the xy plane with a goniometer eyepiece indicate the existence of an angle of 8.3±1.5°. However, if the event is projected onto a ground glass and each grain of track B is delineated with a pencil mark as it is brought into focus, then it appears that the particle made a large-angle scatter at a point B', about 4 microns away from the origin, as shown in the insert of Fig. 2. If this interpretation is correct, then the initial projected angle between the two recoil tracks could be as large as 18.5±0.5°.

THREE-BODY DECAY SCHEMES

Owing to the buckling and distortion of steep tracks caused by the drying and coalescence of the gelatin, the possibility must also be considered that the two angular estimates are spurious and that the event might be a case of coplanar decay into three charged particles. As a test of coplanarity the analytical function,[4]

$$F=\tan\beta_2 \sin\alpha_1-\tan\beta_1 \sin\alpha_2-\tan\beta_0 \sin(\alpha_2-\alpha_1)=0,$$

was applied to the measurements. If one assumes $(\alpha_2-\alpha_1)=8.3°$, then $F=0.11\pm0.02$. Using the upper limit of 18.5° for $(\alpha_2-\alpha_1)$ gives $F=-0.21\pm0.02$. On the basis of the average angle between the recoil tracks, the deviation from coplanarity is small and reconcilable with a distortion effect. One must therefore consider the possibility that the decay was at rest and coplanar.

If one assumes that particles A and B are singly charged and are either protons or deuterons, momentum balance of the following decay schemes have been investigated:

Tracks A B C

(a) $H^{2*}\rightarrow H^1+H^1+\pi^-+Q_a$.

(b) $H^{3*}\rightarrow H^1+H^2+\pi^-+Q_b$.

(b′) $H^2+H^1+\pi^-+Q_{b'}$.

On the basis of 3-body decay, the resultant momentum $\mathbf{P}$ of the momenta of $\mathbf{P}_A$ and $\mathbf{P}_B$ has been computed from the relationship $P^2=P_A{}^2+P_B{}^2+2P_AP_B\cos\theta$, where θ is defined as the angle between tracks A and B in the xz plane. If the assumptions are correct, then $P=P_\pi$. The results are summarized in Table II, together with the Q and the Δ values for the proposed mechanisms. The Δ value[5] represents the difference between the binding energies of the last neutron and the Λ^0 particle in the excited fragment.

This analysis shows that the decay at rest of a deuteron into two protons and a pi meson is untenable, as the resultant momentum of the two recoil particles is 25 percent less than the measured momentum of the meson. Since it is not possible to postulate the emission of a massive neutral particle in order to conserve momentum, it is highly improbable that fragment F could be a deuteron. This evidence, taken in conjunction

TABLE I. Track characteristics of excited triton and its decay products.

Track	F	A	B	C
Range, microns	1330±10	23.7 ±1	49.3 ±5	12 900±500
Identity		H^1	H^1	π^-
Kinetic energy (H^1), Mev		1.43±0.04	2.31±0.15	26.63±0.9
Momentum (H^1), Mev/c		51.8 ±0.8	65.9 ±2.2	90.2 ±1.7
Identity		H^2	H^2	
Kinetic energy (H^2), Mev		1.77±0.05	2.93±0.2	
Momentum (H^2), Mev/c		81.5 ±1.2	104.9 ±3.5	

[4] G. Goldhaber, Phys. Rev. **89**, 1188 (1953).
[5] Bonetti, Levi Setti, Panetti, Scarsi, and Tomasini, Nuovo cimento **11**, 210 (1954); **11**, 331 (1954).

TABLE II. Momentum balance for assumed 3-body decay mechanisms.

Mechanism	P_A	P_B	P momenta in Mev/c	$(P-P_\pi)$	Q Mev	Δ Mev
(a) $H^2(2p\pi)$	51.8±0.8	65.9±2.2	67.5±12	−22.8±10	30.4±1	−4.24±1
(b) $H^3(pd\pi)$	51.8±0.8	105 ±3.5	98.9±21	8.7±19	31.0±1	0.42±1
(b′) $H^3(dp\pi)$	81.5±1.2	65.9±2.2	84.2±11	−6.0±9	30.7±1	0.11±1

with the scattering measurements, indicates that the fragment is indeed a triton.

As shown in Table II, a fair momentum balance is achieved assuming that an excited triton decayed at rest into a deuteron, a proton, and a pi meson. Since the recoil particles cannot be uniquely identified, two possibilities have been considered: (b) with track A taken as a proton and track B as that of a deuteron, and (b′) with these roles inverted. In decay mechanism (b′) the small difference between P and P_π is readily bridged by the experimental error in the measurement of the momenta and the angles between the tracks. However, this mechanism leads to the conclusion that the Δ value is vanishingly small. This is unlikely, since one would expect the excited triton to reach its ground state before the occurrence of mesonic decay.

FOUR-BODY DECAY SCHEME

The difficulty of the small value of Δ resulting from the assumption of a 3-body decay, can be avoided by postulating the emission of a fourth neutral particle:

$$\text{(c)}\quad H^{3*}\rightarrow H^1+H^1+n^0+\pi^-+Q_c.$$

The energy of the neutron can be estimated by means of a momentum component balance. Selecting the y-axis coincident with the initial direction of emission of the pi meson and assuming that the initial projected angle between the recoil tracks is 18.5°, the momentum vectors are resolved as follows:

$$\text{(1)}\quad \mathbf{P}_\pi=90.2\mathbf{u}_1=0\mathbf{i}+90.2\mathbf{j}+0\mathbf{k}.$$

$$\text{(2)}\quad \mathbf{P}_A=51.8\mathbf{u}_2=0\mathbf{i}-42.3\mathbf{j}+30.3\mathbf{k}.$$

$$\text{(3)}\quad \mathbf{P}_B=65.9\mathbf{u}_3=5.0\mathbf{i}-15.0\mathbf{j}-63.9\mathbf{k}.$$

The corresponding momentum vector of the neutron, $\mathbf{P}_n$, from conservation of momentum components, is:

$$\text{(4)}\quad \mathbf{P}_n=47.3\mathbf{u}_4=-5.0\mathbf{i}-32.9\mathbf{j}+33.6\mathbf{k}.$$

The corresponding energy of the neutron is 1.2±0.2 Mev. A similar analysis based on a projected angle of 8.3° between the recoil tracks yields 1.0±0.2 Mev. Because of the uncertainty in the projected angle, the energy of the neutron varies between an upper limit of 1.4 Mev and a lower limit of 0.8 Mev. For purposes of computing the Q-value, the kinetic energy of the neutron has been taken as 1.1±0.3 Mev, yielding $Q_c=31.5\pm1$ Mev. The corresponding Δ value is 3.1±1 Mev which is now of the same order of magnitude as that observed by other investigators.[5,6]

[6] Debenedetti, Carelli, Tallone, and Vigone, Nuovo cimento **12**, 466 (1954).

COMPARISON OF EXCITED TRITON DECAYS

Several examples of the emission and decay of heavy fragments from cosmic-ray stars are on record.[7] The closest analogy to the present event, insofar as mesonic decay can be established, is the example of a meson-active triton described by Bonetti and co-workers.[5] In their observation the fragment also originates in a large star, and scattering and grain density measurements along its 13-mm track length identifies the particle as a triton. On coming to rest, the fragment decays into two colinear particles, momentum balancing on the basis of: $H^{3*}\rightarrow He^3+\pi^-+Q=41.7\pm1$ Mev. More recently, a second example of the identical process has been reported by Debenedetti *et al.*[6] in which the energy release in the decay of the triton is estimated at 42.1 ±4.2 Mev. The characteristics of these three examples of the mesonic decay of excited tritons are compared in Table III. The present event differs from the other two examples in that it represents a complete breakdown of the tritium atom into fundamental particles.

It is also of interest to compare the present event with decay processes of heavier fragments ($Z\leq2$) in which the emission of a pion is clearly established.[8] The most striking feature is the emission of a meson with a kinetic energy of about 25 Mev,[9,10] and a total energy release of essentially the same magnitude as that produced in the decay of the Λ^0 particle, *viz.*, ∼37 Mev. In the first observation of this phenomenon Danysz and Pniewski[11] suggested that the heavy fragment contained one of its nucleons in an excited state, possibly by the substitution of a neutron with a Λ^0 particle, forming a relatively stable unit which has been designated a "V-particle nuclear fragment." Cheston and Primakoff[12] have made a theoretical study of the relative stability of such fragments and conclude that for a simple structure such as a "V-deuteron,' consisting of a proton bound to a Λ^0 particle, the unit

[7] For a recent bibliography see Freier, Anderson, and Naugle, Phys. Rev. **94**, 677 (1954).

[8] C. F. Powell, Nuovo cimento **12**, Suppl. No. 2, 165 (1954).

[9] Hill, Salant, Widgoff, Osborne, Pevsner, Ritson, Crussard, and Walker, Phys. Rev. **94**, 797(A) (1954). They observed an event initiated by 1.5-Bev pi mesons from the Cosmotron from which an excited alpha particle is emitted. This decays at rest with the formation of a 25-Mev pion, a 5.3-Mev proton, and a 3.5-Mev He^3 nucleus. Momenta balance on an assumed decay: $He^{4*}\rightarrow\pi^-+H^1+He^3+Q=33.8$ Mev.

[10] Naugle, Freier, and Ney, Phys. Rev. **96**, 829(A) (1954). They report a very exceptional event in which a K-meson initiates a star one of whose heavy fragments decays at rest. A 23.5±0.5 Mev pion is observed among the disintegration products.

[11] M. Danysz and J. Pniewski, Phil. Mag. **44**, 348 (1953).

[12] W. Cheston and H. Primakoff, Phys. Rev. **92**, 1541 (1953).

TABLE III. Comparison of meson-active triton decays.

Event	Bonetti[a]	Debenedetti[b]	Present
Star type	$22+3n$	$21+7p$	$21+5p$
Range of H^{3*}, microns	13 000	1490	1330
Decay products	$He^3+\pi^-$	$He^3+\pi^-$	$2H^1+n^0+\pi^-$
Kinetic energy of π^-, Mev	39.4±1	39.8±4	26.6±0.9
Energy of recoil particles, Mev	$He^3=2.7\pm0.6$	$He^3=2.5\pm0.5$	$H^1=1.43\pm0.04$ $H^1=2.31\pm0.15$ $n^0=1.1\ \pm0.3$
Q-value, Mev	41.7±1	42.1±4.2	31.5±1
Δ-value, Mev	5.1±1.1	6.0±4.2	3.1±1[c]
Binding energy of H^{3*}, Mev	2.9±1.1	2.5±4.2	5.4±1
Time of flight, sec	$>3\times10^{-10}$	4×10^{-11}	4.2×10^{-11}

[a] See reference 5.
[b] See reference 6.
[c] The Δ value has been computed from the isotopic weights listed by E. Segrè [*Experimental Nuclear Physics* (McGraw-Hill Book Company, Inc., New York, 1953), Vol. 1, p. 745], using the values of the physical constants proposed by J. W. M. DuMond and E. R. Cohen [Revs. Modern Phys. **25**, 691 (1953)]. The mass of the Λ_0-particle was computed on the basis of the Q-value of 36.92 ±0.22 Mev observed by M. W. Friedlander *et al.* [Phil. Mag. **45**, 533 (1954)]. When these constants are used the nuclear masses of the particles entering in the computation of Δ are as follows: proton =938.232 Mev, neutron = 939.52, deuteron =1875.534, triton =2808.802, π-meson =139.40, Λ^0-particle =1114.5, and He^3 =2808.27. The Δ values cited by Bonetti and Debenedetti, recomputed with these constants, are 5.59 and 5.99 Mev, respectively.

would be stable for $\approx10^{-10}$ sec with equal probabilities of decay via the following modes:

(1) $H^{2*}\rightarrow p+n+175$ Mev—nonmesonic decay.

(2) $H^{2*}\rightarrow p+p+\pi^-+\approx35$ Mev or $p+n+\pi^0+\approx35$ Mev } mesonic decay.

The present example is a close approximation to decay mode (2) in which the "V-triton" furnishes an energy release of 31.5±1 Mev. Following this model, $H^{3*}\rightarrow2p+n+\pi^-+Q$, 36.9 Mev are released by the initial decay of the Λ^0 particle into a proton and a meson. A part of this energy is consumed in breaking the nuclear bonds existing in the tritium nucleus, the remainder appearing as kinetic energy shared by the disintegration products. The difference between $Q_{\Lambda0}$ and the observed Q is thus a measure of the binding energy of the excited triton. On the basis of decay scheme (c) this binding energy is 5.4±1 Mev. In a normal tritium atom the binding energy is 8.48 Mev. This implies that the Λ^0 particle is less strongly bound in nuclear matter than is the neutron.

The smaller binding energy of the Λ^0 particle in the excited triton is also demonstrated by the two events in which the triton decays via He^3 formation (Table III). Thus the Q of 41.7±1 Mev observed by Bonetti implies that the He^3-nucleus is more tightly bound than the excited triton by 4.8±1 Mev. If we consider that the binding energy of normal He^3 is 7.72 Mev, the binding energy of the excited triton is 2.9±1 Mev. This is to be compared with the binding energy of the triton in the present example (5.4±1 Mev) and with its normal value of 8.48 Mev.

The event was observed in 60 cc of emulsion examined for pion terminations.[1] No systematic search was made for the emission of unstable heavy fragments. However, in the subsequent high-power examination of stars with ejected pi mesons, a total of 3 associated unstable fragments (nonmesonic decays) were noted among 422 stars of this special character. In evaluating the relative frequency of this process it is well to note that track F would probably not have been observed by itself in a low-power survey of the emulsion.

ACKNOWLEDGMENTS

Opportunity is taken to thank the members of the Office of Naval Research Project for the high-altitude balloon exposure. Appreciation is expressed to Howard Smith for assistance with the computations. The writer is indebted to R. H. Dalitz of Cornell University for a discussion of this event. Appreciation is expressed to N. Seeman and M. M. Shapiro of the Naval Research Laboratory for the mass determination of the fragment.

Scattering of 192-Mev Electrons from the Deuteron*†

JOHN A. MCINTYRE AND ROBERT HOFSTADTER
Department of Physics and High-Energy Physics Laboratory, Stanford University, Stanford, California
(Received December 10, 1954)

Elastic scattering of 192-Mev electrons from deuterium has been studied using both solid (CD_2) and high-pressure gas targets. The results obtained by these two methods are in agreement and yield the following conclusions: (1) The range of the neutron-proton potential is between 1 and 4×10^{-13} cm if a square potential well is assumed and if the deuteron wave functions predicted by the binding energy of the deuteron are used. (2) It is, however, impossible with the present data to eliminate the possibility of other charge distributions for deuterium such as uniform or Gaussian.

Inelastic electron scattering from deuterium was also investigated, and promises to give independent information of the deuteron structure.

I. INTRODUCTION

THE reduced wavelength of electrons with energy in the neighborhood of 200 Mev is about 10^{-13} cm. Consequently the scattering of a beam of such electrons from charged objects such as the various atomic nuclei which have these dimensions yields information about the size and structure of the nuclei. Investigations of this type have been carried out already for gold and lead nuclei which have radii of about 7×10^{-13} cm and it has been found possible to determine two parameters which specify the charge distribution in these nuclei.[1]

In considering what nuclei to study next, several factors were apparent which made the deuteron an attractive possibility. (1) The deuteron is the only nucleus in which the two-body character of nuclear forces is isolated for study. (2) The deuteron is large enough so that some information about its structure should be obtainable with the electrons available. (3) The "size" of the deuteron has been determined by one method only, i.e., by using the value of the binding energy.[2] While there is no reason to doubt the result obtained by that method, an independent check is desirable. (4) It was found some time ago[3] that scattering studies with deuterium as well as hydrogen were feasible with solid (e.g., CH_2) targets because of the significant change in scattered electron energy due to recoil of the struck nucleus. Thus, the electrons scattered from deuterium nuclei may be separated from most of the electrons scattered from the heavier carbon nuclei.

The results of scattering 192-Mev electrons from CD_2 targets are reported in this paper. Since absolute cross sections have not yet been obtained experimentally, the scattering from hydrogen was also studied in CH_2. Hydrogen was found to scatter essentially as a point charge.‡ Since calculations have been made for point-charge scattering,[4] it is necessary only to determine the ratios of deuterium to hydrogen scattering at various angles in order to obtain the absolute cross sections for deuterium.

Finally, scattering experiments were carried out by using D_2 and H_2 gas targets with pressures ranging from 137 atmospheres to about half this value.[5] The results from these experiments are in agreement with those obtained with the solid targets.

II. APPARATUS

Several improvements have been made in the apparatus previously described.[1,6] A CsBr(Tl) scintillator has been placed on the electron-beam axis beyond the scattering chamber. The scintillator is viewed with a telescope in the room where pulse counting is carried on, and the electron beam is then steered to its correct position on the axis. A remotely-controlled lead slit has also been installed at the entrance to the analyzing magnet; this slit width determines the spread in scattering angle accepted by the analyzing magnet. Finally, the high-pressure gas-target chamber mentioned above is now available for use. It can be filled and emptied from the remote counting room in about five minutes.

The CD_2 and CH_2 targets used for most of the runs were 0.200 in. and 0.115 in. thick, respectively. Thicker targets were also tried but were rejected, because of an indirect effect of the energy loss in the target. Since the incident electrons lose energy in the target and hence are incident at slightly different energies, the recoil energy taken away by the struck nucleus is

* The research reported here was supported jointly by the Office of Naval Research and the U. S. Atomic Energy Commission, and by the U. S. Air Force, through the Office of Scientific Research of the Air Research and Development Command.

† Aided by a grant from the Research Corporation.

[1] Hofstadter, Hahn, Knudsen, and McIntyre, Phys. Rev. **95**, 512 (1954); Yennie, Ravenhall, and Wilson, Phys. Rev. **95**, 500 (1954); D. G. Ravenhall and D. R. Yennie, Phys. Rev. **96**, 239 (1954).

[2] See, for example, J. M. Blatt and V. F. Weisskopf, *Theoretical Nuclear Physics* (John Wiley and Sons, Inc., New York, 1952), p. 52.

[3] Hofstadter, Fechter, and McIntyre, Phys. Rev. **91**, 422 (1953).

‡ *Note added in proof.*—Newer data on hydrogen obtained by R. S. McAllister and R. Hofstadter at larger scattering angles reveal the effect of the magnetic moment of the proton. Also, a slit correction in the analyzing magnet has been omitted in this paper since it is small compared to other uncertainties in the data (e.g. 10 percent at 90° and 20 percent at 120°).

[4] N. F. Mott, Proc. Roy. Soc. (London) **A135**, 429 (1932); W. A. McKinley, Jr., and H. Feshbach, Phys. Rev. **74**, 1759 (1948).

[5] Hofstadter, McAllister, and Wiener, Phys. Rev. **96**, 854 (1954).

[6] Hofstadter, Fechter, and McIntyre, Phys. Rev. **92**, 978 (1953).

different if the scattering occurs at the front than if it occurs at the back of the target. Hence, the elastically-scattered electrons at a given angle exhibit this energy difference. The targets, therefore, had to be thin enough so that this energy difference would not be larger than the spread of energy in the incoming beam of electrons. The target thicknesses so determined yielded negligible energy spreading due to collision straggling and bremsstrahlung. For most of the experiments reported here, the spread in energy in the electron beam was set at $\frac{1}{2}$ percent and the slit at the exit of the analyzing magnet was set for $\frac{1}{2}$ percent energy acceptance band. Again, for most of the experimental runs, the slit at the entrance of the analyzing magnet which determines the solid angle subtended by the magnet was set at $\frac{1}{4}$ in. wide (about one-third maximum) by $1\frac{1}{4}$ in. high (maximum). Selection of the small width was dictated by a recoil effect: *viz.*, electrons scattered at different angles give up different energies to the recoil nucleus. Thus, if the scattered electrons detected are to have less than a given spread in energy, the spread in angle accepted by the analyzing magnet must be limited.§ The energy spread in electrons scattered was about 1.5 Mev due to the different effects mentioned. This small spread insured that inelastically-scattered electrons in the disintegration of the deuteron would not be accepted as elastically-scattered electrons.

The gas targets for both deuterium and hydrogen were used with a maximum pressure of 137 atmospheres. At this pressure, none of the "thick-target" effects discussed above was important. However, the effects of multiple scattering in the walls of the pressure chamber must be considered. These effects have been found to be less than 5 percent.[7]

The beam was monitored as before with a helium-filled ionization chamber. Such a chamber is known to become nonlinear at sufficiently high beam currents. For these experiments this nonlinearity was at most 5 percent. The nonlinearity was determined by using a secondary-electron-emitter monitor of a type developed by Fechter and Tautfest[8] and built for our use by A. W. Knudsen and B. R. Chambers.

III. PROCEDURE

When taking data the analyzing magnet was set at a particular angle and the number of scattered electrons of a particular energy was determined for a fixed number of beam electrons. The analyzing-magnet field was then changed and the number of scattered electrons of a different energy determined. Such determinations yield curves such as that shown in Fig. 1 for electrons scattered through an angle of 80° from a CH_2 target. The C and H peaks are due to elastically-scattered electrons from carbon and hydrogen, respectively. The other peaks are due to scattered electrons which have

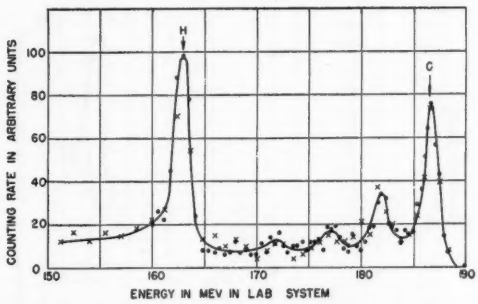

FIG. 1. Scattering from a CH_2 target at 80°. The C and H peaks are due to electrons scattered elastically from carbon and hydrogen, respectively. The remaining peaks are due to electrons scattered inelastically from carbon.

lost energy by exciting levels in carbon nuclei.[9] The electrons in the H peak have lost energy because of recoil of hydrogen nuclei. To obtain the elastic scattering from hydrogen alone, the scattering from a pure carbon target is measured and a subtraction is made. It is evident that the subtraction is only of the order of 10 percent and so should not contribute more than a few percent error.

It might at first seem surprising that there should be more elastic scattering from hydrogen than from carbon since Coulomb scattering is proportional to Z^2. However, the carbon nucleus appears considerably different from a point charge at these electron energies, and because of this, carbon elastic scattering at large angles drops more than a factor of 18 $(=6^2/2)$ below point-charge scattering. At the smaller scattering angles, however, the C peak grows toward its Coulomb value of 18 times the H peak. Since the hydrogen recoil also becomes smaller at small angles, the H peak is not as well isolated from the C peak at these angles.

What has been said of hydrogen scattering from solid targets holds also for deuterium scattering. In addition, however there are two adverse effects: (1) The deuteron recoil is roughly half that of hydrogen so that the deuteron elastic peak is considerably closer to the carbon elastic peak. For example, at 80° it would appear at 174 Mev (compare to Fig. 1). Thus, at the smaller angles at least, where the recoil is small, there is a larger carbon background to be subtracted than for the hydrogen case. (2) The finite size of the deuteron manifests itself at the larger angles by a considerable decrease in the deuteron elastic scattering. Figure 2 shows how much smaller the deuterium scattering is than the hydrogen scattering at 110°. Naturally, the carbon subtraction for deuterium is more serious at 110° also. In addition, Fig. 2 shows deuterium scattering at a "small angle," 50°, where again the carbon subtraction is large. At angles between these values the carbon subtraction for deuterium is less serious.

§ This effect, of course, limits the thickness of the target also.

[7] Measurements made by R. W. McAllister and R. Hofstadter.

[8] G. W. Tautfest and H. R. Fechter, Phys. Rev. **96**, 35 (1954).

[9] Such inelastic peaks have already been reported for beryllium by McIntyre, Hahn, and Hofstadter, Phys. Rev. **94**, 1084 (1954). More recent data on carbon taken by J. Fregeau and R. Hofstadter with better resolution show additional carbon levels.

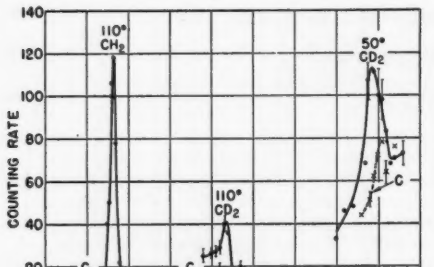

FIG. 2. Scattering from CH_2 and CD_2 targets at 110° and 50°. Scattering from a pure-carbon target is also shown. The ordinate scale for the two angles shown is different for each. Uncertainties shown for the ordinates are due to counting statistics alone.

The carbon-subtraction problem is eliminated entirely when the high-pressure gas target is used. However, the hydrogen scattering from the gas target is only about one-sixth that from the 0.115-in. CH_2 target, and the deuterium scattering is one-tenth that from the 0.200-in. CD_2 target. Thus, for deuterium, scattering from the gas target was not carried out for angles larger than 90°. Hydrogen data over a larger range of angles have been taken with the gas target; these will be reported in a subsequent publication.[10]

To compare experiment with theory, the elastic-scattering relative yields are plotted against center-of-mass scattering angle. For the Born approximation, and to first order in β, the scattering can be analyzed in the center-of-mass system in the usual way.[11] The deuterium scattering takes place at a center-of-mass energy of 175 Mev and the hydrogen scattering at 160 Mev for 192-Mev incoming electrons.

All theoretical calculations of the scattering for deuterium and hydrogen are made for a Dirac electron scattering from a static charge. An error at the largest angles for hydrogen is made by this procedure chiefly due to neglect of the anomalous magnetic moment of the hydrogen nucleus. However, at the present time, the experimental data do not warrant a more detailed calculation. The Born approximation is used in all of the form-factor calculations for deuterium.[12]

IV. RESULTS

Figure 3 shows the angular distribution obtained for electrons scattered from hydrogen with the theoretical scattering from a point charge plotted for comparison. The fit is as good as the statistics warrant, and in the following, the hydrogen nucleus will be assumed to scatter as a point charge and all absolute cross sections quoted will be based on this assumption.‡

The results obtained by scattering from deuterium are given in Fig. 4. The hydrogen points in this figure were taken for normalization purposes during the deuterium runs and represent different data from the points in Fig. 3. Since only two hydrogen points were taken during each deuterium run, and since these two points were plotted to best fit the theoretical curve, the hydrogen data in Fig. 4 do not test the theory as well as the data in Fig. 3.

The deuterium points in Fig. 4 deviate from point-charge scattering by a factor of 10 at the large angles. Four theoretical curves[12] have been plotted to determine what information can be gained from the deuterium data. Each solid curve gives the angular distribution for scattering from the charge distribution of a proton that is bound in a square potential well with the binding energy of the deuteron. The range of the potential for each curve is noted in Fig. 4. The dotted curve gives the angular distribution for scattering from a uniform charge distribution with radius 2.1×10^{-13} cm. The root-mean-square radius of each charge distribution is also given in the figure. Of the four curves, only the zero-range deuterium curve can be eliminated as a possible fit. The other two deuterium curves roughly enclose the experimental points so that one can say that if the charge distribution of the deuteron is that expected from nuclear theory, then the radius of the potential well between neutron and proton is probably between 2 and 3×10^{-13} cm and certainly between 1 and 4×10^{-13} cm. If the predictions of nuclear theory are disregarded, however, a uniform charge distribution of radius 2.1×10^{-13} cm is also a possibility (a Gaussian charge distribution would fit equally as well). It is

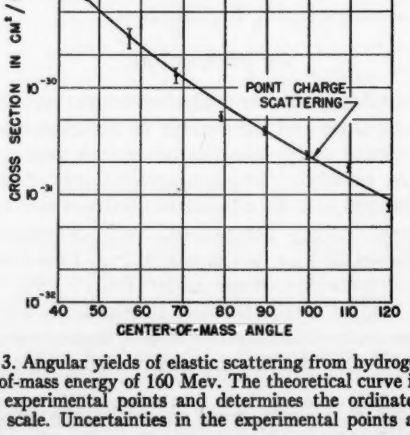

FIG. 3. Angular yields of elastic scattering from hydrogen with center-of-mass energy of 160 Mev. The theoretical curve is fitted to the experimental points and determines the ordinate cross-section scale. Uncertainties in the experimental points are statistical.

[10] Data taken by R. W. McAllister and R. Hofstadter.

[11] Here $\beta=v/c$, where v is the velocity of the nucleus in the center-of-mass system. For hydrogen at electron energies of 200 Mev, $\beta=0.175$.

[12] The scattering from deuterium for two square-well nuclear potential ranges has been calculated by J. H. Smith, Ph.D. dissertation, Cornell University, 1951 (unpublished). [A previous calculation by M. E. Rose, Phys. Rev. 73, 282 (1948) is in error.]

interesting that the root-mean-square radii of the deuteron charge distributions and the uniform charge distribution which fit the data can be as greatly different as 30 percent. Clearly the present data do not allow a very precise determination of the deuteron structure, but it is also clear from Fig. 4 that data of accuracy of 10 percent would give considerable information about the deuteron structure and the neutron-proton potential. Such data should be attainable without making major changes in the present apparatus. It should be noted in Fig. 4 that the root-mean-square radii are given in the barycentric coordinates of the deuteron while the nuclear potential ranges are given in the relative neutron-proton coordinates (twice the barycentric coordinates).

In addition to elastic scattering from deuterium, there is also inelastic scattering of electrons which have lost energy in disintegrating the deuteron. Figure 5 shows the energy spectrum of electrons scattered from deuterium and hydrogen gas at 70°. The hydrogen elastic peak represents scattering from protons at rest while the wider inelastic deuterium peak represents scattering from the moving proton in the deuterium nucleus. The shape of the inelastic peak, therefore, should yield information on the velocity or momentum distribution of the proton in the deuteron. Thus, the elastic scattering gives the wave function of the proton through its measure of the charge distribution while the inelastic scattering gives information about the wave function of the proton in the momentum representation through its measure of the velocity distribution. Calculations are now in progress at Stanford University by V. Jankus to investigate what information can be gained from the inelastic data.

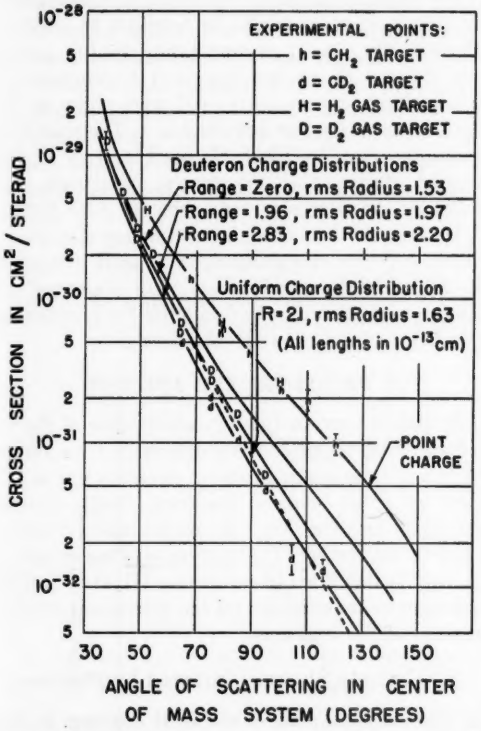
EXPERIMENTAL POINTS:
h = CH2 TARGET
d = CD2 TARGET
H = H2 GAS TARGET
D = D2 GAS TARGET
Deuteron Charge Distributions
Range = Zero, rms Radius = 1.53
Range = 1.96, rms Radius = 1.97
Range = 2.83, rms Radius = 2.20
Uniform Charge Distribution
R = 2.1, rms Radius = 1.63
(All lengths in 10⁻¹³ cm)
POINT CHARGE
CROSS SECTION IN CM² / STERAD
ANGLE OF SCATTERING IN CENTER OF MASS SYSTEM (DEGREES)

FIG. 4. Angular yields of elastic scattering from deuterium with center-of-mass energy of 175 Mev. Hydrogen points were taken for normalization. Data were taken in five runs, all runs being normalized by the hydrogen points. The ordinate scale is determined by assuming hydrogen scattering is point-charge scattering. The curves are all determined by the Born approximation. The two curves calculated from deuteron wave functions with nuclear potential ranges of 1.96 and 2.83×10^{-13} cm were calculated by Smith (see reference 12). "Range" in the figure means the range of a square-well potential in relative neutron-proton coordinates (neutron at rest), while the "rms radius" is given in barycentric coordinates of the deuteron (one-half the value of the relative coordinates). Statistical uncertainties in the experimental points are all smaller than the heights of the letters except where indicated.

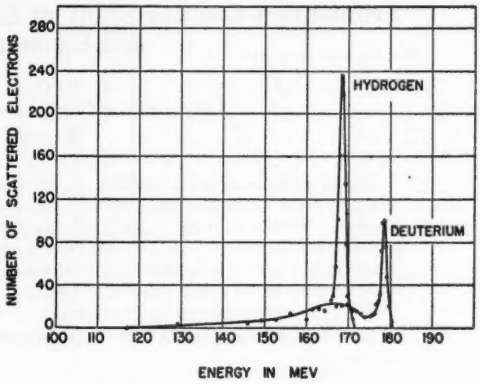

FIG. 5. Scattering from hydrogen and deuterium at 70° using gas targets.

V. CONCLUSIONS

Three conclusions may be drawn from the data presented:

(i) The range of the neutron-proton potential is between 1 and 4×10^{-13} cm if a square potential well is assumed and if the deuteron wave functions predicted by the binding energy of the deuteron are used.

(ii) The present data for deuterium are not accurate enough to eliminate the possibility of other charge distributions such as uniform and Gaussian.

(iii) Inelastic scattering from deuterium should also yield information about the internal dynamics of the deuteron.

VI. ACKNOWLEDGMENT

The authors wish to thank Dr. B. Hahn and E. Chambers for assistance in taking data; Dr. D. G. Ravenhall, Dr. R. H. Dalitz, Dr. D. R. Yennie, Professor L. I. Schiff, and V. Jankus for a number of helpful suggestions; and A. W. Knudsen, B. R. Chambers, and G. Siegner for building and improving the new parts of the apparatus.

Scintillation Counter Study of Energy Spectra of Cosmic-Ray Photons and Electrons at 11 200 Feet*

C. N. CHOU AND MARCEL SCHEIN
Department of Physics, University of Chicago, Chicago, Illinois

(Received December 9, 1954)

An apparatus designed to measure cascade showers initiated by photons and electrons of energies in the range of 1 Bev to 30 Bev was used to measure the energy spectra of cosmic-ray photons and electrons at Climax, Colorado (altitude 11 200 feet). The apparatus consisted of four anthracene-in-polystyrene plastic scintillators, interposed with 2.00 cm, 2.25 cm, and 2.25 cm of lead plates, respectively. Four trays of G-M counters and a set of anticoincidence G-M counters were used simultaneously with the scintillators.

More than 10 000 events were recorded and analyzed. The results show that in the energy range of 2 to 20 Bev, the integral energy distributions can be represented by a power law expression of the form $N(>E) = \text{const}\ E^{-s}$, with s equal to 1.6 ± 0.2 for the photon component and s equal to 1.5 ± 0.2 for the electron component.

SEVERAL experiments pertaining to the energy spectra of cosmic-ray photons and electrons have been reported.[1–12] These experiments were mostly carried out with G-M counter arrangements or with cloud chambers. The highest energy that has been measured with good precision was of the order of magnitude of several hundred Mev up to a few Bev. The previous results[13] reported here showed that large plastic scintillation counters could be used advantageously for the measurement of cascade showers initiated by photons or electrons up to energies of at least several Bev. Indeed it has been proved that large anthracene-in-polystyrene plastic scintillators are relatively simple to construct, convenient to handle, and the data obtained can be analyzed with the aid of cascade theory reasonably well.

I. EXPERIMENTAL ARRANGEMENT

The apparatus used was the same as the one used in a previous experiment concerning the study of penetrating showers produced by cosmic rays.[14] (Hereafter this paper will be referred to as I.) The arrangement was shown in Fig. 1 of I. It consisted of four anthracene-in-polystyrene plastic scintillators (one of size $18\times9\times1.8$ cm^3, two of size $18\times18\times0.9$ cm^3, and one of size $18\times18\times1.8$ cm^3), interposed with lead plates of thicknesses of 2.00 cm, 2.25 cm, and 2.25 cm, respectively. Four trays of G-M counters and a set of anticoincidence counters were used simultaneously with the scintillators for the registration of high-energy photons and electrons at Climax (altitude 11 200 feet). Each individual event corresponding to the passage of an electron or photon triggered a synchroscope. The triggering arrangements used were those of S_2^m, $AB-S_2^S$, and $AB-S_2^m$ described in I. The lead block PB and the graphite block G (see Fig. 1 of I) were not used during this experiment. Electrons were selected by the triggering arrangements $AB-S_2^m$ and S_2^m. In the case of determining the energy spectrum of photons, only the triggering S_2^m was used. Altogether more than 10 000 useful events were registered and analyzed, with roughly equal number for photons and electrons [see subsection III(b) below].

II. PROCEDURE AND ANALYSIS

Only events were analyzed in which none of the side counters E was triggered. This means that we selected predominantly single photons or electrons not accompanied by other ionizing particles. Singly charged penetrating particles were measured mainly for the purpose of calibration. The analysis was essentially the same as that described in subsection III(1) in I. These measurements are also used for the determination of the intensities of the μ mesons.

(a) Cascade Showers Initiated by Photons

In these events, none of the G-M counters in trays A or B was triggered, and no scintillation pulse or only very small scintillation pulse (with respect to minimum ionization particles) was registered in the top scintillator S_3. A cascade shower developed as the photon traversed the scintillators S_2, S_4, and S_1 and the interposed lead plates. The energy of the primary photon was then determined from cascade theory in exactly the same way as described previously, i.e., by fitting with graphs to curves representing the number of electrons expected from shower theory at the depth of the different scintillators for photons of different

* Supported in part by the joint program of the Office of Naval Research and the U. S. Atomic Energy Commission.

[1] L. Janossy and B. Rossi, Proc. Roy. Soc. (London) **A175**, 88 (1940).
[2] K. Greisen, Phys. Rev. **63**, 323 (1943).
[3] W. E. Hazen, Phys. Rev. **65**, 67 (1944).
[4] B. Lombardo, Jr., and W. E. Hazen, Phys. Rev. **68**, 74 (1945).
[5] H. Bridge and B. Rossi, Phys. Rev. **71**, 379 (1947).
[6] B. Rossi, Revs. Modern Phys. **21**, 104 (1949).
[7] J. Clay, Physica **14**, 569 (1949).
[8] Carlson, Hooper, and King, Phil. Mag. **41**, 701 (1950).
[9] J. Clay and E. van Alphen, Physica **17**, 711 (1951).
[10] Baroni, Cortini, Milone, Scarsi, and Vanderhaege, Nuovo cimento **9**, 867 (1952).
[11] C. Cernigoi and G. Poiani, Nuovo cimento **11**, 41 (1954).
[12] Lovati, Mura, Succi, and Tagliaferri, Nuovo cimento **12**, 526 (1954).
[13] C. N. Chou, Phys. Rev. **90**, 473 (1953).
[14] C. N. Chou and Marcel Schein, Phys. Rev. **97**, 206 (1955).

energies. As previously described, all pulse heights from the scintillators had been converted into equivalent number of minimum ionization particles. Due to the large thickness of lead above them, the G-M counters in tray C could be triggered only for showers of primary energy greater than about 10 Bev. G-M counters in tray D should not be triggered for photons of energies less than about 10^6 Bev. A correction was made for events which could be produced by neutron-initiated stars at the lead plate interposed between the scintillators S_3 and S_2 with the production of one or more π^0 mesons, which decayed into photons to initiate the showers. The frequency of these events was calculated from the actually observed known rate of nuclear interactions in the scintillator S_3.

(b) Cascade Showers Initiated by Electrons

For events of this kind it was required that one G-M counter both in tray A and in tray B was triggered. Accordingly a scintillation pulse of a height of that of a minimum ionization particle was registered in the top scintillator S_3. A cascade shower developed in the scintillators S_2, S_4, and S_1 as the electron traversed the interposed lead plates. The energy of the primary electron was determined in a way very similar to that described in subsection (a) for the photon-initiated showers.

III. RESULTS

All the experimental data are plotted in Figs. 1, 2, and 3. In the energy range of less than 3 Bev, the sensitivity of identifying a cascade shower dropped off because in the analysis, allowance was made for the fluctuation in the shower theory. This range of allowance falls below the minimum pulse required in the present analysis when the energy is less than 3 Bev. On the other hand, for energies higher than 15 or 20 Bev, because of the greater probability of actuating one or more of the anticoincidence G-M counters E by the secondaries of the shower initiated by a high-energy primary, the effective solid angle of accepting the incoming flux of particles was estimated to be decreased by a factor of from 2 to 4 in going from 15 Bev to 30 Bev or higher. Hence a multiplying factor of this order of magnitude should be allowed for in interpreting the results.

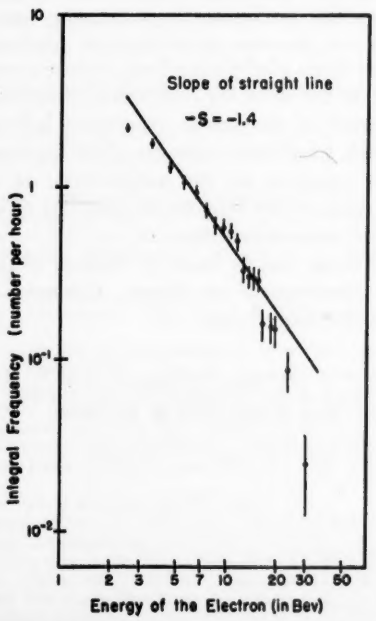

FIG. 1. Integral energy spectrum of cosmic-ray electrons at an altitude of 11 200 feet (with coincidence triggering).

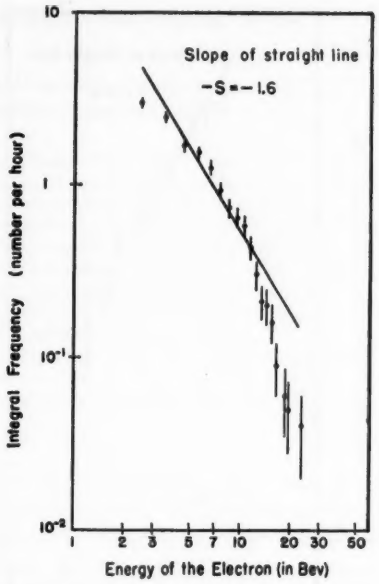

FIG. 2. Integral energy spectrum of cosmic-ray electrons at an altitude of 11 200 feet (without coincidence triggering).

(a) Energy Spectrum of Cosmic-Ray Electrons at 11 200 Feet

The results concerning the electron component obtained with the triggering arrangements $AB-S_2^m$ and the triggering S_2^m, respectively, are shown in Fig. 1 and Fig. 2. Straight lines best fitted with experimental points were drawn through the most reliable range of energies from 3 to 15 Bev. The integral frequency *vs* energy relation can be expressed by a power law of the form E^{-s}, with s equal to 1.4 ± 0.2 in Fig. 1 and s equal to 1.6 ± 0.2 in Fig. 2. Within experimental error these two exponents agree with each other.

The flux was determined for single electrons defined as above. For energies greater than 3 Bev, the observed rates were 2.5 per hour for the triggering arrangement $AB-S_2^m$ and 3.0 per hour for the triggering arrange-

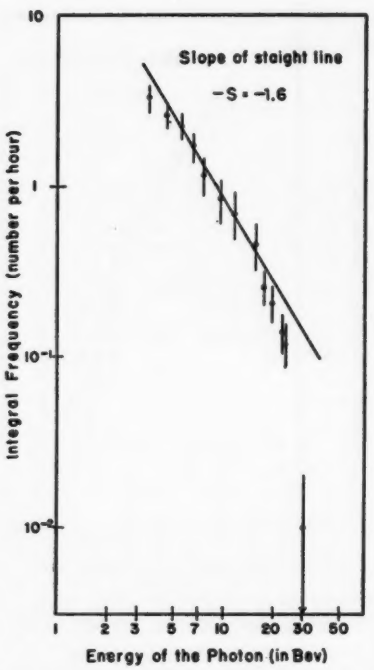

FIG. 3. Integral energy spectrum of cosmic-ray photons at an altitude of 11 200 feet.

ment $S_2{}^m$. This corresponds to an average rate of about 0.40 cm^{-2} $sterad^{-1}$ $hour^{-1}$.

(b) Energy Spectrum of Cosmic-Ray Photons at 12 000 Feet

The data referring to photons must be corrected for the contribution of neutron-initiated events in the lead plate between the scintillators S_3 and S_2. It is assumed that at the high-energy range dealt with in the present experiment, neutrons have approximately the same flux as protons. From the results in paper I we estimate the contributions of these neutron-initiated events and subtract them from the observed values. The corrected data thus obtained are plotted in Fig. 3. One sees that in the energy range from 3 to 15 Bev, a power-law spectrum holds for the integral frequency *vs* energy. The exponent of this distribution is equal to -1.6 ± 0.2. Within experimental error this value does not differ from the value for the electron spectrum.

At this high altitude (11 200 feet) most photons must be due to the decay of π^0 mesons from nuclear interactions of the incoming primaries. Based upon the observed spectrum of primary cosmic rays, the theoretical expected value of the exponent s is 1.7 or 1.8 for threshold energies of meson production of 1 or 2 Bev respectively.[15]

(c) Flux of Unaccompanied Single or Associated Penetrating Particles

From the results obtained with the triggering arrangement $AB-S_2{}^S$, we find that the rate of unaccompanied single or closely associated penetrating particles capable of traversing 12.5 cm of lead or more was about 13 cm^{-2} $sterad^{-1}$ $hour^{-1}$. They were probably mostly μ mesons. Now in the analysis of the hard component of the cosmic rays,[16] the vertical intensity of mesons with range greater than 167 g cm^{-2} of lead at the altitude of the present experiment was equal to about 58 cm^{-2} $sterad^{-1}$ $hour^{-1}$. If we take into account the fact that we detected and measured only unaccompanied single or closely associated penetrating particles, the two results are not inconsistent with each other.

IV. CONCLUDING REMARKS

The results of the present experiment show that at least in the energy range of 3–20 Bev, the integral energy distributions of the cosmic ray electrons and photons at an altitude of 11 200 feet can be represented by a power law of the form E^{-s}, with s equal to 1.6 ± 0.2 for the photon component and s equal to 1.5 ± 0.2 for the electron component. These values agree with the theoretical prediction for the energy spectra of electrons and photons assumed to be predominantly due to the decay of π^0 mesons from nuclear interactions initiated by the incoming cosmic-ray primaries.

The results of the present experiment indicate that large plastic scintillation counters of the type used here are quite adequate for the measurement of cascade showers initiated by photons or electrons of energies from 1 Bev up to tens of Bev.

The authors wish to thank R. Hansen of the High Altitude Observatory at Climax, Colorado, for his very valuable cooperation.

[15] P. Budini in *Kosmische Strahlung*, edited by W. Heisenberg (Springer Verlag, Berlin, Germany, 1953), pp. 418–424.
[16] B. Rossi, Revs. Modern Phys. **20**, 537 (1948).

Čerenkov Counter Flux Measurement of Cosmic-Ray Alphas at 41°*

NAHMIN HORWITZ†
Department of Physics, University of Minnesota, Minneapolis, Minnesota
(Received August 30, 1954; revised manuscript received December 22, 1954)

A Čerenkov counter inside a Geiger counter telescope was flown by balloon to a residual atmospheric depth of 16 g/cm². The purpose of the experiment was to measure the flux of cosmic-ray alpha particles and to investigate the usefulness of a Čerenkov counter for flux measurements on the more heavily charged cosmic-ray components. A Čerenkov counter was used because of its inherent discrimination against slow secondary particles. The pulse height distribution obtained showed a partially resolved peak at approximately 4 h_0, where h_0 is the mean pulse height corresponding to a fast proton. This is experimental confirmation of the Z^2 dependence for Čerenkov radiation. There were 3024 events which gave pulse heights corresponding to alphas. There is evidence that 451 were due to side showers, 651 were due to nuclear interactions, an additional 478 were due to either side showers or interactions, and 1444 were due to primary alphas. This leads to the value 99±16 particles/m²-steradian-second, as the extrapolated flux at the top of the atmosphere. There is also an indication of peaks corresponding to carbon and oxygen. There is evidence that the geometry factor of the telescope was appreciably increased for the heavy components due to the action of delta rays.

PURPOSE AND MOTIVATION

THIS paper reports an experiment whose primary goal was to determine the flux of cosmic-ray alpha particles at geomagnetic latitude 41°. A secondary goal was to learn something of the usefulness of a Čerenkov counter for flux measurements on cosmic-ray components with charge $3 \leq Z \leq 9$.

It is now generally accepted that cosmic rays are simply very high-energy atomic nuclei. Multiply-charged particles in cosmic rays were discovered in 1948 by Freier *et al.*[1] who sent photographic emulsions and cloud chambers to the top of the atmosphere by balloon. Ultimately we would like to know the flux and energy spectrum of each charge component, as this kind of information should be very helpful in solving the fundamental problem of the origin and history of cosmic rays.

PAST MEASUREMENTS OF THE ALPHA FLUX

Table I summarizes some past measurements[2–9] of the alpha flux. Consider how well these flux values determine an energy spectrum. Over the latitude-sensitive region, the integral energy spectrum for the total flux is approximated quite closely by:

$$I(E_t) = K/E_t^{\gamma}, \tag{1}$$

where E_t is the total energy of the particle, $I(E_t)$ is the flux of particles with energy greater than E_t, and γ has the value 1.0. Since most cosmic rays are protons, it is generally assumed that the proton component has an inverse power-law energy spectrum with exponent equal to 1.0 also. This assumption is probably correct unless, as was pointed out by Kaplon *et al.*,[10] the total

TABLE I. Summary of some past measurements of the alpha flux.

Geomagnetic latitude	Cutoff energy (total in Bev/nuc.)	Method	Experimenter	Flux (particles per m²-steradian-sec)
0	7.6	inefficient Geiger counter	Singer[a,b]	14±20
30	4.9	emulsion	Goldfarb[c] *et al.*	60±10
41	2.75	proportional counter	Perlow[d] *et al.*	110±20
41	2.75	inefficient Geiger counter	Singer[e,b]	140±60
	1.68	cloud chamber	Linsley[f]	135±20
51	1.54	emulsion	Goldfarb[c] *et al.*	340±120
55	1.30	scintillation counter	Ney[g] *et al.*	340
55	1.30	proportional counter	Davis[h] *et al.*	310±30
55	1.30	cloud chamber	McDonald[i]	230±60

[a] See reference 2.
[b] These flux values were calculated from Singer's data on the assumption that his equipment looked only at fast protons and fast alphas. If slow protons were also present, this method will give an alpha flux which is too high.
[c] See reference 3.
[d] See reference 4.
[e] See reference 5.
[f] See reference 6.
[g] See reference 7.
[h] See reference 8.
[i] See reference 9.

* This work supported by the joint program of the U. S. Atomic Energy Commission and the Office of Naval Research. This paper is a summary of a thesis submitted in partial fulfillment of the requirements for the Ph.D. degree at the University of Minnesota.
† National Science Foundation Fellow. Present address: Radiation Laboratory, University of California, Berkeley, California.
[1] Freier, Lofgren, Ney, Oppenheimer, Bradt, and Peters, Phys Rev. 74, 213 (1948).
[2] S. F. Singer, Phys. Rev. 80, 47 (1950).
[3] Goldfarb, Bradt, and Peters, Phys. Rev. 77, 751 (1950); see also *Progress of Cosmic Ray Physics*, edited by J. G. Wilson (North Holland Publishing Company, Amsterdam, 1952), p. 221.
[4] Perlow, Davis, Kissinger, and Shipman, Phys. Rev. 88, 321 (1952).
[5] S. F. Singer, Phys. Rev. 76, 701 (1949).
[6] J. Linsley, Phys. Rev. 93 (1954). (Corrected flux value given in a private communication.)
[7] E. P. Ney and D. M. Thon, Phys. Rev. 81, 1069 (1951).
[8] Davis, Caulk, and Johnson, Phys. Rev. 91, 431 (1953). (Corrected flux value was given to Professor E. P. Ney in a private communication.)
[9] F. B. McDonald (private communication to Professor E. P. Ney, 1953).
[10] Kaplon, Peters, Reynolds, and Ritson, Phys. Rev. 85, 295 (1952).

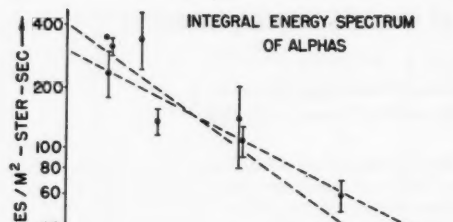

FIG. 1. The points represent flux values measured at various geomagnetic latitudes. The values of E_t are the cut-off energies at the corresponding latitudes. The dotted lines have slopes corresponding to $\gamma=1.0$ and 1.4 in the spectrum $I(E_t)=K/E_t^{\gamma}$.

flux measurements included a large amount of albedo (the higher energy protons would make relatively more albedo and this would tend to flatten the total flux spectrum). In any case, the value 1.0 is a lower limit for the exponent in the proton energy spectrum.

Similar attempts to fit the C,N,O, and $Z\geq 10$ components indicate a value of about 1.4 for the exponent in their energy spectra.[10] One would probably expect alphas to have an integral energy spectrum with exponent between the values 1.0 and 1.4. Figure 1 is a graph of the results listed in Table I. The dotted lines are not attempts at best fits to the data but rather show the slopes corresponding to the values 1.0 and 1.4. As can be seen, the data are not sufficiently self-consistent to decide between what we expect are the two limiting values. Equipment which can give more precise results should therefore be developed and should be used in a series of flux measurements at different latitudes.

APPLICATION OF A ČERENKOV COUNTER TO ALPHA FLUX MEASUREMENTS

In past counter experiments one usually identified primary alphas by measuring ionization loss. In principle, one should obtain a pulse-height distribution showing resolved peaks due to the cosmic rays with charge 1, 2, etc. The results have not been precise, however, because of the presence of background due to: (1) slow secondary protons originating in the residual atmosphere above the equipment, (2) proton induced nuclear interactions occurring in the detector, (3) showers of fast singly-charged particles originating in the air surrounding the equipment.

There is some evidence that the most serious problem is slow secondaries. A number of experiments which did not attempt to discriminate against slow particles also did not obtain any alpha peak. On the other hand, the Naval Research Laboratory group which flew proportional counters[4,8] included absorbers in their telescopes to eliminate slow particles and did succeed in partially resolving the alpha peak. In addition, the experiment which will be described in this paper and a recent experiment by Bohl[11] had provision to eliminate slow particles, and both succeeded in partially resolving the alpha peak.

An alternative to including an absorber in the equipment is to use a Čerenkov counter because it, in effect, has the absorber "built in." As is well known, a slow proton gives less Čerenkov light than a fast one. Therefore the pulse from such a particle will not cause background in the region of pulse heights expected for alphas.

The Čerenkov counter seems like an inviting tool for counter measurements on the very heavy components also. Here background usually was due to nuclear interactions in which a few evaporation particles lost a great deal of energy and gave very large pulses. However, in order to give as much Čerenkov light as a fast oxygen nucleus, the interaction would have to produce essentially 64 fast mesons.

Čerenkov counters had been used for balloon flight experiments during the past few years by Winckler and Anderson[12] in their studies of the albedo problem. They were recently adapted to flux measurements of multiply charged cosmic rays by Linsley.[6] Several years ago Ney[7] developed the first scintillation counter equipment suitable for balloon flight flux measurements of heavies. The present experiment is an outgrowth of that work, but it is built around a Čerenkov counter.

DESCRIPTION OF THE EQUIPMENT

In essence, the equipment consists of a Geiger counter telescope to define a solid angle in space from which particles will be accepted, a Čerenkov counter to determine their charge, some devices to identify background events, and apparatus to record the information obtained.

Trays A, B, and C, which are shown in solid black in Fig. 2, form the Geiger counter telescope. The equipment records only those events which cause a coincidence between these three trays. Thin-wall (30-mg/cm²) counters were used in tray A to reduce the number of nuclear interactions occurring just above the radiator.

If f_v is the number of particles per m² per second per steradian coming from the vertical, and N is the observed counting rate of the telescope, then

$$N=Gf_v, \qquad (2)$$

where G is a constant determined by the geometry of the telescope and the angular distribution of the incident radiation. The geometry factor for this

[11] L. Bohl (to be published).
[12] J. R. Winckler and K. Anderson, Phys. Rev. **93**, 596 (1954).

telescope for an isotropic flux was 9.5 ± 1 cm²-steradian.

Between trays A and B (Fig. 2) is the Čerenkov counter. The radiator is a cylindrical slab of Lucite 4 in. in diameter and 1 in. thick. The Lucite is optically coupled by a film of Canada balsam to the cathode of a Dumont K1198 photomultiplier (an end-window photomultiplier with a 5-in. diameter photocathode). This tube was operated with the cathode at ground potential and the collecting anode at plus 1220 volts. A positive output signal was taken from the tenth dynode, amplified, and displayed on a cathode ray tube (CRT). It is assumed that the deflection on the CRT is proportional to the voltage output of the photomultiplier which in turn is proportional to the amount of Čerenkov light made in the Lucite. This means the pulses from the photomultiplier must be free of saturation effects. The Dumont tubes are presumably free of saturation for signals in which the instantaneous currents are less than 12 ma.[13]

Let i be the instantaneous tube current, C be the output capacity of the tube, V_0 be the output voltage signals, and t be the duration of the pulse in the photomultiplier. Then if the current pulse is approximated by a square wave,

$$i=CV_0/t. \tag{3}$$

Taking C equal 10 $\mu\mu$f, and assuming spread in transit time makes $t\geqslant 5\times10^{-9}$ second, we see from Eq. (3) that the instantaneous current will be less than 12 ma if the output signals are less than 6 volts. The amplifiers were designed so that the maximum signal required (i.e., full scope deflection) was 5 volts.

If a proton interacts in the Lucite, making four fast mesons, the detector will indicate that an alpha came through. The same thing would happen if a narrow shower of fast particles originating in the air above the apparatus passed through the detector. In order to identify these events as background, an attempt was made to make the detector indicate whenever more than one particle passed through the telescope. This was done by placing the Geiger counters in tray B

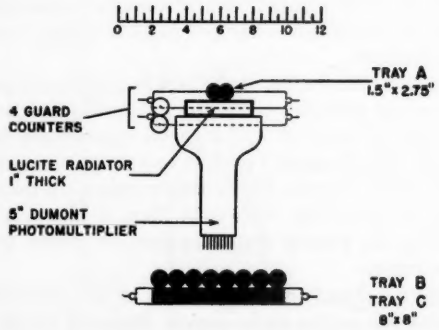

FIG. 2. Čerenkov counter telescope.

[13] B. R. Linden, Nucleonics 11, 31 (1953).

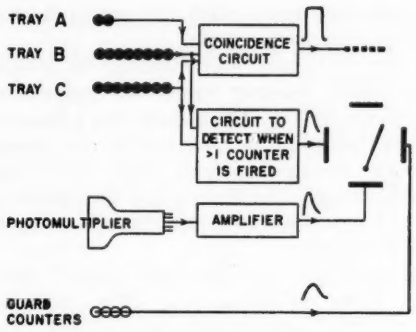

FIG. 3. Method of recording events.

perpendicular to those in tray C and having an electronic circuit which would indicate whenever more than one Geiger counter was tripped simultaneously in either tray. There were 8 Geiger counters in each tray so the bottom 64 square inches was effectively divided into 64 separate units, and the detector could tell whenever particles passed through more than one of these units simultaneously. In a further attempt to determine which events were really due to alphas and which to background, four guard counters were placed alongside the Lucite radiator to detect side showers.

Figure 3 illustrates the method of recording. The pulses from the photomultiplier are amplified and then fed to the vertical deflection plates of a cathode-ray tube. The CRT, however, is normally cut off. A coincidence between trays A, B, and C produces an enabling gate which is applied to the grid of the CRT and turns it on. A camera takes continuous pictures of the CRT. Thus if a single fast particle passes through the telescope, a vertical line, whose height is proportional to the square of the charge of the particle, will be recorded on the film.

The outputs of both tray B and tray C are also fed to a circuit which detects those cases in which more than one Geiger counter in a tray is fired simultaneously. When this happens a signal is fed to one of the horizontal deflection plates. When a guard counter is triggered, a signal is fed to the other horizontal deflection plate. Thus if a nuclear interaction takes place, the pulse on the film will appear tipped to one side, and if a side shower takes place, it will be tipped to the other side.

It was desired to record pulses ranging in size from 0 to $80h_0$, where h_0 is the mean pulse height corresponding to a fast proton. In order to do this, two cathode-ray tubes were used (like two scales on a voltmeter). One tube covered the range 0 to $9h_0$ and the other covered the range 0 to $80h_0$.

A watch with a second hand, a thermometer, and a Wallace and Tiernan pressure gauge were mounted on an instrument panel which was photographed by the same camera which photographed the cathode-ray tubes. The camera lens was always open so a light would

flash on the instrument panel (but not on the cathode-ray tubes) once every minute.

All the equipment was mounted in a spherical gondola whose diameter was 30 in. and whose wall thickness was 0.03 in. The gondola was pressure tight, and thus the equipment remained in one atmosphere of pressure during the flight. (This was to prevent corona discharge.) The Wallace and Tiernan gauge was connected by a hose to a lead-through fitting in the wall of the gondola.

The equipment was flown by balloon[14] from San Angelo, Texas, on Februrary 2, 1954. It reached an altitude of 16 g/cm² at 9:30 A.M. C.S.T. and remained within 1 g/cm² of this altitude until 3:28 P.M. C.S.T. At 3:28 P.M. the equipment, suspended from a parachute, was released from the balloon and floated to earth. The equipment was recovered in good condition, and its operating characteristics appeared to be the same as before the flight.

RESULTS

When the apparatus is operated at sea level it is responding primarily to fast μ mesons. The pulse height distribution obtained is shown in Fig. 4. The dotted curve represents a Poisson distribution of mean 30. The good fit implies that on the average, a fast meson causes 30 photoelectrons to be collected at the first dynode. It will be useful to have an idea of the

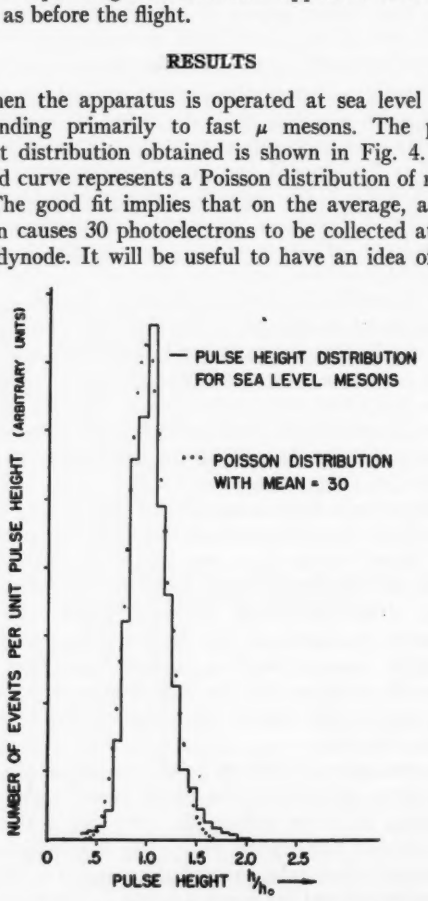

FIG. 4. The pulse height distribution for sea level mesons can be fitted quite closely by a Poisson distribution with mean 30. (The disagreement at the peak is probably due to the effects of personal bias in measuring the pulse heights.)

[14] The balloon flight was made by Office of Naval Research Project Skyhook.

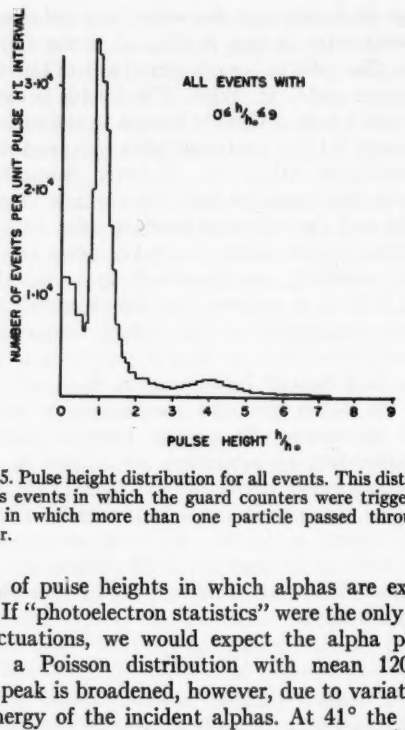

FIG. 5. Pulse height distribution for all events. This distribution includes events in which the guard counters were triggered and events in which more than one particle passed through the detector.

region of pulse heights in which alphas are expected to lie. If "photoelectron statistics" were the only source of fluctuations, we would expect the alpha peak to follow a Poisson distribution with mean 120. The alpha peak is broadened, however, due to variations in the energy of the incident alphas. At 41° the cut-off kinetic energy is 1.75 Bev/nuc. A particle with this energy gives 87 percent of the saturation amount of Čerenkov light. Thus at 41° the alpha particles will give amounts of Čerenkov light varying between 87 and 100 percent of the saturation value. Furthermore, a few percent of the alphas will give large pulses because they produce knock-on electrons in the Lucite which also give Čerenkov light. Combining these effects leads to the prediction that essentially no alphas will give pulses less than $2.7h_0$ and only a few percent will give pulses greater than $5.4h_0$.

Figure 5 shows the pulse height distribution obtained at high altitude for all events with pulse heights in the range 0 to $9h_0$. This distribution includes all events in which a guard counter was discharged and all events in which more than one particle passed through the telescope.

It seems fairly clear that there is a group of pulses due to fast particles of charge 1, a group due to fast particles of charge 2, and a group representing background. The Z equals 1 peak is very large compared to the Z equals 2 peak, which simply points up the difficulty in measuring the alpha flux, if there is any tendency for proton events to produce pulses in the alpha region.

Figure 6 shows an enlarged view of the pulse height distribution in the alpha region. Since all events are included in this pulse height distribution, the only discrimination involved is the inherent discrimination of a Čerenkov counter against slow particles. It is of

interest to note that this, in itself, is enough to bring out a partially resolved alpha peak. The solid arrow was drawn under the proton peak, and the dotted arrow was drawn at four times the pulse height corresponding to the proton peak. The fact that the alpha peak falls essentially at the dotted arrow is an experimental verification of the Z^2 dependence of Čerenkov radiation. The shaded lines are drawn at h equals $2.7h_0$ and $5.4h_0$. As was mentioned above, all but a small percentage of alphas are expected to lie within these limits. The area under the curve between the two lines corresponds to 3024 events. Of course, many of these pulses are to be classed as background and the next job is to try to determine which events are the true alphas.

It seems reasonable to say that all events in which the guard counters are triggered are not single alphas that passed vertically downward through the telescope. Therefore, these events are not what we are interested in and are to be classed as background (it was for this reason that the guard counters were included in the equipment). There is a check on this assumption. If indeed the guard counter events are not associated in any way with alphas, then their pulse height distribution should not show any structure in the alpha region. Figure 7 shows the pulse height distribution for the guard counter events only. Again the shaded lines define the region in which alphas are to be expected. Outside the lines there are no alphas, so all these pulses must be background. The distribution inside the shaded lines follows an interpolation of the curve outside. This is what we would expect if these events were all background as is being assumed. There are 451 guard counter events in the alpha region (i.e., between the shaded lines).

Next consider the events in which more than one counter in trays B or C were triggered. As has been mentioned, it was hoped that this device would identify background due to proton-induced nuclear interactions taking place in the Lucite radiator. However, it is also possible for an alpha to cause more than one Geiger

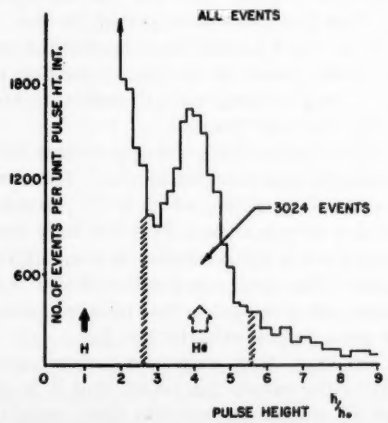

FIG. 6. An enlarged view of the alpha region shown in Fig. 5.

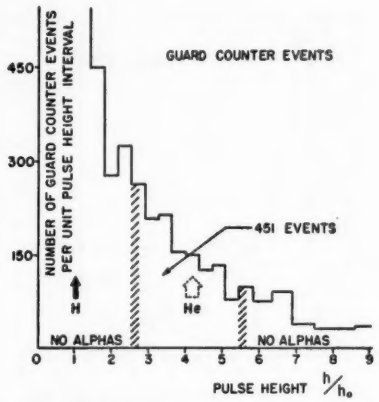

FIG. 7. The pulse height distribution for events in which a guard counter was discharged. There is no "structure" in the alpha region, which is consistent with the assumption that all these events are background due to side showers.

counter to be triggered simultaneously. This can come about in 3 ways. First there is about 7 ± 3 g/cm² of matter between the Lucite and tray C. An alpha can go through the radiator, give a Čerenkov pulse of the right size, then interact in this matter and the resultant shower can trip more than one Geiger counter. Second, it is possible that a delta ray made by the alpha will trigger an additional Geiger counter, and third, a small number of alphas traveling at large angles will be able to pass obliquely through two adjacent counters. If true alphas do occasionally cause more than one Geiger counter to be fired, than the pulse height distribution for the multiple counter events should show an alpha peak superimposed on the background due to proton interactions in the Lucite. Qualitatively this is what was found. Figure 8 shows the pulse height distribution for these multiple counter events. Again the shaded lines indicate the region in which alphas are expected. Note that a small peak does appear and it does lie roughly within the shaded lines. Outside the lines there should be few alphas. To get the background in the alpha region, an interpolation was made and is indicated by the dotted line. The area under the peak but above the dotted line represents true alphas and amounts to 247 events. This is 17 percent of the total number of events which were finally believed to be alphas. The area under the dotted line represents background and amounts to 651 events.

The pulse height distribution for what remained after using these two devices to identify background events is shown in Figure 9. These are the pulses which appeared straight on the film. The dotted curve is the pulse height distribution obtained from sea level mesons, and it is therefore what one would expect to get at altitude if there were nothing but fast protons. There is not appreciable broadening in the main proton peak but there is an extra group of small pulses presumably due to single slow secondaries.

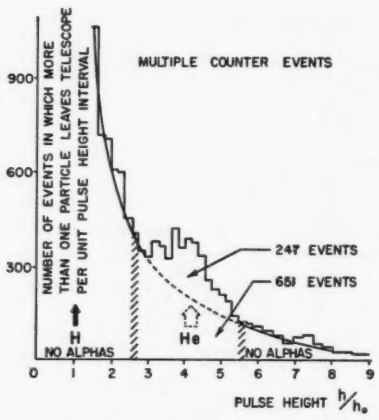

FIG. 8. The pulse height distribution for events in which two or more counters in tray B or C are triggered simultaneously. Here there *is* "structure" in the alpha region. 247 events are due to alphas and 651 are due to proton-induced interactions.

This group does not blot out the alpha region because the pulses are small, but had this been a device which measured ionization loss, those particles would have given pulses on the other side of the proton peak. This, of course, is the principle advantage of the Čerenkov counter.

Figure 10 shows an enlarged view of the alpha region. Now that the guard counter and multiple counter events have been subtracted out, the alpha peak is more clearly resolved, but since the valley doesn't drop to zero, there must still be background. This means that the other devices were not 100 percent efficient in detecting nonalpha events. There are two kinds of background here. One is caused by the tail of the proton peak. These pulses do not actually extend into the alpha region but do contribute to the curve to the left of the alpha peak. The other background is probably caused by nuclear interactions which failed to trip two

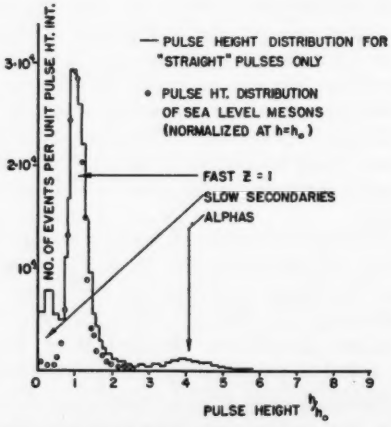
— PULSE HEIGHT DISTRIBUTION FOR "STRAIGHT" PULSES ONLY
• PULSE HT. DISTRIBUTION OF SEA LEVEL MESONS (NORMALIZED AT h=h₀)
FAST Z = 1
SLOW SECONDARIES
ALPHAS
NO. OF EVENTS PER UNIT PULSE HT. INT.
3·10⁴
2·10⁴
10⁴
0 1 2 3 4 5 6 7 8 9
PULSE HEIGHT h/h₀

FIG. 9. The pulse height distribution for "straight" pulses only. Events in which guard counters or multiple counters in trays B or C were triggered are *not* included.

Geiger counters, and these events would give pulses of all heights. To estimate the magnitude of this background in the alpha region, we would like to make an interpolation as was done before, but before interpolating it is necessary to subtract out the proton tail. This can be done because it has the same shape as the known meson tail. After the protons are subtracted out, it is assumed that the remaining pulses outside the alpha region are all nuclear interactions. These are shown in solid black in Fig. 11. It is this solid black curve which is used to interpolate the background into the alpha region. This interpolation is indicated by the heavy dotted line.

An alternative method of estimating the background is to use data obtained while the balloon is ascending. Here one takes the data obtained at an altitude sufficiently high that there are appreciable numbers of protons which can produce interactions, but sufficiently low so that there are no alphas. Then all large pulses

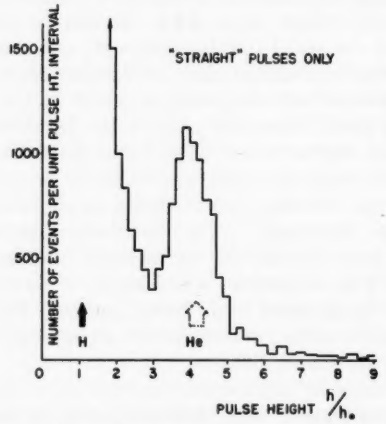

FIG. 10. An enlarged view of the alpha region shown in Fig. 9.

must be background. Of course since we are dealing with protons which have been degraded in energy, this may only give a lower limit for the background at altitude. The background estimated in this way is shown by the lower dotted line. This method has been used by various people in the past. Note that the two methods, at least in the case of a Čerenkov counter, give significantly different results.

The value obtained using the upper curve was taken as the estimated remaining background. This correction amounts to 478 particles, which is 33 percent of the total number of true alphas. This is a large correction and means there is the possibility of a significant error in the result. This points up the fact that in a counter experiment one must get a well resolved peak if one hopes to get a precise value for the flux.

After making this correction, there are 1197 "straight" pulse events remaining, and it is assumed they are all alphas. In addition there were the 247 multiple counter events which are believed to be alphas.

The time during which this total of 1444 events occurred is 355.5±1 minutes. A mean free path of 50 g/cm² for the absorption of alphas in the 16 g/cm² of air above the equipment and in the first cm of Lucite in the radiator was used to extrapolate the counting rate to the top of the atmosphere. We finally obtain as the result of this experiment the value [see Eq. (2)]:

$$f_v = \frac{(1444)}{e^{-17/50}\,(355.5)(60)(9.5\times10^{-4})}$$

$$= 99 \text{ particles/m}^2\text{-steradian-second},$$

for the flux of alpha particles at the top of the atmosphere at a geomagnetic latitude of 41 degrees.

Since the value of the flux is based on 1444 events, the statistical uncertainty is less than 3 percent. More important possible sources of error, however, are the value of the geometry factor, and the magnitude of the background corrections. It is estimated that the flux value is correct to within ±16 percent.

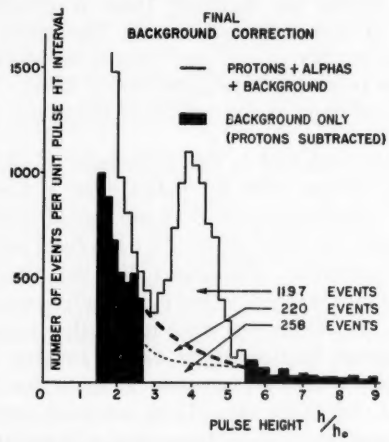

FIG. 11. The final background correction. The upper curve is a repetition of Fig. 10. The solid black curve is what one obtains after subtracting out the proton tail. The heavy dotted line is the estimated background in the alpha region based on an interpolation of the solid black curve. The light dotted line is the estimated background based on data taken while the balloon was ascending.

Figure 12 shows the summary of alpha flux values that was given in Fig. 1 with three additions. The dot with the arrow next to it represents the result of this experiment. The two dots just below it represent the results of Bohl's[11] double scintillation counter and Linsley's[15] Čerenkov counter triggered cloud chamber. All three experiments were flown from Texas last February. As can be seen, the three points are reasonably consistent and lie somewhat below the previous values. It would be very interesting now to have these experiments repeated at other latitudes in order to get a better idea of the integral energy spectrum of primary alphas.

[15] J. Linsley, Phys. Rev. **96**, 829(A) (1954).

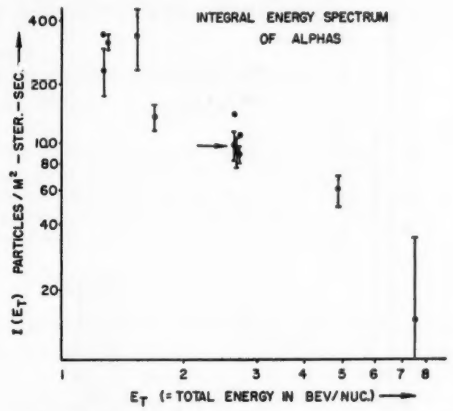

FIG. 12. This is a repetition of Fig. 1 except that three new points have been added at $E_t = 2.75$ Bev/nuc. The point with the arrow is the result of this experiment. The two points just below it are due to Bohl and Linsley.

The behavior of the Čerenkov counter in the $3 \leqslant Z \leqslant 9$ region is shown in Figs. 13 and 14. Figure 13 gives the pulse height distribution in the range $9h_0$ to $80h_0$ for those events which gave "straight" pulses (i.e., events which triggered a guard counter or more than one counter in trays B or C are not included). The regions of pulse heights which one expects to correspond to the various elements are indicated along the abscissa. These regions have been determined by using (1) the Z^2 dependence for Čerenkov light, (2) the amplifier calibration curve, and (3) the fact that the peaks are smeared downward by 13 percent due to variations

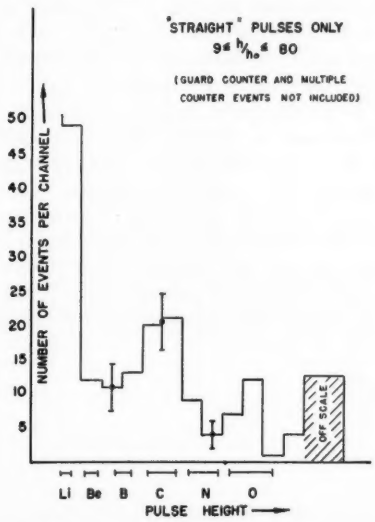

FIG. 13. Pulse height distribution in the range $9h_0$ to $80h_0$ for those events which gave "straight" pulses only (i.e., events which triggered a guard counter or more than one counter in trays B or C are not included).

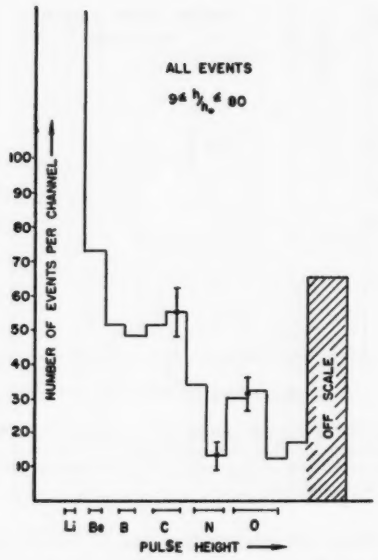

FIG. 14. Pulse height distribution for all events in the range $9h_0$ to $80h_0$.

in the energy of the primaries and then smeared out symmetrically an additional few percent due to other fluctuations.

There are no resolved peaks in the Li, Be, B region; however, there is some indication of partially resolved carbon and oxygen peaks. In judging the usefulness of a Čerenkov counter for measurements on the more heavily charged components on the basis of Fig. 13, one should remember that (1) the distribution involves rather few events (69 in the C,N,O region), and this makes resolution difficult; and (2) the effect of variations in energy spreads out the peaks to a serious extent (one would be better off in this respect if the experiment were done at the equator).

Figure 14 is the pulse height distribution for all events. There were a total of 209 events which gave pulses in the C,N,O region. Of these 25 triggered a guard counter, 115 triggered multiple counters in trays *B* and *C* and the remaining 69 gave "straight" pulses. If one believes that proton-induced nuclear interactions will not give pulses in the C,N,O region when one uses a Čerenkov counter, then all 209 events must be associated with true C,N,O's. (This is possible since C,N,O's have a large probability of making delta rays which could trigger a guard counter or a second Geiger counter.) Extrapolating the total counting rate to the top of the atmosphere using a mean free path of 35 g/cm², one obtains a C,N,O flux of 17 particles/m²-steradian-second. This is to be compared with the value 6 particles/m²-steradian-second obtained with emulsions.[10] Thus, either there are background events that are not associated with C,N,O's, or the geometry factor is 2 or 3 times bigger for C,N,O's than for protons. Linsley has obtained results with his Čerenkov-triggered cloud chamber which indicate the geometry factor is increased for the heavy components. This happens because some heavies which pass through the Lucite radiator but miss one of the trays of the telescope get recorded anyway because a delta ray triggers the missed tray. Figure 14 shows that when multiple counter events are included, there is considerable fill-in to the left of the carbon peak. This would imply that the number of nuclear interactions which give Čerenkov pulses in the neighborhood of $25h_0$ to $35h_0$ is of the same order as the number of boron and carbon nuclei.

The data obtained in this experiment is consistent with the picture that all pulses from a Čerenkov counter corresponding to $Z>6$ are indeed associated with a heavy nucleus, but for $Z<6$ the event may be a nuclear interaction. The large C,N,O flux along with Linsley's results indicate that in a counter experiment in the C,N,O region one must realize that acceptable paths cannot be defined by Geiger counters alone. The C,N,O's have an extension in space due to the action of their delta rays. Thus, one must use either Geiger counter trays of large area or some counter which can differentiate between a heavy nucleus and a delta ray it may produce.

ACKNOWLEDGMENTS

I wish to express my sincere appreciation to Professor E. P. Ney for his continued encouragement and interest in this work; to John Linsley and Leland Bohl for helpful advice and many stimulating discussions; to the National Science Foundation for providing a fellowship under which this work was done; and to the Office of Naval Research which supports the Minnesota cosmic ray research program.

Photodisintegration of Carbon-12 by 330-Mev Bremsstrahlung*

SHELDON D. SOFTKY
Radiation Laboratory, Department of Physics, University of California, Berkeley, California
(Received November 17, 1954)

The excitation function for the reaction $C^{12}(\gamma,3\alpha)$ from 330-Mev bremsstrahlung has been measured. Ilford C2 600μ emulsions were irradiated and scanned for three-prong stars which satisfied conservation of momentum for the disintegration. Of the forty-six stars found, none were from quanta bigger than 42 Mev and so an upper limit for the cross section was estimated up to 100 Mev. From this it can be seen that there are no prominent resonances up to 100 Mev other than those already known.

THE reaction $C^{12}(\gamma,3\alpha)$ has been extensively studied for gamma energies below 70 Mev by Telegdi,[1-3] Goward and Wilkins,[4-6] and Millar and Cameron.[7] The present paper describes an experiment on this reaction, using the 330-Mev bremsstrahlung of the Berkeley synchrotron. As in previous experiments with the $(\gamma,3\alpha)$ reaction, nuclear emulsions were exposed directly to the synchrotron beam, developed, and scanned for three-prong stars. Using 600μ thick Ilford C-2 emulsions, a "cold development" procedure was employed which held distortion of the emulsion to a minimum. It was necessary to bleach the exposed plates for two days in hypo to decrease background fog, and even then the maximum usable exposure yielded only about thirty-three stars per cm^2 of exposed emulsion. Ranges of all prongs as well as horizontal projections of angles were measured, and only those stars accepted which conserved linear momentum for the disintegration in the plane normal to the beam. A total of forty-six stars were accepted and an excitation curve was obtained. No stars were found for quanta over 42 Mev, so an upper limit for the cross section above this energy was estimated. A comparison of the measured cross section with that of Goward and Wilkins[6] indicated poor scanning efficiency in this experiment, so the extrapolated upper limits were obtained by normalizing the excitation curve to the cross section of reference 6. The histogram in Fig. 1 represents the measured curve, with numbers of stars shown in each interval; the dotted curve is that of reference 6 obtained from 70-Mev bremsstrahlung.

The estimated upper limits for the cross section (after corrections for losses from the emulsion surfaces) are:

$$\bar{\sigma} \text{ from } 42 \text{ to } 50 \text{ Mev} \leqslant 0.32\times10^{-28} \text{ cm}^2,$$
$$\bar{\sigma} \text{ from } 50 \text{ to } 70 \text{ Mev} \leqslant 0.25\times10^{-28} \text{ cm}^2,$$
$$\bar{\sigma} \text{ from } 70 \text{ to } 100 \text{ Mev} \leqslant 0.49\times10^{-28} \text{ cm}^2.$$

Comparison of these values with the dotted curve of Goward and Wilkins of Fig. 1 based on 1700 stars shows

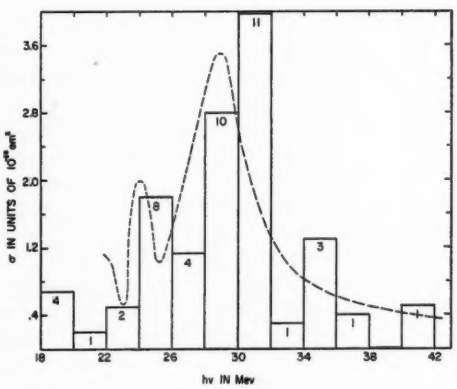

FIG. 1.

that there are no prominent resonances below 100 Mev other than those already known.

I am grateful to Professor A. C. Helmholz for advice and assistance, to the synchrotron crew for the exposures, and to Mr. R. P. Michaelis for development of the plates.

* This work was performed under the auspices of the U. S. Atomic Energy Commission.

[1] Hanni, Telegdi, and Zünti, Helv. Phys. Acta 21, 203 (1948).
[2] V. L. Telegdi and W. Zünti, Helv. Phys. Acta 23, 745 (1950).
[3] V. L. Telegdi and M. Eder, Helv. Phys. Acta 25, 55 (1952).
[4] F. K. Goward and J. J. Wilkins, Proc. Phys. Soc. A64, 201 (1951).
[5] F. K. Goward and J. J. Wilkins, Proc. Phys. Soc. A64, 1056 (1951).
[6] F. K. Goward and J. J. Wilkins, Atomic Energy Research Establishment, Harwell Report G/M 127, 1952 (unpublished).
[7] C. H. Millar and A. G. W. Cameron, Can. J. Phys. 31, 723 (1953).

Relation between Multiple Coulomb Scattering and Residual Range in Nuclear Emulsion*

R. G. GLASSER
Department of Physics, University of Chicago, Chicago, Illinois
(Received July 8, 1954; revised manuscript received October 4, 1954)

Measurements of multiple Coulomb scattering were carried out on 101 artificially produced stopping protons from the end of the track to a point where the residual range was 2500μ. These measurements yield a new relation between range and multiple scattering which can be represented by a power law. The mass dependence was derived theoretically and checked by measuring 20 positive pions. The general relationship is:

$$\langle|\eta|\rangle_{Av}=(19.0\pm0.3)R^{-(0.607\pm0.016)}(M_P/M)^{(0.393\pm0.016)}(t/50)^{\frac{1}{2}},$$

where $\langle|\eta|\rangle_{Av}$ is the mean absolute sagitta due to multiple scattering, R is the range, t the cell length, M is the particle mass, and M_P the mass of the proton. All lengths are measured in microns. This relationship leads to a set of schemes for making scattering measurements on stopping tracks in order to determine the mass of the particle with the maximal efficiency. The precision possible on an individual track is limited, but a sequence of tracks, each of which need not be too long, can give a very satisfactory precision, free from the systematic errors inherent in ionization measurements.

INTRODUCTION

In recent years the attempt to clarify the nature and relationships of the various heavy mesons has assumed great importance. The mass of the heavy mesons themselves is one of the important experimentally definable parameters of the particles, and methods for determining this in photographic emulsions are receiving renewed interest at the present time. These techniques had been somewhat neglected ever since the artificial production of pions made possible more powerful techniques for determining the mass of both pions and muons by combining the photographic emulsion with other instruments. The techniques applicable in emulsion normally use the range as one parameter in the two-parameter system needed to specify the particle mass. The other parameter used is then either ionization, measured by photometric track density, gap number density or gap length density, or multiple Coulomb-scattering. The latter method may not be capable of giving as precise statistical information on individual tracks as some of the others, but it has the advantage that it is free from some of the systematic errors due to plate condition and processing techniques that are often inherent in the ionization measurements. Corrections for these effects involving the making of careful calibrations on each individual plate and even on each region of the plate can sometimes be made. The number of cases of the new particles are few enough, and the number of postulated particles involved are numerous enough, to make desirable as many independent measurements on each track as possible.

The method of multiple scattering has received extensive theoretical[1–9] and experimental[5,10–16] treatment as a means of momentum determination, with special relevance to fast tracks. Some measurements have been made on slow tracks,[17] but the information obtained is for only a limited velocity range, and the measurements do not easily lend themselves to accurate mass determination. Bose and Choudhuri[18] used scattering measurements to distinguish mesons from protons. Lattimore used the range-scattering method for quantitative mass determination of pions.[19] More recently Biswas, George, and Peters[20] and Dilworth, Goldsack, and Hirschberg[21] have proposed a scattering scheme for mass determination, using available range-energy relations and the theoretical law of multiple scattering. It is of interest to check the validity of scattering formulas as applied to tracks of stopping particles. This investigation was undertaken to determine directly the range-scattering relation for stopping particles, with special reference to particles in the heavy meson and hyperon mass ranges.

Artificially accelerated protons provided a means of unambiguously identifying the particles without con-

* Supported in part by a joint program of the Office of Naval Research and the U. S. Atomic Energy Commission.

[1] B. Rossi and K. Greisen, Revs. Modern Phys. **13**, 241 (1941) contains also references to earlier work.

[2] G. Molière, Z. Naturforsch. **3a**, 78 (1948).

[3] H. S. Snyder and W. T. Scott, Phys. Rev. **76**, 220 (1949); **78**, 223 (1950).

[4] W. T. Scott, Phys. Rev. **85**, 245 (1952).

[5] Martin J. Berger, Phys. Rev. **88**, 59 (1952).

[6] B. D'Espagnat, J. phys. et radium **13**, 74 (1952).

[7] R. Mertens, Compt. rend. **236**, 1753 (1953).

[8] H. A. Bethe, Phys. Rev. **89**, 1256 (1953).

[9] E. P. Wigner, Phys. Rev. **94**, 17 (1954).

[10] Goldschmidt-Clermont, King, Muirhead, and Ritson, Proc. Phys. Soc. (London) **A61**, 183 (1948).

[11] Y. Goldschmidt-Clermont, Nuovo cimento **7**, 331 (1950).

[12] P. H. Fowler, Phil. Mag. **41**, 169, 413 (1950).

[13] L. Voyvodic and E. Pickup, Phys. Rev. **81**, 471, 890 (1951); **85**, 91 (1952).

[14] Gottstein, Menon, Mulvey, O'Ceallaigh, and Rochat, Phil. Mag. **42**, 708 (1951).

[15] I. B. McDiarmid, Phys. Rev. **84**, 851 (1951).

[16] W. Bosley and H. Muirhead, Phil. Mag. **43**, 63 (1952).

[17] M. G. K. Menon and O. Rochat, Phil. Mag. **42**, 1232 (1951).

[18] D. M. Bose and B. Choudhuri, Nature **147**, 240 (1941).

[19] S. Lattimore, Nature **161**, 5181 (1948).

[20] Biswas, George, and Peters, Proc. Indian Acad. Sci. **38**, 418 (1953).

[21] Dilworth, Goldsack, and Hirschberg, Nuovo cimento **11**, 113 (1954).

fusion with other particles, such as deuterons, tritons, and α particles. This condition can only be attained with difficulty in cosmic ray plates with the large number of particles necessary. The positive pions were identified by their decay into muons of definite range. This could also be done in cosmic ray plates, but the probability of having all particles in the plate and the pions still nearly parallel to the surface of the plate is very small. The range-scattering relation was obtained to an accuracy consistent with its possible use in multiple scattering measurements for mass determination. Beyond the points checked by this experiment, the velocity of the particles is high enough that one should be able to reliably use range-energy relationships and the multiple scattering relationships which are well established to extend the measurements to longer tracks.

The relationship thus established can be most effectively used by extracting the maximum information about the multiple scattering from each track. This can be done most effectively by a method of varying the cell-length, so as to make the mathematical expectation of the sagitta the same in all cells. This allows a great increase in the number of cells over the number obtainable by using constant cell lengths. Even with this refinement, the errors involved in a mass measurement on an individual track are comparatively large; however, applied to a small group of tracks, whose lengths need not be excessively long, a very reliable mass estimate can be obtained which is independent of the estimates which include the inherent uncertainties in ionization measurements.

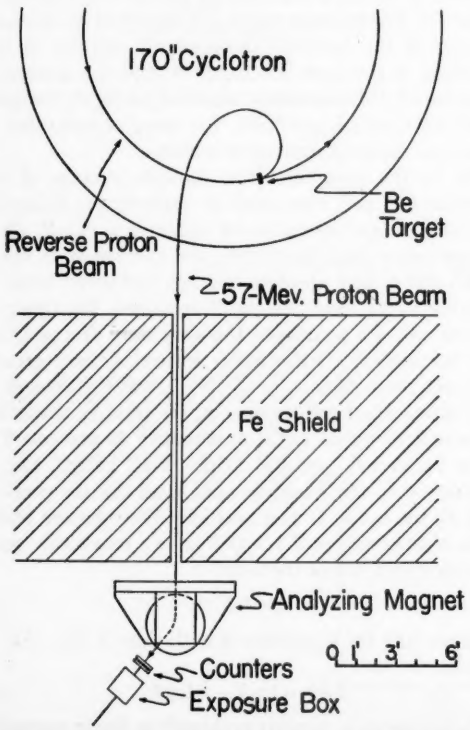

FIG. 1. Schematic drawing of arrangement for exposing plates to 57-Mev protons. Counters and plates not to same scale as cyclotron.

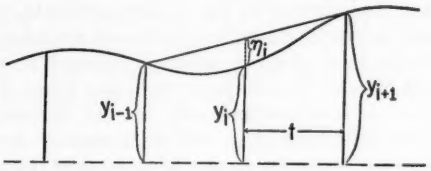

FIG. 2. Projection of a track on the plane of the emulsion. y is the coordinate measured. η is the sagitta, t is the cell length.

EXPERIMENTAL PROCEDURE TO DETERMINE THE SCATTERING RELATION

Protons, scattered off the beryllium target in the beam of the University of Chicago 460-Mev synchrocyclotron were bent first in the fringing field of the cyclotron and then in a "steering" magnet with the current adjusted so that it corresponded to a proton energy of 57 Mev, in an arrangement first attempted by Fermi, Sugarman, and Haber (see Fig. 1).[22] The beam then entered the 600-micron Ilford G-5 emulsion where many of the protons stopped. Since the identity of the particles was uniquely determined by looking for particles which stopped in a region of the emulsion which corresponds to the range of protons of the momentum given by the magnetic field, it was possible to pick out protons unambiguously.

Measurements of multiple Coulomb scattering were carried out on 101 of these protons which stopped in the emulsion and which had a projected length in the emulsion of more than 3000 microns. This criterion for the measured proton tracks does not bias the results, since the scattering in the plane perpendicular to the plate is independent of the scattering in the plane parallel to the plate; only the former can affect the probability of the particle scattering out of the emulsion, while only the latter is measured in this experiment.

For the purpose of establishing accurately the relation between range and multiple scattering, the multiple scattering was measured with a constant cell length, chosen to be 50 microns, which is a cell length such that the scattering all along the track is significantly above noise along the total measured length. The measurements were made from the stopping end of the proton track, back for a distance of 2500 microns. These measurements by the coordinate method were made on the precision scattering stage of Professor Schein's laboratory, which has been used and described previously.[5,23] Figure 2 shows a drawing representing the projection of a section of a track on the plane of the

[22] Fermi, Sugarman, and Haber, University of Chicago, Institute for Nuclear Studies Accelerator Progress Report, 1953 (unpublished).

[23] Lord, Fainberg, and Schein, Phys. Rev. 80, 970 (1950).

emulsion. As indicated in Fig. 2, the coordinate, y_i, of the track perpendicular to the direction of motion of the stage in the plane of the emulsion, is measured at equal intervals of cells. To eliminate the linear trend of the track, which is determined only by the direction in which the plate is lined up, and get a number characteristic of the scattering alone, the sagittae of the track in successive cells,

$$\eta_i = y_i - \tfrac{1}{2}(y_{i-1} + y_{i+1}), \tag{1}$$

were obtained. From these data it was possible to obtain the correct empirical multiple scattering law for protons, as will be explained later.

To get a check on the mass dependence, similar measurements were carried out for positive pions. These were produced in the 46-Mev positive pion beam of the University of Chicago synchrocyclotron and were unambiguously identifiable as pions by the fact that each had a muon of range 600 ± 30 microns coming from its stopping, with an electron from the end of the muon track. Since these were to be used only as a check on the predicted mass dependence of the new scattering law, 20 pions gave sufficient statistical accuracy. Because pions have less kinetic energy at a given residual range and hence scatter more at the same range than protons, a cell length of only 30 microns was used for these pions compared to the cell length of 50 microns for protons.

We may define the noise as the apparent residual scattering measured, in the absence of any true Coulomb scattering. It is mostly due to error in determination of the actual position of the path of the particle, due to the fluctuations in the position of the grains of the emulsion. For most of the range of the measurements, the true scattering was very large compared with the noise-level. The noise on these tracks was measured by using a very short cell length, 10 microns, such that after a distance of 250 microns from the end of the track the actual scattering in this distance became negligible, and the measurements gave only an estimate of the spurious contributions, which are the noise. The noise level estimate thus obtained was $\langle|\eta_{\text{noise}}|\rangle_{Av} = 0.09\mu$, as compared with 0.10μ obtained by measuring tracks of particles of such high energy that no true scatter was detectable. It is reasonable to have a lower value for these slow tracks, since the greater grain density means that more information is available to set the position of the microscope filar by. Hence, the value of 0.09μ was adopted and used as a correction for noise.

In all these measurements it was decided to ignore any effect such as the changing dip and inclination of the track to the direction of motion of the stage. The dip angle was necessarily less than 6° and the inclination of the track direction to the direction of motion of the stage was held under 20° at all points. Any variation within this limit was accepted as something to be averaged into all tracks, both those used in determining the range and those whose masses are to be measured by this means, so that any systematic error should automatically cancel out.

ANALYSIS OF THE DATA

In general, the true range-energy relation cannot be exactly represented by any simple analytic expression. In a limited region of ranges and energies it can be represented for a given particle in the form

$$E = kR^{-n}, \tag{2}$$

where E is the energy, R the range, and k an empirical constant. In a region where the nonrelativistic approximation momentum × velocity $= 2E$ is valid, the multiple scattering relation verified at higher energies can be represented for a given particle and a given cell length by

$$\langle|\eta|\rangle_{Av} = lE^{-1}, \tag{3}$$

where l is the sagitta of the track and l is approximately constant. Then the direct scattering-range relation is obtained in the form

$$\langle|\eta|\rangle_{Av} = KR^{-n}, \tag{4}$$

where K is a new constant. A relation of the same form as (4) may be approximately valid for slow particles even though some of the assumptions used in deriving it may not be exactly correct. For this reason it was decided to try to fit the data for the protons to such an equation. For protons and a cell length of 50 microns, the use of the accepted range energy relation in G-5 emulsion in the form $R = 10.6E^{1.68}$, and the scattering constant of 25.0 commonly accepted at higher energies, leads to $K = 15.7$, $n = 0.595$, for energies measured in Mev and ranges measured in microns.

To fit the data, first the absolute average of the sagittae (η_i) was computed at each range. Following the well-known procedure for applying a cutoff, those values larger than four times the average were eliminated and a new absolute average computed until no sagittae larger than the cutoff remained. By this procedure only 1.5 percent of the data were dropped, but the fluctuations in the mean scattering were greatly reduced. Since each value of $\langle|\eta_i|\rangle_{Av}$ was the average of 101 independent measurements, the relative statistical error of each value was approximately 10 percent. The noise correction was also made to all values. Let us denote by x_i the quantity $\langle|\eta_i|\rangle_{Av}$ at the ith position and R_i the range at this position. Then we are trying to fit a set of values of x_i which have a reasonably great precision to a law of the form

$$x_i = KR_i^{-n}. \tag{5}$$

If we take the logarithm of both sides in Eq. (5), we obtain

$$\log x_i = \log K - n \log R_i. \tag{6}$$

This represents a familiar problem[24] in linear regression

[24] Harold Cramér, *Mathematical Methods of Statistics* (Princeton University Press, Princeton, 1946), p. 548.

of $\log x_i$ on $\log R_i$. Since the distribution of $\log x_i$ is a rather complicated one, the exact solution is difficult. However, for our purposes this distribution can be approximated well enough by a normal or Gaussian distribution if the distribution of x_i is narrow enough. One has

$$\log x_i = \log E(x_i) + \frac{\log e}{E(x_i)}[x_i - E(x_i)] - \frac{\log e}{2E^2(x_i)}[x_i - E(x_i)]^2 + \cdots, \quad (7)$$

where $E(x)$ represents the mathematical expectation of x. Then

$$E(\log x_i) = \log E(x_i) - \frac{\log e}{2E^2(x_i)} E([x_i - E(x_i)]^2) + \cdots. \quad (8)$$

The second term on the right side of (8) represents a shift in the $\log x_i$ axis of all points by 0.00123 (as computed from the experimental data) which represents the multiplication of all values of x_i by 1.003. A correction for this will be made but all higher terms will be still smaller and hence can be disregarded. From (7) the following relation can be derived:

$$E([\log x_i - E(\log x_i)]^2) = \frac{\log^2 e}{E^2(x_i)} E([x_i - E(x_i)]^2) + \cdots. \quad (9)$$

Relations (8) and (9) will be used later.

Under the assumption that $\log x_i$ is approximately normally distributed, one can then try to fit the data to a law of the form (6), by the method of least squares.[25] The result of this fitting gives

$$\log x_i = 1.275 - 0.607 \log R_i, \quad (10)$$

which by the use of (8) is equivalent to

$$\langle |\eta_i| \rangle_{Av} = 18.9 R_i^{-0.607}, \quad (11)$$

or, if one keeps in mind the correction factor of 1.003 for the second term in (8) mentioned above, the constant becomes 19.0. We can estimate the errors in the coefficient in (10) by the well known estimates for the linear regression problem, as given by Cramér[24]:

$$s(1.275) = \sigma^* N^{-\frac{1}{2}},$$

$$s(0.607) = \sigma^* N L^{-\frac{1}{2}},$$

$$\sigma^{*2} = \frac{1}{N-2} \sum_{i=1}^{N} (\langle \log x_i \rangle_{Av} - 1.275 + 0.607 \log R_i)^2, \quad (12)$$

$$L = \frac{1}{N} \sum_{i=1}^{N} (\log R_i - \langle \log R_i \rangle_{Av})^2,$$

where $s(x)$ is the estimate of the standard deviation in the quantity represented by x. We get from this that the proton range-scattering relation can be expressed in the form

$$\langle |\eta_i| \rangle_{Av} = (19.0 \pm 0.3) R_i^{-(0.607 \pm 0.016)}. \quad (13)$$

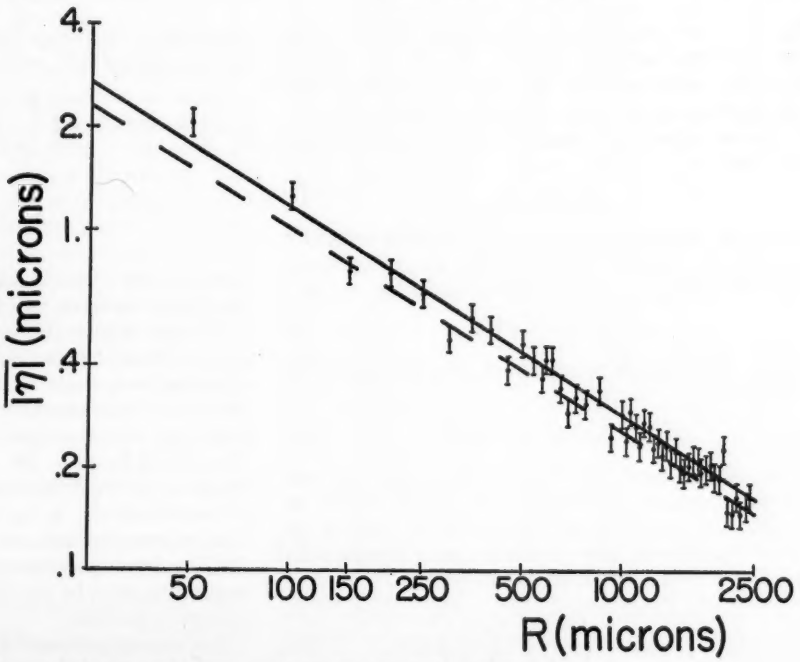

FIG. 3. Scattering *vs* range for protons. Cell length is 50μ. Each point represents the average of 101 measurements. Full curve is the new range-scattering relation. Dashed curve is the old semi-theoretical relation. Errors shown are only the statistical errors.

[25] P. G. Hoel, *Introduction to Mathematical Statistics* (John Wiley and Sons, New York, Inc., 1947), p. 78.

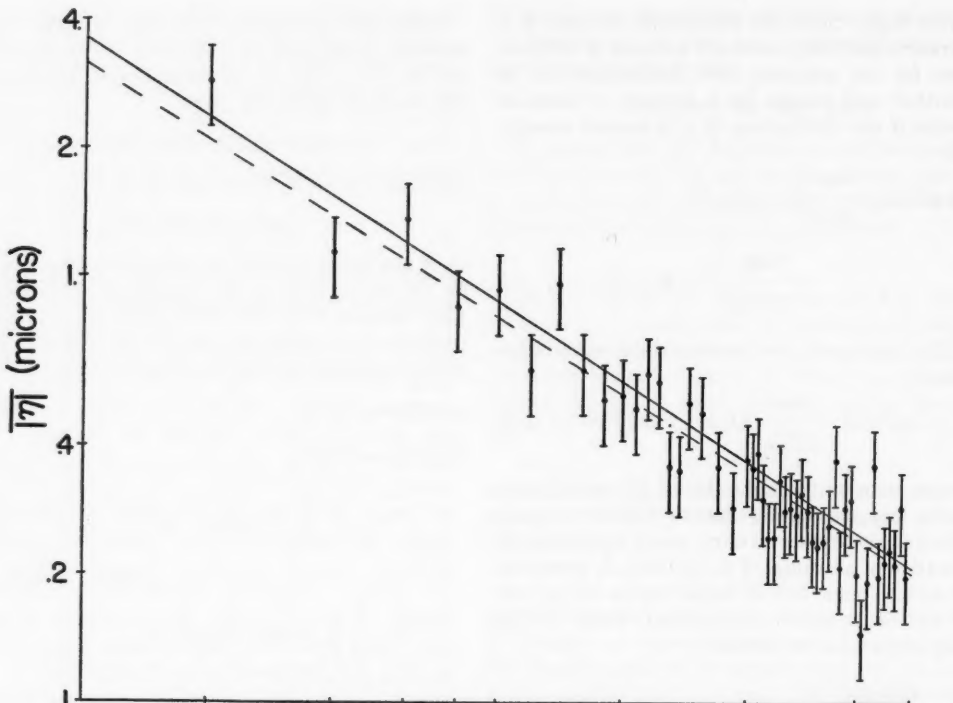

FIG. 4. Scattering *vs* range for pions. Cell length is 30μ. Each point represents the average of 20 measurements. Full curve is the new relation. Dashed curve is the old relation. Errors shown are only the statistical errors.

In Fig. 3 are shown the proton sagittae at each range, the curve obtained from the new relation (13), and the old curve obtained from the equation resulting from the argument given at the beginning of this section.

We can express the general range energy relation in the form

$$R=Mf(v), \tag{14}$$

where $f(v)$ is a function only of the particle velocity v, and M is the mass of the particle. The scattering relation can be expressed to a good approximation in the form

$$\langle|\eta|\rangle_{Av}=g(v)t^{\frac{1}{2}}/M, \tag{15}$$

where $g(v)$ is another function of velocity alone. Then we have

$$\langle|\eta|\rangle_{Av}=M^{-1}t^{\frac{1}{2}}k(R/M), \tag{16}$$

from the two preceding relations. If, as we have seen, we can represent the relation for protons with a 50-micron cell length by an equation of the form of (4), we will have for the general relation, since the functional form of $k(x)$ is determined by this relation:

$$\langle|\eta|\rangle_{Av}=K\left(\frac{M_P}{M}\right)^{1-n}\left(\frac{t}{50}\right)^{\frac{1}{2}}R^{-n}, \tag{17}$$

where M_P is the proton mass. Inserting the values of K and n given by (13), we have

$$\langle|\eta|\rangle_{Av}=(19.0\pm0.3)\left(\frac{M_P}{M}\right)^{(0.393\pm0.016)}\times\left(\frac{t}{50}\right)^{\frac{1}{2}}R^{-(0.607\pm0.016)}. \tag{18}$$

Formula (18) then should represent, for a given mass, the relation between range and multiple scattering.

The first of Eqs. (12) gives an estimate of the standard deviation of $\log x_i$. Equation (9) gives the relation of this estimate to the relative deviation of x_i (standard deviation of x_i divided by the expectation of x_i). From these two values we get the relative deviation 0.097. Since this is based on 101 measurements at each point, the estimate of the relative deviation of $\langle|\eta|\rangle_{Av}$, based on N measurements, is $(\sqrt{101})\times0.097/\sqrt{N}=0.98/\sqrt{N}$. This estimate includes any effect due to correlation of the successive measurements on a given track and is larger than given by treating the η_i as statistically independent quantities.

The mass dependence of Eq. (18) was checked by the measurements on the pions. The data were treated in

the same way as for the proton measurements to obtain the sagittae. Figure 4 shows the pion points, the curve predicted by (18) and the curve predicted by the use of the range-energy relation and an extrapolation of the usual multiple scattering law. The fit of the curve obtained from (18) was tested by the method of least squares, and a χ^2 value (M value) of 41 was obtained. If the fit were perfect, a χ^2 value of 49 with a standard deviation of 7 would be expected, so that the fit is very good. Another way of demonstrating that the mass dependence predicted is correct is to determine the mass of the pion from these measurements. The mass ratio of the pion to the proton yielded a value of 0.147 $\pm$0.012, in excellent agreement with the established value of 0.149.[26]

CONSTANT SAGITTA METHOD

Constant cell-length measurements, as used in the establishment of the multiple scattering-range relation will not give as much information from a given track as will the constant sagitta method of varying the cell length. In this method the cell length is varied in such a manner that the expected sagitta due to scattering is in every cell the same. As can be seen from Eq. (18) the relation $t=\text{const}\times R^{0.405}$ will accomplish this, where the constant is chosen to give the desired cell length. The measurement was started at a point of the track such that $R=t_0$, where t_0 is the initial cell length. That is, the cell length-range relation is used in the form

$$t=t_0(R/t_0)^{0.405}, \tag{19}$$

where t_0 is the initial cell size and the first cell begins at a distance t_0 from the end of the track.

To determine the optimum cell size a statistical analysis was made of the error as a function of cell length. The limiting factor in the precision of measurement is the sagitta due to noise, that is, the contribution when the effect due to true scattering is negligible. It was assumed for the purposes of this computation that both noise and true scattering distributions can be represented by independent Gaussian distributions. The non-Gaussian character of the distribution should produce errors which will be negligible compared to the statistical errors involved. It then turns out that, just as for fast tracks, the optimum cell size is that for which $\langle|\eta|\rangle_{Av}=(\sqrt{6})\langle|\eta_{\text{noise}}|\rangle_{Av}$, where η is the correct sagitta (due to true scattering plus noise) and η_{noise} is the sagitta due to just noise (as determined in this experiment). From (18) and (19) we get for the true scattering

$$\langle|\eta|\rangle_{Av}=0.0535(M_P/M)^{0.393}t_0^{0.893}, \tag{20}$$

or, since $\langle|\eta_{\text{noise}}|\rangle_{Av}=0.09\mu$,

$$t_0=4.4(M/M_P)^{0.44}. \tag{21}$$

For protons, formula (21) gives 4.4μ; for pions, 1.9μ; and for a particle of mass $1000m_e$, 3.4μ as the optimum

[26] Smith, Birnbaum, and Barkas, Phys. Rev. **91**, 765 (1953).

TABLE I. Ranges at which measurements are to be made for constant sagitta measurements and the mass estimates based on these measurements.

1. Initial cell length (t_0) $=8\mu$

8.0	189.1	550.0	1059.4	1699.3	2458.7	3330.7
16.0	217.9	594.4	1118.3	1769.9	2541.0	3423.9
26.6	248.4	640.2	1178.5	1841.7	2624.4	3518.1
39.6	280.6	687.4	1239.1	1914.7	2708.9	3613.4
54.9	314.5	736.1	1301.0	1988.9	2794.5	3709.8
72.4	350.0	786.2	1364.2	2064.3	2881.2	3807.3
92.0	387.0	837.7	1428.7	2140.9	2968.9	3905.9
113.5	425.5	890.8	1494.5	2218.6	3057.7	4005.7
136.9	465.5	945.5	1561.6	2297.5	3147.6	
162.1	507.0	1001.8	1629.9	2377.5	3238.6	

$M/M_P=(0.344/\langle|\eta|\rangle_{Av})^{2.54}$

2. Initial cell length (t_0) $=5\mu$

5.0	175.2	522.1	1010.0	1622.3	2347.9	3179.5
10.0	196.3	544.9	1052.9	1674.2	2408.2	3247.7
16.6	218.4	588.5	1096.5	1726.8	2469.1	3316.5
24.8	241.4	622.9	1140.8	1780.0	2530.6	3385.8
34.3	265.4	658.1	1185.8	1833.9	2592.7	3455.7
45.2	290.3	694.1	1231.5	1888.4	2655.5	3526.2
57.4	316.2	730.9	1277.9	1943.6	2718.9	3597.3
70.8	343.0	768.5	1325.0	1999.4	2782.9	3668.9
85.4	370.7	806.9	1372.8	2055.9	2847.5	3741.1
101.2	399.3	846.0	1421.3	2113.0	2912.7	3813.9
118.1	428.7	885.9	1470.5	2170.8	2978.5	3887.3
136.1	459.0	926.5	1520.4	2229.2	3044.9	3961.2
155.1	490.1	967.9	1571.0	2288.2	3111.9	

$M/M_P=(0.226/\langle|\eta|\rangle_{Av})^{2.54}$

3. Initial cell length (t_0) $=4\mu$

4.0	174.5	527.7	1026.0	1650.5	2391.1	3229.0
8.0	193.0	556.7	1063.8	1696.3	2444.4	3289.2
13.3	212.3	586.3	1102.1	1742.7	2498.2	3349.8
19.8	232.3	616.5	1141.0	1789.6	2552.4	3410.9
27.4	253.1	647.3	1180.5	1837.0	2607.1	3472.4
36.1	274.6	678.7	1220.6	1884.9	2662.3	3534.4
45.8	296.8	710.7	1261.2	1933.3	2717.9	3596.8
56.5	319.7	743.4	1302.4	1982.2	2764.0	3659.7
68.2	343.4	776.7	1344.1	2031.6	2820.5	3723.0
80.8	367.7	810.6	1386.3	2081.5	2877.5	3786.8
94.3	392.7	845.1	1429.0	2131.9	2934.9	3851.0
108.7	418.4	880.1	1472.3	2182.8	2992.8	3915.7
123.9	444.7	915.7	1516.1	2234.2	3051.2	3980.8
139.9	471.7	951.9	1560.4	2286.0	3110.0	
156.8	499.4	988.7	1605.2	2338.3	3169.3	

$M/M_P=(0.185/\langle|\eta|\rangle_{Av})^{2.54}$

4. Initial cell length (t_0) $=3\mu$

3.0	174.7	532.7	1038.8	1674.4	2428.4	3292.6
6.0	190.2	557.2	1070.8	1713.3	2473.6	3343.7
10.0	206.3	582.1	1103.2	1752.5	2519.1	3395.1
14.8	222.9	607.5	1136.0	1792.1	2565.0	3446.9
20.6	240.1	633.3	1169.2	1832.1	2611.2	3499.0
27.1	257.8	659.5	1202.8	1872.4	2657.7	3551.4
34.4	276.0	686.2	1236.8	1913.1	2704.6	3604.1
42.5	294.7	713.3	1271.2	1954.1	2751.8	3657.1
51.3	313.9	740.8	1306.0	1995.5	2799.3	3710.4
60.8	333.6	768.8	1341.2	2037.2	2847.2	3764.0
71.0	353.8	797.2	1376.7	2079.3	2895.4	3818.0
81.8	374.5	826.0	1412.6	2121.7	2943.9	3872.3
93.3	395.7	855.2	1448.9	2164.5	2992.7	3926.9
105.4	417.4	884.8	1485.6	2207.6	3041.9	3981.8
118.1	439.5	914.8	1522.6	2251.1	3091.4	
131.4	462.1	945.2	1560.0	2294.9	3141.2	
145.3	485.2	976.0	1597.8	2339.1	3191.3	
159.7	508.7	1007.2	1635.9	2383.6	3241.8	

$M/M_P=(0.146/\langle|\eta|\rangle_{Av})^{2.54}$

TABLE II.

Particle	Track length used	t_0[a]	No. of cells	Mass (units m_e)
Chicago τ	1040μ	4μ	48	850±400
Brookhaven K^- (1)	2400	3	106	1350±400
	2400	4	93	1350±400
	2400	8	45	1400±500
Brookhaven K^- (2)	3700	3	115	1250±350
	3800	5	86	1000±300
Brookhaven K^+	3300	4	90	1050±300

[a] In the table, t_0 is the initial cell used as explained in the text. The Brookhaven particles referred to were kindly lent to the author by J. Hornbostel and E. O. Salant of Brookhaven National Laboratories [Phys. Rev. 93, 902 (1954)]. These authors quote mass values for K^-(1) of 1050±150, 1200±300, and 1080±220 from gap-length *vs* range, scattering *vs* range, and magnetic rigidity *vs* range. Hill, Salant, and Widgoff also give mass values for some Brookhaven particles in a later article [Phys. Rev. 95, 1699 (1954)].

value of t_0. Table I gives a set of values of ranges at which measurements should be made for the first 4000μ of a constant sagitta scheme following Eq. (19) for $t_0=3$, 4, 5, and 8μ.

Application of the method to mass determination on heavy mesons studied in this laboratory is in progress. Some of the mass values obtained are shown in Table II.

Other schemes for constant sagitta measurement which have been proposed, such as those of the Bombay[20] and Brussels[21] groups, have been based on reasoning similar to that following Eq. (4). They give a different dependence of cell length on range for constant sagitta. The difference is not large but may introduce a significant bias into measurements on groups of tracks of various lengths.

CONCLUSION

A new range-multiple scattering relationship in photographic emulsion has been determined which has a precision adequate for use in mass measurements on stopping particles. The scattering at low energies increases beyond the amount predicted by use of a constant scattering factor. We define the scattering factor as

$$\frac{180}{\pi}\frac{p\beta\langle|\eta|\rangle_{Av}}{t^{\frac{1}{2}}}.$$

If one assumes the range-energy relation represented by $R=10.6E^{1.68}$, as in the first paragraph of the section on "Analysis of the Data," then the scattering factor would increase with decreasing energy and would be about 28 at 18 Mev and approach 30 at very low energies. At the lower energies second order effects, such as the increase in path length due to scattering in a given cell and due to an inclination of the track to the average direction (which determines the position of the base line), certainly affect the value of the scattering factor. An additional factor which must be considered is the question whether the present theories correctly estimate the cross section for single scattering at low energies. The numerical estimate which can be made on the basis of the various theories does not seem to account correctly for the increase in the scattering factor. The fact that the cause of this increase is not understood is, of course, irrelevant to the use of the relation established here for mass measurement.

The precision which can be given by use of a scattering measurement has previously been slightly overestimated by using idealized models to represent the statistical situation. The main contribution to the increased variance in a scattering measurement over that predicted by the simple models is the correlation between successive values of η because they contain a common scattering. There is also some contribution from the non-Gaussian character of the distribution, although most of this is removed through applying the cutoff.

The formulation given in this paper allows one to make mass measurements of reasonable precision, even on the comparatively short tracks which are very common and very hard to deal with. On a long track, as frequently observed in pellicle stacks, it enables one to increase the precision of the measurement since the slower a track is the more information is contained in its scattering per unit length. The precision resulting from various numbers of cells and the corresponding track length are given in Table III.

TABLE III. Percentage statistical error in mass measurements based on multiple scattering on stopping tracks of mass $M=1000m_e$.

Available range (microns)	No. of cells	Error on one track	Error on 25 tracks
1000	45	45%	8.9%
3000	81	33%	6.7%
6000	131	26%	5.3%
10 000	178	23%	4.5%
50 000	350	14%	3.0%

ACKNOWLEDGMENTS

The author wishes to express his primary gratitude to Professor Marcel Schein whose constant support and advice made this work possible. Thanks are also due Dr. Theodore Bowen and Mr. David Haskin for their aid in the cyclotron exposure and the latter for the development of the plates. Mr. David Williams and Mr. Edgar Waehrer did some of the computations. Dr. Salant and Dr. Hornbostel were very gracious in lending plates containing artificially produced K mesons. Professor H. L. Anderson and Mr. L. Kornblith are to be thanked for making the cyclotron available.

Note added in proof.—C. C. Dilworth [Nuovo cimento 11, 203 (1954) discusses the constant sagitta method as used by various groups and compares its effectiveness as estimated by the various authors with other methods.

Infrared Divergence in Bound State Problems

F. ROHRLICH
Department of Physics, State University of Iowa, Iowa City, Iowa
(Received December 20, 1954)

The proof, in the iteration solution, that all infrared divergences exactly cancel for all physical processes and to all orders in the coupling constant, leads to apparent difficulties in bound state problems. These difficulties are resolved.

IN a recent paper by Jauch and the author[1] a proof was presented concerning the cancellation of all infrared divergences in physically meaningful expressions. This cancellation was shown to hold for all types or processes in quantum electrodynamics and to all orders in the coupling constant. Part of the proof consisted in a calculation in the interaction picture which lends itself to a simple physical interpretation of the details of this cancellation. However, when the same physical picture is used for certain bound state problems, the argument seems to fail. This leads to a contradiction, since the infrared divergences must clearly cancel also in bound state problems. In fact, the proof could have been carried out in the bound interaction picture, since a transformation from this picture to the free interaction picture cannot introduce infrared divergences.[2]

THE PROBLEM

In order to exhibit the difficulty clearly, it is sufficient to consider a typical case, *viz.*, the radiative corrections to the two-photon annihilation of positronium. As is well known, this annihilation can take place only from states of even charge-parity. Furthermore, these same states cannot decay into three photons because of conservation of parity.

But, as was shown in IRD, radiative corrections always give rise to infrared divergences and these are always exactly canceled by soft photon emission in addition to the original process. Applied to our case, this would mean that the radiative corrections to two-photons annihilation are infrared divergent, and that these divergences are exactly canceled by the annihilation into three photons, one of which is very soft. But since the latter process is forbidden by selection rules, this infrared divergence seems to remain uncompensated.

Similar difficulties arise with the compensation of the radiative corrections of three-photon annihilation by four-photon annihilation including one very soft photon, etc.

Clearly, there is no difficulty in pair annihilation in flight, since then the parity is not a good quantum number and no such selection rules arise.

[1] J. M. Jauch and F. Rohrlich, Helv. Phys. Acta 27, 613 (1954). This paper will be quoted as IRD.

[2] In this connection it must be noted that convergence problems of the iteration solution are here irrelevant, since the proof must hold in each power of α separately.

THE SOLUTION

The soft photon emission gives rise to a divergence which can be expressed as a factor b multiplying the original transition probability [see IRD, Eq. (5)],

$$b=\frac{e^2}{(2\pi)^3}\sum\int\frac{d^3k}{2\omega}\left|\frac{p\cdot e}{p\cdot k}-\frac{p'\cdot e}{p'\cdot k}\right|^2, \tag{1}$$

where p and p' are the initial and final momenta of the emitting electron path, and the summation is to be carried out over the two *transverse* polarization directions of the emitted soft photon.

The divergence in b is exactly canceled by the term

$$r=2(\rho_1+\rho_2), \tag{2}$$

which arises from the radiative corrections. One finds [see IRD Eqs. (12) and (20)]:

$$\rho_1=-\frac{i\alpha}{4\pi^3}\sum\int\frac{p'\cdot e p\cdot e}{(p'\cdot k)(p\cdot k)}\frac{d^4k}{k^2} \tag{3}$$

and

$$\rho_2=-\frac{\alpha}{\pi}\int\frac{d\omega}{\omega}. \tag{4}$$

In Eq. (3), the summation is to be carried out over all polarization directions of the virtual photon, i.e., over transverse, longitudinal, and scalar photons.

Consider now the nonrelativistic limit of the process in question. If p refers to a negaton and p' to a positon, this limit is exactly the lowest order approximation of a positronium annihilation process. The corresponding state vector of the initial state can be regarded as the first term in an expansion of the exact state vector in free particle states.

In this limit b vanishes, so that r cannot contain contributions from *transverse* photons. That this is indeed the case follows easily from Eq. (3). In the limit only the longitudinal and scalar photons contribute to the sum and yield

$$\lim\rho_1=-\frac{\alpha}{\pi}\int\frac{d\omega}{\omega},$$

which exactly cancels ρ_2. We conclude that the infrared divergences which arise from longitudinal and scalar virtual photons in the radiative corrections always cancel *within* r.

It follows, therefore, that the description of positronium in terms of the bound interaction picture, but without radiative corrections, does not involve infrared divergences, since the Coulomb wave functions take the place of the nontransverse photons.

In this picture, the radiative corrections to positronium annihilation can only involve transverse photons. These correspond to retardation effects, and they do not give rise to infrared divergences as a whole.

These arguments show that the absence of the term b because of selection rules is not only *possible* without affecting the correct cancellation of the divergences, but is indeed necessary. There is thus no further contradiction.

It should be remarked that the vanishing of b in the nonrelativistic limit is well known in the three-photon decay of positronium. The cross section for this process *vanishes* when the energy of one of the photons approaches zero. This fact, in turn, may seem to be in contradiction with the substitution law, according to which the matrix elements of the double Compton effect and of three-photon annihilation differ only in the meaning of the momentum four-vectors involved. The cross section for the double Compton effect is known to show an *infrared divergence* when one of the emitted photons vanishes. However, this apparent contradiction is also easily resolved when one observes that, although the matrix elements of these two processes are related by the substitution law, the corresponding cross sections differ in their densities of final states which accounts for the difference.

Finally, a word may be added about bound state problems involving external fields. These take a position in a certain sense intermediate between the scattering problem described by the iteration solution and the positronium problems discussed above. Again, there exist no terms of the type b, but instead of them there occur certain diagrams in the expansion in powers of the external field, which may be called higher Born approximations, and which contain infrared divergences. These again exactly cancel the divergences arising from radiative corrections. Examples of this situation are known in calculations of level shifts in electrostatic and magnetostatic fields. The proof of the exact cancellation of infrared divergences in external field problems follows from the proof given in IRD and the remark that external fields are classical limits of quantized fields; external field problems can thus be regarded as special cases of problems involving the interaction of quantized fields only.[3]

I would like to thank Professor L. M. Brown for an interesting discussion, in which he convinced me that some of the implications of the IRD paper are not obvious.

[3] Methods of computation can be devised which differ from the usual Born expansions in external field problems and which avoid the appearance of infrared divergences. The existence of such methods may be thought of as explicit proof of the spurious character of these divergences and their eventual disappearance in the final expressions for these problems, no matter which methods are adopted. Compare R. G. Newton, Phys. Rev. **96**, 523 (1954).

Variational Principle for Scattering with Tensor Forces*

S. I. RUBINOW†
Physics Department, Massachusetts Institute of Technology, Cambridge, Massachusetts
(Received October 4, 1954)

A reformulation of the variational principle in differential form for the phase shift δ_l of a central-force scattering problem is presented. This is considered to be the most simple that can be formed in terms of the inside-wave function representing the difference between the wave function and an appropriately chosen asymptotic form. It is then generalized by means of matrix notation so as to provide corresponding variational principles for the three parameters that arise in scattering with tensor forces, the two phase shifts δ_α, δ_β and the mixture parameter ϵ. These all develop from the differential formulation of Schrödinger's equation and do not depend on the integral equation formulation as does the one originally presented by Schwinger for the phases δ_α and δ_β, and the extension of it by Blatt and Biedenharn to the parameter ϵ.

INTRODUCTION

THE variational principle for the phase shift in scattering problems based upon the integral equation formulation of Schrödinger's equation was first given by Schwinger.[1] This could be applied to problems with either central forces,[2] or tensor forces.[3] Recently, Biedenharn and Blatt[4] have shown how the principle may be extended so as to be applicable to the mixture parameter that arises in the latter case.

Both Schwinger[5] and Hulthén[6] have also introduced variational principles for the phase shift which are based on Schrödinger's equation in differential form with central forces. These are often more feasible for numerical computation than the integral equation formulation, and have in fact been improved upon in recent years.[7–12] In the present note, we wish to give the analogous extension to tensor forces of this differential formulation of the variational principle. This requires three stationary expressions for the three parameters (two phase shifts plus mixture parameter) that arise in this case. These will be found in Secs. II and III.

Before proceeding to this, we first provide in Sec. I a new formulation of the variational prlnciple for the phase shift which is slightly simpler than ones now in use. The point of view adopted will also help indicate why so many formulations have appeared in the literature. The procedure is then generalized in a natural way to tensor forces with the aid of matrix notation.

* Supported in part by the joint program of the U. S. Atomic Energy Commission and the Office of Naval Research.
† Now at Division of Applied Science, Harvard University, Cambridge, Massachusetts.
[1] J. Schwinger, hectographed notes, Harvard University, 1947 (unpublished).
[2] J. M. Blatt and J. D. Jackson, Phys. Rev. **76**, 18 (1949).
[3] F. Rohrlich and J. Eisenstein, Phys. Rev. **75**, 705 (1949).
[4] J. M. Blatt and L. C. Biedenharn, Phys. Rev. **86**, 399 (1952); L. C. Biedenharn and J. M. Blatt, Phys. Rev. **93**, 1387 (1954).
[5] J. Schwinger, Phys. Rev. **78**, 135 (1950); **72**, 742 (1947).
[6] L. Hulthén, Kgl. Fysiograf. Sällskap. Lund, Förh. **14**, No. 21, 257 (1944); *Den 10. Skandinaviske Matematiker Kongres 1946* (Jul. Gjellerups Vorlag, Copenhagen, 1947), p. 201.
[7] W. Kohn, Phys. Rev. **74**, 1763 (1948).
[8] L. Hulthén, Arkiv Mat. Astron. Fysik **35A**, 25-1 (1948).
[9] S. S. Huang, Phys. Rev. **76**, 1878 (1949).
[10] T. Kato, Phys. Rev. **80**, 475 (1950).
[11] L. Hulthén and S. Skavlem, Phys. Rev. **87**, 297 (1952).
[12] H. Feshbach and S. I. Rubinow, Phys. Rev. **88**, 484 (1952).

I. REFORMULATION OF THE VARIATIONAL PRINCIPLE FOR $k\cot\delta_l$

Our work here is an extension in many ways of the point of view adopted in reference 12, but, for completeness, we repeat the necessary equations and definitions.

The radial part u/r of the Schrödinger wave function for a state of orbital angular momentum l satisfies the equation,

$$\left[\frac{d^2}{dr^2}+k^2-\frac{l(l+1)}{r^2}+U(r)\right]u(r)=0, \tag{1}$$

with the usual notation. The boundary conditions on $u(r)$ are that

$$\left.\begin{aligned} &u(0)=0,\\ &u(\infty)=\cot\delta_l\sin(kr-\tfrac{1}{2}l\pi)+\cos(kr-\tfrac{1}{2}l\pi)\end{aligned}\right\}. \tag{2}$$

It is desirable to formulate the problem in terms of a wave function which is essentially nonzero only in the region where the potential $U(r)$ is important. To this end, introduce the asymptotic function u_∞ defined by the equation

$$u_\infty=\cot\delta_l F_l+G_{l\infty}, \tag{3}$$

where $F_l=krj_l(kr)$, $G_l=-krn_l(kr)$, with j_l, n_l the well-known spherical Bessel functions. These functions have the required asymptotic property at infinity, i.e.,

$$\left.\begin{aligned} &\lim_{r\to\infty}F_l=\sin(kr-\tfrac{1}{2}l\pi),\\ &\lim_{r\to\infty}G_l=\cos(kr-\tfrac{1}{2}l\pi)\equiv G_{l\infty}.\end{aligned}\right\} \tag{4}$$

The use of $G_{l\infty}$ instead of G_l in the definition of u_∞ avoids dealing later on with the objectionable singular behavior of G_l in the neighborhood of the origin. It may be noted that

$$\left[\frac{d^2}{dr^2}+k^2-\frac{l(l+1)}{r^2}\right]F_l=0, \tag{5}$$

and that

$$\left[\frac{d^2}{dr^2}+k^2\right]G_{l\infty}=0, \tag{6}$$

while, of course,

$$\lim_{r\to\infty} u = \lim_{r\to\infty} u_\infty .$$

Now introduce the inside-wave function y defined by

$$y = u_\infty - u. \tag{7}$$

Then the equation for y is

$$\frac{d^2y}{dr^2} + k^2 y - \frac{l(l+1)}{r^2}(y - G_{l\infty}) + U(y - u_\infty) = 0. \tag{8}$$

The boundary conditions in terms of y become

$$y(0) = G_{l\infty}(0) = \cos(\tfrac{1}{2}l\pi),$$

$$y(\infty) = 0.$$

Also useful is the equation for $(y - G_{l\infty})$,

$$\left[\frac{d^2}{dr^2} + k^2 - \frac{l(l+1)}{r^2} + U\right](y - G_{l\infty}) - \cot\delta_l U F_l = 0. \tag{9}$$

There are two different expressions that may be formed directly for $k\cot\delta_l$, neither of which is, by itself, stationary. However, most of the variational principles given may be looked on as an appropriate combination of these expressions (an exception is Eq. (10) of Kato's article[10]). Our present point of view is to form them at the very outset in terms of the inside-wave function y so that there will be no explicit dependence on $k\cot\delta_l$ of the expression to be varied. The first of these may be obtained from Eq. (9) by multiplying by $(y - G_{l\infty})$ and integrating. There results in a straightforward manner after some partial integrations, the equation

$$0 = (k\cot\delta_l)B - C, \tag{10}$$

where

$$B = \frac{1}{k}\int_0^\infty dr U F_l (y - G_{l\infty}), \tag{11}$$

$$C = \int_0^\infty dr \left\{ -\left(\frac{dy}{dr}\right)^2 + k^2 y^2 + \left[U(r) - \frac{l(l+1)}{r^2}\right](y - G_{l\infty})^2 \right\}. \tag{12}$$

On the other hand, if we multiply Eq. (9) by F_l, Eq. (5) by $(y - G_{l\infty})$, integrate, and subtract, we obtain after partial integration a second equation for $k\cot\delta_l$:

$$k\cot\delta_l = k\cot\delta_{lB}(1 + B), \tag{13}$$

where $k\cot\delta_{lB}$ is just the Born approximation,

$$\frac{1}{k\cot\delta_{lB}} = \frac{1}{k^2}\int_0^\infty dr U F_l^2. \tag{14}$$

Equations (10) and (13) may be looked on as a fundamental set of equations for $k\cot\delta_l$, and, in fact, they were already given for the case of the S-state phase shift ($l = 0$) by Hulthén.[8] However, the starting point of most of the variational principles has been to multiply Eq. (8) by $(y - u_\infty)$ and integrate (or, as originally, to work with the equation for u). If, rather, Eqs. (10) and (13) are considered directly, it is observed that they have the important property that their variations with respect to variation in the wave function y are proportional to each other. Thus, from Eq. (10),

$$\delta(k\cot\delta_l) = \frac{\delta C}{B} - \frac{C}{B^2}\delta B.$$

It follows from Eq. (12) that, in view of the differential Eq. (8) for y,

$$\delta C = 2\cot\delta_l \int_0^\infty dr U F_l \delta y = (2k\cot\delta_l)\delta B. \tag{15}$$

Consequently,

$$\delta(k\cot\delta_l) = (k\cot\delta_l)\delta B/B.$$

On the other hand, it follows directly from Eq. (13) that

$$\delta(k\cot\delta_l) = (k\cot\delta_{lB})\delta B.$$

In both cases the variation in $k\cot\delta_l$ is proportional to δB. Therefore, it should not be surprising if we could discover very many combinations of Eqs. (10) and (13) such that the contributions from each to $\delta(k\cot\delta_l)$ cancel each other, i.e., these combinations form stationary expressions. This is indeed the case. The question of choosing among them appears to be merely a matter of selecting the one most feasible for numerical computation. The simplest combination appears to be the following one:

$$k\cot\delta_l = (k\cot\delta_{lB})(1 + B)^2 - C. \tag{16}$$

It is easy to verify that, in view of Eqs. (13) and (15), this is a stationary expression for $k\cot\delta_l$. From the present point of view, previously given variational principles for $k\cot\delta_l$ represent somewhat more cumbersome combinations of Eqs. (10) and (13).

II. GENERALIZATION TO TENSOR FORCES

We now wish to extend the foregoing procedure to the case of tensor forces. A general discussion of the scattering theory with spin-orbit coupling has been given in reference 4. It suffices here to restrict ourselves to the mathematical details. Consider a tensor force interaction,

$$V = V_c + V_t(r) S_{12},$$

coupling the ${}^3S_1$ and ${}^3D_1$ states of a neutron-proton system, where S_{12} is the usual tensor operator,

$$S_{12} = \frac{3(\boldsymbol{\sigma}_1\cdot\mathbf{r})(\boldsymbol{\sigma}_2\cdot\mathbf{r})}{r^2} - \boldsymbol{\sigma}_1\cdot\boldsymbol{\sigma}_2.$$

The extension of the analysis for a spin-orbit interaction coupling any two orbital angular momentum states is

trivial. Let the ${}^3S_1$ and ${}^3D_1$ state radial wave functions be denoted by u and w, respectively.

These are coupled by the following two equations[13]:

$$\frac{d^2u}{dr^2}+k^2u+W_cu+2\sqrt{2}W_tw=0,$$
$$\frac{d^2w}{dr^2}+k^2w-\frac{6}{r^2}w+(W_c-2W_t)w+2\sqrt{2}W_tu=0. \tag{17}$$

The boundary conditions at the origin are

$$u(0)=w(0)=0,$$

while, at $r=\infty$, there are two linear combinations of the asymptotic forms of u and w that are possible. These are denoted by the letters α and β. Thus,

$$\left.\begin{aligned}\lim_{r\to\infty}u&=\cos\epsilon[\cot\delta_\alpha\sin(kr)+\cos(kr)],\\ \lim_{r\to\infty}w&=\sin\epsilon[\cot\delta_\alpha\sin(kr-\pi)+\cos(kr-\pi)],\end{aligned}\right\}\text{solution }\alpha;$$

$$\left.\begin{aligned}\lim_{r\to\infty}u&=-\sin\epsilon[\cot\delta_\beta\sin(kr)+\cos(kr)],\\ \lim_{r\to\infty}w&=\cos\epsilon[\cot\delta_\beta\sin(kr-\pi)+\cos(kr-\pi)],\end{aligned}\right\}\text{solution }\beta.$$

The quantity ϵ is called the mixture parameter as it determines the amount of admixture of pure ${}^3S_1$ and pure ${}^3D_1$ waves at infinity.

The problem at hand is to derive variational principles for δ_α, δ_β, and ϵ analogous to Eq. (16). This can be accomplished most easily with the use of matrix notation. The equations will be numbered so as to indicate the corresponding equations of Sec. I. First, introduce the asymptotic functions,

$$u_{\alpha\infty}=\cos\epsilon[\cot\delta_\alpha F_0+G_{0\infty}],\quad u_{\beta\infty}=-\sin\epsilon[\cot\delta_\beta F_0+G_{0\infty}],$$
$$w_{\alpha\infty}=\sin\epsilon[\cot\delta_\alpha F_2+G_{2\infty}],\quad w_{\beta\infty}=\cos\epsilon[\cot\delta_\beta F_2+G_{2\infty}].$$

Furthermore, define inside-wave functions normalized to unity at the origin, i.e.,

$$\cos\epsilon y_\alpha=u_{\alpha\infty}-u_\alpha,\quad -\sin\epsilon y_\beta=u_{\beta\infty}-u_\beta,$$
$$-\sin\epsilon v_\alpha=w_{\alpha\infty}-w_\alpha,\quad -\cos\epsilon v_\beta=w_{\beta\infty}-w_\beta.$$

Then

$$y_{\alpha,\beta}(0)=v_{\alpha,\beta}(0)=1,$$
$$y_{\alpha,\beta}(\infty)=v_{\alpha,\beta}(\infty)=0.$$

Now introduce the vector U by the equation

$$U=\begin{pmatrix}u\\ w\end{pmatrix},$$

and define the scalar product of two vectors U_1 and U_2 by the bracket notation

$$\{U_1,U_2\}=\int_0^\infty dr(u_1^*u_2+w_1^*w_2).$$

In addition, let

$$F_\alpha^\infty=\begin{pmatrix}\cos\epsilon F_0\\ \sin\epsilon F_2\end{pmatrix},\quad G_\alpha^\infty=\begin{pmatrix}\cos\epsilon G_{0\infty}\\ \sin\epsilon G_{2\infty}\end{pmatrix},$$
$$F_\beta^\infty=\begin{pmatrix}-\sin\epsilon F_0\\ \cos\epsilon F_2\end{pmatrix},\quad G_\beta^\infty=\begin{pmatrix}-\sin\epsilon G_{0\infty}\\ \cos\epsilon G_{2\infty}\end{pmatrix}.$$

Then we may define, in analogy with Eq. (3), the asymptotic vector

$$U^\infty=\cot\delta F^\infty+G^\infty, \tag{3A}$$

with either subscript α or β applicable. Further, let

$$Y=U^\infty-U \tag{7A}$$

or, explicitly,

$$Y_\alpha=\begin{pmatrix}\cos\epsilon y_\alpha\\ -\sin\epsilon v_\alpha\end{pmatrix},\quad Y_\beta=\begin{pmatrix}-\sin\epsilon y_\beta\\ -\cos\epsilon v_\beta\end{pmatrix}.$$

With the following definitions of operators,

$$T=\begin{pmatrix}d^2/dr^2 & 0\\ 0 & d^2/dr^2-6/r^2\end{pmatrix},\quad T_2=\begin{pmatrix}0 & 0\\ 0 & -6/r^2\end{pmatrix},$$
$$W=\begin{pmatrix}W_c & 2\sqrt{2}W_t\\ 2\sqrt{2}W_t & W_c-2W_t\end{pmatrix},$$

Eq. (17) may be written as

$$TU+k^2U+WU=0. \tag{1A}$$

Also,

$$TF^\infty+k^2F^\infty=0, \tag{5A}$$
$$(T-T_2)G^\infty+k^2G^\infty=0. \tag{6A}$$

These last two equations combined yield

$$TU^\infty-T_2G^\infty+k^2U^\infty=0,$$

and consequently, the equation for Y is

$$TY-T_2G^\infty+k^2Y+W(Y-U^\infty)=0. \tag{8A}$$

For convenience, it may be indicated that the equation for $(Y-G^\infty)$ is

$$T(Y-G^\infty)+k^2(Y-G^\infty)+W(Y-G^\infty)-(\cot\delta)WF^\infty=0. \tag{9A}$$

All the operations necessary for obtaining Eq. (16) may now be carried out in completely analogous fashion so that it is sufficient to write down the corresponding equations. Thus,

$$0=(k\cot\delta)B-C, \tag{10A}$$

in which we use the same symbols as before but they

[13] J. M. Blatt and V. F. Weisskopf, *Theoretical Nuclear Physics*, (John Wiley and Sons, Inc., New York, 1952), Chap. II, Sec. 5D.

have the following extended meaning:

$$B=\frac{1}{k}[F^{\infty}, W(Y-G^{\infty})]. \tag{11A}$$

$$C=[Y, (T-T_2)Y]+[(Y-G^{\infty}), T_2(Y-G^{\infty})] +k^2(Y,Y)+[(Y-G^{\infty}), W(Y-G^{\infty})]. \tag{12A}$$

In addition,

$$k\cot\delta=(k\cot\delta_B)(1+B), \tag{13A}$$

with

$$\frac{1}{k\cot\delta_B}=\frac{1}{k^2}(F^{\infty},WF^{\infty}). \tag{14A}$$

The term in C involving second derivatives of the wave function has been symmetrized by means of a partial integration. The variational principle for the two phase shifts δ_α and δ_β is given by

$$k\cot\delta=(k\cot\delta_B)(1+B)^2-C. \tag{16A}$$

It is to be understood that where a subscript is omitted, either α or β may be inserted. The equation (16A) for $k\cot\delta_\alpha$ is stationary with respect to simultaneous variations of the wave functions y_α, v_α and similarly with β replacing α. It is an analog in differential form of the Schwinger variational principle[1,3] for the phase shifts with tensor forces. It may be easily seen that Eq. (16A) reduces to Eq. (16) if the tensor coupling is zero by letting W_t and $\epsilon\to 0$. Then δ_α reduces to the ordinary S-wave phase shift δ_0 and δ_β becomes the D-wave phase shift δ_2. For the benefit of completeness, we write out the expressions for B and C in long form.

$$B_\alpha=\cos^2\epsilon\cdot\frac{1}{k}\int_0^\infty dr[W_cF_0(y_\alpha-G_{0\infty}) +\tan\epsilon\cdot 2\sqrt{2}W_tF_2(y_\alpha-G_{0\infty}) -\tan\epsilon\cdot 2\sqrt{2}W_tF_0(v_\alpha+G_{2\infty}) -\tan^2\epsilon\cdot(W_c-2W_t)F_2(v_\alpha+G_{2\infty})],$$

$$C_\alpha=\cos^2\epsilon\int_0^\infty dr\left\{-\left(\frac{dy_\alpha}{dr}\right)^2+k^2y_\alpha{}^2+W_c(y_\alpha-G_{0\infty})^2 +\tan^2\epsilon\left[-\left(\frac{dv_\alpha}{dr}\right)^2+k^2v_\alpha{}^2 +\left(W_c-2W_t-\frac{6}{r^2}\right)(v_\alpha+G_{2\infty})^2\right] -2\tan\epsilon\cdot 2\sqrt{2}W_t(y_\alpha-G_{0\infty})(v_\alpha+G_{2\infty})\right\},$$

$$\frac{1}{k\cot\delta_{B\alpha}}=\cos^2\epsilon\cdot\frac{1}{k^2}\int_0^\infty dr[W_cF_0{}^2+2\tan\epsilon\cdot 2\sqrt{2}W_tF_0F_2 +\tan^2\epsilon\cdot(W_c-2W_t)F_2{}^2],$$

$$B_\beta=\cos^2\epsilon\cdot\frac{1}{k}\int_0^\infty dr[\tan^2\epsilon\cdot W_cF_0(y_\beta-G_{0\infty}) -\tan\epsilon\cdot 2\sqrt{2}W_tF_2(y_\beta-G_{0\infty}) +\tan\epsilon\cdot 2\sqrt{2}W_tF_0(v_\beta+G_{2\infty}) -(W_c-2W_t)F_2(v_\beta+G_{2\infty})],$$

$$C_\beta=\cos^2\epsilon\int_0^\infty dr\left\{\tan^2\epsilon\left[-\left(\frac{dy_\beta}{dr}\right)^2+k^2y_\beta{}^2 +W_c(y_\beta-G_{0\infty})^2\right]-\left(\frac{dv_\beta}{dr}\right)^2+k^2v_\beta{}^2 +\left(W_c-2W_t-\frac{6}{r^2}\right)(v_\beta+G_{2\infty})^2 +2\tan\epsilon\cdot 2\sqrt{2}W_t(y_\beta-G_{0\infty})(v_\beta+G_{2\infty})\right\},$$

$$\frac{1}{k\cot\delta_{B\beta}}=\cos^2\epsilon\cdot\frac{1}{k^2}\int_0^\infty dr\{\tan^2\epsilon\cdot W_cF_0{}^2 -2\tan\epsilon\cdot 2\sqrt{2}W_tF_0F_2+(W_c-2W_t)F_2{}^2\}.$$

III. VARIATIONAL PRINCIPLE FOR THE MIXTURE PARAMETER ϵ

In Eq. (16A), it has been assumed that the correct value of the mixture parameter ϵ was inserted in the expressions on the right-hand side. But the value of this parameter is not really known, and we must supplement the stationary equations for δ_α and δ_β with a third stationary expression if we are to render the value of ϵ correct to second order. The possibility of carrying out the same operations as for Eq. (16A) in "mixed" form yields such a stationary expression. Thus, multiply Eq. (9A) for $(Y_\alpha-G_\alpha{}^\infty)$ by $(Y_\beta-G_\beta{}^\infty)$ and vice versa, integrate, and add. We obtain in exactly similar fashion to (10A) the following equation:

$$0=(k\cot\delta_\alpha)B_\beta{}'+(k\cot\delta_\beta)B_\alpha{}'-2C', \tag{10B}$$

where

$$B_\alpha{}'=\frac{1}{k}[(Y_\alpha-G_\alpha{}^\infty), WF_\beta{}^\infty],$$

$$B_\beta{}'=\frac{1}{k}[(Y_\beta-G_\beta{}^\infty), WF_\alpha{}^\infty],$$

$$C'=[Y_\alpha, (T-T_2)Y_\beta]+k^2(Y_\alpha,Y_\beta) +[(Y_\alpha-G_\alpha{}^\infty), (W+T_2)(Y_\beta-G_\beta{}^\infty)],$$

with the term in C' involving second derivatives appropriately symmetrized. In addition, corresponding to Eq. (13A), we obtain

$$\begin{aligned} k\cot\delta_\alpha&=(k\cot\delta_B')B_\alpha', \\ k\cot\delta_\beta&=(k\cot\delta_B')B_\beta', \end{aligned} \tag{13B}$$

in which $k\cot\delta_B'$ is a kind of "mixed" Born approximation,

$$\frac{1}{k\cot\delta_B'}=\frac{1}{k^2}(F_\alpha^\infty,WF_\beta^\infty). \tag{14B}$$

The difference in form of Eqs. (13A) and (13B) arises from the fact that, for Eq. (13B),

$$[F_\beta, T(Y_\alpha-G_\alpha^\infty)]-[(Y_\alpha-G_\alpha^\infty), TF_\beta]=0,$$

whereas, for Eq. (13A),

$$[F_\alpha, T(Y_\alpha-G_\alpha^\infty)]-[(Y_\alpha-G_\alpha^\infty), TF_\alpha]=k.$$

Substituting Eqs. (13B) into (10B), we obtain

$$0=(k\cot\delta_B')B_\alpha'B_\beta'-C'. \tag{16B}$$

This expression is stationary with respect to variations in all four wave functions, y_α, y_β, v_α, and v_β, as may be readily verified. Also, it contains no explicit dependence on $k\cot\delta_\alpha$ or $k\cot\delta_\beta$ and consequently may be used to solve for $\tan\epsilon$ (as a function of $\tan\epsilon$, it is a quartic algebraic equation). Therefore, it is proper to consider Eq. (16B) as an implicit stationary expression for $\tan\epsilon$. However, it appears more correct to consider Eqs. (16A) and (16B) as three simultaneous stationary equations for the three scattering parameters. A procedure for using them that suggests itself is to guess a value of $\tan\epsilon$, use Eq. (16A) for obtaining $k\cot\delta_\alpha$ and $k\cot\delta_\beta$, and then use Eq. (16B) as a corrector equation for $\tan\epsilon$, inserting in it the varied wave functions already determined by rendering Eq. (16A) stationary.

We append below the explicit expressions for the primed quantities.

$$\begin{aligned}B_\alpha'=\cos^2\epsilon\cdot\frac{1}{k}\int_0^\infty dr[&-\tan\epsilon\cdot W_cF_0(y_\alpha-G_{0\infty})\\&+2\sqrt{2}W_tF_2(y_\alpha-G_{0\infty})\\&+\tan^2\epsilon\cdot 2\sqrt{2}W_tF_0(v_\alpha+G_{2\infty})\\&-\tan\epsilon\cdot(W_c-2W_t)F_2(v_\alpha+G_{2\infty})],\end{aligned}$$

$$\begin{aligned}B_\beta'=-\cos^2\epsilon\cdot\frac{1}{k}\int_0^\infty dr[&\tan\epsilon\cdot W_cF_0(y_\beta-G_{0\infty})\\&+\tan^2\epsilon\cdot 2\sqrt{2}W_tF_2(y_\beta-G_{0\infty})\\&+2\sqrt{2}W_tF_0(v_\beta+G_{2\infty})\\&+\tan\epsilon\cdot(W_c-2W_t)F_2(v_\beta+G_{2\infty})],\end{aligned}$$

$$\begin{aligned}C'=\cos^2\epsilon\int_0^\infty dr\Big\{&-\tan\epsilon\Big[-\Big(\frac{dy_\alpha}{dr}\Big)\Big(\frac{dy_\beta}{dr}\Big)\\&+k^2y_\alpha y_\beta+W_c(y_\alpha-G_{0\infty})(y_\beta-G_{0\infty})\Big]\\&+\tan\epsilon\Big[-\Big(\frac{dv_\alpha}{dr}\Big)\Big(\frac{dv_\beta}{dr}\Big)+k^2v_\alpha v_\beta\\&+\Big(W_c-2W_t-\frac{6}{r^2}\Big)(v_\alpha+G_{2\infty})(v_\beta+G_{2\infty})\Big]\\&-2\sqrt{2}W_t(y_\alpha-G_{0\infty})(v_\beta+G_{2\infty})\\&+\tan^2\epsilon\cdot 2\sqrt{2}W_t(y_\beta-G_{0\infty})(v_\alpha+G_{2\infty})\Big\},\end{aligned}$$

$$\begin{aligned}\frac{1}{k\cot\delta_B'}=\cos^2\epsilon\cdot\frac{1}{k^2}\int_0^\infty dr\\\times[&-\tan\epsilon\cdot W_cF_0^2+(1-\tan^2\epsilon)2\sqrt{2}W_tF_0F_2\\&+\tan\epsilon\cdot(W_c-2W_t)F_2^2].\end{aligned}$$

Note that in applying the above expressions to Eq. (16B), the common factor of $\cos^2\epsilon$ may be dropped from all of them.[14]

[14] *Note added in proof.*—The author is indebted to L. Sartori for pointing out to him that T. Regge and M. Verde, Nuovo cimento **10**, 997 (1953) have extended Hulthen's second formulation (see reference 8) to the three independent elements of the K matrix.

Equivalent Two-Body Method for the Triton*

HERMAN FESHBACH† AND S. I. RUBINOW‡
Department of Physics and Laboratory for Nuclear Science, Massachusetts Institute of Technology, Cambridge, Massachusetts
(Received November 12, 1954)

A method for developing equivalent two-body problems for the binding energy of the triton has been derived from the variational principle. The method has been applied to two central-force problems. In the first, the exponential well of Rarita and Present is discussed and the method is shown to give excellent results. In the second, the central-force term in the Lévy potential including the repulsive core is investigated. It is estimated that the Lévy potential including the tensor term will give the correct order of binding energy to the triton.

INTRODUCTION

THE problem of solving the quantum-mechanical three-body problem has received from the very outset considerable attention from nuclear physicists. This is natural inasmuch as the binding energy of the triton provides a first test of any nuclear potential that has been found to predict the experimentally known deuteron and nucleon-nucleon scattering data. It is also now known to be a sensitive test of the particular shape of the potential that is assumed.

The mathematical difficulty that is immediately encountered is the lack of separability of Schrödinger's equation. Since the classic work of Hylleraas[1] on the ground state of the helium atom, the problem has been almost exclusively attacked by use of the Ritz variational method. Among the large-scale applications of this method to the triton problem, we may mention the work of Rarita and Present,[2] and, more recently, in connection with the use of tensor forces, the work of Schwinger, Feshbach, and co-workers.[3–8] The last-named work[8] represents at this time the culmination of this effort in providing a Yukawa-type tensor interaction that fits all the known low-energy two-body experimental data and also predicts within the error of the variational method the experimental values of the triton- and alpha-particle binding energies. Among other methods of attack on the problem that have been tried, the work of Svartholm[9] is noteworthy: he has made use of the more powerful variation-iteration method. A direct numerical procedure for solving the associated integral equation[10] has also been attempted.

Because of the tremendous amount of labor that is involved in these computations, more approximate methods for obtaining reasonably accurate solutions have always been desired. Furthermore, the large state of flux of the nuclear two-body potential has, unfortunately, rendered obsolete a vast amount of the work that has been accomplished in the past, and the recent introduction of a hard-core meson-theoretic potential[11] threatens to do the same for much of the recent work, insofar as the use of a particular well shape is concerned.

This paper is designed to provide a simple means of providing approximate eigenvalue solutions for any given potential. We shall work with the S state only. The extensions required for the inclusion of tensor forces are not difficult to outline, though the required analysis would be very lengthy. The most notable effort in this direction in the past was Feenberg's "equivalent" two-body method.[12] This method is based on plausibility arguments which at best can be shown to hold for a restricted class of potentials.[13] It is not known whether it gives an upper or lower bound to the energy, although the latter has been surmised from the results of various examples.

In what follows, an "equivalent" two-body method is introduced in which the essential approximation employed is to give the wave function a particular functional form.[14] This leads to a true two-body equation, of which the lowest eigenvalue is an upper bound of the lowest eigenvalue of the original three-body equation. The equation is given once and for all except that the "effective" two-body potential energy that has to be introduced is an integral of the original three-body potential energy.

EFFECTIVE TWO-BODY METHOD

It is assumed that the center-of-mass motion is removed, and for simplicity only central potentials will be considered so that, consequently, the triton in its ground state is in a $^2S_1$ state. The variational principle

* Supported in part by the joint program of the Office of Naval Research and the U. S. Atomic Energy Commission.

† Now Guggenheim Fellow on leave from the Massachusetts Institute of Technology; at Harvard University, Cambridge, Massachusetts.

‡ Now at Harvard University, Cambridge, Massachusetts.

[1] E. A. Hylleraas, Z. Physik **48**, 469 (1928).
[2] W. Rarita and R. D. Present, Phys. Rev. **51**, 788 (1937).
[3] W. Rarita and J. Schwinger, Phys. Rev. **59**, 436 (1941).
[4] E. Gerjuoy and J. Schwinger, Phys. Rev. **61**, 138 (1942).
[5] H. Feshbach, Phys. Rev. **61**, 544(A) (1942).
[6] R. G. Sachs and J. Schwinger, Phys. Rev. **70**, 41 (1946).
[7] R. E. Clapp, Phys. Rev. **76**, 873 (1949).
[8] R. L. Pease and H. Feshbach, Phys. Rev. **81**, 142 (1951).
[9] N. Svartholm, thesis, Lund, 1945.
[10] S. I. Rubinow, Phys. Rev. **86**, 388 (1952).
[11] M. M. Lévy, Phys. Rev. **88**, 72, 725 (1952).
[12] E. Feenberg, Phys. Rev. **47**, 850 (1935).
[13] E. Feenberg and S. S. Share, Phys. Rev. **50**, 253 (1936).
[14] It should be mentioned that such an approach was already suggested by the pioneer work of E. P. Wigner [Phys. Rev. **43**, 252 (1933)] in this field.

for Schrödinger's equation may then be written as

$$0=\delta\int_0^\infty dr_1\int_0^\infty dr_2\int_{|r_1-r_2|}^{r_1+r_2} dr_3 r_1 r_2 r_3 \times\left\{\left(\frac{\partial\psi}{\partial r_1}\right)^2+\left(\frac{\partial\psi}{\partial r_2}\right)^2+\left(\frac{\partial\psi}{\partial r_3}\right)^2 +\frac{r_1^2+r_3^2-r_2^2}{2r_1r_3}\frac{\partial\psi}{\partial r_1}\frac{\partial\psi}{\partial r_3}+\frac{r_1^2+r_2^2-r_3^2}{2r_1r_2}\frac{\partial\psi}{\partial r_1}\frac{\partial\psi}{\partial r_2} +\frac{r_2^2+r_3^2-r_1^2}{2r_2r_3}\frac{\partial\psi}{\partial r_2}\frac{\partial\psi}{\partial r_3} +\frac{m}{\hbar^2}[V_1(r_1)+V_2(r_2)+V_3(r_3)]\psi^2-\frac{m}{\hbar^2}E\psi^2\right\}, \quad (1)$$

where (r_1,r_2,r_3) represent the three nucleon interdistances (see Fig. 1) of the triton and ψ is a function of (r_1,r_2,r_3) only. The potentials $V_i(r_i)$ represent the result of taking the appropriate spin average. Again for simplicity we have taken the spin dependence of the wave function as $(1/\sqrt{2})\alpha(1)[\alpha(2)\beta(3)-\beta(2)\alpha(3)]$. Introducing the other possible spin dependence, $(1/\sqrt{6})\{\alpha(1)[\alpha(2)\beta(3)+\beta(2)\alpha(3)]-2\beta(1)\alpha(2)\alpha(3)\}$, and its associated spatial wave function would lead eventually to a pair of coupled two-body Schrödinger equations. For most potentials considered up to now, this additional complication does not lead to significant effects and for this reason we have not included it. If Eq. (1) is considered as a variational principle for the energy, it is known that the trial function $\psi=\exp[-\frac{1}{2}\lambda(r_1+r_2+r_3)]$ yields excellent results for the binding energy, with λ considered as a variational parameter. Such a trial function bears out the idea that the triton in its ground state is spherical and essentially symmetric in the behavior of its constituent particles. This is generalized by letting

$$\psi=\varphi(\tfrac{1}{2}(r_1+r_2+r_3)), \quad (2)$$

where φ is an unspecified arbitrary function of the perimetric length of the triangle formed by the three particles. It is now desirable to change variables so that this length becomes one of the independent variables.

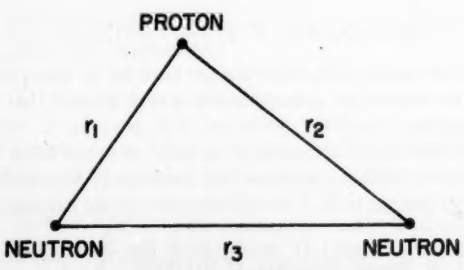

FIG. 1. The triton interdistances r_1, r_2, and r_3.

Thus, let

$$R=\tfrac{1}{2}(r_1+r_2+r_3), \quad R_2=r_2, \quad R_3=r_3. \quad (3)$$

Then, since φ is a function of R only, the integration over the other variables (R_2,R_3) may be performed. The volume element is now

$$\int_0^\infty dr_1\int_0^\infty dr_2\int_{|r_1-r_2|}^{r_1+r_2} dr_3 r_1 r_2 r_3 =\int_0^\infty dR\int_0^R dR_2\int_{R-R_2}^R dR_3(2R-R_2-R_3)R_2R_3, \quad (4)$$

and Eq. (1) becomes

$$0=\delta\int_0^\infty dR\frac{R^5}{8}\left\{\left(\frac{d\varphi}{dR}\right)^2+\frac{m}{\hbar^2}V_{eff}\varphi^2-\frac{m}{\hbar^2}\frac{14}{15}E\varphi^2\right\}, \quad (5)$$

where

$$V_{eff}=\frac{8}{R^5}\int_0^R dR_2\int_{R-R_2}^R dR_3(2R-R_2-R_3)R_2R_3 \times\{V_1(r_1)+V_2(r_2)+V_3(r_3)\}. \quad (6)$$

If the potentials are now assumed to be all the same shape, so that $V_i(r_i)=V_iv(r_i)$, with V_i constant, Eq. (6) becomes

$$V_{eff}=(V_1+V_2+V_3)\cdot\frac{8}{R^5} \times\int_0^R dR_2(R^2R_2^2-RR_2^3+\tfrac{1}{6}R_2^4)v(R_2). \quad (7)$$

A particular form of $\varphi(R)$ may, of course, still be specified. The choice $\varphi=e^{-\lambda R}$ naturally reduces to the previously mentioned calculation in a very simple way. The best choice of the form of $\varphi(R)$ is the solution of the equation obtained from the variation indicated in Eq. (5):

$$\frac{1}{R^5}\frac{d}{dR}\left(R^5\frac{d\varphi}{dR}\right)-\frac{14}{15}k^2\varphi+U_{eff}\varphi=0, \quad (8)$$

where $k^2=(m/\hbar^2)|E|$ and $U_{eff}=-(m/\hbar^2)V_{eff}$. Letting $\varphi(R)=F(R)/R^{5/2}$, this becomes

$$\frac{d^2F}{dR^2}-\frac{14}{15}k^2F-\frac{15}{4}\frac{1}{R^2}F+U_{eff}F=0. \quad (9)$$

It may now be noted that this is exactly the form of the Schrödinger equation for the deuteron in which $\psi=[F(R)/R]Y_{lm}$. The reduced mass has the value $(14/15)m$ instead of m, and there is a centrifugal potential energy term $[+(15/4)R^{-2}]$ corresponding to setting the orbital quantum number $l=\frac{3}{2}$. This is a very important term and is contributed by the kinetic energy, independent of the choice of potential energy.

The potential energy that is to be inserted in this equation is not the actual two-body potential, but the "averaged" potential given by Eq. (7). It might perhaps be more apt to call the combination $[-U_{eff}+(15/4)R^{-2}]$ the true effective potential of the problem, as can be readily seen by the form of the equation. This completes the reduction to an "effective" two-body equation. It may perhaps bear repeating that the lowest eigenvalue associated with Eq. (9) remains an upper bound of the true eigenvalue of the original triton problem.

For purposes of illustration, assume Eq. (9) is to be solved for an exponential well nucleon-nucleon interaction. Let $V_i(r_i)=-V_i e^{-r_i/R_0}$, and let R_0 be chosen as the unit of length. For this case U_{eff} becomes, after performing the integration indicated in Eq. (7),

$$U_{eff}=(14/15)(U_1+U_2+U_3)R_0^2u(R),$$

where

$$u(R)=\frac{8}{R^5}\frac{15}{14}\Big\{4-6R+2R^2+e^{-R}\times\Big[-4+2R+2R^2+\frac{R^3}{3}-\frac{R^4}{6}\Big]\Big\}. \quad (10)$$

The function $u(R)$ decreases monotonically from the value 1 at the origin to zero value at infinity. The attractive potential $(-U_{eff})$ is plotted in Fig. 2, as well as the combination $[-U_{eff}+(15/4)R^{-2}]$, with $(U_1+U_2+U_3)R_0^2$ set equal to 5.128. This corresponds

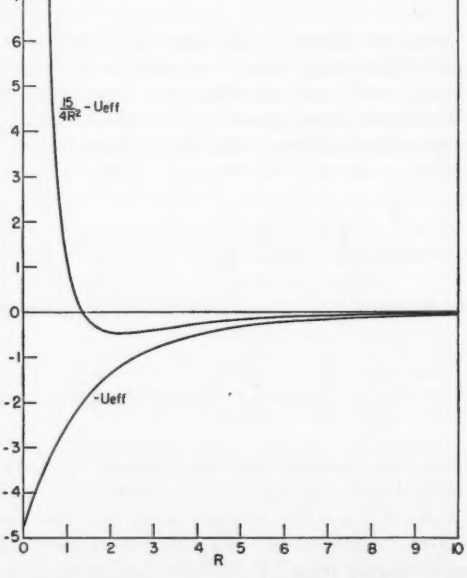

FIG. 2. The effective potential $(-U_{eff})$ and the net effective potential $[(15/4)R^{-2}-U_{eff}]$ with $(U_1+U_2+U_3)R_0^2=5.128$. The unit of length is $R_0=0.678\times10^{-13}$ cm, and unit well depth corresponds to 90.3 Mev.

to a choice of neutron-proton and neutron-neutron singlet and triplet well depths which fit the low-energy scattering data.[15] Numerical integration of the equation for this case yields a binding energy value of 11.02 Mev, compared to the experimental value of 8.50 Mev. This is, surprisingly, only about 1 percent deeper than the value that is obtained with the trial function $e^{-\lambda R}$, which is probably a reflection of the "goodness" of the latter trial function.

As a second illustration, it will easily be shown that a two-body potential of infinitesimally small range will produce infinite binding of the triton.[16] For, suppose the nucleon-nucleon potential is a delta function,

$$V_2(r_2)=-V_2\delta(\mathbf{r}_2),$$

of such a strength that

$$\frac{1}{4\pi}\int d\tau_2 V_2(r_2)=-V_2.$$

It follows directly from Eq. (7) for the effective potential that $U_{eff}=(U_1+U_2+U_3)\cdot 8/R^3$, and such a singular potential is well known to have an infinite binding energy.

APPLICATION TO HARD-CORE POTENTIALS; THE LÉVY POTENTIAL

Recent calculations based on various approximations in the meson theory of nuclear forces have indicated that as the distance between nucleons decreases, the force between nucleons eventually becomes very strongly repulsive. A similar result has been suggested by the success of a hard-core model proposed on a phenomenological basis by Jastrow.[17] We shall be interested here in formulating an equivalent two-body method for S potentials of this type and shall apply the method to a potential proposed by Lévy[11] which has the merit of giving an adequate description of low-energy two-nucleon phenomena. The potential under consideration here is:

$$V(r)=\begin{cases}\infty & r<r_0\\ V_0v(r) & r>r_0,\end{cases}$$

where r is the distance between any two nucleons. The wave function must satisfy the following boundary conditions:

$$\psi(r_1,r_2,r_3)=0 \quad \text{if} \quad r_i\leq r_0, \quad i=1,2,3.$$

A few qualitative remarks are in order at this point. In the absence of a hard core it is well known that an attractive two-body potential will lead to a triton structure which is considerably more compact than the deuteron, with a corresponding increase in the binding energy per particle. This is illustrated by the calculation

[15] J. M. Blatt and J. D. Jackson, Phys. Rev. **76**, 18 (1949).
[16] L. H. Thomas, Phys. Rev. **47**, 903 (1935).
[17] R. Jastrow, Phys. Rev. **78**, 135 (1950).

in the preceding section where the two-body exponential potential required to yield the correct deuteron binding energy gave a triton binding energy far in excess of the experimental value. A simple explanation of this effect will now be given so that the modification introduced by hard-core potentials may be understood.

Let $u(r)$ be the solution of the deuteron problem with potential $V(r)$. Insert then the trial function $\psi=u(r_1)u(r_2)$ into the variational principle [Eq. (1)] for the binding energy of the triton, letting $V_i(r_i)=V(r_i)$. We find immediately that the resultant variational energy equals twice the binding energy of the deuteron plus an average over potential $V(r_3)$ which will always increase the calculated binding energy if the usual monotonic potentials are employed for V. This potential energy term is not balanced by a corresponding kinetic energy term, so that for the narrow deep potentials customarily used this term will be large. For hard-core potentials the physical situation is changed drastically. Since the wave function ψ must go to zero whenever $r_i\leq r_0$ and in particular $r_3\leq r_0$, the function $u(r_1)u(r_2)$ is no longer an admissible trial function for the three-body problem. New kinetic energy terms are introduced because the wave function must be so distorted as to be zero not only whenever r_1 and r_2 equal r_0 but also when $r_3=r_0$. It is no longer possible to make even the mild statement that the binding energy of the triton is at least twice the binding energy of the deuteron. As we shall see below this kinetic energy effect is large. Of course similar remarks apply to any potential which is not essentially monotonic, the hard-core potential being an extreme case where this effect is probably a maximum.

Let the potential in variational principle (1) be

$$V_i(r_i)=\begin{cases}\infty & r_i<r_0\\ V_i v(r_i) & r_i>r_0.\end{cases} \tag{11}$$

A trial function which obeys the boundary conditions and which is still simple in form is

$$\psi(r_1,r_2,r_3)=\begin{cases}0 & r_i\leq r_0\\ (r_1-r_0)(r_2-r_0)(r_3-r_0)\varphi(r_1+r_2+r_3) & \text{elsewhere.}\end{cases} \tag{12}$$

As we did in the previous section, we introduce appropriate new coordinates:

$$R=r_1+r_2+r_3-3r_0,\quad R_2=r_2,\quad R_3=r_3, \tag{13}$$

and integrate over (R_2,R_3). A complication arises from the limits of integration, for the volume element is now

$$\int_{r_0}^{\infty}dr_1\int_{r_0}^{\infty}dr_2\int_{[|r_1-r_2|,r_0]}^{r_1+r_2}dr_3,$$

where the brackets signify "the greater of the two quantities." However, the integration over (R_2,R_3) is straightforward and is carried through once and for all for the kinetic energy. It is convenient to introduce the nondimensional variable $\rho=R/r_0$. The equation analogous to (5) is then

$$0=\delta\int_0^{\infty}d\rho a_2(\rho)\left\{\left(\frac{d\varphi}{d\rho}\right)^2+\frac{a_1(\rho)}{a_2(\rho)}\varphi\frac{d\varphi}{d\rho}+\frac{a_0(\rho)}{a_2(\rho)}\varphi^2+\frac{k^2r_0^2n(\rho)}{a_2(\rho)}\varphi^2-r_0^2U_{\text{eff}}\varphi^2\right\}, \tag{14}$$

where

$$a_2(\rho)=\rho^8[0.2\rho^3+2.6\rho^2+9\rho+9],\quad 0\leq\rho\leq 1,$$

$$=\frac{1}{256}[39.8\rho^{11}+517.4\rho^{10}+2367\rho^9+3639\rho^8-1194\rho^7-3301.2\rho^6+4796.4\rho^5+822\rho^4-3825\rho^3+819\rho^2+1092.6\rho-448.2],\quad \rho>1;$$

$$a_1(\rho)=\rho^7[\rho^3+18\rho^2+69\rho+72],\quad 0\leq\rho\leq 1,$$

$$=\frac{1}{256}[253\rho^{10}+3402\rho^9+16\,557\rho^8+28\,824\rho^7-1638\rho^6-25\,956\rho^5+20\,706\rho^4+9432\rho^3-12\,087\rho^2-342\rho+1809],\quad \rho>1;$$

$$a_0(\rho)=\rho^6[\rho^3+45\rho^2+198\rho+210],\quad 0\leq\rho\leq 1,$$

$$=\frac{1}{256}[451\rho^9+6723\rho^8+40\,572\rho^7+87\,948\rho^6+21\,546\rho^5-76\,230\rho^4+12\,012\rho^3+32\,796\rho^2-2133\rho-7461],\quad \rho>1;$$

$$n(\rho)=\rho^8\left[\frac{0.6}{11}\rho^3+0.6\rho^2+2\rho+2\right],\quad 0\leq\rho\leq 1,$$

$$=\frac{1}{256}\left[\frac{101.4}{11}\rho^{11}+119.4\rho^{10}+542\rho^9+812\rho^8-306\rho^7-747.6\rho^6+1142.4\rho^5+180\rho^4-915\rho^3+201\rho^2+262.8\rho-\frac{1195.2}{11}\right],\quad \rho\geq 1; \tag{15}$$

$$U_{\text{eff}}=(U_1+U_2+U_3)\frac{1008}{a_2(\rho)}\int_1^{\rho+1}dxx(x-1)^2$$

$$\times(\rho+1-x)^5\left[\frac{1}{14}(\rho+1-x)^2+\frac{1}{3}(\rho+1-x)+\frac{1}{3}\right]v(x),\quad 0\leq\rho\leq 1,$$

$$=(U_1+U_2+U_3)\frac{10\,080}{a_2(\rho)}\int_1^{(\rho+1)/2}dx\cdot x^2(x-1)^2$$

$$\times\left\{\frac{1}{140}x^6-\left[\frac{1}{10}\left(\frac{\rho+1}{2}\right)+\frac{1}{30}\right]x^5\right.$$

$$+\left[\frac{3}{5}\left(\frac{\rho+1}{2}\right)^2+\frac{2}{5}\left(\frac{\rho+1}{2}\right)+\frac{1}{30}\right]x^4$$

$$-\left(\frac{\rho+1}{2}\right)\left[2\left(\frac{\rho+1}{2}\right)^2+2\left(\frac{\rho+1}{2}\right)+\frac{1}{3}\right]x^3$$

$$+\left(\frac{\rho+1}{2}\right)^2\left[\frac{7}{2}\left(\frac{\rho+1}{2}\right)^2+\frac{14}{3}\left(\frac{\rho+1}{2}\right)+\frac{4}{3}\right]x^2$$

$$-\left(\frac{\rho+1}{2}\right)^3\left[3\left(\frac{\rho+1}{2}\right)^2+5\left(\frac{\rho+1}{2}\right)+2\right]x$$

$$\left.+\left(\frac{\rho+1}{2}\right)^4\left(\frac{\rho+1}{2}+1\right)^2\right\}v(x)$$

$$+(U_1+U_2+U_3)\frac{1008}{a_2(\rho)}$$

$$\times\int_{(\rho+1)/2}^{(\rho+1)/2+1}dxx(x-1)^2(\rho+1-x)^5$$

$$\times\left[\frac{1}{14}(\rho+1-x)^2+\frac{1}{3}(\rho+1-x)+\frac{1}{3}\right]v(x),$$

$$\rho>1;\quad(16)$$

with $x=r_2/r_0$. All the numbers given in these equations are exact. It should be noted that the point $\rho=0$ corresponds in the original problem to the point $r_1=r_2=r_3=r_0$, while the point $\rho=1$ corresponds to $R=4r_0$. The associated differential equation is

$$\frac{d}{d\rho}\left(a_2\frac{d\varphi}{d\rho}\right)+\left[\frac{1}{2}\frac{da_1}{d\rho}-a_0\right]\varphi-k^2r_0^2n(\rho)\varphi$$

$$+U_{\text{eff}}r_0^2a_2\varphi=0.\quad(17)$$

Or, setting $[a_2(\rho)]^{\frac{1}{2}}\varphi=F(\rho)$, the effective two-body equation becomes

$$\frac{d^2F}{d\rho^2}-k^2r_0^2\frac{n(\rho)}{a_2(\rho)}F-c(\rho)F+U_{\text{eff}}r_0^2F=0,\quad(18)$$

where $c(\rho)=a_0/a_2-\frac{1}{4}(a_1/a_2)^2$. The ratio $n(\rho)/a_2(\rho)$ is remarkably constant for the entire range of values of ρ and varies monotonically from a minimum value of $2/9=0.2222\cdots$ at $\rho=0$ to a maximum value of $0.2316\cdots$ at $\rho=\infty$. Hence the effective mass is smaller by a factor of about 4.5 than that of a corresponding deuteron equation. The binding energy will therefore be magnified by the factor 4.5 (as contrasted with the factor 15/14 in the previous case). Of greater importance is the term U_{eff} and the centrifugal repulsive term $c(\rho)$. For small values of ρ, $c(\rho)\sim 22/3\rho^2$ so that F goes to zero at $\rho=0$ like $\rho^{2.25}$, where the exponent is approximate. Note that the wave function φ and therefore ψ is singular at $\rho=0$, since

$$\varphi=F(\rho)/a_2^{\frac{1}{2}}\underset{\rho\to 0}{\longrightarrow}\rho^{-1.75}.$$

Of course ψ is nevertheless quadratically integrable because of the high dimensionality of the configuration space for the three particles.

We have obtained U_{eff} and integrated Eq. (18) numerically for the central-force term in the Lévy potential. Since the Lévy potential contains noncentral tensor terms as well, the calculation gives at best an upper bound to the energy. A lower bound may be obtained by increasing the strength of the central Lévy potential until it, unaided by a tensor term, would bind the deuteron with the experimental binding energy. This may be accomplished by increasing the well depth by 42.5 percent. We expect that such a potential would give a greater binding in the three-body problem than

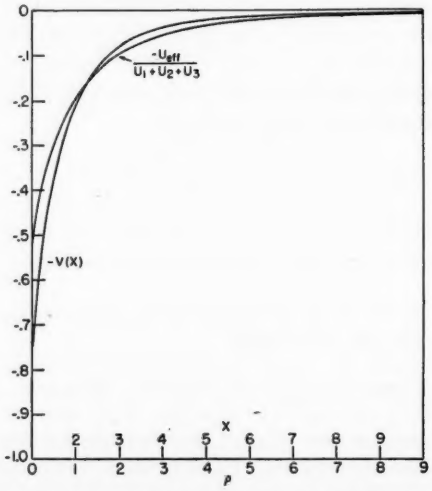

FIG. 3. The Lévy well-shape function $-v(x)$ as compared to the effective two-body well shape $-U_{\text{eff}}(\rho)/(U_1+U_2+U_3)$. The unit of length is the core radius $r_0=0.38(1.40\times10^{-13})$ cm, and unit well depth corresponds to 147 Mev.

the original Lévy potential including the tensor term, since the tensor term is expected to be less effective in binding H^3 than in binding H^2.

To summarize, we have calculated the binding energy of H^3 using two values of $U_i r_0^2$, (1) 10.57 and (2) 15.06, with a $v(x)$ equal to

$$v(x)=\frac{1}{x^2}\left[\frac{2}{\pi}K_1(0.76x)+0.075\left(\frac{2}{\pi}K_1(0.38x)\right)^2 +0.013xe^{-0.38x}\right], \quad x\geq 1, \quad (19)$$

and with $r_0=0.38(1.4\times10^{-13})$ cm. We expect the binding energy to be between the two results. The potential $v(x)$ is a very deep but narrow potential hole. The well depth at $\rho=1$ gives a value of V_i of 1189 Mev and 1690 Mev for the two cases. In Fig. 3, we have plotted $-v(x)$ as well as the effective potential well shape $-U_{\text{eff}}/(U_1+U_2+U_3)$.

In Fig. 4, we give the total equivalent two-body potential including the centrifugal term for the Lévy central potential (case 1) and also the stronger adjusted Lévy central potential, case (2). We see that the effective potential is almost completely canceled by the kinetic repulsion for the original Lévy central potential. As we expected from our earlier qualitative discussion, the insistence on making the wave function go to zero at $r_i=r_0$ is costly in kinetic energy; the stronger centrifugal term, as compared to the case in the preceding section, arises from the linear terms inserted in the variational form (12) in order to meet the boundary conditions. As we see from Fig. 4, only a very small attractive potential pocket remains. One can immediately infer that there is no binding in case (1). In case (2) the well is considerably deeper and broader and binding is obtained. The binding energy calculated by integrating Eq. (18) numerically is found to be 13.3 Mev.

From this we conclude that the binding energy calculated with the complete Lévy potential including the tensor term would be between zero and 13.3 Mev, in

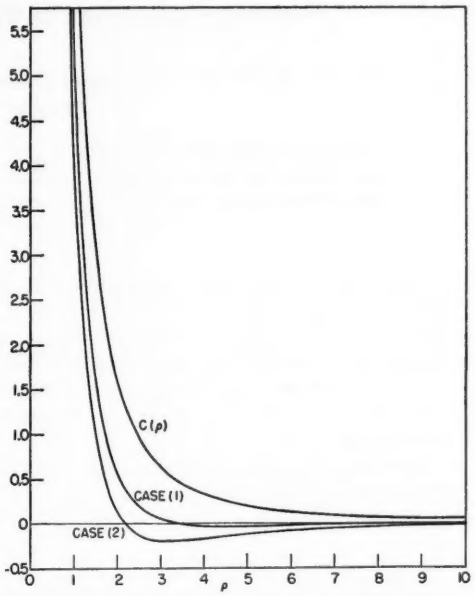

FIG. 4. The centripetal repulsion function $c(\rho)$ and the net effective potentials for (1) the Lévy central potential, and (2) the Lévy central potential with well depth adjusted to give the correct value of the binding energy of the deuteron. The units are the same as for Fig. 3.

short, of the right order of magnitude. This is of some interest since it indicates that, if the Lévy potential is correct,[18] strong three-body forces are not needed in the understanding of the triton. It indicates that the kinetic effects of the repulsive core are large and may be enough to at least partially insure saturation of nuclear forces in heavier nuclei.

The authors wish to take this opportunity to thank Mrs. Barbara Levine of the Joint Computing Group for performing the necessary numerical computations.

[18] The original derivation from meson theory was found to be faulty. See A. Klein, Phys. Rev. 89, 1158 (1953).

Variation Calculation of the Polarizability of the Deuteron

B. W. Downs
Stanford University, Stanford, California
(Received December 9, 1954)

The polarizability of the deuteron in a uniform electric field is calculated by a variation method. The result obtained by Ramsey, Malenka, and Kruse is rederived and improved in accuracy, and the modification of the deuteron wave function produced by the electric field is calculated.

IN a recent paper, Ramsey, Malenka, and Kruse[1] presented an approximate calculation of the electric polarizability of the deuteron. The purpose of the present paper is to rederive their result from a variation principle and to improve the accuracy. The modification of the deuteron wave function produced by the electric field is also found.

The Schrödinger equation for the relative motion in the center-of-mass system of a deuteron in a uniform electric field is

$$(H_0+H'-E)\psi=0. \tag{1}$$

The perturbation is $H'=-\frac{1}{2}e\mathcal{E}z$; z is the component of the relative n-p separation vector along the electric field, $\mathcal{E}$. A trial function $\psi=\psi_0+\mathcal{E}\phi$ is taken; ϕ may depend on $\mathcal{E}$. ψ_0 is the normalized, even-parity ground-state wave function, which satisfies the equation:

$$(H_0-E_0)\psi_0=0. \tag{2}$$

With the assumed trial function, the lowest energy level satisfies the variational inequality:

$$E\leqq\frac{\int(\psi_0^*+\mathcal{E}\phi^*)(H_0+H')(\psi_0+\mathcal{E}\phi)d\tau}{\int(\psi_0^*+\mathcal{E}\phi^*)(\psi_0+\mathcal{E}\phi)d\tau}. \tag{3}$$

In Eq. (3) and all subsequent expressions, the appropriate spin sums are implied. With Eq. (2), Eq. (3) can be written:

$$E\leqq E_0+\mathcal{E}^2\left\{\frac{1}{\mathcal{E}}\int\psi_0^*H'\phi d\tau+\frac{1}{\mathcal{E}}\int\phi^*H'\psi_0d\tau+\int\phi^*(H_0-E_0)\phi d\tau-E_0\left[\int\psi_0^*\phi d\tau+\int\phi^*\psi_0d\tau\right]^2\right\}+O(\mathcal{E}^3). \tag{4}$$

ϕ is taken to be that function which minimizes the right-hand side (rhs) of Eq. (4). Both ψ_0 and ϕ can be considered to be three-component wave functions, each component being associated with one of the possible values of the z component of the spin.[2] The rhs of Eq. (4) can be minimized by equating to zero its variation with respect to one component of ϕ^*. This process yields a differential equation for ϕ:

$$(H_0-E_0)\phi=-\frac{1}{\mathcal{E}}H'\psi_0+2E_0\psi_0\left\{\int\psi_0^*\phi d\tau+\int\phi^*\psi_0d\tau\right\}+O(\mathcal{E}). \tag{5}$$

The polarizability is determined by that term of $E-E_0$ which is quadratic in $\mathcal{E}$. From Eq. (4) it is clear that only that part of ϕ which is of zero order in $\mathcal{E}$ affects the polarizability. If ϕ is expressed as the sum of an even parity function and an odd parity function, Eq. (5) shows that only the odd parity function has a term of zero order in $\mathcal{E}$.[3] If only those quantities which affect the polarizability are considered, Eq. (5) becomes

$$(H_0-E_0)\phi=-\frac{1}{\mathcal{E}}H'\psi_0=\frac{e}{2}z\psi_0. \tag{6}$$

The polarizability is $\alpha=-2(E-E_0)/\mathcal{E}^2$; with this and Eq. (6), Eq. (4) yields[4]

$$\alpha=-\frac{2}{\mathcal{E}}\int\psi_0^*H'\phi d\tau=e\int\psi_0^*z\phi d\tau. \tag{7}$$

The odd parity solution of Eq. (6) is

$$\phi=\frac{e}{2}\int G(\mathbf{r},\mathbf{r}')z'\psi_0(\mathbf{r}')d\tau'; \tag{8}$$

$G(\mathbf{r},\mathbf{r}')$ is the deuteron Green's function.[5] With Eq.

[1] Ramsey, Malenka, and Kruse, Phys. Rev. 91, 1162 (1953).

[2] The singlet spin function need not be considered, because the perturbation H' does not connect singlet and triplet spin states.

[3] If the even parity function has a zero-order term, it must be a multiple of ψ_0; this cannot affect the polarizability.

[4] As a result of the variation process, Eq. (7) is an equality. That Eq. (7) is exact can be seen from an examination of Eq. (1): If $\psi=\psi_0+\mathcal{E}\phi$ is considered to be an eigenfunction, and ϕ is expressed as the sum of an even parity function and an odd parity function, then Eq. (1) can be separated into an even parity equation and an odd parity equation. These two equations show that Eq. (7) is exact and that the zero-order term of ϕ has odd parity and satisfies Eq. (6).

[5] Equation (8) can also be derived from perturbation theory, in analogy with the derivation by Ramsey *et al.* of their Eq. (5).

(8), Eq. (7) becomes

$$\alpha=\frac{e^2}{2}\int\int\psi_0^*(\mathbf{r})zG(\mathbf{r},\mathbf{r}')z'\psi_0(\mathbf{r}')d\tau'd\tau. \tag{9}$$

Equation (9) is the expression for α obtained by Ramsey *et al.*[1] by means of the Schrödinger perturbation theory. They approximated Eq. (9) by replacing the Green's function for the deuteron with that for a free particle. From Eqs. (6) and (8), it is clear that this approximation is equivalent to the assumption that the n-p interaction vanishes for odd parity states (Serber interaction). Ramsey *et al.*[1] have shown that, with the free-particle Green's function, Eq. (9) can be separated conveniently into contributions arising from the ground-state S wave alone (α_{SS}), from the D wave alone (α_{DD}) and from cross terms involving both S and D waves (α_{SD}).

Equation (8) has been used to calculate the modification ϕ_S of the ground-state S wave in two cases: The n-p interaction V_d is taken to be (1) a Serber interaction and (2) a (scalar) square well interaction for odd-parity states. In calculations which involve only the ground-state S wave, the spin functions can be omitted; the S wave ψ_S is taken to be the Hulthén wave function:

$$\psi_S=N\{e^{-\gamma r}-e^{-(\gamma+\beta)r}\}/r, \tag{10}$$

N is so chosen that the ground state is 96 percent S state. $\gamma^2=(2\mu/\hbar^2)\epsilon$; $\epsilon=-E_0=2.226$ Mev, and μ is the reduced mass. The Hulthén range parameter β is taken to be $\beta=6.0\gamma$.

Case 1. V_d a Serber Interaction

With the free-particle Green's function $G_f(\mathbf{r},\mathbf{r}')$ and $\psi_0=\psi_S$, Eq. (8) yields

$$\phi_S^{(1)}=\frac{e\mu}{\hbar^2}N\cos\theta\left\{\frac{1}{4\gamma}re^{-\gamma r}-\frac{1}{\beta^2(2\gamma+\beta)^2}\left[\frac{2(1+\gamma r)}{r^2}e^{-\gamma r}-\frac{2}{r^2}e^{-(\gamma+\beta)r}-\frac{2(\gamma+\beta)}{r}e^{-(\gamma+\beta)r}-\beta(2\gamma+\beta)e^{-(\gamma+\beta)r}\right]\right\}. \tag{11}$$

With this $\phi_S^{(1)}$ and Eq. (7), one gets[1]

$$\alpha_{SS}^{(1)}=0.56\times10^{-39}\ \text{cm}^3. \tag{12}$$

Case 2. V_d a Square Well

The n-p interaction in odd parity states is taken to be that (scalar) square well which is appropriate to the deuteron ground state:

$$V_d(r)=\begin{cases}-V_0=-33.73\ \text{Mev} & r\leqq a=2.100\times10^{-13}\ \text{cm},\\ 0 & r>a.\end{cases} \tag{13}$$

With $\psi_0=\psi_S$, Eq. (6) becomes

$$\left\{-\frac{\hbar^2}{2\mu}\nabla^2+V_d(r)-E_0\right\}\phi_S^{(2)}=\frac{e}{2}z\psi_S. \tag{14}$$

Equation (14) can be solved by setting[6]

$$\phi_S^{(2)}=f(r)\cos\theta. \tag{15}$$

With Eq. (15), Eq. (14) yields

$$\left\{\frac{d}{dr}r^2\frac{d}{dr}-\frac{2\mu}{\hbar^2}r^2V_d(r)-\gamma^2r^2-2\right\}f(r)=-\frac{e\mu}{\hbar^2}r^3\psi_S(r). \tag{16}$$

Equation (16) can be solved for $f(r)$ by means of a one-dimensional Green's function $g(r,r')$:

$$f(r)=-\frac{e\mu}{\hbar^2}\int g(r,r')r'^3\psi_S(r')dr'. \tag{17}$$

The Green's function for Eq. (16) is[7]

$$g(r,r')=-\frac{\gamma}{1.48659}U_{\mathrm{I}}(r_<)U_{\mathrm{II}}(r_>). \tag{18}$$

$r_<$ is the smaller of r, r'; $r_>$ is the larger.

$$U_{\mathrm{I}}(r)=\begin{cases}j_1(\rho r) & r\leqq a,\\ -1.970706ij_1(i\gamma r)+0.0274676n_1(i\gamma r) & r>a,\end{cases}$$
$$U_{\mathrm{II}}(r)=\begin{cases}j_1(\rho r)-5.59266n_1(\rho r) & r\leqq a,\\ -0.765008i[j_1(i\gamma r)+in_1(i\gamma r)] & r>a.\end{cases} \tag{19}$$

j_1 and n_1 are spherical Bessel functions; $\rho^2=\gamma^2[(V_0/\epsilon)-1]$. Since V_d is not exact, it seems best to express $\phi_S^{(2)}$ in such a way that the influence of the potential is manifestly small. This can be done by solving Eq. (14) directly for $\phi_S^{(2)}$:

$$\phi_S^{(2)}=(e/2)\int G_f(\mathbf{r},\mathbf{r}')z'\psi_S(r')d\tau'-\int G_f(\mathbf{r},\mathbf{r}')V_d(r')\phi_S^{(2)}(\mathbf{r}')d\tau'. \tag{20}$$

The first term on the rhs of Eq. (20) is $\phi_S^{(1)}$, which was calculated for Case 1; in the second term, the $\phi_S^{(2)}$ to be used is given by Eqs. (15) and (17). Thus

$$\phi_S^{(2)}=\phi_S^{(1)}+\frac{e\mu}{\hbar^2}\int G_f(\mathbf{r},\mathbf{r}')V_d(r')\times\cos\theta'\left\{\int g(r',r'')r''^3\psi_S(r'')dr''\right\}d\tau'. \tag{21}$$

[6] H' connects the S state only with P states.

[7] This one-dimensional Green's function was calculated for a square well with $\rho a=1.830600$ and $\gamma a=0.4865936$. The Wronskian of the functions U_{I} and U_{II} which are given in Eq. (19), calculated for $r<a$, agrees with that calculated for $r>a$ to six figures.

Since $V_d(r')=0$ for $r'>a$, the r'' integral in Eq. (21) need only be evaluated for $r'\leqq a$. In the r'' integral, which was evaluated exactly, the term which arises from the $e^{-(\gamma+\beta)r''}$ term of ψ_S is small[8] compared to that which arises from the $e^{-\gamma r''}$ term of ψ_S for $r'\leqq a$. This small contribution was neglected in the subsequent r' integration. For the r' integration, the integrand was expanded in a power series, whose values differed from those of the original expression by less than 1 percent for $r'\leqq a$. With the resulting $\phi_S^{(2)}$, Eq. (7) yielded[9]

$$a_{SS}^{(2)}=a_{SS}^{(1)}+\delta a_{SS}, \quad \delta a_{SS}=0.020\times10^{-39}\ \text{cm}^3. \quad (22)$$

The author is indebted to Professor L. I. Schiff for suggesting this problem and for his guidance throughout its solution.

[8] The ratio of the term which arises from $e^{-(\gamma+\beta)r''}$ to that which arises from $e^{-\gamma r''}$ is -0.112 at $r'=0.10a$, -0.061 at $r'=0.50a$, and -0.032 at $r'=a$. The contribution of this term to δa_{SS} would be about -0.001×10^{-39} cm^3. With this estimate, Eq. (22) would read $\delta a_{SS}=0.019\times10^{-39}$ cm^3.

[9] *Note added in proof.*—J. Sawicki, Acta phys. Polon. **13**, 225 (1954), has used a different variation technique to obtain $a_{SS}\approx0.32\times10^{-39}$ cm^3. His method yields a lower limit for a_{SS}.

PHYSICAL REVIEW VOLUME 98, NUMBER 1 APRIL 1, 1955

Derivation of the Feynman-Dyson Rules from Time-Independent Theory

SAUL T. EPSTEIN
The University of Nebraska, Lincoln, Nebraska
(Received December 15, 1954)

The Feynman-Dyson rules for computing the scattering matrix are derived starting with the time-independent Schrödinger equation. Although no essentially new results are obtained, it is interesting to trace the connection between the time-dependent and time-independent methods starting from the time-independent end rather than, as is usually done, starting from the time-dependent interaction representation. In particular, a theorem due to R. J. Eden plays an important role in our discussion.

I. INTRODUCTION

THE Feynman-Dyson rules[1] for the calculation of scattering matrix elements differ from the rules of the older formulations of perturbation theory in two essential ways: (A) One can immediately write down the net contribution of all virtual processes which can be represented by the same "Feynman diagram" whereas in the older theory each virtual process was treated separately. (B) Not only is momentum conserved at each "vertex" (as in the older theory), but also energy is conserved at each "vertex."

These rules were originally derived by Dyson[1] from the time-dependent Schrödinger equation in the interaction representation, and by Feynman[1] from his Lagrangian formulation of quantum mechanics. In this note we will derive the Feynman-Dyson rules starting from the time-independent Schrödinger equation. We feel that this derivation may be of interest for two reasons: (i) It is hoped that the derivation of the Feynman-Dyson rules from the time-independent Schrödinger equation for problems in the continuum may suggest ways of further clarifying the connection between the "relativistic two-body equation"[2] and the time-independent Schrödinger equation for bound states. (ii) Our work may also be considered as a contribution to the discussion[3] of the connection between the Feynman-Dyson and the time-independent definitions of the scattering matrix. Our approach is different from that of most authors in that we start from the time-independent theory rather than from the time-dependent theory, and although no essentially new results are obtained in this way it does seem of interest to look at the connection from the "other end." In particular, we will find that a theorem due to Eden[4] will play an important role in our discussion.

In the next section we will carry through a derivation of the Feynman-Dyson rules and in the final section we will make a connection with the "adiabatic switch-on, switch-off method."[5]

II. DERIVATION OF THE FEYNMAN-DYSON RULES

The state vector for the time-independent scattering problem with interaction V satisfies the well-known equation:[6]

$$\psi=\phi-2\pi i\delta_+(E-H_0)V\psi, \quad (1)$$

where $H_0\phi=E\phi$, and where

$$\delta_+(x)=\tfrac{1}{2}\delta(x)-\text{p.v.}\frac{1}{2\pi ix}, \quad (2)$$

[1] R. P. Feynman, Phys. Rev. **76**, 749 and 769 (1949); F. J. Dyson, Phys. Rev. **75**, 486 and 1736 (1949).
[2] E. E. Salpeter and H. A. Bethe, Phys. Rev. **84**, 1232 (1951); J. Schwinger, Proc. Nat. Acad. Sci. U. S. **37**, 452 and 455 (1951).
[3] See F. J. Belinfante and C. Møller, Kgl. Danske Videnskab. Selskab, Mat.-fys. Medd. **28**, No. 6 (1954) for a detailed discussion of the problem and references to the literature.
[4] R. J. Eden, Proc. Roy. Soc. (London) **A198**, 540 (1949).
[5] B. A. Lippmann and J. Schwinger, Phys. Rev. **79**, 469 (1950).
[6] P. A. M. Dirac, *Quantum Mechanics* (Clarendon Press, Oxford, 1947), third edition, pp. 197–199.

p.v. standing for principal value. Some useful representations of these singular functions are

$$\delta_+(x)=\lim_{\eta\to 0}-\frac{1}{2\pi i}\frac{1}{x+i\eta},\quad \delta(x)=\lim_{\eta\to 0}\frac{\eta}{\pi(x^2+\eta^2)} \tag{3a}$$

and

$$\delta_+(x)=\frac{1}{2\pi}\int_0^\infty d\tau e^{i\tau x},\quad \delta(x)=\frac{1}{2\pi}\int_{-\infty}^\infty d\tau e^{i\tau x}. \tag{3b}$$

What we are interested in computing is the matrix element $(\phi',V\psi)$ on the energy shell,[5] i.e., with $H_0\phi'=E\phi'$. In the usual way, we write this matrix element as $(\phi',T\phi)$ whence from (1), using the representation (3a), we see that

$$T=V[1-(E+i\eta-H_0)^{-1}V]^{-1}$$
$$=V[E+i\eta-H_0-V]^{-1}[E+i\eta-H_0],$$

which on the energy shell becomes

$$T=i\eta V[E+i\eta-H_0-V]^{-1}, \tag{4a}$$

or

$$T=\frac{2V}{\delta(0)}\delta_+(E-H_0-V). \tag{4b}$$

We now use the representation (3b) to write (4b) as

$$T=\frac{1}{\pi\delta(0)}\int_0^\infty d\tau e^{iE\tau}Ve^{-i(H_0+V)\tau},$$

which, on the energy shell, becomes

$$T=\frac{1}{\pi\delta(0)}\int_0^\infty d\tau e^{iH_0\tau}Ve^{-i(H_0+V)\tau}$$
$$\equiv\frac{1}{\pi\delta(0)}\int_0^\infty d\tau V(\tau)U(\tau,0), \tag{5}$$

where $V(\tau)=e^{iH_0\tau}Ve^{-iH_0\tau}$ and $U(\tau,0)=e^{iH_0\tau}e^{-i(H_0+V)\tau}$.

From its definition we see that $U(\tau,0)$ satisfies the equations

$$dU(\tau,0)/d\tau=-iV(\tau)U(\tau,0),\quad U(0,0)=1, \tag{6}$$

whence we may also write

$$U(\tau,0)=P\exp\left(-i\int_0^\tau V(\tau')d\tau'\right), \tag{7}$$

where P is Dyson's chronological ordering operator. Further, by comparing (5) and (6), we see that

$$T=\frac{i}{\pi\delta(0)}\int_0^\infty dU(\tau,0)=\frac{i}{\pi\delta(0)}[U(\infty,0)-1]. \tag{8}$$

With this result, we have completed the derivation of part (A) of the Feynman-Dyson rules, since by using the form (7) for $U(\infty,0)$ we can analyze the perturbation expansion of $U(\infty,0)-1$ into "Feynman diagrams."

To establish part (B) of the Feynman-Dyson rules, we must now show that we can replace $U(\infty,0)-1$ by $(U(\infty,-\infty)-1)/2$ since $U(\infty,-\infty)$ is the Feynman-Dyson scattering matrix and the factor $\frac{1}{2}$ is needed in order to get the proper connection between T and the scattering matrix.[5] However, in agreement with other authors,[3] we are thus far able to derive this result only by the use of perturbation theory. If we use perturbation theory then, as we stated earlier, we can analyze $U(\infty,0)-1$ into "Feynman diagrams" and we can also analyze $U(\infty,-\infty)-1$ into the *same* diagrams. The difference between the contribution of a diagram in the two cases arises from the fact that if E_k is (minus) the sum of the energies at the kth vertex in a diagram, then in the case of $U(\infty,0)-1$ one will get a factor of

$$(2\pi)^{-1}\int_0^\infty d\tau_k e^{iE_k\tau_k}=\delta_+(E_k),$$

while in the case of $U(\infty,-\infty)-1$ one will get a factor of

$$(2\pi)^{-1}\int_{-\infty}^\infty d\tau_k e^{iE_k\tau_k}=\delta(E_k),$$

i.e., the energy conservation mentioned in the introduction. Hence if there are N vertices in a diagram we must compare

$$\prod_{k=1}^N\delta_+(E_k)\quad\text{with}\quad\prod_{k=1}^N\delta(E_k).$$

This we do by use of a theorem due to Eden[4] according to which

$$\prod_{k=1}^N\delta_+(E_k)=Z\delta_+\left(\sum_{k=1}^N E_k\right),\quad \prod_{k=1}^N\delta(E_k)=Z\delta\left(\sum_{k=1}^N E_k\right),$$

where Z is a function which need not concern us here. Now the fact that we are on the energy shell means that $\sum_{k=1}^N E_k=0$ and therefore

$$\delta_+\left(\sum_{k=1}^N E_k\right)=\tfrac{1}{2}\delta\left(\sum_{k=1}^N E_k\right)$$

so that from Eden's theorem we may conclude that on the energy shell we may replace

$$\prod_{k=1}^N\delta_+(E_k)\quad\text{by}\quad\tfrac{1}{2}\prod_{k=1}^N\delta(E_k)$$

and hence that we may replace $U(\infty,0)-1$ by $[U(\infty,-\infty)-1]/2$, which completes the derivation of the Feynman-Dyson rules.

III. DISCUSSION

Equation (8) in the preceding section is apparently derived without approximation. However in its derivation we used the representation (3b) which is perhaps

not as satisfactory as using a limiting process as in (3a). If in fact we do need to use such a process, then in order to derive (8) it appears that we must assume the validity of the representation:

$$\delta_+(E-H_0-V)=\lim_{\eta\to 0}\frac{1}{2\pi}\int_0^\infty d\tau e^{-\eta\tau+iE\tau}$$

$$\times P\exp\left(-i\int_0^\tau (H_0+Ve^{-\eta\tau'})d\tau'\right). \quad (9)$$

To see this, we introduce (9) into (4a) and, defining

$$V'(\tau)=V(\tau)e^{-\eta\tau},$$

$$U'(\tau,0)=e^{iH_0\tau}P\exp\left(-i\int_0^\tau (H_0+Ve^{-\eta\tau'})d\tau'\right),$$

we find

$$T=\eta\int_0^\infty d\tau V'(\tau)U'(\tau,0).$$

But from its definition $U'(\tau,0)$ satisfies

$$dU'(\tau,0)/d\tau=-iV'(\tau)U'(\tau,0), \quad U'(0,0)=1,$$

whence we can write

$$U'(\tau,0)=P\exp\left(-i\int_0^\tau V'(\tau')d\tau'\right)$$

and[7]

$$T=i\eta(U'(\infty,0)-1), \quad (8')$$

[7] If we would start with the representation

$$\delta_+(x)=\lim_{\eta\to 0}\frac{1}{2\pi}\int_0^\infty d\tau e^{ix\tau-\eta\tau},$$

which is equivalent to (3b) and presumably not subject to any doubt, then one can derive from (4a), after an integration by parts, that

$$T=i\eta\left(\eta\int_0^\infty d\tau U(\tau,0)e^{-\eta\tau}-1\right).$$

From this one can "derive" an expression which is in a certain sense intermediate between (8) and (8') by writing

$$T=i\eta\left(\int_0^\infty dZU\left(\frac{Z}{\eta},0\right)e^{-Z}-V\right)$$

and saying that in the limit as $\eta\to 0$ this becomes what we might write, in a sort of "mixed representation" of singular functions as

$$T=i\eta(U(\text{“}\infty\text{,”}0)-1).$$

which just corresponds to (8). We have as yet been unable to give an *a priori* proof of the general validity of (9).

It is interesting to complete the derivation of the Feynman-Dyson rules by using this representation. To do this we consider the perturbation expansion of $U'(\infty,0)-1$. Now the $\prod_{k=1}^N \delta_+(E_k)$ will appear as

$$\prod_{k=1}^N\left(-\frac{1}{2\pi i}\right)\frac{1}{E_k+i\eta}$$

which, from Eden's theorem, we may replace by

$$\frac{1}{2}\prod_{k=1}^N\frac{1}{\pi}\frac{\eta}{E_k^2+\eta^2}.$$

One readily sees that this replacement is equivalent to replacing

$$\prod_{k=1}^N\frac{1}{2\pi}\int_0^\infty d\tau_k e^{iE_k\tau_k-\eta\tau_k} \quad \text{by} \quad \frac{1}{2}\prod_{k=1}^N\frac{1}{2\pi}\int_{-\infty}^\infty d\tau_k e^{iE_k\tau_k-\eta|\tau_k|},$$

which in turn is equivalent to replacing $U'(\infty,0)-1$ by $[U''(\infty,-\infty)-1]/2$, where

$$U''(\infty,-\infty)=P\exp\left(-i\int_{-\infty}^\infty V''(\tau)d\tau\right),$$

and where

$$V''(\tau)=V(\tau)e^{-\eta|\tau|}.$$

Thus we have established a connection with the "adiabatic switch-on, switch-off method"[5] but, in agreement with other authors,[3] only by the use of a perturbation expansion.

I wish to thank Professor H. Jehle for a very interesting discussion.

Letters to the Editor

PUBLICATION of brief reports of important discoveries in physics may be secured by addressing them to this department. The closing date for this department is five weeks prior to the date of issue. No proof will be sent to the authors. The Board of Editors does not hold itself responsible for the opinions expressed by the correspondents. Communications should not exceed 600 words in length and should be submitted in duplicate.

Shell Theory for the Nuclei with Mass 19*

MARTIN G. REDLICH
Department of Physics, University of Wisconsin, Madison, Wisconsin
(Received February 2, 1955)

CALCULATIONS for the nuclei with $A=19$ have been made on the basis of a shell model with a harmonic oscillator central potential to represent the O^{16} core, central Gaussian interactions between pairs of outer nucleons, and energy differences between $1d_{3/2}$, $2s_{1/2}$, and $1d_{5/2}$ single-particle levels equal to the ones observed for levels with these spins and parity + in O^{17}. The model and all parameters save one are the ones which have been used in previous calculations[1] for $A=18$. One parameter, the depth of the two-nucleon potential, $-V_0$, will later be changed from the value 70.8 Mev, which, for the range used, gives the correct H^2 binding energy.

The basic wave functions were taken in j-j coupling form. Earlier calculations[2] had indicated that the configurations $(d_{5/2})^3$ and $(d_{5/2})^2s_{1/2}$ do not alone account for the data. It is necessary to take into account all configurations of the $1d$, $2s$ shell. They can be grouped as follows: The ones with no $d_{3/2}$ particles, which lie lowest, are of Type 0, those with one or more than one $d_{3/2}$ particles are of Type 1 or 2, respectively. For the Type 0 configurations, ordinary and space-exchange forces lead to a ground state with $J=5/2$ or $1/2$; spin-exchange and space-and-spin-exchange forces yield $J\geq 7/2$. The ground state of F^{19} has $J=1/2$, and therefore an equal mixture of the first two forces was used, just as for $A=18$.

For each (T,J) of Table I the matrix of the two-nucleon potential was calculated. The submatrix for the Type 0 and 1 configurations was diagonalized and the characteristic vector for the lowest characteristic (i.e., energy) value was obtained. The Type 2 configurations were taken into account by further subdiagonalization and perturbation theory. For $V_0=-70.8$ Mev, the (1/2,5/2) state lies below the (1/2,1/2) state, contrary to experiment (see Table II). This order is reversed with a decrease in the $d_{3/2}-d_{5/2}$ energy difference; that is, with larger admixtures of the higher configurations. To effect this, calculations have been made with $-V_0$ arbitrarily increased to 103.2 Mev.

TABLE I. Weights of various configurations in percent, for $V_0=-103.2$ Mev.

State (T,J)	Type Config.	0 $d_{5/2}^3$	0 $d_{5/2}^2s_{1/2}$	0 $s_{1/2}^2d_{5/2}$	0 $s_{1/2}^3$	Type 0 total	Type 1 total	Type 2 total
(1/2,1/2)		9	40	···	30	79	14	7
(1/2,5/2)		50	10	19	···	79	11	10
(3/2,5/2)		68	0	19	···	87	3	10
(3/2,1/2)		···	88	···	···	88	2	10

Table I contains the weights (quantum-mechanical probabilities) of various configurations. Type 0 configurations are by far predominant. Nonetheless interaction between these and the higher configurations indicates that $j-j$ coupling is not accurate; this calculation may therefore be considered to be of "intermediate coupling" character.

Comparison with experiment.—The calculations account only for states with parity +. For O^{19}, the lowest of these has $J=5/2$. Other results are compared in Table II with data already available. For the larger depth there is agreement with experiment for the energy differences between (1) the 5/2+ and 1/2+ states of F^{19} and (2) the ground states of O^{19} and F^{19}, as well as the ft values of two allowed β transitions: (3) $Ne^{19}(\beta^+)F^{19}$, which is favored and (4) $O^{19}(\beta^-)F^{19}$ (5/2+), which is unfavored. It seems noteworthy that the last ft value is obtained despite the fact that the configuration $(d_{5/2})^3$ has weights 50 and 68 percent in the initial and final states.

TABLE II. Comparison of theory with experiment. [$E(T,J)$ = energy of lowest state with (T,J); μ = magnetic moment.]

Datum	Relevant nucleus or nuclei	Theory, with $V_0=-70.8$ Mev	Theory, with $V_0=-103.2$ Mev	Experiment[a]
$E(1/2,5/2)-E(1/2,1/2)$	F^{19}	−0.08	0.17	0.200 Mev ±0.002
$\mu(1/2,1/2)$	F^{19}		2.94	2.628 nm
$T_{1/2}(E2,\gamma\text{-transition})$	F^{19}		2.3×10^{-7}	1.0×10^{-7} sec ±0.2
$E(3/2,1/2)-E(3/2,5/2)$	O^{19}		0.45	1.47 Mev ±0.02
$E(3/2,5/2)-E(1/2,1/2)$	O^{19}, F^{19}	5.39	8.47	7.7[b] Mev
ft value for $(1/2,1/2)\rightarrow(1/2,1/2)$	$Ne^{19}\rightarrow F^{19}$		1570	1700 ±170
ft value for $(3/2,5/2)\rightarrow(1/2,5/2)$	$O^{19}\rightarrow F^{19}$	128 000	367 000	355 000 ±100 000

[a] Data are taken from F. Ajzenberg and T. Lauritsen, Revs. Modern Phys. (to be published).
[b] This number equals the maximum β-decay energy of O^{19} to the 5/2 state of F^{19} + the 200-kev γ-ray energy + 3.67 Mev calculated Coulomb energy difference − ($n-H^1$) atomic mass difference.

There is disagreement with experiment for (5) the magnetic moment of the ground state and (6) the half-life of the 5/2+ state of F^{19}, as well as (7) the energy of the 1/2+ state of O^{19}. The quantities (3), (5), (6), and (7) appear to change only slightly with a decrease in depth to 70.8 Mev; the other quantities, however, decrease substantially, as is seen in Table II. Calculations of these and other data with a Yukawa

two-nucleon potential and the Rosenfeld mixture of forces have been made in England.[3]

I am grateful to Professor E. P. Wigner for suggesting this investigation and to him and Dr. I. Talmi for their advice and interest.

* Supported by the U. S. Atomic Energy Commission.

[1] M. G. Redlich, Phys. Rev. **95**, 448 (1954).
[2] M. G. Redlich, Princeton University dissertation, January, 1954 (unpublished).
[3] J. P. Elliott and B. H. Flowers (to be published).

Spin and Lifetime of the 439-kev Excited State of Hg^{202}†

FRANZ R. METZGER

Bartol Research Foundation of The Franklin Institute, Swarthmore, Pennsylvania

(Received February 11, 1955)

USING a source of Tl^{202} at a temperature of 1000°C, we have observed nuclear resonance fluorescence from the 439-kev excited state of Hg^{202}.

The angular distribution of the resonance radiation, measured at angles ranging from 102 to 147 degrees, is reproduced in Fig. 1. It agrees, within the experimental uncertainty, with the distribution expected for an excited state with spin 2 and a ground state with spin 0. The angular distribution measurement thus confirms the tentative assignment[1] of spin 2 to the 439-kev level in Hg^{202} which was based on measured K/L and $(L_I+L_{II})/L_{III}$ ratios and on the systematics[2] of the first excited states of even-even nuclei.

The angular distribution experiments were performed with a gaseous source of thallium iodide. In such a source the recoil due to the radiation preceding the 439 kev level, i.e., the neutrino recoil accompanying electron capture, is still effective when the gamma radiation is emitted. The resonance fluorescence effect is therefore large and easily measured. However, the electron capture transition energy of Tl^{202} is not known and the lifetime of the 439-kev transition cannot be deduced from such an experiment. In order to determine the lifetime, a solid or liquid source has to be used. In this case, the neutrino recoil is dissipated before the gamma emission takes place and the gamma emitting nuclei are in thermal equilibrium with the surroundings. The broadening of the gamma line due to the thermal motion can then be calculated and the lifetime can be deduced from the magnitude of the resonance fluorescence effect.

Such a pure "thermal" source can be realized by using metallic thallium. At 1000°C the vapor pressure of thallium is approximately 13 mm Hg.[3] If sufficient amounts of inactive metal are added as a carrier, the percentage of the activity present in the vapor phase can be made negligible even at 1000°C.

The metal source was prepared by electroplating

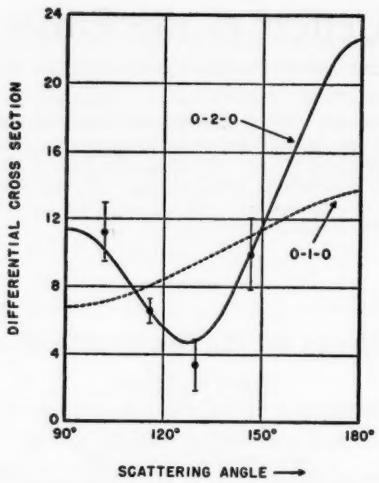

FIG. 1. Angular distribution of the resonance radiation from the 439-kev level of Hg^{202}. The solid line represents the theoretical angular distribution for an excited state with spin 2 and a ground state with spin 0. The dashed line represents the theoretical distribution for an excited state with spin 1. The differential cross section in arbitrary units is plotted as the ordinate.

thallium out of an ammonia solution ($p_H=10$) to which several hundred milligrams of hydroxylamine hydrochloride had been added. With a current density of 50 ma/cm² at the platinum electrodes, more than 95 percent of the activity were plated out in two hours.[4]

Based on the magnitude of the resonance fluorescence effect with this metal source, the lifetime τ_γ of the 439-kev transition in Hg^{202} was calculated to be $(3.5\pm0.7)\times10^{-11}$ second. Using a total conversion coefficient of 4×10^{-2} for this electric quadrupole transition, the lifetime for the 439-kev level becomes $(3.4\pm0.7)\times10^{-11}$ second.

The corresponding 411-kev transition in Hg^{198} had previously been found[5] to have a lifetime of $(3.3\pm0.3)\times10^{-11}$ second, i.e., in spite of its smaller energy it is somewhat faster. However, only a survey of more of the even-even Hg isotopes will show whether there exists a trend towards smaller $E2$ transition probabilities as the closed neutron shell at $N=126$ is approached.

As was mentioned earlier, the measurements with gaseous sources could be used to determine the lifetime provided the electron capture transition energy were known. On the other hand, with the lifetime known from the experiments with the metallic source, the measurements with the gaseous source can be used to determine the electron capture transition energy. Preliminary results have been obtained, but further experiments will be necessary in order to ascertain the correctness of the assumptions made with respect to the recoiling molecules.

It is a pleasure to thank Professor W. B. Keighton for his help in the chemical preparation of the sources, Mr. W. B. Todd for his assistance in taking the data,

and Mr. J. B. Bulkley of the Radioactivity Center at the Massachusetts Institute of Technology for his cooperation in arranging the necessary cyclotron bombardments.

† Assisted by the joint program of the Office of Naval Research and the U. S. Atomic Energy Commission.

[1] Bergström, Hill, and de Pasquali, Phys. Rev. **92**, 918 (1953).
[2] G. Scharff-Goldhaber, Phys. Rev. **90**, 487 (1953); P. Preiswerk and P. Stähelin, Helv. Phys. Acta **24**, 623 (1952).
[3] *Handbook of Chemistry and Physics* (1952/53) (Chemical Rubber Publishing Company, Cleveland, 1952), p. 1990.
[4] We thank Professor R. G. Wilkinson of Indiana University for his advice concerning the plating process.
[5] F. R. Metzger and W. B. Todd, Phys. Rev. **95**, 853 (1954).

Self-Energy Effects on Meson-Nucleon Scattering According to the Tamm-Dancoff Method

J. C. TAYLOR
Peterhouse, Cambridge, England
(Received January 24, 1955)

IN a paper with the foregoing title, Visscher[1] has shown that the self-energy effects in the Tamm-Dancoff method (as modified by Dyson) give rise to an unphysical pole in the meson-nucleon wave function. We show here that a simple and natural modification of the usual way of eliminating the negative frequency components removes this difficulty.

We use Visscher's notation. Define

$$X(\mathbf{p})=[X^+(\mathbf{p})u+X^-(\mathbf{p})w](M/E_p)^{\frac{1}{2}}$$
$$=[(\Psi_0^*(0)b_{\mathbf{p}u}a_{-\mathbf{p}\alpha}\Psi(0))u + (\Psi_0^*(0)b_{\mathbf{p}w}{}^*a_{-\mathbf{p}\alpha}\Psi(0))w](M/E_p)^{\frac{1}{2}},$$

where w is a negative-energy solution of the Dirac equation; and

$$-i\gamma_4(p\cdot\gamma-iM)N(p)=\tfrac{3}{4}iG^2\Omega_R(p\cdot\gamma),$$

where Ω_R is the finite self-energy function defined by Visscher. We suppose the meson negative-frequency components eliminated, since they are not our concern; and we leave out the meson self-energy term for simplicity. Then the second-order equation has the form

$$(\epsilon-H_p-\omega_p)[1-\gamma_4N(p)]X(\mathbf{p}) = \int\gamma_4K(\mathbf{p},\mathbf{k})X(\mathbf{k})d\mathbf{k}, \quad (1)$$

where $p=(\mathbf{p},\epsilon-\omega_p)$ and K represents the interaction terms. Visscher drops negative energy components from (1), to give the approximate equation

$$(\epsilon-E_p-\omega_p)[1-(\bar{u}(\mathbf{p})N(p)u(\mathbf{p}))M/E_p]X^+(\mathbf{p}) = \int(M/E_p)^{\frac{1}{2}}(\bar{u}(\mathbf{p})K(\mathbf{p},\mathbf{k})v(\mathbf{k}))(M/E_k)^{\frac{1}{2}}X^+(\mathbf{k})d\mathbf{k}, \quad (2)$$

and a zero of the factor in the square bracket causes the unwanted pole in $X^+(\mathbf{p})$.

We propose the following alternative prescription. First transfer the square bracket in (1) to the right-hand side, then separate and drop the negative frequency components, to give

$$(\epsilon-E_p-\omega_p)X^+(\mathbf{p})=\int(M/E_p)^{\frac{1}{2}}(\bar{u}(\mathbf{p})\{[1-\gamma_4N(p)]^{-1} \times K(\mathbf{p},\mathbf{k})\}v(\mathbf{k}))(M/E_k)^{\frac{1}{2}}X^+(\mathbf{k})d\mathbf{k}. \quad (3)$$

A natural further approximation gives

$$(\epsilon-E_p-\omega_p)X^+(\mathbf{p})=(\bar{u}(\mathbf{p})[\gamma_4-N(p)]^{-1}u(\mathbf{p}))M/E_p \times\int(M/E_p)^{\frac{1}{2}}(\bar{u}(\mathbf{p})K(\mathbf{p},\mathbf{k})v(\mathbf{k}))(M/E_k)^{\frac{1}{2}}X^+(\mathbf{k})d\mathbf{k} \quad (4)$$

as our alternative to Eq. (2).

The factor in front of the integral in (4) can be written

$$[L(u^2)]^{-1}[1-(\bar{u}(\mathbf{p})N(-p)u(\mathbf{p}))M/E_p], \quad (5)$$

where $u=\gamma\cdot p/(iM)$, and $L(u^2)$ is a function defined by Feldman.[2] This is verified by noting that N is connected with Feldman's function $f(u)$ by the equation

$$-\tfrac{1}{3}\gamma_4N(p)=cf(u).$$

Feldman has found the zeros of $L(u^2)$ (when $\mu=0$), and none of them is real. Therefore, Eq. (4) does not have the difficulty of Eq. (2).

[1] W. M. Visscher, Phys. Rev. **96**, 788 (1954).
[2] G. Feldman, Proc. Roy. Soc. (London) **223A**, 112 (1954).

Photoproduction of π^+ Mesons from Hydrogen Near Threshold*

J. E. LEISS,† C. S. ROBINSON, AND S. PENNER
Department of Physics, University of Illinois, Urbana, Illinois
(Received January 27, 1955)

THE total cross section for photoproduction of π^+ mesons very close to threshold has been investigated, following the method of a preliminary experiment.[1] π^+ mesons and their μ^+ decay mesons were stopped in a carbon absorber surrounding the target. Since the positrons from the decay of the stopped μ^+ mesons are emitted with an energy spectrum peaked around 36 Mev,[2] a large fraction will escape with considerable energy and can be counted. Since the decay of the stopped μ^+ mesons is isotropic, the positrons leaving the absorber will be essentially isotropic, regardless of the angular distribution of the emitted π^+ mesons. Except for small corrections due to geometry

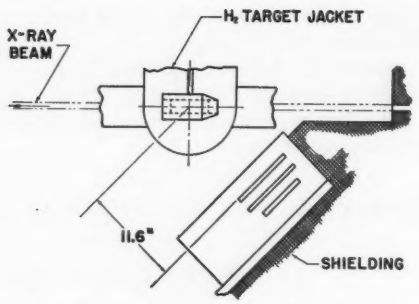

FIG. 1. Experimental arrangement, showing hydrogen target, absorber around target, counters, and shielding.

effects and to positron energy loss in the target and absorber, the spectrum and angular distribution of positrons leaving the absorber are independent of the energy of the photon which initiated the reaction.

The geometry used is shown in Fig. 1. The liquid hydrogen target is a cylinder $1\frac{1}{4}$ in. in diameter and 4 in. long with 0.001-in. brass windows for the x-ray beam. The beam diameter at the target was 0.681 in. The hydrogen target was surrounded by a hollow carbon cylinder 6 in. long with 0.500-in. wall, to stop most mesons produced by photons of less than 185 Mev. Triple coincidences in the three $\frac{3}{8}$-in. plastic scintillators were counted. Background from hydrogen, due to pair production, is small and was subtracted on the basis of counting rates below meson threshold. Activation curves were obtained in 2-Mev steps from 140 to 200 Mev.

The cross sections determined from the activation curves[3,4] must be corrected for the counting efficiency, composed of three factors: (1) the fraction of mesons which stop in the hydrogen or carbon ($\sim$90 percent); (2) the solid angle of the counters ($\sim$0.13 steradian); (3) the fraction of positrons heading for the detector which are counted ($\sim$50 percent). The efficiency has been calculated using Monte Carlo methods and the Illiac and is believed accurate to <10 percent.

Using arguments given by Bernardini and Goldwasser,[5] one can express the total cross section by

$$\sigma_T/4\pi\chi = A_0 + A_2\eta^2,$$

where

$$\chi = (k/\nu)(1+\nu/M)^{-1}(1+\omega/M)^{-1}, \quad \eta = k/\mu c,$$

ν = photon momentum or energy, and k and ω = meson momentum and energy, respectively. The best straight-line fit to our data in a plot of $\sigma_T/4\pi\chi$ *vs* η^2 gives $A_0 = (1.60\pm0.10)\times10^{-29}$, $A_2 = (1.20\pm0.56)\times10^{-29}$. See Fig. 2. The errors shown for the points are statistical only. In a similar plot for the 90° cross section, using data of this experiment together with that of other work at higher energies[6] (near threshold $\sigma_T/4\pi \cong \sigma_{90°}$), one obtains $A_0 = (1.56\pm0.06)\times10^{-29}$, $A_2 = (1.46\pm0.19)\times10^{-29}$. This shows that A_0 is insensitive to the energy range assumed, and is therefore reasonably well determined.

Using a weighted mean value of $A_0 = (1.57\pm0.05)\times10^{-29}$ and the value 1.4 ± 0.1 for the ratio of π^- to π^+ photoproduction in deuterium at threshold,[7] we have determined the renormalized symmetric coupling constant g, and the coupling constant f of the Chew cutoff theory[7] to be $g^2 = 11.7\pm0.7$, $f^2 = 0.069\pm0.004$.

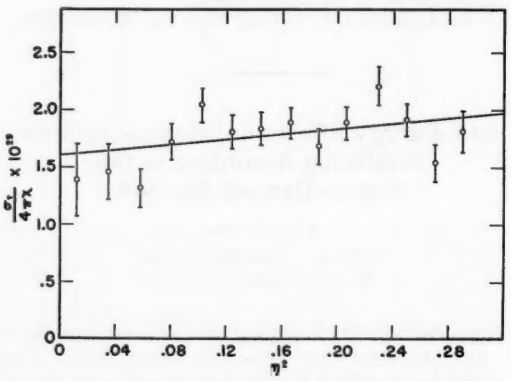

FIG. 2. Total cross section, $\sigma_T/4\pi\chi$, plotted *versus* η^2. Solid curve is $\sigma_T/4\pi\chi = (1.60+1.20\eta^2)\times10^{-29}$. The range of photon energy for the points is from 152.8 to 178.7 Mev.

Using the foregoing data, the π^-/π^+ ratio in deuterium,[8] and the branching ratio in the Panofsky experiment,[9] one may calculate[10,11] a threshold value for the difference of the S-wave scattering phase shifts, $(\alpha_1-\alpha_3)/\eta = 10.5° \pm 1.3°$. (Bethe and de Hoffmann[11] obtain $10.7°\pm2.5°$ from the data of Bernardini and Goldwasser.) This result, when compared with the value $\sim17°$ from scattering experiments at higher energies, is further evidence that $\alpha_1-\alpha_3$ does not depend linearly on η. It should be noted, however, that this interpretation of the Panofsky experiment, based on charge independence, is in some doubt because of the $\pi^- - \pi^0$ mass difference.

The authors are indebted to Professor G. Bernardini and Professor A. O. Hanson for many helpful discussions and suggestions.

* This work supported in part by the U. S. Atomic Energy Commission, Office of Naval Research, and the National Science Foundation.

† Now at Betatron Section, National Bureau of Standards, Washington, D. C.

[1] C. S. Robinson and J. E. Leiss, Phys. Rev. **95**, 638(A) (1954).
[2] Sagane, Dudziak, and Vedders, Phys. Rev. **95**, 863 (1954).
[3] L. Katz and A. G. W. Cameron, Can. J. Phys. **29**, 518 (1951).
[4] A. S. Penfold and J. E. Leiss, Phys. Rev. **95**, 637(A) (1954).
[5] G. Bernardini and E. L. Goldwasser, Phys. Rev. **95**, 857 (1954).
[6] J. E. Leiss and C. S. Robinson, Phys. Rev. **95**, 638(A) (1954).
[7] G. F. Chew, Phys. Rev. **95**, 1669 (1954).
[8] Sands, Teasdale, and Walker, Phys. Rev. **95**, 592 (1954).
[9] Panofsky, Aamodt, and Hadley, Phys. Rev. **81**, 565 (1951).
[10] J. Orear, Phys. Rev. **96**, 176 (1954).
[11] H. A. Bethe and F. de Hoffmann, Phys. Rev. **95**, 1100 (1954).

Nuclear Surface Energy and the Diffuseness of the Nuclear Surface

W. J. Swiatecki

Institute for Mechanics and Mathematical Physics and The Gustaf Werner Institute for Nuclear Chemistry, Uppsala, Sweden

(Received October 1, 1954)

IN the course of an attempt to interpret the empirical magnitude of the nuclear surface energy $S(4\pi R_0^2 S = 15$ Mev, $R_0 = 1.4\times10^{-13}$ cm), we have found reasons to believe that this quantity is intimately related to the diffuseness of the nuclear surface and should in fact provide a measure of the thickness of the surface region. Estimates given below suggest that to account for the observed S it is necessary to assume the thickness of the region in which nucleons experience an appreciable one-sided resultant force and the density is falling to be of the order $6-8\times10^{-13}$ cm. An estimate of some of the most obvious consequences of such a value did not seem to lead to contradictions with known properties of nuclei. Some arguments which appear to support it are discussed in the following Letter. It is suggested that the use of a nuclear potential with sloping sides in which the rise occurs in a distance of $6-8\times10^{-13}$ cm merits attention.

Since the surface energy is intimately connected with the deficiency in binding of particles in the surface, it is clear that any attempt at a quantitative account of the nuclear surface energy will come up against difficulties due to our insufficient understanding of the nature of the effects responsible for nuclear cohesion.[1-3] The idea behind the present attempt is to by-pass this difficulty in the same way that the individual particle model by-passes the question of nuclear interactions, that is, by using the fact that it appears to be possible with some success to replace the effect of interactions by an over-all potential acting on independent particles. This is a prescription which often enables one to make predictions about phenomena which in fact depend on the presence of nuclear interactions without having to specify these explicitly (the nuclear shell model). We have examined the consequence of this prescription for the question of the surface energy. The estimate of S which follows can be regarded as an attempt to apply the ideas of the independent particle model to the calculation of the surface energy.

In practice the problem is essentially that of estimating the surface energy of a Fermi gas of particles moving in some potential well with sloping sides. The total energy (kinetic plus potential) of any one particle in such a well *remains constant* as the particle enters the surface region and the appearance of a surface energy for the Fermi gas as a whole is then due to the circumstance that the faster particles penetrate further into the surface region, which thus becomes enriched in high-total-energy particles. A somewhat more general way of looking at this is to say that when filling a region of space with particles obeying the exclusion principle, the number of particles that can be accommodated in a given energy interval is proportional to the volume of ordinary space available. Since the more energetic (fast) particles are more difficult for the cohesive forces to contain, they will explore a greater volume (by an amount proportional to the surface area) and consequently more of them can be accommodated. We would like to stress that on the basis of the individual-particle model the surface energy is thus due to a simple effect of rather general validity (faster particles explore greater volumes) and to point out the immediate connection between the surface energy and the slope of the potential in the surface region. (The extra energy should increase with decreasing slope.)

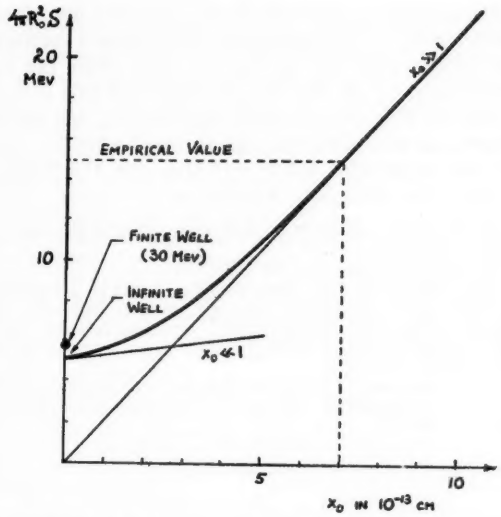

FIG. 1. The surface energy per unit area (defined as the energy associated with a number of particles in a volume touching unit area of surface minus the energy of the same number of particles inside the nucleus) for a Fermi gas with $T_0 = 22$ Mev bounded by a potential which rises to infinity with a constant slope equal to T_0/x_0. (Compare reference 5.) (The effect of levelling off the potential at about 30 Mev can be neglected due to the small number of particles in the region in question. The effect vanishes for $x\to\infty$ and is greatest for a square well ($x_0=0$) when it increases S by 12.5 percent as shown in the figure.) The curve plotted is an interpolation between the limits $x_0\to0$ and $x_0\to\infty$. The finite value of S at $x_0=0$ is a quantum mechanical effect which can be traced to the more efficient use of the available space by particles with a shorter wavelength.

A quantitative illustration is given in Fig. 1, which shows the surface energy for a semi-infinite Fermi gas (Fermi energy T_0) bounded by a region of linearly increasing potential, plotted as function of a thickness x_0, the distance in which the potential increases by T_0. The only parameter entering the calculation is T_0. No assumptions about nuclear forces have been made. At $x_0 = 1-2\times10^{-13}$ cm, $4\pi R_0^2 S$ is 5–6 Mev,[4] to be compared with the empirical 15 Mev. In terms of specific assumptions about nuclear interactions, one could think of effects that would tend to increase or decrease the

surface energy (many-body forces, clustering into alpha particles, etc.). The significance of the present estimate lies in the fact that so long as these effect can be represented by an over-all potential (and this is suggested by the validity of the shell model), one would come back to a value ~ 6 Mev for $x_0 = 1-2\times10^{-13}$ cm. To obtain the value $4\pi R_0^2 S = 15$ Mev with $T_0 = 22$ Mev we must assume $x_0 = 6-8\times10^{-13}$ cm.

[1] H. A. Bethe and R. F. Bacher, Revs. Modern Phys. **8**, 83 (1936), especially p. 164.
[2] E. Feenberg, Phys. Rev. **60**, 204 (1941).
[3] W. J. Swiatecki, Proc. Phys. Soc. (London) **A64**, 226 (1951).
[4] Note that E. Feenberg, reference 2, or D. L. Hill and J. A. Wheeler, Phys. Rev. **89**, 1102 (1953), especially p. 1125, would give $4\pi r_0^3 S = 28$ Mev at $x_0 = 0$. The discrepancy by a factor 5 is discussed in reference 2.
[5] W. J. Swiatecki, "The effect of a potential gradient on the density of a degenerate Fermi gas," Proc. Phys. Soc. (London) (to be published).

Average Nuclear Potentials and Densities

W. J. Swiatecki

Institute for Mechanics and Mathematical Physics and The Gustaf Werner Institute for Nuclear Chemistry, Uppsala, Sweden

(Received October 8, 1954)

ACCORDING to the preceding Letter,[1] the empirical magnitude of the nuclear surface energy, interpreted on the basis of the individual-particle model, suggests a nuclear potential well with rather gently sloping sides. In the present note we shall discuss some consequences of such a potential. For definiteness, let us consider the nucleus divided into an inner region $r<R_1$ where no average force is present and a surface region where particles experience a constant inward force. The implied potential wells and estimates of the associated densities of a Fermi gas are given in Fig. 1 for $A = 27, 64, 125, 216$. The densities are based on the semi-infinite distribution used in (1) and disregard therefore effects of shells, the curvature of the nuclear surface, etc. From other work[2] it then appears that for the small potential gradient assumed here the simple Fermi relation, stating the proportionality of the density ρ and the $\frac{3}{2}$ power of the maximum kinetic energy $T(r)$, is adequate.[3] It will be noted that the wells do not appear to be inconsistent with a shell model potential (intermediate between square well and oscillator potential). For medium and large A, a region of constant density is implied. For small A, all nucleons should be regarded as subject to a field of force.

As a rule the density distributions are more compact than the corresponding potential wells. This is due to (a) the more rapid fall off of density ($\frac{3}{2}$ power of T) which expresses the statistical preference for particles to congregate in a region of deep potential, and (b) the finite nucleon separation energy (~ 8 Mev) which means that about a quarter of the potential rise occurs beyond the turning point of the fastest particle where the density is practically zero.

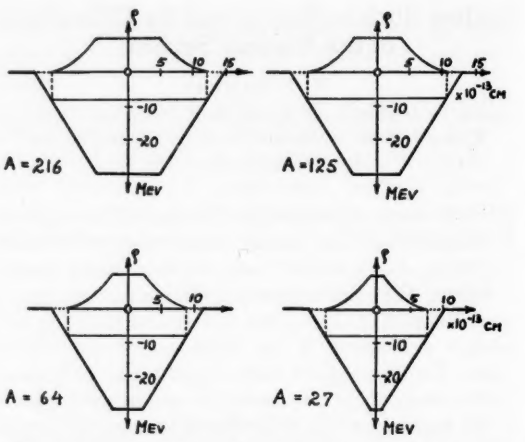

FIG. 1. Potential wells and Fermi densities for $A = 27, 64, 125, 216$. The depth of the wells is 30 Mev, the Fermi energy $T_0 = 22$ Mev, the gradient at the surface T_0/x_0 with $x_0 = 7\times10^{-13}$ cm. With these density distributions the equivalent radius $\bar{R}$, defined as the radius of the sphere which would contain all the particles at a constant (the central) density, can be approximated by $\bar{R} \doteq R_{\frac{1}{2}} + x_0/2$ to better than 3.6 percent. We have taken $\bar{R} = 1.4 \times 10^{-13} A^{\frac{1}{3}}$ cm.

The above refers to average nucleon densities. It is interesting to examine the neutron and proton densities (ρ_N, ρ_Z) separately. For a nucleus with $N>Z$, the zero point energies for neutrons are greater than for protons (Fermi energies $T_N > T_Z$) and the faster neutrons will, therefore, penetrate farther into the surface region, this enrichment of the surface in neutrons being inversely proportional to the gradient of the potential across the surface.[4] A simple estimate of the effect can be made by using $T_N/T_Z = (N/Z)^{\frac{1}{3}}$, when the difference in effective neutron and proton radii $\bar{R}_N - \bar{R}_Z$ becomes $\frac{2}{3}[(N-Z)/A]x_0$.[5] (For notation see caption to Fig. 1.)

Figure 2 shows, as a function of A, the values of $\bar{R}_N$ and $\bar{R}_Z$, as well as $R_{\frac{1}{2}}$, the radius at which the average potential has half its central value. If $R_{\frac{1}{2}}$ is taken to represent an average interaction radius for nucleons interacting with a potential well with sloping sides, then the curves for $R_{\frac{1}{2}}$ and $\bar{R}_Z$ illustrate the different radii appropriate for the interpretation of experiments with particles which are (nucleons) and are not (electrons or muons) subject to specifically nuclear interactions. The effect being associated with a sloping potential the difference between $R_{\frac{1}{2}}$ and $\bar{R}_Z$ should provide a measure of the thickness of the surface region. The empirical difference between the two sets of radii (about 20 percent) is consistent in order of magnitude with Fig. 2, based on a value $x_0 = 7\times10^{-13}$ cm (but not with $x_0 = 1-2\times10^{-13}$ cm).

A value of x_0 considerably greater than $1-2\times10^{-13}$ cm is suggested by very simple considerations. The thickness of the region in which a particle crossing a

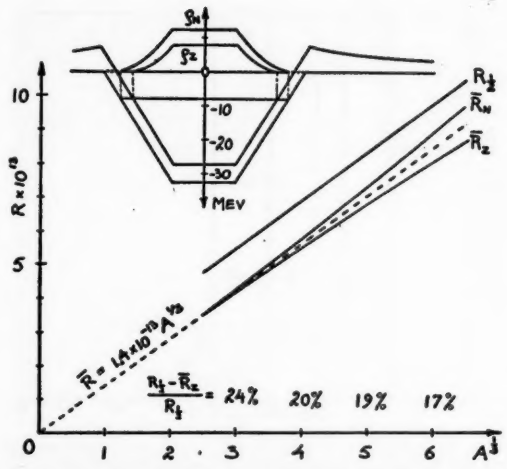

FIG. 2. The neutron and proton wells and densities for $A=216$, the equivalent radii $\bar{R}_N$, $\bar{R}_Z$ and the radius $R_{\frac{1}{2}}$ at half-depth of the average potential well. $\bar{R}$ has been taken as $1.4\times10^{-13}A^{\frac{1}{3}}$ cm, though one would be nearer to the experimental results by choosing $R_{\frac{1}{2}}\sim1.4\times10^{-13}A^{\frac{1}{3}}$ cm (to agree with high-energy neutron cross sections) and have the "electromagnetic" radius $\bar{R}_Z$ come out ~20 percent less. The resulting value of $\bar{R}\sim1.1\times10^{-13}A^{\frac{1}{3}}$ cm corresponds to greater nucleon densities, which in turn imply a well depth of $8+(1.4/1.1)^2\times22=44$ Mev. It may be significant that a well depth ~40 Mev is also suggested by recent evidence from low-energy neutron scattering experiments [R. K. Adair, Phys. Rev. 94, 737 (1954)]. With a greater value of T_0 the arguments of the preceding Letter would lead to a smaller estimate for x_0.

sharp discontinuity in the density would experience an appreciable resultant force would be twice the range of the forces. For a Fermi gas of particles the least diffuseness in the density at the surface is about $(2\pi)^{-1}$ times the wavelength of the fastest particle present (1×10^{-13} cm for a nucleus) realized when the gas is bounded by an infinite square well. This would give $x_0\sim(1+2\times1.4)\times10^{-13}=3.8\times10^{-13}$ cm. Since the density distribution is actually determined by some such resultant field of force and not by an infinite force at a sharp surface (square well), the density would diffuse further and there is no difficulty in understanding a final diffuseness of $x_0=7\times10^{-13}$ cm. On the contrary a value $x_0=1-2\times10^{-13}$ cm would be hard to explain.

The rather diffuse potential wells discussed above are not necessarily inconsistent with the recent analyses of high-energy electron scattering experiments which suggest that the transition region ΔR in which the *proton density* falls from 90 percent to 10 percent of its central value is around 2.4×10^{-13} cm,[6] or between 2.5 and 4.5×10^{-13} cm.[7] The considerations of the present note give $\Delta R=0.717(2Z/A)^{\frac{1}{2}}x_0$. Thus, for Au, $\Delta R=4.3\times10^{-13}$ cm if $x_0=7\times10^{-13}$ cm, or $\Delta R=3.1\times10^{-13}$ cm if $x_0=5\times10^{-13}$ cm.

Quantitative estimates apart, we would like to stress the qualitative considerations underlying this and the preceding Letter, namely the observation that faster particles are expected to explore greater volumes and that this points to a connection between the magnitude of the surface energy, the diffuseness of the nuclear surface, and the enrichment of the surface in neutrons.

[1] W. J. Swiatecki, preceding Letter [Phys. Rev. 98, 203 (1955)].
[2] W. J. Swiatecki, "The effect of a potential gradient on the density of a degenerate Fermi gas," Proc. Phys. Soc. (London) (to be published).
[3] For example, this relation gives $\rho=0$ at $T=0$; the more correct density calculated according to reference 2 would give $\rho=2.1$ percent of the central density.
[4] Compare reference 1. This is a way of stating the first of the two arguments suggested by M. H. Johnson and E. Teller [Phys. Rev. 93, 357 (1954)] to account for a greater neutron radius than proton radius. The second effect, associated with the region of exponential decay of wave functions, should be negligible in our case (see reference 3).
[5] A more general expression for T_N/T_Z, which corrects for the smaller proton radius implied by the effect under discussion, leads to $\bar{R}_N-\bar{R}_Z=\frac{2}{3}[(N-Z)/A](1/x_0+1/3\bar{R})^{-1}$.
[6] G. Ravenhall, Stanford University (private communication).
[7] G. Brown, University of Birmingham (private communication).

Angular Distribution of Pions from θ^0 Decay*

R. M. STERNHEIMER
Brookhaven National Laboratory, Upton, New York
(Received February 14, 1955)

IN view of the possibility of counter experiments to detect the θ^0 particles, it seems of interest to calculate the expected distribution in angle between the π^+ and π^- mesons as a function of the kinetic energy of the θ^0. The derivation follows closely that given by Rossi[1] for the π^0 decay. For the sake of generality, the masses of the decay particles will be taken as different, m_1 and m_2.

As shown by Rossi,[1] the probability that in a two-body decay, one of the outgoing particles has total energy E_1 in the laboratory system is given by

$$dn/dE_1=m_0/(2p_0p_1^*), \tag{1}$$

where dn=fractional number of decays in dE_1, m_0, and p_0 are the mass and momentum of the decaying particle, p_1^*=momentum of the emitted particles in the rest system. Hence, if θ is the angle between the emitted particles in the laboratory,

$$\frac{dn}{d\theta}=\frac{m_0}{2p_0p_1^*}\left|\frac{dE_1}{d\theta}\right|. \tag{2}$$

The conservation equations are[2]

$$(E_1^2-m_1^2)^{\frac{1}{2}}\sin\theta_1-(E_2^2-m_2^2)^{\frac{1}{2}}\sin\theta_2=0, \tag{3}$$

$$(E_1^2-m_1^2)^{\frac{1}{2}}\cos\theta_1+(E_2^2-m_2^2)^{\frac{1}{2}}\cos\theta_2=p_0, \tag{4}$$

$$p_0^2+m_0^2=(E_1+E_2)^2, \tag{5}$$

where θ_1 and θ_2 are the laboratory angles of the emitted particles with the direction of the incoming particle,

E_1 and E_2 are their total energies in the laboratory system. Upon solving Eqs. (3)–(5) for $\theta=\theta_1+\theta_2$, one finds

$$\cos\theta=\frac{E_1E_2-A}{(E_1^2-m_1^2)^{\frac{1}{2}}(E_2^2-m_2^2)^{\frac{1}{2}}}, \tag{6}$$

where

$$A\equiv(m_0^2-m_1^2-m_2^2)/2. \tag{7}$$

Upon differentiating Eq. (6), one obtains (using $\partial E_2/\partial E_1=-1$),

$$-\sin\theta d\theta=\cos\theta\left[\frac{E_2-E_1}{E_1E_2-A}\frac{E_1}{(E_1^2-m_1^2)^{\frac{1}{2}}}+\frac{E_2}{(E_2^2-m_2^2)^{\frac{1}{2}}}\right]dE_1. \tag{8}$$

From (2) and (8), one finds

$$\frac{dn}{d\theta}=\frac{m_0}{2p_0p_1^*}\left|\tan\theta\Big/\left[\frac{E_1-E_2}{E_1E_2-A}+\frac{E_1}{(E_1^2-m_1^2)^{\frac{1}{2}}}-\frac{E_2}{(E_2^2-m_2^2)^{\frac{1}{2}}}\right]\right|. \tag{9}$$

$dn/d\theta$ is found by first calculating θ for several assumed values of E_1 from (6), and then $dn/d\theta$ from (9). In these expressions, $E_2=E_0-E_1$, where $E_0=$ total energy of the incident particle. The extreme values of E_1 are obtained when $\theta=0°$ or 180°. Figure 1 shows $dn/d\theta$ for θ^0 particles of various kinetic energies T_0. There are two regions of T_0: (1) For $T_0<378$ Mev, the velocity v_0 of θ^0 is less than the velocity v_1^* of the π's in the θ^0 rest system. There is a minimum angle θ_s corresponding to symmetric decay about the incident direction ($\theta_1=\theta_2$, $E_1=E_2=E_0/2$). θ_s is given by

$$\cos\theta_s=(\tfrac{1}{4}E_0^2-A)/(\tfrac{1}{4}E_0^2-m_1^2). \tag{10}$$

$dn/d\theta$ becomes infinite at $\theta=\theta_s$, since the denominator of (9) vanishes for $E_1=E_2$. This case is similar to π^0 decay. (2) For $T_0>378$ Mev, $v_0>v_1^*$, the possible values of θ extend from 0° to a maximum θ_m. By a method given previously,[3] it can be shown that for $m_1=m_2$, θ_m is given by

$$\tan\theta_m=(1-v_0^2)^{\frac{1}{2}}/(v_0^2-v_1^{*2})^{\frac{1}{2}}. \tag{11}$$

At $\theta=\theta_m$, $dn/d\theta$ becomes infinite since $\partial\theta/\partial E_1=0$ [Eq. (2)]. The curves of $dn/d\theta$ have two branches between θ_s and θ_m, because for a given θ in this region, there are two possible values of E_1, which lead to the two values of $dn/d\theta$. The total $dn/d\theta$ is the sum of the terms due to the two branches.

We note that for case (1), θ is close to θ_s for a large fraction of the decays. Thus for $T_0=100$ Mev, θ lies between θ_s ($=101.8°$) and 110° for ~65 percent of the decays. Similarly, for $T_0=500$ Mev [case (2)], θ lies between θ_s ($=50.3°$) and θ_m ($=61.1°$) for ~95 percent of the decays. This correlation between T_0 and the most likely value of θ could be used to estimate the energy of the incident θ^0 particles in a suitable counter experiment.[4] Moreover, the existence of a minimum angle θ_s for case (1) and of a maximum angle θ_m for case (2) may be used to put an upper or a lower limit on T_0.

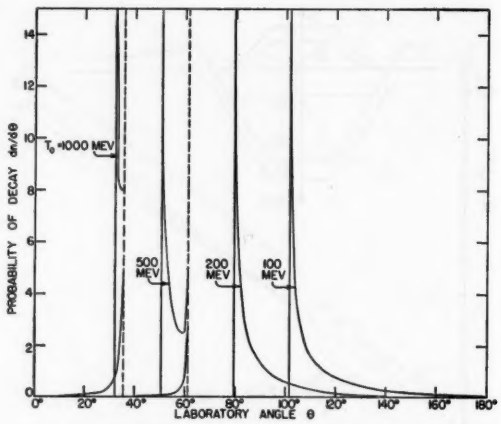

FIG. 1. Probability of decay $dn/d\theta$ as a function of the angle θ between the pions, for various kinetic energies T_0 of the θ^0 particle. The full vertical lines correspond to the angle θ_s for symmetric decay; the broken vertical lines correspond to the maximum angle θ_m.

I would like to thank Dr. R. Madey for suggesting this problem and for helpful discussions.

* Work performed under the auspices of the U. S. Atomic Energy Commission.

[1] B. Rossi, *High Energy Particles* (Prentice-Hall, Inc., New York, 1952), pp. 192, 198.

[2] It is assumed that the units are such that $c=1$.

[3] R. M. Sternheimer, Phys. Rev. **93**, 642 (1954).

[4] Equation (9) can also be used to obtain the distribution in θ for the Λ^0 decay. In this case, for $T_0<252$ Mev, when the velocity v_0 of Λ^0 is less than the velocity v_π^* of the pion in the Λ^0 rest system, all angles θ are possible. For $T_0>252$ Mev, $v_0>v_\pi^*$, there is a maximum angle θ_m, and the spectrum is double-valued between $\theta=0°$ and θ_m, where $dn/d\theta$ becomes infinite.

Angular Correlation in Two-Photon Annihilation in Quartz*

L. A. PAGE, M. HEINBERG, J. WALLACE, AND T. TROUT
University of Pittsburgh, Pittsburgh, Pennsylvania

(Received January 7, 1955)

A NARROW component has been found in the angular correlation of two-quantum annihilation radiation in fused quartz at room temperature, while crystalline quartz exhibits no such anomaly. A brief description of the experimental evidence follows.

Measurements are being made of the angular correlation, *circa* 180°, between two photons in coincidence, arising when a positron has entered a thick absorbing

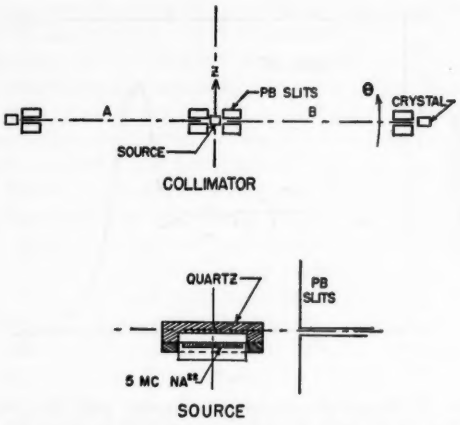

FIG. 1. Apparatus. Each detector-crystal is 120 cm from source. The x-axis is perpendicular to the plane of the paper.

sample. The apparatus measures essentially the z-component of total momentum of the two photons detected (see Fig. 1). Collimator-detector system A remains fixed, while identical system B may be rotated in the plane normal to an axis, x, centered on the region in the sample where the annihilation events take place. The geometry is thus similar to that first used by DeBenedetti *et al.*,[1] except that here it is arranged that the detectors see, for practical purposes, only radiation from the sample itself.

Some experimental work on a "crystal" of native graphite to measure the relative width-at-half-maximum for different basal plane orientations showed that the crystal structure's effect should be less than 1 percent[2] and the apparatus and circuitry is reliable to approximately 0.2 percent (based on some 10^7 coincidences, with the slit width $\Delta\theta=5\times10^{-3}$ radian). We do not know at this time, nor are we concerned about, the orientation of the crystal axes of the particular sample in use.

Geometrically identical fused and crystal quartz samples, denoted by F and C, respectively, were compared first as regards relative half-width, and with moderate resolution, $\Delta\theta=5\times10^{-3}$ radian. The positron source,[3] five mC of Na^{22}, provides some twenty coincidences/second of which less than 0.5 percent are accidentals. The result was (width C)/(width F)$\sim$1.2 uncorrected for finite resolution of apparatus. The nominal half-width is 12×10^{-3} radian.

There is a difference in shape between the F-curve and the C-curve occurring mainly for angles between the half-value points. Figure 2(a) shows the F- and C-curves superposed, for $\Delta\theta=5\times10^{-3}$ radian. The "difference," $(F'-C)/C_{\max}$ denoted by γ, is shown as Fig. 2(b). F' is the F-rate arbitrarily normalized. The geometry was then narrowed a factor of two, with $\Delta\theta=2.5\times10^{-3}$ radian, and the resulting difference is Fig. 2(c). Finally, with $\Delta\theta=0.8\times10^{-3}$ radian, the F'- and

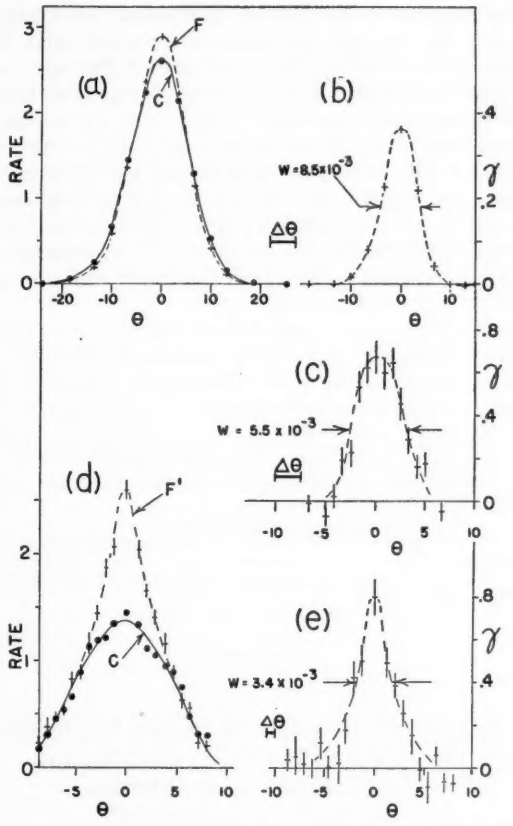

FIG. 2. Angular correlation curves for fused and crystal quartz. Angle θ is in units of 10^{-3} radian. Half-width, w, is in radians.

C-curves of Fig. 2(d) were run, yielding the difference curve Fig. 2(e). The half-width of the difference curve has thus narrowed, without affecting its area significantly.

The best estimate of the fraction of two-quantum annihilation belonging to this narrow component is to be had from the data of curves (a) and (b) which have good statistics. Actually an empirical integration has been made by moving scintillator A by half-inch steps parallel to the x-axis, running complete θ dependence at each step; this procedure eliminates from consideration the finite extension of the scintillators (only $1\frac{1}{4}$ inches) in the x-direction. It is this method which gives difference curve (b) whose area relative to the total two-quantum area for the F-sample is found to be 0.176 ± 0.015. The remaining curves of the figure are based on one x-position only.

The ultimate half width of the narrow component in fused quartz seems to be $\sim3\times10^{-3}$ radian, while the broader component, taken to be that for crystalline quartz, appears to be $\sim11\times10^{-3}$ radian.

That the narrow component should appear in fused quartz and not in crystalline quartz is reminiscent of

the behavior of the long-life component found some years ago by Bell and Graham for annihilation in quartz and various other substances.[4] Perhaps the narrow component of the two photons may stem from a simple positron-electron system with v/c sensibly less than 1/137. If the narrow component should be formed only "in parallel" with the long-half-life component, one might expect the narrow fraction to be one-third of the long-half-life fraction of Bell and Graham, which was 0.29.[4] Perhaps a portion of the two-quantum events supposed to arise from the triplet state appear in the narrow component.

The present experiment is being extended to include other materials under various conditions. Preliminary work on teflon, at room temperature, indicates an angular correlation similar to that for fused quartz.

* Work done in the Sarah Mellon Scaife Radiation Laboratory and supported by the Office of Ordnance Research.

[1] DeBenedetti, Cowan, Konneker, and Primakoff, Phys. Rev. 77, 205 (1950).

[2] University of Pittsburgh (unpublished).

[3] We are indebted to Dr. A. J. Allen for the preparation of the source.

[4] R. E. Bell and R. L. Graham, Phys. Rev. 87, 236 (1952); 90, 644 (1953).

Angular Distribution of Pickup Deuterons for 95-Mev Protons on Carbon, and Implications as to Internal Interactions in Carbon*

W. SELOVE

Harvard University, Cambridge, Massachusetts

(Received January 24, 1955)

THE angular distribution of the sharp energy group of deuterons observed in this reaction has been analyzed by Born-approximation pickup theory, to give the internal momentum distribution of the picked-up neutrons. The momentum distribution shows relatively strong high-momentum components, and these in turn indicate the presence of a strong short-range interaction in carbon.

A previous brief report[1] described the sharp energy distribution of deuterons observed in this reaction. The sharply defined group has been studied for laboratory angles between 6° and 60°. At the largest angles, the group still is clearly recognizable, although because of the increasing relative intensity of a continuum distribution of deuterons, the absolute cross section to be attributed to the "line" is uncertain to a factor of perhaps two. An energy distribution at 42° is shown in Fig. 1, and Fig. 2 shows the angular distribution of the sharp group.

Following Chew and Goldberger,[2] a Born-approximation calculation of the reaction yields from the angular distribution the internal momentum distribution of the picked-up neutron. CG show that the differential cross section $\sigma(\theta)$ is proportional to $N(\mathbf{n})F(q)$, where $N(\mathbf{n})$ is the momentum distribution density of neutrons of momentum $\mathbf{n}$ and $F(q)$ is a factor which is a function of the internal momentum of the formed deuteron; if one uses a Hulthén wave function for the deuteron then $F(q)$ has a relatively weak angular dependence. In the present case it falls by a factor of about $2\frac{1}{2}$ while the center-of-mass differential cross section is falling by 40, over the angular range covered.

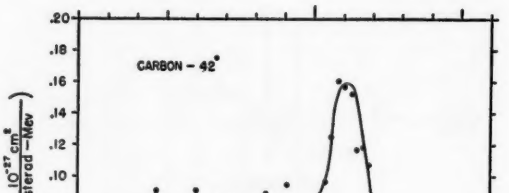

FIG. 1. Energy distribution of deuterons from the $C^{12}(p,d)$ reaction at 95 Mev. Statistical uncertainty is shown for two representative points.

Some discussion is in order with regard to the interpretation of the deuteron pickup results in terms of internal momentum distributions, in view of the fact that in the same type of theory applied by Butler[3] at low energies with very good success, the results do not seem to depend on the internal wave function $u(r)$ of the picked-up nucleon. In fact the effect of Butler's procedure is that the internal contribution to the

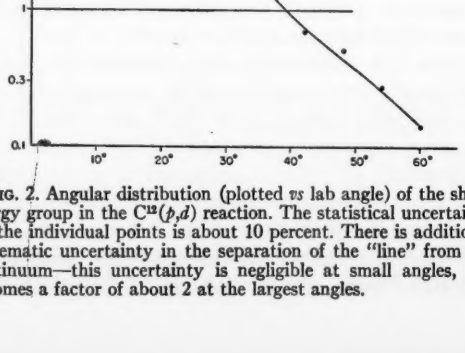

FIG. 2. Angular distribution (plotted *vs* lab angle) of the sharp energy group in the $C^{12}(p,d)$ reaction. The statistical uncertainty for the individual points is about 10 percent. There is additional systematic uncertainty in the separation of the "line" from the continuum—this uncertainty is negligible at small angles, but becomes a factor of about 2 at the largest angles.

overlap integral $\int \exp(i\mathbf{n}\cdot\mathbf{r})u(\mathbf{r})d\mathbf{r}$ is omitted entirely. This omission does not have a dominating effect on the magnitude of the integral,[4] since at low energies the wavelength $2\pi/n$ is not small compared to the nuclear radius, so that a considerable contribution to the integral comes from the region outside the nucleus. Indeed, at low energies it has been pointed out[3] that a variety of different approximations can lead to angular distributions resembling Butler's. At higher energies, on the other hand, the dominant contribution to the integral comes from the region inside the nucleus. It is just for this reason that one may hope the high-energy data can give information on the momentum distribution inside the target nucleus. An incidental characteristic accompanying this dominance of the inner contribution is that minima and secondary maxima become less pronounced, in the angular distribution.

The momentum density obtained from the data of Fig. 2 refers to a single state. If the independent-particle model is valid, this momentum distribution is that of a single-particle orbit, and the corresponding wave function $u(r)$ can be obtained by Fourier inversion. For this, the orbital angular momentum number l must be known. One could identify this l-value as 0 or 1 (the only probable values) if information were available on the behavior of $N(\mathbf{n})$ for $n\to 0$. The kinematics of the reaction are such that at 95 Mev the value of n even for the forward angles has a minimum corresponding to about 8 Mev kinetic energy, and this does not permit the determination of the behavior of N for $n\to 0$. Such a determination could be made by using protons of energy about twice the Q of the reaction, so about 30 to 35 Mev; at that low an energy, however, the theory is probably less accurate.

Direct Fourier inversion of the momentum "wave function" $[N(\mathbf{n})]^{\frac{1}{2}}$ to get the configuration-space wave function $u(r)$ is thus not possible unambiguously because of lack of information on the behavior of N outside the range for n of 0.65 to 2.3×10^{13} cm^{-1}, covering equivalent kinetic energies of about 9 to 120 Mev. However, calculations have been made using various reasonable extrapolations at low and high n, and the region covered by the data serves to determine the dominant characteristics of $u(r)$. Namely, the fact that the momentum spectrum falls off as slowly as it does at high n can be accounted for only by a $u(r)$ which has high curvature near the origin. The potential $V(r)$ which is required to produce this u can be obtained by applying the Schrödinger operator to u. The result is that to account for the momentum spectrum in this way requires a $V(r)$ which for $r>1.0\times 10^{-13}$ cm is not well determined but may be of the order of -20 to -30 Mev up to $r\sim 3$ or 4×10^{-13} cm, but which for $r<1.0\times 10^{-13}$ cm drops to a narrow hole of the order of 200 Mev deep. Present analysis indicates that the behavior of $V(r)$ for small r is similar for either of the assumptions $l=0$ or $l=1$; the behavior at large r appears to be given more reasonably on the assumption $l=1$.

These results suggest the interpretation that the potential felt by a nucleon in carbon includes a short-range strong interaction, presumably to be associated with local fluctuations occurring when two nucleons are near each other. It is not clear whether local fluctuations of the strength indicated here can be reconciled with the high degree of success of the independent-particle model.[5] At the same time, evidence of strong correlation effects inside the nucleus has recently appeared in the coincidences observed in high-energy photonuclear reactions.[6]

Some comments are appropriate on the relation of the present results to other information concerning the momentum distribution, and on the validity of the theory. As to the first: the momentum distribution obtained here is substantially in agreement with that obtained by York[7]; the present measurements give more specific information because of the better energy resolution available with a proton beam, and give information out to higher momenta. Relatively strong high-momentum components in carbon have also been inferred by Temmer.[8] The "Chew-Goldberger" (CG) distribution introduced[2] to describe York's results fits the present data but clearly is not to be considered correct at very much higher energies. The CG distribution corresponds to a Hulthén wave function with $\beta=\infty$—i.e., with infinite curvature at the origin. The results of the present note indicate that for internal nucleon kinetic energies above 150 Mev or so the momentum distribution $N(\mathbf{n})$ will fall off more rapidly than the n^{-4} behavior of the CG function. A Hulthén wave function with a finite value of β would give asymptotically an n^{-8} behavior at high n. The falsely high N given by the CG distribution for extremely high momenta does not affect the results of some calculations involving the effect of the momentum distribution, but may affect others, depending on the specific way in which $N(\mathbf{n})$ enters. Thus Lax and Feshbach[9] have obtained good agreement in photomeson production using the CG distribution, but Henley[10] found it to be too strong at high n to agree with the proton-produced meson distribution, and empirically introduced a modified momentum distribution having a stronger cutoff. Cladis,[11] Wolff,[12] and Wilcox[13] have studied the momentum distribution by quasi-elastic scattering of high-energy protons, and have concluded that the CG distribution is unsatisfactory. However, it can be shown that the disagreement they obtain is due to the artificially high value of the CG distribution at high n. From the results of the quasi-elastic experiments the behavior of $N(\mathbf{n})$ can be inferred for internal nucleon kinetic energies up to 30 Mev or so—in this range the results are essentially in agreement with the present results; it is difficult to extract from these experiments information on higher momenta.

As to the validity of the theory, there is unfortunately good reason to believe that just for the high momenta, which are of special interest, the simple theory may become inadequate. The theory is essentially based on the idea that the incoming proton interacts with only one target nucleon at a time. If, however, the high internal momenta occur only when two target nucleons are near each other, then the single-interaction model is inappropriate. Nevertheless, perhaps the qualitative conclusions drawn by the use of this theory have enough validity to be of interest.

* Assisted by the joint program of the Office of Naval Research and the U. S. Atomic Energy Commission.

[1] W. Selove, Phys. Rev. **92**, 1328 (1953).

[2] G. F. Chew and M. L. Goldberger, Phys. Rev. **77**, 470 (1950); hereafter referred to as CG.

[3] S. T. Butler, Proc. Roy. Soc. (London) **A208**, 559 (1951). Several authors have discussed the relation of a Born approximation calculation to the apparently different technique used by Butler. For a thorough discussion, see E. Gerjuoy, Phys. Rev. **91**, 645 (1953).

[4] Except for a certain large effect at one minimum. See P. B. Daitch and J. B. French, Phys. Rev. **87**, 900 (1952).

[5] In recent work of Brueckner, Eden, and Francis, they answer this question affirmatively.

[6] M. Q. Barton and J. H. Smith, Phys. Rev. **95**, 573 (1954); H. Myers *et al.*, Phys. Rev. **95**, 576 (1954).

[7] J. Hadley and H. York, Phys. Rev. **80**, 345 (1950).

[8] G. M. Temmer, Phys. Rev. **83**, 1067 (1951).

[9] M. Lax and H. Feshbach, Phys. Rev. **81**, 189 (1951).

[10] E. M. Henley, Phys. Rev. **85**, 204 (1952).

[11] Cladis *et al.*, Phys. Rev. **87**, 425 (1952).

[12] P. A. Wolff, Phys. Rev. **87**, 434 (1952).

[13] J. M. Wilcox, University of California Radiation Laboratory report UCRL-2540, April, 1954 (unpublished).

Low-Energy Photoproduction of π^0 Mesons from Hydrogen: Total Cross Section*

F. E. Mills and L. J. Koester, Jr.

Department of Physics, University of Illinois, Urbana, Illinois

(Received January 27, 1955)

TOTAL cross sections for the photoproduction of neutral pions from threshold to 240 Mev have been measured with the use of a liquid hydrogen target. One of the π^0 decay photons was detected in a scintillation counter telescope composed of an anticoincidence counter, a $\frac{1}{4}$-in. Pb converter, and two counters in coincidence separated by a $\frac{1}{2}$ in. thick Al absorber.

The product of efficiency times solid angle for the γ-ray telescope was calculated by a Monte Carlo method with the Illinois digital computer. This calculation included the following: (1) geometry effects arising from the finite size of source and detector, (2) pair production and depth distribution of pair production in the Pb converter, (3) radiation loss and straggling of the pair electrons, (4) ionization loss and straggling of the pair electrons, (5) multiple scattering of the pair electrons, and (6) preabsorption of the photons in material preceding the telescope. Results

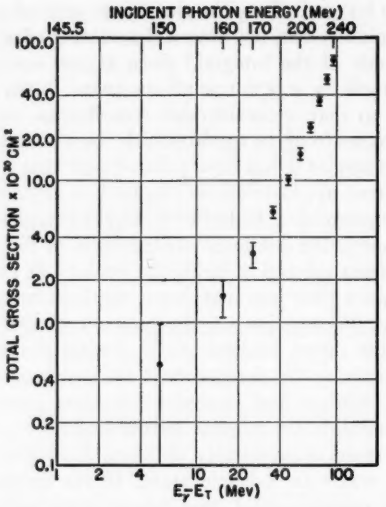

FIG. 1. Values of σ^0_{total} as a function of the difference between incident photon energy in the laboratory system and the threshold energy.

of this calculation are in satisfactory agreement with measured efficiencies of a similar counter at Cornell.[1]

Counting rates at an angle of 85° to the x-ray beam were measured as the betatron energy was increased in 10-Mev steps from 120 to 250 Mev. The photon difference method yielded the counting rate per incident photon as a function of incident photon energy.

This counting rate per photon, $I_{85°}$, is related to the photomeson cross section by integrating the spectrum of decay photons over the detector efficiency.[2] The photomeson cross section is assumed to be

$$\sigma^0(\theta)=A_0+A_1\cos\theta+A_2\cos^2\theta.$$

Then the total cross section is

$$\sigma^0_{\text{total}}=4\pi[A_0+\tfrac{1}{3}A_2].$$

In the resulting expression[2] for $I_{85°}$, the term involving A_1 is negligibly small, while the ratio of the coefficient of A_2 to that of A_0 is approximately $\frac{1}{3}$. Thus the data are essentially a measure of σ^0_{total}. Because this ratio is not exactly $\frac{1}{3}$ at all energies, a value must be assumed for the ratio A_2/A_0; but the results are very insensitive to this value.[3] Cross sections presented in Fig. 1 are based on the assumption that $A_2/A_0=-0.6$.

The logarithmic plot in Fig. 1 shows that between 170 and 240 Mev, σ^0_{total} is proportional to $(E_\gamma-E_T)^{2.2}$, where E_γ is the incident photon energy and E_T the threshold energy. This large exponent is not surprising because σ^0_{total} arises almost entirely from the "enhanced" P-state (isotopic spin$=\frac{3}{2}$, $J=\frac{3}{2}$) of the meson-nucleon system and is extremely sensitive to the corresponding phase shift δ_{33}. When the theoretical connection between σ^0_{total} and δ is established, these measurements may be used to determine δ_{33}.

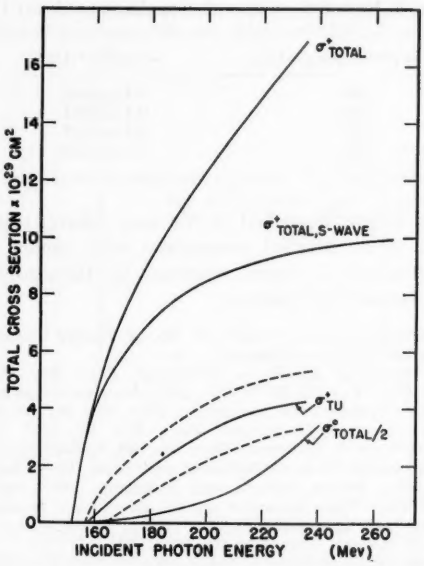

FIG. 2. Values of the total cross section for photoproduction of π^+ mesons after the S-wave and "enhanced" P-wave contributions are subtracted, as a function of incident photon energy in the laboratory system. The dotted lines indicate statistical errors involved in the subtraction.

Unlike σ^0_{total}, the π^+ photoproduction cross section, σ^+_{total}, includes substantial contributions from the S-state and other "unenhanced" states. Charge independence implies that the enhanced state contribution to σ^+_{total} is just one-half that to σ^0_{total}. Thus the quantity[4]

$$\sigma^+_{TU}\equiv\sigma^+_{total}-\sigma^+_{T,\,S\text{-wave}}-\tfrac{1}{2}\sigma^0_{total}$$

represents the contributions to σ^+_{total} made by all the unenhanced states except the gauge invariant S-state term.

This residual cross section σ^+_{TU} is plotted in Fig. 2.[5] The magnitude of σ^+_{TU} relative to that of $\frac{1}{2}\sigma^0_{total}$ indicates that, below 200 Mev, the unenhanced contributions to σ^+_{total} are greater than the enhanced.

More complete results will be submitted in the near future. The authors wish to thank Professor A. O. Hanson and Professor G. Bernardini for many valuable discussions.

* Supported in part by the U. S. Atomic Energy Commission and the Office of Naval Research.

[1] G. Cocconi and A. Silverman, Phys. Rev. 88, 1230 (1952).

[2] The principal ideas in this calculation are developed in a letter from A. Borsellino to G. Bernardini.

[3] Changing the ratio A_2/A_0 from -1 to -0.6 changes σ^0_{total} by 10 percent at 240 Mev and by successively smaller percentages at the lower energies.

[4] Professor E. L. Goldwasser has performed an analogous subtraction with the differential cross sections (private communication).

[5] The curves for σ^+_{total} and $\sigma^+_{total,\,S\text{-wave}}$ were obtained from measurements of the following authors: G. Bernardini and E. L. Goldwasser, Phys. Rev. **95**, 857 (1954); M. Beneventano *et al.* (to be published); Leiss, Robinson, and Penner (to be published).

Low-Energy Photoproduction of π^0 Mesons in Hydrogen: Differential Cross Sections at 135°*

LOUIS J. KOESTER, JR.

Department of Physics, University of Illinois, Urbana, Illinois

(Received January 27, 1955)

DIFFERENTIAL cross sections for the reaction $h\nu+p\rightarrow\pi^0+p$ have been measured for incident photon energies between 180 and 215 Mev by observation of the recoil protons (Fig. 1). The target and monitor were those used by Bernardini and Goldwasser,[1] with the exception that the cylinder of liquid hydrogen was only $\frac{7}{8}$ in. in diameter. The protons were detected in Ilford G-5 nuclear emulsions placed at angles of 17.5° with respect to the 226-Mev bremsstrahlung. Emulsion stacks 1 in.×3 in. in area and 1.8 mm thick were composed of two pellicles and a plate, each 600 microns thick.

Proton tracks found by surface scanning of the first pellicle are followed through the stack to their endings. Then range and angle measurements determine the energy and angle of the event. The observed protons correspond to π^0 mesons emitted at $135°\pm6°$ in the center-of-mass system. A measured background of approximately 30 percent arises from the 0.0005-in. brass wall of the target and is subtracted.

If only S- and P-states of the meson-nucleon system are considered, the cross section for neutral pions may be written

$$d\sigma^0/d\Omega=\sigma_S{}^0(\theta)+\sigma_{SP}{}^0(\theta)+\sigma_P{}^0(\theta),$$

where the subscripts denote S- and P-states and S-P interference. The energy dependence and angular distribution of the cross sections at higher energies[2,3] have indicated consistently that neutral photomesons are produced mainly in P-states. On the basis of charge independence, however, the connection between phase shifts involved in scattering and photoproduction of mesons requires[4] that the low-energy S-state contribution be at least

$$\sigma_S{}^0(\theta)\gtrsim 0.02\chi\nu\eta^2A_0{}^+,$$

where $\chi\nu=\eta(1+\nu/M)^{-1}(1+\omega/M)^{-1}$, η is meson momentum in units of μc, ν is photon energy, ω is meson total energy, M is nucleon total energy, and where $A_0{}^+=1.5\times10^{-29}$ cm^2/sterad is the S-state part of the π^+ photoproduction determined by Bernardini and Goldwasser.[1] In this lower limit, the S-wave would have the same dependence on meson momentum as the P-wave and could not be detected in the energy dependence of the cross sections.

By making the assumption that the nucleon recoil part of photoproduction is similar for all three types of pions (Watson's Model I),[4] and by using the average value[5] $\langle\sigma^-/\sigma^+\rangle=1.4$ of the negative-to-positive photo-

pion ratio between threshold and 250 Mev, a more realistic estimate obtained for $\sigma_S^0(\theta)$ is

$$\sigma_S^0(\theta)\approx 1.1\times 10^{-30}\chi\nu\{0.2+0.2\eta^2\}\ \text{cm}^2/\text{sterad}.$$

Then the interference term becomes

$$\sigma_{SP}^0(\theta)\approx -1.1\times 10^{-30}\chi\nu\eta\cos\theta\ \text{cm}^2/\text{sterad},$$

when the P-state term[6] used is

$$\sigma_P^0(\theta)\approx 3.3\times 10^{-30}\chi\nu\eta^2(1-0.6\cos^2\theta)\ \text{cm}^2/\text{sterad}.$$

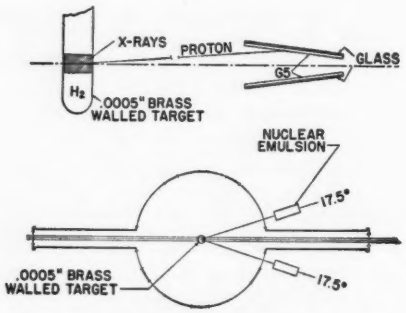

FIG. 1. Schematic diagram of liquid target and nuclear emulsion detectors.

Figure 2 illustrates the role of the interference term. The differential cross section may be written

$$d\sigma^0/d\Omega = A_0+A_1\cos\theta+A_2\cos^2\theta.$$

Values of $A_0+A_2\cos^2\theta$ shown as the dotted curve are deduced from total cross sections measured in the counter experiment[7] by setting $A_2=-0.6A_0$. Addition of the interference term $A_1\cos\theta=\sigma_{SP}^0(\theta)$ yields the solid curve, in closer agreement with the measured differential cross sections.

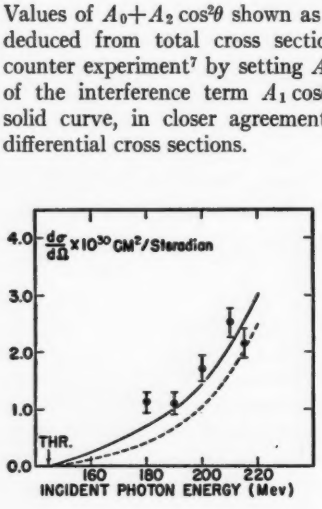

FIG. 2. Differential cross sections at 135° in the center-of-mass system *versus* laboratory photon energies. For discussion of curves see text.

Because the monitoring system was the same as that used by Bernardini and Goldwasser,[1] a direct comparison of results gives the neutral-to-positive production ratios of Table I.

Cross sections presented above are based on measurements of about half of the observed tracks. Complete results will be described in the near future, together with a more detailed comparison with theory. The author wishes to thank Professor G. Bernardini for many valuable discussions.

TABLE I. Neutral-to-positive photoproduction ratios at 135°.

Incident photon energy (Mev)	$\sigma^0(135°)/\sigma^+(135°)$
180	0.14±0.03
190	0.12±0.02
200	0.16±0.03
210	0.21±0.02

* Supported in part by the U. S. Atomic Energy Commission and the Office of Naval Research.

[1] G. Bernardini and E. L. Goldwasser, Phys. Rev. **94**, 729 (1954); Phys. Rev. **95**, 857 (1954), and private communication.
[2] Panofsky, Steinberger, and Steller, Phys. Rev. **86**, 180 (1952); A. Silverman and M. Stearns, Phys. Rev. **88**, 1225 (1952); G. Cocconi and A. Silverman, Phys. Rev. **88**, 1230 (1952).
[3] Goldschmidt-Clermont, Osborne, and Scott, Phys. Rev. **89**, 329 (1953); Walker, Oakley, and Tollestrup, Phys. Rev. **89**, 1301 (1953). More complete reports have been received as preprints from these authors.
[4] K. M. Watson, Phys. Rev. **95**, 228 (1954).
[5] G. Bernardini, private communication.
[6] The total cross sections of reference 7 are used to determine the coefficient of this term.
[7] F. E. Mills and L. J. Koester, Jr., preceding Letter [Phys. Rev. **97**, 210 (1955)].

System of Even-Even Nuclei*

GERTRUDE SCHARFF-GOLDHABER AND J. WENESER
Brookhaven National Laboratory, Upton, New York
(Received January 20, 1955)

PREVIOUS investigations of even-even nuclei have yielded the following main results:

(1) While the ground state has presumably always the character (spin and parity) 0+, the first excited state has 2+ with very few exceptions.[1,2]

(2) The character of the second excited state, where known, is either 4+, 2+, 0+, or (odd, ±).[2]

(3) The energy of the first excited state, E_1, increases as the number of neutrons or protons approaches the end of a shell, and shows a very pronounced peak at the filled shell.[2,3] As a rule E_1 varies less when two protons are added to the nucleus, than when two neutrons are added.[2]

We have now studied second excited states in the region $36\leqslant N\leqslant 88$ in more detail, and have found the following:

(1) The characters of the second excited states, where known, are preponderantly 2+, occasionally 4+, 0+, and (odd, −), whereas second excited states of a rotational band,[4] occurring for $90\leqslant N\leqslant 108$, have always the character 4+.

(2) The energy of the second excited state, E_2, shows a dependence on A similar to E_1.[5] In Fig. 1 the ratio

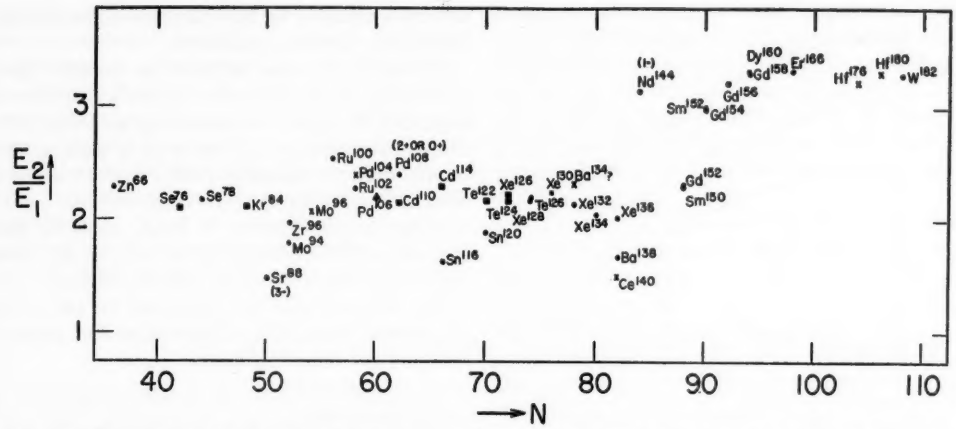

FIG. 1. Ratio of energies E_2/E_1 as function of neutron number N ($36 \leqslant N \leqslant 108$). The character of the second excited state of the nucleus is denoted by ▲(0+), ■(2+), × (4+), and • (not known, unless given in parentheses).

E_2/E_1 is plotted against N. For $N \leqslant 88$, it is seen that this ratio is remarkably constant, fluctuating around 2.2, except where I_2 is odd. Rotational states, with E_2/E_1 approaching 3.33, are also shown. In Fig. 2, E_2/E_1 is plotted against E_1, omitting points with odd I_2. Here the distinction between the two groups is even more striking. Group (a), consisting of nuclei with rotational states ($90 \leqslant N \leqslant 108$), covers a small range of energies between $70 \leqslant E_1 \leqslant 125$ kev. Group (b) begins at $E_1 \approx 330$ kev and extends to almost 2 Mev. Above 1200 kev, all points refer to nuclei whose neutron or proton number is magic. In this region a few deviations toward lower values for E_2/E_1 occur. The gap between groups (a) and (b) indicates an abrupt transition which occurs as N changes from 88 to 90. Again we find that N, rather than A, seems to determine the nature of the system of excited states of a nucleus. This is brought out strikingly by recent work on the dual decay of Eu^{152} (12 yr),[6,7] which yields for Sm^{152} ($N=90$) $E_1=123$ kev, $E_2=367$ kev, $E_2/E_1=3.0$ and for Gd^{152} ($N=88$) $E_1=344$ kev, $E_2=754$ kev, $E_2/E_1=2.19$.

(3) In group (b), two intensity rules govern the electromagnetic transitions: (I) Between a second and first 2+ state the transition is usually mainly $E2$, with only a small $M1$ admixture. (II) The probability for the $E2$ part of this transition relative to that for the competing transition to the ground state is much higher than would be expected on the basis of the single-particle model. Both these intensity rules were pointed out by Kraushaar and Goldhaber,[8,9] and have meanwhile been supported by further examples.

(4) Coulomb excitation data[10] for group (b) indicate that the probability for a transition from the first excited state to the ground state are 10 to 20 times higher than would be expected on the basis of a single-particle model.

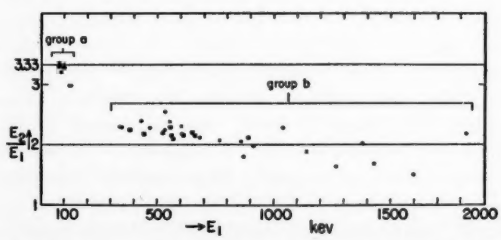

FIG. 2. Ratio of energies E_2/E_1 as function of E_1 for $36 \leqslant N \leqslant 108$. The character of the second excited state of the even-even nucleus is denoted by ▲(0+), ■(2+), × (4+), and • (not known). Points for nuclei with odd spin for the second excited state are omitted from this figure.

The uniformity and simplicity of the empirical pattern over a large range of even-even nuclei of group (b) suggest that the pattern arises from a single feature. Two facts are especially suggestive: the pattern exists in nuclei immediately adjacent to those in which the Bohr-Mottelson rotational pattern is manifest, and it also obtains very near to closed shells where the coupling must be weak. It is therefore tempting to assume that the Bohr-Mottelson model[11] in the region of weak to moderate coupling should yield the above results.

We first consider the limit of zero coupling. The first and second excited states, due to core excitations, are at $\hbar\omega$, $2\hbar\omega$ above the ground state; thus $E_2/E_1=2$. At $2\hbar\omega$ lies a degenerate triplet, of characters 0+, 2+, 4+. Intensity rule II follows from the favored nature of one phonon jumps. Also, there is no $M1$ radiation, because the current is directly proportional to the velocity of the fluid. The collective nature of the excitation gives rise to fast $E2$ transitions.

The theory has been extended into the weak to moderate coupling region by a Tamm-Dancoff calculation, which we have, however, only been able to carry out with a cutoff at three phonons. The Bohr-Mottelson Hamiltonian is modified by the introduction of forces between the outer nucleons; for reasons of definiteness

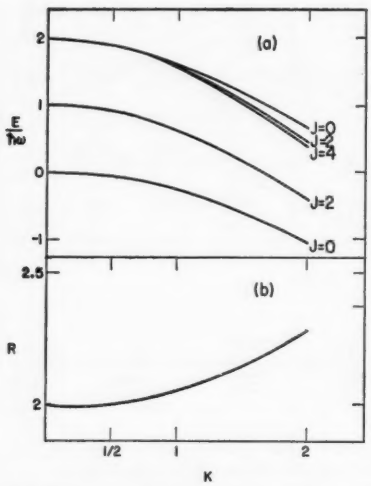

FIG. 3. (a) The energy levels as a function of the coupling strength K. $K=0.67[(\hbar^2/2B)/\hbar\omega]^{\frac{1}{2}}k$, where B denotes the mass parameter and k the coupling parameter. (b) $R=E_2/E_1$, where E_1, E_2 denote the energy above the ground state of the first and second $2+$ state respectively. The anharmonic terms are not included.

and simplicity, the outer nucleons are taken as $(f_{7/2})^4$, and $E(J=2, s=2)=3\hbar\omega$, $E(J, s=4)\sim 6\hbar\omega$.[12] The choice of other, perhaps more realistic conditions, does not appear to change the qualitative conclusions. In addition, it is necessary to increase the mass parameter B by a factor 5 to fit the experimental data.[13] The results of the calculations of the energy levels are shown in Fig. 3. For the range of coupling strength shown, the intensity rules are found to be essentially the same as in the zero-coupling case, with the exception that a weak $M1$ component is introduced. The $E2$ transition probability between the first $2+$ state and the ground state also remains nearly the same; for zero coupling the ratio of the transition probability to that given by the simple shell model is:

$$\mathfrak{M}(\text{coll})/\mathfrak{M}(\text{shell})=\left[\frac{9}{16\pi^2}Z^2\left(\frac{\hbar^2/2B}{\hbar\omega}\right)R^4\right]\Big/\left(\frac{1}{25}R^4\right)\sim 25,$$

where $\hbar^2/2B=0.008$ Mev, $\hbar\omega=0.75$ Mev, $Z=40$.

The addition of possible anharmonic terms affects the position of the energy levels. Reasonable assumptions result in effects opposite to that of the coupling between the core and the particles and of similar magnitude. Hence, superposition of anharmonic terms and coupling does not affect the general agreement with the empirical results, although it may change the sequence of the triplet levels.

These ideas are proving valuable for the interpretation and construction of decay schemes. However, the existence of the triplet of levels together with the natural extension of the intensity rules for all these levels need further examination.

Although it seems difficult to explain the great uniformity of the pattern without a collective model approach, it would be interesting to study the alternative interpretation in terms of a shell model. The electromagnetic intensity rules I and II would follow directly from seniority considerations.[9] It is conceivable that the simple behavior of E_2/E_1 could be obtained, and moderate speed-up factors of the $E2$ transition probability are possible for suitable mixing.

We wish to thank M. Goldhaber for many valuable discussions, and Betty Oppenheim for assistance in carrying out the calculations.

* Work performed under the auspices of the U. S. Atomic Energy Commission.

[1] M. Goldhaber and A. W. Sunyar, Phys. Rev. **83**, 906 (1953).
[2] G. Scharff-Goldhaber, Phys. Rev. **90**, 587 (1953).
[3] P. Preiswerk and P. Stähelin, Nuovo cimento **10**, 1219 (1953).
[4] A. Bohr and B. R. Mottelson, Phys. Rev. **90**, 717 (1953).
[5] See also M. Nagasaki and T. Tamura, Progr. Theoret. Phys. **12**, 248 (1954). We are indebted to the authors for a prepublication copy of their paper.
[6] E. L. Church and M. Goldhaber, Phys. Rev. **95**, 626(A) (1954).
[7] Slattery, Lu, and Wiedenbeck, Phys. Rev. **96**, 465 (1954).
[8] J. J. Kraushaar and M. Goldhaber, Phys. Rev. **89**, 1081 (1953).
[9] A. de-Shalit and M. Goldhaber, Phys. Rev. **92**, 1211 (1953).
[10] G. Temmer and N. P. Heydenburg, Phys. Rev. (to be published).
[11] A. Bohr and B. R. Mottelson, Kgl. Danske Videnskab. Selskab, Mat.-fys. Medd. **27**, No. 16 (1953); D. C. Choudhury, Kgl. Danske Videnskab. Selskab, Mat.-fys. Medd. **28**, No. 4 (1954).
[12] The symbol s denotes the seniority number. A. R. Edmonds and B. H. Flowers, Proc. Roy. Soc. London **A215**, 120 (1952), discuss the configuration $(f_{7/2})^4$.
[13] See also K. W. Ford, Phys. Rev. **95**, 1250 (1954); A. W. Sunyar, Phys. Rev. (to be published). Their results may suggest a similar change in B for the region $90 \leqslant IV \leqslant 126$.

First-Forbidden Nonunique Beta Spectra in Re^{186}†

F. T. PORTER, M. S. FREEDMAN, T. B. NOVEY, AND F. WAGNER, JR.

Chemistry Division, Argonne National Laboratory, Lemont, Illinois

(Received January 24, 1955)

THE anomaly of the isotropic β-γ angular correlation[1] and the apparent[2] alpha shape of the first inner beta group in Re^{186} led us to an examination of the beta spectrum in coincidence with the 137-kev gamma. Six-mm-diameter samples of Re^{186} (10 $\mu g/cm^2$) volatilized onto 100-$\mu g/cm^2$ aluminum backing, containing <0.1 percent Re^{188}, were measured in the double-lens spectrometer at a transmission of 6 percent with a resolution of 6 percent. Gammas were counted at 3 percent geometry in NaI(Tl) crystal 1 in. behind the sample, and betas with a 1-mm-thick×11-mm-diameter anthracene disk, using 24-in. Lucite light guides and DuMont 6292 photomultipliers. Amplified shaped pulses were counted in fast ($2\tau_F=0.12$ μsec) coincidence and then in slow coincidence ($2\tau_F=2.6$ μsec) with the

output of single-channel gamma and beta pulse analyzers set to accept only the 137-kev gamma photopeak (and higher energy gammas) and to reject beta noise. The beta photomultiplier was cooled to −80°C.

Considerable effort was devoted to ascertaining the efficiency for measuring coincidences. A long low tail on the beta pulse amplitude distribution (due to backscattering from anthracene) extended into the noise region, leading to a small (1.4 percent) loss in coincidence efficiency at the lowest energy observed, 148 kev. Real/chance >10 for all points below 760 kev. The

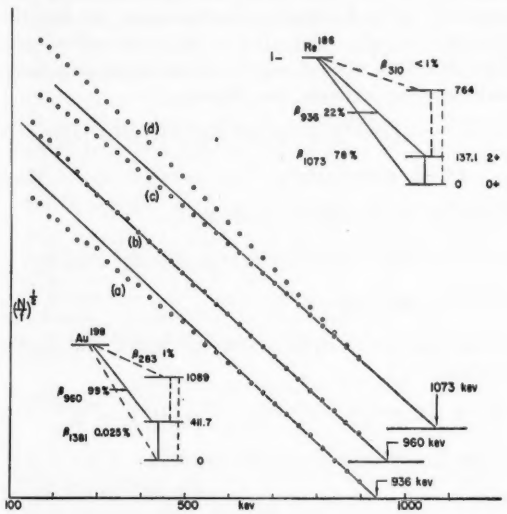

FIG. 1. Kurie plots of: (a) Re^{186} coincidence spectrum; (b) Au^{198} coincidence spectrum; (c) Re^{186} ground-state transition by subtraction; (d) Re^{186} total singles spectrum.

resolving time and its small dependence on beta energy were determined with independent Re^{186} sources to ±5 percent and monitored during the 70-hr experiments at frequent intervals. Six to eight complete spectra constituted each experiment, accumulating *ca* 4000 coincidences at each point. Corrections were made for finite resolving times of the analyzers and slow coincidence circuits and for other small (0.1 percent) effects. The magnetic spectrometer resolution correction was made by using constants derived from the profile of the 137-kev K line.[3] Figure 1(a) exhibits the Kurie plot calculated with shielding-corrected Fermi function.

To illustrate the performance of the coincidence spectrometer, Fig. 1(b) shows the Kurie plot of Au^{198} taken in coincidence with the 411-kev gamma, under conditions identical in all respects save that the gamma pulse amplitude was lowered slightly below that of the Re^{186} 137-kev gamma by reducing the light collection efficiency. The volatilized sample (70 $\mu g/cm^2$) contained <0.5 percent Au^{199}. The 300-kev component in Au^{198} accounts for the magnitude of the upturn below 300 kev.

Comparison of the Re^{186} results with the allowed experimental (coincidence and singles) shape for Au^{198} shows a downward deviation below 500-kev amounting to 13±2 percent reduction in the momentum spectrum at 300 kev and clearly not of the alpha type. A slight upturn below 300 kev may be due to the weak 300-kev group.[4] E_0=936 kev, in excellent agreement with the ground state E_0 of 1074 kev[2] and the gamma energy[5] of 137.1±0.2 kev.

We have also observed (not illustrated) the same downward deviation in Re^{186} using a low-pressure proportional-counter beta detector, which produces smaller pulses with increasing beta energy, opposite to the behavior of the scintillation detector.

We have observed an angular anisotropy of the 137-kev gamma with 500-kev betas $[W(180°)-W(90°)/W(90°)=+0.08\pm0.02]$, and are now determining its energy dependence which is needed to obtain the true "isotropic" shape from the observed coincidence beta spectrum, owing to the restricted range of beta and gamma detection angles employed. Thus we present no values for "shape" factors as yet.

Ignoring this small correction (<2 percent), we subtract the observed coincidence spectrum from the singles spectrum [Fig. 1(d)], normalizing so as to secure E_0=1073 kev (936+137), and the resultant ground-state curve [Fig. 1(c)] shows a shape similar to the inner group and a relative abundance of 78±2 percent.[6]

The only spin assignment for Re^{186} consistent with the similar ft values and shapes for the two prominent beta branches and with the small but definite beta-gamma angular anisotropy as 1−, in agreement with the conclusions of Koerts,[4] who found, however, an allowed shape for the inner group in coincidence.

Together with the cases of RaE,[7] whose curvature is in the opposite direction, and Sb^{124},[8] observable only from 2.32 to 1.60 Mev, these confirm the existence of first-forbidden nonunique spectral shapes. In agreement with theoretical predictions a beta-gamma angular anisotropy is associated with an energy-dependent shape factor, contrary to two cases, Rb^{86} and Tm^{170},[9,10] in which even larger correlations are found with allowed shapes.

† Based on work performed under the auspices of the U. S. Atomic Energy Commission.

[1] J. P. Hurley and P. S. Jastram, Phys. Rev. **95**, 627 (1954).

[2] Guss, Killion, and Porter, Phys. Rev. **95**, 627 (1954); F. T. Porter (private communication).

[3] A resolution correction using these constants applied to a P^{32} spectrum taken under identical conditions yielded a Kurie plot straight (above 300 kev) to within the expected statistical fluctuations of 0.2 percent.

[4] Leo Koerts, Phys. Rev. **95**, 1358 (1954).

[5] Paul Day (private communication—bent-crystal spectrometer).

[6] F. R. Metzger and R. D. Hill, Phys. Rev. **82**, 646 (1951).

[7] Lidofsky, Benczer, Macklin, and Wu, Bull. Am. Phys. Soc. **30**, No. 1, 47 (1955); E. A. Plassmann and L. M. Langer, Phys. Rev. **96**, 1593 (1954).

[8] Langer, Lazar, and Moffat, Phys. Rev. **91**, 338 (1953).

[9] Pohm, Lewis, Talboy, and Jensen, Phys. Rev. **95**, 1523 (1954).

[10] Graham, Wolfson, and Bell, Can. J. Phys. **30**, 459 (1952).

Possible Experiments to Determine the Transition Matrix for p-p Scattering*

REINHARD OEHME
Institute for Nuclear Studies, University of Chicago, Chicago, Illinois
(Received January 28, 1955)

RECENTLY, it became possible to perform scattering experiments with polarized proton beams on unpolarized hydrogen targets.[1] It is the purpose of this note to point out that for given energy and scattering angle one may obtain up to eleven independent relations between the parameters of the p-p transition matrix, provided it is experimentally possible to perform all necessary single, double, and triple scattering experiments. The targets are always unpolarized and only one hydrogen scattering is necessary.

The unit vectors in the direction of the incoming and the scattered beam in the center-of-mass system are denoted by $\mathbf{k}_i$ and $\mathbf{k}_f$ respectively. We define further the unit vectors $\mathbf{m}\sim\mathbf{k}_i-\mathbf{k}_f$, $\mathbf{l}\sim\mathbf{k}_i+\mathbf{k}_f$, $\mathbf{n}=\mathbf{m}\times\mathbf{l}\sim\mathbf{k}_i\times\mathbf{k}_f$, and $\mathbf{n}_1=\mathbf{n}\times\mathbf{k}_i$. The transition matrix between states of two free protons with positive energy will be written in the general form[2]

$$T=\alpha+\beta\boldsymbol{\sigma}_1\cdot\mathbf{n}\boldsymbol{\sigma}_2\cdot\mathbf{n}+\gamma(\boldsymbol{\sigma}_1+\boldsymbol{\sigma}_2)\cdot\mathbf{n}+\delta\boldsymbol{\sigma}_1\cdot\mathbf{m}\boldsymbol{\sigma}_2\cdot\mathbf{m}+\epsilon\boldsymbol{\sigma}_1\cdot\mathbf{l}\boldsymbol{\sigma}_2\cdot\mathbf{l},$$

where α, β, etc. are complex functions of energy and of $\cos\vartheta=\mathbf{k}_i\cdot\mathbf{k}_f$. Aside from an absolute phase there are nine real functions of ϑ to be determined at a fixed energy. Once these functions are known for $0\leq\vartheta\leq\pi/2$, their behavior for $\vartheta>\pi/2$ is determined by the Pauli principle. Let $\mathbf{P}^{\text{in}}=\langle\boldsymbol{\sigma}_1\rangle_{\text{in}}$ be the polarization of the proton beam impinging on the hydrogen target. In addition to the cross section Q^u for $\mathbf{P}^{\text{in}}=0$ the observable quantities are the polarization $\mathbf{P}^p=\langle\boldsymbol{\sigma}_1\rangle_{\text{out}}$ in the scattered beam and the correlation function $C^p(\mathbf{p},\mathbf{q})=\langle\boldsymbol{\sigma}_1\cdot\mathbf{p}\boldsymbol{\sigma}_2\cdot\mathbf{q}\rangle_{\text{out}}$. The superscripts u and p refer to unpolarized and polarized incident proton beams respectively. We find for these quantities:

$$\mathbf{P}^p=(\mathbf{P}^u+\mathfrak{T}\mathbf{P}^{\text{in}})/(1+\mathbf{P}^u\cdot\mathbf{P}^{\text{in}}),$$

where[3]

$$\mathfrak{T}_{ik}=\text{Tr}(\sigma_{1i}T\sigma_{1k}T^\dagger)/\text{Tr}(TT^\dagger)$$

and

$$C^p(\mathbf{p},\mathbf{q})=[C^u(\mathbf{p},\mathbf{q})+\mathbf{Z}(\mathbf{p},\mathbf{q})\cdot\mathbf{P}^{\text{in}}]/(1+\mathbf{P}^u\cdot\mathbf{P}^{\text{in}}),$$

where

$$C^u(\mathbf{p},\mathbf{q})+\mathbf{Z}(\mathbf{p},\mathbf{q})\cdot\mathbf{P}^{\text{in}}=\text{Tr}(T(1+\boldsymbol{\sigma}_1\cdot\mathbf{P}^{\text{in}})T^\dagger\boldsymbol{\sigma}_1\cdot\mathbf{p}\boldsymbol{\sigma}_2\cdot\mathbf{q})/\text{Tr}(TT^\dagger).$$

The function $C^p(\mathbf{p},\mathbf{q})$ represents the expectation value of the product $\boldsymbol{\sigma}_1\cdot\mathbf{p}\boldsymbol{\sigma}_2\cdot\mathbf{q}$. It is obtained by measuring in coincidence the components of the polarization of the "scattered" beam ($\mathbf{k}_f$) and of the "recoil" beam ($-\mathbf{k}_f$) in the directions $\mathbf{p}$ and $\mathbf{q}$ respectively.[4] Restricting ourselves to triple scattering, the polarization $\mathbf{P}^{\text{in}}$ of the beam impinging on the hydrogen target (second target) is always orthogonal to $\mathbf{k}_i$. Furthermore, by measuring the asymmetry, we can determine only those components of the polarization of the corresponding beam which are orthogonal to its direction of propagation in the laboratory system. With these restrictions, we may measure eleven independent quantities which will be given in terms of the parameters $a=\alpha+\beta$, $b=\alpha-\beta$, $c=\delta+\epsilon$, $d=\delta-\epsilon$, $e=2\gamma$; α, β, etc., are the coefficients in the transition matrix. The parameters, a, $b+c$, d, and e depend only on triplet elements of the transition matrix, whereas $b-c$ is proportional to T (singlet). Furthermore, we find that $a(\pi-\vartheta)=-a(\vartheta)$, $b(\pi-\vartheta)=-c(\vartheta)$, $c(\pi-\vartheta)=-b(\vartheta)$, $d(\pi-\vartheta)=d(\vartheta)$, $e(\pi-\vartheta)=e(\vartheta)$. From single and double scattering experiments, we obtain:

$$Q^u=\tfrac{1}{2}\{|a|^2+|b|^2+|c|^2+|d|^2+|e|^2\}, \quad (1)$$

$$Q^u(\mathbf{P}^u\cdot\mathbf{n})=\text{Re}(ae^*); \quad (2)$$

analyzing in coincidence leads to[5,6]

$$Q^uC^u(\mathbf{n},\mathbf{n})=\tfrac{1}{2}\{|a|^2-|b|^2-|c|^2+|d|^2+|e|^2\}, \quad (3)$$

$$Q^uC^u(\mathbf{m},\mathbf{l})=\text{Im}(de^*). \quad (4)$$

Straightforward triple scattering gives the further relations:[3,5,6]

$$Q^u(\mathbf{n}\cdot\mathfrak{T}\mathbf{n})=\tfrac{1}{2}\{|a|^2+|b|^2-|c|^2-|d|^2+|e|^2\}, \quad (5)$$

$$Q^u(\mathbf{m}\cdot\mathfrak{T}\mathbf{n}_1)=-\text{Re}(ab^*+cd^*)\cos(\vartheta/2)-\text{Im}(be^*)\sin(\vartheta/2). \quad (6)$$

These two quantities are neither symmetric nor antisymmetric with respect to $\vartheta=\pi/2$. Thus measurements in the angular region $\pi/2<\vartheta<\pi$ give two further independent relations between the parameters a, b, etc. in the angular region $0<\vartheta<\pi/2$. Instead of the "scattered" beam for $\vartheta>\pi/2$, one may use the recoil beam for $\mathbf{k}_f$ in the angular region $0<\vartheta<\pi/2$. The relations so obtained are

$$Q^u(\mathbf{n}\cdot\mathfrak{T}\mathbf{n})_{\pi-\vartheta}=Q^u(\mathbf{n}\cdot\mathfrak{T}'\mathbf{n})_{\text{recoil}}=\tfrac{1}{2}\{|a|^2-|b|^2+|c|^2-|d|^2+|e|^2\}, \quad (7)$$

$$Q^u(\mathbf{m}\cdot\mathfrak{T}\mathbf{n}_1)_{\pi-\vartheta}=-Q^u(\mathbf{l}\cdot\mathfrak{T}'\mathbf{n}_1)_{\text{recoil}}=-\text{Re}(ac^*-bd^*)\sin(\vartheta/2)+\text{Im}(ce^*)\cos(\vartheta/2), \quad (8)$$

where $\mathfrak{T}'_{ik}$ is obtained by replacing σ_{1i} by σ_{2i} in $\mathfrak{T}_{ik}$. Analyzing in coincidence, one obtains from triple scattering experiments the three additional relations[7]:

$$Q^u\mathbf{Z}(\mathbf{m},\mathbf{l})\cdot\mathbf{n}=\text{Im}(bc^*-ad^*), \quad (9)$$

$$Q^u\mathbf{Z}(\mathbf{m},\mathbf{n})\cdot\mathbf{n}_1=\text{Im}(ab^*+cd^*)\sin(\vartheta/2)-\text{Re}(be^*)\cos(\vartheta/2), \quad (10)$$

$$Q^u\mathbf{Z}(\mathbf{n},\mathbf{l})\cdot\mathbf{n}_1=\text{Im}(ac^*-bd^*)\cos(\vartheta/2)+\text{Re}(ce^*)\sin(\vartheta/2). \quad (11)$$

In Eqs. (4), (6), and (8)–(11) we have neglected relativistic corrections.

For $\vartheta=\pi/2$ the relations (2) and (9) vanish whereas (10) and (11) become identical. There remain therefore six independent relations between the coefficients $b(\pi/2)=-c(\pi/2)$, $d(\pi/2)$, and $e(\pi/2)$, i.e., between five real parameters which determine the transition matrix $T(\pi/2,\phi)$ except for an absolute phase factor. For angles $0<\vartheta<\pi/2$, one can obtain eleven relations for nine parameters. The experimental quantities are of course not single-valued functions of these parameters, but the ambiguities may be reduced by comparing solutions for different angles and energies. At lower energies also a phase shift analysis can be helpful. A more complete discussion, especially of the correlation experiments, will be published later.

The author is very grateful to Professor G. Wentzel for interesting discussions. Thanks are also due Professor M. L. Goldberger, Dr. S. Cohen, Dr. Leona Marshall, and Dr. H. Miyazawa for helpful comments.

* Work supported by the U. S. Atomic Energy Commission.

[1] Ypsilantis, Wiegand, Tripp, Segrè, and Chamberlain, Bull. Am. Phys. Soc. **29**, No. 8, 19 (1954).

[2] L. Wolfenstein and J. Ashkin, Phys. Rev. **85**, 847 (1952); R. H. Dalitz, Proc. Roy. Soc. (London) **A65**, 175 (1952).

[3] R. Oehme, Phys. Rev. **98**, 147 (1955), Eqs. (12) and (13).

[4] We find

$$C^p(\mathbf{p},\mathbf{q})=\frac{N(\mathbf{p},\mathbf{q})+N(-\mathbf{p},-\mathbf{q})-N(\mathbf{p},-\mathbf{q})-N(-\mathbf{p},\mathbf{q})}{N(\mathbf{p},\mathbf{q})+N(-\mathbf{p},-\mathbf{q})+N(\mathbf{p},-\mathbf{q})+N(-\mathbf{p},\mathbf{q})},$$

where $N(\mathbf{p},\mathbf{q})$ is the number of events in which the spin of the "scattered" proton is in the direction $\mathbf{p}$ and the spin of the "recoil" proton in the direction $\mathbf{q}$.

[5] L. Wolfenstein, Phys. Rev. **96**, 1654 (1954). The author is indebted to Professor Wolfenstein for sending him a copy of this paper.

[6] H. P. Stapp, Bull. Am. Phys. Soc. **29**, No. 8, 19 (1954); the author wishes to thank Dr. Leona Marshall for showing him a preprint of this paper.

[7] These are practically quadruple scattering experiments, but they might be somewhat easier than straightforward quadruple scattering.

Electron Scattering from the Proton*†‡

ROBERT HOFSTADTER AND ROBERT W. MCALLISTER

Department of Physics and High-Energy Physics Laboratory, Stanford University, Stanford, California

(Received January 24, 1955)

WITH apparatus previously described,[1,2] we have studied the elastic scattering of electrons of energies 100, 188, and 236 Mev from protons initially at rest. At 100 Mev and 188 Mev, the angular distributions of scattered electrons have been examined in the ranges 60°–138° and 35°–138°, respectively, in the laboratory frame. At 236 Mev, because of an inability of the analyzing magnet to bend electrons of energies larger than 192 Mev, we have studied the angular distribution between 90° and 138° in the laboratory frame. In all cases a gaseous hydrogen target was used.

We have found that deviations in excess of Mott scattering are readily apparent at large scattering angles. The early results (reported at the Seattle meeting, July, 1954) at smaller angles showed the expected agreement with the Mott formula within experimental error. Deviations from the Mott formula such as we have found may be anticipated at large angles because of additional scattering from the magnetic moment of the proton.[3] We have observed this additional scattering but in an amount smaller than predicted by theory.

The experimental curve at 188 Mev is given in Fig. 1. It may be observed that the experimental points do not fit either the Mott curve or the theoretical curve of Rosenbluth,[3] computed for a point charge and point (anomalous) magnetic moment of the proton. Furthermore, the experimental curve does not fit a Rosenbluth curve with the Dirac magnetic moment and a point charge. The latter curve would lie close to the Mott curve and slightly above it. Similar behavior is observed at 236 Mev.

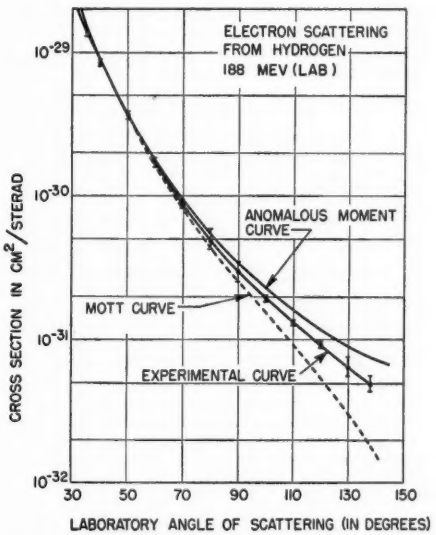

FIG. 1. The figure shows the experimental curve, the Mott curve, and the point-charge, point-magnetic-moment curve. The experimental curve passes through the points with the attached margins of error. The margins of error are not statistical; statistical errors would be much smaller than the errors shown. The limits of error are, rather, the largest deviations observed in the many complete and partial runs taken over a period of several months. Absolute cross sections given in the ordinate scale were not measured experimentally but were taken from theory. The radiative corrections of Schwinger have been ignored since they affect the angular distribution hardly at all. The radiative corrections do influence the absolute cross sections. Experimental points in the figure refer to areas under the elastic peaks taken over an energy interval of ±1.5 Mev centering about the peak. The data at the various points are unchanged in relation to each other when the energy interval is increased to ±2.5 Mev about the peak; the latter widths include essentially all the area under the peak.

The correct interpretation of these results will require a more elaborate explanation (probably involving a good meson theory) than can be given at the moment, although Rosenbluth already has made weak-coupling calculations in meson theory which predict an effect of the kind we have observed.[4]

Nevertheless, if we make the naive assumption that the proton charge cloud and its magnetic moment are both spread out in the same proportions we can calculate simple form factors for various values of the proton "size." When these calculations are carried out we find that the experimental curves can be represented very well by the following choices of size. At 188 Mev, the data are fitted accurately by an rms radius of $(7.0\pm2.4)\times10^{-14}$ cm. At 236 Mev, the data are well fitted by an rms radius of $(7.8\pm2.4)\times10^{-14}$ cm. At 100 Mev the data are relatively insensitive to the radius but the experimental results are fitted by both choices given above. The 100-Mev data serve therefore as a valuable check of the apparatus. A compromise value fitting all the experimental results is $(7.4\pm2.4)\times10^{-14}$ cm. If the proton were a spherical ball of charge, this rms radius would indicate a true radius of 9.5×10^{-14} cm, or in round numbers 1.0×10^{-13} cm. It is to be noted that if our interpretation is correct the Coulomb law of force has not been violated at distances as small as 7×10^{-14} cm.

These results will be reported in more detail in a paper now in preparation.

We wish to thank Dr. D. R. Yennie for his generous aid in discussions of the theory.* We wish to thank Mr. E. E. Chambers for assistance with several phases of the work. In the early phases of this research, the late Miss Eva Wiener made important contributions.

* The research reported in this document was supported jointly by the U. S. Navy (Office of Naval Research) and the U. S. Atomic Energy Commission, and the U. S. Air Force through the Office of Scientific Research of the Air Research and Development Command.

† Aided by a grant from the Research Corporation.

‡ Early results were reported at the Seattle Meeting of the American Physical Society [Phys. Rev. **96**, 854(A) (1954)]. More recent results were presented at the Berkeley meeting of the American Physical Society [Bull. Am. Phys. Soc. **29**, No. 8, 29 (1954)].

[1] Hofstadter, Fechter, and McIntyre, Phys. Rev. **92**, 978 (1953).

[2] Hofstadter, Hahn, Knudsen, and McIntyre, Phys. Rev. **95**, 512 (1954).

[3] M. N. Rosenbluth, Phys. Rev. **79**, 615 (1950).

[4] See also the classical calculation of L. I. Schiff reported in Rosenbluth's paper.

Capture of Negative K Mesons*

J. Hornbostel and E. O. Salant

Brookhaven National Laboratory, Upton, New York

(Received February 16, 1955)

SEARCH for negative K mesons has been continued[1] with essentially the same arrangement as previously reported,[2] but with 2.8-Bev protons. The stack of stripped emulsions now receives a collimated beam of negative particles of momentum 316 Mev/c (average spread ±8 Mev/c) emitted from a Be target at 4° to the proton beam.

Each emulsion was scanned, near its edge through which the beam entered, for tracks of the beam direction (within $\pm1°$) and of about twice minimum grain density, appropriate to the K mesons. All such tracks were then followed to their ends.

In this way, 13 stars made by K^- mesons at the end of their range were found; 3 stars made by K^- mesons in flight were found in ~58 cm of K-meson track followed. Therefore, the K^- mean-free path for star-producing collisions approximately equals the geometric mean-free path of emulsion (27 cm).

The flux of K^- mesons relative to π^- mesons in the emulsions (beam tracks of minimum grain density, g_{min}) was 2×10^{-5}. The mass of each K^- particle, from preliminary measurements of momentum *vs* range, in some cases of grain count *vs* range and, for K mesons producing stars in flight, of scattering *vs* grain count, was consistent with the tau mass within about 10 percent.

In five K^- stars, described in Table I and, for four cases, in Fig. 1, a charged unstable heavy particle (UHP) is emitted. The other K^- stars show 1 to 7 heavy prongs and, in all but two cases, a single light track consistent with a pion of ~100 Mev, and have visible energies $\lesssim$300 Mev, sufficiently less than the 500 Mev available to allow the possibility of Λ^0 emission.[3]

In Fig. 1, tracks (1) are due to K^- coming to rest at S, tracks (2) to the UHP, tracks (3) to light particles emerging from the end of tracks (2) at P, tracks (5) to light particles from S, and tracks (4) and (6)–(11) to stable particles.

TABLE I. Characteristics of K^--capture stars with unstable heavy particle emission. F=star made in flight; (a) possibly bound; (b) particle present, unanalyzed; (c) high energies have no upper limits; (d) energies were calculated for pions. Errors include both statistical and systematic uncertainties.

NK	Unstable heavy particle Identity	Energy Mev	Light secondary at P energy (c, d) Mev	Light particle at S energy (d) Mev	Visible star energy Mev
8	Σ^+	10	$93_{-14}{}^{+?}$	$63_{-6}{}^{+16}$	480
1	$\Sigma^\pm$	30	$120_{-40}{}^{+?}$	$57_{-6}{}^{+16}$	490
5	Σ^- or Λ^0 bound	10 $\gtrsim$18	18, π^-	none	420 $\gtrsim$380
4	$Y^{\pm(a)}$	~120	$120_{-40}{}^{+?}$	none	$\gtrsim$410
14F	(b)		none	(b)	

In star $NK8$, particle (2) comes to rest at P. From scattering and range, its mass is $(0.7_{-0.3}{}^{+0.4})m_p$. The energy of particle (3) is consistent with a pion from the charged hyperon Σ^+ (Q=110 Mev). Accordingly, the UHP can be identified as Σ^+.

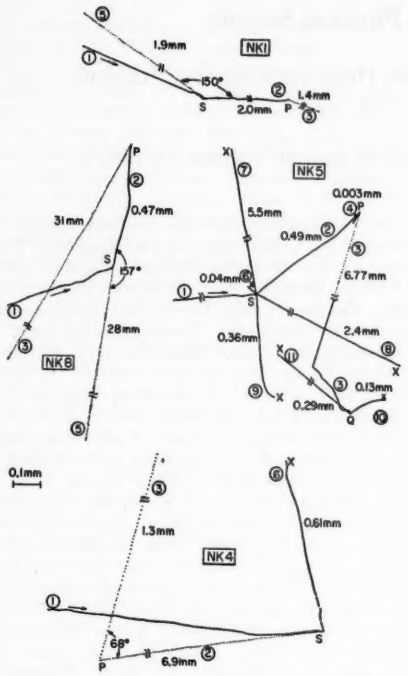

FIG. 1. Drawings of K^--capture stars. (1) incoming K^- meson; (2) unstable heavy particle; (3) light secondary particle; (5) light particle; (4), (6)–(11) stable particles. × = stops in emulsion. Angles are in space.

Star *NK*1 resembles *NK*8. It differs in that the scattering indicates that particle (2) has probably not come to rest at P but decays in flight and has an average kinetic energy of about 30 Mev. Because of saturated grain count, it is a heavy particle, probably a free $\Sigma^{\pm}$, though possibly bound.

In *NK*5, particle (3) is an 18-Mev π^-, making a σ star. Particle (2) comes to rest at P; its mass, from scattering and range, is $(2.6_{-1.1}{}^{+1.4})m_p$. If the event at P is a decay, the UHP could be He^{4*} or H^{4*}, with a bound Λ^0; decay products could be $3p+n+\pi^-+27$ Mev,[4,5] or, for example, $He^3+n+\pi^-+33$ Mev (assuming 3 Mev for Λ^0 binding), respectively. In any case, one or more neutrons must take up the residual energy and balance momenta of particles (3) and (4). Alternatively, the UHP could be Σ^-, captured at P.

In star *NK*4, particle (2) gives a track $(2.85 \pm 0.08)g_{\min}$ for its entire path, hence $m \geq m_Y$. Its kinetic energy is 0.1 mc^2, hence momentum and energy can be balanced at S by a neutron if the UHP is $\Sigma^{\pm}$, by nuclear recoil if it is D^*, but not at all if it is T^*. Particle (2) produces in flight the backward track (3), $p\beta \geq 100$ Mev/c, $1.1g_{\min}$. If particle (3) is a pion from free decay of $Y^{\pm}$, then $Q = 250_{-60}{}^{+?}$ Mev, an unknown value; decay into a muon or electron, likewise unknown, would be compatible with the data. Alternatively, the UHP could be $\Sigma^{\pm}$ making a zero-pronged star in flight (for which the probability $\sim 10^{-3}$) and decaying at rest; this would not conform to theoretical schemes.[6]

We thank J. D. Leek, E. R. Medd, and J. E. Smith for microscopy, M. D. Carter and P. Simack for processing, J. W. Quinn for help with the experiments, and the Cosmotron staff for unfailing cooperation.

* Work performed under the auspices of the U. S. Atomic Energy Commission.

[1] J. Hornbostel and E. O. Salant, Bull. Am. Phys. Soc. **30**, No. 1, 63 (1955).
[2] J. Hornbostel and E. O. Salant, Phys. Rev. **93**, 902 (1954).
[3] Herbert DeStaebler, Jr., Phys. Rev. **95**, 1110 (1954).
[4] Hill, Salant, Widgoff, Osborne, Pevsner, Ritson, Crussard, and Walker, Phys. Rev. **94**, 797 (1954).
[5] Naugle, Ney, Freier, and Cheston, Phys. Rev. **96**, 1383 (1954).
[6] M. Gell-Mann and M. Goldhaber (private communications).

Proceedings of the American Physical Society

Minutes of the 1954 Thanksgiving Meeting Held at Chicago, Illinois, November 26–27, 1954

(Corresponding to *Bulletin of the American Physical Society*, Volume 29, No. 7)

OF the 1953 Thanksgiving Meeting the Secretary reported that it was the first held in Chicago after a gap of two years in the sequence, and that the number of contributed papers was unexpectedly low, suggesting that the November meeting had yielded to the March meeting its former rank of third largest of the year. It is a pleasure to report that the 1954 Thanksgiving meeting was again held at Chicago and made a good recovery,—not however quite to the level of recent March meetings. There were 168 contributed papers, and the registration at the meeting amounted to 610. Invited papers, nearly all of them from the Midwestern area, numbered 15. Our Division of Solid-State Physics organized a half-day symposium. The meeting was, as heretofore, excellently administered by Mrs. Dorothy C. Johnson, to whom we owe not a single but a recurrent debt.

The banquet of the Society was held on the Friday evening in the Quadrangle Club. This time every available place was taken, to a total of 157. The after-dinner speakers were N. E. Bradbury of Los Alamos, who spoke on his Laboratory, and F. Zernike of Groningen.

The Council met on the Friday, and elected to Fellowship one candidate and to Membership three hundred and sixty-six; the names are appended.

Elected to Fellowship: R. K. Wangsness.

Elected to Membership: Alexander Abashian, Robert Abbey, Angelo A. Alaggia, Harvey A. Alperin, Elmer L. Amma, John Melvin Anderson, *Baxter Hardin Armstrong, Adriaan Hendrik Willem Aten, Jr., Frank LeRoy Baimonte, Thomas L. Bailey, *John Arnold Baldwin, Jr., John C. Ballinger, *George Barnes, James Russell Beacham, Michael Beer, Arlene Dale Berger, *Robert Lewis Berger, *Arnold Berman, William Harrison Bice, William Pierson Bickham, *Olexa Myron Bilaniuk, *Adam Marian Bincer, *Robert L. Bingham, *Normand Conrad Blais, Lenore Julia Bloswick, Grenfell P. Boicourt, Hoyt A. Bostick, Albert Bouillon, Roger Earl Boyd, Chester Griswold Bragaw, Jr., *Alfred Ephraim Brenner, *Norman Wheeler Briggs, *Edward Hays Brooks, L. Carlton Brown, Rollin Lombard Brown, Jack Ray Buckingham, *Audley Oliver Burford, Robert Mercer Burger, *Peter Nicholas Burgoyne, Robert S. Buritz, Carlton Edwin Burley, *Benjamin Screven Burton, Jr., *Julian Jakob Bussgang, *Sidney Roy Butler, Anthony E. Cahill, Gordon Hillyard Cameron, *Anthony Vincent Campise, *Edward Hill Carlson, Boyd Balford Cary, Jr., Leonardo Castillejo, *Robert John Cence, *Sewell Preston Champe, *Ren Chiba, Chung Ying Chih, *Oong Choi, *Charles Henry Church, Stig Melker Claesson, *Roland J. A. Cloutier, *Mitchell Simmons Cohen, *Terry Cole, Robert J. Collins, *Eugene David Commins, Walter Dale Compton, Samuel P. Cook, *James William Corbett, *Robert G. Cunningham, George William Curtis, George Boudislavov Cvijanovich, *Robert Alan Dannels, *Frederick Jerome Darnell, Cyrano Tuillio DeDominicis, Marvel Demeur, Daniel Francis Demsey, *Carl Dulgeroff, Herbert Spencer Dunkerley, *Gordon Harold Dunn, Marvin Emerson Ebel, *Richard Malvin Edelstein, Martin H. Edwards, *Jacob Enoch, Albert Tromly Ellis, *Albert Eskowitz, Edward Allen Fagen, Philo Taylor Farnsworth, *Marvin E. Feldman, Bernard R. Felix, Morton A. Fineman, Richard W. Fink, *David Bibb Fischbach, Kenneth Henry Fishbeck, Jean Collins Flint, Donald Gordon Flom, *James Franklin Foley, *Howland Auchincloss Fowler, William Frati, Jerome Heyde Fregeau, Steven Max Fulda, *Ellis Nelson Fuls, Heinz Gabloffsky, Martin F. Gellert, V. L. Gentry, *Thomas Henry George, Hans-Jürg Gerger, Umberto Ferdinando Gianola, Bud H. Gibbs, *John Browning Gibson, *Sheldon Lee Glashow, Rolfe Eldridge Glover, III, Robert Owen Gorson, Dwight L. Gravitte, Jerome Boley Green, Ignatius Cartwright Griesacker, Russell Winston Hall, Jr., Archibald Cameron Hollis Hallett, Clay Jeter Halley, Jr., James Hamilton, Paul Handler, Mortimer Wm. Hans, Kenneth James Harker, Raymond Jay Hart, *Kenneth L. Hartt, *Tsuneo Hashi, *Marvin Hass, Herman Ralph Haymond, *Eugene Robert Heath, *Louis Charles Hebel, Robert Russell Heikes, David M. Heinz, *Jerome David Herniter, John Wells Hilborn, David Allen Hill, John R. Hoffman, *John Francis Hon, Robert Sanchez Hooper, George Robert Hopkins, Hisashi Horie, Morton Bernard Hornstein, Andre Henri Houriet, Donald Lawrence Hoyt, John Charles Hubbs, William L. C. Hui, Charles Angas Hurst, *Rudolph Chia-Chao Hwa, *Hiaetsugu Ikegami, *Francis Joseph Jackson, Hans H. Jaffe, D. C. Jameson, *Allen Ira Janis, Charles Minor Johnson, Llewellyn H. Jones, Selig N. Kaplan, *James Lyle Kassner, Jr., Ralph William Kavanagh, Mitsuji Kawai, Donald W. Keefer, *Ralph W. Kilb, John Joseph Kinsella, Edward A. Kmetko, Paul E. Kolk, *Carol Kolm, Roman Krawec, *Sol Krongelb, Isao Kumabe, James Morrison Lambert, *Sigurd Larsen, *Edgar Miller Layton, Jr., *David Morris Lee, Otto Lee, *Rene Albert Levesque, Warren Burton Lewis, *Sideny Liebes, Jr., *Joseph Isaac Lipson, Albert Edward Litherland, Elizabeth Alden Little, John Bascom Little, Raymond Clare Lloyd, *Leroy Robert Loewenstern, Jere Johns Lord, *Elihu Lubkin, Fred Everett Luborsky, J. D. Lydick, *Hannibal Hamlin Madden, Jr., *Ernest Ilya Malamud, Robert Allan Mapleton, Kenneth I. Marks, *Robert Bruce Marr, Daniel Mattis, *Robert Wallace McAllister, *Wilson Melville McClelland, Jr., Lewis Isaac Mendelsohn, Leslie H. Meredith, Arthur John Meyerott, Harold Abe Miller, *William Frederick Miller, *William Raymond Mills, Jr., *Albert Hugh Mitchell, *Kenneth Virgil Moore, *Richard Moore, A. Gregory Morris, *Robert Gemmill Morris, *Earl Raymond Mosburg, Jr., Burton Harlow Muller, *George Raymond Murray, Jr., Nishtala Appala Narasimham, Robert Ernest Naylor, Jr., Herschel Neumann, *Edward Joseph Ney, *Larry Mark Noble, *Hugh Nutley, *Ordean Silas Oen, Thomas Alphonsus O'Halloran, Howard John Okoomian, Neill Clinton Ostrander, Harry White Parr, *Laurence Passell, *Helmut Paul, *Emmanuel C. Paxhia, Israel Pelchowitch, Harry James Peppiatt, *John D. Reppy, Robert W. Perry, *Martin D. Peter, Benajmin Petkof, *James P. Phelps, *John Joseph Pinajian, George Pish, Walter George Planet, Jr., Harmon Hastings Plumb, Philippe

Pluvinage, *Gerald Leslie Pollack, John William Preiss, *Charles Aubrey Preskitt, Jr., James Henry Prindle, *William Ira Pyle, Robert Harold Quint, *Melukote KrishnaRao RamaSwamy, *Philip Lee Randolph, Bernard Rappaport, Fritz Herbert Reder, Peter John Redmond, Marvin Lee Reeves, *Gilbert Henry Reiling, Julian Reinheimer, *Jacques S. Renau, George Michael Rentzepis, *Dale Wilson Rice, *Marvin Rich, *Robert Graham Rich, Jr., Harold Owen Wilson Richardson, *Burton Richter, Wolfgang Riezler, David Zav Robinson, *Kenneth Walter Robinson, *Byron P. Roe, *Onofre Rojo, Edward George Roka, Herbert H. Rosen, *Mervine Rosen, David Dewey Roshon, Jr., *Lawrence Rosler, *Thomas Dean Rossing, *Paul Frederick Roth, Carl Albert Rouse, Frank Sherwood Rowland, *James Edward Russell, Marvin Winfred Russell, Monroe S. Sadler, *Walter L. Sadowski, *Julius Alexander Salacz-Dohnanyi, Jürg Xaver Saladin, Gary Saul Sales, *William Henry Sandmann, *Jack Sandweiss, *Richard Cassell Sapp, *Myriam Paula Sarachik, *Lynn Redmon Sarles, Leopoldo G. Colin Scherer, Victor E. Scherrer, Robert Ellsworth Schlier, *Jack Schneps, George J. Schulz, Paul F. Schutt, Edmond Victor Schwartz, Norman Edward Schofield, Joseph Paul Seiden, *Stanley T. Sekula, *Kamal Kishore Seth, *John Richard Shepanski, William Danks Shephard, Motoichi Shibuya, Masao Shimizu, *Benjamin Francis Sherman, Jr., Jacob Sherman, *Walter Allen Shropshire, Jr., *Joseph Wright Simmons, *Leon Judah Slutsky, James Yeoman Smith, *Robert Clinton Smith, *William Hurst Snedegar, Jr., Irvin Henry Solt, Jr., *Charles Michael Sommerfield, David Hugh Sowle, *William Edward Spicer, Valentine Spiegel, Jr., William J. Spry, Jr., *Robert K. Squire, *Devanatha Srinivasan, Paul Steiner, Alec Thompson Stewart, John Wescott Stewart, *Turner van Cortlandt Stokes, Harold Leon Stolov, *Robert Gilbert Stone, Alan Jay Strauss, *Edward Henry Stupp, *Jerome Douglas Swalen, Robert Henderson Swick, Raymond Edmund Szupillo, *Yoshiro Takano, *Kenji Takumi, Tomoyasu Tanaka, *Menasha Joseph Tavsner, *Herbert Lydon Taylor, *Ralph Aloysius Tobin, Ivan Tolstoy, *James Roland Travis, J. Kenneth Trolan, *William Wadsworth True, Harold Clyde Trueblood, John George Trulio, Benson Leland Tucker, Simpei Tutihasi, Leopoldo B. Valdes, A. Van Itterbeck, *Franklin James Vaughn, *William H. Venable, Jr., *Jack Vorona, *Charles Noel Waddell, *Bernard Lawrence Walsh, Jr., Donald Harris Webb, *Medford S. Webster, Johannes Weertman, *Steven Weinberg, *John David Weisner, *Rainer Weiss, Herman Benjamin Weissman, Samuel I. Weissman, *James Herbert Werntz, Jr., *Howard Wayne Wicklein, Rolf Wideroe, *Irwin Wieder, *Tor Wiedling, *John Frederick Wild, Thomas Walley Williams, III, James Leroy Willows, *Peter Joseph Wojtowicz, Peter N. Wolfe, *Eugene YouShe Wong, Ralph E. Woodard, *Henry Wyle, Leonard Zablow, Roy Lawrence Zastrow, Edwin Leopold Zebroski, *Walter Ziffer, Robert Walker Zimmerer, and *Walter Zobel.

*—Student.

KARL K. DARROW, *Secretary*
American Physical Society
Columbia University,
New York 27, New York

Errata Pertaining to Papers G8, G11, H7, I3, I4, K4, and V8

G8, by E. G. Grimsal. In the footnote*, instead of "Supported in part by the National Research Council," read "Supported in part by the Research Council."

G11, by G. M. Seidel and V. A. Johnson. Insert footnote to the title: "* Work assisted by Signal Corps Contract."

H7, by Berol L. Robinson and Richard W. Fink. In line 14, "were" should read "was." The last sentence should read, "We observed gamma rays at 395±10 kev and 550±30 kev, ··· and which are attributed to Cs^{129}."

I3, by R. L. Stearns, J. W. Robson, and E. C. Gregg. The sentence "The spectrum compared favorably with that calculated by Schiff assuming a 20-mil molybdenum target," should read "The spectrum compared favorably with the Schiff thin-target spectrum."

I4, by J. W. Robson, R. L. Stearns, and E. C. Gregg. Instead of

$$n(T)=\int_{T-T/2}^{T+\Delta T/2} E(T')\left[\int NA(\psi,E_2)\frac{\partial 6}{\partial \psi}B(E_2)\frac{\partial \psi}{\partial T}dE_2\right]ZdT',$$

read

$$\int_{T-\Delta T/2}^{T+\Delta T/2} E(T')\left[\int NA(\psi,E_\gamma)\frac{\partial 6}{\partial \psi}B(E_\gamma)\frac{\partial \psi}{\partial T}dE_\gamma\right]dT'.$$

K4, by W. M. MacDonald. The last sentence should be removed. A footnote should be added to the title: "* This work was carried out at Princeton University."

V8, by A. B. Bhatia. In the fourth sentence "part" should read "§," and "these secular equations" should read "the appropriate secular equation."

PROGRAMME

FRIDAY MORNING AT 10:00

Cobb 110

(K. A. BRUECKNER presiding)

Theoretical Physics

A1. Quantum Theory of Noise. NORMAN ROSTOKER AND HANS EKSTEIN, *Armour Research Foundation.*—Most of the current theories of noise are semiclassical. Our approach differs in that it is entirely quantum-mechanical. It consists in formulating an operator for the spectral density of a fluctuating dynamical variable that is based on an analysis of the method of measurement. An essential feature of the spectral density operator is that it involves replacement of classical dynamical variables by time-dependent Heisenberg operators. The expectation value of the spectral density includes fluctuations of statistical origin as well as fluctuations of quantum-mechanical origin. It can be computed for any physical system when the initial state has been specified. A practical application has been made to a system in thermodynamic equilibrium. The physical system employed is similar to the one discussed by Callen and Welton[1] except that we consider degenerate eigenstates. The resultant expectation value of the spectral density of current fluctuations is in agreement with Nyquist's law.

[1] H. B. Callen and T. A. Welton, Phys. Rev. **83**, 34 (1951).

A2. Quantum Correction to the Shot Effect. HANS EKSTEIN AND NORMAN ROSTOKER, *Armour Research Foundation.*—Classically, a beam of electrons produces a fluctuating current at a detector characterized by a spectral density that is independent of frequency. The fluctuations in current are simply due to charge discreteness. Quantum corrections would be expected due to the wave-like character of the electron and due to correlation between different electrons such as is required by the Pauli principle. In this paper we consider only free noninteracting electrons and disregard the Pauli principle so that the problem can be reduced to a one-electron problem. A quantum correction is obtained whose origin is in the wave-like character of the electron. While it would be difficult to observe the quantum effect in ordinary circuits, the result is of fundamental interest. For an electron of definite momentum and kinetic energy $\hbar\omega_0$ due to motion in the x direction the spectral density of fluctuations of the current in the x direction indicates particle-like behavior for $\omega \ll \omega_0$ in which case the classical result obtains. At frequencies of the order of ω_0, the behavior is "wave-like" exhibiting a singularity in the spectral density similar to what would be expected for a photon of frequency ω_0.

A3. Quantized Linear Theory of Gravitation.* F. J. BELINFANTE AND J. C. SWIHART,† *Purdue University.*—In this year's Washington Meeting (Phys. Rev. **95**, 630 (1954), abstracts M2–M3), we have proposed a quantum theory of gravitation. This theory's Lagrangian contains the gradient of the Dirac wave function of the matter field in the interaction terms. We know of no existing general proof of the covariance of the commutation relations and of the existence of an interaction representation for a theory with such a Lagrangian. (We need the interaction representation for formulating an auxiliary condition to be satisfied by the gravitational field.) A direct proof of this covariance and of the integrability of the generalized Schroedinger equation (condition for existence of an interaction representation) is in this case rather involved. Our first attempts had negative results, as orally announced in Washington. More recently, we have found that the theory *is* Lorentz-covariant, and that an interaction representation *does* exist, if we ignore certain paradoxes which are no special features of the present theory but present themselves in every quantum field theory of the conventional type. (Compare Phys. Rev. **76**, 461 (1949), abstract H6, for a similar paradox.)

* For details, see J. C. Swihart, Ph.D. Thesis, Purdue University.
† Supported in part by the National Science Foundation.

A4. Relativistic Energy of Two-Electron Atoms. TA-YOU WU AND G. E. TAUBER, *National Research Council of Canada.*—It is shown that in the existing calculations of the relativistic corrections of the energy of helium-like atoms which are based on a perturbation treatment starting with the nonrelativistic approximation, a correction, also of the order $(v/c)^2$, has been neglected. This additional correction arises from the singular behavior of the relativistic wave functions at the origin and the failure of the usual perturbation method to take proper account of this effect up to the order $(v/c)^2$. A variational method has been suggested which is a modified form of Hylleraas' classic work so as to take account of this singular behavior. Calculations for the ground state of helium have been carried out for a 3-parameter approximation, and a correction of about $+14.5$ cm^{-1} is obtained in addition to the recent result of Sucher and Foley for the same 3-parameter approximation. The "surface integral" term found by Berestetskii and Landau and by Sucher and Foley has also been discussed on the basis of the work of Breit and of Møller.

A5. On the Infrared Divergence. F. ROHRLICH AND J. M. JAUCH, *State University of Iowa.*—The absence of infrared divergences in quantum electrodynamics in physically meaningful cross sections and related expressions is proven rigorously for any process and to all orders in the coupling constant. Two partly complementary methods are available: (a) Using the iteration solution of the S matrix the cancellation between the radiative correction and the emission of one additional soft photon can be shown explicitly to any order. (b) The collective effect of an undetermined number of soft photons can be expressed by a multiplicative factor to the basic process, which contains in closed form *all* radiative corrections. By this method, the results of Bloch and Nordsieck are found correct in a certain approximation. The divergence found by Pauli and Fierz is in contradiction with the general proof of renormalization by Dyson and Salam. This divergence is due to an unjustified extrapolation of the approximation used for the collective soft photon emission. All difficulties caused by the infrared divergences are thereby resolved.

A6. Tabulation of F Coefficients. M. FERENTZ AND N. ROSENZWEIG, *Argonne National Laboratory.*—The combination F of Clebsch-Gordan and Racah coefficients,[1]

$$F_k(LL'J'J) = (-)^{J'-J-1}[(2J+1)(2L+1)(2L'+1)]^{\frac{1}{2}} \times C_{1-1}^{LL'k} W(JJLL'; kJ'),$$

occurs in the angular correlation function for $\gamma-\gamma$, $\alpha-\gamma$,

and $\beta-\gamma$ cascades. We are preparing a table of this F coefficient which will include the following range of the arguments: Integral and half-integral values of J and J' up to 12; all useful combinations of L and L' up to 6; k up to 6. The calculations are performed on Argonne's Electronic Digital Computer (AVIDAC); manual transcription of the results has been eliminated. The table will be published as an Argonne report (ANL-5324). The applicability of the F coefficient and the construction of the table will be discussed.

[1] See L. C. Biedenharn and M. E. Rose, Revs. Modern Phys. **25**, 729 (1954) and also F. Frauenfelder (to be published).

A7. Lamb Shift of the 1S Level of Deuterium. G. HERZBERG, *National Research Council, Canada.*—According to modern quantum electrodynamics, the $1S$ level of hydrogen and deuterium is predicted to lie 0.271 cm^{-1} above the energy given by the Dirac theory. In order to determine this shift experimentally, the absolute wavelength of the L_α line of D was determined by means of a 3-meter vacuum grating spectrograph in fifth order. Lines of the series 6^1S-n^1P and 6^1S-n^3P of Hg^{198} were used as standards. The wavelengths of these standards were obtained by the combination principle from lines in the visible and near ultraviolet regions. Both the lines of mercury and the line of deuterium were observed in absorption. In this way, from five independent plates the wavelength of the L_α line of deuterium has been found to be 1215.3379 ± 0.0004 A. This value refers to an unresolved doublet. Taking account of the relative intensity of the two doublet components (2:1) and the temperature of the absorbing column (80°K), a shift of the 1^3S level of $0.25_7+0.03$ cm^{-1} results. The small deviation from the predicted value is well within the accuracy of the measurements.

A8. Fine Structure of Positronium.* R. WEINSTEIN, M. DEUTSCH, AND S. BROWN, *M.I.T.*—Previous experiments[1] on the Zeeman splitting of the 1^3S state of positronium have been extended, using 3360 mc instead of 3000 mc for the resonant frequency, and using improved methods of magnetic field measurement. The resonant value of the magnetic field was increased by 6 percent, and, within the experimental error, ΔW was found to be independent of magnetic field. Improved methods of magnetic field measurement also resulted in a decrease of the error. The best value of the singlet-triplet splitting of the ground state, calculated to order α^5 from the Zeeman splitting is $\Delta W=(2.0338\pm0.0004)\times10^5$ mc, compared with a theoretical value[2] of 2.0337×10^5 mc. A cavity has been developed to provide circularly polarized microwaves for a more accurate investigation of the degeneracy of the $1^3Sm=\pm1$ states.

[1] Weinstein, Deutsch, and Brown, Phys. Rev. **94**, 758(A) (1954).
[2] R. Karplus and A. Klein, Phys. Rev. **86**, 257 (1952).
* This work was assisted in part by the joint program of the Office of Naval Research and the U. S. Atomic Energy Commission, and in part by the U. S. Signal Corps and the U. S. Air Material Command.

FRIDAY MORNING AT 10:00

Kent 106

(A. S. LANGSDORF, JR., presiding)

Neutrons

B1. Neutron Spectrometer for 100–500 Kev Region. G. J. PERLOW, *Argonne National Laboratory.*—A recoil spectrometer has been constructed consisting of two closely spaced cylindrical proportional counters arranged with axes parallel. The interiors of the counters communicate via a proton collimator equivalent to a set of holes in a plate. A collimated neutron beam impinges on one counter so that forwardly directed recoils from a hydrogenous gas filling may pass through the proton collimator into the second counter. A coincidence between the two counters indicates a useful event, which is measured by the sum of the two pulse heights. The spectrum of pulse heights yields the spectrum of incident neutrons. The gas (methane) pressure is chosen for the energy region of interest, the present unit having 3.7 cm Hg. At a given pressure, the lower energy limit is reached when the collimator thickness becomes a considerable fraction of the recoil range, while the upper energy limit is determined by the total available path length. When the recoil range lies between one and two counter diameters, an asymmetric broadening appears on the low energy side of the resolution function. Pulses contributing to the tail plus pulses from higher energy events are removed by setting suitable acquirements on the ratio of the pulse heights from the two counters. With the collimator used, a trial using neutrons from $Li^7(p,n)$ gave a half-maximum line width of 14 percent at 200 kev.

B2. Neutron Transmission Measurements at the New Argonne Reactor, CP-5. L. M. BOLLINGER, D. A. DAHLBERG, R. E. COTÉ, H. E. JACKSON, AND G. E. THOMAS, *Argonne National Laboratory.*—The Argonne neutron velocity selector, used previously at CP-3′, has been modified and re-installed at the new reactor CP-5. The high flux from CP-5 made it feasible to block all but 2 of the original 6 chopper slits. This change enables us to use a 60-meter flight path. The new detector is a $4\frac{1}{2}$ by $4\frac{1}{2}$ inches boron-loaded liquid scintillator viewed by 4 photomultipliers. It produces a counting rate of about 4 counts per minute per μsec channel width at 1 kev and gives a high enough rate to permit full speed operation for energies above 10 ev. The mean neutron capture time in the counter of 0.4 μsec hardly influences the over-all resolution of the system, which is about 0.08 μsec/meter at full speed. The time analyzer has been made more flexible; its 100 channels may now be divided into two groups which can be independently placed to cover different flight time intervals. The total neutron cross sections of Th^{232} and U^{238} have been the first subject for investigation. All parameters of the 22, 23, and 69-ev resonances in Th^{232} and for those at 6.6, 21, 37, 66, and 102 ev in U^{238} were obtained. New structure was observed above 100 ev.

B3. Total Neutron Cross Sections in the Kev Region: Be, B, C, F, Ti, Ni, and Bi. CARL T. HIBDON AND ALEXANDER LANGSDORF, JR., *Argonne National Laboratory.*—Transmission cross sections as a function of neutron energy have been measured, by the method previously used,[1] For Be (1–55), B (1–160), C (1–160), F (1–160), Ti (1–55), Ni (1–160), and Bi (1–55); the energy range in kev is shown in parentheses. Only F, Ti, Ni, and Bi exhibit resonance structure in this energy region. The three previously known resonances in F now located at 28.2, 49.7, and 99.5 kev are found to be much

narrower and with higher peak cross sections as a result of improved resolution. The prominent features of the curve for titanium are a high peak at 18 kev with an unresolved lesser peak at 23 kev and two previously unknown peaks at 38 and 53 kev. Smaller peaks occur between 3 and 4 kev. The data for Ni are complicated, there being resonance peaks at 4.6, 5.2, 13, 16, 29, 65, 99, 111, 126, 144, and 160 kev. Of these, the ones at 16, 65, 144, and 160 kev are the most prominent. For Bi, the total cross section shows prominent resonances at 2.2, 12, 16, 34, and 47 kev with lesser ones near 4 to 5 kev. The high-energy side of a resonance below one kev was also observed.

[1] Hibdon, Langsdorf, and Holland, Phys. Rev. **85**, 595 (1952).

B4. Slow Neutron Scattering by Liquid Helium. D. G. HURST AND D. G. HENSHAW, *Chalk River Laboratories.*—Measurements of the scattering by liquid helium[1] have been continued with 1.04 A neutrons over the angular range 4.3° to 75° at several temperatures between 1.6°K and 4.2°K. The pattern shows a pronounced peak in the region of 19°. Beyond the peak the scattering falls to about two-thirds of the peak value decreasing with increasing angle with a broad weak maximum in the region of 40°. Details of the pattern vary slightly with temperature but no pronounced changes occur on going through the λ point. Transmission measurements with a gadolinium filter gave a rough indication of the energy losses accompanying scattering. At large angles the energy changes are similar to those for scattering from free helium atoms.

[1] D. G. Henshaw and D. G. Hurst, Phys. Rev. **91**, 1222 (1953).

B5. Inelastic Scattering of Neutrons by Fe, F, Mn and I.* J. J. VAN LOEF AND D. A. LIND, *University of Wisconsin.*—A collimator of a modified Preston and Stelson type has been used to define a beam of neutrons generated by the $Li^7(p,n)$ reaction. Using a neutron beam with an energy spread of 80 kev and disk scatterers of Fe, Teflon, Mn, and I gamma rays resulting from inelastic scattering have been observed with a NaI scintillation spectrometer. The excitation curve for the 850-kev gamma ray from Fe has been determined from threshold to 1.8-Mev neutron energy. The cross section at 1.2 Mev is 0.59 ± 0.06 b. In addition the angular distribution of gamma rays at 1.2 Mev was determined. The excitation curve is in agreement with Kiehn's results.[1] Excitation curves were taken for the 113 and 198 kev lines of F up to 1.8 Mev. In addition a line of 1.37 Mev was observed above a threshold of 1.57 Mev. Only one line at 126 kev was observed from Mn up to 1.2-Mev neutron energy. A preliminary value for the cross section at 1.2 Mev is $\approx 1b$. Radiations of 30, 60, 140, 200, 435, 650, and 725 kev were observed from I. A level scheme based on the excitation curve will be presented.

* Research supported by the U. S. Atomic Energy Commission and the Wisconsin Alumni Research Foundation.
[1] Kiehn and Goodman, Phys. Rev. **95**, 989 (1954).

B6. $\gamma-\gamma$ Coincidences Produced by Inelastic Scattering of 2.5-Mev Neutrons. W. R. FAUST, V. E. SCHERRER, AND B. A. ALLISON,* *Naval Research Laboratory.*—Neutrons from the $D(d,n)He^3$ reaction are used to bombard a small radiator placed inside a 1.0-inch diameter hole drilled through a 5-inch diameter by 3-inch thick NaI(Tl) crystal. Coincidences between the He^3 reaction monitor and crystal pulses gate the multichannel analyzer which records the distribution of spectrometer pulses, and thereby effectively collimates the neutrons in a narrow beam along the crystal axis. Cascade γ rays arising from neutron bombardment of the radiator produce maxima in the pulse-height distribution at their primary energy and at all possible sums of their initial energies.[1] The large crystal thus acts as a coincidence unit with a resolving time approximately equal to the decay time of the phosphor. The spectrometer efficiency for single-, double- and triple-coincidence events at 1 Mev is 40 percent, 20 percent, and 10 percent, respectively. The pulse-height distribution obtained using a Mn radiator with this spectrometer will be discussed.

* Now at University of Pennsylvania, Philadelphia, Pennsylvania.
[1] Wiedenbeck, Phys. Rev. **95** (1954).

B7. Cascade γ Rays from 2.5-Mev Neutron Bombardment of Gold, Iodine, and Chromium. V. E. SCHERRER, W. R. FAUST, AND B. A. ALLISON,* *Naval Research Laboratory.*—A coincidence γ-ray spectrometer with high efficiency for single-, double-, and triple-cascade events has been used to observe pulse-height distributions produced by 2.5-Mev neutron bombardment of gold, iodine, and chromium. The decay scheme for gold as deduced from the coincidence data shows γ rays at 0.98, 1.38, and 1.98 Mev each separately in cascade with a 0.25-Mev γ ray. There is also a 0.54-Mev γ ray not in cascade with the others. These results are consistent with previous data.[1,2] Pulse-height distributions for iodine indicate several cascade γ rays. Cr shows some cascade γ rays and is in agreement with other data.[3]

* Now at University of Pennsylvania, Philadelphia, Pennsylvania.
[1] Wiedenbeck, Phys. Rev. **68**, 1 (1945).
[2] Goldburg and Williamson, Phys. Rev. **95**, 769 (1954).
[3] Peacock and Deutsch, Phys. Rev. **69**, 306 (1946).

B8. Anomalous Absorption of Neutrons in Single Crystals. J. W. KNOWLES, *Chalk River Laboratories.*—Two nearly perfect calcite crystals, two inches thick, were set in the parallel arrangement of a two crystal neutron spectrometer and the gamma rays from neutron capture by the calcium of the second crystal were measured with a NaI scintillation detector. A maximum percentage change in gamma-ray intensity of 2.5 ± 0.6 occurred near the angle of Laue reflection. An application of the dynamical diffraction theory gave a "dispersion curve" variation with angle for the gamma-ray intensity. The theory agreed quantitatively with the experimental observation. In a second experiment concerning a search for anomalous absorption of neutrons incident at the Bragg angle, the transmission of neutrons by a 2-mm thick $3(CdSO_4)\cdot 8H_2O$ crystal was measured and compared with the transmission of x-rays. The incident radiations (1.30 A neutrons and 0.708 A x-rays) were selected by reflection from calcite crystals. When the 2-mm crystal was set near the position of Laue reflection the x-ray transmission increased from 1.5×10^{-4} to 4.5×10^{-4} but the neutron transmission decreased from 3.3×10^{-2} to 2.9×10^{-2}, this decrease being equal to the reflected intensity. Both observations could be explained by the measured mosaic block size of 0.4 mm in the crystal.

B9. Problems in the Analysis of Neutron Resonance Data.* V. L. SAILOR, H. H. LANDON, H. L. FOOTE, JR., AND R. E. WOOD,† *Brookhaven National Laboratory.*—During recent years the need for precise measurements of the Breit-Wigner parameters of slow neutron resonances has steadily increased. Ordinarily the "true" shape of a resonance cannot be directly observed because of the distortion introduced by instrument resolution, Doppler broadening, and the presence of neighboring resonances. Precise corrections for these effects are complicated and require laborious computations. Such computations, however, become practical with the assistance of modern computing machines. Methods for treating certain cases have been developed, programmed, and are in routine use on a type 409.2R Remington-Rand punched-card computer at Brookhaven. The following cases will be discussed: (1) Least squares analysis for cases where instrument resolution, Doppler broadening, and scattering can be neglected (applies generally to resonances lying in region from thermal

to ~0.3 ev); (2) Least squares analysis of the wings of a resonance including the interference between resonant scattering and potential scattering; and, (3) "Shape" analysis of the central region of resonance with corrections for instrument resolution and Doppler broadening. The results obtained from each type of analysis will be illustrated and the limitation of the methods will be discussed.

* Research performed under contract with the U. S. Atomic Energy Commission.
† Doctoral candidate at the University of Utah.

B10. Radiation Width Variations in the Neutron Resonances of Eu and In.* H. H. LANDON AND V. L. SAILOR, *Brookhaven National Laboratory.*—The parameters of the lowest energy resonances in europium and indium have been determined from total cross-section measurements using the BNL crystal spectrometer. The data have been analysed for variations of the radiation width parameter from resonance to resonance. The preliminary results are indicated in the table.

Target isotope	Resonance energy ev	Γ_γ ev
Eu^{151}	0.327	0.070
	0.461	0.093
	1.056	0.094
In^{115}	1.456	0.072
	3.85	0.087

The method of analysis used to make account of Doppler effect in the observed cross section will be presented. The limits of error of the above results will be discussed, but preliminary estimates indicate that the radiation width in the first resonance in Eu is definitely smaller than the second and third which appear most likely to be the same. The widths of the two levels in In are also significantly different. The remaining one-level parameters for each resonance will be presented.

* Research performed under contract with the U. S. Atomic Energy Commission.

FRIDAY MORNING AT 10:00

Eckhart 133

(C. P. SLICHTER presiding)

Magnetism; Magnetic Resonance

C1. A Classical Theory of the Temperature Dependence of Magnetic Crystalline Energy. CLARENCE ZENER, *Westinghouse Research Laboratories.*—An analysis has been made of the consequences of certain assumptions regarding the magnetic crystalline energy. These assumptions are: (i) the crystalline energy of a single atomic spin is a function only of its direction cosines, (ii) the only effect of temperature is to introduce deviations in these localized directions from the macroscopic magnetization direction, (iii) these deviations are the resultant of a very large number of small independent deviations, thereby giving rise to a random walk distribution function. The analysis then consists simply of taking an average of the crystalline energy using the appropriate random walk function. Upon expressing this energy as a sum of surface harmonics of the direction cosines, the coefficient E_n of the nth harmonic is found to vary as the saturation magnetization raised to the power of $n(n+1)/2$. The first harmonic satisfying cubic symmetry, beyond the zeroth order, is of fourth order, leading to the exponent of 10, in precise agreement with the observed data for K_1 of iron. An exponent of 21 is predicted for K_2 of iron. Disagreement with the data for Ni indicates the invalidity of our assumptions for this metal.

C2. Magnetic Coercive Force in Alloys of Iron and Nitrogen. J. KERR AND C. WERT, *University of Illinois.*—The increase in magnetic coercive of iron caused by the addition of two of the nitrides of iron has been measured. By appropriate heat treatment platelets of the compounds $Fe_{16}N_2$ and Fe_4N in different degrees of dispersion have been precipitated from solid solution. The course of the formation of the nitrides was followed using well known internal friction techniques. The coercive force was also measured at invervals during the nitride formation; hence it was possible to determine how the coercive force varied with the amount of precipitate which had been formed up to a given time. Electron microscope studies of the material were made to show particle shapes and sizes. The chief finding of the investigation is that the fineness of dispersion of the precipitate is of great importance in determining the coercive force increase. At least one critical particle size exists, this occurs when the largest dimension of the platelets is about 1500 A°. For platelets of this size the coercive force is a maximum. This critical dimension is about the same as the critical size found for precipitates of carbide in iron.

C3. Relation of Magnetic Structure to Electrical Conductivity in NiO and Related Compounds. R. R. HEIKES, *Westinghouse Research Laboratories.*—A qualitative theory, based on an atomic model, is presented in an effort to understand the electrical properties of NiO. Its insulating nature is shown to arise from the action of the Pauli exclusion principle. If one generalizes this theory to include all stoichiometric binary compounds, having a transition element as cation and an element from group V or VI as anion, a rather startling correlation between the magnetic and electric properties is predicted. Ferromagnetic compounds should be good conductors with a positive temperature coefficient of resistivity while antiferromagnets should be insulators with a negative temperature coefficient of resistivity. The available data indicate that this correlation does exist.

C4. Magnetic Domain Patterns Observed by the Kerr Effect in BiMn Alloy. B. W. ROBERTS AND C. P. BEAN.—The high resistivity[1] of ferromagnetic BiMn alloy allows deep penetration of light into the alloy surface which, combined with the high magnetocrystalline anisotropy, gives rise to a large magneto-optic Kerr rotation. Magnetic domain patterns are easily observed in reflection as alternate light and dark bands through nearly-crossed Nicol prisms or through the polarizing arrangement of a Bausch and Lomb metallograph. Several domain pattern types have been observed. A repetitious zig-zag or "rick-rack" pattern is usually found when the incident polarized light is nearly parallel to the C_0 axis which is also the direction of moment orientation at room temperature. In other crystallites, domain patterns are irregular and similar to those found on cobalt.[2] When light strikes a crystallite perpendicular to the C_0 axis, a system of parallel domains is observed. These propagate across grain boundaries. A

few spiral domain configurations have been observed which are not related to surface structure.

[1] K. Kondo, J. Phys. Soc. Japan **5**, 307 (1950).
[2] Williams, Foster, and Wood, Phys. Rev. **82**, 119 (1951).

C5. Antiferromagnetism of Ytterbium Sesquioxide at Liquid Helium Temperatures. WARREN E. HENRY, *United States Naval Research Laboratory.*—The study of exchange interaction between rare earth ions as related to overlap of wave functions for unpaired $4f$ electrons is of interest. The superposition of magnetic moment isotherms[1] in the liquid helium range for Ce^{+++} (in cerium nitrate hexahydrate), which has one unpaired f electron, shows smallness of exchange and negligible overlap of wave functions. The problem of studying exchange at small interionic distances, arising from the instability of Ce_2O_3, is partly solved by taking advantage of the small variation of lattice parameters among the rare earth oxides and using ytterbium sesquioxide (obtained from Professor F. H. Spedding) in which the Yb^{+++} has one unpaired hole (13 electrons in an f shell of capacity 14). Magnetization studies were carried out ballistically at 10 temperatures in the range, 1.3° to 4.2°K and in magnetic fields up to 58 000 gauss. $M(H/T)$ curves disclosed (1) nonsuperposition of magnetic moment isotherms indicating interaction and (2) positive curvature for sections of the lower temperature isotherms, indicating a possible transition. When M is plotted against temperature for fixed magnetic fields, maxima in the magnetic moment curves appeared, showing antiferromagnetism. The Néel (antiferromagnetic transition) temperature is about 2.5°K in small fields and is reduced to about 1.5°K at 30 000 gauss. At 1.5°K, 35 000 gauss suppressed the antiferromagnetism, which means that the molecular field is of the order of 35 000 gauss.

[1] W. E. Henry, Phys. Rev. **95**, 603A (1954).

C6. Relaxation Time Modification by Double Nuclear Resonance. B. HERZOG AND E. L. HAHN, *IBM Watson Laboratory and Columbia University.*—The continuous nuclear resonance of nucleus A which is coupled to a different nucleus B, whose resonance is being observed, should modify the spin-spin relaxation time T_2 of B. Since the lifetime T_2' of the B spin echo envelope depends on random fluctuations of the local field, forced reorientation of A nuclei should affect this contribution to T_2 strongly. The resonance of A ought to affect the static local field broadening, and high rate of A flipping should average it to a smaller value. Experimentally, very low and even zero field *cw* proton resonance in paradichlorobenzene increases T_2' of Cl^{35} quadrupole echoes[1] (~34 mc) e.g., from its natural value of 1.1 ms to 5.9 ms, and produces a narrowing of the Cl^{35} static line width. The *cw* pure quadrupole resonance of Na (~400 kc)[2] in $NaClO_3$ and $NaBrO_3$ modifies T_2' for Cl^{35} (~30 mc) and Br^{81} (~150 mc) quadrupole echoes. For sufficiently large dipole-dipole Zeeman decoupling[1] of Na, T_2' passes through a minimum when the Na reorientation rate becomes comparable to the local dipolar field frequency spread of the halogen line width. Faster reorientation increases T_2' beyond its value without Na resonance. Utilizing these effects upon the halogen echo, the Zeeman splitting of the Na quadrupole interaction was measured.

[1] Bloom, Norberg, Hahn, and Herzog, Phys. Rev. **93**, 638, 639 (1954).
[2] Itoh and Kusaka, J. Phys. Soc. Japan **9**, 434 (1954).

C7. Strong Crystal Field Theory of Magnetic Resonance for d^3 Configurations. C. M. HERZFELD, *U. S. Naval Research Laboratory.*—The conventional theory of paramagnetic resonance of some ionic Cr^{+3} compounds assumes a crystal field splitting of the F state of Cr^{+3}, small compared to the separation of the free ion terms ^4F and ^4P. The splitting estimated from this theory using experimental values of g is larger than the ^4F, ^4P separation for the Cr alums and a Cr^{+3} fluoride. This paper presents calculations assuming that the crystal field breaks down Russell-Saunders coupling. Three d electrons are oriented separately in the crystal field and then coupled by electrostatic repulsion. The ground state, $^4\Gamma_2$, interacts strongly only with $^4\Gamma_5$. Angular wave functions for these levels are calculated, using a novel method based on the isomorphism of the cubic crystal rotation group with the symmetric permutation group S_4, from the idempotent generators of the irreducible representations of S_4. With these wave functions the spin-orbit coupling and external magnetic field perturbations are calculated and an equation for the effective g derived. This equation, with experimental values of g, gives crystal field splittings greater than the separation of ^4F and ^4P for the Cr alums and fluoride, and for some Mo fluorides.

C8. Nuclear Spin Relaxation in Alkali Metals Near Their Melting Points. R. E. NORBERG, *Washington University and* D. F. HOLCOMB, *Cornell University.**—Spin echo measurements of the relaxation times T_1 and T_2 previously reported[1] for metallic Li^7 and Na^{23} have been repeated (for Larmor frequencies ν_0 between 3 and 15 mc/sec), using the method of Carr and Purcell[2] to obtain T_2. In agreement with the previous results, T_2 in both metals is found to decrease suddenly upon melting. No corresponding reduction of T_1 is observed. Use of the Carr-Purcell technique excludes diffusion through magnetic field inhomogeneities as the source of the reduced T_2's found in the liquids. To test the possible quadrupolar nature[1] of the high temperature interactions, T_1 and T_2 have been measured for the Li^6 and Li^7 resonances in a metallic sample enriched to 94 percent Li^6. T_2 for both resonances decreases suddenly at the melting point. In the liquid $T_2(Li^6)/T_2(Li^7) \leqslant 3$, if the comparison is made at constant ν_0. This small ratio excludes quadrupolar interactions. In the liquid, T_2 for both Li^6 and Li^7 decreases as ν_0 is increased. Since the correlation frequency for the self diffusive motion in liquid lithium and sodium is much greater than ν_0, and yet $T_1 > T_2$ there, the short high temperature T_2's apprently arise either from an interaction unaffected by diffusion or from magnetic local z fields with no components effective for spin lattice relaxation.

* This work carried out at the University of Illinois.
[1] D. F. Holcomb and R. E. Norberg, Phys. Rev. **93**, 919(A) (1954).
[2] H. Y. Carr and E. M. Purcell, Phys. Rev. **94**, 630 (1954).

C9. Calculation of the g-Factor of Metallic Lithium.* P. N. ARGYRES† AND A. H. KAHN,‡ *University of California, Berkeley.*—We have performed the calculation of the g-factor of metallic lithium by means of the method of Y. Yafet.[1] This is an extension of Bardeen's method[2] enabling one to include spin-orbit interaction in the calculation of electronic wave functions in alkali metals. Seitz's empirical potential for the lithium atom[3] was used to represent the potential within the W.-S. sphere. The result obtained for the shift from the free electron g is $\delta g = -3.0 \times 10^{-5} \sin^2\theta_0$, where θ_0 is the angle between the electronic wave vector and the magnetic field. A perturbation calculation based on plane waves gives a result an order of magnitude smaller than that of the above method. Experimental measurements of the g-factor of metallic lithium have been performed by Feher.[4] He finds $\delta g < 10^{-4}$; the shift is too small to be measured at present.

* This research has been assisted in part by the Office of Naval Research and the U. S. Signal Corps.
† Now at Westinghouse Research Laboratories.
‡ Now at Department of Physics, University of Illinois.
[1] Y. Yafet, Phys. Rev. **85**, 478 (1952).
[2] J. Bardeen, J. Chem. Phys. **6**, 367 (1938).
[3] F. Seitz, Phys. Rev. **47**, 400 (1935). We are indebted to Professor J. Bardeen for providing the correct potential used by Professor Seitz.
[4] G. Feher, Phys. Rev. (to be published).

FRIDAY MORNING AT 10:00

Mandel Hall

(W. H. ZINN presiding)

Invited Papers

D1. The Use of Glaser Bubble Chambers in Photographing Nuclear Events. R. H. HILDEBRAND, *University of Chicago.* (30 min.)

D2. Nuclear Alignment in Liquid Helium 3. B. WEINSTOCK, *Argonne National Laboratory.* (30 min.)

D3. Nuclear Properties of Elements 98, 99, 100. W. H. STUDIER, *Argonne National Laboratory* (30 min.)

FRIDAY MORNING AT 10:00

Oriental 104

(RALPH BRAY presiding)

Semiconductors, I

E1. Oscillatory Hall Effect, Magnetoresistance, and Magnetic Susceptibility of a Graphite Single Crystal. TED G. BERLINCOURT AND M. C. STEELE, *United States Naval Research Laboratory.*—Oscillatory dependences upon magnetic field at low temperatures have previously been observed in the magnetic susceptibility (de Haas-van Alphen effect) of a graphite single crystal by Shoenberg[1] and in the magnetoresistance by Berlincourt and Logan.[2] We have observed oscillations in the Hall coefficient as well and have also measured the magnetoresistance and magnetic susceptibility of the same graphite crystal at liquid helium temperatures in magnetic fields up to 25 kilogauss. In all cases the oscillations are periodic in reciprocal field and exhibit the same period $\beta/E_0=2.15\times10^{-8}$ gauss^{-1} for the magnetic field parallel to the hexagonal axis. The phases, however, are different in that magnetoresistance minima lag minima in diamagnetism by approximately $\pi/2$ in reciprocal field, while Hall coefficient minima lag minima in diamagnetism by roughly $\pi/4$.

[1] D. Shoenberg, Trans. Roy. Soc. (London) **A245** (1952).
[2] Ted G. Berlincourt and John K. Logan, Phys. Rev. **93**, 348 (1954).

E2. Donor Impurities in Graphite. G. HENNIG AND M. DZURUS, *Argonne National Laboratory.*—In graphite, the nearly empty conduction and nearly full valence bands barely touch or possibly overlap very slightly; therefore graphite is intermediate in properties between metals and semiconductors. The electrical properties of graphite, like those of real semiconductors, are sensitive to the presence of those impurities which charge the electron population of the band structure. The impurities can be introduced at lattice imperfections in clusters of about three to five, but only one in such a cluster will ionize. They can also be introduced in two-dimensional layers between the graphite layer planes (so-called lamellar compounds), but even then only about one in four will ionize. The ionized fraction is very nearly temperature-independent. Because of the fractional ionization, acceptors and donors can be studied quantitatively only if they can be introduced electrolytically. Such a study has been described earlier by us for acceptors.[1] Donors can be introduced electrolytically in liquid ammonia. The effect of these added donors on the Hall coefficient, resistance, and magnetoresistance will be described. The results seem to confirm the calculations of Carter and Krumhansel,[2] which predict that the valence and conduction bands are not symmetrical at the zone boundaries.

[1] G. Hennig, J. Chem. Phys. **19**, 922–29 (1951).
[2] J. L. Carter and J. A. Krumhansel, J. Chem. Phys. **21**, 2238 (1953).

E3. Electronic Relaxation Time in Graphite. JOHN E. ROBINSON, *Argonne National Laboratory.*—The major contributions to the electronic transport properties of graphite come from electrons whose kinetic energy to the first approximation is not a quadratic function of wave number but is more nearly proportional to the modulus of the wave number vector as measured from the edge of the first Brillouin zone. As a pilot investigation, the elastic, incoherent scattering by a Coulomb field of electrons in a two-dimensional graphite layer is discussed. The kinetic energy relative to the band edge is proportional to $|\mathbf{k}|$, where $\mathbf{k}$ is measured from a zone corner. The condition for the validity of treating the scattering in terms of orbital concepts is independent of electronic energy. The relaxation time appropriate to current decay is found to be independent of electronic energy.

E4. Electrical and Optical Properties of GaSb Films. R. J. COLLINS, F. W. REYNOLDS AND G. R. STILWELL, *Bell Telephone Laboratories.*—Films of gallium antimonide were prepared by evaporation of the compound from shallow tungsten heaters. The deposition was carried out at pressures below 10^{-5} mm of Hg onto a warm (100°C) glass substrate and completed in 3–5 sec. Before the films were removed from the vacuum they were annealed for four hours at 450°C. Electron diffraction studies showed only the structure of the compound. The films were shown to be continuous and to have crystallite size of 600–1000 A with the electron microscope. All films prepared to date were p type with room temperature resistivities and Hall coefficients of 0.05–0.5 ohm cm and electron mobilities of ~50 cm^2/volt sec, respectively. The transmittance and reflectance were determined from 0.5 to 3.0 microns. With the film at room temperature, using chopped radiation, photoconductivity was observed for wavelengths shorter than 1.8 microns. The half-response point corresponded to an energy of 0.75 ev. When cooled to 77°K the response increases and shifts to shorter wavelengths, from which a temperature dependence of the energy gap can be calculated to be $\sim3\times10^{-4}$ ev/°C.

E5. Usually Large Magnetoresistive Effects in InSb for Specialized Boundary Conditions.* R. K. WILLARDSON, T. C. HARMAN, P. F. CHOQUARD, AND A. C. BEER, *Battelle Memorial Institute.*—In the usual determination of transverse galvanomagnetic effects, the boundary condition $j_y=0$ is applied. If less restrictive transverse boundary conditions are realized, interesting phenomena are observed in high-mobility semi-

conductors. One example is the behavior of the Hall-effect gyrator.[1] Another is the greatly augmented magnetoresistive effects discussed by Weiss and Welker,[2] particularly those resulting from the geometry of the Corbino disk. For large values of μH, simplified analysis gives $\Delta\rho/\rho_0 \cong (9\pi/32)\mu_0^2 H^2$. This would predict values for $\Delta\rho/\rho_0$ of greater than 300 at 80°K and 10 000 gauss for the hyperpure specimens of InSb in which electron mobilities of over 200 000 cm²/sec-volt were measured. However, for such large magnitudes of μH, electron orbit quantization effects should probably be taken into account[3] in the formulation of the Boltzmann equation. Calculations are compared with experimental data as a function of magnetic field at several temperatures.

* Supported in part by Wright Air Development Center.
[1] R. F. Wick, J. Appl. Phys. 25, 741 (1954).
[2] H. Weiss and H. Welker, Z. Physik 138, 322 (1954).
[3] A. H. Wilson, *The Theory of Metals* (Cambridge University Press, Cambridge, 1953), p. 210.

E6. The Crystal Structure of Indium Bismuthide. W. P. BINNIE, *Purdue University.**—Indium bismuthide prepared by L. M. Roth by fusing in a melt equal atomic proportions of each element. From single-crystal analysis the structure is shown to be the B-10 type,[1] the most well-known example of which is PbO. The tetragonal unit cell has dimensions $a=b=4.999$ A and $c=4.773$ A and contains two molecules of InBi. Extinctions are consistent with the space group $P4/nmm$. The In atoms are located at (0,0,0) and $(\frac{1}{2},\frac{1}{2},0)$ and the Bi atoms at $(0,\frac{1}{2},Z)$ and $(\frac{1}{2},0,\bar{Z})$ with $Z=\sim 0.39$, so that each In atom is surrounded tetrahedrally by four Bi atoms and each Bi atom is bonded to four In atoms which form a square on one side of it.

* Work supported by Signal Corps contract.
[1] Struktur Bericht 1, 89 (1913–1928).

E7. Semiconducting Properties of Iron Oxide Thermistor Material.* J. J. BROPHY, N. ROSTOKER, AND L. V. AZAROFF, *Armour Research Foundation.*—The semiconducting properties of iron oxide thermistor material containing 10 percent each of copper and titanium ions as impurities have been examined. This material, prepared by sintering the oxide powders, is found to have the crystal structure of alpha Fe_2O_3, indicating simple substitution of copper and titanium for iron ions in the lattice. The resistivity is a logarithmatic function of temperature having an activation energy of 0.52 electron volt. Hall effect and Seebeck effect studies of the semiconductor show that this variation is due to thermal activation of carriers to conduction levels. The carriers are found to be electrons with mobility of about 1.0 cm²/volt second. Concurrent with the origin of electrical conduction is ferromagnetic behavior, and a saturation magnetic moment of 2.0 emu/g at room temperature is observed above magnetic saturation at about 5000 oersteds. A discrepancy between donor concentration determined from extrapolated carrier density measurements and the known concentration of impurity atoms appears to indicate a type of cancellation between the effect of copper and titanium atoms.

* Work supported by Bureau of Ordnance, Department of the Navy.

Post-Deadline Papers, if Any

FRIDAY AFTERNOON AT 2:00

Oriental 104

(WALTER KOHN presiding)

Semiconductors, II

G1. Pressure Dependence of Absorption Edge in Germanium and Silicon. W. SPITZER, C. O. BENNETT, AND H. Y. FAN, *Purdue University.**—The effect of pressure on the edge of fundamental absorption in the near infrared was investigated for germanium and silicon up to 1000 kg/cm². The samples were placed in a chamber with windows and with dry nitrogen under pressure. For germanium, the edge (up to an absorption coefficient of 100 cm⁻¹) showed a parallel shift to higher energies under pressure, amounting to $(8.2\pm1)\times10^{-6}$ ev kg⁻¹ cm². The absorption edge in silicon showed similar behavior with a shift of about 5×10^{-6} ev kg⁻¹ cm²; this result is less accurate than for germanium. The value for germanium is comparable to but somewhat larger than the pressure coefficient of energy gap, about 5.5×10^{-6} ev kg⁻¹ cm², deduced from the variation of intrinsic resistivity.[1] Such results are not available for silicon. Shifts of the absorption edge with temperature for silicon and germanium have been measured by M. Becker[2] and others in this laboratory: -5×10^{-4} ev/°K for germanium and -4.5×10^{-4} ev/°K for silicon. According to the observed pressure shifts, the effect of lattice dilation accounts only for a small fraction of the temperature shift.[2]

* Work supported by a Signal Corps contract.
[1] See W. Paul and H. Brooks, Phys. Rev. 94, 1128 (1954), and references given there.
[2] H. Y. Fan, Phys. Rev. 82, 900 (1951).

G2. Single-Crystal Layers of Germanium Semiconductors. W. M. BECKER AND K. LARK-HOROVITZ, *Purdue University.**—Using grinding and etching techniques, germanium layers a few microns thick have been prepared from single crystals. X-ray diffraction indicates that these layers are single crystals. Whereas germanium films deposited from the vapor are always p type with abnormally small mobilities (1–150 cm²/volt sec), these single-crystal layers, like the bulk material they are made from, are n type or p type with mobilities comparable to bulk material of the same resistivity. These films having been mounted in a high vacuum opposite a polonium source, conductivity and Hall effect are measured as a function of alpha particle irradiation. Both n-type and p-type material varying in resistivity from 0.01 ohm-cm to 30 ohn-cm have been investigated. The efficiency of carrier removal depends on the position of the Fermi potential at the start, being highest for the lowest resistivity material. Both hole and electron traps are introduced by irradiation as indicated by the initial resistivity increase of both n-type and high-resistivity p-type samples. The efficiency for electron removal is far greater than for hole removal.

* Supported by a Signal Corps contract.

G3. Low-Temperature Electrical Conductivity of Germanium. S. H. KOENIG AND G. R. GUNTHER-MOHR, *IBM Watson Laboratory.*—The variation of current with applied voltage in germanium crystals at liquid helium temperatures has been measured. The variation is ohmic at very low voltages, then has a region in which the logarithm of the current is linear in voltage, followed in turn by a negative resistance region in which the current increases orders of magnitude for

very small changes in voltage. The dependence on temperature, the importance of surface treatment, nature of contacts, and geometry will be discussed. The conduction thus resembles that of gas discharges at low pressure except that the current density depends only on the applied field for sample thicknesses from 10^{-2} to 1 cm. Previous observations[1] have been interpreted as due to carrier multiplication by collision ionization of impurity centers. Preliminary measurements of both "ionization" and "deionization" time show them to be less than 5×10^{-7} sec. The initial investigations were undertaken by Dr. P. J. Price and Dr. G. L. Tucker of this laboratory.

[1] E. M. Conwell, Phys. Rev. **94**, 1068 (1954); Dresselhaus, Kip, and Kittel, Phys. Rev. **92**, 827 (1953); Sclar, Burstein, Turner, and Davisson, Phys. Rev. **91**, 215 (1953).

G4. The Segregation Coefficient of As in Germanium as a Function of Crystal Growth Variables.* D. C. JILLSON AND A. C. SHECKLER, *General Electric Electronics Laboratory.*—The segregation coefficient of arsenic during the growth of single crystals of germanium has been studied as a function of the orientation, the growth rate, and the temperature gradient across the liquid-solid interface. For a given low temperature gradient, values of the segregation coefficient for ⟨111⟩ and ⟨112⟩ orientations differ at all growth rates studied (down to ½ inch per hour) and are converging on a zero rate value of about 0.02. This is contrary to previously published data presumably taken at higher temperature gradients. At higher rates of growth, a log-log plot of carrier concentration *vs* weight fraction not pulled departs from linearity, indicating that the segregation coefficient is not constant. Reasons considered for this departure from theoretical assumptions are inadequate stirring, appreciable solid-state diffusion, gain or loss of impurity, segregation of a second impurity, and crystalline imperfection.

* This work was supported by Air Force Contract.

G5. Minority Carrier Lifetime as a Function of Crystal Growth Variables.* A. C. SHECKLER AND D. C. JILLSON, *General Electric Electronics Laboratory.*—Lifetime of minority carriers in *N*-type germanium has been studied as a function of the crystal growth rate and of the temperature gradient in the region of the liquid-solid interface during growth. For a given low temperature gradient the recombination center density increased for a high rate of growth and remained constant or decreased for lower growth rates. Available data indicate the same effect with a steeper gradient, but at different growth rates. Simple segregation of an impurity atom cannot account for the observed variation in recombination center density.

* This work was supported by Air Force Contract.

G6. Minority Carrier Extraction in Germanium. RALPH BRAY, *Purdue University.**—Application of an electric sweep field to high-resistivity Ge samples with low resistance end contacts produces a decrease or increase in sample resistance, corresponding to propagation by drift of an excess (injection) or deficiency (extraction) in concentration of minority carriers along the sample from the forward biased contact. Which effect is observed should depend on whether the equilibrium concentration of minority carriers at the contact is greater or less than in the interior. This is determined by the method of making the contact. With increasing field in extraction, and for transit times$\ll$lifetime, the increase in resistance saturates at a value corresponding to less than total minority carrier extraction. For a 25 ohm-cm *p*-type sample, extraction shifts the peak in resistivity *vs* temperature from 297° to 327°K. Increases in resistance $\leq$factor of 3 were observed in the near-intrinsic range. Measurements of lifetime on the same sample, whether from observation of transient recovery after extraction or after injection, are in good agreement, as would be expected for recovery after extraction by thermal generation. Extraction may be applied for modulation of diodes and transistors and extension of temperature and power range of their operation.

* Work supported by Signal Corps Contract.

G7. (Abstract withdrawn.)

G8. The Hall Coefficient in Anisotropic Media.* E. G. GRIMSAL,† *Louisiana State University.*—An expression has been obtained for the Hall coefficient in the case of the anisotropic two-band model. The derivation is classical, except inasmuch as the interaction of the electrons with the lattice is included by the use of effective masses. The absence of integrals over the Fermi surface permits the retention of the anisotropy of the effective masses. When the anisotropy is neglected, the expression obtained in the case of vanishing magnetic field reduces to the expression usually given for the Hall coefficient for small fields.

* Supported in part by the National Research Council.
† Now at Canisius College.

G9. A Physical Model of Semiconductors. J. G. BARREDO,* *Instituto Rocasolano, Consejo Superior Investigaciones, Madrid.*—A physical model of semiconductors described by the equation $I=zFK\Sigma^{\alpha}(4qzd/m)^{\frac{1}{2}}N^{\alpha}t^{-\frac{1}{2}}+V/R$ is given (I=current; z and q=charge of the dipole and carrier, respectively; d=half of the length of the dipole; m=mass; t=time; α=order of the reaction; K=constant; F=faraday).[1] It was verified experimentally, with oscillographic precision, for germanium diodes and diffusion junction rectifiers between liquid nitrogen temperature and 300°C. It describes how current can be increased by increasing the number of dipoles Σ or carriers N by nuclear bombardment or other means.

* c/o Jones Laboratories, University of Chicago, Chicago, Illinois.
[1] Preliminary work, J. G. Barredo, Phys. Rev. **83**, 243 (1951); J. Chem. Phys. **19**, 1065 (1951).

G10. Theory of the Magnetic Rectifier.* KURT LEHOVEC, ALMA MARCUS, AND KURT SCHOENI, *Sprague Electric Company.*—A theoretical investigation was made of the rectifying properties of a slab of intrinsic semiconducting material placed in crossed electric and magnetic fields, when opposite sides are treated to give widely different surface recombination velocities. Surface and volume recombination rates were assumed to be linear functions of the deviation from equilibrium carrier densities. It was concluded that saturation values are reached in the case of forward as well as reverse currents at large electric fields. The ratio of the saturation currents equals the ratio of the surface recombination velocities. Both saturation values are inversely proportional to the magnetic field in-

tensity. The derivation of surface and volume recombination constants from measurements of the current voltage characteristic will be discussed.

* Work carried out in part under contract with the U. S. Army Signal Corps.

G11. Verification of the Bridgman Relation for a Mixed Semiconductor. G. M. SEIDEL AND V. A. JOHNSON, *Purdue University.*—It has been shown that the Lorentz solution of the Boltzmann equation for a semiconductor containing both electrons and holes leads to a set of current density equations whose coefficients satisfy the Onsager relation; and consequently the Bridgman relationship $T\eta_i=\kappa_i P$ holds, where T, η_i, κ_i, P are, respectively, the temperature, isothermal Nernst coefficient, isothermal thermal conductivity, and Ettingshausen coefficient. With the assumed independence of electrons and holes, the current density equations are put into the form used by Callen;[1] the current densities used are the electric current density and the heat current density defined by $Q=TS$ where S is entropy current density. The various coefficients need not be evaluated to show that the Onsager relations hold, but can be left in the integral form as functions of energy, mean free path, and Fermi-Dirac distribution function. Once it is verified that the coefficients of the current density equations do satisfy the Onsager relation, the Bridgman relation follows automatically.

[1] H. B. Callen, Phys. Rev. **73**, 1349 (1948).

G12. Generalized Deformation Potential Theory for *n*-Type Ge.† WILLIAM P. DUMKE, *University of Chicago and Chicago Midway Laboratories.* Introduced by E. N. Adams, II. —The deformation potential theory has been re-examined taking into account the ellipsoidal shape of the surfaces of constant energy in reciprocal lattice space, and the effect of shear-wave scattering in *n*-type Ge. We find that if scattering by compressional waves is the dominant scattering process, a simple relaxation time exists proportional to $E^{-\frac{1}{2}}$, just as for spherical energy surfaces. However, the scattering due to shear waves is strongly anisotropic and cannot be described by a simple relaxation time. We have been able to show that when shear wave scattering is taken into account, the distribution function for electrical conduction takes the usual form $f_1=-e\mathbf{E}\cdot\langle\bar{\tau}\rangle\ddagger\cdot\nabla_p f_0$, except that the relaxation time is a second rank tensor with components that depend on direction. Preliminary calculations indicate that shear-wave scattering is the dominant scattering mechanism for *n*-type Ge.

† This research was supported in part by the United States Air Force.
‡ This notation is used in place of the authors' tau with a double bar, which the printer does not have.

FRIDAY AFTERNOON AT 2:00

Kent 106

(R. M. STEFFEN presiding)

Radioactive Nuclei; Positrons

H1. Gamma Rays from Proton Bombardment of Li^6.† S. BASHKIN AND R. R. CARLSON, *State University of Iowa.*—A NaI scintillation spectrometer, limited to 1.5 Mev gamma rays, detected 0.43 ± 0.02 Mev radiation when Li^6 was bombarded with protons of energy 180 kev to 415 kev. Spectrometer efficiency was measured using beta-gamma coincidences and a Au^{198} source. The thick target yield was $(7\pm4)\times10^{-13}$ gammas per proton at 180 kev and $(170\pm35)\times10^{-13}$ at 415 kev. This gamma ray was interpreted as part of the cascade decay[1] of the broad, third excited state of Be^7 at about 6.4 Mev, since the spectrometer, when unlimited, detected gamma rays corresponding to transitions to the ground and 0.43 Mev state in Be^7. The ratio of the partial radiation width for the latter transition to the total radiation width was >0.01 by comparison of the intensity of 0.48 Mev radiation from Li^{7*} produced after a lengthy bombardment at 365 kev (none) with the amount of 0.43 Mev radiation produced during the bombardment. This limit, together with the known properties of the ground and first excited states of Be^7, requires the transitions to these states from the capture state to be of the same multipole type and order and the spin of the capture state to be $\frac{1}{2}$ or $\frac{3}{2}$.

† Supported in part by U. S. Atomic Energy Commission.
[1] Erdman, Warren, James, and Alexander, Bull. Am. Phys. Soc. 29, No. 6, 23(A) (1954).

H2. Electron-Neutrino Angular Correlation in the Beta Decay of Neon-19. D. R. MAXSON, J. S. ALLEN, AND W. K. JENTSCHKE, *University of Illinois.*—The electron-neutrino angular correlation in the beta decay of Ne^{19} has been measured by observing the energy spectrum of F^{19} recoil ions. The constant λ in the angular correlation function $(1+\lambda v_e/c\cos\theta_{e\nu})$ was found to be $\lambda=-0.21\pm0.08$, indicating that the beta-decay interaction is of the form *STP* and not *VTP*. The observed angular correlation leads to the result $C_S^2|\int 1|^2/C_T^2|\int\boldsymbol{\sigma}|^2=0.69\pm0.17$, which is consistent with $C_S^2\simeq C_T^2$ if the nuclear configuration is $(d_{5/2})_{\frac{1}{2}}^3$, but not if the configuration is $(s_{\frac{1}{2}})_{\frac{1}{2}}^3$. Most of the F^{19} recoils carried one unit of negative charge, but singly charged positive ions were also detected. The coincidence rate due to positive ions was about 10 percent of that due to negative ions. No doubly charged recoils were observed.

H3. Decay of $_{22}Ti^{51}$ (5.8 min). S. B. BURSON, W. C. JORDAN, AND J. M. LEBLANC, *Argonne National Laboratory.*—The radiations from Ti^{51} have been studied with a scintillation coincidence spectrometer. Gamma rays of 0.32, 0.61, and 0.92 Mev are resolved. Their intensities are estimated to be in the ratio 100:1:5, respectively. The 0.32 and 0.61-Mev gamma rays are in coincidence. Two beta-ray components are resolved; one of approximately 2.4 Mev is in coincidence with the 0.32-Mev gamma ray, and one of 1.8 Mev is in coincidence with the 0.92-Mev radiation. No indication of a beta transition to the ground state of V^{51} is observed. The total disintegration energy is concluded to be 2.7 ± 0.2 Mev. This value is consistent with energy systematics of odd mass beta-ray emitters.

H4. Anisotropic Gamma Radiation from Aligned Nd^{147} Nuclei.* E. AMBLER AND R. P. HUDSON, *National Bureau of Standards,* AND G. M. TEMMER, *Department of Terrestrial Magnetism, Carnegie Institution of Washington.*—We have aligned Nd^{147} nuclei using the same low-temperature method as that already reported for Ce^{141} nuclei.[1] Alignment again occurs in a plane perpendicular to the axis of symmetry

(z axis) in the paramagnetic salt used to cool the nuclei. Separate observations were made on the angular distributions of the 530-kev and 92-kev gamma radiations. For the 530-kev gamma ray, an anisotropy $\epsilon = -0.29$ was observed at the lowest temperature reached ($\simeq 0.003$°K). Assuming spin $9/2^-$ for Nd^{147} we conclude that the gamma transition is $E2$, and that the spins involved in the decay chain are $9/2^- \rightarrow 9/2^+ \rightarrow 5/2^+$. No significant anisotropy was observed for the 92-kev gamma ray and it is concluded that this transition is a mixture of $M1$ and $E2$ radiation. The spins involved in the decay chain are $9/2^- \rightarrow 7/2^+ \rightarrow 5/2^+$. From the temperature dependence of the anisotropy we deduce a value 0.22 ± 0.05 nm for the magnetic moment of Nd^{147}. This rather small value (together with our value of 0.16 ± 0.06 nm for Ce^{141}) may not be meaningful because of possible internal magnetic field effects. This, however, does not affect our other conclusions.

* Assisted by the Office of Naval Research.
[1] Ambler, Hudson, and Temmer, Phys. Rev. **95**, 625 (1954); also Phys. Rev. (to be published).

H5. Inner Bremsstrahlung from A^{37}.† TORSTEN LINDQVIST AND C. S. WU, *Columbia University.*—Recent investigations[1,2] on the distribution of inner bremsstrahlung from electron capture processes of Fe^{55} and Cs^{131} have shown that the theoretical predictions[3,4] which take account only of the K-electron capture are not adequate in interpreting the low-energy region of the distribution. We have recently reinvestigated the inner bremsstrahlung from A^{37} with particular emphasis on the low-energy region. The NaI crystal used in the scintillation spectrometer is permanently canned in a container with a window of thin Al foil (1 mil). The observed spectrum is corrected for the NaI crystal detection efficiency, geometrical factor, photopeak to Compton-electron ratio, and resolution of the system. It is concluded that the intensity of the low-energy photons is much more than that which can be accounted for by Morrison and Schiff's treatment. A better agreement can be obtained if one considers the p-electron capture and takes the Coulomb effect into the treatment as is shown by Glauber and Martin.[5]

† This work was supported by the U. S. Atomic Energy Commission.
[1] L. Madansky and F. Rasetti, Phys. Rev. **94**, 407 (1954).
[2] B. Saraf, Phys. Rev. **94**, 642 (1954).
[3] P. Morrison and L. I. Schiff, Phys. Rev. **58**, 24 (1940).
[4] J. M. Jauch, Oak Ridge National Laboratory, ORNL-1102, 1951 (unpublished).
[5] R. J. Glauber and P. C. Martin, Phys. Rev. **95**, 572 (1954).

H6. Disintegration of Niobium-91 and -92. R. W. HAYWARD, D. D. HOPPES, AND H. ERNST, *National Bureau of Standards.*—The radiations from the 60-day Nb^{91} and the 10-day Nb^{92} isotopes have been investigated using magnetic lens, scintillation-pulse height, and coincidence counting techniques. Isotopic identification has been made from threshold energies of the following reactions: $Mo(d,\alpha)Nb$, $Nb(\gamma,xn)Nb$, $Zr(d,xn)Nb$, and $Y(\alpha,xn)Nb$. In Nb^{91} two gamma rays were observed, a 1.21-Mev gamma ray 6.1 times the intensity of the unconverted portion of a strongly converted 0.104-Mev isomeric transition of $M4$ multipolarity. The 1.21-Mev gamma ray is in coincidence with Zr x-rays, indicating appreciable K capture. This gamma ray is the same as that occurring in the disintegration of Y^{91}. In Nb^{92} three gamma rays were observed with the following energies and relative intensities per disintegration: 0.930 Mev (0.98), 0.900 Mev (0.01), and 1.83 Mev (0.02). The first two gamma rays are in coincidence with each other and all are in coincidence with Zr x-rays. Decay schemes based on the experimental results will be proposed.

H7. Electromagnetic Radiations of Cs^{132}.† BEROL L. ROBINSON AND RICHARD W. FINK, *University of Arkansas.*—A sample of Cs^{132} was prepared by bombarding "Specpure" CsCl with 80-Mev protons in the University of Rochester 130-inch cyclotron[1] and by subsequent radiochemical purification. The half-life was 6.2 ± 0.2 days by gamma counting. Scintillation spectrometer studies showed gamma rays at 669 ± 3 kev, 1100 ± 40 kev, and 1265 ± 20 kev, the ratio of the intensities being $1000 : (7 \pm 2) : (8 \pm 2)$, respectively. By means of an x-ray-gamma coincidence experiment, the branching ratio to the 669-kev state was found to be 0.9 ± 0.2. Major sources of error in this measurement arise from uncertainties in the absolute calibration of a Cs^{137} standard, and in the decay constants of Cs^{132} and Cs^{131} which were present as a contaminant. From the branching ratio we deduce that electron capture to the ground state of Xe^{132} is forbidden and that Cs^{132} has $I \geq 2$, in agreement with shell model predictions. Gamma-gamma coincidences were observed, but the 1265-kev gamma ray is not coincident with the 669-kev transition. We observed a gamma ray at 365 ± 6 kev, which decayed with a half-life of about 30 hours, and which is attributed to Cs^{129}.

† Supported in part by the U. S. Atomic Energy Commission.
[1] The bombardment was performed through the courtesy of Professor E. O. Wiig and the Rochester cyclotron crew.

H8. Radioactive Tl^{204} and Bi^{207}. L. S. CHENG, VIRGINIA C. RIDOLFO, M. L. POOL, AND D. N. KUNDU, *Ohio State University.*—An activity from a deuteron bombardment of thallium has been recorded for ten years with an ionization chamber. The half-life is $2.5 + 0.03$ years. The activity is chemically thallium, and the beta spectrum was shown, by absorption measurements made with a Geiger counter and nucleometer, to be identical with that of the 4.0-year Tl^{204}. An activity of four years could not be found. From a lead bombardment an activity was found which showed a half-life of 8.0 ± 0.6 years based upon observations for eleven years. Chemically the activity is bismuth and the electromagnetic spectrum in a scintillation spectrometer is identical with that of the 50-year Bi^{207}. The five neighboring activities in Tl, Pb, and Bi were identified, however, essentially as recorded in the literature, by chemical separations, characteristic radiations, and half-lives.

H9. Extranuclear Effects on the Directional Correlation of the Ta^{181} Gamma Rays.* H. PAUL AND R. M. STEFFEN, *Purdue University.*—The directional correlations of the Ta^{181} gamma rays have been measured before by McGowan,[1] who found the anisotropies to be strongly influenced by the source composition. To investigate the role of the time-dependent quadrupole interaction in the 480-kev excited state of Ta^{181}, the correlation of the 132-kev–480-kev cascade displayed by solutions of Hf^{181} of different viscosities was measured using a coincidence scintillation spectrometer. The viscosity was changed by adding different amounts of glycerine to the solutions and by varying the temperature. In contradistinction to similar experiments[2] with In^{111}, Hf^{181} in different solvents with equal viscosities shows strongly different directional correlations. This might be traced to the formation of complex Hf ions in some of the cases. A spin assignment different from McGowan's is suggested which agrees fairly well with the angular correlation results,[1] but is consistent also with expected gamma lifetimes and recent Coulomb-excitation data.

* Supported by the U. S. Atomic Energy Commission.
[1] F. K. McGowan, Phys. Rev. **95**, 471 (1954).
[2] P. B. Hemmig and R. M. Steffen, Phys. Rev. **92**, 823 (1954).

H10. Gamma-Gamma Correlation of Pb_2^{04m}. SOL RABOY AND VICTOR E. KROHN, *Argonne National Laboratory.*—The angular correlations of the 913–374-kev and 913–898-kev gamma-ray pairs of Pb^{204m} have been measured in liquid media (deuteron-irradiated thallium foils dissolved in HNO_3 and H_2SO_4). The anisotropy ($[W(180°)/W(90°)]-1$) of the delayed coincidences is 0.34 ± 0.02 for the 913–374-kev cascade and 0.44 ± 0.02 for the 913–898-kev cascade. The anisotropy as a function of the delay between the gamma rays was investigated and no attenuation was observed as the delay was increased from 0.185 to 0.550 microsecond. A ten percent

attenuation of the anisotropy during this time would be consistent with the data, but the aforementioned errors do not include an allowance for possible attenuation. Solid angle corrections of eight percent have been made with the assumption that the $P_4(\cos\theta)$ and higher terms can be neglected for this purpose.

H11. Alpha-Gamma Directional Correlation in Th^{228}. T. B. NOVEY, *Argonne National Laboratory.*—Measurements of the alpha-gamma directional correlation in the even-even alpha particle emitters have indicated[1,2] the presence of an attenuation of the anisotropy expected for the 0–2–0 spin sequence. It has been suggested[3] that this effect is due to the presence of electric quadrupole interactions in the crystalline sources. Recent work on Am^{241} has shown[4] that by the use of liquid film sources the quadrupole effect may be greatly attenuated; however, the expected correlation for this type of decay is not adequately provided by theory at present. Results of measurements with liquid film sources to Th^{228} will be presented showing the extent of the effect of the crystalline field interaction in a case where the unique directional correlation function $\sin 2\theta$ is expected.

[1] Beling, Feld, and Halpern, Phys. Rev. **84**, 155 (1951).
[2] G. M. Temmer and J. M. Wyckoff, Phys. Rev. **92**, 913 (1953).
[3] A. Abragam and R. V. Pound, Phys. Rev. **89**, 1306 (1953).
[4] T. B. Novey, Phys. Rev. (to be published).

H12. Angular Correlation of Photons from Positron Annihilstion in Light Metals. A. T. STEWART* AND R. E. GREEN,† *Dalhousie University.*—The angular correlation of gamma rays from positron annihilation in the light metals Li, Be, Na, Mg, Al, K, and Ca, has been measured. Two flat NaI scintillation crystals were placed about 5 m apart, with a source of annihilation radiation midway between them. The coincident counting rate was observed as a function of the angle defined by the position of the source and two counters. The half-width of the measured angular correlation curve is directly related to the average momentum of the center of mass of the annihilating pair. A measure of the momentum may be given by defining an effective Fermi energy in terms of the following assumptions: (1) the positrons are thermalized before annihilation; (2) they annihilate only with electrons of a free electron gas; and (3) the momentum of the annihilating electron is carried away by the two photons. The Fermi energies so determined are: Li, 4.6±0.5; Be, 13.6±0.9; Na, 3.3±0.4; Mg, 7.4±0.5; Al, 11.1±0.9; K, 2.1±0.3; and Ca, 4.8±0.4 electron volts. It is interesting to note that these results are in good agreement with values calculated from the free electron theory.

* Member of the staff of Atomic Energy of Canada Limited, on temporary appointment to Dalhousie University during the academic term 1953–54.
† Now at McGill University, Montreal, Quebec.

FRIDAY AFTERNOON AT 2:00

Eckhart 133

(J. H. WILLIAMS presiding)

Apparatus of Nuclear Physics; Other Nuclear Topics

I1. Magnetic Analyzer for Nuclear Reactions. T. D. HANSCOME AND D. K. WILLETT, *Naval Research Laboratory.*—A 60-degree magnetic spectrograph has been constructed for application to Q measurements using the NRL 2-Mev Van de Graaff. The central radius of curvature is 32.14 cm. Six 1×3 inch nuclear track emulsions are arranged on tangents along the focus curve. The range of radii accommodated is approximately 30 to 40 cm. The magnetic field is regulated to better than one part in 50 000 by use of the nuclear magnetic resonance of the proton. The energy dispersion is 0.13 percent per mm at the center of the camera. The position of a monoenergetic group can be determined to ±0.2 mm. For a target of negligible thickness and 0.02-in. width, the resolution is 1000. The polonium alpha line is 7 kev wide, giving a practical resolution for thin targets of 750. The resolution and stability of the Van de Graaff permitted the use of 0.010-in. slits on the incident beam. The calibration is very nearly linear in the momentum. Normal oxygen targets (NiO) were bombarded with deuterons at 1.61 Mev. The proton groups were observed at the expected points on the plates. The width of the $C^{12}(d,p)C^{13}$ group (5.2 kev) from carbon contamination confirms that the line width for the $O^{16}(d,p)O^{17}$ groups is due to target thickness.

I2. Amplitude and Frequency Stabilized Adjustable High-Frequency Oscillator.* R. C. MOBLEY AND B. R. ALBRITTON, JR., *Louisiana State University.*—During development of the deflection system for an "Ion Buncher,"[1] need was found for a highly amplitude- and frequency-stable rf oscillator tunable in 100 kc/sec steps from 5.0 to 9.5 Mc/sec. This need has been met through development of a circuit which automatically maintains a free-running amplitude-controlled 5.0 to 9.5 Mc/sec oscillator in phase lock with any desired harmonic, between the 50th, and 95th, of a fixed-frequency 100-kc/sec Mecham Bridge crystal oscillator. To accomplish this the 100-kc/sec sine wave from the crystal oscillator is amplified, clipped, and differentiated to produce pulses 20 mμsec long. These pulses are then mixed in a 6BN6 gated beam tube with the sine wave from the free-running oscillator. The resultant phase-sensitive signal, after further amplification at 500 kc/sec and rectification, biases a reactance tube across the tank circuit of the free-running oscillator so as to maintain a fixed phase relationship between the two oscillators.

* This work was supported in part by the University Council of Research, Lousiana State University.
[1] R. C. Mobley, Phys. Rev. **88**, 360 (1952).

I3. A Determination of the Bremsstrahlung Spectrum Produced by 18-Mev Electrons.* R. L. STEARNS, J. W. ROBSON,† AND E. C. GREGG, *Case Institute of Technology.*—A relative measurement of the energy spectrum of the Case betatron has been obtained by performing a magnetic analysis of Compton electrons ejected from a 38-mil beryllium scatterer. The electrons in the forward direction pass through a 60° magnet and are detected by means of a plastic scintillator (Plastifluor B) and a Du Mont 6292 photomultiplier. The raw data were corrected for multiple-scattering effects and converted through the known Compton cross section to a photon distribution.[1] The spectrum compared favorably with that calculated by Schiff[2] assuming a 20-mil molybdenum target. The agreement was within the statistical accuracy of the experiment (about ±5 percent) except at the lowest energy (5.65 Mev), at which

point the discrepancy is attributed to the failure of the multiple-scattering calculations.

* This work supported by the U. S. Atomic Energy Commission.
† Now at the University of Arizona, Tuscon, Arizona.
[1] See following abstract.
[2] L. Schiff, Phys. Rev. **70**, 87 (1946).

I4. Emergent Electron Distribution Resulting from Bremsstrahlung Incident on a Thin Scatterer.* J. W. ROBSON,† R. L. STEARNS, AND E. C. GREGG, *Case Institute of Technology.*—In deducing the bremsstrahlung spectrum incident on a thin foil from the observed energy distribution of Compton electrons one must consider multiple scattering in the foil as well as the usual Compton cross section. The number of electrons reaching the detector when it is set to detect electrons of kinetic energy T is given by

$$n(T)=\int_{T-\Delta T/2}^{T+\Delta T/2} E(T')\left[\int NA(\psi,E_2)\frac{\partial\sigma}{\partial\psi}B(E_2)\frac{\partial\psi}{\partial T}dE_2\right]ZdT',$$

where $E(T')$ is the detector efficiency, N is a constant depending on the scatterer, $A(\psi,E_2)$ is the probability of an electron being detected, $\partial\sigma/\partial\psi$ is the Klein-Nishina cross section per unit electron angle, and $B(E_2)$ is the desired photon distribution. Also $A(\psi,E_2)=\int p(\theta,\theta_m)W(\theta,\psi)d\theta$, where $p(\theta,\theta_m)$ is the probability of an electron of kinetic energy T being multiply scattered through an angle θ; this probability was evaluated using the results of Bethe, Rose, and Smith. $W(\theta,\psi)$ is the probability of such an electron being detected.

* This work supported by the U. S. Atomic Energy Commission.
† Now at the University of Arizona, Tucson, Arizona.
[1] Bethe, Rose, and Smith, Proc. Am. Phil. Soc. **78**, 573 (1938).

I5. Coupling of Betatron and Phase Oscillations in a Synchrotron. E. A. CROSBIE AND M. HAMERMESH, *Argonne National Laboratory.*—The coupled equations for radial position, momentum, and phase oscillations in a synchrotron are treated by use of difference equations. The effect of a radial variation in the accelerating radio-frequency voltage is included in the treatment; any resultant damping of one type of oscillation is shown to be necessarily accompanied by equal antidamping of oscillations of the other type. A simple treatment of the adiabatic variation of parameters for systems of linear differential or difference equations is given.

I6. A Crystal Technique for Measuring Cyclotron Beam Energies. PHILIP YUSTER, SOL ROCKLIN, WARREN RAMLER, AND CHARLES DELBECQ, *Argonne National Laboratory.*—A lithium fluoride crystal, when irradiated with deuterons from a cyclotron, develops a yellow color; if the deuterons are stopped within the crystal there is a sharp demarcation in color between the irradiated and unirradiated portions. It has been found that the measurement of the depth of penetration of the color into lithium fluoride crystals can be used to determine accurately and rapidly the energy of deuterons in a cyclotron beam. A single exposure of a crystal to the deuteron beam can be used to determine not only the energy of the deuterons but also the angular orientation of the beam trajectories.

I7. A New Technique for Observing Cyclotron Phase Grouping.* STEWART D. BLOOM, *Brookhaven National Laboratory.*—The phase grouping of the beam on the Brookhaven 18-in. cyclotron has been observed to be of the order of 1–2 mμsec out of 54 mμsec (18.6 Mc), in agreement with theoretical prediction.[1] The measurement was accomplished by allowing the 1-ma, 2.6-Mev deflected proton beam to impinge upon an appropriate target, and then looking for coincidences between the resultant γ rays due to (p,γ) processes, and rf voltage "pips" occurring once per rf cycle. The rf-coincidence technique utilized the new Philips 6218 beam-deflection tube in fundamentally the same manner as originally proposed,[2] with the exception of the introduction of the γ-detection signal on the first focusing grid. In the present work resolution times of 0.5–1.0 mμsec were used, though better resolutions are achievable. The immediate intention is to apply this method to the general problem of inelastic neutron scattering using time-of-flight techniques. Also an investigation is being made of the possibilities of the method in observing the decay of metastable states.

* Research carried out under the auspices of U. S. Atomic Energy Commission.
[1] B. L. Cohen, Rev. Sci. Instr. **24**, 589 (1953).
[2] Bruysten, Groendijk, and Mantz, Communication News **XIII**, No. 1, 13 (1953).

I8. The Synchro-Microtron. H. F. KAISER, *Naval Research Laboratory.*—Among several methods proposed[1] for increasing the maximum particle energy of the microtron is considered the use of an auxillary magnetic field over the region of the final microtron orbit so that further acceleration of electrons in this orbit could proceed in a rising field as in a synchrotron. Here an extension of this idea will be discussed in which the field will rise in a stepwise or quasi-stepwise way. The field system is regarded as a transmission line carrying a current wave at nearly particle speed. In one form it is operated as two semicircular parts for each of which the "delay time" is nearly the orbital period. The effect is a constant current during each period which rises stepwise in time. A similar effect is obtained with a circular line beginning at the resonator and terminating in its characteristic impedance. If field and energy increments satisfy $T_n=(2\pi/cc)[(E_n+\Delta E)/(H_n+\Delta H)]$, acceleration is possible to an energy limited by the field attainable. The system exhibits regions of phase stability, which, moreover, is preserved even when the average rate of field rise is slightly nonlinear.

[1] H. F. Kaiser, Phys. Rev. **95**, 667 (1954).

I9. A Theory of Cavity Ionization. L. V. SPENCER AND F. H. ATTIX, *National Bureau of Standards.*—Measurements by Attix and De La Vergne[1] of the cavity ionization produced by γ rays, as a function of the wall material, do not agree with the predictions of the Bragg-Gray theory, which neglects effects due to the travel of fast secondary electrons generated in inelastic collisions. These effects depend strongly on the difference between the atomic numbers of the gas and wall materials. We propose a new theory in which only collisions transferring energies less than a cut-off Δ are dissipative. The parameter Δ may be related to the cavity size. Calculations based on this theory agree well with the measurements of Attix and De La Vergne. They also indicate a variation in the ionization per gram of air as a function of cavity size which agrees with measurements by Gray.[2] According to these new considerations, measurements with extrapolation to zero cavity size have at best a questionable interpretation.

[1] F. H. Attix and L. De La Vergne (to be published).
[2] L. H. Gray, Proc. Roy. Soc. (London) **A156**, 578 (1936).

I10. Performance Characteristics of the BNL Research Electrostatic Accelerator.* C. M. TURNER, *Brookhaven National Laboratory.*—Preliminary tests have been carried out with accelerated hydrogen ion beams in the revised BNL research electrostatic accelerator following the incorporation of effective x-ray suppression at the anode end of the 8-foot-long acceleration tube.[1] A capillary arc type source with capillary probe is presently used. General performance specifications are as follows: (1) nominal rating, 3.5 Mev, 50 microampere analyzed proton beam, 25 mr/hr x-ray intensity beside tank; (2) maximum present rating, 4.0-Mev, 75-microampere proton beam, 150 mr/hr beside tank; (3) proton yield, 50–75 percent; (4) maximum power in the total ion beam (focusable

to a 3/32-in.-diameter spot), approximately 1 kilowatt; (5) voltage stability without regulation, 0.2 to 0.3 percent.

* Work performed under the auspicies of the U. S. Atomic Energy Commission.
[1] C. M. Turner, Phys. Rev. **95**, 599(A) (1954).

I11. The Effect of Temperature upon the Scintillation Efficiency of NaI(Tl). L. A. WEBB AND R. F. JOHNSON, *U. S. Naval Radiological Defense Laboratory.*—Studies have been made of the effect of temperature upon the scintillation efficiency of crystals of NaI(Tl) over the range of 5°C to 45°C. The samples used were 1-in.×1-in. diameter crystals sealed in standard commercial packages with MgO reflecting surfaces. The samples were coupled to a 6292 photomultiplier tube by means of a special light pipe which permitted the change of temperature of the crystal package only, while the operating conditions of all other components remained constant. All temperatures were controlled by means of circulating oil. Crystal temperature *vs* the pulse height output of the Cs^{137} total absorption line as recorded by a gamma-ray scintillation spectrometer shows a coefficient of -0.12 ± 0.02 percent per centigrade degree. This value agrees quite well with that obtained by others.[1]

[1] "Round Table Discussion of Photomultiplier and Phosphors," Scintillation Counter Symposium, 1954; Nucleonics **12**, No. 3, 28 (1954).

I12. Double-Scattering Experiment with 96-Mev Protons.* KARL STRAUCH, *Harvard University.*—The external cyclotron beam (energy 96 Mev, spread 2 Mev) has been used to perform a double-scattering experiment. When both scatterers were carbon, it was possible to make sure that the majority of detected protons were elastically scattered in both targets. Although not as certain, the same fact is believed to be true with the other targets investigated. The first and second scatterings took place at average energies of about 87 Mev and 66 Mev, respectively. Measured values of $\epsilon=R-L/R+L$ are as follows:

Target 1	Target 2	θ_1	θ_2	ϵ
Cu	Cu	26°	18°	$4.3\pm1.7\%$
C	Cu	8.5°	18°	$0.3\pm1.8\%$
C	C	8.5°	18°	$1.7\pm2.0\%$
C	C	15°	15°	$3.0\pm1.6\%$†
C	C	20°	20°	$3.6\pm1.6\%$†
Be	Be	20°	20°	$3.1\pm1.8\%$†

These results will be discussed and compared with other experiments.

* This work was supported by the joint program of the Office of Naval Research and the U. S. Atomic Energy Commission.
† Correction for geometric inhomogeneity of first scattered beam has been applied.

I13. Elastic Scattering of 0.41 and 0.66 Mev Gamma Rays* by Tin and Lead. A. K. MANN, *University of Pennsylvania.*—Collimated beams of 0.41- and 0.66-Mev gamma rays were scattered from tin and lead targets and the absolute differential cross sections for elastic scattering measured at five angles between 15 and 75 degrees. The scattered radiation was detected with a NaI scintillation counter to select only the energy region of elastic scattering. At the smaller angles, the degraded radiation from Compton scattering was subtracted empirically by comparing the tin and lead scattering with that from an aluminum target containing the same number of electrons. At these energies the predominant mode of elastic scattering should be Rayleigh scattering from the tightly bound electrons. Within the experimental error of about 10 percent the measured differential cross sections for lead at both 0.41 and 0.66 Mev do not differ significantly from the calculation of Rayleigh scattering made by Franz,[1] using the Thomas-Fermi model. For tin at 0.66 Mev the measured values at large angles appear to be less than those given by Franz, but no such disagreement is evident at 0.41 Mev.

* Supported in part by the Air Research and Development Command.
[1] W. Franz, Z. Physik. **98**, 314 (1935).

FRIDAY AFTERNOON AT 2:00

Cobb 110

(J. M. JAUCH presiding)

Invited Papers

K1. The Photodisintegration of Deuterium. A. O. HANSON, *University of Illinois.* (30 min.)

K2. A Partial-Wave Analysis of the Experimental Photomeson Cross Sections and Its Interpretation. K. M. WATSON, *University of Wisconsin.* (30 min.)

Theoretical Nuclear Physics

K3. Coulomb Effects in the (d,p) Reaction.* R. W. HOCKNEY AND P. V. C. HOUGH, *University of Michigan.*—The Schrodinger equation for the motion of a neutron and a proton in the field of a nucleus is transformed by standard techniques to a differentio-integral equation for the motion of the proton when the neutron is bound in a particular harmonic oscillator state. The Coulomb force on the proton gives rise to a source term in Born approximation. As a slight justification for the Born approximation, the most important neutron impact parameters are found to be somewhat larger than the nuclear radius. For 7.8-Mev deuterons incident on O^{16} and leading to the 0.88-Mev, 2*s* state in O^{17}, the Coulomb amplitude in the forward direction is about one-third the Butler amplitude and interferes destructively, thereby reducing the theoretical cross section by almost a factor 3 and establishing reasonable agreement with experiment.[1] The nuclear radius required to fit the position of the first minimum in the experimental angular distribution is reduced from $\sim6\times10^{-13}$ cm to $\sim4\times10^{-13}$ cm, the formula $R=1.4\ A^{\frac{1}{3}}$ giving 3.5.

* Supported by the Michigan Memorial Phoenix Project and by the U. S. Atomic Energy Commission.
[1] W. J. Childs and W. C. Parkinson, private communication. Burge *et al.*, Proc. Roy. Soc. (London) **A210**, 534 (1952).

K4. Isotopic Spin Impurity in Light Nuclei. W. M. MACDONALD. *University of California, Berkeley.*—The validity of the total isotopic spin quantum number T^2, which exists under the assumption of "charge independent" nuclear forces of the form $\Sigma(a+b\tau_i\cdot\tau_j)$, is impaired only by the Coulomb potential. Charge independence must therefore be renounced unless the Coulomb potential can explain the isotopic spin impurity determined experimentally from violations of the isotopic spin selection rule on electric dipole transitions.[1] The impurity introduced by the Coulomb potential has been calculated, taking into account first the interaction of outside nucleons

among themselves and with the core of nucleons in closed shells. Secondly, we have calculated the effect on isotopic spin impurity of the interaction of nucleons in closed shells. This latter "core impurity," neglected in previous work[1] has been found to be larger by a factor of ten than that due to nucleons outside closed shells. The isotopic spin impurity of the normal states of nuclei with $A \leq 20$ has been found to vary in intensity (squared amplitude of higher isotopic spin states) from $\sim 3\times10^{-3}$ for He^4 to 2×10^{-2} for Ne^{20}. This work was performed under the auspices of the U. S. Atomic Energy Commission.

[1] L. A. Radicati, Proc. Phys. Soc. (London) **66A**, 139 (1953); **67A**, 39 (1953).

K5. Supermultiplet Structure and Spin Dependent Forces.* R. W. KING, *National Research Council.*—While Wigner's supermultiplet formalism provides the most natural theoretical explanation of the empirical difference between favored and unfavored β decay, it does not permit favored negatron decay for odd A nuclei with $A > 3$. There is considerable experimental evidence from the decay of $T_z = \frac{3}{2}$ nuclei to excited states of $T_z = \frac{1}{2}$ nuclei that is contrary to such a restriction. An explanation of this group of favored negatron transitions is proposed on the basis of a deviation from the supermultiplet formalism due to spin dependent nuclear forces. An expression for the energy difference between the $T_z = \frac{3}{2}$, $S = \frac{1}{2}$ parent state and the $T_z = \frac{1}{2}$, $S = \frac{1}{2}$ daughter state belonging to the same supermultiplet contains at least two spin dependent terms opposite in sign to the Coulomb energy difference. Super allowed negatron decay is thus possible within supermultiplets of the $[4^k+3+2]$ or $[4^k+2+1]$ type for any A where the energy gained by these two spin dependent terms is greater than the coulomb energy difference between the parent and daughter state. Empirically such a condition seems to prevail for $A \lesssim 25$. Some needed experimental measurements will be discussed.

* Work supported by the U. S. Atomic Energy Commission.

K6. Molecular Excitation in Beta Decay. MURRAY CANTWELL,* *Washington University.*—A theoretical study has been made of the formation, following the beta decay of one of the nuclei of a tritium molecule, of the daughter helium-tritide molecule ion in the various rotational states associated with the first three vibrational levels of its ground electronic state. It is predicted that a sample of tritium will emit about 2×10^{13} photons per second per gram with a wave number of approximately 3100 cm^{-1} due to the radiative deexcitation of the first excited vibrational level of the ground electronic state of the daughter molecule ion. The effect of the type of beta-decay coupling on the distribution of the helium-tritide molecule ion over its excited vibrational states is less than one percent because of the relatively small beta electron velocity in tritium. In addition general curves have been constructed giving the probability that a diatomic molecule will remain bound after the beta decay of one of its nuclei as a function of the beta-energy release, of the internuclear potential well parameters, and of the number of stable vibrational levels in the electronic state of the daughter molecule.

* NSF fellow, assisted by joint program of the Office of Naval Research and the U. S. Atomic Energy Commission.

K7. The Importance of Parentage of Nuclear States for Nuclear Reaction Phenomena.* D. H. WILKINSON,† *Brookhaven National Laboratory* AND A. M. LANE, *AERE, Harwell, England.*—The concept of fractional parentage of nuclear states is briefly reviewed. It is pointed out that many dynamical properties of nuclear systems—transition rates and level widths—are directly controlled by products of the coefficients of fractional parentage for common parents—the "parentage overlap"—between initial and final states. Illustrations are given from a range of nuclear reactions including radiative transitions, high and low energy stripping, pickup, and photonuclear processes. It is particularly to be emphasized that, because of the occurrence of the coefficients of fractional parentage and certain (vector coupling) weighing factors in the expression for the transition rate, one may find reduced and radiative widths very considerably less than the "single particle" values even though the states concerned are wholly of an independent particle character.

* Work partially done at Brookhaven National Laboratory under the auspices of the U. S. Atomic Energy Commission.
† On leave from the Cavendish Laboratory.

K8. An Intermediate Coupling Model of Lithium-6. R. H. ADKINS AND J. G. BRENNAN, *The Catholic University of America.*—Horie and Yoshida[1] have obtained a wave function for the ground state of lithium-6 from a $(p)^2$ configuration. This has been done by imposing the requirements that the known magnetic moment and electric quadrupole moment be reproduced. This work has been re-examined and it is found that two wave functions from a $(p)^2$ configuration satisfy these requirements. One of these wave functions corresponds to that of Horie and Yoshida; the other differs considerably from it. An attempt has been made to make a selection between these two within the scope of an intermediate coupling model neglecting configuration interaction. The results are not conclusive, but there seems to be an indication that a modified Hall and Powell potential[2] which has the latter of these two wave functions as its lowest state gives a more satisfactory energy level structure for this nucleus.

[1] H. Horie and S. Yoshida, Progr. Theoret. Phys. **6**, 829 (1951).
[2] H. H. Hall and J. L. Powell, Phys. Rev. **90**, 912 (1953).

K9. Tensor Force Interaction Energies for Configurations Important in O^{18} and F^{18}.* D. R. BACH, C. R. LUBITZ, AND P. V. C. HOUGH, *University of Michigan.*—The two-nucleon jj configurations $d_{5/2}d_{5/2}$, $d_{5/2}d_{3/2}$, $d_{3/2}d_{3/2}$, $d_{5/2}s_{1/2}$, $d_{3/2}s_{1/2}$, $s_{1/2}s_{1/2}$ are probably responsible[1] for all the low-lying even parity states in the polyad of mass 18. Matrix elements of the tensor force have been calculated for these configurations in terms of the radial integrals I_l of the harmonic oscillator wave functions.[2] Energies of states of isobaric spin $T=1$ have been obtained both by the Slater method and using the tensor algebra of Racah[2]; those of $T=0$ have been calculated by the second method only. The dependence of the level scheme in O^{18} and F^{18} on the relative strength of central and tensor forces, and on the two ranges and shapes is under investigation.

* Supported in part by the U. S. Atomic Energy Commission.
[1] M. G. Redlich, Phys. Rev. **95**, 448 (1954).
[2] I. Talmi, Phys. Rev. **89**, 1065 (1953).

K10. Excited States of C^{12} and O^{16}.* L. I. SCHIFF, *Stanford University.*—The matrix element for the electric monopole transition in O^{16} computed from the pair emission lifetime[1] has roughly the same magnitude as the matrix element between the ground and 7.68-Mev states in C^{12} estimated from inelastic electron scattering,[2] assuming that the latter is also electric monopole.[3] Both matrix elements are much smaller than would be expected on the basis of an alpha particle model, an elastic fluid model, or a $1S \rightarrow 2S$ transition of a single proton. It seems possible that this can be explained on the independent particle model (IPM) if two particles change their states. The transition is then forbidden if the IPM is taken literally, but becomes allowed if some interaction between particles is admitted in addition to that which is included on the average in the IPM. An estimate of the magnitude of this residual interparticle interaction that is required to explain the matrix elements will be presented.

* Supported in part by the Office of Scientific Research, Air Research and Development Command.
[1] Devons, Goldring, and Lindsey, Proc. Phys. Soc. (London) **A67**, 134 (1954).
[2] R. Hofstadter and J. H. Fregeau, private communication.
[3] G. Harries, Proc. Phys. Soc. (London) **A67**, 153 (1954).

FRIDAY AFTERNOON AT 2:00

Mandel Hall

(S. K. ALLISON presiding)

Invited Papers

L1. The Temperature of the Primitive Earth. H. C. UREY, *University of Chicago.* (30 min.)

L2. Review of the MURA High-Energy Accelerator Programme. D. W. KERST, *University of Illinois.* (30 min.)

SATURDAY MORNING AT 9:30

Oriental 104

(F. F. RIEKE presiding)

Nonmetallic Solids, Mostly Crystals

P1. Electrical Conduction in Plastics. RAYMOND J. MUNICK, *Argonne National Laboratory.*—Electric current from specimens of Lucite, fluorothene, polystyrene, polyethylene, and Teflon was found to consist of two parts. One part decreases with time elapsed from initial voltage application as t^{-n} with n around 1,[1] depends on voltage changes, and changes little with temperature from 25 to 49°C although it attains a maximum in magnitude for Lucite and fluorothene around −30 and −55°C, respectively. The other part appears almost steady, depends on voltage, and increases exponentially as the reciprocal absolute temperature[2] from 25 to 49°C with activation energies around 1 electron volt.[3] The almost steady part shows a slight decrease with time, which is more rapid at higher temperatures, an effect which others have observed for crystalline insulators.[3] The conductivities indicated by the steady current are less than 10^{-19} mhos cm^{-1}.

[1] Warner, Muller, and Nordlin, J. Appl. Phys. 25, 131 (1954); P. Ehrlich, J. Appl. Phys. 25, 1056 (1954).
[2] N. W. Ramsey, Nature 172, 214 (1953); Fowler and Farmer, Nature 171, 1020 (1953); 173, 317 (1954); 174, 136 (1954).
[3] A. J. Joffe, *The Physics of Crystals* (McGraw-Hill Book Company, Inc., New York, 1928), Lecture VIII.

P2. Mechanism of High-Speed-Waterdrop Erosion of Methyl Methacrylate Plastic. OLIVE G. ENGEL, *National Bureau of Standards.*—The erosion that waterdrops cause when they strike solid surfaces at very high velocities has become important because of the damage produced when high-speed aircraft fly through rain. This erosion is essentially the same as that which occurs in steam turbines because of the waterdrops present in wet steam. The process has been studied for the past twenty-five years, but no clear understanding of the complete damage mechanism (or mechanisms) has emerged. The damage that results from these high-speed liquid-to-solid collisions is a function both of the impact properties of the waterdrop and of the properties of the material against which impingement occurs. Under impact conditions the waterdrop is essentially hard, but unlike a sphere of hard material it retains its liquid property of flow. A parallel study of the damage produced on methyl methacrylate plastic by the impingement of steel spheres and deforming lead pellets has contributed information in regard to the mechanism of the high-speed-waterdrop erosion of this plastic. Results of the parallel study will be described. The mechanism can be extrapolated with safety only to other brittle materials of low tensile strength the other characteristic properties of which are similar to those of methyl methacrylate plastic.

P3. Generation of Electron Traps by Plastic Flow. WERNER KÄNZIG AND MASAYASU UETA, *University of Illinois.*—Vacancy clusters generated by moving dislocations act as effective electron traps, and change the photographic properties of the alkali halides considerably. This has been investigated, using additively colored KCl and electrolytically colored NaCl. Electrons were released from the F centers by irradiation of F light. In a plastically deformed crystal these electrons are immediately captured by vacancy clusters and have not much chance to return to a negative ion vacancy. Therefore, the F band bleaches much faster than in the case of undeformed crystals. Measurements of the bleaching rates permit an estimation of the concentration of traps generated by plastic flow. About 10^{17} traps per cm^3 are formed by a plastic strain of 10 percent. The filled traps give rise to a very broad absorption band, centered in the near infrared. Photochemical processes, such as the formation of F', R, and M centers by irradiation of F light, are strongly affected by the presence of these traps. In additively colored KCl these centers cannot be formed after sufficient plastic deformation.

P4. The Thermal Formation of Colloids from F Centers in KCl Crystals. H. PAGNIA AND F. STÖCKMAN,* *Institute of Technology, Darmstadt, Germany* (introduced by K. LARK-HOROVITZ).—The thermal formation of colloids from F centers has been investigated in KCl crystals. Additively colored crystals have been tempered at temperatures between 250° and 400°C and the absorption spectra have been measured at intervals of some minutes. Results: the colloid band does not grow directly from the F band but appears only after some intermediate steps from which two agree with the M and R band. After tempering for a long time an equilibrium concentration of colloids is established which equals the difference of the excess potassium concentration and the equilibrium concentration of F centers at the temperature of tempering. The absorption band of the colloid shifts to longer wavelengths after tempering at higher temperatures, but its position does not depend upon the concentration of the colloids. According to the theory of M. Savastianova[1] this means that the colloids become larger if they grow at higher temperatures and that their size only depends upon this temperature.

* Now at Purdue University, Lafayette, Indiana.
[1] M. Savastianova, Z. Physik 64, 262 (1930).

P5. Optical and Electrical Properties of Lithium Fluoride X-Rayed at Liquid Nitrogen Temperature. C. J. DELBECQ, P. PRINGSHEIM, AND P. H. YUSTER, *Argonne National Laboratory.*—When a lithium fluoride crystal is irradiated with x-rays at −190°C, absorption bands are formed at 242 mμ (*F* band) and at 340 mμ. It has been found previously that upon slow warming, such a crystal shows a large luminescence glow peak at about −133°C;[1] in the present investigation it has been found that the 340 mμ band almost completely disappears and the *F* band decreases appreciably between −170 and −120°C with a maximum rate of disappearance in both cases at about −134°C. When a lithium fluoride crystal, after irradiation at −190°C, is placed in an electric field and warmed slowly, the electrical conductivity of the crystal is observed to pass through a large maximum at about −130°C. This electrical conductivity is interpreted as being due to the migration of positive holes after being thermally released from their traps (*V* centers); the luminescence occurs when the positive holes are annihilated at electron excess centers, in this case the 340 centers and *F* centers. Experiments will be described which support this interpretation of the origin of luminescence and electrical conductivity.

[1] J. A. Ghormley and H. A. Levy, J. Phys. Chem. **56**, 548 (1952).

P6. Photoelastic Observation of the Expansion of Alkali Halides on Irradiation. W. PRIMAK, P. H. YUSTER, AND C. J. DELBECQ, *Argonne National Laboratory.*—Alkali halides crystals subjected to a nonuniform irradiation by x-rays or high-energy deuterons were found to become anomalously birefringent. The effect is shown to have been due to the photoelastic birefringence accompanying a nonuniform dilatation. The phenomenon was studied in detail in lithium fluoride. The dilatation due to irradiation is calculated from the measured birefringence with the aid of elasticity theory and is found to be about $2(10^{-4})$ at the end of the range after a bombardment of about 10^{18} d/cm². From a comparison of the absorption with the absorption of other crystals which had been carefully studied, the color center concentration is found to be about $2(10^{19})$/cm³. Thus the dilatation is about equal to the volume of vacancies associated with the color centers. Since an intrinsic property of the body of material has been studied, the effect cannot be attributed to a surface alteration, a criticism which has been leveled [F. Seitz, Revs. Modern Phys. **26**, 74 (1954)] against other determinations of density changes accompanying color center formation.

P7. Elastic Constants and Specific Heat of KCl at Elevated Temperatures.* F. D. ENCK† AND C. B. COOPER, *University of Maryland.*—Measurements of the adiabatic elastic constants of KCl have been made in the region 300° to the melting point (1043°K) by a dynamical method developed by Balamuth. Recently determined values of C_p have been used to obtain the isothermal values of the compressibility. The behavior of the elastic constants and the compressibility are compared with the theoretical predictions of Born and Furth and reasonable agreement is obtained. Values of C_v have been obtained, using values for the coefficient of linear expansion (α_l) measured by Eucken and Dannohl, and they would indicate that there is a drop in C_v above 700°K, but that this drop is considerably less than that found by Eucken in the case of NaCl. There is strong evidence that Eucken's values of α_l are systematically high at temperatures above 700°K; in fact, if the high temperature values of α_l are discarded in favor of an extrapolation from low temperature results, the Dulong-Petit law is valid up to the melting point.

* Supported by the Office of Naval Research.
† Now at Franklin and Marshall College.

P8. Thermal Ionization of Interstitials in Cubic Zinc Sulfide. H. D. VASILEFF, *Sylvania Electric Products Inc.*—The theory[1] of thermal ionization of impurities in polar crystals is applied to interstitials in cubic zinc sulfide. The interaction energy of the trapped electron with the optical vibrational modes is included in the electronic wave equation and the normal coordinate dependence of the electronic wave function and energy is determined through Simpson's[2] method. This leads to an evaluation of the displacement constant c and the configurational constant S occurring in the theory. The numerical evaluation of the frequency factor indicates that it has the form $s(E,T)$ at moderately high temperatures T but depends only on the trap depth E at low temperatures. For interstitials in cubic ZnS, $E=0.61$ ev, $S=1.2$, $s(E,320°\text{K})=10^{3.6}$ sec^{-1}, as deduced from an effective ionic charge of $e^*=0.5e$ for the lattice. These results are in reasonable agreement with experiment.

[1] H. D. Vasileff, Phys. Rev. **95**, 618 (1954).
[2] J. H. Simpson, Proc. Roy. Soc. (London) **A197**, 269 (1949).

P9. Photoconductivity and Photodesorption in Zinc Oxide.* DAVID B. MEDVED.† *University of Pennsylvania.*—Conductivity and photoconductivity processes in zinc oxide have been studied as functions of light intensity, pressure, and temperature. Most of the experiments were performed on very thin samples of sintered zinc oxide. The results are in agreement with the theory of chemisorption and conductivity developed by Miller,[1] Morrison,[2] and Melnick.[3] These experiments show that: (1) the rise of the photoconductivity in thin samples reaches saturation in several minutes or seconds (dependent on incident intensity) instead of increasing indefinitely. (2) The rates of rise and decay show that the kinetics involve an expression of the Elovich form $-(dn/dt)=ae^{bn}$. (3) The variation of the saturation values with intensity follows the logarithmic law developed by Melnick from considerations of the Elovich equation for the rate of chemical adsorption. (4) Measurements of pressure as a function of time in the range of 10^{-6} mm of Hg indicate that the incident light causes a photodesorption of the gas from the surface concomitant with the photoconductivity.

* Supported in part by contract with U.S.A.F.
† Now at Convair, San Diego, California.
[1] P. H. Miller and S. R. Morrison, Tech. Rep. No. 5, N6-onr-24914, August 6, 1952.
[2] S. R. Morrison, Tech. Rep. No. 4, N6-onr-24914.
[3] D. A. Melnick, Bull. Am. Phys. Soc. **29**, No. 3, 40, Paper X5 (March 18, 1954).

P10. Photoconductivity of Pyrolytic Layers of Boron.* C. H. HAYN AND VINCENT P. JACOBSMEYER, *Saint Louis University.*—Layers of elementary boron were deposited on tantalum ribbons at 807°C, 1060°C, 1260°C, 1377°C, and 1500°C by the pyrolysis of diborane gas. The activation energy as a function of deposition temperature was investigated by means of photoconductive measurements. For these studies evacuated Pyrex tubes, provided with quartz windows, were used. The boron sample was centered in the tube. Contact was made to the boron surface by two tungsten probes under pressure. Radiation from a G.E. tungsten projection lamp passed through a monochromator was the source of illumination. The activation energy was determined from the wavelength corresponding to half-maximum on the normalized photosensitivity curve. The following results were obtained for the five samples of boron: 0.75 ev for the 807°C sample, 1.66 ev for the60°C10 sample, 1.28 ev for the 1260°C sample, 0.81 ev for the 1377°C sample and 1.50 ev for the 1500°C sample. Comparing these results with data obtained from photoemission studies, it is found that the two samples having the highest activation energies are those which have the larger work functions. X-ray studies showed sharp diffraction lines for the 1060°C and 1500°C samples, while the pattern for the region around 1200°C was very diffuse.

* Supported by the National Science Foundation.

P11. Photoconductivity in Para-Terphenyl Single Crystals.* G. J. GOLDSMITH AND D. E. HILL, *Purdue University.*—The photoconductivity of terphenyl single crystals was investigated. One observes a strong absorption edge at 3400 A with a structureless band extending to the limit of observation, 2000 A. Photoconductivity was found to be present within this absorption band with a threshold corresponding to that of the absorption edge. Photocurrents up to about two orders of magnitude greater than the dark current are observed with the light sources available. The photocurrent is proportional to the light intensity. A sample illuminated perpendicularly to the field shows saturation of photocurrent. Illumination parallel to the field does not produce photocurrent saturation. The current increased far more rapidly when the positive electrode was illuminated than when the illuminated electrode was negative: predominant hole conduction. The photoconductivity increases more slowly with temperature than does the dark conductivity (see preceding abstract) giving an activation energy of the order of 0.2 ev.

* This work supported in part by a Motorola Research grant.

P12. Dark Conduction in Para-Terphenyl Single Crystals.* D. E. HILL AND G. J. GOLDSMITH, *Purdue University.*—Single crystals of para-terphenyl were prepared by growth in vacuum from the melt. Samples free from visible imperfections were selected and silver paste electrodes applied to the ends perpendicular to the cleavage faces. The samples were mounted in a specially designed chamber provided with a vacuum jacket and facilities for controlling the temperature. The conductivity as a function of temperature was measured using a vibrating reed electrometer as the detection device. It was found that the conductivity σ varied exponentially with reciprocal temperature with an activation energy $\epsilon = 1.2$ ev assuming intrinsic semiconduction.

$$(\sigma = \sigma_0 e^{-\epsilon/2kT}).$$

The field dependence of the current was linear up to fields of about 1000 v/cm and increased at higher fields. The resistivity at low fields at room temperature is 10^{-14} ohm-cm. A waiting period of about two hours after application of the field was necessary to reach steady-state currents at room temperature. These results are consistent with those found by others for similar organic compounds containing conjugated bonding.

* This work supported in part by a Motorola Research grant.

[1] See, e.g., Eley, Parfitt, Perry, and Taysum, Trans. Faraday Soc. 49, 79 (1953).

P13. Time-Average Light Output from Electroluminescent Phosphors. S. NUDELMAN* AND F. MATOSSI, *U. S. Naval Ordnance Laboratory.*—The time-average light output from cubic and hexagonal ZnS:Cu and Zn(S,Se):Cu electroluminescent phosphors has been investigated as a function of field strength, frequency, and time using sinusoidal and square wave field shapes. All observations were made with appropriate filters to determine the field influence on the green and blue emission bands independently. In general, the time-average light output in both bands grows with frequency up to 20 000 cps, the limit of our measurements. However, a phosphor with a slow natural decay of the green band shows a plateau-like region between 1000 to 4000 cps for the green light output. The field strength dependence follows a power law, with exponents ranging from 4 to 8. At low frequencies, square waves produce a greater light output than sine waves of the same peak to peak voltage. Fatigue measurements at 5000 cps indicated that the light output dropped from 25 to 75 percent of its starting value within a 24 hour period. The light output decreased according to a power law over most of this time.

* Also at the University of Maryland.

P14. Electroluminescence Excited with Short Field Pulses. F. MATOSSI AND S. NUDELMAN,* *U. S. Naval Ordnance Laboratory.*—Repetitious field pulses with pulse times from 2500 to 40 microseconds duration were applied to several electroluminescent phosphors. The slopes of the decay curves for both the green and blue luminescence bands become steeper as the pulse duration decreases. The heights of the luminescence peaks excited at the leading and the trailing edges of the pulses also depend on the pulse duration. In this respect, bands with fast and with slow natural decay behave differently. The results are interpreted as confirming previous conclusions about the influence on the decay curves of polarization charges piling up near the electrodes. For short pulses, these charges do not have time to accumulate. This tends to make the slopes approach the fast natural decay of some bands (blue band of a Sylvania cell). For other bands (green band of Sylvania cell), the decreased number of filled traps also tends to make the decay faster for short excitation pulses.

* Also at the University of Maryland.

P15. Electroluminescence in ZnS Single Crystals. D. R. FRANKL, *Sylvania Electric Products Inc.*—Watson *et al.*[1] have shown that 60 cycle half-wave voltage excitation of electroluminescent ZnS single crystals results in emission having two major peaks per cycle. The spectral distributions and absolute intensities of these peaks have been measured by means of a calibrated photomultiplier and a series of interference filters. The two peaks have essentially the same spectrum, a broad peak at about 4500 A, and have intensities of the order of 10^{12} photons/sec in the brightest crystals at average field strengths of the order of 10 kv/cm. The crystal current is almost purely conductive, and is nearly exponential with voltage. The in-phase emission intensity is essentially a function of the current alone.

[1] Watson, Dropkin, and Halpin, Phys. Rev. 94, 777(A) (1954).

SATURDAY MORNING AT 9:30

Kent 106

(H. A. BETHE presiding)

Mesons

Q1. Photomeson Production from Hydrogen. BERNARD T. FELD, *M.I.T.**—The available data on charged and neutral photomeson production from hydrogen, from threshold to ~450-Mev photons, can be fitted on the assumption of *s*- and *p*-wave meson production only. The most reasonable interpretation requires a resonance in the state of ordinary and isotopic spin $\frac{3}{2}$, positive parity, at a photon energy of ~350 Mev. The observed angular distributions require appreciable electric quadrupole photon absorption, in addition to magnetic dipole absorption, in this state, especially at the higher energies.

The (complex) amplitudes for the absorption processes involved exhibit reasonable dependence on photon energy, with the exception of the phase of the electric dipole absorption which appears to be anomalously large near threshold. An alternative "Yang-type" solution cannot be excluded on the basis of the present data, but the ambiguity could be resolved by the observation of the state of polarization of the recoil protons from the neutral photomeson production.

* Work done as Guggenheim Fellow and Visiting Professor at the Institute of Physics, University of Rome, Italy.

Q2. Pion Photoproduction Ratios. D. C. PEASLEE, *Purdue University.*—Measurements[1] of the pion production ratio $\rho=\pi^+/\pi^-$ from nuclear bombardment by 300-Mev bremsstrahlung have been interpreted in terms of (i) Coulomb field effects; (ii) limitations on the final states of the recoil nucleon; (iii) intrinsic reduction of $p(\gamma,\pi^+)n$ relative to $n(\gamma,\pi^-)p$; (iv) variation of the effective neutron to proton ratio at the nuclear surface. Simple formulas fitted to the data indicate that (i) and (ii) are appreciable for the elements studied; a rough value of $\rho_0\approx 0.9$ results for (iii); no information on (iv) is obtainable from the crude interpretation. A plot of total yields corrected for (i) and (ii) indicates considerable transparency for light nuclei, going over to the usual $A^{\frac{1}{3}}$ law for $A>16$.

[1] Voss, Palfrey, and Haxby, Bull. Am. Phys. Soc. **29** (5), 19 (1954); R. M. Littauer and D. Walker, Phys. Rev. **86**, 838 (1952).

Q3. Photoproduction of π^0 Mesons in Hydrogen.* L. J. KOESTER, *University of Illinois.*—The photoproduction of π^0 mesons at low energies has been investigated by observing the recoil protons from a 2.2-cm diameter liquid hydrogen target. The proton detectors were stacked emulsions placed at an angle of 17.5° with the x-ray beam. Proton energies were obtained by range measurements. The betatron energy was 225 Mev. On the basis of about half of the observed tracks, the differential cross sections obtained for photoproduction of π^0 mesons at a center-of-mass angle of 133°±8° are, in units of 10^{-30} cm²/steradian:

1.3±0.3 at 183±4.5 Mev, 1.4±0.3 at 192±4.5 Mev,
1.7±0.4 at 200.5±4 Mev, and 2.1±0.5 at 208±3.5 Mev.

The energy dependence of the differential cross section at 135° may, in principle, be used together with the total cross section to distinguish between a pure P-wave $(5-3\cos^2\theta)$ angular distribution and an S-wave, P-wave mixture $(A_0+A_1\cos\theta+A_2\cos^2\theta)$. If, however, $A_2\approx 4A_1$, this discrimination is not feasible. The relation of these results to those of other laboratories will be discussed.

* Supported in part by the Office of Naval Research and the U. S. Atomic Energy Commission.

Q4. Elastic Photoproduction of π^0 Mesons for Helium.* E. L. GOLDWASSER, L. J. KOESTER, AND F. E. MILLS, *University of Illinois.*—The activation curve for the photoproduction of π^0 mesons from liquid helium has been observed. Detection of the π^0 mesons was accomplished by observing the π^0 decay γ-ray pairs in two γ-ray telescopes. The betatron maximum energy was varied from 150 to 190 Mev. Conservation of energy requires that all π^0 mesons produced by photons with energies between 138 and 158 Mev arise from the elastic process, $h\nu+\mathrm{He}^4\rightarrow\pi^0+\mathrm{He}^4$. Results of this experiment clearly indicate the production of π^0 mesons by photons in this energy bin. Production of S-wave mesons through this process is forbidden by angular momentum selection rules. Spin flipping interactions are forbidden by the Pauli principle. Therefore P-wave production can arise only through magnetic dipole absorption. For these reasons, a suppression of the cross section for single nucleon interactions is expected. However, a comparison of activation curves for helium and hydrogen indicates roughly equal cross sections per nucleon. A contribution from cooperative interactions of the four nucleons of helium could compensate for the expected suppression. A measurement of this cooperative contribution gives information about the form factor for the nucleons in the helium nucleus.

* Supported in part by the Office of Naval Research and the U. S. Atomic Energy Commission.

Q5. The Scattering of π Mesons by Nuclei. LEONARD S. KISSLINGER.*—The elastic scattering of π mesons by nuclei was calculated using the generalized optical model. This model[1,2] has the simplicity of the old optical model in that the scattering can be described by a potential independent of the individual coordinates of the nucleons and depending only on the coordinates of the scattered particle. It is superior to the old optical model in that the potential describing the elastic scattering depends not only on the nucleon density but also on its gradient. The predominant p-wave dependence of the meson-nucleon scattering necessitates the inclusion of the gradient of the density in the real part of the potential. As is usually done the imaginary part of the potential is assumed to be proportional to the nucleon density. Using a Gaussian density distribution, the scattering of 62-Mev mesons by C^{12} was calculated, the results obtained being in reasonable agreement with experiment.

* National Science Foundation Predoctoral Fellow.
[1] Kenneth W. Watson, Phys. Rev. **89**, 578 (1953).
[2] N. C. Francis and K. W. Watson, Phys. Rev. **92**, 291 (1953).
[3] Byfield, Kessler, and Lederman, Phys. Rev. **86**, 17 (1952).

Q6. Differential Cross Sections for Pion-Proton Scattering at 150 and 170 Mev.* F. FEINER, J. ASHKIN, J. P. BLASER, AND M. O. STERN, *Carnegie Institute of Technology.*—Measurements using counter techniques have been made on the angular distribution of 150-Mev π^+ and π^- mesons scattered by liquid hydrogen. Both the elastic and charge exchange reactions have been observed. The distributions were measured at eight angles ranging from 30° to 157° in the laboratory system. Phase shifts resulting from analysis of the data, as well as conclusions concerning the importance of d-wave scattering will be presented. Preliminary data on similar measurements for 170-Mev π^+ and π^- mesons will also be given.

* Supported in part by the U. S. Atomic Energy Commission.

Q7. Scattering of 165-Mev Pions by Protons.* M. GLICKSMAN AND H. L. ANDERSON, *The University of Chicago.*—The elastic scattering of positive pions, and the elastic and charge exchange scattering of negative pions in liquid hydrogen were measured at 165 Mev. The differential cross sections for these processes were measured, and in addition, the total cross sections were determined from transmission measurements. For π^+ the transmission measurements gave 188.2±5.4 mb, while the integral of the differential measurements was 188.6±11.5 mb. For π^- the integral of the differential elastic scattering cross sections was 22.5±1.5 mb, while for the charge exchange process the integral was 42.5±1.3 mb. From this the total cross section for π^- including the radiative capture process was found to be 65.7±2.0 mb. The total cross section determined from the transmission measurement for π^- was found to be 67.5±1.5 mb. In our preliminary analysis of the data three distinct sets of phase shifts were found with the values:

	Set No. 1	Set No. 2	Set No. 3
α_1	9°	9°	6°
α_3	−18°	−17°	−37°
α_{11}	−7°	−5°	11°
α_{13}	2°	1°	−7°
α_{31}	1°	97°	68°
α_{33}	63°	34°	26°

* Research supported by a joint program of the Office of Naval Research and the U. S. Atomic Energy Commission.

Q8. Scattering of 23-Mev Positive Pions on Hydrogen. JAY OREAR, *Columbia University.*—The 90-Mev π^+ beam of the Chicago cyclotron was slowed down to a mean energy of

25 Mev by absorbers placed 50 inches in front of the 45° deflecting magnet. G5 plates were placed at the conjugate focus, 50 inches behind the magnet. As of September 24, four scatterings on hydrogen had been found with barycentric angles of 79°, 83°, 89°, and 106°. This corresponds to a total cross section of about 4 mb for scatterings greater than 50°. A value of $-2.1°$ is obtained for α_3 by using the recipe ($\alpha_{33}=0.235\eta^3$).[1] For $(-1°<\alpha_3<4°)$, the cross section would be less than 2.4 mb. Independent evidence that α_3 cannot be positive (or near zero) at 23 Mev is the observed angular distribution. Any positive value (or negative value down to $-1°$) of α_3 gives a strong backward scattering which would make the four angles obtained here highly improbable. As α_3 becomes more negative the Coulomb interference changes from destructive to constructive which greatly increases the forward scattering. The proposal[1] that $\alpha_3=-0.11\eta$ is a good fit to all the low-energy data is supported by these preliminary results.

[1] J. Orear, Phys. Rev. **96**, 176 (1954).

Q9. Scattering of 195-Mev Pions by Deuterium.* W. SKOLNIK, *University of Chicago.*—A preliminary measurement of the scattering cross section for 195-Mev negative pions has been made. A liquid deuterium target was placed in an external 195±5 Mev pion beam from the Chicago synchrocyclotron. The attenuation of the beam by the deuterium was measured with four scintillation counters in coincidence. Two small counters were placed before the target and two large counters behind. Sufficient copper absorber was used between the final two counters to cut out proton and deuteron recoils. The attenuation measurement yielded a total cross section of 212±8 mb. Preliminary measurements on the differential cross sections for pions either elastically or inelastically scattered were made and will be described in detail.

* Research supported by a joint program of the Office of Naval Research and the U. S. Atomic Energy Commission.

Q10. Interaction of 46 Mev π^+ Mesons in Deuterium.* D. BODANSKY AND A. M. SACHS, *Columbia University.*—Elastic and inelastic scattering and the absorption of 46+5 Mev π^+ mesons in liquid deuterium have been studied. Out-coming particles are detected at several angles, and their mass and energy are determined by pulse-height analysis in the plastic scintillators of the detecting telescope. Mesons of energy greater than 23 Mev and protons of energy greater than 50 Mev are counted. Pulse heights in three counters are measured for each event by photographing an oscilloscope trace. For events with pulse heights in relevant regions, the ratio of events from the empty target to those from deuterium is 0.1 at 90 deg, 2 at 45 deg, and increases rapidly at smaller laboratory angles. Differential cross sections for all scattering where the scattered meson has energy greater than 23 Mev are 0.6±0.2 mb/sterad, 0.7±0.1 mb/sterad, and 1.15±0.2 mb/sterad in the laboratory system for scattering angles of 45, 90, and 135 degrees respectively. Energy distributions of the scattered mesons are obtained. For the absorption process, $\pi^+ + D \rightarrow P + P$, differential cross section measurements at five angles are consistent with a distribution of $0.3+1.5\cos^2\theta$ mg/sterad in the center-of-mass system.

* Research supported by joint contract of the Office of Naval Research and the U. S. Atomic Energy Commission.

Q11. Interactions of 1.5-Bev π^- Mesons.* W. D. WALKER† AND J. CRUSSARD, *University of Rochester.*—Further studies[1,2] have been made on $\pi^- - P$ and $\pi^- - N$ interactions at 1.5 Bev. Approximately 25 percent of the $\pi^- - P$ collisions seem to be elastic. A considerable fraction of these elastic scatterings seems to be a diffraction scattering produced by the absorption of the incoming π^- beam in inelastic processes. There is a large angle tail on the angular distribution of the elastically scattered π's which is not accountable as a diffraction scattering. From the angular distribution of the elastically scattered π's and the ratio of inelastic to elastic collisions it seems necessary to suppose that a considerable number of the inelastic collisions occur with impact parameters of 10^{-13} cm or more. This outside edge of the nucleon is rather transparent to the π's however. The inelastic collisions usually result in the production of a single additional π. The angular distributions of the products do not seem to be consistent with either a statistical model or an excited nucleon[3] model of meson production.

* Supported by the U. S. Atomic Energy Commission.
† Now at Physics Department, University of Wisconsin.
[1] Crussard, Walker, and Koshiba, Phys. Rev. **94**, 736 (1954).
[2] Walker, Crussard, and Koshiba, Phys. Rev. **95**, 852 (1954).
[3] S. J. Lindenbaum and L. C. L. Yuan, Bull. Am. Phys. Soc. **29**, No. 4, 50 (1954).

Q12. Search for Improbable Meson Decays.* S. LOKANATHAN AND J. STEINBERGER, *Columbia University.*—We have searched unsuccessfully for two possible meson decay processes with apparatus considerably more sensitive than has heretofore been used. In order to detect the process $\mu^+ \rightarrow e^+ + \gamma$, π^+ mesons monitored by a counter telescope were allowed to come to rest in a carbon target. Two detectors are placed at opposite sides of the target, one sensitive to the 50-Mev electrons, the other made sensitive to the γ rays by means of $\frac{1}{4}$ in. of Pb converter. The system is calibrated by means of electrons from normal μ decay. We place an upper limit of 2×10^{-5} for the fraction of μ mesons which decay in this way. In order to detect the electrons in the process $\pi^+ \rightarrow e^+ + \nu$, and to separate them from the accompanying μ-decay electrons, positive pions are stopped in a thin polyethylene target. With a 4-counter telescope, we measure the absorption spectrum in polyethylene of all electrons emerging from the target, as well as that fraction which comes not later than 5×10^{-8} sec following a pulse in a telescope in the incident beam. Comparison of the two absorption curves makes it possible to distinguish the 70-Mev $\pi^+ - e^+$ electrons from the μ-decay spectrum. We find that the fraction of π's decaying in this fashion is less than 5×10^{-5}.

* This work was performed under the joint program of the Office of Naval Research and the U. S. Atomic Energy Commission.

SATURDAY MORNING AT 9:30

Eckhart 133

(JOHN MARSHALL presiding)

Reactions of Transmutation, I

R1. Search for Excited States of Be^8. R. E. HOLLAND, D. R. INGLIS, AND F. P. MOORING, *Argonne National Laboratory.*—In an attempt to verify the existence of some of the reported extra states of the simple nucleus Be^8, further[1] momentum analyses have been made of two reactions under various conditions. The reaction $B^{10}(d,\alpha)Be^8$ has been ob-

served with a solid-backed target at several angles between 60° and 120° and bombarding energies between 2 and 3.2 Mev. The reaction B^{11} $(p,\alpha)Be^8$ has been observed under similar conditions and also with a thin-backed natural *B* target near the forward direction. In spite of rather good resolution and statistics, no evidence has been found for any excited state except the broad 3-Mev state up to about 10 Mev. At an energy corresponding in $B^{11}(p,\alpha)$ to 7 Mev in Be^8 a sharp alpha group is found which has been shown by comparison with a B^{10} target to arise from an intense reaction in the B^{10} content of the natural *B* target.

[1] R. Malm and D. R. Inglis, Phys. Rev. **92**, 1326 (1953).

R2. The $B^{11}(n,\alpha)Li^8(\beta)Be^{8*}(2\alpha)$ Reaction from 12 to 20 Mev.* G. M. Frye, Jr., A. H. Armstrong, and L. Rosen, *Los Alamos Scientific Laboratory.*—Ilford 200-μ C-2 plates loaded with B^{11} were exposed to monoenergetic neutrons produced at various angles to the 3.5-Mev deuteron beam of the large Los Alamos electrostatic accelerator incident upon a tritium gas target. The plates were then scanned for the distinctive "hammer stars" resulting from the reaction $B^{11}(n,\alpha)Li^8(\beta)Be^{8*}(2\alpha)$. A total of 442 such events were found which satisfied the requirements of conservation of energy and momentum. Using Ilford's data for the B^{11} loading, one obtains the following cross sections: $E_n=12.5$ Mev, $\sigma=29\pm7$ mb; 13.0 Mev, 42 ± 8 mb; 14.7 Mev, 30 ± 6 mb; 15.4 Mev, 41 ± 8 mb; 16.8 Mev, 21 ± 5 mb; 17.5 Mev, 26 ± 5 mb; 18.8 Mev, 21 ± 4 mb; 19.7 Mev, 16 ± 3 mb; 19.9 Mev, 15 ± 3 mb. These cross sections do not include the contribution from the Be^8 ground state, as its disintegration energy of 0.1 Mev is not enough to given perceptible alpha tracks. In essentially all the cases Li^8 was left either in the ground state or in the first excited state at 1 Mev. The values for the excitation energy of Be^8 were similar to those obtained previously,[1] showing the broad level at 3 Mev and possibly additional levels at 4.3 and 7.4 Mev.

* Work performed under the auspices of the U. S. Atomic Energy Commission.
[1] F. C. Gilbert, Phys. Rev. **93**, 499 (1954).

R3. Alpha-Alpha Angular Correlation in $B^{11}(p,\alpha\alpha)He^4$.* E. H. Geer,† E. B. Nelson, and E. J. Wolicki,† *State University of Iowa.*—The angular correlation was measured at proton energies of 163 and 290 kev with thin targets on thin backings, in a plane normal to the proton beam. The shape of the 2.9-Mev level was estimated from the alpha energy spectrum,[1] and the theoretical correlation functions were integrated over the level. The experimental correlations, expressed in terms of the center-of-mass angle, were, for 163 kev, $W=1-1.97\cos^2\theta+1.28\cos^4\theta$, and, for 290 kev, $W=1+1.62\times\cos^2\theta-1.25\cos^4\theta$. The data at 163 kev are consistent with a spin of 2+ in C^{12} and 2+ but not 0+ in Be^8. The data at 290 kev cannot be explained on the basis of a pure 1−, 2−, or 3+ state in C^{12} but probably result from an interference between the states of 0.67 and 1.4 Mev.

* Supported in part by the U. S. Atomic Energy Commission.
† Now at the Naval Research Laboratory.
[1] W. Whaling (private communication).

R4. Angular Distributions and Excitation Functions of $C^{12}(d,p)$ Reaction. K. W. Jones, M. T. McEllistrem, R. A. Douglas, D. F. Herring, and E. Silverstein, *University of Wisconsin.*—Measurements were conducted in a large (4 ft×5 ft) gas scattering chamber. A gridded ion chamber mounted on a 23 in. rotating arm served as principal detector. Differentially pumped gas targets (C_3H_8 or C_4H_{10}) were used to obtain absolute cross sections good to about 6 percent. Excitation curves for $C^{12}(d,p)C^{13}$ were taken at 25, 83, and 161 degrees from 1.857 to 3.45 Mev and at 54, 125, and 154 degrees from 2.58 to 3.3 Mev. Resonances occurred at 2.05, 2.35, 2.51, (2.67)?, 2.74, (2.92)?, 3.01, and 3.10 Mev. Angular distributions were taken on and off several of the resonances. At $E_d=1.86$ Mev the angular distribution showed a large back angle cross section (21 mb at 145 degrees C.M.) with a small forward angle peak (7 mb) at 25 degrees C.M., which peak corresponds to the first stripping maximum expected on Butler's theory for $l_n=1$. As the energy was increased the forward stripping peak cross section increased and became larger than the back angle peak. The magnitude of the stripping maxima changed markedly when taken on and off observed resonances; constructive and destructive interference of stripping and resonant contributions is indicated.

R5. Energy Spectrum of Photoprotons from Carbon. W. E. Stephens and A. K. Mann, *University of Pennsylvania.*—The photoprotons ejected from a 6 mg per cm² thick carbon foil by 23-Mev bremsstrahlung have been observed in nuclear emulsions. The ranges of 408 protons which entered the emulsions in the proper direction were measured. The proton energy distribution has a peak at 5.5 Mev and a width at half-maximum of about 2.8 Mev. These values confirm the previous determination[1] of the giant resonance in carbon which had been obtained from yield curve data. The width of the proton spectrum is consistent with transitions from a single broad level in C^{12} to the ground state of B^{11} but transitions to the first excited state of B^{11} appear to be inhibited.

* Supported in part by the Air Research and Development Command.
[1] J. Halpern and A. K. Mann, Phys. Rev. **83**, 370 (1951).

R6. *Q* Values for the $O^{17}(d,p)O^{18}$ and $O^{18}(d,p)O^{19}$ Reactions. H. D. Holmgren, T. D. Hanscome, and D. K. Willett, *Naval Research Laboratory.*—The Naval Research Laboratory 60° magnetic spectrograph has been employed to study the energies of the protons emitted from isotopically enriched targets[1] of oxygen bombarded with deuterons from the *NRL* 2-Mev Van de Graaff generator. Targets of both normal and enriched oxygen were studied to identify the proton groups from O^{17} and O^{18}. The energies of the reaction protons were measured for 1.390 and 1.976 Mev incident deuterons at an angle of 90° to the direction of the beam. In addition to the proton groups from O^{16} and carbon, three intense groups and two very weak groups of protons were observed when the enriched oxygen targets were bombarded. The three intense groups were assigned to the $O^{18}(d,p)O^{19}$ reaction with *Q* values 1.735 ± 0.008, 1.641 ± 0.008, and 0.264 ± 0.013 Mev. Since the energies of the two weak groups were considerably higher than the energy expected for the ground-state transition of the $O^{18}(d,p)O^{19}$ reaction, these groups were attributed to the $O^{17}(d,p)O^{18}$ reaction with *Q* values 3.393 ± 0.016 and 3.861 ± 0.016 Mev. The *Q* values for the $O^{18}(d,p)O^{19}$ reaction are in agreement with the work at Minnesota and Cal. Tech.[2] The two proton groups attributed to the $O^{17}(d,p)O^{18}$ reaction indicate levels in O^{18} at 1.977 and 2.445 Mev above the ground state.

[1] We are indebted to A. O. C. Nier for furnishing the enriched oxygen and to the Minnesota Van de Graaff group for helping in preparing the targets.
[2] Stratton, Famularo, Holmgren, and Stuart, Bull. Am. Phys. Soc. **29**, 5 (1954); Thirion, Cohen, and Whaling, Bull. Am. Phys. Soc. **29**, 6 (1954).

R7. Gamma-Ray Thresholds in the $F^{19}(d,n\gamma)Ne^{20}$ Reaction. J. W. Butler, *Naval Research Laboratory.*—When an excited nucleus decays by gamma emission to the ground state following the emission of a neutron at threshold, then the threshold in question may be considered also a "gamma-ray threshold." Two such thresholds have been observed by bombarding a thin target of CaF_2 with deuterons from the NRL 2-Mev Van de Graaff generator, and counting the gamma pulses between 9.7 and 11.9 Mev in a 3-in.×3-in. sodium iodide crystal. There are breaks in the excitation curve at 1.15- and 1.35-Mev bombarding energy indicating levels in Ne^{20} at 11.69 and 11.87 Mev, respectively. Both levels appear to decay to the ground state.

R8. Excitation Functions of Radioactive Products from the Interaction of High-Energy Protons with Lead.* E. BAKER, A. CARETTO, J. CUMMING, G. FRIEDLANDER, J. HUDIS, AND R. WOLFGANG, *Brookhaven National Laboratory.*—Excitation functions of radionuclides produced by proton bombardment of lead between 0.6 and 3 Bev are presented. Yields of isotopes of F, Na, Mg, and P increase rapidly from the order of 10 microbarns at 600 Mev to the order of a millibarn at about 2 Bev. Thus at these high energies production of such light elements—which cannot result from the usual spallation or fission processes—becomes a relatively probable event. In the medium mass region, from Mn to Ba, cross sections of neutron excess isotopes (as produced by 340 Mev Bi fission[1]) remain approximately constant or decrease by about a factor of two with increasing energy. By contrast yields of neutron deficient nuclides increase rapidly until at about 2 Bev they become comparable with those of the neutron excess nuclides. No clearly defined fission peak as appears with Bi at 340 Mev was found with Pb at Bev energies.

* Work performed under the auspices of the U. S. Atomic Energy Commission.

[1] W. F. Biller, UCRL 2067.

SATURDAY MORNING AT 9:30

Cobb 110

(T. H. OSGOOD presiding)

Invited Paper

S1. Ultrasonic Light Modulators for Spectroscopy and the Measurement of Very Short Time Intervals. E. A. HIEDEMANN, *Michigan State College.* (30 min.)

General Physics, I

S2. Intensity Distribution Among Spectral Orders in a Grazing Incidence Spectrograph.* D. E. BEDO AND D. H. TOMBOULIAN, *Cornell University.*—Relative intensity measurements in soft x-ray continuous spectra emitted by relativistic electrons or x-ray targets require a knowledge of the distribution of intensity among various spectral orders. An investigation was undertaken for the comparison of the beam intensity in a given order with that of the incident beam. The narrow emission bands of C, Be, and Al were used as sources. For the particular spectrograph equipped with a lightly ruled grating (grazing angle of incidence fixed at 4.64°) theoretical considerations[1] predict the enhancement of spectral intensity in orders zero, one, and two at $\lambda=35$, 55, and 90 A, respectively. Furthermore the fraction of the incident intensity diffracted into the first order should vary from 0.5 percent at 60 A to 9 percent at 200 A; in the second order from 1 percent at 100 A to 6 percent at 200 A. Intensity ratios based on the synchrotron continuum, emission bands, and line spectra compare favorably with the calculated values.

* Supported by the Office of Ordnance Research, U. S. Army.

[1] Calculations by Dr. G. C. Sprague (to be published).

S3. The Determination of Polydisperse Aerosol Size Distributions from the Analysis of Light Scattering Data.* T. L. GILBERT, *Armour Research Foundation of Illinois Institute of Technology.*—The problem of calculating the size distribution, $n(r)$, of a polydisperse aerosol from the light scattered at various angles, $I(\cos\theta)$, or the extinction at various wavelengths, $I(2\pi/\lambda)$, is equivalent to solving an integral equation of the first kind, $I(x)=\int K(x,r)n(r)dr$, where $K(x,r)$ is the scattered light or extinction for a monodisperse aerosol with particles of radius r. If the function, $I(x)$, obtained from experimental measurements is used, this equation will, in general, have no solution because of experimental errors. As a consequence, previously used methods, which attempt to approximate this nonexistent solution, are completely unreliable. An exact solution of a modified equation, obtained by using a kernel derived from the bilinear expansion of the exact kernel by discarding all but a finite number of terms, will exist. A new approximate method will be presented for calculating that size distribution which represents the optimum compromise between experimental errors and the error introduced by using the approximate kernel.

* Work supported by Geophysics Research Directorate of the Air Force Cambridge Research Center.

S4. A Mass Spectrometric Study of Gaseous Species in the Si–SiO_2 System. RICHARD F. PORTER AND PAUL SCHISSEL, *University of Chicago,* AND MARK G. INGHRAM, *University of Chicago, and Argonne National Laboratory.*—A combination of mass spectrometric and Knudsen effusion techniques have been employed to study the molecular composition of the equilibrium vapor over solid SiO_2 and Si–SiO_2 mixtures at temperatures between 1500°K and 1950°K. Gaseous molecules effusing from the Knudsen cell enter directly into the ionization chamber of the mass spectrometer.[1] Ion currents of SiO^+ and SiO_2^+ were observed. Appearance potentials for the two species are 10.8 ± 0.5 and 11.7 ± 0.5 ev, respectively. A peak at mass 88 is tentatively ascribed to $Si_2O_2^+$. The low voltages required to produce SiO_2^+ together with temperature dependence measurements show that SiO_2^+ must be formed by direct ionization of effusing SiO_2 gas and cannot be formed in a secondary mechanism involving SiO^+. With the calculated partial pressure of SiO inside the Knudsen cell and estimating relative ionization cross sections of 1 and 1.5 for SiO^+ and SiO_2^+, respectively, we obtain the partial pressure of SiO_2 from the ion current ratio of SiO_2^+ to SiO^+. With an estimated uncertainty of within a factor of three, the partial pressure of SiO_2 gas is 5×10^{-7} atmos over SiO_2 solid at $T=1925$°K. From the temperature dependence curve for SiO_2, we obtain for SiO_2 (quartz) = SiO_2 (gas); $\Delta H_{298}^\circ=130\pm7$ kcal.

[1] W. A. Chupka and M. G. Inghram (to be published).

S5. Equilibrium Charge Distribution of Energetic Nitrogen Ions. H. L. REYNOLDS, L. D. WYLY,* AND A. ZUCKER, *Oak Ridge National Laboratory.*—The equilibrium charge distribution of nitrogen ions in Formvar was measured as a function of the nitrogen energy from 6 to 26 Mev. The fringing magnetic field of the cyclotron was used to separate the charge groups resulting from the passage of the nitrogen ion beam through Formvar foils of sufficient thickness to insure an equilibrium charge distribution. At 26 Mev, 41 percent of the

ions are completely stripped while at 10 Mev 3.5 percent are completely stripped. The ratio of the loss to capture cross sections for the first two electrons is proportional to $V^{3.9}$. The ratio of the loss to capture ratio for the third electron is proportional to $V^{2.7}$. The capture and loss cross sections for the first electron are equal at an energy of 28.2 Mev, and for the second electron at 13.3 Mev.

* Permanent address: School of Physics, Georgia Institute of Technology Atlanta, Georgia.

S6. Measurement of the Ionization Yield of Low Energy Ions in a Gas.* RALPH A. LOWRY AND GLENN H. MILLER, *Iowa State College.*—A large cylindrical ionization chamber has been used to study the ionization yield of 50 to 250 kev ions in various gases. The ions are selected from the kevatron beam by a magnetic and electrostatic analyzer and enter the chamber by means of a 0.004 inch diameter open window. A differential pumping system permits pressures up to 10 mm Hg to be maintained in the chamber. The chamber is alternately operated as a proportional counter and an ionization chamber to measure the rate with which the primary ions enter the chamber and the ionization produced by them, respectively. A detailed description of the apparatus and measuring technique will be given. The results for protons in nitrogen gas will be presented.

*Work was performed in the Ames Laboratory of the U. S. Atomic Energy Commission.

S7. Specific Heat of He^3-He^4 Solutions. P. J. PRICE AND P. B. LINHART, *IBM Watson Laboratory.*—The effect of small amounts of dissolved He^3 isotope on the specific heat of liquid helium is of interest to the study of quantum liquids. No direct measurements have been reported, but the molar specific heat C may be calculated from measurements on the saturated vapor by means of a thermodynamic formula. For small concentrations X of He^3

$$C(X,T)=(1-X)C(0,T)+RXf(T)+O(X^2),$$

where

$$f=5/2-Td^2/dT^2[T\ln(\partial p_3^*/\partial X)_{X=0}].$$

We have calculated f from 1.2° to the lambda point, using values of the partial fugacity $p_3^*(X,T)$ calculated from Sommers' data.[1] f exceeds the "ideal gas value" $\frac{5}{2}$ appreciably at 1.6°, and rises steeply to more than 30 near the lambda point. The interpretation of this result will be discussed.

[1] H. S. Sommers, Jr., Phys. Rev. **88**, 113 (1952).

S8. The Mechanism of Photochemical Reactions Catalyzed by Red-Mercuric Sulfide. L. L. GROSSWEINER AND S. GORDON, *Argonne National Laboratory.*—Visible light irradiation of suspended red-HgS in acid solutions of ferrous-ferric sulfate will induce oxidation in the presence of oxygen and reduction in oxygen-free systems.[1] Continued work shows that similar irradiations in distilled water containing oxygen will induce hydrogen peroxide formation. The initial yields are linear with absorbed light intensity, while the maximum yields are limited by a photoactivated back-reaction which destroys hydrogen peroxide. It is consistent with these and the earlier results to assume that the primary products are H and OH formed respectively from the capture of conduction electrons from excited HgS by absorbed hydrogen ions and from the anodic discharge of HgS particles by water. It is believed that the OH recombines to water and oxygen, not hydrogen peroxide. For these primary reactions to be energetically favorable, it is estimated that the energy of an electron in a low conduction level of HgS is about 4 to 5 ev compared to vacuum. The energetics of the over-all photochemical conversion of water and oxygen to hydrogen peroxide depends only on the valence-to-conduction band gap and is exothermic for this system.

[1] L. I. Grossweiner and S. Gordon, J. Chem. Phys. **22**, 1139 (1954).

S9. Calculation of the Compressibility of Polyethylene from the Energy of Interaction between $(-CH_2-)$ Groups. WERNER BRANDT, *E. I. Du Pont de Nemours & Company.*—Polyethylene consists essentially of long $(-CH_2-)$ chains arranged in a partly crystalline structure. The crystalline regions are assumed to be interconnected by chains penetrating regions of lower degrees of order. Considering the interaction of all chains in such an imperfect lattice, a semiempirical potential energy function of molecular interaction is derived under the assumption that each $(-CH_2-)$ group of a chain interacts with each of the surrounding lattice groups according to a Lennard-Jones potential $4\epsilon[(\sigma/r)^{12}-(\sigma/r)^6]$. The intermolecular force constants of a $(-CH_2-)$ group are determined from the density of polyethylene and from the heat of sublimation per $(-CH_2-)$ group at 0°K. They are found to be $\sigma=4.19$A and $\epsilon/k=38.4$°K. The volume dependence of the potential function leads to the compressibility of polyethylene and its dependence on pressure. The theoretical results are in agreement with experimental data[1-3] up to 40 000 kg/cm².

[1] P. W. Bridgman, Proc. Am. Acad. Arts Sci. **76**, 71 (1948).
[2] W. Parks and R. B. Richards, Trans. Faraday Soc. **45**, 203 (1949).
[3] C. E. Weir, J. Research Natl. Bur. Standards **46**, 207 (1951).

S10. Direct Production of Spectroscopic Specimens from Single Crystals by Controlled Growth from a Vapor; Infrared Absorption Anisotropy and Induced Molecular Motion in a Single Crystal of Benzene. SOLOMON ZWERDLING, *Lincoln Laboratory, M.I.T.*, AND RALPH S. HALFORD, *Columbia University.*—A method has been developed for growing from the vapor phase, thin section single crystals of very low melting substances for use in polarized infrared spectrometry. The method consists of evacuating a special cell, developing a thermal gradient across it at low temperature, and controlling vapor admittance by capillary flow until the critical nucleation pressure is reached. Following nucleation, growth is completed below the critical pressure. A single crystal of benzene 100μ thick and 300 mm² area was grown in 15 hours. The extinction axes were determined between crossed polaroids using visible light. Polarized and unpolarized infrared spectra were measured from 650 to 4000 cm^{-1}. Spectra interpretation was based upon D_{6h} point symmetry for benzene vapor, C_i site symmetry and V_h^{15} factor group symmetry for the unit cell containing 4 molecules. Since crystalline benzene is biaxial orthorhombic, the interpretation is simplified. The results indicated that incident radiation was parallel to the b axis, and the a and c axes were parallel to the extinction axes. Absorption due to "intrinsic" moments and to crystal "induced" moments were analyzed in different orders of approximation. Splitting of frequencies under the "static" crystal field and under site-factor group correlations were examined, as well as several additional spectral features.

S11. Normal Coordinate Treatments and Calculated Thermodynamic Properties of Phosphoryl Chloride, Phosphoryl Fluoride, Thiophosphoryl Chloride, and Thiophosphoryl Fluoride.* JOSEPH S. ZIOMEK, EDWARD A. PIOTROWSKI, AND EDWARD N. WALSH, *De Paul University.*—The infrared and Raman spectra for phosphoryl chloride, phosphoryl fluoride, thiophosphoryl chloride, and thiophosphoryl fluoride were collected and examined for the most probable values for the wave numbers, intensities, and depolarization factors. The values adopted for the fundamentals are as follows: for $POCl_3$, 192.85, 267.39, 337.44, 486.24, 581.2, and 1289.9 K; for POF_3, 337, 476, 483, 875, 982, and 1395 K; for $PSCl_3$, 172, 247, 247, 430, 538, and 753 K; and for PSF_3, 276, 402, 440, 695, 874, and 940 K. Also normal coordinate treatments on the basis of the most probable model C_{3v} were conducted for these same molecules. These treatments gave the above listed wave numbers as those of the fundamentals.

Moreover, the F matrix elements obtained for these molecules were determined in such a manner that those potential constants for the PCl_3 group had nearly the same values in both $POCl_3$ and $PSCl_3$, those for the PF_3 group had nearly the same values in both POF_3 and PSF_3, the one for the PO group had nearly the same value in both $POCl_3$ and POF_3, and the one for the PS group had nearly the same value in both PSF_3 and $PSCl_3$. Finally, the above spectral data were used to calculate the values of the thermodynamic properties for these substances up to a rigid rotator harmonic oscillator approximation for temperatures from 200°K to 1000°K.

* Supported by the Office of Ordnance Research.

SATURDAY MORNING AT 9:30

Mandel Hall

(JOHN BARDEEN presiding)

Symposium of the Division of Solid-State Physics

T1. Recent Experiments on High-Pressure Phenomena at Chicago. A. W. LAWSON, *University of Chicago.* (30 min.)

T2. P-V Isotherms of 10 000 Atmospheres st 4.2°K for Four Alkali Metals and Some Condensed Gases. C. A. SWENSON, *M.I.T.* (30 min.)

T3. Properties of Germanium and Silicon at High Pressures. H. BROOKS, *Harvard University.* (30 min.)

T4. Effect of Hydrostatic Pressure on the Superconducting Transition. M. D. FISKE, *General Electric Research Laboratory.* (30 min.)

SATURDAY MORNING AT 9:30

Judd 126

(K. M. WATSON presiding)

Invited Papers in Theoretical Physics

U1. Neutron-Proton Mass Difference and Structure of the Nucleon. R. G. SACHS, *University of Wisconsin.* (30 min.)

U2. Nuclear Saturation and the Independent-Particle Model of the Nucleus. K. A. BRUECKNER, *Indiana University.* (30 min.)

U3. Calculations of Energy-Levels for Intermediate Nuclei. K. W. FORD, *Indiana University.* (30 min.)

U4. Some Considerations Concerning Relstivistic Two-Particle Wave-Equations. Z. V. CHRAPLYVY, *St. Louis University.* (30 min.)

SATURDAY AFTERNOON AT 1:30

Oriental 104

(CYRIL S. SMITH presiding)

Metals

V1. Diffusion of Copper and Zinc in Ordered and Disordered CuZn.* ALAN B. KUPER AND CARL T. TOMIZUKA, *University of Illinois.*—Radioactive tracer diffusion measurements have been made using Cu^{64} and Zn^{65} diffusing into single crystals of CuZn of approximately 48 atom percent Zn (β brass). At this composition, the alloy orders at about 466°C (T_c). β brass orders rapidly with no change in volume or structure. Diffusion coefficients have been determined at 7 points between about 350° and 850°C for each element. In the disordered phase, data above T_c+10°C may be represented by: $D_{Zn}=0.013e^{-21\,200/RT}$; $D_{Cu}=0.020e^{-23\,200/RT}$. The transition from D to D' is being studied from 470° to 430°C. In the ordered phase, preliminary results indicate that below T_c-55°C: $D_{Zn}'\cong 77\cdot e^{-35\,600/RT}$; $D_{Cu}'\cong 5.6e^{-32\,900/RT}$. From these data it can be seen that $D_{Zn}'\rightarrow D_{Cu}'$ at low temperatures. The existence of a Kirkendall effect in β brass[1] rules out an interchange mechanism for diffusion. The low temperature data suggest a vacancy rather than an interstitial mechanism.

* Supported in part by the U. S. Atomic Energy Commission.

[1] R. Resnick and R. W. Balluffi, private communication.

V2. Effect of Low Concentrations of Impurity on Diffusion in Silver. E. SONDER, *University of Illinois.*— In order to obtain information on the effect of impurities in the one percent range on the activation energy of diffusion, diffusion coefficients for antimony and silver tracers into single crystals of silver doped with antimony are being measured. Partially complete data show the following. 1. The diffusion rate of antimony tracer is not changed by adding as much as 0.8 percent antimony impurity to the silver lattice. 2. There is an appreciable (about 50 percent) increase in the diffusion rate of silver tracer in these alloys. There seems to be little if any change in the activation energy for silver self-diffusion in these alloys of up to 1.6 percent antimony. This result is similar to that obtained on the silver lead system by other investigators.[1]

[1] Hoffman and Turnbull, J. Appl. Phys. **23**, 1409 (1952).

V3. Interpretation of Dimensional Changes on Dezincification of Alpha Brass. DAVID D. VAN HORN AND WILLIAM J. COOLEY, *Knolls Atomic Power Laboratory.**—Small wires and square plates of alpha brass were dezincified in vacuum at various temperatures and the dimensional changes were followed as a function of the amount of zinc removed. Dimensional changes in both geometries were found to be linear functions of the amount of zinc removed. Since these relationships are independent of temperature, it is reasonable to assume that all the vacancies introduced remain within the material, "precipitating" out to form the observed porosity. If one assumes no volume change results on agglomeration of vacancies, the observed dimensional changes can be related to the accumulated lattice strain resulting from the introduction of vacancies. Greater dimensional changes in the diffusion direction are attributed to the additional effect of loss of surface lattice sites due to the concurrent diffusion of copper atoms. The ratio of the intrinsic diffusivities of copper and zinc is calculated along with the lattice strain introduced by vacancies. The lattice strain is 0.12 times the concentration of vacancies; the ratio of diffusivities of copper to zinc is 0.11.

* Operated by the General Electric Company for the U. S. Atomic Energy Commission.

V4. Effect of Quench on the Structure of Au−Cd. MONROE S. WECHSLER, *Oak Ridge National Laboratory.*—Experiments initiated at Columbia University and continuing at ORNL have shown that quenches from 450°C cause a ten percent increase in the electrical resistivity of Au−Cd of approximately 50 atomic percent composition. This alloy is ordered in the Cs−Cl structure at temperatures several degrees above room temperature. At-temperature x-ray spectrometer measurements were made in the range of temperatures from room temperature to approximately 15°C below the melting point (~620°C) in order to determine whether the increase in resistivity is the result of the quenching-in of a less ordered structure or possibly to a new phase formed at the high temperature. It was found, however, that the alloy is highly ordered at temperatures near the melting point and that no new phase is formed. Experiments were also performed on the annealing kinetics of the effect of quench. It was found that the increase in resistivity anneals out in the order of 100 minutes at 70°C and that the process has an activation energy of 0.6 ev. Interpretation will be given in terms of the motion of lattice vacancies.

V5. Expansion of Copper Bombarded by 19-Mev Deuterons. HENRY A. KIERSTEAD, *Argonne National Laboratory.*— The deuteron bombardment-induced expansion of copper reported earlier[1] has been investigated in more detail by using an improved apparatus of greater sensitivity and reliability, and the annealing characteristics of the volume change have been studied. Bombardment by 1.15×10^{17} 19-Mev deuterons per cm² at liquid nitrogen temperature produces a volume increase of 0.034 percent, averaged over the range of the deuteron. About 10.8 percent of this effect recovers on annealing to −105°C, none between −105°C and −25°C, 2.9 percent between −25°C and 0°C, none between 0°C and 190°C, 3.6 percent between 190°C and 260°C, and 2.9 percent just below 400°C. About 80 percent of the volume change remains after annealing to 400°C. Using the Seitz theory to calculate the number of atoms displaced per 19-Mev deuteron, we find that the final volume change corresponds to about one-tenth of an atomic volume per displaced atom. In the range studied the volume change is about proportional to the bombardment. Room-temperature bombardment produces only about one-tenth as much volume change as is produced by liquid nitrogen bombarment followed by annealing to room temperature. Dr. Siegel of this laboratory reports no change in the lattice constant, within the error (0.02 percent) of the x-ray measurement.

[1] W. R. McDonell and H. A. Kierstead, Phys. Rev. **93**, 247 (1954).

V6. Effect of Vacancies and Interstitials on the Electrical Properties of Copper. F. J. BLATT, *University of Illinois*— In order to interpret resistance measurements on metal. during irradiation and upon subsequent anneal, a knowledge of the effect on the resistivity of a small concentration of vacancies and interstitials is necessary. The change in resistivity due to vacancies in copper has been calculated by Jongenburger.[1] In an analogous manner, the change in resistivity due to interstitials was obtained. The scattering potential used was the Hartree potential of singly ionized copper, and the shielding was adjusted to give the correct Friedel sum.[2] The effect of the relaxation of the lattice was neglected.[3] The result, $\Delta\rho_{\text{int}}=1.4$ μohm-cm/atom percent, which is nearly the same as $\Delta\rho_{\text{vac}}=1.25$ μohm-cm/atom percent,[1] does not agree with the conclusions of Overhauser.[4] The effect of lattice imperfections on the thermoelectric power[5] has also been determined.

[1] P. Jongenburger, Appl. Sci. Research **B3**, 237 (1953).
[2] J. Friedel, Phil. Mag. **43**, 153 (1952).
[3] D. L. Dexter, Phys. Rev. **87**, 768 (1952).
[4] A. W. Overhauser, Phys. Rev. **94**, 1551 (1954).
[5] C. A. Domenicali and F. A. Otter, Phys. Rev. **95**, 1134 (1954).

V7. Formation Energy of Lattice Vacancies in Gold.* J. W. KAUFFMAN AND J. S. KOEHLER, *University of Illinois.*—High purity (99.999 percent or better) large grained polycrystalline gold wires were rapidly quenched from given temperatures in the range 500°C to 900°C to liquid nitrogen temperature. The wires were heated in a helium atmosphere by electric current and quenched by a jet of cooled helium gas; they were then immediately immersed in liquid nitrogen. The quench produces an increase in the electrical resistance up to 0.8 percent which is completely annealed out at higher temperatures. The increase in resistance is interpreted as due to lattice vacancies that are in equilibrium at the temperature at which the quench is made. The slope of the log of the resistance increase *versus* the reciprocal of the temperature at quench gives 1.28 ± 0.03 ev for the energy of formation of a vacancy. For a particular specimen the data show a sharp break at low temperatures to a plateau. The residual resistance at 4°K was measured in order to estimate the relative purity of the specimens. The lower the temperature at which the plateau appeared the lower was the impurity content. Appreciable recovery occurs in the range −20°C to 0°C.

* This research reported in part by the U. S. Atomic Energy Commission.

V8. Vibration Spectra and Specific Heats of Cubic Metals. Part I: Theory and Application to Sodium. A. B. BHATIA,* *National Research Council, Canada.*—A model for monovalent metals is proposed on the basis of which the secular equations determining the frequencies of the normal modes of vibration

are derived for body- and face-centered cubic metals. In contrast to the two force constants occurring in the Born-von Karman model, these equations contain three force constants which may be identified with the three independent elastic constants of a cubic metal. The limitations of the model are discussed. In Part III of this paper, the frequency spectrum of sodium and hence its specific heat C_v at constant volume is calculated by solving these secular equations. It is found that the agreement between the observed and calculated values of C_v is more satisfactory in the entire relevant (and especially at low temperatures) temperature range than that obtained by Bauer[1] using the customary two force constant model.

* National Research Laboratories Postdoctorate Fellow.
[1] E. Bauer, Phys. Rev. 92, 58 (1953).

V9. A Theory of Steady-State Creep Based on Dislocation Climb. J. WEERTMAN, *Naval Research Laboratory* (introduced by J. R. WEERTMAN).—A theory of steady-state creep is developed using Mott's model of dislocations climbing over barriers. The assumed rate-controlling process is the flow of vacancies from barriers where they are being produced by dislocation climb to barriers where they are being destroyed. The concentration of vacancies at a barrier is determined by equating the work done when a dislocation climbs in a stress field in which it moves in the slip direction as it climbs to the change in the Gibb's free energy caused by the creation or destruction of vacancies. If the barriers are immobile dislocations the creep equation that results from the analysis is: creep rate $=$ const $(\sigma^m/kT)\exp(-Q/kT)$ where σ is the stress, m is a constant (reasonable values being $4<m<6$), Q is the activation energy of self-diffusion, and k and T have their usual meanings. This equation should be valid only in the approximate stress range of 10^7 to 4×10^8 dynes/cm^2. At higher stresses the theory predicts that the creep rate will increase at a greater rate with stress; at lower stresses with a smaller stress dependence.

V10. Internal Friction in Some Fe-Al Alloys. C. WERT, *University of Illinois*.—The internal friction of alloys of Fe and Al close to the composition Fe_3Al has been partially investigated. Two well-defined peaks of damping as a function of temperature have been observed in polycrystalline specimens. For a frequency of about 1 cps, one of these peaks occurs near 700 deg C, the other near 500 deg C. The high-temperature peak had a high maximum, the lower peak had a much smaller maximum. These peaks are tentatively ascribed to the grain-boundary relaxation and the short-range-order relaxation, respectively. In addition to these well defined peaks at these relatively high temperatures, there is a further component of damping at lower temperatures which is almost certainly of magnetic origin. It is strongly amplitude dependent and exists below the magnetic Curie temperature (some 300 deg C) at least as far down as room temperature. It is not present in hot-rolled material but appears after such material has been given a high temperature anneal.

V11. Properties of CdS Films Deposited in Vacuo. ARTHUR BRAMLEY, *A. B. Du Mont Laboratories*.—The presence of metallic Cd in evaporated films of CdS was reported recently by Gottesman and Ferguson. The present experiments indicate that the properties of CdS films depend strongly on evaporation techniques. CdS evaporated on cold surfaces contains conducting impurities whereas no evidence of impurities was found in fractionally distilled CdS evaporated on hot surfaces. Films with impurities have low photoconductive sensitivity and low dark resistance while films evaporated on hot surfaces have high dark resistance and a sensitivity comparable to the best CdS crystals prepared by Frerichs method. Baking both types of films in air at 300°C for 2 hours had no permanent effect on either dark resistance or sensitivity, although the dark resistance of the insensitive variety increased temporarily by a factor of 10. No loss of sensitivity appeared in evaporated films exposed to air for 1 year. The nature of the impurities in the evaporated film is uncertain because the low temperature of evaporation (<900°C) and the absence of oxidation during the baking cycle militate against free Cd.

V12. Some Notes on the Low Temperature Resistance Minimum. R. W. SCHMITT AND M. D. FISKE, *General Electric Research Laboratory*.—The effect of changing the microstructure of copper and copper-zinc alloys on the low temperature resistivity minimum has been investigated. No evidence has been found to indicate that such changes either produce a minimum or influence a minimum otherwise present. These results do not confirm the proposal of Blewitt, *et al.*[1] that grain boundaries can produce such a minimum. The experiments on copper-zinc alloys also indicate that zinc, as an impurity in copper, is not responsible for causing a minimum. The latter result is contrary to a report of Gerritsen and Linde.[2]

[1] Blewitt, Coltman, and Redman, Phys. Rev. 93, 891 (1954).
[2] A. N. Gerritsen and J. O. Linde, Physica 18, 877 (1952).

V13. The Effect of Plastic Deformation on the Surface Resistivity of Copper Wires. J. ARON AND D. KAHN, *Lewis Flight Propulsion Laboratory*.—The change in the surface resistivity of 0.05 cm copper wire resulting when the wire was subjected to an elongation of 10–15 percent was measured by microwave techniques as follows. Five copper wires were first electropolished and annealed 5 hours at 500°C in vacuum. Each wire was successively made the center conductor of an open ended coaxial line[1] which formed part of one arm of an impedance bridge operated around 9600 megacycles. The unbalance of the bridge due to the insertion of the wire was measured as a function of the applied frequency. If the resistivity of the copper wire is directly computed from the average Q, the result obtained is about 20 percent higher than the dc value and this sets an upper limit for the combined effect of the irregularities of the surface of the wire and losses inherent to the coaxial line employed. Immediately after each wire was pulled it was replaced in the cavity and its surface resistivity measured again. In each case, this was found to have become two to three times as large as before. The surface resistivity of these wires subsequently decreased with time while they were held at room temperature indicating that an annealing process occurs whereby the surface approaches its normal state.

[1] A. C. Beck and R. W. Dawson, Proc. Inst. Radio Engrs. 38, 1181 (1950).

SATURDAY AFTERNOON AT 1:30

Kent 106

(MARCEL SCHEIN presiding)

Cosmic Rays

Invited Paper

W1. Multiple Photon Production in Electron-Positron Annihilstion. S. N. GUPTA, *Purdue University.* (30 min.)

Contributed Papers

W2. Changes in Amplitude of the Cosmic-Ray 27-Day Intensity Variation with Solar Activity.* PETER MEYER AND J. A. SIMPSON, *University of Chicago.*—Both cosmic-ray neutron and ionization chamber intensity observations reveal that the amplitude of the 27-day recurring intensity variation has been changing over an interval of several years. This phenomenon has been studied using ionization chamber data for the period 1936–1946 and neutron intensity data for 1951–1953. The amplitude of the 27 day intensity variation over these years displays minima and a maximum closely related in time to the minima and maxima of the approximately 11 year cycle in general solar activity. Thus, these results provide additional evidence that solar active regions are related to the 27-day cosmic ray primary intensity variations.

* Assisted by the Office of Scientific Research, Air Research and Development Command, U. S. Air Force.

W3. Identity of Shower Particles in Stars in Region 1–2x Minimum Ionization. E. PICKUP AND A. HUSAIN,* *National Research Council, Canada.*—Grain counting and scattering measurements have been made on about 100 long ($\lesssim 12$ mm) shower tracks from cosmic ray stars in photographic emulsion, which was exposed in a O.N.R. "Skyhook" flight. The particles have fallen into π meson, proton, and deuteron groups and one fairly certain K-meson ($m=960\ m_e$). The results appear to be in generally good agreement with the latest Bristol results[1] indicating few mesons with mass $\sim 1000\ m_e$. The possible presence of other heavy mesons and hyperons will also be discussed.

* National Research Laboratories Postdoctorate Fellow.
[1] C. F. Powell, Nuovo cimento Suppl., 11, Ser. 9 (1954).

W4. Delayed Disintegration of Nuclear Fragments. W. F. FRY, J. SCHNEPS, AND M. S. SWAMI, *University of Wisconsin.*—Nuclear emulsions, exposed to cosmic rays, and to 3-Bev protons and 1.4-Bev negative π mesons from the Brookhaven Cosmotron, were scanned for double stars where the secondary star appeared to have been produced by a stopped nuclear fragment. Seventeen examples of such double stars were observed out of 29 000 stars produced by 3-Bev protons; 6 such examples out of 7000 cosmic-ray stars, and 1 example out of 200 stars produced by 1.4-Bev π mesons. In one example, the energy release from the breakup of the fragment was measured and found to be 176 ± 3 Mev which is consistent with the decay of a Λ^0 particle bound in a B_e nucleus. The energy release in a second event, which is interpreted as the mesonic decay of a L_i* fragment, is considerably greater than the decay energy of a Λ^0 particle. In most of the remaining cases the connecting track is shorter than 25 microns. These events are consistent with the non-mesonic decay of a bound Λ^0 particle in a fragment of $Z \geqslant 3$.

[1] W. F. Fry and G. R. White, Nuovo cimento 11, 551 (1954).

W5. Evidence for Gamma Rays from Hyperons or Heavy Mesons Produced by Cosmotron Protons. S. L. RIDGWAY AND GEORGE B. COLLINS, *Brookhaven National Laboratory.*—In the experiment similar to that of Garwin[1] a search was made for gamma emission from downstream of the target, assuming that hyperons or heavy mesons produced in the target in proton-nucleon collisions decaying with lifetime in the $\sim 10^{-10}$ second region may decay by π^0 emission. In two considerably different arrangements with collimators that observed a 2-in. long region downstream, and a gamma-sensitive 20-Mev threshold fast triple coincidence counter at angles of 55° and 90° to the beam, there was observed, at 3 Bev, an intensity of gamma rays downstream of the target that was $\sim 10^{-3}$ of the π^0 gamma intensity of the target, and an energy dependence with a threshold approximately 1.2 Bev, consistant with the hypothesis of associated production. Observing the intensity decrease with target upstream motion, there appears a fast decaying component with mean survival distance between 1.1 and 1.8 cm, and a slower component.

* Work performed under the auspices of the U. S. Atomic Energy Commission.
[1] R. L. Garwin, Phys. Rev. 90, 274 (1953).

W6. Chi Meson Produced by 3-Bev Protons.* R. D. HILL, *University of Illinois,* AND E. O. SALANT AND M. WIDGOFF, *Brookhaven National Laboratory.*—K mesons have been found in Ilford G5 stripped emulsions exposed to radiations from a copper target bombarded by 3-Bev protons of the Cosmotron. One K meson emerging at 90° to the proton beam was observed to decay at rest 9.4 cm from the target, giving a flat out-going track of 5.25 cm in a single strip. Both the scattering angle and blob density measurements showed significant changes along the outgoing track. On a plot of $p\beta$ *vs* ratio of blob density to plateau density, five equally spaced points, each based on 9 mm of track, fell very closely on the curve determined for pions by Fleming and Lord.[1] Our plateau blob density, determined from $\mu-e$ decay electrons, agreed with that of Fleming and Lord. Identification as a pion was supported by the variation of $p\beta$ with range. Hence this K is a χ^+ meson. The value of $p\beta$ at the start of the outgoing track was (163 ± 10) Mev/c. If one assumes that the χ^+ meson decays at rest into a π_0 (263.7 m_e) and a π^+ (273.4 m_e), then its mass is $(950\pm 40)\ m_e$ and the Q value of its decay is (211 ± 20) Mev, agreeing with that of the θ^0 meson.[2]

* Work performed under auspices of the U. S. Energy Commission.
[1] Fleming and Lord, Phys. Rev. 92, 511, (1953).
[2] Thomas, Burwell, Cohn, Huggett, and Karzmark, Phys. Rev. 95, 661, (1954).

W7. New Evidence Concerning the Specific Identity of the θ^0 Decay Fragments and the Statistics of the θ^0 Particle.* J. R. BURWELL, R. W. HUGGETT, AND R. W. THOMPSON, *Indiana University.*—In view of the preliminary analysis of τ decay by Dalitz,[1] there is indication that the θ and τ mesons may represent different K-particle families. From the point of view of the θ meson, the argument depends essentially on the fact that the two decay fragments are both pions, rather than a pion and a muon. Therefore it may be of interest to report

some new results which favor the two pion scheme. The status of previous evidence on this point is summarized in a recent paper.[2] The new evidence is based on the dynamic methods of analysis which provides means for the absolute determination of parent and fragment masses. In the case of θ^0 decay, the dynamic distinction between pion and muon fragments is difficult since those fragments are quite relativistic in the center-of-mass system. However, a substantial set of decay data from the large Indiana magnet chamber is now available and a straightforward fitting procedure indicates that, to 99 percent confidence level, both fragments are pions. Conversely, assuming equal fragment masses, the best value is 285 m_e, with an error certainly small enough to exclude two muons.

* Assisted by the U. S. Office of Ordnance Research and by grant of the Frederick Gardner Cottrell Fund of the Research Corporation.
[1] R. H. Dalitz, Phys. Rev. 94, 1046 (1954).
[2] Thompson, Burwell, Huggett, and Karzmark, Phys. Rev. 95, 1576 (1954).

W8. New Examples of the Anomalous V^0 Particles.* R. W. HUGGETT, J. R. BURWELL, AND R. W. THOMPSON, *Indiana University.*—Since the first resolved example of the anomalous V^0 particle was reported,[1] a limited number of additional examples have been found by various groups. Although the existence of the phenomenon now appears to be firmly established, the nature and decay scheme of the neutral parent particle (or particles) is not yet known. The object of this paper is to report two new V^0 decay events of fortuitous quality and to discuss the relationship of this new data to the previous data and to the various conjectures that have been made as to the decay scheme.

* Assisted by the U. S. Office of Ordnance Research and by grant of the Frederick Gardner Cottrell Fund of the Research Corporation.
[1] Thompson, Buskirk, Etter, Karzmark, and Rediker, Phys. Rev. 90, 329 (1953).

W9. Evidence for Charge Asymmetry of the $V^{\pm}$ Particles.* Y. B. KIM, J. R. BURWELL, R. W. HUGGETT, AND R. W. THOMPSON, *Indiana University.*—Analyses have been made on 13 V^+ and 18 V^- decays obtained in the large magnetic cloud chamber.[1] The distribution of transverse momentum for V^+ suggests a 2-body decay with $p' \sim 220$ Mev/c, the c.m. momentum. For V^-, the distribution appears broader and the mean is lower. Also, the V^+ lifetime appears longer than that of V^-. Such a charge asymmetry has not been previously observed in the magnetic cloud chamber work. In 3 V^+ events, the values of p' are consistent with a unique $p' = 222 \pm 5$ Mev/c. Thus the present data provide preliminary evidence for a long-lived particle $K^+(\sim 1000\ m_e) \rightarrow L^+ + (\pi^0, \nu,$ or $\gamma)$. In one V^- event, $p' < 140$ Mev/c; therefore, the V^- data cannot represent 2-body decay of a homogeneous group. In another V^- event, the charged secondary is a π^- ($\pi - \mu$ decay). This event is consistent with $\tau^- \rightarrow \pi^- + 2\pi^0$ or $V^- \rightarrow \Delta^0 + \pi^-$. However, not many of the V^- events can be attributed to these decay schemes. Also, very few $V^{\pm}$ events can be attributed to $K^{\pm}(\sim 1450\ m_e) \rightarrow \mu^{\pm} + 2\nu$.

* Assisted by the U. S. Office of Ordnance Research and by grant of the Frederick Gardner Cottrell Fund of the Research Corporation.
[1] Thompson, Buskirk, Etter, Karzmark. and Rediker, Phys. Rev. 90, 329 (1953).

W10. Charged V Particle Production in a Proton-Proton Collision.* M. M. BLOCK† AND E. M. HARTH,‡ *Naval Research Laboratory*, W. B. FOWLER, R. P. SHUTT, A. M. THORNDIKE, AND W. L. WHITTEMORE, *Brookhaven National Laboratory.*—A 20 atmosphere hydrogen-filled diffusion cloud chamber, in a magnetic field of 9500 gauss, was exposed to an external 2.6-Bev proton beam at the Brookhaven Cosmotron. A p-p collision was observed in which two positively charged particles, which were not coplanar with the beam track, were produced; one (a), traveled 6 cm and decayed through an angle of 12.5°, and the other (b) went 3 cm, where it appeared to have decayed through an angle of only 2°. The ratio of the ionizations of this track after and before the point of apparent decay was ~1.5–2, which makes the given interpretation quite likely in spite of the somewhat uncertain decay angle. The decay product of b is identified as a proton by momentum and ionization measurements; we assume that b is a hyperon with the decay scheme $\Lambda^+ \rightarrow p + \pi^0 + 115$ Mev. From the kinetics of the p-p collision, particle a is identified as a K particle of $\sim 1000\ m_e$. The reaction scheme, $p + p \rightarrow \Lambda^+ + K^+ + N$, where N is a neutron, is proposed and is internally consistent with our data. This implies that the K^+ meson observed is a boson.

* Work performed under the auspices of the U. S. Atomic Energy Commission.
† On military leave of absence from Duke University, Durham, North Carolina.
‡ Now at Duke University, Durham, North Carolina.

SATURDAY AFTERNOON AT 1:30

Eckhart 133

(D. R. INGLIS presiding)

Reactions of Transmutation, II; Neutron-Yielding Reactions, Electric Excitation

X1. Neutrons in Coincidence with Photoprotons.* A. C. ODIAN, W. RANKIN, P. C. STEIN, AND A. WATTENBERG, *M.I.T.*—Further studies have been made at the MIT synchrotron of those neutrons which are in coincidence with high energy photoprotons. A plastic scintillation counter telescope detected protons with an energy spread of about 10 Mev. The neutron detector was approximately 5 percent efficient and had no energy selectivity. Targets of Li, D_2O, and H_2O were employed. The neutrons from deuterium had the kinematically predicted spiked angular distribution when the proton energy and angle were held fixed. With the same proton energy and angle, the neutrons from Li and oxygen came off about the same angle as from deuterium, but with an angular spread whose width depended upon the photon energy. The spread in neutron angle from Li and O had a width at half-maximum of about 50° for 140-Mev photons and about 33° for 252-Mev photons.

* This work was supported in part by the joint program of the Office of Naval Research and the U. S. Atomic Energy Commission.

X2. The Angular Distribution of Neutrons from the Reaction $D(d,n)He^3$ at 100 Kev.* J. C. FULLER AND D. C. RALPH, *Louisiana State University.*—The relative intensity of neutrons resulting from 100 Kev deuterons incident on a thick deuterated paraffin target has been measured by means of nuclear emulsions exposed at six laboratory angles ranging

from 0° to 150°. The yields in center of mass coordinates agree well with the relation $n'(\theta')=n'(90)[1+A(E)\cos^2\theta']$, and require an asymmetry coefficient $A(E)=0.48\pm0.09$. A comparison of these data with previous results[1–3] in the low-energy region will be made.

* Supported in part by a grant by the Research Corporation.
[1] I. Bartholdson, Arkiv Fysik 2, 271 (1950).
[2] P. Baker and A. Waltner, Phys. Rev. 88, 1213 (1952).
[3] Eliot, Roaf, and Shaw, Proc. Roy. Soc. (London) 216, 57 (1953).

X3. $Li^7(d,n)Be^8$ Neutron Spectrum and Differential Cross Section. C. C. TRAIL* AND C. H. JOHNSON, *Oak Ridge National Laboratory.*—The neutron spectrum and differential cross sections for the $Li^7(d,n)Be^8$ reaction have been obtained at 2-Mev bombarding energy with a neutron spectrometer described previously.[1] The spectrum at 120° indicated only one excited state in Be^8 (at 3 Mev) up to an excitation of 9 Mev in agreement with the 0° data.[1] The neutron angular distributions for the two states were measured by observing the spectrum at fourteen angles from 0° to 135°. Each spectrum exhibited, in addition to the two groups, a continuum which results from the three-body breakup of Be^9. In order to plot the angular distributions, this continuum was subtracted in an arbitrary but consistent manner. Absolute cross sections were obtained by normalizing the yield at 0° to the cross section obtained with a weighed LiF target. The cross section for the ground-state group decreases from 3.2 ± 0.3 mb/steradian at 0° to 1.7 ± 0.2 for angles larger than 40°. That for the 3-Mev state decreases from 6.7 ± 0.7 mb/steradian at 0° to approximately 4.5 mc/steradian for angles greater than 90°. Butler curves for $l_p=1$ give a qualitative description of the forward yield but not of the yield at larger angles.

* Now at argonne National Laboratory.
[1] C. C. Trail and C. H. Johnson, Phys. Rev. 95, 1363 (1954).

X4. Neutron Yields as a Function of Energy in the Reactions $Li^7(d,n)Be^8$ and $Be^9(d,n)B^{10}$.* D. C. RALPH AND F. E. DUNNAM, *Louisiana State University.*—Neutron yields from the deuteron bombardment of lithium and beryllium have been studied over an incident deuteron energy range of 70–110 kev. Incident deuterons were supplied by a Cockcroft-Walton accelerator, and neutron yields were measured with an anthracene scintillator. Gamow plots of the data give lines with slopes in agreement with the experiments of Sawyer and Phillips[1] on the charged particle yield for these reactions. The theoretical interpretation of these results will be discussed.

* Assisted in part by Research Corporation.
[1] G. A. Sawyer and J. A. Phillips, LADC-1578 (1953).

X5. $Be^9(n,2n)Be^8$ Reaction. J. M. FOWLER, S. S. HANNA, AND G. E. OWEN, *The Johns Hopkins University.**—The $Be^9(n,2n)Be^8$ reaction has been studied at a neutron energy of 3.7 Mev using the $D(d,p)He^3$ reaction as a neutron source. The inelastic neutrons were observed with two large *trans*-stilbene counters operated in coincidence, and the neutron flux was monitored with the protons from the $D(d,p)H^3$ reaction. The pulse-height spectrum from one of the counters was measured with a multichannel analyzer which was gated by coincidences between the pulses from the two counters. The scintillators intercepted a solid angle of 0.114 steradian at the scatterer. In order to obtain the cross section for this process, observations were made in a plane containing the incident neutron at the following pairs of angles: 30°–30°, 60°–60°, 67°–67°, 80°–80°, and 0°–90°. These spectra all showed evidence of two discrete neutron groups, suggesting the mechanism $Be^9(n,n')Be^{9*}(n'')Be^8$. The observed neutron energies indicated an excitation energy of Be^9 consistent with the known value of 2.43 Mev.

* Assisted by a contract with the U. S. Atomic Energy Commission.

X6. Angular Distribution of Gamma Rays from Coulomb Excitation. P. H. STELSON AND F. K. MCGOWAN, *Oak Ridge National Laboratory.*—To test the semiclassical theory of angular distribution of gamma-rays following Coulomb excitation given by Alder and Winther,[1] we have carried out measurements on the 330- and 358-kev gamma rays in Pt^{194} and Pt^{196}. These gamma rays are especially suitable because of the large coefficients for P_2 and P_4 characteristic of 0–2–0 transitions and because angular correlation measurements have shown no observable influence of extranuclear fields. The experimental and theoretical values for the energy-dependent coefficients, a_2 and a_4, for a thick target are listed beneath. The observed energy dependence deviates considerably from the theory. In addition, larger differences have been bound for medium weight nuclei ($Z=40$ to 50), indicating a Z dependence for the energy-dependent coefficients.

Proton energy Mev	(a_2) exp	(a_2) theory	(a_4) exp	(a_4) theory
2.5	$+0.800\pm0.015$	$+0.696$	-0.068 ± 0.010	-0.019
3.0	$+0.709\pm0.010$	$+0.683$	-0.054 ± 0.005	-0.020
3.5	$+0.637\pm0.008$	$+0.667$	-0.023 ± 0.007	-0.022
4.0	$+0.590\pm0.007$	$+0.652$	-0.011 ± 0.004	-0.026
4.5	$+0.534\pm0.015$	$+0.636$	-0.006 ± 0.007	-0.035
5.0	$+0.478\pm0.008$	$+0.623$	$+0.001\pm0.003$	-0.040

[1] K. Alder and A. Winther, Phys. Rev. 91, 1578 (1953).

X7. Electric Excitation of Heavy Nuclei with Protons.* CLYDE MCCLELLAND, HANS MARK, AND CLARK GOODMAN, *M.I.T.*—The low-lying energy levels of seventeen heavy nuclides, including isotopes of hafnium, tantalum, wolfram, rhenium, and platinum have been studied by electric excitation with protons.[1,2] The results have been interpreted in terms of the hypothesis of nuclear rotational levels of Bohr and Mottelson.[3] Approximate intrinsic electric quadrupole moments (Q_0) have been determined for these nuclides from the energies and electric excitation cross sections of the various levels. The values of Q_0 obtained by these two methods are in good agreement for isotopes of highly deformed nuclei (hafnium) but as the shell at 126 neutrons and 82 protons (Pt^{195}) is approached the value of Q_0 obtained from the excitation energy exceeds the value obtained from the cross section by a factor of seven.

* Supported by the joint program of the U. S. Office of Naval Research and the U. S. Atomic Energy Commission.
[1] T. Huus and C. Zupancic, Dan. Mat. Fys. Medd. 28, No. 1 (1953).
[2] C. L. McClelland and Clark Goodman, Phys. Rev. 91, 760 (1953).
[3] A. Bohr and B. R. Mottelson, Dan. Mat. Fys. Medd. 27, No. 16 (1953).

X8. Electric Excitation of Nuclei Near the Closed 50 Proton and Neutron Shells.* HANS MARK, CLYDE MCCLELLAND, AND CLARK GOODMAN, *M.I.T.*—Energy levels of several nuclei near the closed 50 proton and neutron shells have been studied by electric excitation with protons. Two elements (zirconium and niobium) near the closed 50 neutron shell have no energy levels which have large electric excitation cross sections. Several nuclei (palladium, silver, cadmium and iodine) near the closed 50 proton shell have levels with large electric excitation cross sections. The 325- and 436-kev γ rays from natural silver, which are due to levels of nearly equal energies[1] in Ag^{107} and Ag^{109}, have been studied in detail using thick and thin targets. The yield of these γ rays as a function of proton energy agrees well with the electric quadrupole excitation function between 1.5 and 3.5 Mev. Reduced electric quadrupole transitions probabilities obtained from excitation cross-section measurements for levels in palladium, silver, cadmium and iodine are smaller by factors of ten to fifty than those obtained from the energies of the transitions assuming rotational excitation.[2]

* Supported by the joint program of the U. S. Office of Naval Research and the U. S. Atomic Energy Commission.
[1] N. Heydenburg and G. Temmer, Phys. Rev. 95, 861 (1954).
[2] A. Bohr and B. R. Mottelson, Dan. Mat. Fys. Medd. 27, No. 16 (1953).

SATURDAY AFTERNOON AT 1:30

Cobb 110

(A. H. WEBER presiding)

General Physics, II

Y1. Some Tabulations of Cosmic Abundances. J. Y. SMITH, *The Ohio State University.*—Tentative values of cosmic abundance are assigned to 286 natural nuclear species, after correlating published data on abundance values for 83 elements and multiplying each value by an isotopic percent. Differing tabulations are assembled with each of 285 nuclides (excluding hydrogen-1) identified by proton, neutron, mass, and isotopic number and by an abundance value which is the prime criterion of tabulation. One table ranks in order of abundance the 285 nuclides with P, N, M, I, and abundance values, and additionally for each nuclide, an index as stable or unstable and with or without isomeric states. Another table comprises four columnar sets with the nuclides alternatively grouped under 121 N numbers, 210 M numbers and 50 I numbers along with the initial 83 P numbers. Abundance value for a P, N, M, or I number is the sum of values for nuclides having that number (isotones, isobars, etc.). After ranking each columnar set by abundance, with a counting of the nuclides bearing each number, all four sets are assembled for inspection of possible coincidences or near-coincidences across the rows of the same relative abundance rank. A third table illustrates alterations in such horizontal alignments, and in vertical clusters, arising from differing methods for initial evaluations of abundance.

Y2. The Branching Ratio of K^{40} and the Age of Meteorites. G. J. WASSERBURG, *University of Chicago*, AND R. J. HAYDEN, *Argonne National Laboratory.*—The A^{40}/K^{40} ratios and the Pb^{206}/U^{238} and Pb^{207}/U^{235} ages of various coexisting potassium feldspars and uraninites were determined. The argon was released from the minerals by fluxing with NaOH at 600°C. The radiogenic A^{40} content was determined using an isotopic dilution technique. A^{38} was used as a tracer. The branching ratio was calculated assuming the Pb−U age and using a decay constant $\lambda=0.55\times10^{-9}$ yr^{-1}. The Pb^{206}/U^{238} and Pb^{207}/U^{235} ages determined agreed within 2 percent for each sample investigated. Nine samples ranging in age from 2.7×10^8 to 1.9×10^9 yr were run. The value obtained for the branching ratio was $\lambda_\epsilon/\lambda_\beta=0.085\pm0.005$. No systematic decrease in the branching ratio was observed with the age of the sample indicating no significant loss of argon due to diffusion. The A^{40}/K^{40} ages of two stony meteorites were determined using the method described. An isotopic dilution technique was used to determine the potassium content. K^{41} was used as a tracer. The isotopic ratios were determined by a surface ionization technique using a mass spectrometer with 60° deflection and a 12-inch radius of curvature. The following ages were obtained: Beardsley, $4.82\pm0.2\times10^9$ yr, Forest City $4.58\pm0.2\times10^9$ yr.

Y3. Potassium-Argon Ages of Lepidolites. G. W. WETHERILL, L. T. ALDRICH, AND G. L. DAVIS, *Carnegie Institution of Washington.*—The radiogenic argon content of several lepidolites has been determined by a mass-spectrometric isotopic dilution technique, using A^{38} as a stable isotope tracer. Potassium analyses were made with a flame photometer. Using the decay constants $\lambda_{\beta^-}=5.06\times10^{-10}$ yr^{-1} and $\lambda_K/\lambda_{\beta^-}=0.090$ the following ages have been calculated and compared with Rb−Sr ages on the same mineral specimens.

Sample	K−A age	Rb−Sr age
Bikita, S. Rhodesia	2750	3400
Bonneville, Wyoming	2570	3020
Bagdad, Arizona	1610	1900
Ohio City, Colorado: White	1500	1740
Coarse	1540	1750

The potassium-argon age of Bikita lepidolite agrees with reliable uranium-lead and thorium-lead ages of a monazite sample from this locality. The argon content of the atmosphere has been found to be 0.93$_4$ percent by this same technique, in excellent agreement with earlier volumetric analyses.

Y4. Low-Energy Electron Diffraction Studies of a Germanium Crystal Surface. H. E. FARNSWORTH, R. E. SCHLIER, AND R. M. BURGER, *Brown University.**—A beam of primary electrons at normal incidence in the energy range below 250 ev is diffracted from an etched (100) crystal face. Because of the low penetration, surface contamination is easily detected. Attempts to clean the crystal surface by prolonged outgassing in a high vacuum near the melting point were unsuccessful, although some weak diffraction beams from the germanium crystal were observed, thus indicating that the adsorbed gas layer had been reduced very appreciably in thickness. However, after subsequent bombardment of the crystal surface by argon ions in a low pressure discharge, followed by a very short annealing (a few minutes at 500°C), intense, sharp diffraction beams characteristic of a germanium lattice were observed in the two principal azimuths. The manner in which residual gas was later adsorbed is discussed. Some anomalies in the diffraction pattern are described. Studies of controlled adsorption of various gases are in progress.

* Assisted by Project Lincoln, U. S. Air Force.

Y5. Low-Energy Electron Diffraction Studies of a Titanium Crystal Surface. R. E. SCHLIER, H. E. FARNSWORTH, AND T. H. GEORGE, *Brown University.**—A primary electron beam in the energy range below 250 ev is incident normally on an etched (0001) crystal face. After prolonged outgassing in a high vacuum at temperatures up to 750°C (the transition point is at approximately 850°C), intense sharp diffraction beams were observed which are not characteristic of the titanium lattice. Subsequent bombardment by argon ions in a low-pressure discharge removed the surface layer which produced this diffraction pattern. Damage to the crystal lattice caused by ion bombardment was removed by a very short annealing (a few minutes at 500°C), after which an intense sharp diffraction pattern characteristic of the titanium surface lattice was observed in the two principal azimuths. This diffraction pattern was not obtained by ion bombardment unless the crystal had been outgassed previously by heating at 700°C to 750°C for many hours. Observations on the subsequent adsorption of residual gas is described. Certain anomolies in the diffraction pattern have been observed. Studies of controlled adsorption of various gases are in progress.

* Assisted by Office of Ordnance Research, U. S. Army.

Y6. Measurement of Ionizing Radiation by Frequency Variation Using Ferroelectric Material. HANS KOHN RICHARDS AND EUGENE D. DENMAN, *Oak Ridge National Laboratory.*—A method of measuring ionizing radiation by frequency variation was reported at the American Physical Society Meeting, November, 1952. At that time, the frequency variation of an oscillator was produced by a moving vane electrometer as the reactance elements. To eliminate moving parts, the electrometer has been replaced by a ferroelectric capacitance. Barium titanate ($\frac{1}{2}$ mm thick, area one mm^2) silverplated on opposite

sides had capacitance values between 10 and 15 $\mu\mu$F. This capacitance was connected to a similar one and also to the center electrode of an ionization chamber. Both were in series as elements of the frequency determining network of an oscillator, but connected electrostatically in parallel. The center electrode and connected capacitance areas were charged to 200 to 300 volts. The ferroelectric capacitance decreased with increase in charge and therefore the oscillator frequency increased. The oscillator was controlled by a 2 megacycles quartz crystal which permitted a frequency variation of several thousand cycles/sec. The sensitivity, limited by the finite leakage resistance of the material, permitted measurements of dose rates as low as 10 mr/hr. This limitation was minimized by measuring the beat frequency of identical oscillators, one of which was connected to the ionization chamber, thus the sensitivity was extended to lower values.

Y7. Duration of Mercury Arcs in Evacuated Bulbs Coated with Rare Earths. B. PEARSON DE LANY AND PAUL L. COPELAND, *Illinois Institute of Technology.*—Previous experiments[1] have shown that the distribution of observed durations for the low pressure mercury arc is exponential when the cathode spot is unanchored or when it is anchored at one point of the junction between a tungsten-coated wall and the mercury pool. In the present study interior surfaces of experimental tubes were coated with rare earths obtained by heating misch metal in vacuum. Added mercury wet the coated wall, and the cathode spot after several minutes of operation ordinarily was confined to points on the junction between the mercury pool and the film. The position of the spot changed from time to time. For a given mode of anchoring an exponential distribution of lives would be expected, but the decay constant for the distribution varies from point to point along the curve of contact. In this case, a simple exponential distribution of the observations is not obtained. There are too few observations in the middle range, and the distribution is characterized by occasional observations of very long arc duration.

[1] P. L. Copeland and W. H. Sparing, J. Appl. Phys. **16**, 302 (1945).

Y8. Statistics of the Exponential Distribution of Exponential Populations Applied to the Distribution of Arc Lives. PAUL L. COPELAND AND B. PEARSON DE LANY, *Illinois Institute of Technology.*—As a means of describing the observed distribution of arc lives in rare-earth-coated, mercury arc tubes, certain statistics of exponential populations, $\exp(-t/l)dt/l$ continuousiy distributed in average life according to the law $dN=-kdl\exp(-kl)$, where l represents the average duration of simple exponential constituents, have been computed. For the same expected duration, $1/k$, the statistical fluctuation of individual observations is three times as large as for the simple exponential. This combination of exponentials gives many more small observations, and the number of individuals surviving many times longer than the average is several orders of magnitude greater than for the simple exponential distribution. The proportion of individuals surviving until time T as computed from

$$p=\int_0^\infty kdle^{-kl}\int_T^\infty e^{t/l}\frac{dt}{l}$$

$$=\int_0^\infty kdle^{-(kl+T/l)}$$

is compared with experimental results from a series of 1000 observations.

Y9. Evapor-ion Pump Developments.* MELVIN J. BINA, IGOR ALEXEFF, AND RICHARD M. SANDERS, *University of Wisconsin.*—Further advances have been made with the Evapor-ion pump[1] which utilizes both gettering and ionization pumping to reach pressures down to 5×10^{-8} mm Hg. Titanium wire is fed onto a heated post, evaporates, and condenses on the pump wall, where gettering occurs. The ionization system, now much improved, pumps inert gas atoms by ionizing them in an electric field and driving them into the ever increasing titanium layer on the pump wall. Argon is pumped at 160 liters/sec at 7.2×10^{-6} mm with a pump power input of about 3 kw. Chemically active gases are pumped at about 10^4 liters/sec. Operating time at present is limited either by erosion of the post by molten titanium or deposits upon it. The lifetimes of several post materials have been compared. In starting, pressure in the pump is reduced from forepump level to below the threshold of glow discharges by use of a primer, a tungsten wire from which a small amount of titanium is evaporated by conduction current heating.

* Work supported by the Wisconsin Alumni Research Foundation, the U. S. Atomic Energy Commission, and the National Science Foundation.
[1] Divatia, Davis, and Herb, Phys. Rev. **93**, 926 (1954).

Y10. A Physical Theory for Capillary Flow. E. E. MILLER, *University of Wisconsin.*—The motion of fluids which incompletely fill the voids between the solid grains of a porous medium (exemplified in the action of a blotter) has important technological applications in soils, petroleum extraction, chemical engineering, etc. The problem is complicated by marked hysteresis effects in the dependence of the flow properties of the medium upon liquid content. By assuming that the gas-liquid interface shapes within the pores are governed by the standard differential equation of surface tension, and that the flow within the tortuous microscopic channels obeys the differential equation of viscous flow, a nonlinear differential equation for macroscopic flow is deduced. This equation is obtained in fully reduced form and exhibits hysteresis in an interesting and simple way. The reduced variables, deduced from the similitude properties of the basic differential equations, provide several direct predictions susceptible to experimental test. They also suggest useful applications such as scale modeling of systems, reduction of the essential diversity of medium types, etc. Although little of the experimental work already in the literature provides information on the applicability of this theory, that which does so appears to be favorable.

Y11. On the New Fundamentals of Fluid Dynamics. M. Z. V. KRZYWOBLOCKI, *University of Illinois* (introduced by C. E. MANDEVILLE).—The author points out that fundamentally the mechanics of continuum can give correct answers in the case of incompressible media. Application of continuum equations to compressible media gives answers to the first approximation only. Principally, the phenomena in gases should be considered on the basis of the statistical mechanics due to the physical structure of a gas. The approach from the kinetic theory point of view is obvious. Some remarks on the mathematical part of the problem, like ergodic theorem, invariant measure, etc., close the presentation.

Y12. Field Effect of Space Charge in the Intermittent Glow in Hydrogen. HERMAN RITOW.—Gill, Mitra, and Clark found that the effective tube capacity during discharge was many orders larger than that caused by the geometry of the tube and electrodes. Two methods are developed for measuring the charge on the electrodes at the moment of flash initiation. This charge is shown experimentally to be approximately 10^{-7} coulombs for each square centimeter of the smaller of the two electrodes. This means the electrostatic field at this electrode is of the order of 10^6 volts per cm. Since the emission field of the electrode metal is of the same order, the possibility exists that field emission plays a role in initiating a flash along with photoionization and exponential avalanche formation.

SATURDAY AFTERNOON AT 1:30

Mandel Hall

(ARNOLD NORDSIECK presiding)

Invited Papers

Z1. Hyperfine Splitting in Electron-Spin Resonances of Donors in Silicon. R. C. FLETCHER, *Bell Telephone Laboratories.* (30 min.)

Z2. Theory of the Hyperfine Splitting of Donor States in Silicon. WALTER KOHN, *Bell Telephone Laboratories and Carnegie Institute of Technology.* (30 min.)

Z3. Recent Developments in the Effective-Mass Theory for Semiconductors. J. M. LUTTINGER, *Bell Telephone Laboratories and University of Michigan.* (30 min.)

SUPPLEMENTARY PROGRAMME

SP1. Quantized Spin Paramagnetism in a Free Radical Near Magnetic Saturation. WARREN E. HENRY, *United States Naval Research Laboratory.**—Paramagnetism of free radicals was predicted[1] on the basis of the existence of an unpaired, bound electron and then experimentally confirmed[2] by susceptibility and microwave resonance measurements. However, despite the spin-only g value and negligible spin-orbit coupling of the Banfield and Kenyon free radical, its use in adiabatic demagnetization is impaired by exchange interaction. Diphenyl picryl hydrazil, the subject of this investigation, is more magnetically dilute. We have carried out magnetization experiments in the range, 1.3° to 4.2°K and in magnetic fields up to 50 000 gauss. The magnetic moments were determined ballistically as the sample was moved relative to a coil system.[3] The magnetization, when plotted against H/T, gives isotherms (at 1.3°, 2.0°, 3.0°, and 4.2°K) which superpose. They fall on a Brillouin function for $g=2$ and $J=S=\frac{1}{2}$. Our results are in general agreement with the Leiden[4] work at low fields, except that at the lower temperatures, we do not observe a drop in $M(H/T)$. The measurements confirm the smallness of exchange interaction and indicate some usefulness of diphenyl picryl hydrazil as a paramagnetic coolant.

* To be given at the end of Session C if the Chairman rules that time permits.

[1] N. W. Taylor and G. N. Lewis, Proc. Nat. Acad. Sci. **11**, 456 (1925).

[2] Garstens, Singer, and Ryan, Phys. Rev. **96**, 53 (1954); J. Kenyon and S. Sugden, J. Chem. Soc. 170 (1932); Holden, Kittel, Merritt, and Yager, Phys. Rev. **75**, 1614 (1949).

[3] W. E. Henry, Phys. Rev. **88**, 559 (1952).

[4] Gerritsen, Okkes, Gijman, and van den Handel, Physica **20**, 13 (1954).

Author Index to Papers Presented at the 1954 Thanksgiving Meeting

Adkins, R. H. and J. G. Brennan—K8
Ambler, E. and R. P. Hudson—H4
Argyers, P. N. and A. H. Kahn—C9
Aron, J. and D. Kahn—V13
Bach, D. R., C. R. Lubitz, and P. V. C. Hough—K9
Baker, E., A. Caretto, J. Cumming, G. Friedlander, J. Hudis, and R. Wolfgang—R8
Barredo, J. G.—G9
Bashkin, S. and R. R. Carlson—H1
Becker, W. M. and K. Lark-Horovitz—G2
Bedo, D. E. and D. H. Tomboulian—S2
Belinfante, F. J. and J. C. Swihart—A3
Berlincourt, Ted G. and M. C. Steele—E1
Bhatia, A. B.—V8
Bina, Melvin J., Igor Alexeff, and Richard M. Sanders—Y9
Binnie, W. P.—E6
Blatt, F. J.—V6
Block, M. M., E. M. Harth, W. B. Fowler, R. P. Shutt, A. M. Thorndike, and W. L. Whittemore—W10
Bloom, Steward D.—I7
Bodansky, D. and A. M. Sachs—Q10
Bollinger, L. M., D. A. Dahlberg, R. E. Coté, H. E. Jackson, and G. E. Thomas—B2
Bramley, A. B.—V11
Brandt, Werner—S9
Bray, Ralph—G6
Brophy, J. J., N. Rostoker, and L. V. Azaroff—E7
Brueckner, K. A.—U2
Burson, S. B., W. C. Jordan, and J. M. LeBlanc—H3
Burwell, J. R., R. W. Huggett, and R. W. Thompson—W7
Butler, J. W.—R7
Cantwell, Murray—K6
Cheng, L. S., Virginia C. Ridolfo, M. L. Pool, and D. N Kundu—H8
Collins, R. J., F. W. Reynolds, and G. R. Stilwell—E4
Copeland, Paul L. and B. Pearson de Lany—Y8
Crosbie, E. A. and M. Hamermesh—I5
Chraplyvy, Z. V.—U4
de Lany, B. Pearson, and Paul L. Copeland—Y7
Dumke, William P.—G12
Delbecq, C. J., P. Pringsheim, and P. H. Yuster—P5
Ekstein, Hans and Norman Rostoker—A2
Enck, F. D. and C. B. Cooper—P7
Engel, O. G.—P2
Farnsworth, H. E., R. E. Schlier, and R. M. Burger—Y4
Faust, W. R., V. E. Scherrer, and B. A. Allison—B6
Feiner, F., J. Ashkin, J. P. Blaser, and M. O. Stern—Q6
Feld, Bernard T.—Q1
Ferentz, M. and N. Rosenzweig—A6
Fiske, M. D.—T4
Fletcher, R. C.—Z1
Ford, K. W.—U3
Fowler, J. M., S. S. Hanna, and G. E. Owen—X5
Frankl, D. R.—P15
Frye, G. M., Jr., A. H. Armstrong, and L. Rosen—R2
Fry, W. F., J. Schneps, and M. S. Swami—W4
Fuller, J. C. and D. C. Ralph—X2
Geer, E. H., E. B. Nelson, and E. J. Wolicki—R3

Gilbert, T. L.—S3
Glicksman, M. and H. L. Anderson—Q7
Goldsmith, G. J. and D. E. Hill—P11
Goldwasser, E. L., L. J. Koester, and F. E. Mills—Q4
Grossweiner, L. L., and S. Gordon—S8
Grimsal, E. G.—G8
Gupta, S. N.—W1
Hanscome, T. D. and D. K. Willett—I1
Hanson, A. O.—K1
Hayn, C. H. and Vincent P. Jacobsmeyer—P10
Hayward, R. W., D. D. Hoppes, and H. Ernst—H6
Heikes, R. R.—C3
Hennig, G. and M. Dzurus—E2
Henry, Warren E.—C5, SP1
Herzberg, G.—A7
Herzfeld, C. M.—C7
Herzog, B. and E. L. Hahn—C6
Hibdon, Carl T. and Alexander Langsdorf, Jr.—B3
Hiedemann, E. A.—S1
Hildebrand, R. H.—D1
Hill, D. E. and G. J. Goldsmith—P12
Hill, R. D., E. O. Salant, and M. Widgoff—W6
Hockney, R. W. and P. V. C. Hough—K3
Holland, R. E., D. R. Inglis, and F. P. Mooring—R1
Holmgren, H. D., T. D. Hanscome, and D. K. Willett—R6
Huggett, R. W., J. R. Burwell, and R. W. Thompson—W8
Hurst, D. G. and D. G. Henshaw—B4
Jillson, D. C. and A. C. Sheckler—G4
Jones, K. W., M. T. McEllistrem, R. A. Douglas, D. F. Herring, and E. Silverstein—R4
Kaiser, H. F.—I8
Känzig, Werner and Masayasu Ueta—P3
Kauffman, J. W. and J. S. Koehler—V7
Kerr, J. and C. Wert—C2
Kerst, D. W.—L2
Kierstead, H. A.—V5
Kim, Y. B., J. R. Burwell, R. W. Huggett, and R. W. Thompson—W9
King, R. W.—K5
Kisslinger, Leonard S.—Q5
Koenig, S. H. and G. R. Gunther-Mohr—G3
Knowles, J. W.—B8
Koester, L. J.—Q3
Kohn, Walter—Z2
Kuper, A. B. and C. T. Tomizuka—V1
Landon, H. H. and V. L. Sailor—B10
Lawson, A. W.—T1
Lehovec, Kurt, Alma Marcus, and Kurt Schoeni—G10
Lindqvist, Torsten and C. S. Wu—H5
Lokanathan, S. and J. Steinberger—Q12
Lowry, Ralph A. and Glenn H. Miller—S6
Luttinger, J. M.—Z3
McClelland, Clyde, Hans Mark, and Clark Goodman—X7
MacDonald, W. M.—K4
Mann, A. K.—I13
Mark, Hans, Clyde McClelland, and Clark Goodman—X8
Matossi, F. and S. Nudelman—P14
Maxson, D. R., J. S. Allen, and W. K. Jentschke—H2
Medved, David B.—P9
Meyer, Peter and J. A. Simpson—W2
Miller, E. E.—Y10
Mobley, R. C. and B. R. Albritton, Jr.—I2
Munick, Raymond J.—P1
Norberg, R. E. and D. F. Holcomb—C8
Novey, T. B.—H11
Nudelman, S. and F. Matossi—P13
Odian, A. C., W. Rankin, P. C. Stein, and A. Wattenberg—X1
Orear, Jay—Q8
Pagnia, H. and F. Stöckman—P4
Paul, H. and R. M. Steffen—H9
Paul, W.—T3
Peaslee, D. C.—Q2
Perlow, G. J.—B1
Pickup, E. and A. Husain—W3
Porter, R. F., P. Schissel, and Mark G. Inghram—S4
Price, P. J. and P. B. Linhart—S7
Primak, W., P. H. Yuster, and C. J. Delbecq—P6
Raboy, Sol and Victor E. Krohn—H10
Ralph, D. C. and F. E. Dunnam—X4
Reynolds, H. L., L. D. Wyly, and A. Zucker—S5
Richards, Hans Kohn and Eugene D. Denman—Y6
Ridgway, S. L. and George Collins—W5
Ritow, Herman—Y12
Roberts, B. W. and C. P. Bean—C4
Robinson, Berol L. and Richard W. Fink—H7
Robinson, John E.—E3
Robson, J. W., R. L. Stearns, and E. C. Gregg—I4
Rohrlich, F. and J. M. Jauch—A5
Rostoker, Norman and Hans Ekstein—A1
Sachs, R. G.—U1
Sailor, V. L., H. H. Landon, H. L. Foote, Jr., and R. E. Wood—B9
Scherrer, V. E., W. R. Faust, and B. A. Allison—B7
Schiff, L. I.—K10
Schlier, R. E., H. E. Farnsworth, and T. H. George—Y5
Schmitt, R. W. and M. D. Fiske—V12
Seidel, G. M. and V. A. Johnson—G11
Sheckler, A. C. and D. C. Jillson—G5
Skolnik, W.—Q9
Smith, J. Y.—Y1
Sonder, E.—V2
Spencer, L. V. and F. H. Attix—I9
Spitzer, W., C. O. Bennett, and H. Y. Fan—G1
Stearns, R. L., J. W. Robson, and E. C. Gregg—I3
Stelson, P. H. and F. K. McGowan—X6
Stephens, W. E. and A. K. Mann—R5
Stewart, A. T. and R. E. Green—H12
Strauch, Karl—I12
Studier, W. H.—D3
Swenson, C. A.—T2
Trail, C. C. and C. H. Johnson—X3
Turner, C. M.—I10
Urey, H. C.—L1
Van Horn, David D. and William J. Cooley—V3
Vasileff, H. D.—P8
van Loef, J. J. and D. A. Lind—B5
v. Krzywoblocki, M. Z.—Y11
Walker, W. D. and J. Crussard—Q11
Watson, K. M.—K2
Wasserburg, G. J. and R. J. Hayden—Y2
Webb, L. A. and R. F. Johnson—I11
Wechsler, Monroe S.—V4
Weertman, J.—V9
Weinstein, R., M. Deutsch, and S. Brown—A8
Weinstock, B.—D2
Wert, C.—V10
Wetherill, G. W., L. T. Aldrich, and G. L. Davis—Y3
Wilkinson, D. H. and A. M. Lane—K7
Willardson, R. K., T. C. Harman, P. F. Choquard, and A. C. Beer—E5
Wu, Ta-You and G. E. Tauber—A4
Yuster, Philip, Sol Rocklin, Warren Ramler, and Charles Delbecq—I6
Zener, Clarence—C1
Ziomek, J. S., E. A. Piotrowski, and E. N. Walsh—S11
Zrgyres, P. N. and A. H. Kahn—C9
Zwerdling, Solomon and Ralph S. Halford—S10

MINUTES OF THE 1954 WINTER MEETING AT THE UNIVERSITY OF CALIFORNIA, BERKELEY, CALIFORNIA, DECEMBER 28–30, 1954

(Corresponding to *Bulletin of the American Physical Society*, Volume 29, No. 8)

THE 1954 Winter meeting of the American Physical Society was held at Berkeley, California, on Tuesday, Wednesday, and Thursday, December 28, 29, and 30, 1954. This was a joint meeting of the Society and the American Association for the Advancement of Science (AAAS), whose meetings were held throughout all of the same week on the campus of the University of California. As a result, our Society sponsored a joint session with the Third Berkeley Symposium on Mathematical Statistics and Probability before our own meetings began. This was Session A, Monday afternoon. A supplementary bulletin, issued by the very efficient and active Local Committee headed by W. A. Nierenberg, called attention to a Symposium on Biological and Medical Physics.

This meeting of the Society was by far the largest meeting in the history of the West Coast both from the point of view of the number of papers given and of the attendance.

There were 163 contributed papers, 4 post-deadline papers, and 28 invited papers. The sessions were well attended with standing room only the situation at a number of them. There were nearly 600 present at the session of invited papers on high-energy physics and more than 500 members and guests registered for the meetings.

The dinner of the Society was held on Thursday evening, at the Men's Faculty Club. Professor A. C. Helmholz was the presiding officer and Professor R. T. Birge the principal speaker. His topic, "Science and Pseudo-Science," was informative, interesting, and at times amusing. There were about 200 members, wives, and guests at this very fine dinner.

The Local Committee did an outstanding job in making this a very smoothly run and pleasant meeting. A cocktail party, jointly sponsored by the Department of Physics and the Staff of the Radiation Laboratory at Berkeley and Livermore, was held in the Claremont Hotel just before the dinner of the Society. Other arrangements, such as coffee hours for which the wives of the Physics Department Staff were responsible, and tours of the bay area and of the Radiation Laboratory made this a very successful meeting.

Editorial note: The following information, which modesty prevented Secretary Kaplan from supplying, was provided by a source of the highest reliability. "A. C. Helmholz, who presided at the dinner on Thursday evening, announced that this was the last meeting at which Dr. Joseph Kaplan was serving as the Pacific Coast Secretary. After a brief description of the distinguished services which Dr. Kaplan had rendered, those present gave a rising vote of thanks to him. Dr. Kaplan responded by introducing his successor, Dr. William A. Nierenberg."

This was the last meeting of the writer as Local Secretary for the Pacific Coast. The success of this meeting was due in great part to the fine work of the new Secretary and his cooperative colleagues in Berkeley. I wish now formally to thank him and his colleagues, as well as all of the outstanding physicists in the West with whom I have had the privilege of planning these meetings. Finally, my best wishes to Dr. W. A. Nierenberg for a long, pleasant, and successful term as Local Secretary.

J. KAPLAN, *Local Secretary for the Pacific Coast*
University of California
Los Angeles 24, California

Errata Pertaining to Papers D4, H1, H2, H3, and P15

D4, by John C. Burgess. In line 3, instead of Stanford, California, read Stanford Research Institute. In equation (2), instead of $\bar{Q}_m^2>0.75$, read $\bar{Q}_m^2<0.75$.

H1, by J. K. Trolan, J. P. Barbour, E. E. Martin, and W. P. Dyke. In the byline read Linfield College, instead of Winfield College.

H2, by George Barnes. In the byline read Linfield College, instead of Winfield College.

H3, by W. P. Dyke, J. P. Barbour, J. K. Trolan, and E. E. Martin. In the byline read Linfield College, instead of Winfield College. Also, in the next to the last sentence read "Excessive transport which would otherwise undesirably alter the gross cathode geometry," instead of "Excessive transport which would otherwise undesirably after the gross cathode geometry."

P15, by Harry R. Bowman and Lloyd G. Mann. Ninth line: Instead of 1.2 Mev, read 0.9 Mev. Tenth line: Instead of 14 ± 2 Mev, read 9.5 ± 1.5 Mev.

PROGRAMME

MONDAY AFTERNOON AT 1:30

145 Dwinelle Hall

(MINA REES, presiding)

Statistical Mechanics

Joint Session with the Third Berkeley Symposium on Mathematical Statistics and Probability

Invited Papers

A1. Hopf-Wiener Equation System and Matrix Factorization. NORBERT WIENER, *M.I.T.* (30 min.)

A2. Foundation of Kinetic Theory of Gases. MARK KAC, *Cornell University.* (30 min.)

A3. Effect of Dimensionality on Long-Range Order in Crystals. ELLIOTT MONTROLL, *O.N.R.* (30 min.)

TUESDAY MORNING AT 10:00

310 Le Conte Hall

(R. F. BACHER presiding)

B1. High-Energy Interactions at the Cosmotron. R. P. SHUTT, *Brookhaven National Laboratory.* (30 min.)

B2. The Unstable Particles. C. D. ANDERSON, *California Institute of Technology.* (30 min.)

B3. S-Particles and Charged Heavy Particles. A. LAGARRIGUE, *Ecole Polytechnique* (Paris). (30 min.)

B4. Theoretical Views on the New Particles. M. GELL-MANN, *University of Chicago.* (30 min.)

THURSDAY MORNING AT 10:00

4 Le Conte Hall

(A. L. BENNETT, presiding)

Contributed Papers

C1. Quantitative Fluid Flow Visualization with Streaming Birefringence.* HAROLD WAYLAND, *California Institute of Technology.*—Birefringence of flow was studied in the annular space between a fixed outer and a rotating inner cylinder. With dielectric walls and well collimated light beam, quantitative measurements were possible within 0.1 mm of the wall. For an aqueous colloidal solution of bentonite, shear stress could be evaluated by birefringence measurements only when, for a given birefringence, the angle of extinction was the same in the unknown flow as in a known laminar flow. In turbulent shear flow this is not generally true. For a pure liquid, ethyl cinnamate, the angle of extinction remained at 45° to the streamlines, within experimental error, under all flow conditions obtainable; thus even in turbulent shear flow the birefringence probably arises primarily from the principal stresses. Assuming birefringence proportional to mean shear stress permits construction of a velocity profile across the gap, yielding the correct value of velocity of moving wall within limits of experimental error. Thus in two-dimensional shear flow one can measure the mean shear stress by means of streaming birefringence of a pure liquid.

* This work was carried on at the Centre de Recherche sur les Macromolecules of the CNRS at Strasbourg, France, with the aid of a fellowship of the John Simon Guggenheim Memorial Foundation.

C2. Effects of Attenuating Materials on Detonation Induction Distances in Gases.* MARJORIE W. EVANS, FRANK I. GIVEN, AND WILLIAM E. RICHESON, JR., *Stanford Research Institute.*—Detonation induction distance, x_d, is the distance from ignition point to beginning of detonation in a detonable gas. It varies with composition of gas, method of ignition, and pressure. Theory predicts that it depends upon the distance required to form a precompression shock wave of strength comparable to that of the detonation wave. Absorption of precompression waves at the walls of a cylindrical tube should lead to delay in formation of the detonation wave, or with sufficient absorption to complete suppression. The validity of this concept was tested using a stoichiometric H_2-O_2 mixture at initial pressure of 1 atmosphere, with spark ignition. The value of x_d was established in a smooth-walled steel tube of 2-inch inside diameter, and was then determined for tubes of similar diameter but with porous sintered bronze walls. Results were obtained for several thicknesses and porosities of wall material, the acoustic properties of which were known. Results showed that attenuating wall materials had a pronounced effect, more than doubling x_d in some instances. It was larger for 1-inch than for ½-inch thick walls, and for coarse than for fine wall material.

* This research was supported by Soundrive Engine Company, Los Angeles, California.

C3. Growth, Coalescence, and Decay of Vortices in a Jet Accompanying Pfeifentone. A. B. C. ANDERSON.—A shadowgraph system has been developed enabling one to take two successive shadowgraphs of microsecond time exposure and separated by a suitable time interval, whose magnitude may be varied at will. These shadowgraphs show the vortex train in the jet at successive instants. With this, studies of a carbon dioxide jet discharging into the atmosphere from an orifice (0.250 in. diameter and 0.093 in. thick) terminating a cylindrical resonant cavity (0.80 in. diameter and 12.0 in. long) were made. Typical results show that in flow regimes where a regular system of vortices shed from an orifice tend to coalescence downstream, a uniform train of larger and more evenly spaced vortices result. When two vortices coalesce, the downstream vortex tends to enlarge permitting the upstream vortex to move inside of the downstream vortex, leading to their coalescence. Pure tones are accompanied by a smooth and even array of vortices; complex tones by a somewhat distorted and irregular array. In one flow regime, a double train of vortices whose axes make a considerable angle with respect to each other, emerges from the orifice. Each train contains an alternate set of vortices shed by the orifice. The plane made by the two axes of the two trains may remain fixed or may rotate in space about the axis of the orifice.

C4. I. Shock Front Structure in Argon. JOHN W. BOND, JR., *Los Alamos Scientific Laboratory.*—One-dimensional steady-state shocks in argon of such strength that one degree of ionization is of importance are considered. The equilibrium region behind the shock front is determined by assuming the ideal-gas equation of state and using the Saha equation. The equilibrium conditions are specified by the ordinary shock equations. The non-equilibrium region which defines the shock front may be considered in two parts. The first part is that in which the translational degrees of freedom of the gas atoms are first excited and then become equilibrized. If the "local" temperature at which translational equilibrium is achieved is sufficiently high, energy will be transferred to other degrees of freedom which, in the case of argon, are those of electronic excitation and ionization. The relaxation time for complete thermal equilibrium to be reached is determined by consideration of the individual atomic interactions that take place. Finally, recombination of the electrons and the ions is treated by a method of detailed balancing. Thus the luminous region behind the shock front is preceded by a high-temperature region whose width decreases with increasing shock velocity.

C5. Detonation in Gas at Low Pressure. ARTHUR L. BENNETT AND HENRY W. WEDAA, *U. S. Naval Ordnance Test Station.*—A tube with driver section 97 cm long and an experimental section 444 cm long was used. The driver and 215 cm of the experimental section are 12 cm in diameter. A smooth transition section 46 cm long leads to a 10-cm square section 183 cm long fitted with windows. Detonation in the experimental section is initiated by spark ignition of $C_2H_2+O_2$ and ensuing detonation in the driver section. The driver is separated from the experimental section by a zip-tape diaphragm so that the initial pressures may be different. Detonation velocity is determined by CRO recording, at 1.5×10^5 cm/sec, of the pulses from accurately located ionization probes throughout the experimental section. For $2H_2+O_2$ the average velocity over the last 110 cm in 10^5 cm/sec (for the pressure in mm Hg) is: 2.82(400); 2.72(100); 2.65(50); 2.55(20). The observed velocities show no appreciable dependence on the ratio of initial driver pressure to that of hydrogen-oxygen over the limited ratio explored (0.42 to 2.5 for various experiments). The light at 46 cm from the end collimated by slits ⅜ mm wide 3 to 25 mm long (175 mm separation) was measured by an *S*4 photomultiplier and high speed CRO. At 400 mm pressure the light rises immediately to a peak, then falls about 25 percent within 10 μsec, then decays another 20 percent over the 150 μsec recorded. At lower initial pressures, the rise becomes less steep, about 2 μsec at 50 mm, 5 μsec at 20 mm, and 7 μsec at 10 mm.

C6. Shock Waves in Air Produced by Waves in a Plate. WILLIAM A. ALLEN, JOE M. MAPES, AND EARLE B. MAYFIELD, *U. S. Naval Ordnance Test Station.*—A shadowgraphic technique has been used to measure surface motion of a series of steel plates while they deform under impact caused by ½-in. diameter steel cylinders fired into their back surfaces at about 3000 ft/sec. Shadowgraphs show two air shock waves separated about 3 μsec in time. Extrapolation of the air shocks back into the metal indicates that the second wave is associated with a disturbance that travels through steel at the same velocity as the initial longitudinal sound wave. This second disturbance appears associated with the actual plastic deformation of the free surface.

C7. Velocity of Explosively-Induced Shock in Steel. SAMUEL KATZ, *Stanford Research Institute.*—The velocity of explosively induced shock in steel has been measured by a new method. The test specimen is a rectangular steel plate with the two large surfaces covered with uniform layers of *C*-3 explosive and initiated at diagonally opposite edges. The two shocks generated in the steel collide at normal incidence and produce severe shock twinning and other grain deformation in a sharply defined, narrow zone whose width is related to the explosive thickness. The shock velocity is given by $v_s=v_e \sin d$, where d is the angle between the deformed zone and the loaded surface, and v_e is the detonation velocity. $v_s=4.93\pm0.13$ mm/μsec for mild steel, and 4.5 mm/μsec for 18–8 stainless steel. These values compare with those of Pack *et al.*[1] of 5.24 mm/μsec and of Allen[2] of 4.6 mm/μsec, both for mild steel. The hydrodynamic theory,[3] based on an extrapolation of Bridgman's data for an incident explosive pressure of 0.17 megabars, particle velocity 0.163 mm/μsec, and initial density 1.6 g/cm³, predicts a shock velocity in iron of 5.2 mm/μsec.

[1] Pack, Evans, and James, Proc. Phys. Soc. (London) **60**, 1 (1948).
[2] W. A. Allen, J. Appl. Phys. **24**, 1180 (1953).
[3] G. E. Duvall (private communication).

TUESDAY MORNING AT 10:00

3 Le Conte Hall

(V. F. LENZEN, presiding)

Contributed Papers

D1. On the Scattering of Electromagnetic Waves by a Bounded Lattice of Parallel Cylinders,* V. TWERSKY, *Sylvania Electric Products Inc.*—The two-dimensional problem of the scattering of a plane electromagnetic wave by a bounded lattice of parallel cylinders is treated. The lattice cell is a rectangle; the lattice itself is in the form of a slab of infinite length and finite thickness. Starting with a "self-consistent" representation for the field in terms of cylindrical waves, we derive expressions for the reflected, internal and transmitted waves in terms of certain sets of plane waves. The amplitudes and propagation coefficients of these plane waves are given by certain algebraic equations. The result is applied to determine the conditions for perfect reflection and maximum transmission (or equivalently, to derive expressions for the centers and widths of the stopping and pass bands), and to the artificial dielectric. The present results are either generalizations of, or equivalent to, certain results obtained originally by Ewald, Darwin, Laue, or Kohler. However, the present derivation, which is based on the boundary value problem of the bounded array, allows for more careful consideration of certain features; e.g., Darwin's postulated equations are here derived on the basis of Maxwell's equations subject to certain restrictions, the existence of a "medium" (with or withouts sharp boundaries) is not assumed, etc.

*Work supported by Signal Corps contract.

D2. A Modified Holtzmark Distribution. S. GASIOROWICZ, M. NEUMAN, AND R. RIDDELL, JR., *University of California, Berkeley.*—The probability distribution of the force due to a random distribution of particles generating a Newtonian potential (the so-called Holtzmark distribution) is of considerable importance in astrophysical applications.[1] One of the difficulties encountered in working with this distribution is that moments, beginning with the second one, do not exist. The divergence of these moments is a reflection of the singularity of the potential at the origin, i.e., there is no mechanism for preventing a particle from getting close to the origin. Clearly the nearest neighbors call for a more careful dynamical treatment, where the correlations are not disregarded. A distribution, excluding N nearest neighbors from statistical consideration, has been derived. Its characteristic function is given by

$$\psi^{(N)}(k)=\frac{1}{\Gamma(N)}\int d\bar{n}(r)[\bar{n}(r)]^{N-1}\times\exp\left\{\int_r^\infty d\bar{n}(r')(e^{-ik\cdot F(r')}-1)-\bar{n}(r)\right\}$$

where $F(r')$ is the force at r' and $d\bar{n}(r')$ the average number of particles in a volume d^3r. This distribution yields $(N+1)$ finite moments. This work was performed under the auspices of the U. S. Atomic Energy Commission.

[1] S. Chandrasekhar, Revs. Modern Phys. 15, 1 (1943).

D3. On Dynamical Friction. R. RIDDELL, JR., M. NEUMAN, AND S. GASIOROWICZ, *University of California, Berkeley.*—This dynamical friction may be defined as the expectation value of the force acting on a particle which moves in a field of force due to other particles.[1] This quantity has been studied in two ways: (i) a hydrodynamical approach in which the modification of the distribution function of a system due to the introduction of a test particle moving with a fixed velocity has been investigated under the assumption of small deviations from equilibrium, and (ii) a statistical approach using the modified Holtzmark distribution, for which second moments exist has been investigated. Here a uniform density was assumed and $\langle F(Z(t))_{Av}\rangle$, where $Z(t)$ is the orbit subject to the (fluctuating) force, was expanded. Explicit expressions for the coefficient of dynamical friction were obtained in the limit of high and low densities. The two approaches serve to complement each other in that the first seems more suited to long relaxation times, whereas the expansion used in the statistical approach appears most valid if these times are short. This work was performed under the auspices of the U. S. Atomic Energy Commission.

[1] J. Kirkwood, J. Chem. Phys. 14, 180 (1946).

D4. Apparent Limit of Convergence of the Perturbation Series Solution for the Free Undamped Duffing Equation with Hardening Spring. JOHN C. BURGESS, *Stanford, California.*—The exact solution of the equation

$$\ddot{q}+\kappa^2(q+\mu^2q^3)=0,\quad \mu^2>0 \tag{1}$$

has been given by Weigand* in terms of a complete elliptic integral of the first kind. This solution can be expanded in a power series in the dimensionless maximum displacement $\bar{Q}_m\equiv Q_m(\frac{3}{4}\mu^2)^{\frac{1}{2}}$,

$$\eta^2=1+\bar{Q}_m^2-\frac{\bar{Q}_m^4}{24}+\frac{\bar{Q}_m^6}{24}-\cdots,\quad \bar{Q}_m^2>0.75, \tag{2}$$

where Q_m is the maximum value of q and $\eta\equiv\omega/\kappa$, ω being the circular frequency of the motion. Solution of (1) by the perturbation method yields a power series in $\bar{Q}_m$ that is identical to (2) in the first four terms, the extent to which both series were evaluated, but does not provide a limit of convergence. It is usual to state only that the perturbation parameter must be "small enough." Comparison of the two series suggests that the limit of convergence of the perturbation series solution for (1) is $\bar{Q}_m^2=0.75$.

* A. Weigand, "Die Berechnung freier nichtlinearer Schwingungen mit Hilfe der elliptischen Functionen," Forschung, Bd. 12, No. 6, 274–284 (1941).

D5. Integral Equation Solution of Space-Charge Wave Propagation. PHILIP PARZEN, *The Johns Hopkins University.*—Previous solutions[1] of the propagation of space-charge waves in a drift tube with infinite longitudinal magnetic focusing field result in a complicated transcendental equation for the propagation constant, which can be solved only numerically. An integral equation method is given for obtaining approximate closed expressions for the propagation constant. For the important practical case where the ratio of drift tube radius to beam radius is infinite, using Ramo's notation,

$$\left(\frac{T}{\gamma_0}\right)^2=\frac{2}{(\gamma_0 a)^2}\frac{1}{I_0K_0+I_1K_1},$$

where I and K are modified Bessel functions of argument $\gamma_0 a$. This method is easily extended to the case in which the charge density and beam velocity vary across the beam. The effect of a varying velocity is to cause propagation constants of the two modes to differ from the beam wave number by different amounts.

[1] S. Ramo, Proc. Inst. Radio Engrs. 27, 757 (1939).

D6. The Statistical Thermodynamics of Isotope Effects. I. Theory of Equilibrium Processes.* IRWIN OPPENHEIM, *National Bureau of Standards.*—A statistical mechanical theory of isotope effects on the thermodynamic properties of gases and liquids has been developed. Use has been made of the expansion of the quantum mechanical partition function in powers of $\hbar$[1] to obtain expansions of the thermodynamic properties of the type

$$G = G_{\text{classical}} + \Lambda^{*2} G_1 + \Lambda^{*4} G_2 + \cdots,$$

where Λ^* is the mean de Broglie wavelength. The results are valid in intermediate temperature ranges where the effects of statistics are not important. The differences in various thermodynamic properties of isotopes are computed with the aid of classical radial distribution functions and the computations are applicable to dense gases and liquids near the critical point. An alternative formulation in terms of the Wigner distribution function has also been derived. Results may be expressed in terms of an effective temperature defined in terms of the mean kinetic energy.

* Supported in part by the U. S. Atomic Energy Commission, Division of Research.
[1] J. G. Kirkwood, Phys. Rev. **44**, 31 (1933).

D7. Statistical Thermodynamics of Isotope Effects. II. The Equation of State of the Hydrogen Isotopes at Intermediate Densities.* ABRAHAM S. FRIEDMAN AND IRWIN OPPENHEIM, *National Bureau of Standards.*—The equation of state for a dense gas is expressed in terms of reduced thermodynamic variables. These are given in terms of a classical part and a quantum mechanical part. The latter is dependent on the quantum mechanical parameter Λ^* and the derivative, with respect to the reduced volume, of a series of integrals of the radial distribution functions.[1] A generalized table of quantum mechanical compressibility factors is obtained. Using the classical 6–12 Lennard-Jones intermolecular force constants for hydrogen,[2] the differences in the compressibility factors of the six isotopic hydrogen molecules are computed. The results for $Z_{H_2} - Z_{D_2}$ (where $Z = pV/NkT$) are in excellent agreement with the experimental values[3] over a wide temperature and density range.

* Supported in part by the U. S. Atomic Energy Commission Division of Research.
[1] See preceding abstract.
[2] White, Friedman, and Johnston, Phys. Rev. **79**, 235(A) (1950).
[3] A. S. Friedman, dissertation, Ohio State University (1950); H. L. Johnston *et al.*, MDDC—850.

D8. Polarizability of the Deuteron. B. W. DOWNS, *Stanford University.*—By means of a variation method the polarizability of the deuteron in a uniform electric field has been calculated under the assumption that the ground state of the deuteron is an S state. A trial function $\psi_0 + E\psi_1$ is used to obtain an expression for the polarization energy. $E\psi_1$ is the odd parity modification of the ground state wave function, ψ_0, introduced by the perturbing electric field, E. This expression for the polarization energy is minimized with respect to ψ_1. This process leads to a differential equation for $\psi_1 \cdot \psi_1$ and the polarizability have been calculated for two cases: the n-p interaction in the deuteron was taken to be (1), a Serber interaction and (2), a square well interaction for odd parity states. The extension of this calculation to include the deuteron D wave will be discussed. A comparison will be made with the previous work of Ramsey, *et al.*[1]

[1] Ramsey, Malenka, and Kruse, Phys. Rev. **91**, 1162 (1953).

TUESDAY MORNING AT 10:00

1 Le Conte Hall

(L. I. SCHIFF, presiding)

Contributed Papers

E1. Stars Formed by Protons of 3.2 Bev from the Bevatron. JOSEPH LANNUTTI, GERSON GOLDHABER, AND STEPHEN J. GOLDSACK, *University of California, Berkeley.*—Stacks of nuclear emulsions have been exposed to the primary beam of the Bevatron at a nominal energy of 3.2 Bev. It is estimated that most of the collimated relativistic particles in the emulsions are protons of the full energy. A summary of the statistics on 118 stars with $N_H \geq 2$ formed by such particles is as follows:

No. of prongs	2–5	6–10	11–15	16–20	21–25	>25
No. of stars	45	38	20	8	4	3

Scattering and grain density measurements have been made on 70 tracks longer than 3 mm, and with grain density less than five times minimum to determine the energy and nature of the particle. The results among tracks >1.4 minimum were: π mesons, 9; protons, 38. The corresponding number for shower particles were 14 and 5. Four shower particles were too energetic to be identified. These tracks came from 270 stars. After solid-angle corrections this corresponds to a mean production of approximately one charged π meson per interaction. This work was performed under the auspices of the U. S. Atomic Energy Commission.

E2. Energy Dependence of Photoyields of N^{17}.* D. D. REAGAN, *Stanford University.*—Yield curves of N^{17} arising from electron and x-ray bombardment have been measured for the elements O, F, Ne, Mg, and Al. N^{17} was identified by its delayed neutrons which made the measurement of low yields feasible. It is clear, in spite of the low yields, that for the more complex reactions the cross section is very broad, energy-wise, and increases in the region of 150–350 Mev.

* Supported by the joint program of the Office of Naval Research and the U. S. Atomic Energy Commission.

E3. Angular Distribution of Bremsstrahlung Photons. JOHN D. ANDERSON, ROBERT W. KENNEY, AND CHARLES A. MCDONALD, JR., *University of California, Berkeley.*—The angular distribution of photons in the full-energy bremsstrahlung spectrum from the Berkeley synchrotron has been measured with a pair spectrometer at 200-, 250-, and 300-Mev photon energy. From the 20-mil platinum target, the full widths at half maximum were observed to be 8.9 ± 0.1, 8.6 ± 0.1, and 7.7 ± 0.2 milliradians respectively. This is in gross agreement with the value 9.2 ± 0.6 milliradians obtained by Rosengren[1] from the same target at 17-Mev photon energy in the full-energy bremsstrahlung spectrum from the Berkeley synchrotron. The angular distribution from the 20-mil Pt target was found to fit very nearly an exponential with a discrepancy at the origin which may be accounted for by the finite target width. The observed distributions will be compared with the theoretical distributions of Schiff and of Lanzl and Hanson. This

work was performed under the auspices of the U. S. Atomic Energy Commission.

[1] J. W. Rosengren, University of California Radiation Laboratory Repor No. UCRL-1999 (1952).

E4. Photodisintegration of Deuterons by High Energy Gamma Rays. DWIGHT R. DIXON AND KENNETH C. BANDTEL. *University of California, Berkeley.*—Bremsstrahlung of 335-Mev electrons was incident on a liquid deuterium target. The protons were detected with a telescope consisting of twelve scintillation counters. Pulses from the counters were combined, delayed, presented on an oscilloscope and recorded photographically. The height of the pulse from the first counter determines the dE/dx of a particle and the number of succeeding pulses determines the range. This allows one to identify the protons and measure their energy. Correction for nuclear absorption and scattering of protons has been determined experimentally using proton beams of various energies from the 184-in. cyclotron. Cross sections have been measured at laboratory angles of 49°, 75°, 106°, and 141° and at nine energies ranging from 136 Mev to 292 Mev with statistical errors of about ten percent. Results are consistent with those from Cornell University, Illinois Institute of Technology and California Institute of Technology. This work was performed under the auspices of the U. S. Atomic Energy Commission.

E5. Analysis of High-Energy Photons from the Cyclotron Target. HARLAN SHAW, DAVID COHEN, BURTON J. MOYER, AND CHARLES WADDELL, *University of California, Berkeley.*—Pair spectrometer techniques have improved considerably over those employed in earlier data,[1] allowing more clear answers to be given on the spectra contributed by proton bremsstrahlung and by π^0 decay. In particular, the symmetry properties of the total π^0 radiation may be subjected to closer scrutiny in order to show the presence or absence of other radiative processes in observable amounts. Characteristics of the bremsstrahlung radiation offer information concerning the nature of the collisions of high-energy protons with nuclei. The degree to which the nucleus may act as an integral unit in these collisions, as distinguished from a swarm of nucleons, enters into the interpretations of the bremsstrahlung spectra. A few instrumental features will be described. This work was performed under the auspices of the U. S. Atomic Energy Commission.

[1] W. E. Crandall and B. J. Moyer, Phys. Rev. 92, 749 (1953).

E6. Interaction of 95-Mev Protons with He^4.* J. M. TEEM,† W. SELOVE, AND U. E. KRUSE,‡ *Harvard University.*—The external proton beam of the Harvard cyclotron was used to bombard a liquid helium target, and the energy spectra of protons and deuterons scattered in the interaction were observed with a scintillation counter telescope by measuring simultaneously their range and specific ionization. The differential cross section for elastic scattering was measured from the region of the nuclear-Coulomb interference into the backward hemisphere. Notably, the results fail to show the characteristic diffraction minimum observed for lower incident energies or with heavier target nuclei, indicating the high transparency of He^4 for protons of this energy. The angular distribution of the deuterons from the reaction $He^4(p,d)He^3$ was also studied, and these results analyzed in terms of "pick-up" theory[1] to yield information concerning the momentum density function for a neutron in He^4. Inelastic proton spectra were measured at several angles and will be discussed.

* Assisted by the joint program of the U. S. Atomic Energy Commission and the Office of Naval Research.
† Present address, California Institute of Technology.
‡ Present address, The University of Chicago.
[1] G. F. Chew and M. L. Goldberger, Phys. Rev. 77, 470 (1950).

E7. Elastic and Inelastic Scattering of 90-Mev Neutrons by Deuterons. LEROY KERTH AND BYRON L. YOUTZ. *University of California, Berkeley.*—The angular distribution of the cross section for the elastic scattering of 90-Mev neutrons by deuterons has been measured, using counters to identify the particles by dE/dx and energy. Comparison with the data of Stern and Bloom[1] (for elastic scattering of protons by deuterons) shows agreement indicating the charge symmetry of nuclear forces. Comparison with calculations of Chew[2] and of Horie *et al.*[3] shows qualitative agreement. The pseudo elastic scattering of neutrons by the bound protons of the deuteron has also been investigated. The data is in disagreement with the calculations of Chew[4] but is in agreement with the data of Hadley[5] at 270 Mev. This work was done under the auspices of the U. S. Atomic Energy Commission.

[1] Stern, UCRL-2236; Bloom, UCRL-2237.
[2] Chew, Phys. Rev. 74, 809 (1948).
[3] Horie, Tamura, and Yoshida, Progr. Theoret. Phys. 8, 341 (1952).
[4] Chew, Phys. Rev. 84, 710 (1951).
[5] Hadley, UCRL-1542 (1951).

E8. The Production of High Energy Neutrons and Deuterons from the Stripping of Helium. WARREN HECKROTTE, *University of California, Berkeley.*—The differential cross sections for the production of high-energy neutrons and deuterons from the interaction of 490-Mev helium nuclei with heavier target nuclei have been previously measured at this laboratory.[1] The production of neutrons from the He^3 results from the stripping off of one or both of the protons of He^3. One would not, however, expect the two protons to be stripped off simultaneously, so that one need consider the effect of only one proton being stripped off. In calculating the differential cross sections it is necessary to include the interaction between the neutron and the remaining proton after the stripping event. Because of the virtual level of the singlet n-p state, the effect of this interaction reduces substantially the width of momentum distribution of the neutron from what would be obtained by neglecting this interaction. The calculation for the deuteron production is similar except that the interaction between the neutron and proton leads to binding. The calculated and experimental results will be compared. This work was performed under the auspices of the U. S. Atomic Energy Commission.

[1] Schecter, Crandall, Millburn, and Ise, University of California Radiation Laboratory Report 2685.

E9. Interactions of 380-Mev Alpha Particles in Ilford G.5 Emulsion. DORA F. SHERMAN, *Radiation Laboratory, University of California, Berkeley.*—The study of stars produced by α particles in nuclear research emulsion begun by Eugene Gardner[1] has been extended to α particles of 380-Mev. Ilford G.5 emulsion has been used. The mean free path for star production is 18.1 ± 1 cm. The frequency distribution of the number of prongs per star is given in the table:

Number of prongs	1	2	3	4	5	6	7	8
Percent	2.6%	36.3	23.2	18.7	9.2	7.1	2.1	0.8

The most interesting feature of these stars is the frequent occurrence of fast singly charged particles which usually emerge at a small angle to the forward direction. Of these stars, 40.5 percent have one such grey prong, 19.8 percent have two, and 4.9 percent have three, in addition to black prongs. About one-eighth of the stars consist entirely of fast single charged particles. This includes all the one-prong stars in the table, 18 percent of the two-prong stars, and 10 percent of the three-prong stars. The above data were obtained by area scanning. An efficiency check was made by scanning along the track. In neither case were any "zero-prong" stars observed. Observation of the number of stars with a prong of range less than 50 microns, permits placement of a lower limit of 20 percent on the number of events occurring in light nuclei. This work was performed under the auspices of the U. S. Atomic Energy Commission.

[1] Eugene Gardner, Phys. Rev. 75, 379 (1949).

TUESDAY AFTERNOON AT 2:00

1 Le Conte Hall

(E. TELLER, presiding)

Theoretical Physics

Invited Papers

F1. Reactions and Models of Light Nuclei. R. F. CHRISTY, *California Institute of Technology.* (30 min.)

F2. Some Implications of Causality for Scattering. R. KARPLUS AND M. A. RUDERMAN, *University of California, Berkeley.* (30 min.)

F3. Application of the Monte Carlo Method to the Theory of Liquids. A. W. ROSENBLUTH AND M. N. ROSENBLUTH, *Los Alamos Scientific Laboratory* (at present on leave to the Radiation Laboratory, Berkeley). (45 min.)

F4. On the Classical Field Theory of Nuclear Forces. M. H. JOHNSON, *Lockheed Research Laboratory,* AND E. TELLER, *University of California, Berkeley.* (45 min.)

TUESDAY AFTERNOON AT 2:00

4 Le Conte Hall

(G. SEABORG, presiding)

Invited Paper

G1. Radio Chemical Studies on Nuclear Reactions at the Cosmotron. J. M. MILLER, *Department of Chemistry, Columbia University, and Brookhaven National Laboratory.* (30 min.)

Contributed Papers

G2. Long-Lived Radioactive Aluminum-26. J. R. SIMANTON, R. A. RIGHTMIRE, A. L. LONG, AND T. P. KOHMAN, *Carnegie Institute of Technology.*—There is theoretical[1] and experimental[2] evidence for a level in Al^{26} below the 6-second 0+ level. The ground state apparently lies 4.0 Mev above that of Mg^{26}, probably has a 5+ configuration, and evidently is very long-lived. Weak β and γ radioactivity has been observed in aluminum carrier isolated from magnesium bombarded by deuterons, the specific activity remaining constant through numerous chemical separations. The most prominent radiations correspond to positron emission to the 1.83-Mev first excited state of Mg^{26}. The yield indicates a half-life of $\sim 10^6$ years, consistent with a $5+ \rightarrow 2+$ (second-forbidden) transition.

[1] R. W. King and D. C. Peaslee, Phys. Rev. **90**, 1001 (1953); P. Stähelin, Helv. Phys. Acta **26**, 691 (1953); Phys. Rev. **92**, 1076 (1953); S. A. Moszkowski and D. C. Peaslee, Phys. Rev. **93**, 455 (1954).
[2] Montalbetti, Katz, and Goldemberg, Phys. Rev. **91**, 659 (1953); Haslam, Roberts, and Robb, Can. J. Phys. **32**, 361 (1954); Kluyver, van der Leun, and Endt, Phys. Rev. **94**, 1795 (1954); C. P. Browne, Phys. Rev. **95**, 860 (1954).

G3. Radiations of Ba^{128}–Cs^{128}. J. M. HOLLANDER AND M. I. KALKSTEIN, *Radiation Laboratory, University of California, Berkeley.*—The chain Ba^{128}–Cs^{128} has been prepared in the 184-inch cyclotron by the reaction $Cs^{133}(p,6n)Ba^{128}$, and their radiations have been studied with a 50-channel scintillation spectrometer, a scintillation coincidence spectrometer, and a magnetic lens beta-ray spectrometer. Gamma rays of energy 440 kev and 980 kev have been observed belonging to the decay of Cs^{128}. A 270-kev gamma ray is observed in the decay of Ba^{128}. The beta-ray spectrometer data indicate three positron groups of end-point energies 3.0, 2.5, and 1.5 Mev with relative abundances of 7:3:0.3, respectively. These belong to the decay of Cs^{128} which decays mainly by positron emission with a ratio of β^+/EC of 3:1. Coincidence data will also be given and a decay scheme presented. This work was performed under the auspices of the U. S. Atomic Energy Commission.

G4. Gamma Rays in the Alpha Decay of 100^{254}. F. ASARO, F. STEPHENS, AND I. PERLMAN, *University of California, Berkeley.*—By alpha particle-gamma ray coincidence measurements, L x-rays and gamma rays of 42 ± 4 ($[2 \pm 1] \times 10^{-2}$ percent) and 94 ± 2 kev ($[4.4 \pm 1] \times 10^{-2}$ percent) were observed in the decay of 100^{254}. The L x-rays and the 42-kev gamma ray are interpreted as the transition in the daughter nucleus from the first excited state to the ground state. The abundance of L x-rays corresponded to a 15 percent alpha particle population to the first excited state. The spin of this level is established as two, even parity, from the conversion coefficient of the 42-kev gamma ray and other criteria. The 94-kev gamma ray is interpreted as an $E2$ transition from the second to the first even spin state. Reasonable estimates of a conversion coefficient indicate that the alpha particle population to the second excited state lies between 0.3 and 0.8 percent. After correction for energy differences, the alpha particles population to the second even spin state of even-even nuclei is a maximum for thorium emitters (no values below thorium), progressively decreases to a minimum for curium and then increases progressively for californium and element 100. This behavior was qualitatively predicted in Rasmussen's treatment of spheroidal nuclei.[1] This work was performed under the auspices of the U. S. Atomic Energy Commission.

[1] J. O. Rasmussen, Jr., University of California Unclassified Report, UCRL 2431 (1954).

G5. Alpha Groups and Angular Correlation of Am^{243}. F. STEPHENS, J. HUMMEL, F. ASARO, AND I. PERLMAN, *University of California, Berkeley.*—Using an alpha particle spectrograph, we have continued a study of Am^{243} showing alpha groups of 5.340 (0.17 percent), 5.309 (0.16 percent), 5.267 (87.1 percent), 5.224 (11.5 percent), and 5.169 (1.1 percent) Mev. We have also examined the angular correlation between alpha particles and the prominent 75-kev gamma ray. The data were best fit by the function, $W(\theta)=1-0.11\cos^2\theta$. The anisotropy in the correlation contributed by alpha particles which do not directly populate the 75-kev level was less than 3 percent. The spins of Am^{243} and Np^{239} have been measured at 5/2[1] and 1/2,[2] respectively. If the 75-kev gamma ray, which is an $E1$[3] transition, terminates at the ground state (spin 1/2) of Np^{239}, the only spin possible for the 75-kev level permitting any angular correlation is 3/2. Furthermore the theoretical correlation for this 5/2–3/2–1/2 sequence is $W(\theta)=1-0.14\cos^2\theta$, which is in good agreement with the observed correlation. This line of reasoning is inconsistent with the spin of 2.5 ± 0.2 calculated for the 75-kev level on the basis of the alpha particle energies and the Bohr-Mottelson theory. This work was performed under the auspices of the U. S. Atomic Energy Commission.

[1] J. Conway and R. McLaughlin, Phys. Rev. **94**, 498 (1954).
[2] J. Conway and R. McLaughlin, Phys. Rev. (to be published) (1954).
[3] F. Asaro and I. Perlman, Phys. Rev. **93**, 1423 (1954).

G6. The Alpha Decay of Pa^{231}. JOHN P. HUMMEL, F. ASARO, AND I. PERLMAN, *University of California, Berkeley.*—Using an alpha-particle spectrograph we have studied the alpha groups of Pa^{231}. Using Rosenblum's[1] energy for the 4.938-Mev group as a standard, the following groups have been observed −5.046 Mev (8.7 percent), 5.018 (23 percent), 5.001 (28 percent), 4.938 (27 percent), 4.843 (1.5 percent), 4.724 (10 percent), 4.667 (1.4 percent), and 4.627 (0.3 percent). These groups are essentially the same as observed by Rosenblum except that the 5.018 and 5.001-Mev groups were previously reported as a single group. (We have completely resolved these groups in a high-resolution run.) Also, the lowest energy group has not previously been reported. These alpha groups lead to a somewhat revised level scheme which accommodates the 27-kev gamma seen by Riou[2] and the 48-kev gamma seen by Mouhasser and Riou.[3] Also, the conversion electron data of Falk-Vairant[4] and gamma data of Moore[5] can be fitted to these levels forming a decay scheme for this nuclide. This work was performed under the auspices of the U. S. Atomic Energy Commission.

[1] Rosenblum, Cotton, and Bouissieres, Compt. rend. **229**, 825 (1949).
[2] M. Riou, Compt. rend. **234**, 1157 (1952).
[3] A. Mouhasser and M. Riou, Compt. rend. **238**, 2520 (1954).
[4] P. Falk-Vairant and M. Riou, J. phys. et radium **14**, 65 (1954).
[5] R. Moore, thesis, Ohio State University, AECU-2757 (1953).

G7. Tantalum Spallation and Fission Induced by 340-Mev Protons. WALTER E. NERVIK AND GLENN T. SEABORG, *University of California, Berkeley.*—Tantalum metal has been irradiated with 340-Mev protons in the 184-in. Berkeley cyclotron. Nuclides formed as spallation and fission products were separated chemically, identified, and their formation cross sections calculated. A very broad fission peak which extends from about mass number 20 to mass number 132 is observed. The maximum fission yield occurs in the region of the nuclide Kr^{83} and analysis of a set of contour curves fitted to the data indicates that either Hf^{166} or Lu^{166} is "the most probable fissioning nucleus." Comparison of the fission data of tantalum, bismuth, and uranium under the same bombardment conditions indicates that asymmetric fission is much more probable in tantalum than in either of the other elements. The total cross section for fission of tantalum with 340-Mev protons is estimated to be 4.1 mb. In the spallation region, neutron emission is observed to be the predominant reaction. Integration under the spallation yield curve indicates that of those tantalum target nuclei which received at least enough excitation energy to reach the region of "the most probable fissioning nucleus" less than one percent undergo fission; the remainder undergo spallation reactions. This work was performed under the auspices of the U. S. Atomic Energy Commission.

G8. Fission-Spallation Competition in Heavy Elements. R. A. GLASS, R. J. CARR, J. W. COBBLE, AND G. T. SEABORG, *University of California, Berkeley.*—A study of the competition of the fission and spallation processes in excited heavy element nuclei has led to some rather unexpected observations. In the alpha-particle-induced reactions (20 to 50 Mev) in Pu^{239}, for example, the spallation product excitation functions, while giving low cross sections as anticipated, showed the same shape as those predicted for nonfissioning nuclei by the statistical model. Further, for some reactions the emission of a proton in an $(\alpha,p2n)$ reaction was found to be favored over neutron emission in a similar three- article emission $(\alpha,3n)$ reaction. The integrated fission yield curves obtained by radiochemical analysis yielded total fission cross sections and were used to fix the nuclear radius. Such well-defined spallation excitation functions can be used to elucidate some of the factors governing the fission process itself in a comparison of different nuclear types. Data obtained for the Pu^{238}, Pu^{239}, and Pu^{242} spallation yields thus indicate the effects of mass type on the fissionability of nuclei. These results also can be interpreted on the basis of a statistical model. Certain features of noncompound nuclei effects also present in these reactions will be discussed. This work was performed under the auspices of the U. S. Atomic Energy Commission.

G9. Isomeric States in the Chain $Mo^{90}\rightarrow Nb^{90}\rightarrow Zr^{90}$. H. B. MATHUR AND E. K. HYDE, *University of California, Berkeley.*—In the decay of 5.7-hour Mo^{90} three distinct isomers of the odd-odd isotope Nb^{90} are produced. Nb^{90m_1} has a half-life of 24 seconds and Nb^{91m_2} has a half-life of 10 to 20 milliseconds. The ground state of Nb^{90} is the well-known 14.6-hour activity. Study of its radiations showed a delayed transition of 2.3-Mev energy in the even-even nucleus Zr^{90}. The chemical and spectrometer evidence supporting these assignments will be discussed. This work was done under the auspices of the U. S. Atomic Energy Commission.

G10. Decay Scheme of Np^{238}*. J. O. RASMUSSEN, *University of California, Berkeley,* AND H. SLÄTIS, *The Nobel Institute of Physics, Stockholm.*—The results of beta spectroscopic studies[1–3] and scintillation counter and coincidence studies[4] on Np^{238} are analyzed. The decay gives rise to a hard beta group of 1260 kev proceeding to the 44.2-kev state and three soft beta groups populating the levels near 1 Mev. Gamma transitions of 44.2, 102.0, 927, 941, 986, and 1030 kev occur. A beta-decay scheme is proposed involving six levels of the daughter nucleus Pu^{238}, namely, the known ground rotational band levels of energies (in kev) 0, 44.2, 146.2 and a higher cluster of levels at 1030, 1073, and either 1087 or 985. The decay scheme is discussed in respect of its consistency with the strong coupling approximation of the Bohr-Mottelson unified nuclear model. In particular, it is proposed that the levels at 1030 and 1073 kev probably constitute the two lowest rotational members of the first gamma-vibrational band in the strong coupling model.

* Work performed in part under the auspices of the U. S. Atomic Energy Commission.
[1] Freedman, Jaffey, and Wagner, Phys. Rev. **79**, 410 (1950).
[2] Slätis, Rasmussen, and Atterling, Phys. Rev. **93**, 646 (1954).
[3] Rasmussen and Passell, unpublished results.
[4] Rasmussen, Stephens, Strominger, and Åström (unpublished results)

G11. Gamma Rays of Ra^{225} and Tl^{209}. I. PERLMAN, F. STEPHENS, AND F. ASARO, *University of California, Berkeley.*—We have studied the gamma spectra associated with two of the beta emitters of the Th^{229} family. Chemically separated Ra^{225} showed L x-rays and a gamma ray at 39.5 ± 2.0 kev. The L x-ray intensity gave a maximum L conversion coefficient of 1.0, clearly indicating an $E1$ transition. The half-life of the 40-kev level was shown to be less than 2×10^{-9} sec.[1] Both the singles beta spectrum and that in coincidence with the 40-kev photon showed end points at 0.32 ± 0.03 Mev. Using coincidence techniques gamma rays of Tl^{209} were identified at 0.12, 0.45, and 1.56 Mev, all of which were in coincidence with one another. Together with the beta energy of 1.99 Mev[2] this yields a total decay energy of 4.12 Mev in reasonable agreement with the calculated value 3.92 Mev.[3] Furthermore, Harvey[4] has found levels in Pb^{209} at 1.56 and 2.03 Mev (among others). The present work is in excellent agreement with these levels and indicates another around 2.13 Mev. This work was performed under the auspices of the U. S. Atomic Energy Commission.

[1] J. Rasmussen and F. Stephens, unpublished data (1954).
[2] Wagner *et al.*, Phys. Rev. **88**, 171(A) (1952).
[3] Glass, Thompson, and Seaborg, J. Inorg. and Nucl. Chem. (to be published).
[4] J. A. Harvey, J. Can. Phys. **31**, 278 (1953).

G12. Neutron Deficient Chains of Mass 187 through 191. W. G. SMITH AND J. M. HOLLANDER, *University of California, Berkeley.*—A radiochemical study of some neutron deficient nuclides in the noble metal region has been undertaken, and several new chains identified. The method used to establish genetic relationships was that of timed chemical separations, where the parent activities are initially produced by cyclotron or linear accelerator bombardments. The following chains have been identified:

$A=191$: $Hg^{191} \xrightarrow{55\ min} Au^{191} \xrightarrow{3.0\ hr} Pt^{191} \xrightarrow{3.0\ day} Ir^{191}$
$A=189$: $Hg^{189} \xrightarrow{\sim20\ min} Au^{189} \xrightarrow{42\ min} Pt^{189} \xrightarrow{10.5\ hr} Ir^{189} \xrightarrow{11\ day} Os^{189}$
$A=188$: $Pt^{188} \xrightarrow{10.0\ day} Ir^{188} \xrightarrow{41\ hr} Os^{188}$
$A=187$: $Au^{187} \xrightarrow{\sim15\ min} Pt^{187} \xrightarrow{2.5\ hr} Ir^{187} \xrightarrow{14\ hr} Os^{187}$

This work was performed under the auspices of the U. S. Atomic Energy Commission.

G13. Occurrence of Technetium-98 in Nature.* EDWARD A. ALPEROVITCH† AND J. MALCOLM MILLER, *Columbia University and Brookhaven National Laboratory.*—A systematic search by neutron activation analysis for naturally occurring long-lived Tc^{98} has been undertaken. Concentrates from various minerals (columbite, yttrotantalite, thortveitite, and chromite) were irradiated in the Brookhaven pile at a thermal neutron flux of $\sim3\times10^{12}$, and examined by scintillation counting for any Tc^{99m}, formed by the (n,γ) process on Tc^{98}. The radiation and decay characteristics of Tc^{99m} (140 kev γ ray, $t_{\frac{1}{2}}=6h$) are sufficiently unique to permit unequivocal identification, provided that no other γ-emitting activities are present in appreciable amounts. Moreover, it must be ascertained that the Tc^{99m} was not formed by the process: $Mo^{98}\ n,\gamma\ Mo^{99} \xrightarrow[67h]{\beta^-} Tc^{99m}$. A chemical procedure, giving decontamination factors of $\sim10^{10}$ from rhenium, molybdenum, and most otner elements, was developed and tested. Of 12 concentrates examined thus far, seven gave positive and two gave negative results; in the three remaining cases the identification was uncertain. In most cases, the formation of the activity from molybdenum could be ruled out with sufficient certainty to leave the (n,γ) process on naturally occurring Tc^{98} as the most plausible explanation. Further work is in progress.

* Supported in part by the U. S. Atomic Energy Commission.
† Present address: University of Illinois, Urbana, Illinois.

TUESDAY AFTERNOON AT 2:00

3 Le Conte Hall

(L. B. LOEB, presiding)

Contributed Papers

H1. Emission from the Single Lattice Step of Clean Tungsten.* J. K. TROLAN, J. P. BARBOUR, E. E. MARTIN, AND W. P. DYKE, *Winfield College.*—Electron emission from the edge of the outermost atom layer of several different crystal faces on tungsten and tantalum has been observed at emitter current densities above 5×10^6 amp/cm^2. This effect appears on a field emission pattern as a high-density emission ring in the normally low current density crystal directions, (110), (211), and (100). When the emitter tip is maintained at a temperature in the range $1700°K<T<2700°K$, and for purposes of viewing the electric field is simultaneously applied in short periodic pulses, the radius of the described emission ring is seen to decrease to zero. After a period of uniformly low emission, another ring appears at the periphery of the low density region, gradually collapses, and is followed in turn by other collapsing rings spaced at nearly equal intervals of time. Through measurements of emitter electron micrographs taken before and after observation of such a series, the collapse of a ring has been associated with the dissolution of the top atom layer from the emitter tip. The ability to observe the transport of the minute amounts of material involved in a single atom layer permits measurement of the dependence of the rate of transport on temperature, radius of curvature, crystal direction, and emitter material under conditions of excellent vacuum and clean surfaces.

* This work supported in part by the Office of Naval Research.

H2. Field Emission from Rhenium: The Emission Pattern Corresponding to Hexagonal Crystal Structure.* GEORGE BARNES, *Winfield College.*—The first field emission patterns from a clean metal having the hexagonal crystal structure (rhenium) are photographed. The fabrication of rhenium field emitter needles having tip radii of the order of 5×10^{-5} cm is described, and electron microscope shadowgraphs of these emitters are shown. Smoothing of the emitter tip by heat treatment is also illustrated by shadowgraphs. Photographs taken before and at intervals during emitter heating in the final vacuum show the development of the clean rhenium field emission pattern; Miller-Bravais indices are assigned to certain of the pattern's dark "holes." The current drawn from the rhenium is proved to be the result of field emission. The rate of contamination of a rhenium emitter as evidenced

by its emission pattern is shown to be less than that for a tungsten emitter under identical vacuum conditions.

* This work supported in part by the U. S. Air Force.

H3. Electrical Stability of the T-F Emitter.* W. P. DYKE, J. P. BARBOUR, J. K. TROLAN, AND E. E. MARTIN, *Winfield College.*—Electrons are emitted from metals in the combined presence of both a high-surface electric field and an elevated cathode temperature, a process which has been called *T–F* emission.[1] Such cathodes have properties which can be useful in electronic devices;[2] however, their employment has been limited by lack of electrical stability and life. In the present work, an intermediate cathode temperature, 2000°K for tungsten, was used to stabilize the electrical performance of the *T–F* emitter during long periods of repetitive pulsed operation at useful power levels and at duty cycles up to about 0.25. Transport mechanisms, primarily evaporation and surface migration, were used to maintain a smooth clean cathode surface whose stability was established during several life tests which are described. Excessive transport, which would otherwise undesirably alter the gross cathode geometry, was minimized by use of intermediate cathode temperatures and surface radii of curvature exceeding about 5×10^{-5} cm, the latter being in the range likely to be useful in practical application. The method is less useful during steady state operation since the cathode is then deformed by large electrostatic forces in the presence of thermal agitation.

* This work supported by the U. S. Air Force and the Office of Naval Research.
[1] W. W. Dolan and W. P. Dyke, Phys. Rev. **95**, 327 (1954).
[2] W. P. Dyke, (to be published).

H4. Electron Mobility in AgCl: Comparison of Experiment with Theory.* FREDERICK C. BROWN, *Reed College.*—Further results are presented on the temperature dependence of electron drift mobility in AgCl.[1] The measurements were made, using crystal counter techniques, on well annealed samples in which the range of conduction electrons was of the order of 10^{-4} cm per volt/cm of electric field strength. Composition, purity and strain of the crystals are important in determining their electronic properties. Some information bearing on these matters is had from optical data. The results for several crystals indicate that electron mobility can be fitted over a wide temperature range by an expression of the form $\mu=2.5\times10^{5}T^{-1}$. This suggests interaction of the slow electrons primarily with acoustic modes of vibration of the lattice but may be the result of a coincidence. It is possible to match experiment with the theory based on interaction with the optical modes[2] taking into account additional scattering by ionized impurity atoms. However, a fairly high concentration of ionized impurities, 10^{17} to 10^{18} atoms per cc, is required. The possibility of scattering by dislocations is considered.

* Partially supported by the Research Corporation and The National Science Foundation.
[1] F. C. Brown, Phys. Rev. **92**, 502 (1953).
[2] F. Low and D. Pines, Phys. Rev. **91**, 193 (1953).

H5. Measurements of Electron Density in Long-Lived Nitrogen Afterglows. ANDREW L. GARDNER, *University of California.**—Microwave methods utilizing the shift of resonant frequency have been used to measure the electron density at points along a system of flowing active nitrogen at pressures of a few mm Hg. The electron density, n, exhibits a decided growth and reaches its maximum more than 0.1 second after the gas has passed the exciting discharge. The magnitude of n and its rate of decay show marked dependence upon the amount of oxygen present in the nitrogen and correlate with light intensity measurements made on a similar flow system by Willey.[1] Measurements were made in which traces of nitric oxide and traces of oxygen were alternately introduced downstream from the exciting discharge. Evidence indicates the ionization of NO by metastable nitrogen molecules is a principal source of electrons. The electrons are then available for collisions in which the metastable $a'\pi g$ state of N_2 may be converted into the radiating $B^3\pi g$ state as proposed by Nicholls.[2]

* Work sponsored by Wright Air Development Center.
[1] E. J. B. Willey, J. Chem. Soc. 336 (1930).
[2] R. W. Nicholls, J. Chem. Phys. **20**, 1040 (1952).

H6. Electric Field Measurements in a Glow Discharge Using a Refined Electron Beam Technique. ROGER WARREN, *University of California, Berkeley.*—A new technique has been developed for measuring electric fields with an electron beam. The electron beam is acted upon simultaneously by both the unknown electric field and a known external transverse magnetic field. By adjusting the magnetic field for a null deflection of the beam, it is possible to determine the electric field, since then the two fields are proportional. In this way, the electric field has been measured in the cathode region of glow discharges at various pressures and currents in air, nitrogen, hydrogen, helium, and argon. Significant deviations from the previously reported linear field variations in the cathode fall have been observed. Electric fields in striations of the positive column have also been examined. Arguments in support of a proposed theory of the cathode region will be presented.

H7. Photoionization by Absorption in a Gas of Radiations from a Discharge in the Same Gas.* C. D. MAUNSELL, *University of California, Berkeley.*—Measurements have been made with a Kingdon cage space charge detector of the positive ions produced in a gas by absorption of radiation excited in a different region in the same gas through bombardment by an electron beam of known energy (0–100 volts). The apparatus was so arranged that neither electrons nor positive ions from the photon source could enter the detector. Absorption coefficients were evaluated by changing the separation between source and detector. No positive ions could be detected in hydrogen. In nitrogen the absorption coefficients corresponded to a cross section per molecule of about 4×10^{-16} cm^2, about fifteen times that observed in the ionization continuum using spectrally dispersed radiation and photographic methods.[1] Argon gave a cross section of the same order as nitrogen. Suggestions as to the processes responsible for these large values will be presented. An attempt is being made to check these observations of photoionization using a similar source but with a parallel plate ionization chamber as detector.

* This work was supported by the Office of Naval Research.
[1] Weissler, Lee, and Mohr, J. Opt. Soc. Am. **42**, 84 (1952).

H8. On Plasma Oscillations in a Static Magnetic Field.* L. WILCOX AND J. E. DRUMMOND, *Electronic Defense Laboratory, Sylvania Electric Products Inc.*—Recent work[1] in the theory of unbounded electron plasma oscillations in a static magnetic field has demonstrated, in an idealized case, the existence of frequency bands in which traveling wave solutions are forbidden at integer multiples of the cyclotron frequency. The extension of these results, based on a rigorous treatment of the Boltzmann equation, to problems more nearly representing the condition of electron plasmas in the laboratory appears to be very difficult.[2] A study of the motion of individual particles provides further insight into the origin of these bands and shows how simplified, macroscopic approaches may be modified to yield qualitative agreement with the rigorous theory. The study shows in detail that the forbidden bands result from a resonant interaction of electrons in disordered motion and space harmonics of the oscillating electric field. Finally the study shows in a semiqualitative manner that the discontinuities in the dispersion relation of Gross tend to disappear rapidly when perturbing effects such as electron drift and close Coulomb interactions are considered.

* Work carried out under U. S. Signal Corps Contract No. DA-36-039-sc-31435.
[1] E. P. Gross, Phys. Rev. **82**, 232 (1951).
[2] J. E. Drummond, L. Wilcox, Proc. Seventh Annual Gaseous Electronics Conference, New York (October, 1954).

H9. Streamers in Positive Point-to-Plane Breakdown in Air.* GILBERT G. HUDSON, *University of California, Berkeley.*—Modification of the method used by Meek and Saxe,[1] and by Amin[2] to include a second photomultiplier, which triggers the CRO, and improvement of the resolution have made it possible to study the streamers that precede the main stroke in positive point-to-plane breakdown in room air. Speeds and time variation of luminosity can be observed. For appropriate values of point radius r and gap length d, a single "set" of streamers precedes each main stroke. Each set consists of a primary streamer (10^8 cm/sec) and a secondary (average speed ~ 1 to 5×10^7 cm/sec) which starts from the anode simultaneously with the primary. The average interval, $\bar{T}$, between the primary and the main stroke depends on r and d (as well as on overvoltage, in the case of a pulsed V). For $r=9.5$ mm and $d=1.5$ cm $\bar{T}\sim0.2$ μsec; the average *secondary* streamer-main stroke delay, $\bar{T}_s$, is about 0.1 μsec. For smaller points ($r\sim1$ mm) $\bar{T}$ may be 5 μsec, or longer. In some gaps (small r and larger d) as many as ten sets (with separations >200 μsec) precede each main stroke. Though the main stroke is difficult to study, because of the electrical pick-up resulting from it, there have been definite indications that it moves toward the anode more rapidly than 10^8 cm/sec.

* This work has been supported by the Office of Naval Research and by the Research Corp.
[1] J. M. Meek and R. F. Saxe, Nature 162, 263 (1948).
[2] M. R. Amin, J. Appl. Phys. 25, 358 (1954).

H10. Contact Charging between Monocrystalline Nonconductors and Metals.* P. E. WAGNER, *University of California.*—Previous data[1] on the electrostatic charge developed by fused quartz and Pyrex spheres when rolled on a Ni surface have been extended to the monocrystalline insulators SiO_2, Al_2O_3, NaCl, KCl, KBr, and KI. The alkali halides charge positively, while the oxides charge negatively. Both fused and crystalline quartz charge similarly to saturation values about ten times higher than values attained by the others. Electron transfer is believed to cause the charging and should lead to a predictable variation of saturation charge with metallic work function, for a given insulator. Experiments designed to measure this variation will be discussed.

* Research supported by the Office of Naval Research.
[1] J. W. Peterson, J. Appl. Phys. 25, 907 (1954).

TUESDAY AFTERNOON AT 2:00

310 Le Conte Hall

(W. A. NIERENBERG, presiding)

Contributed Papers

I1. Electron Spin Resonance in Frozen Metal-Ammonia Solutions. G. FEHER AND R. A. LEVY, *University of California, Berkeley.*—Electron spin resonance has been observed in frozen ammonia solutions of lithium, sodium, potassium, and cesium. In all samples investigated the signals appear to be the result of metallic particles[1] precipitated out of solution during freezing. Temperature dependences of the width, amplitude, and shape of the signals have been studied from 4°K to 180°K, the melting point of the mixtures. Measurements were carried out in a coaxial transmission cavity at 300 megacycles on samples sealed in Pyrex. In frozen sodium-ammonia the line width varies from 0.15 oersted at 4°K to 6 oersteds at 180°K. In frozen lithium-ammonia the line width is temperature independent except for a transition at 77°K. Below 77° the width is 1.5 oersteds; above 77° the width is 4 oersteds. Frozen potassium-ammonia has a line varying from 5 oersteds at 4°K to 20 oersteds at 170°K. Frozen cesium-ammonia has a 13 oersted line below 30°K which disappears at higher temperatures. Its g value of 1.93 ± 0.02 compares favorably with Brooks[2] calculations of 1.94 for metallic cesium. In none of the solutions studied is line width dependent on concentration of metal solute.

[1] G. Feher and A. F. Kip (to be published).
[2] H. Brooks (unpublished results).

I2. Electron Spin Resonance in Liquid Alkali Metals. R. A. LEVY, *University of California, Berkeley.*—Electron spin resonance in a bulk sample of 99.9 percent sodium has been studied at 300 megacycles between 20°C and 140°C. The line width between maximum slopes follows a linear temperature dependence up to the melting point, 97°C, then increases abruptly by 25 percent in less than 5°. From the melting point to 140°C the width remains unchanged at about 16.5 oersteds. The amplitude of the absorption signal did not change on going through the melting point. The results are compatible with the Elliott[1] mechanism for spin lattice relaxation in metals, giving a linear dependence of the inverse relaxation time on resistivity. The resistivity of sodium jumps 35 percent at the melting point.

[1] R. J. Elliott, Phys. Rev. 96, 266 (1954).

I3. Electron Spin Resonance in Irradiated Alkali Halides.* A. M. PORTIS AND D. SHALTIEL, *University of Pittsburgh.*—Electron spin resonance has been observed in samples of LiF and LiCl irradiated for a period of 36 hours with 220 kev x-rays. Both samples show inhomogeneous saturation of the resonance similar to that already reported for F centers in KCl, KBr, and NaCl. The g factors for both lines are within experimental error of the free electron g. Both resonances show a surprising response to the magnetic field modulation in that the signal lags the modulating field by nearly 90°. This effect can be understood in a direct way on the basis of hyperfine broadening of lines which are narrow compared with the modulation frequency. We find no resonance in the crystals before irradiation or after the F band has been bleached. The intensity of the resonance is in general agreement with the strength of the F band. We conclude from this evidence and the similarity with the F center resonances in other alkali halides that we are observing genuine F center resonances. We find no evidence for either the resolved spectrum of 19 lines or the broad peak with a gram of 2.018 reported by Schneider.[1]

* This work was supported in part by the Office of Scientific Research of the Air Research and Development Command.
[1] E. E. Schneider, Phys. Rev. 93, 919 (1954).

I4. Nuclear Magnetic Resonance Spectra of Annular Samples. C. A. REILLY, H. M. MCCONNELL, AND R. G. MEISENHEIMER, *Shell Development Company.*—We have made studies of the nuclear magnetic resonance (NMR) spectra of annular liquid samples. These samples were contained in an annulus between two concentric cylindrical glass tubes, the axes of which are perpendicular to both the static (H_0) and radiofrequency fields in a high resolution NMR spectrometer.[1] The NMR signals from these samples have the appearance of broadened U-shaped doublets, with separations, ΔH, commonly in the range one to five hundred milligauss. Both theory and experiment indicate that

$$\Delta H=4\pi H_0[(\kappa_1-\kappa_2)(a/r)^2+(\kappa_2-\kappa_3)(b/r)^2], \qquad (1)$$

where a, b are the internal and external radii of the inner glass tube, r is the mean radius of the annulus, κ_1, κ_2, and κ_3

are the volume magnetic susceptibilities of (1) material contained in the inner glass tube, (2) glass, and (3) the annular liquid. These observations form the basis of a new, rapid method for the determination of the magnetic susceptibilities of both liquids and solids.

[1] Varian Associates, Palo Alto, California.

I5. Isotope Abundance Ratios by Nuclear Magnetic Resonance. B. E. HOLDER AND M. P. KLEIN, *University of California.*—The Bloch equations for a pair of resonance absorption signals from two isotopes readily lead to an expression for the abundance ratio in terms of the rf amplitude, H_1, the relaxation times, T_1 and T_2, and certain nuclear constants for each of the nuclei. The best signal to noise conditions are realized when the signals are obtained at saturation values of H_1 for the two isotopes. The use of low frequency square wave modulation with the nuclear induction apparatus yields the absorption mode directly. This is in contrast to the sine wave modulation technique which produces the derivative of the absorption curve in a phase sensitive recording instrument. The necessary condition of slow passage is satisfied if the field is swept slowly and the dwell time of the square wave is long compared to the relaxation time. Some experimental data on determination of the natural (H^2/H^1) and (Li^6/Li^7) ratios in paramagnetically relaxed solutions will be presented. This work was performed under the auspices of the U. S. Atomic Energy Commission.

I6. Magnetic Susceptibility Measurements by Nuclear Magnetic Resonance. M. P. KLEIN AND B. E. HOLDER, *University of California.*—Feher and Knight have developed a method for measuring total electronic susceptibilities by nuclear magnetic resonance. The technique makes use of the property that the internal field of a sample subjected to an external field depends explicitly upon the shape and specific susceptibility of the sample. By choosing a sample geometry for which the demagnetizing factors can be theoretically derived, a measurement of the ratio of external to internal field will then determine the specific susceptibility of the sample. The nuclear magnetic resonance of a nuclide contained in the sample provides a direct measurement of the internal field, and the nuclear resonance of the same nuclide in a sample for which the demagnetizing factor is zero, measures the applied field. In practice we employ a sample divided into two sections. For one section the demagnetizing factor is zero, and for the second section the factor is 4π. The nuclear resonance then appears as two lines, the separation being proportional to the susceptibility, $\Delta H/H = 4\pi K$. Thus far only solutions have been studied as the resolution obtainable in solution is higher than for solids. The sensitivity of the method is limited by the homogeneity of the magnetic field and the natural width of the nuclear resonance. This work was done under the auspices of the U. S. Atomic Energy Commission.

I7. Nuclear Magnetic Relaxation in Natural and Synthetic Rubbers.* E. M. BANAS, B. A. MROWCA, AND E. GUTH, *University of Notre Dame.*—Proton magnetic resonance has been observed in unvulcanized natural rubber, Butyl rubber, and Paracril 35 (a 65 parts butadiene, 35 parts acrylonitrile copolymer) from liquid nitrogen to room temperatures. The absorption curves show two more or less abrupt changes of line width with temperature. For unvulcanized natural rubber the first rather sharp drop in line width with increasing temperature occurs at about 125°K. It is at this temperature that Powles and Gutowsky[1] found absorption line narrowing in some tetrasubstituted methanes. This narrowing was attributed to an increased rate of rotation of CH_3 groups about the C_3 symmetry axis. Consequently, this first change could be associated with the onset of CH_3 group rotation in the first two polymers. For unvulcanized Butyl rubber the first sharp drop in line width with increasing temperature occurred in the same temperature region and the line width drops rapidly to about half of its value before leveling off in the vicinity of 150°K. This behavior is consistent with a line narrowing due to rotation in a plane. For Paracril 35 the first rapid decrease in line width with increasing temperature occurs at about 140°K. A second less abrupt change in line width with increasing temperatures occurs in the vicinity of the second-order transition temperature of the polymers.

* Supported in part by the Office of Naval Research.

I8. The Nuclear Magnetic Moments of Rh^{103} and W^{183}. P. B. SOGO AND C. D. JEFFRIES, *University of California, Berkeley.*—The nuclear magnetic moments of Rh^{103} and W^{183} are measured by nuclear induction and found to be: $\mu(Rh^{103}) = -0.08790 \pm 0.00007$ nm and $\mu(W^{183}) = 0.115 \pm 0.001$ nm. The samples consist of metal powders, and the metal shift of the resonance frequencies are calculated to be $(\Delta H_0/H)(Rh^{103}) = (0.25 \pm 0.06)$ percent and $(\Delta H_0/H)$ $(W^{183}) = (2.0 \pm 1)$ percent. Since we have not yet observed the resonances in other than metal samples, these calculated corrections are included in the values quoted above. The ratios of the nuclear magnetic resonance frequencies in the metals to that of D in D_2O containing 1 molar $MnCl_2$ are found to be $\nu(Rh^{103})/\nu(D) = 0.205574 \pm 0.000007$ and $\nu(W^{183})/\nu(D) = 0.27395 \pm 0.00003$. The assistance of The Research Corporation and the U. S. Atomic Energy Commission is gratefully acknowledged.

I9. Direct Measurement of the Nuclear Spin-Lattice Relaxation Time.* J. L. WALSH, A. G. BERGER, J. V. ROGERS, AND W. D. KNIGHT, *University of California, Berkeley.*—A new method for measuring the nuclear spin-lattice relaxation time T_1 is proposed. Oscillating magnetic fields H_1 and H_2 are applied to the sample in directions mutually perpendicular to each other and to a large static field H_0. The frequencies of H_1 and H_2, which are ν_1 and ν_2 respectively, are Larmor frequencies for nuclei in static fields H_0 and $H_0 + \delta H$, respectively, δH being the amplitude of a square wave modulation on H_0. Thus the Larmor frequency is changed from ν_1 to ν_2 and back again in a time equal to the period of the square wave. The field H_1 is supplied by a Pound-Knight oscillator at a level considerably below saturation. H_2 is sufficiently large to cause saturation in a time short compared to the period of the square wave. The electronically integrated curve of power absorption at ν_1 *versus* time is plotted as a function of the period of the square wave. From this curve T_1 can be determined on the assumption that the absorption at frequency ν_1 will rise exponentially with time from the instant δH is removed. The useful limits on this method are for T_1 values from 0.01 to 10 seconds, which is characteristic of many pure metals at temperatures between 1°K and 100°K.

* Supported in part by the Office of Naval Research.

I10. A Diffusion Model for Nuclear Precession Relaxation in Solids. E. L. HAHN AND B. HERZOG, *Watson Scientific Computing Laboratory (IBM).*—A spin dipole field diffusion model is applied to account for the relaxation behavior of free nuclear precession signals from solids where thermal relaxation can be neglected. A configuration of unlike nuclear neighbors B about nucleus A (the precession of A is observed) produces a fluctuating local field at A because of spin-spin coupling among B. We study the case where coupling among A is negligible. The probability that a local magnetic field h_0 at A, due to B, diffuses to another value h_1 in time t is taken from the Ehrenfest model for diffusion of a bound particle between reflecting barriers. The barriers here are represented by $\pm I_B$, where I_B is the total spin of a given B configuration, and the particle unit step is in terms of the local field change at A due to one spin flip in B. The theory predicts the observed dependence of free precession signals on the static field im-

posed by B upon A, and upon spin-spin coupling among B. The experimentally observed effects on A (chlorine) in $NaClO_3$ and para-dichlorobenzene upon decoupling of B by an external magnetic field and upon spin resonance of B are discussed.

I11. Paramagnetic Resonance Absorption in Glass.* R. H. SANDS,† *Washington University.*—A microwave spectrometer operating at 9000 Mc/sec was employed to observe paramagnetic resonance absorption in numerous glass samples furnished by the Corning Glass Works, Corning, New York. Anisotropic spectroscopic splitting factors g of 4.2 and 6.0 were recorded for lines in all glass samples studied. These lines were attributed to an as yet undetermined paramagnetic impurity. The anisotropic g factors must arise from the fine structure produced in the spin states by spin-orbit and Stark interactions. Other lines were recorded near a g of 2, among which were those from Cu^{2+} in network-modifying positions in a soda-lime-silica glass. The resolvable hyperfine structure for these Cu^{2+} ions is evidence for a high degree of short-range order. The fine and hyperfine structure parameters checked well with previous values quoted for the Tutton salts.[1]

* Supported in part by the U. S. Office of Scientific Research, Air Research and Development Command.
† Present address: Stanford University.
[1] A. Abragam and M. H. L. Pryce, Proc. Roy. Soc. (London) **206A**, 164 (1951).

I12. Hyperfine Structure in the Paramagnetic Resonance of Vanadium Ions in Solution.* G. E. PAKE AND R. H. SANDS, *Washington University.*—Paramagnetic resonances of vanadium ions in aqueous, acetone, and ether solutions have been observed. Although attempts were made at preparing valence states V^{3+}, V^{4+}, and V^{5+} in accordance with the procedures of Freed,[1] solutions corresponding in color to V^{3+} and to V^{4+} both gave the same hyperfine pattern of eight $(2I+1)$ lines of different individual widths. The hyperfine coupling constant corresponds to about 120 oersteds, with line spacings being progressively larger toward higher fields as expected in second order[2] for a spectrum centered at 3200 oersteds. The coupling is slightly larger for aqueous than ether solutions, which is not unlikely for solvents forming different complexes with the vanadium ions if the electron promotion hypothesis of Abragam and Pryce[3] for the unexpectedly large hyperfine couplings in such ions is valid. Asymmetric component line shapes for certain solvents and temperatures are interpreted as viscosity effects leading to incomplete averaging of an anisotropic spectroscopic splitting factor of the complexed ion.

* Supported in part by the U. S. Office of Scientific Research, Air Research and Development Command.
[1] S. Freed, J. Am. Chem. Soc. **49II**, 2456 (1927).
[2] B. Bleaney, Phil. Mag. **42**, 441 (1951).
[3] A. Abragam and M. H. L. Pryce, Proc. Roy. Soc. (London) **206A**, 164 (1951).

WEDNESDAY MORNING AT 9:00

310 Le Conte Hall

(E. LOFGREN, presiding)

High-Energy Physics

Invited Papers

J1. European Accelerators. J. R. RICHARDSON, *University of California, Los Angeles.* (30 min.)
J2. Brookhaven 25-Bev Synchrotron. G. K. GREEN, *Brookhaven National Laboratory.* (30 min.)
J3. University of California Bevatron. BRUCE CORK, *University of California, Berkeley.* (30 min.)
J4. Progress with the Stanford Linear Accelerator. W. K. H. PANOFSKY, *Stanford University.* (30 min.)
J5. Design for a Strong-Focusing Electron Synchrotron. M. S. LIVINGSTON, *M.I.T.* (30 min.)

WEDNESDAY AFTERNOON AT 2:30

310 Le Conte Hall

(E. SEGRÈ, presiding)

Invited Papers

K1. Experiments with High-Energy Proton Beams. LEONA MARSHALL, *University of Chicago.* (30 min.)
K2. Polarization Effects on High-Energy Proton-Proton Reactions. R. B. SUTTON, *Carnegie Institute of Technology.* (30 min.)
K3. High-Energy Proton Polarization Studies Involving Triple Scattering. OWEN CHAMBERLAIN, *University of California.* (30 min.)

Contributed Papers

K4. Experimental Determination of the Complete Scattering Matrix in a Proton Carbon Collision. R. TRIPP, C. WIEGAND, T. YPSILANTIS, O. CHAMBERLAIN, AND E. SEGRÈ, *University of California, Berkeley.*—The elastic scattering process of a proton on a particle of spin zero (carbon) is not completely described by the cross section only, but requires the knowledge

of 3 independent parameters which can conveniently be represented by a scattering matrix $g(\theta)+h(\theta)\sigma\cdot n$ where g and h are complex functions of the angle of scattering, σ is the Pauli operator and n is a unit vector perpendicular to the plane of scattering. Besides the amplitudes of g and h only their relative phase has a physical meaning, and for simplicity it is convenient to consider the phase difference β between $g+h$ and $g-h$. A measurement of the scattering cross section and of the polarization gives only two relations and are insufficient to determine the scattering matrix. In order to obtain a third relation we have performed a triple scattering experiment in which the first and second scattering occur in planes perpendicular to each other. After the second scattering the beam is analyzed by a third scattering in a plane perpendicular to the plane of the second scattering and inclined by the same angle θ with respect to the plane of the first scattering. It can be shown that this measurement defines the quantity $\cos(\theta-\beta)$ and hence two possible values of β. This work was done under the auspices of the U. S. Atomic Energy Commission.

K5. Depolarization in Scattering of Polarized Protons by Hydrogen at 310 Mev. T. YPSILANTIS, C. WIEGAND, R. TRIPP, E. SEGRÈ, AND O. CHAMBERLAIN, *University of California, Berkeley.*—The experiment consists in determining how scattering by hydrogen changes the polarization state of a polarized proton beam. The experiment involves three successive scattering processes. The first scattering on beryllium serves to polarize the protons, the second scattering is on (unpolarized) hydrogen, and the asymmetry at the third scattering (carbon) target serves to analyze the polarization of protons leaving the second target. Wolfenstein has shown that there are two significant new quantities determinable in straight-forward triple-scattering experiments. One of these, D, is a measure of the depolarization in the (proton-proton) scattering, and can be studied directly if all three scattering planes are parallel. D is connected to the observed quantities by the relation $e=(DP_1+P_2)P_3/(1+P_1P_2)$ in which P_1, P_2, and P_3 are the respective polarizations that would be induced in an unpolarized beam by the scattering processes at the first, second, or third target, and e is the observed asymmetry at the third scattering. The other new quantity, R, is a measure of the rotation of the spin produced by the second scattering. This rotation is about an axis perpendicular to the plane of scattering and R can be directly measured in a process in which the second scattering plane is perpendicular to the first scattering plane, and the third plane is perpendicular to the second. This work was performed under the auspices of the U. S. Atomic Energy Commission.

K6. Analysis of Triple Scattering and Correlation Experiments. HENRY P. STAPP, *University of California, Berkeley.*—Current triple-scattering experiments measure components of the expectation value of the spin of one of the particles emerging from a $p-p$ collision in which the incident beam is polarized. Another experiment measures simultaneously the spin directions of the two protons which emerge from a collision when the incident beam is unpolarized. These experiments give four new parameters which are characteristics of the $p-p$ system. These, together with the differential cross section and the polarization induced in a single scattering, are expressed in terms of the scattering matrix elements. At $\theta=90°$ there are only three different non-vanishing matrix elements and one may solve for them. There are four possible solutions, and in addition an overall phase factor remains undetermined. The expression for the matrix elements in terms of the $L=0, 1, 2, 3$, $J=0, 1, 2, 3$ phase shifts is obtained. The phase shift analysis will be continued as the experimental results are obtained, and the results reported at the meeting. This work was performed under the auspices of the U. S. Atomic Energy Commission.

K7. Polarization and Cross Section for Inelastic Scattering. M. A. RUDERMAN, *University of California, Berkeley.*—The differential cross section for the inelastic scattering of high-energy nucleons by nuclei has been studied for energy losses ΔE less than 150 $A^{-\frac{1}{3}}$ Mev. To the extent that a nuclear excitation can be considered as either a collective transition or a change of the nuclear configuration, the cross section for exciting either kind of excited state has been compared to that for elastic scattering. For the prescribed range of ΔE and $2pR\sin\theta/2\lesssim 5$, the ratio of the cross section for exciting a collective transition to that for changing the configuration is greater than $0.2\beta^2A^{\frac{5}{3}}$ where β is the deformation parameter[1] of A. Bohr. If a complex potential is used to describe the effective potential within nuclear matter, then in Born approximation the polarization is independent of ΔE, the same as for elastic scattering, as long as only collective transitions are important. The possibility that the 4.4-Mev level of C^{12} can be considered as a collective excitation and the implications for angular distribution, electron scattering, and polarization will be discussed.

[1] A. Bohr, Dansk. Mat. Fys. Medd. **26**, No. 14.

WEDNESDAY AFTERNOON AT 2:30

4 Le Conte Hall

(W. K. H. PANOFSKY, presiding)

Contributed Papers

L1. Heavy Meson and Hyperon Production at the Bevatron. GERSON GOLDHABER, W. W. CHUPP, S. J. GOLDSACK, J. LANNUTTI, AND F. WEBB, *University of California, Berkeley.*—Stacks of nuclear emulsions have been exposed at 90° to the proton beam of the Bevatron (nominal energy 4.8 Bev). The stacks were placed in a re-entrant well at a distance of 10 in. from a plunging target. The only intervening material was the 0.1-in. aluminum wall of the re-entrant well. The stacks are being area-scanned for secondary particles from the target in a region corresponding to a range of 5–6 cm of emulsion. To date, the secondary particles ending or interacting that have been observed are: protons ~700; $\pi+$ 150, $\pi-$ (and μ^- directly from target) 80, μ^+ (directly from target) 5, stars in flight 100, K particles 3. One of the K particles undergoes a scattering in flight of 79°, which is probably a Coulomb scattering from a light element. In emulsion stacks exposed in the direct 3.2 Bev beam (see previous abstract) two events of particular interest were observed among the 2000 proton stars examined. Event A: the interaction of what is possibly a negative hyperon.[1,2] Event B: the emission and interaction of what is probably a 600-Mev α particle. This work was performed under the auspices of the U. S. Atomic Energy Commission.

[1] M. W. Friedlander, Phil. Mag. **45**, 418 (1954).
[2] Johnston and O'Ceallaigh, Phil. Mag. **45**, 424 (1954).

L2. Ionization Loss in Nuclear Emulsions.* JOHN R. FLEMING AND J. J. LORD, *University of Washington.*—Grain density measurements in 400-micron-thick Ilford *G*-5 plates of accelerated particle tracks have been extended.[1,2] Four separate groups of plates were exposed to a beam of 490-Mev pions. Next, the first group was rotated through 90° and exposed to the 1420-Mev pion beam, and then the second, third, and fourth groups respectively to pions of 1100, 800, and 295 Mev. Preliminary normalized blob densities of pions of 295, 490, 1100, and 1420 Mev were found to be 20.3±0.4, 20.0±0.4, 20.5±0.4, and 21.0±0.4 per 100 microns. The effect of the severity of development on the blob density was investigated by developing one plate in the normal manner and another plate without the application of a warm stage. It was found that the ratio between the blob densities of the 490- and 1100-Mev pions on each plate was within 1 percent of being the same even though the degree of development was quite different. The above measurements of grain or blob density are in good agreement with the theoretical calculations of Sternheimer.

* Assisted by the joint program of the Office of Naval Research and the U. S. Atomic Energy Commission.
[1] We are indebted to Dr. R. K. Adair for plates from the cosmotron.
[2] Fleming and Lord, Phys. Rev. **92**, 511 (1953).

L3. π^- Counting by Delayed Coincidence.* K. M. CROWE, R. M. FRIEDMAN, AND H. MOTZ, *Stanford University.*—The counting of π^+ mesons by observing positrons occurring in delayed coincidence with a short-duration primary beam was shown by Alvarez *et al.*, to be a low-background detection scheme of high efficiency. With the Stanford Mark III electron linear accelerator operating at 300 Mev, the beam intensities are sufficient to allow adding magnetic deflection to define the momentum (and charge) of the pions without sacrificing data-gathering rates. With the magnet set for negative particles, we obtain delayed coincidences from some of the π^- mesons which have decayed in flight to μ^-'s. The μ^-'s come to rest in our plastic scintillator (7-in. dia.×10-in. long), and subsequently decay into electrons with essentially the same decay period as the μ^+. The efficiency is high for these events as evidenced by a negative-to-positive yield ratio of ~0.11 on carbon whose π^-/π^+ ratio is approximately one. The following checks have verified the basic scheme. "Negatives" disappear with no magnetic field. They show the correct range-absorption curves for negative μ's; these are somewhat wider than those obtained for positive mesons due to the wider momentum band of the μ's caused by the decay in flight kinematics. The negatives do not show up from bombardment of liquid hydrogen at this energy. The ratio of negatives to positives seems to be insensitive to pion energy.

* Supported by the joint program of the Office of Naval Research and the U. S. Atomic Energy Commission.

L4. π^-/π^+ Ratios in Asymmetric Nuclei.* H. MOTZ, K. M. CROWE, AND R. M. FRIEDMAN, *High-Energy Physics Laboratory, Stanford.*—Using the technique of the preceding abstract, we have measured variations of the negative-positive photopion production ratio for several elements. Large variations have been observed by Littauer and Walker at Cornell University[1] at a laboratory angle of 135°. Our preliminary results at ~300 Mev primary energy at a laboratory angle of 75° are in striking agreement:

	Li	Be	C	S	Ca
L. and W.	2.06±0.18	2.25±0.11	1.06±0.02	0.85±0.03	0.58±0.06
M., C., F.	2.42±0.10	2.61±0.07	1.06±0.02	0.94±0.04	0.70±0.03

In the table we have normalized our carbon ratio to theirs. The probable errors shown are due to counting statistics only. These results are not consistent with more recent work at Cornell (Luckey)[2] and Berkeley (Carrothers),[3] which show less variation with Z. The pion energy, 53±10 Mev, and the electron-beam energy, 300±15 Mev, are measured with a floating-wire technique. We are continuing at different pion energies and with different primary-electron energies. These results will be presented.

* Supported by the joint program of the Office of Naval Research and the U. S. Atomic Energy Commission.
[1] R. M. Littauer and D. Walker, Phys. Rev. **86**, 838 (1952).
[2] D. Luckey, Phys. Rev. **90**, 711 (1953).
[3] J. Carrothers, Ph.D. dissertation, University of California, Berkeley 1952 (unpublished).

L5. Mu Meson Ionization in Argon at Energies 10 to 100 Bev.* ALLAN N. WILSON, *University of California, Berkeley.*—The most probable ionization of cosmic-ray mu mesons has been measured by proportional counters containing argon at 4/3 atmospheres. Energy was measured by magnetic field deflection, the incoming and outgoing directions of the particle being defined by small diameter Geiger counters. Particle deflection occurred *in iron* at 18 500 gauss and over a region of 3.5 feet. Multiple scattering did not seriously limit accuracy of energy measurement. The upper limit of resolution of the system was around 200 Bev. Charged particle identification as mu mesons was inferred by justifying absence of electrons, protons, and pi mesons. By range-interval determination of energy, a relative calibration of the counters was performed on minimum ionizing mesons. The results are in good agreement with the density effect calculations of Sternheimer. The onset of this effect occurs at about 10 Bev for argon at this pressure. The highest point plotted, namely at 85 Bev, represents a weighted mean for all cosmic ray mu mesons above 50 Bev; at this point, Sternheimer's theory gives a value of ionization about 1.59 times minimum, as contrasted with 1.70 by the Bethe-Bloch theory. The experiment also yielded a differential mu meson spectrum at sea level, which agrees well with the generally accepted Rossi curve, but which extends beyond that curve in the region 30 to 100 Bev.

* Assisted by the joint program of the Office of Naval Research and the U. S. Atomic Energy Commission.

L6. Charged Pion Production in Neutron-Proton Collisions.* GAURANG B. YODH, *University of Chicago.*†—The differential cross section and energy spectra for the production of $\pi^\pm$ mesons by the 400-Mev neutron beam of the Chicago synchrocyclotron on liquid hydrogen has been measured at laboratory angles of 90° and 65°, using photographic emulsions as detectors. At 65° (corresponds to 90° in center of mass) roughly equal numbers of positive and negative pions were observed, while at 90° the ratio $\pi^+/\pi^-=2.01\pm0.24$. The experimental cross sections have been reduced to center-of-mass cross sections at a single neutron energy. The differential cross sections at 409-Mev neutron energy are calculated to be:

$$d\sigma^{\pi\pm}/d\omega=(1.07\pm0.39)\mp(1.38\pm0.78)\cos\theta+(0.57\pm1.14)\cos^2\theta\times10^{-29}\ \text{cm}^2/\text{sterad}$$

and the total cross sections are determined to be

$$\sigma(\pi^+)=\sigma(\pi^-)=0.16\pm0.04\ \text{millibarn}.$$

* Research supported by a joint program of U. S. Office of Naval Research and the U. S. Atomic Energy Commission.
† Now at Stanford University.

L7. π^+ Photomeson Production at 180°. Experimental Arrangement. GORDON W. REPP, MARK J. JAKOBSON, AND R. STEPHEN WHITE, *University of California, Berkeley.*—Hydrogen, deuterium, helium, and carbon were bombarded by photons from the Berkeley synchrotron. π^+ mesons were observed at 180° to the beam. The high-pressure low-temperature gas target[1] was used for hydrogen, deuterium, and helium. Additional data on hydrogen and carbon was obtained from polyethylene and carbon. The mesons were deflected out of the photon beam by means of a magnet. The detector consisted of 2 stilbene crystals on light pipes which were viewed by 1*P*21 photomultipliers. A π^+ meson was identified by means of the coincidence between the π^+ meson and the positron from the

μ^+ meson decay.[2] Absolute cross sections were determined with emulsions exposed to π^+ mesons from hydrogen. This work was performed under the auspices of the U. S. Atomic Energy Commission.

[1] White, Jakobson, and Schulz, Phys. Rev. **88**, 836 (1952).
[2] J. Steinberger and A. S. Bishop, Phys. Rev. **86**, 180 (1952).

L8. π^+ Photomeson Production at 180°. Experimental Results. R. STEPHEN WHITE, MARK J. JAKOBSON, AND GORDON W. REPP, *University of California, Berkeley.*—The previous paper gave the details of the experimental procedure. In this paper ratios of the cross sections of deuterium, helium, and carbon to hydrogen will be given for π^+ mesons produced at 180° to the beam. The results will be compared to the phenomenological theory of Chew and Lewis and others.[1] Beam monitoring will be discussed and absolute cross sections will be given. These values will be compared with theoretical predictions.[2] The results will be compared to those of other laboratories. This work was performed under the auspices of the U. S. Atomic Energy Commission.

[1] For a list of references see, e.g., ref. 1 of the above paper.
[2] See, e.g., Brueckner and Watson, Phys. Rev. **86**, 923 (1952); B. T. Feld, Phys. Rev. **89**, 330 (1953); G. F. Chew (to be published).

L9. Scattering and Absorption of 50-Mev π^+ Mesons in Lead. G. SAPHIR, *University of California, Berkeley.*—The interaction of 50±15-Mev π^+ mesons in a $\frac{1}{8}$-inch-thick lead plate have been studied, using a 22-inch cloud chamber in a magnetic field of 5000 gauss. Preliminary cross sections based on 19 100 traversals are: elastic scatters greater than 40 degrees 344±50 mb, stars and stops 1009±75 mb, charge-exchange scattering 37±26 mb. Seven apparently inelastic scatters were found in the forward direction, but six of these are probably $\pi-\mu$ decays just before or within the lead plate. Angular distributions and final results will be presented. This work was performed under the auspices of the U. S. Atomic Energy Commission.

L10. Positron Spectrum from the Decay of the μ Meson. RYOKICHI SAGANE, WALTER DUDZIAK, AND JAMES VEDDER, *University of California, Berkeley.*—Because of the disagreement over the experimental value of ρ (a constant introduced by Michel[1] into the theory of μ-meson decay), an independent measurement was made of this constant with the aid of a 180° β-ray spectrometer. For this experiment the deflected proton beam pulses of the 184-inch cyclotron were used to create low-energy π^+-mesons in a Be target. These low-energy pions, which were stopped in the target, decayed into muons that also stopped in the target. Thus the pion-production target served as a positron source for positrons from the decay of the muon. The spectrum of this positron source was analyzed with a 180° β-ray spectrometer using a fast quadruple coincidence of signals from four plastic crystals. Two types of measurements were made, wherein (a) the distance between the positron source and spectrometer exit slit was kept constant and the magnetic field was varied, and (b) the magnetic field was kept constant and the distance between the source and exit slit varied. A preliminary analysis of the combined results yields $\rho=0.22\pm0.10$. This is in good agreement with the spiral-orbit spectrometer data. This work was done under the auspices of the U. S. Atomic Energy Commission.

[1] L. Michel, Proc. Phys. Soc. (London) **A63**, 514 (1950).

L11. Photomeson Production from H, D, and C. WALTER DUDZIAK, RYOKICHI SAGANE, AND JAMES VEDDER, *University of California, Berkeley.*—Preliminary counter measurements have been made on charged-pion production from hydrogen, deuterium, and carbon at 90° to a photon beam having a maximum photon energy of 300 Mev. For these experiments a 40-inch spiral-orbit spectrometer was used. Pions whose original production energies varied from 14 Mev to 70 Mev were analyzed by the spiral-orbit principle and detected by fast coincidence of pulses from three or four plastic crystals. When the triple-coincidence technique was used, both positive and negative pions were measured at the same time. For these studies a subtraction technique as well as a high pressure deuterium target was used. Data from these preliminary experiments on relative yields of π^+ and π^- mesons will be presented. This work was performed under the auspices of the U. S. Atomic Energy Commission.

L12. π^0 Photoproduction from Protons and Deuterium Nucleons, I.* R. M. WORLOCK AND W. R. SMYTHE, *California Institute of Technology.*—A thin-walled gas target was irradiated with 500 Mev bremsstrahlung from the California Institute of Technology synchrotron. The proton spectrum emerging from the hydrogen, the deuterium, and the empty target was investigated at three angles: 30°, 41°, and 52°. The protons were identified by measurement of specific ionization in the front counter of a three counter scintillation telescope consisting of two counters in coincidence and the rear counter in anti-coincidence. The proton energy was determined by its range, and photon energy was determined by proton energy and angle since the processes studied were two body reactions. The angular resolution was triangular with 4.8° full width and the proton energy resolution was typically 9 Mev. A method involving runs with a lead plug in the telescope was devised to give an accurate background correction. Following are the proton count ratios from deuterium and hydrogen. At proton lab angle of 30°: Proton energy =53 Mev, $D/H=2.23\pm0.17$; 61, 2.04±0.12; 70, 1.56±0.09; 85, 1.51±0.09; 98, 1.56±0.11; 108, 1.71±0.14; 124, 2.05±0.25; 134, 1.93±0.21; 148, 2.35 ±0.40. At 41°: 48, 1.60±0.13; 57, 1.17±0.08; 70, 1.40±0.11; 79, 1.60±0.11; 88, 1.71±0.18; 100, 1.81±0.26; 108, 1.96 ±0.32. At 52°: 46, 1.50±0.10; 52, 1.63±0.13; 57, 1.74±0.20; 62, 2.37±0.21; 70, 2.72±0.32.

* This work was supported in part by the U. S. Atomic Energy Commission.

L13. π^0 Photoproduction from Protons and Deuterium Nucleons, II.* W. R. SMYTHE AND R. M. WORLOCK, *California Institute of Technology.*—From the data described in the preceding abstract the absolute cross section and angular distribution coefficients for the reaction $\gamma+P\rightarrow P+\pi^0$ were obtained for photon laboratory energies from 265 to 450 Mev. The results are approximately 20 percent smaller than those obtained by Oakley[1] at this laboratory using a magnetic spectrometer. There is evidence indicating that in the photoproduction of mesons from deuterium the photon interacts only with one of the nucleons, and the subsequent motion of the second nucleon is determined primarily by its motion in the deuteron prior to the photon interaction. Assuming this hypothesis, the photon on deuteron reaction becomes a two body problem except for smearing due to the initial momentum distribution of the interacting nucleon. The reaction $\gamma+D$ can give the following products: $P+\pi^0+(N)$; $D+\pi^0$; $N+\pi^+ +(N)$; $P+\pi^-+(P)$; $P+N$; $P+\pi^0+(N)$. Only the last three reactions contribute protons. By suitable combination it is possible, using the data from this experiment and known cross sections, to obtain the cross section for production of π^0 mesons from the neutron and proton in the deuteron.

* This work was supported in part by the U. S. Atomic Energy Commission.
[1] D. C. Oakley, thesis, California Institute of Technology, 1954 (to be published).

L14. A Study of the Reaction $H^1(H^2He^3)\pi^0$ at 340-Mev Proton Energy. K. C. BANDTEL, W. J. FRANK, L. HIGGINS, AND B. J. MOYER, *University of California, Berkeley.*—The ratio of the cross section for the reaction $H^1(H^2H^3)\pi^+$ to the above reaction has been determined to be 2.3±0.3 at one angle in the center of momentum system.* This evidence supports

the hypothesis of charge independence. As a further test, the angular distribution of the $H^1(H^2He^3)\pi^0$ is being measured for several angles by identifying the He^3 particle. A pulse height technique for measuring E and dE/dx is being used. The pulse heights are photographed on the sweep of a Tetstronix 517 scope. The angular distribution and yield of the reaction $H^1(H^3H^3)\pi^+$ has been measured,† and a comparison with the $H^1(H^2He^3)\pi^0$ cross section will give information about the hypothesis of charge independence. This work was performed under the auspices of the U. S. Atomic Energy Commission.

* American Physical Society Washington Meeting, 1954.
† Frank, Bandtel, Madey, and Moyer, Phys. Rev. **94**, 1716 (1954).

WEDNESDAY AFTERNOON AT 2:30

1 Le Conte Hall

(J. KAPLAN, presiding)

Contributed Papers

M1. Second-Neighbor Interaction in a Two-Dimensional Graphite Lattice. G. S. COLLADAY AND S. BARSHAY,[1] *U. S. Naval Ordnance Test Station.*—Using a LCAO wave function for the π electrons of a two-dimensional graphite lattice, the energy as a function of wave number vector $E(\mathbf{K})$ can be obtained under the approximation that (I) only interactions between nearest neighbors are included, or (II) interactions between both first and second nearest neighbors are included.[2] Density of states curves for the valence and conduction bands for (I) and (II) have been numerically computed. The desirability of including the second nearest neighbor interaction is indicated by comparing for (I) and (II) the density of states curves for valence and conduction bands, the effective mass of the π electrons, the effective number of conduction electrons, and the resonance energy of graphite.

[1] Now at the University of California, Berkeley.
[2] G. S. Colladay, Bull. Am. Phys. Soc. **29**, No. 6, 11 (1954), abstract B7.

M2. Magnetic Domains in a Single Crystal of Cobalt near 275°C by the Longitudinal Kerr Effect.* EDWARD M. FRYER AND CHARLES A. FOWLER, JR., *Pomona College.*—Hexagonal cobalt passes through a state of zero anisotropy at a temperature of about 275°C.[1] At this temperature the easy direction of magnetization changes from the hexagonal axis to one of the transverse axes. Photographic observations of magnetic domain patterns, by means of the longitudinal Kerr effect[2,3] as this temperature is approached and exceeded, indicate a shift in the domain structure from the one direction to the other. Photographs suggest a gradual widening of the domain wall as the transition temperature is approached, an apparent absence of domains when the crystal is isotropic, followed by a formation of new domains in a transverse direction as the temperature is further increased. On cooling, domains reappear in the original direction, becoming sharper as the crystal is cooled back to room temperature.

* Supported by the Office of Naval Research.
[1] R. M. Bozorth, *Ferromagnetism* (D. Van Nostrand Company, Inc., New York, 1951), p. 555.
[2] C. A. Fowler and E. M. Fryer, Phys. Rev. **94**, 52 (1954).
[3] C. A. Fowler and E. M. Fryer, Phys. Rev. **95**, 564 (1954).

M3. Temperature Dependence of the Heat Capacity of Molybdenite.* EDGAR F. WESTRUM, JR., AND JOHN J. MCBRIDE, *University of Michigan.*—To test the applicability of the recent treatments of thermal properties of lamellar lattices,[1] we have determined the heat capacity and derived thermodynamic functions for a highly purified molybdenite MoS_2 sample and for boron nitride over the range 5 to 300°K. The temperature dependence of the heat capacity of molybdenite is proportional to T^x if x gradually decreases from about three at 7° to less than two at 60°K. An essentially similar result has been found in this laboratory for crystalline boron nitride in contrast to the data reported by others.[2] However, the "sandwich" (S−Mo−S) lamina of molybdenite show as T^2 a dependence as that claimed by DeSorbo[3] for graphite and by Dworkin, Sasmor, and Van Artsdalen[2] for boron nitride. The significance of the temperature dependence is discussed. The entropy (S^0), and enthalpy increment ($H^0-H_0^0$) of molybdenite are 14.96±0.02 cal deg^{-1} $mole^{-1}$ and 2528.±3 cal $mole^{-1}$, respectively, at 298.16°K.

* Supported in part by U. S. Atomic Energy Commission.
[1] Tarassov, Compt. rend. acad. sci. U.R.S.S. **46**, 20, 110 (1945), and others.
[2] Dworkin, Sasmor, and Van Artsdalen, J. Chem. Phys. **22**, 5, 837 (1954).
[3] DeSorbo and Tyler, J. Chem. Phys. **21**, 1660 (1953).

M4. A Second Transition in $AuCu_3$.* G. C. KUCZYNSKI AND M. DOYAMA, *University of Notre Dame.*—The alloy $AuCu_3$, when heated, undergoes a transition from the ordered to the disordered state at about 391°C. Experiments on the kinetics of ordering carried out in this laboratory have shown a discontinuity in the rates of ordering of this alloy when disordered below and above 600°C, suggesting a possible change of phase. Careful specific heat measurements revealed a definite peak between 560° and 590°C. Measurements of the yield point and electrical resistance also showed discontinuities in that range of temperature. It can therefore be concluded that a second phase transition takes place in $AuCu_3$ in the vicinity of 590°C.

* Supported by Office of Naval Research.

M5. Effect of External Stresses upon the Rate of Ordering of AuCu.* A. R. FREDA AND G. C. KUCZYNSKI, *University of Notre Dame.*—AuCu wires were ordered at various temperatures below the critical temperature, under stresses varying from 0 to 200 kg/cm^2. It has been found that in the temperature range between 350° and 400°C the rate of ordering as measured by electrical resistivity was increased greatly in specimens ordered under external stress. Below 350°C no appreciable difference has been noted. Analysis of the results seems to indicate that the rate of nucleation is affected more than the rate of growth of the ordered domains. The effect increases greatly with increase in applied stress. No observable influence of external stress upon the rates of ordering in $AuCu_3$ has been observed.

* Supported by Union Carbon and Carbide Company.

M6. Rectification in Thin Films of PbS. M. SILVER, R. S. WITTE, AND F. MCCAFFREY, *U. S. Naval Ordnance Test Station.*—An induced rectification effect has been observed in chemically deposited PbS cells[1] and has been studied under various conditions of bias, temperature and atmosphere. A similar effect has been observed in evaporated PbS cells at 250°C.[2] The rate of polarization is voltage and temperature dependent. Experiments indicate that the barrier is in the

vicinity of the negative electrode with a back to forward resistance ratio of up to 10 to 1. It is further observed that the forward resistance decreases with time. To the first order, the polarization is atmosphere independent. Experiments have been performed in air (0 percent and 50 percent relative humidity) at atmospheric pressure and in vacuum at 10^{-4} mm of Hg. Rectification was observed with both gold and Aquadag electrodes. Once polarized, the cells exhibit considerable stability in resistance, sensitivity and noise as long as the polarizing bias is maintained. If the bias is removed the cell reverts to the unpolarized state. The rate of recovery is slow at room temperature but increases rapidly with increasing temperature.

[1] Observed independently by David Dutton, University of Rochester (private communication).
[2] Starkiewicz, Sosnowski, and Simpson, Nature 158, 28 (1946).

M7. Donor and Acceptor Ionization Energies in Silicon and Germanium.* A. H. MITCHELL AND C. KITTEL, *University of California, Berkeley.*—An exact theory of impurity states in crystals is developed, and an evaluation is given of the applicability of the Wannier equation to the donor states in Si and Ge in view of the multiple energy minima in the conduction band. The theory is extended to include degenerate bands, and it is shown by two different methods that the Wannier equation is to be replaced by a set of coupled wave equations. The theory is applied to acceptor states in Si and Ge. The agreement with experiment is fairly good for both donors and acceptors.

* This work is supported in part by the Office of Naval Research and the U. S. Signal Corps.

M8. Internal Friction as a Function of Cold Work of Copper Reeds at Low Frequencies. J. J. BRADY, M. B. LARSON, AND T. A. O'HALLORAN, *Oregon State College.*—The internal friction of copper reeds was measured by the resonance method of Jewell[1] for frequencies between 54 and 540 cycles per second. The reeds were annealed in a vacuum by passing a current through them. The Q^{-1} was then measured as a function of strain amplitude between 5×10^{-4} and 5×10^{-3}. Successive measurements were made after subjecting the sample to compressive loads ranging from 1800 lb/in.^{2} to 9000 lb/in.^{2}. For a frequency of 85.5 cps the cold-worked sample had a Q^{-1} greater than the annealed sample for strain amplitudes less than 2×10^{-3} but for greater strain amplitudes the Q^{-1} decreased with cold-working. The samples were polycrystalline.

[1] W. R. Jewell, Rev. Sci. Instr. 24, 5 (1953).

M9. Order-Disorder and Ionic Conductivity in Ag_2HgI_4. JEROME ROTHSTEIN, *Signal Corps Engineering Laboratories.*—Ketelaar[1] has shown ordered Ag_2HgI_4 to consist of full Ag planes, half full Hg planes, and full I planes in the order Hg−I−Ag−I, disordered having the metal atoms randomly distributed over four sites with the I lattice unaffected, ionic conductivity due to Ag only. The specific heat anomaly yields a straight line when its logarithm is plotted *vs* $1/T$, of slope corresponding to 10.7 kcal/mole, 2/3 of which applies to Ag. Close to perfect order, the elementary act of disordering must be the jumping of Ag to vacancies in Hg plane, producing a pair of current carriers (Ag ion and vacancy), so that activation energy of (1/2)(2/3)(10.7) kcal should be observed for ionic conductivity over the anomalous range, 3.6 kcal was observed. The pairs are analogous to Frenkel defects or hole-electron pairs and should relax bimolecularly like Cu_3Au.[2] Activation energies for ionic conduction in ordered and disordered phases (respectively structure-sensitive and intrinsic) correspond respectively to one and one-half vacancies available per elementary act of conduction.

[1] J. A. A. Ketelaar, Z. Krist. 80, 190 (1931) and 87, 436 (1934), Z. phys. Chem. 26B, 327 (1934) and 30B, 53 (1934).
[2] J. Rothstein, Phys. Rev. 94, 1429(A) (1954).

M10. Brillouin Zone Studies of Alloys. III. Matthiessen's Rule for Dilute Magnesium Alloys. E. I. SALKOVITZ, J. PASTERNAK, AND A. I. SCHINDLER, *Naval Research Laboratory.*—An analysis of H. Jones[1] theory of the Brillouin zone structure of magnesium alloys has led Salkovitz and Schindler[2] to suggest that interesting electrical effects might be observed near solute concentrations where electron overlap occurs. Preliminary data on the Hall coefficient[3] have already borne this out. In reference 2 it was suggested that one might find departures from Matthiessen's rule, which states that the temperature change of resistivity ($d\rho/dT$) in dilute alloys is concentration-independent. Therefore the resistivity of a series of dilute binary alloys of magnesium were measured in the temperature range of 20°–35°C in steps of 0.2°C. The solute atoms were Ag, Cd, In, Sn, Al, Tl, or Pb in various concentrations. It was found that as solute atoms were added, $d\rho/dT$ remained relatively constant up to an electron to atom ratio of about 2.013. At this value there was an abrupt drop of 5 percent in the value of $d\rho/dT$ with additional solute atoms. For still greater additions, $d\rho/dT$ continued to decrease slowly. The temperature coefficient of resistivity ($\alpha=d\rho/\rho dT$) decreased rapidly with alloying up to the electron to atom ratio of about 2.013.

[1] H. Jones, Proc. Roy. Soc. (London) A147, 400 (1934).
[2] E. I. Salkovitz and A. I. Schindler, Phys. Rev. 91, 234 (1953).
[3] A. I. Schindler and E. I. Salkovitz, Phys. Rev. 91, 1320 (1953).

M11. Linear Magnetostriction of Some Ternary Cobalt-Iron-Nickel Alloys. H. E. STAUSS AND G. SANDOZ, *Naval Research Laboratory.*—Measurements of linear magnetostriction have been made of ternary cobalt-iron-nickel alloys with high cobalt content. In the case of most of the ternary alloys examined, the linear magnetostrictions that were observed at the highest magnetic inductions attained (approximately saturation magnetostrictions) were less than the published values of saturation magnetostriction for binary cobalt-iron alloys with the same cobalt content. In the restricted range of alloys containing 45- to 60-percent cobalt, the substitution of about 5 percent or less of nickel for iron appeared to result in small increases of magnetostriction up to about 10 percent as compared with binary alloys of like cobalt content. No values of magnetostriction were found in the ternary alloys that were greater than the larger published values for the binary cobalt-iron alloys. Data concerning the change of magnetostriction with magnetic induction are given for the alloys.

M12. Thermal Conductivity of Germanium at Ambient Temperatures. KATHRYN A. MCCARTHY AND STANLEY S. BALLARD,* *Tufts College.*—The thermal conductivity of germanium has been measured by a comparative method[1] in which cast zinc[2] of high purity was used as the standard. The germanium samples, prepared and made available by the Westinghouse Research Laboratories, were stated to contain about 10^{14} electrical impurities per cm^3. Values measured for the thermal conductivity of these samples were: at 35°C, 0.57 watt cm^{-1} °C^{-1}; at 5°C, 0.61 watt cm^{-1} °C^{-1}. These results are in substantial agreement with those reported by Grieco and Montgomery.[3]

* Present address: Scripps Institution of Oceanography.
[1] Ballard, McCarthy, and Davis, Rev. Sci. Instr. 21, 905–907 (1950).
[2] *Zinc and Its Alloys* (National Bureau of Standards, Washington, D. C. 1931), Circular No. 395, pp. 69–71.
[3] A. Grieco and H. C. Montgomery, Phys. Rev. 86, 570 (1952).

M13. Investigation of a Polymorphic Transition in Iron at 130 k.b.* STANLEY MINSHALL, *Los Alamos Scientific Laboratory.*—Propagation of compressive waves generated by high explosives in Armco iron may, under certain conditions, occur with three stable shocks. The characteristics of these have been investigated by means of the pin technique. Data will be presented to show that the three waves are consistent with the hypothesis of a dynamic elastic limit of 6.7 k.b., and a polymorphic transition of about 130 k.b.

* Work done under the auspices of the U. S. Atomic Energy Commission.

THURSDAY MORNING AT 9:00

310 Le Conte Hall

(R. T. BIRGE, presiding)

Nuclear and Electron Resonance

Invited Papers

N1. Cyclotron Resonance in Solids. A. F. KIP, *University of California, Berkeley.* (30 min.)
N2. Nuclear Resonance and the Study of Metals. C. P. SLICHTER, *University of Illinois.* (30 min.)
N3. Paramagnetism of the Transuranic Elements. C. A. HUTCHISON, JR., *University of Chicago.* (30 min.)
N4. Paramagnetic Resonance of Free Radicals. G. E. PAKE, *Stanford University.* (30 min.)

THURSDAY MORNING AT 9:00

3 Le Conte Hall

(W. E. LAMB, presiding)

Invited Paper

O1. Problems of the Diffraction of Light with Demonstrations by Video. F. ZERNIKE, *Groningen, The Netherlands.* (30 min.)

Contributed Papers

O2. The Magnetic Moment of Free Electrons. D. J. BESDIN AND JOSEPH H. ROBINSON III, *Texas Technological College.*—Many elegant methods have been applied to compute the magnetic moment of a system of free electrons confined in a box. If the electron wave functions are required to vanish at the walls, all states are obtained and no distinction need be made between the various orbits. However, an exact and general statistical determination of the moment of the system has not been possible so far because of computation difficulties with the Fermi-Dirac summation. Results reported so far from computing the free energy appear to be not wholly reliable because of H dependence of the limits of summation and the degeneracy-of-states factor. It appears, therefore, that an exact numerical determination may be useful for checking earlier work and indicating trends. We have verified and extended the results at absolute zero temperature obtained previously by one of us for a cylindrical box with a uniform field along the axis.* Results obtained are reminiscent of the deHaas-van Alphen effect, and it is planned to extend the work to higher temperatures.

* D. J. Besdin, Phys. Rev. 79, 417 (1950); unpublished thesis, Rice Institute (1950).

O3. Random Walk Methods in Statistical Mechanics of One-Dimensional Systems.* R. L. SELLS, C. W. HARRIS, AND E. GUTH, *University of Notre Dame.*—We have shown that random walk methods yield in the simplest possible way equations of state and (pair) distribution functions of one-dimensional gases with nearest neighbor interaction only. For such systems Bethe's method of treatment of order-disorder phenomena is exact and an appropriate form of the superposition principle is valid rigorously. The corresponding Born-Green (and/or Kirkwood) type of integral equation can be shown to be linear and of the convolution type. This can be seen most simply by repeated application of the operation of convolution to the pair distribution function for adjacent molecules. This pair distribution function in turn is given simply by Boltzmann's principle and is a Poisson distribution modified by the presence of the interaction potential (with hard core) between the molecules. This study is preliminary to an attempted treatment of a one-dimensional gas where all molecules interact with each other. Such a system will plausibly show a phase transition. In fact the corresponding one-dimensional Ising model does show a phase transition. The existence of this transition can be proved, but the explicit construction of the partition function is difficult. This system is about intermediate between the two- and three-dimensional Ising models with nearest neighbor interaction.

* Supported in part by the Office of Naval Research.

O4. Role of Coordination Number in the Lee-Yang Lattice Gas.* C. W. HARRIS, AND E. GUTH, *University of Notre Dame.*—Lee and Yang[1] considered a lattice gas corresponding to Onsager's solution of a square Ising model. We have considered the lattice gases corresponding to hexagonal, triangular, and kagomé Ising models also. In accordance with physical expectation the critical constant $(\eta_c V_c/kT_c)$ increases with the coordination number from 0.0742 for the hexagonal case to 0.0966 for the square case and further to 0.1182 for the triangular case. The last case comes closest to reality. These lattice gases will be compared with a Lennard-Jones and Devonshire type of two-dimensional cell-gas using a square well interaction between pairs of atoms.

* Supported in part by Office of Naval Research.
[1] T. D. Lee and C. N. Yang, Phys. Rev. 87, 410 (1952).

O5. Effect of the Extended Size of the Nucleus on μ-Meson Pair Photoproduction.* GEORGE RAWITSCHER,† *Stanford University.*—In the case of μ-pair creation by photons, the momentum transfer q to the nucleus is large enough to introduce into the usual point-charge differential Bethe-Heitler cross section a reducing form factor dependent on q and on the shape of the

nucleus. The cross section $d^3\sigma/dEd\Omega$, in which the angle and momentum p of one of the mesons $(-)$ is held fixed, was calculated using the Stanford Card-Programmed-Calculator. The ranges for the parameters $(1.68 \leq p/\mu c \leq 3.72;\ \theta = 10°;\ 4.00 < k/\mu c^2 < 5.70)$ were chosen to correspond to an experiment now in progress at the High-Energy Physics Laboratory. The results for $p/\mu c = 2.73$, folded into the 500-Mev bremsstrahlung spectrum dk/k, and normalized to the corresponding point-charge Bethe-Heitler results are, respectively, 1, 0.318, 0.157, 0.032, 0.028 for $A = 0$, 27, 63, 207, 238. It is felt that for lower energies this form-factor effect will be even more pronounced.

* Partially supported by the joint program of the Office of Naval Research and the U. S. Atomic Energy Commission.
† C. B. P. F., Rio de Janeiro, Brazil, at Stanford under a Fellowship of the Brazilian National Research Council.

O6. Lattice Space Quantization of Coupled Meson and Nucleon Fields.* D. H. HOLLAND, *Stanford University.*—The lattice space quantization method used by Schiff[1] for treating nonlinear mesons is fused in quantizing coupled meson and nucleon fields. Neutral pseudoscalar mesons with pseudoscalar coupling to neutral Dirac nucleons are assumed. Only the fields at the lattice points of a cubic lattice are considered. An appropriate lattice-space Hamiltonian is found and momentum (gradient) terms are treated as perturbations. To zero order the lattice points are uncoupled, so the state function can be written as a product of functions describing a single point. In the representation chosen, finding a particular point function entails the solution of a set of coupled differential equations. These equations can be solved in principle with no assumptions as to the magnitude of the coupling constant g. Linear combinations of the zero-order solutions can be found which diagonalize the perturbation to lowest order and can be interpreted as one-particle momentum eigenstates. Linear combinations of two-particle momentum eigenstates are found which approximately diagonalize the perturbation, and from these scattering cross sections are calculated.

* Supported by the Office of Scientific Research, Air Research and Development Command.
[1] L. I. Schiff, Phys. Rev. **92**, 766 (1953).

O7. Pion-Nucleon s-Wave Phase Shift from $ps-ps$ with Cutoff. CHARLES J. GOEBEL, *University of California, Berkeley.**—An investigation of the pion-nucleon s-wave scattering in the $ps-ps$ theory is made, using a cutoff $\leq$ the nucleon mass, and the ("exact") Foldy nonrelativistic transformation of the Hamiltonian. The calculation of the phase shifts in the 1-meson $T-D$ approximation yields (choosing an appropriate cutoff) a large i-spin dependent term, but this term is spurious since it violates the Gell-Mann and Goldberger[1] "crossing theorem." The spurious term disappears in an (approximate) 3-meson $T-D$ calculation (meson-meson interaction is not included) with the result that no appreciable i-spin dependence is found from this theory.

* Part of a thesis done at the University of Chicago. Supported in part by the U. S. Atomic Energy Commission.
[1] M. Gell-Mann and M. Goldberger (unpublished); but see, e.g., Proc. Fourth Annual Rochester Conference on High Energy Nuclear Physics, p. 29.

O8. A Variational Principle for Tensor Forces. J. L. MCHALE AND R. M. THALER, *Los Alamos Scientific Laboratory.*—In calculating nucleon-nucleon scattering, it proved convenient to formulate the Schwinger variational principle for coupled states[1,2] in terms of quantities $X_{\alpha,\beta}$ and $Y_{\alpha,\beta}$ defined by

$$\varphi_i = \begin{pmatrix} u_J{}^i \\ w_J{}^i \end{pmatrix} \sim \begin{pmatrix} F_{J-1}\delta_{i\alpha} + X_i G_{J-1}\delta_{i\alpha} + Y_i G_{J-1}\delta_{i\beta} \\ F_{J+1}\delta_{i\beta} + X_i G_{J+1}\delta_{i\beta} + Y_i G_{J+1}\delta_{i\alpha} \end{pmatrix}. \quad (1)$$

The α solution corresponds to incident wave in channel $L=J-1$ and, no incident wave in channel $L=J+1$; the β solution corresponds to incident wave in channel $L=J+1$. F_L and G_L are regular and irregular solutions of the homogeneous equation. Time reversal or the Wronskian require $Y_\alpha = Y_\beta$. The stationary expressions for X, Y avoid treating any of them on a special footing, and are similar to Schwinger's expression for eigenphase shifts. Diagonalization of the S matrix requires that the mixture parameter[3]

$$\eta = -(X_\alpha - X_\beta)/2Y \pm [(X_\alpha - X_\beta)^2/4Y^2 + 1]^{\frac{1}{2}}$$

with $\eta_+\eta_- = -1$, and $\tan\delta_\pm = X_\alpha + \eta_\pm Y = X_\beta + (\eta_\pm)^{-1}Y$, where $\delta_\pm$ are eigenphase shifts. Modification of the η condition yields the usual complex phase shifts of the undiagonalized S matrix.

[1] L. C. Biedenharn and J. M. Blatt, Phys. Rev. **93**, 1387 (1954); Phys. Rev. **86**, 399 (1952).
[2] F. Rohrlich and J. Eisenstein, Phys. Rev. **75**, 705 (1949).

O9. Optical Model Analysis of Scattering of 14-Mev Neutrons. I. N. SHERMAN, G. CULLER, AND S. FERNBACH, *University of California, Livermore.*—Calculations of the angular distributions of elastically scattered neutrons and of reaction and total cross sections at 14 Mev have been performed, based on the optical model of the nucleus. The central field was described by a complex potential in the form of a "square well with a tail." The depth and shape of the complex potential were varied in attempts to fit available experimental data. The report will show the best fits for: (a) the experimental angular distributions[1] of C, Al, Cu, Sn, and Pb; (b) the experimental reaction cross sections[2] of B, C, N, Al, Fe, Cu, Cd, Au, and Pb; (c) the experimental total cross sections[3] as a function of atomic number. The complex potentials which yield these fits will be discussed. This work was performed under the auspices of the U. S. Atomic Energy Commission.

[1] Private communication from J. Coon.
[2] Phillips, Davis, and Graves, Phys. Rev. **88**, 600 (1952).
[3] Coon, Graves, and Barschall, Phys. Rev. **88**, 562 (1952).

O10. Optical Model Analysis of Scattering of 14-Mev Neutrons. II. Polarization Effects. S. FERNBACH, G. CULLER, AND N. SHERMAN, *University of California, Livermore.*—The potentials used in the calculations reported in the previous paper have been modified to include a spin-orbit interaction of the form $f(r)\boldsymbol{\sigma}\cdot\mathbf{L}$. A study of variation of polarization and elastic cross section as a function of $f(r)$ and A is under way. Preliminary results indicate that the effect of including the spin-orbit terms is to damp the usual large oscillation in the diffraction pattern, especially at large angles. Experimental angular distributions for scattered protons show the same qualitative features, so that it seems that future proton calculations could profitably include the spin-orbit terms. The absence of minima at the expected angles of the diffraction pattern for scattered 300-Mev nucleons can be explained in the same way. Quantitatively, the results to data show that the maximum percentage polarization of the 14-Mev neutrons varies in a somewhat unpredictable way as a function of A. For $f(r) \approx 2$ Mev over the entire nucleus, a maximum of 95 percent is reached for aluminum, 56 percent for copper, 15 percent for tin, and 63 percent for lead. Keeping $f(r)$ constant over the nucleus but varying its magnitude appreciably affects the maximum percentage polarization as well as the diffraction pattern. In the case of lead, the best value of $f(r)$ was found to be ≈ 0.25 Mev. This work was performed under the auspices of the U. S. Atomic Energy Commission.

O11. On Dirac's Method Using Complex Variables in Quantum Mechanics.* EUGENE GUTH, *University of Notre Dame.*—Dirac[1] introduced essentially the (one-sided) Laplace transform of the radial Schrödinger wave function. This obeys an integral equation similar to that obeyed by momentum transforms. In general, determination of the eigenvalues (and

of the eigenfunctions) needs considerations in the complex plane. It is pointed out, however, that for S-states in a Coulomb field the integral equation reduces to a linear differential equation of the first order and the eigenvalues follow from the postulate of the uniqueness of the wave function. The simple operator calculus involved in the transition from the Hamiltonian to the wave equation for the Laplace transform of the coordinate wave function resembles Heaviside's calculus. To the first power of the radius vector there corresponds differentiation according to the parameter of the Laplace transform, while to the reciprocal of the radius vector there corresponds integration according to the same parameter.

* Supported in part by the Office of Naval Research.
[1] P. A. M. Dirac, Proc. Roy. Soc. (London) **A160**, 48 (1937). Essentially the same method was later developed independently in great detail by H. Kallmann and M. Päsler; cf, e.g., Ann. Physik (6) **2**, 92 (1948).

O12. On the Theory of Successive Orientational Phase Transitions in Two- and Three-Dimensional Systems.* T. E. Lockary and E. Guth, *University of Notre Dame.*—Krieger and James[1] considered a system of three-dimensional rotators fixed in space. For an interaction energy between nearest neighbor rotators which depends only on the angle between their axes and consists of the sum of the first two spherical harmonics, single first- and second-order transitions and even two successive first-order transitions were obtained depending upon the ratio of the coefficients of the spherical harmonics. In the present work a simplified method was developed which was shown to yield all of Krieger and James' principal results. This method was then applied to a two-dimensional system of rotators, the spherical harmonics being replaced by the corresponding cosines. Application of the internal field approximation shows a single second-order transition, a single first-order transition, a first-order transition followed by a second-order transition as the temperature increases, or two second-order transitions depending on the value ratio of the coefficients. The less complete results of the method of Bethe and Chang verify these results qualitatively while changing numerical values slightly in the range accessible to this treatment. Use of more complicated interactions in the internal field approximation indicate the possibility of several successive transitions in the system.

* Supported in part by the Office of Naval Research.
[1] T. J. Krieger and H. M. James, J. Chem. Phys. **22**, 796 (1954).

O13. Two-Dimensional Coulomb Scattering in Quantum Mechanics.* Ming Chen Wang and Eugene Guth, *University of Notre Dame.*—For three-dimensional Coulomb scattering, classical theory, Born approximation, and exact quantum-mechanical theory all lead to the same (Rutherford's) result. For two-dimensional Coulomb scattering (retaining the inverse square law, instead of the logarithmic potential), the exact result contains Planck's constant and gives different results for the Born and the classical limits. This result is of methodological interest.

* Supported in part by the Office of Naval Research.

O14. A Formulation of Probability Theory as a Physical Theory.—A. O. Barut,* *University of Chicago.*—The theory of probability when applied to quantum mechanics appears to be modified and restricted and there is an inconsistency in the use of probability rules. These facts are due to the incompleteness of the probability theory itself in describing the physical world. Probability statements must include the experiment, all possible outcomes of it, as well as the system on which the experiment is carried on. The experiment is taken to be the primary concept. One way of formulating such a completed probability theory is to represent the random variable (experiment) by an Hermitian operator in a Hilbert space, for then the postulates of the inner product in Hilbert space are of the same structure as the postulates of the probability theory. Furthermore the rules for the addition and multiplication of probabilities have no logical connections with the postulates. Such rules must be in agreement with the experiments and it is possible to formulate them in such a way as to contain the superposition principle of physics. The postulates of the quantum theory can then be reduced to a single principle: that "observables are random variables."

* Now at Reed College.

Thursday Morning at 9:00

4 Le Conte Hall

(L. W. Alvarez, presiding)

Contributed Papers

P1. Disintegration of Oxygen by 300-Mev Neutrons. Melvin Otis Fuller, *University of California, Berkeley.*—The 300-Mev neutron beam of the Berkeley cyclotron was used to produce disintegrations of oxygen nuclei in an oxygen-filled cloud chamber situated in a 21 700 gauss pulsed magnetic field. Pictures of the "stars" thus formed were reprojected and measured, permitting identification of most of the ejected particles and computation of their energies and momenta. Each star consisted of one or more tracks due to heavy particles of one or two charges, plus the track of the recoil nucleus. The random selection of 602 stars shows approximate percentages according to total prongs as follows: 2-prong, 42 percent; 3-prong, 29 percent; 4-prong, 12 percent; 5-prong, 12 percent; 6-prong, 4 percent; 7-prong, 1 percent; plus one 8-prong star. Energy measurements of the prongs showed 29 percent as having over 15 Mev, 16 percent over 50 Mev, and 8 percent over 100 Mev. Using 15 Mev as a division point for slow and fast particles, the slow particles were 37 percent alphas, 33 percent protons, and 22 percent deuterons, and the fast particles 66 percent protons, 20 percent deuterons, and 9 percent alphas. The energy spectra of the slow particles show maxima at about 2, 3, and 4 Mev for the protons, deuterons, and alphas, respectively, and have the general form characteristic of evaporation spectra. The fast particles, mostly protons, exhibit energy and angular distributions similar to those previously found for heavier elements using nuclear cascade theory. This work was performed under the auspices of the U. S. Atomic Energy Commission.

P2. An Experimental Ion Source for the 184-inch Cyclotron. Warren Fenton Stubbins, *University of California, Berkeley.*—A PIG type ion source was mounted in the center of the 184-inch cyclotron with extension lips placed on the dees to reduce the dee gap and aperture in the source region according to requirements established by calculations. The operation of the source and the nature of the cyclotron beam were

observed for various conditions of dee voltage, dee bias, source position, and the time sequence of ion injection. A pulse-wise increase of dee voltage at the ion injection time to achieve greater acceptance of ions was investigated. The restrictions imposed on the initial conditions for ions resulted in a decrease in the radial oscillation amplitude by a factor of 2 to 3. The beam current was comparable to that available from the conventional open arc source. The work was performed under the auspices of the U. S. Atomic Energy Commission.

P3. Angle and Energy Distributions of Charged Particles from the Cyclotron Bombardment of Ni and Ag by 200-Mev Protons. L. EVAN BAILEY, *University of California, Berkeley.*—Thin nickel and silver targets have been bombarded by the internal proton beam of the 184-inch synchrocyclotron. Nuclear track plates were used to detect the secondary particles. Absolute cross sections for the production of protons, deuterons, tritons, He^3, and alphas will be presented in the 2- to 70-Mev energy range as a function of angle. Particles were identified by momentum *vs* range. The momentum was determined by the bending in the cyclotron magnetic field. Absolute cross sections were determined by measuring the target's activity, and by comparing it with the activity of a target calibrated in the external cyclotron beam. These cross sections illustrate the relative importance of the cascade (knock-out) process and the evaporation process at different secondary particle energies. This work was performed under the auspices of the U. S. Atomic Energy Commission.

P4. Analysis of the Disintegration Products from the Reactions of 125-Mev Deuterons with Lithium Nuclei. F. C. GILBERT, *University of California, Berkeley.*—A thin lithium (92.5 percent Li^7, 7.5 percent Li^6) target was bombarded with the internal deuteron beam of the 184-inch cyclotron. The resulting fragments were detected in a row of nuclear track plates placed along a radial line from the target. An analysis of the tracks in the emulsions yielded the following information: (a) energy distributions for the production of various fragments from 0° to 70° from the beam direction, (b) the angular distribution of Li^8 nuclei in the reaction $H^2+Li^7 \rightarrow H^1+Li^8$, (c) the range distribution of the alpha particles following the decays of Li^8 and B^8, (d) the electron pickup by Li^8 ions as a function of their velocity, (e) the range of Li^8 nuclei in emulsion. In addition, absolute cross sections are obtained for processes (a) and (b) by means of exposures in the monitored external beam of the cyclotron. This work was performed under the auspices of the U. S. Atomic Energy Commission.

P5. External Proton Beam at the Cosmotron.* O. PICCIONI, D. CLARK, R. COOL, G. FRIEDLANDER, AND D. KASSNER, *Brookhaven National Laboratory.*—A system for ejection of protons from the Cosmotron by magnetic deflection has been devised.[1] After rf turnoff, the beam passes through a Lucite target which causes a decrease in orbit radius of about 4 inches in the next revolution. The beam then passes through a 1 in.×3 in. gap in a 30 in. long electromagnet placed near the inner edge of a straight section without having previously been disturbed by the magnet's fringing field. The protons are deflected outward by about 3° and arrive near the outer edge of the next straight section where they are given an additional outward deflection by a second magnet. Tests with the first magnet in place have produced at the position of the second magnet a proton beam about half the intensity of the circulating beam and with a cross section of about 1½ in.×5 in. The system can be used with either sharp or slow rf turnoff, thus preserving for the external beam the choice of time spreads between 1 and about 25 milliseconds now available with the internal beam.

* Research performed at Brookhaven National Laboratory, under the auspices of the U. S. Atomic Energy Commission.
[1] A substantially similar system has been independently proposed for the Bevatron by B. Wright, Rev. Sci. Instr. 25, 429 (1953).

P6. Nuclear Interactions of Cosmic Rays in Aluminum.* W. W. BROWN,† *University of California, Berkeley.*—A method of detecting and observing cosmic-ray nuclear interactions in thin metal foils is described. Five aluminum foils, from 5 to 70 mg cm^{-2} thick×20×23 cm mounted horizontally in a cloud chamber, form the cathodes of a proportional counter system. The anodes are 3-mil tungsten wires strung between the foils. The gas, argon saturated with isoamyl alcohol, is common to the cloud chamber and counter system. Amplified pulses from the counters trigger the expansion of the chamber and cut off the high voltage rapidly enough so that the positive ions generated by the triggering particles are still in position for track formation. The amplifier bias is set high enough to favor observing heavily ionizing particles. Nuclear interactions occurring in the gas and foils at sea level are observed. Their absolute rate of occurrence in argon, 0.52 hr^{-1} per gram atom, agrees with previous measurement. The ratio of the rates in Al and A, when corrected for absorption effects of the foils, is about the same as the ratio of the geometric nuclear areas.

* Assisted by the joint program of the Office of Naval Research and the U. S. Atomic Energy Commission.
† Now at North American Aviation, Inc., Downey, California.

P7. Some Results on Heavy Charged Mesons. R. ARMENTEROS, B. GREGORY, P. HENDEL, A. LAGARRIGUE,* L. LEPRINCE-RINGUET, F. MULLER, AND C. PEYROU, *Ecole Polytechnique, Paris.*—The results to be presented were obtained at the Pic du Midi in the French Pyrenees (9000 feet), with two cloud chambers placed one above the other.[1] The upper is in a magnetic field 2500 gauss; the lower is a multiplate chamber containing 15 copper plates 1 cm thick. The nuclear interactions of the secondaries of fast $V^{\pm}$ particles in the lower chamber indicate a large majority of μ mesons among the positive secondaries, but a considerable proportion of π mesons among the negative secondaries. Most of the particles with π-meson secondaries could be hyperons. We observe a significant positive excess for the slow charged $V^{\pm}$ particles (time of flight 1 or 2×10^{-9} sec) and a very large (27 to 1 or 2) positive excess for the S particles (time of flight larger than 5×10^{-9} sec). From the study of slow $V^{\pm}$ mesons and S particles we conclude the existence of two kinds of K particles with μ-meson secondaries. One is the K_{μ},[1] which has a mass of 914±18, probably a two-body decay, and a positive charge. The other has a shorter mean life, a three-body decay, and probably a larger mass.

* Now at the University of California.
[1] Gregory, Lagarrigue, Leprince-Ringuet, Muller, and Peyrou, Nuovo cimento II, 292 (1954), and Report of the Padua Conference (to be published).

P8. Analysis of Charged *V* Events.* W. H. ARNOLD, J. BALLAM, A. L. HODSON, R. RONALD RAU, GEORGE T. REYNOLDS, S. B. TREIMAN, AND V. A. VAN LINT, *Princeton University.*—Two interesting cases of V^+ events have been observed in a double cloud chamber operated at Echo Lake, Colorado (10 600 feet). Event 161–48942 consists of a charged particle, not visible in the upper chamber, which comes to rest in the second plate of the lower chamber and decays. The secondary then proceeds back up into the upper chamber and is visible for 33 cm. The secondary momentum is 145±5 Mev/c. Assuming it is a μ meson its momentum at the point of decay must have been 220±5 Mev/c, which is close to the value for p^* for the K_{μ}[1] particle. Event 164–50818 is a charged V whose secondary makes a star in the argon gas of the upper chamber. The primary has a momentum of 740±130 Mev/c and is lightly ionizing. It therefore is unlikely that it is a hyperon. The secondary track is short but preliminary measurements of its momentum indicate that although it could be part of a charged τ decay it is more likely that it belongs to a

θ^+.[2] A general analysis of charged V events will also be presented.

* Supported by the Office of Naval Research and U. S. Atomic Energy Commission.
[1] Gregory, Lagarrigue, Leprince-Ringuet, Muller, and Peyrou, Nuovo cimento **II**, 292 (1954).
[2] Hodson, Ballam, Arnold, Harris, Rau, Reynolds, and Treiman, Phys. Rev. (to be published).

P9. Specific Ionization of High-Energy Electrons.* W. C. BARBER, *High-Energy Physics Laboratory, Stanford.*—The measurements of specific ionization described previously[1] have been improved in accuracy and extended to lower electron energies. The improved accuracy results from tests of the Faraday cup which indicate that its absolute error is under 2 percent while relative errors from changes in primary energy are less than 0.5 percent. Measurements over the energy range 1–35 Mev were made in H_2, He, and N_2. At minimum ionization, the gases showed 7.58, 6.16, and 5.34 ion pairs per cm at N.T.P., respectively. If the data are compared with the theory of energy loss, using constants given by Sternheimer[2] and taking into account the size of the ion chamber, the number of electron volts to produce an ion pair is calculated to be 38.5, 44.3, and 34.4, respectively. The relativistic increase in ionization agrees with the calculated increase in energy loss within 1 percent for N_2, but is a few percent less for He and H_2. Calculations indicate that this discrepancy may result from production of Čerenkov radiation.

* Supported by the joint program of the U. S. Navy (Office of Naval Research) and the U. S. Atomic Energy Commission.
[1] W. C. Barber, Phys. **93**, 942 (1954).
[2] R. M. Sternheimer, Phys. Rev. **88**, 851 (1952).

P10. Stripping Electrons from Accelerated O and Ne Ions.* EDWARD L. HUBBARD AND EUGENE J. LAUER, *University of California, Berkeley.*—Electrons were stripped from O and Ne ions accelerated by the 4-Mev Van de Graaff by passing the ions through a $\frac{1}{8}$-in.-diam., 20-in.-long tube filled with gas. Magnetic deflection was used to select the energy and charge of the incident ions and to determine the distribution of ionic charges in the stripped beam. Gas was admitted to the center of the tube and pumped away from both ends so that it was not necessary for the beam to pass through any foils. As the pressure was increased, the peak of charge distributions first shifted toward higher charges and then became constant as equilibrium was established between capture and loss of electrons. The pressure of argon at the center of the tube required for equilibrium was 40μ, corresponding to a thickness of 3.5×10^{16} atoms cm^{-2}. At equilibrium in argon the average ionic charges were

3.3-Mev O	6.1-Mev O	8.7-Mev O	3.1-Mev Ne	7.1-Mev Ne	10.3-Mev Ne
3.5	4.8	5.2	3.3	4.9	6.0

The charge distributions were bell-shaped with a width at half-maximum of 1.8. Little or no dependence on the stripper gas was observed.

* This work was done under the auspices of the U. S. Atomic Energy Commission.

P11. Analysis of Electron Stripping Data.* ROBERT L. GLUCKSTERN, *Yale University.*†—The stripping experiments in the preceding abstract have been compared with the predictions of a model due essentially to Bell[1] and originally applied to the capture and loss of electrons for fission fragments in gases. For lighter ions it appears desirable to modify the capture and loss cross sections to take account of the possibility of loss or capture of two or more electrons in a single stripper atom. The results for the dependence of the average charge on ionic atomic number and on energy are in good agreement with the experiments, and the predicted charge-state widths at half-maximum are all about 2.3, slightly larger than observed. A slightly increased average charge is predicted for strippers of higher atomic number. The observed variation of charge distribution with stripper thickness was converted into capture and loss cross sections on the assumption of single-jump events, and the results agreed reasonably well with those predicted. Double-jump events cannot be ruled out by the experiment, and there is some slight indication that they are present.

* This work was supported by the U. S. Atomic Energy Commission.
† This work was performed at the University of California, Berkeley.
[1] G. I. Bell, Phys. Rev. **90**, 548 (1953).

P12. Absolute Cross Section for the Reaction $C^{12}(\gamma,n)C^{11}$.* W. GEORGE, W. BARBER, AND D. REAGAN, *High-Energy Physics Laboratory, Stanford.*—Stacked foils were exposed to the direct beams of both the Mark II (38-Mev) and Mark III (270-Mev) linear accelerators, to obtain the activation curve for the reaction in the energy range 18–250 Mev. The shape of the cross-section curve was found by the photon-difference method. The threshold and peak characteristics compare reasonably with previous results,[1] but the curve has a high-energy tail extending even beyond 38 Mev. The shape of the tail is not well known, but the total effect is unlikely to be due to meson production. The value of the total cross section up to 38 Mev, $\int\sigma(k)dk$, was found to be 0.0505 ± 0.002 Mev-barns, with a peak at 22.5 Mev of 7.5 millibarns; up to 25 Mev, 0.0293; and up to 250 Mev, $\sim$0.060.

* Supported by the joint program of the U. S. Navy (Office of Naval Research) and the U. S. Atomic Energy Commission.
[1] Montalbetti, Katz, and Goldemberg, Phys. Rev. **91**, 659 (1953).

P13. Fission of Bismuth by 22-Mev Deuterons.* A. W. FAIRHALL, *University of Washington.*—High-purity (99.998 percent) bismuth metal bombarded with 22-Mev deuterons is being studied by radiochemical techniques for possible fission products. Activation analysis shows uranium and thorium absent in detectable amounts. Elements between zinc and barium are being examined. Some show activities which must surely come from traces of impurity in the target. Others, such as strontium, yttrium, and palladium, show activities which can only be fission products. These yields are very low, corresponding to cross sections of the order of 10^{-31} cm^2.† Preliminary results indicate a sharply rising fission-yield curve in the region of mass numbers 92 and 93, with a dip occurring at mass number 105. The indication so far is that the mass-yield curve is rather narrow, and possibly asymmetric. The latest results, and their correlation with Fong's theory of fission,[1] will be discussed.

* Supported in part by the U. S. Atomic Energy Commission.
† Preliminary studies were made with 15-Mev deuterons at *M.I.T.* At this energy the yields were a factor of about 20 lower.
[1] P. Fong, Phys. Rev. **89**, 332 (1953); privately circulated notes.

P14. The Decay of Bi^{207}. D. E. ALBURGER AND A. W. SUNYAR, *Brookhaven National Laboratory.**—Bi^{207} has been found to decay by electron capture accompanied by gamma rays of energies 570 ± 2 kev, 1.0639 Mev, and 1.78 ± 0.01 Mev having relative transition intensities of 1:0.90:0.10 and K-conversion intensities of 1.7, 8.2 and 0.022 electrons per 100 disintegrations, respectively. Electron capture branches 90 percent to the $i_{13/2}$ state at 1.634 Mev and 10 percent to a level at 2.35 Mev. The latter branch proceeds by L capture only as shown from the x-ray spectrum in coincidence with $1.78+0.57$ sum pulses. This information places the decay energy to the 2.35-Mev level at 50 ± 40 kev and the total Bi^{207} decay energy at 2.40 ± 0.04 Mev. The 1.78-Mev transition has a K-conversion coefficient of 2.4×10^{-3} in agreement with $E2$. Angular correlation experiments confirm the $1.06-0.57$, $13/2\rightarrow5/2\rightarrow1/2$ cascade but the $1.78-0.57$ cascade shows an approximately isotropic distribution when measured using a 50 μC liquid source of $BiSO_4$ in dilute H_2SO_4. We assume that the latter correlation is washed out by electronic effects associated with electron capture. An

investigation of the 1.78−0.57 correlation is now being made with an electroplated source. All other data are consistent with an assignment of $h_{9/2}$ to the 2.35-Mev level. A spin $\geq 7/2$ for this state is supported. Fast coincidence techniques have been used to show that the 0.57 Mev level has a half-life of $<4\times10^{-10}$ sec.

* Under contract with the U. S. Atomic Energy Commission.

P15. Gamma Rays Accompanying Spontaneous Fission of Cf^{252}. HARRY R. BOWMAN AND LLOYD G. MANN, *University of California, Livermore.*—The gamma-ray spectrum in coincidence with Cf^{252} spontaneous fissions has been measured using a source of 113 fissions per minute. A parallel plate ionization chamber and NaI(Tl) crystals were used to drive a coincidence circuit of one-microsecond resolving time. The sodium iodide crystals ranged in size from 1½ inch diameter ×1 inch to 3×2 inches and were corrected for pulse height distribution by the method used by Gerhart.[1] The gamma spectrum extends to about 5 Mev, with an average energy of 1.2 Mev. The total energy release via gamma radiation is 14±2 Mev per fission, indicating an average of 12 gamma rays per fission. This work was done under the auspices of the U. S. Atomic Energy Commission.

[1] Gerhart, Carlson, and Sherr, Phys. Rev. **94**, 917 (1954).

THURSDAY MORNING AT 9:00

1 Le Conte Hall

(K. MACKENZIE, presiding)

Invited Paper

Q1. Electron Scattering and Nuclear Structure. R. HOFSTADTER, *Stanford University.* (30 min.)

Contributed Papers

Q2. Theory of Nuclear Excitation in Inelastic Electron Scattering.* C. J. MULLIN AND E. GUTH, *University of Notre Dame.*—When nuclear excitation is induced by electron bombardment, the inelastically scattered electrons are always accompanied by electrons which have lost energy by bremsstrahlung. The inelastically scattered electrons can be observed only if the electron energy is sufficiently high so that the inelastic peaks (peaks in the energy distribution of the electrons scattered through a fixed angle) rise well above the background of "bremsstrahlung electrons." Recently, Hofstadter *et al.*[1] at Stanford have observed inelastic peaks in the energy distributions of 190-Mev electrons scattered on Be^9 and C^{12}. A theoretical study of the inelastic scattering process has been made in an attempt to deduce the properties of the excited levels of the scattering nuclei from the experimental scattering data. Definite conclusions about the spin and parity of an excited level cannot be made unless some assumptions are made about the form of the nuclear wave functions. In preliminary calculations, the inelastic scattering cross section has been evaluated by a method similar to that developed by Schiff;[2] nuclear wave functions of the harmonic oscillator type suggested by the shell model have been used.

* Supported in part by the Office of Naval Research.
[1] McIntyre, Hahn, and Hofstadter, Phys. Rev. **94**, 1084 (1954). J. A. McIntyre and R. Hofstadter, Abstract I-1, Seattle Meeting Am. Phys. Soc., July, 1954.
[2] L. I. Schiff, Phys. Rev. (to be published).

Q3. Phase Shift Analysis of High-Energy Electron Scattering.* D. G. RAVENHALL AND D. R. YENNIE, *Stanford University.*—Further results of a phase shift analysis of high-energy electron scattering[1] will be reported. Previously, the experimental data of Hofstadter *et al.* on gold at several energies[2] have been compared with cross sections obtained by using a "smoothed uniform" charge distribution.[3] The effect of altering the central charge density has now been investigated, in an attempt to improve the agreement with these experiments, and in order to examine the extent to which the experiments determine the charge distribution. Some results will also be presented for other nuclei whose distortion (i.e., intrinsic quadrupole moment) is small enough that the assumption of a spherically symmetrical charge distribution is justified.

* Supported in part by the Office of Scientific Research, Air Research, and Development Command.
[1] Yennie, Ravenhall, and Wilson, Phys. Rev. **95**, 500 (1954).
[2] Hofstadter, Hahn, Knudsen, and McIntyre, Phys. Rev. **95**, 512 (1954).
[3] D. G. Ravenhall and D. R. Yennie, Phys. Rev. (to be published).

Q4. A Modified Born Approximation for Electron Scattering Calculations.* D. R. YENNIE, D. G. RAVENHALL, AND B. W. DOWNS, *Stanford University.*—It has been shown previously that for heavy elements the Born approximation is inadequate for calculating high-energy electron scattering.[1] However, after the problem of scattering in a central potential has been solved exactly (by numerical methods), additional effects can be treated by perturbation theory. Since the unperturbed scattering waves are known only through their partial wave decomposition, this method leads to a tedious, though straightforward, computation. We have found an analytic approximation to the complete unperturbed scattering wave which restores the perturbation calculation to the simplicity of the Born approximation; the approximation is good in the neighborhood of the nucleus. In this region the approximate function is very nearly a plane wave with normalization and wave number altered from that of the incident wave; in addition the wave fronts are slightly curved. This modified Born approximation will be used to estimate the sensitivity of electron scattering to small changes in the radial charge distribution.

* Supported in part by the Office of Scientific Research, Air Research, and Development Command.
[1] Yennie, Ravenhall, and Wilson, Phys. Rev. **95**, 500 (1954).

Q5. Electric Quadrupole Effects in Scattering of High-Energy Electrons by Heavy Nuclei.* B. W. DOWNS, D. G. RAVENHALL, AND D. R. YENNIE, *Stanford University.*—Using a modified Born approximation,[1] we have calculated the contributions to the differential scattering cross section which arise from the static quadrupole moment and from the collective electric quadrupole transitions[2] (excitation of low-lying collective rotational states of the target nucleus[3]). For nuclei having large intrinsic quadrupole moments these contributions partially smooth the diffraction wiggles in the scattering curves calculated by the method of Yennie *et al.*;[4] the theoretical curves are thus brought into better agreement

with the experimental data.[5] The quadrupole charge distribution and the extent to which its details affect the scattering cross section will be discussed. Results will be presented for scattering of 183-Mev electrons by tantalum.

* Supported in part by the Office of Scientific Research, Air Research and Development Command.
[1] Yennie, Ravenhall, and Downs, preceding abstract.
[2] L. I. Schiff, Phys. Rev. 96, 765 (1954).
[3] A. Bohr and B. R. Mottelson, Kgl. Danske Videnskab. Selsk., Mat.-Fys. Medd. 27, 16 (1953).
[4] Yennie, Ravenhall, and Wilson, Phys. Rev. 95, 500 (1954).
[5] B. Hahn and R. Hofstadter, paper presented at this meeting.

Q6. W.K.B. Approximation to Phase Shifts.* S. P. HEIMS, D. R. YENNIE, AND D. G. RAVENHALL, *Stanford University.*—The computing time required to evaluate exactly the phase shifts for the nuclear electron scattering[1] at very high energies increases roughly as the square of the energy. For this reason the W.K.B. approximation for the phase shifts is being reconsidered. Using this approximation, E. Baranger[2] has obtained cross sections at 150 Mev for mercury that agree well with those obtained by the exact method, and the accuracy of the W.K.B. approximation improves as the energy increases. The phase integral is evaluated numerically rather than by the analytic approximation used by Baranger. Phase shifts and cross sections obtained by this method will be compared with those obtained by the exact method.

* Supported in part by the Office of Scientific Research, Air Research and Development Command.
[1] Yennie, Ravenhall, and Wilson, Phys. Rev. 95, 500 (1954).
[2] E. Baranger, Phys. Rev. 93, 1127 (1954).

Q7. On the Radiative Correction to Electron Scattering.* H. SUURA, *Stanford University.*—The radiative correction to the high-energy electron scattering by heavy nuclei due to the one-virtual-photon processes is examined for all orders in the Born approximation with respect to the external field. The terms associated with the infrared catastrophe can be separated out quite generally, and are expected to give the same fractional decrease in transition probability as in the first Born approximation. This assumes that the elastic scattering is a continuous function of the distance from the energy shell; this is true for a non-Coulomb potential and is being investigated in the Coulomb case. The magnitude of the remaining terms is also being calculated in the second Born approximation.

* Supported by the Office of Scientific Research, Air Research, and Development Command.

Q8. Nuclear Dispersion Contribution to High-Energy Electron Scattering.* L. I. SCHIFF, *Stanford University.*—In the calculation of high-energy electron scattering from nuclei, the interaction may be divided into a static part that arises from the expectation value of the nuclear Coulomb field, and a dynamic part that takes account of the existence of excited states of the nucleus. The static part gives rise to elastic scattering and can be treated numerically for any assumed charge distribution, to all orders in the interaction.[1] The dynamic part gives rise to inelastic scattering in first order, and to dispersive contributions to both elastic and inelastic scattering in second order. These contributions involve sums over virtual intermediate states of the nucleus; they are are readily formulated but cannot be evaluated in closed form. An estimate of the magnitude of the dispersion terms is made with the help of the closure relation for the nuclear states. It is found to be small, although not negligible, in some cases of physical interest.

* Supported in part by the Office of Scientific Research, Air Research, and Development Command.
[1] Yennie, Ravenhall, and Wilson, Phys. Rev. 95, 500 (1954).

Q9. High-Energy Electron Scattering in Rh, Ta, W, and U.† BEAT HAHN AND ROBERT HOFSTADTER, *Stanford University.*—Recent improvements in experimental technique have made it possible to measure more accurately the angular distribution of high-energy electrons (180 Mev) scattered by heavy and medium nuclei. Small differences in scattering cross sections of two nuclei can be established by measuring ratios of counting rates at each scattering angle. Scattering ratios of gold with respect to hydrogen have been measured, as well as ratios with respect to Rh, Ta, W and U. Ta, W, and U definitely show less pronounced diffraction wiggling in the angular distribution than Pb^{208}, Au, and Bi. It is fairly difficult to fit the experimental results for Ta, W, and U with phase shift calculations to a spherically symmetric charge distribution. A possible explanation of these relatively smooth angular distributions may involve nuclear-quadrupole effects.*

† Supported by the joint program of the Office of Naval Research and the U. S. Atomic Energy Commission, and by the U. S. Air Force through the Office of Scientific Research of the Air Research and Development Command. Also aided by a grant from the Research Corporation.
* Downs, Ravenhall, and Yennie, paper presented at this meeting.

Q10. Electrodisintegration of the Deuteron.* V. Z. JANKUS, *Stanford University.*—Calculations have been made on the disintegration of the deuteron in high-energy electron impact. With increase of momentum transfer the inelastic cross section increases at the expense of the elastic, while the sum of the two remains approximately equal to the Mott cross section. The energy spectrum of the scattered electron has been obtained using the Møller potential. In this calculation it was necessary to take account of the proton-neutron interaction in the final S state. The influence of this interaction on the states of higher angular momentum has been found to be much smaller. The results indicate that the cross section is sensitive to the effective range of proton-neutron forces, especially at high momentum transfers, such as produced by 300-Mev electrons scattered at 60°.

* Supported in part by the Office of Scientific Research, Air Research, and Development Command.

THURSDAY AFTERNOON AT 1:30

310 Le Conte Hall

(PAUL KIRKPATRICK, presiding)

Division of Electron Physics

Invited Papers

R1. Physical Properties of Germanium Surfaces. C. G. B. GARRETT, *Bell Telephone Laboratories.* (30 min.)

R2. Experiments at Very Low Pressures. D. H. ALPERT, *Westinghouse Electric Corporation.* (30 min.)

R3. Radio Astronomy. RONALD N. BRACEWELL, *Sydney Radio Physics Laboratory* (now visiting University of California, Berkeley). (30 min.)

R4. The Upper Atmosphere. JOSEPH KAPLAN, *University of California, Los Angeles.* (30 min.)

THURSDAY AFTERNOON AT 1:30

4 Le Conte Hall

(J. R. RICHARDSON, presiding)

Contributed Papers

S1. Radioactivity of Co^{57}. BERND CRASEMANN AND D. L. MANLEY,* *University of Oregon.*—By the reaction $Mn^{55}(\alpha,2n)$, Co^{57} (270 day) has been prepared, separated chemically, and its disintegration investigated with a magnetic lens spectrometer. A helical baffle permitted a study of the low energy positron spectrum without interference from conversion electrons. Preliminary results of this work indicate that Co^{57} decays to two excited states of Fe^{57} by positron emission and electron capture. From the conversion electron spectrum, the energy of two previously known gamma rays was determined as 0.133 ± 0.002 and 0.119 ± 0.002 Mev, with relative gamma intensities of 3 and 97 percent. These transitions presumably are magnetic quadrupole and electric dipole, respectively, in accordance with conversion coefficient measurements of Alburger and Grace.[1] The *K*-capture/positron ratio for transitions to the second excited state of Fe^{57} is $(6.7\pm3.5)\times10^3$. Two positron groups have maximum energies 0.312 ± 0.020 and 0.194 ± 0.010 Mev, relative abundance 70 and 30 percent, and log(ft) values of approximately 8.1 and 7.6. A new half-life measurement is in progress. A tentative decay scheme is proposed.

* Now at Department of Radiological Physics, University of Rochester.
[1] D. E. Alburger and M. A. Grace, Proc. Phys. Soc. (London) **67A**, 280 (1954).

S2. Radioactivity of Sn^{109}. M. D. PETROFF, S. W. MEAD, AND W. O. DOGGETT, *University of California, Berkeley.*—An 18-minute radioactivity produced by bombarding CdS enriched in Cd^{106} with 15-Mev alphas has been assigned to Sn^{109}. The bombarding energy was chosen such as to favor strongly the reaction $Cd^{106}(\alpha,n)Sn^{109}$. The analysis was based primarily on the observation of the chemically separated Sn in a magnetic lens beta-ray spectrometer. Two internal conversion peaks corresponding to γ rays of energies 0.073 and 0.678 Mev were found to decay with an approximately 18-minute half-life, and the related growth of a peak identified with the 0.205 Mev γ of In^{109} was also observed. After the decay of the 18-minute component, the remaining spectrum included the two strongly converted γ-rays observed by McGinnis.[1] The half-lives, energies, and K/L ratios were in agreement with McGinnis' findings. Other data, obtained with a trochoid analyser and a continuously recording pulse-height analyzer, indicate that both *K*-capture and positron emission are involved in the Sn^{109} decay. The presence of other short lives, such as the 50-minute Sn^{108}, makes accurate determination of the half-life difficult. Our present estimate is 18 ± 2 minutes. This work was performed under the auspices of the U. S. Atomic Energy Commission.

[1] C. L. McGinnis, Phys. Rev. **81**, 739 (1951).

S3. Proton Bremsstrahlung.* HANS MARK, CLYDE MCCLELLAND, AND CLARK GOODMAN, *Massachusetts Institute of Technology.*—The bremsstrahlung emitted when protons are scattered by nuclei is an important background effect in electric excitation experiments.[1] This process has been investigated in some detail using protons between 1 and 3 Mev. The emitted bremsstrahlung spectrum, the yield of 150-kev photons as a function of proton energy and the cross section for the production of 150-kev photons have been determined for various materials. The results are in reasonable agreement with a semi-classical calculation based on the treatment of Landau and Lifschitz.[2] It has also been possible to observe x-rays characteristic of absorbers placed between the target and the detector which are caused by the photoelectric absorption of high energy bremsstrahlung photons.

* Supported by the joint program of the Office of Naval Research and the U. S. Atomic Energy Commission.
[1] C. Zupancic and T. Huus, Phys. Rev. **94**, 205 (1954).
[2] L. Landau and E. Lifshitz, *The Classical Theory of Fields* (Addison Wesley Press, Cambridge).

S4. N–P Scattering at 20 Mev.* R. B. DAY, R. L. MILLS, J. E. PERRY, JR., AND F. SCHERB, *University of California, Los Alamos Scientific Laboratory.*—Using the $T(d,n)He^4$ reaction as a source of high-energy neutrons, we have measured the neutron total cross section of hydrogen in a transmission experiment. The detector was a stilbene scintillation counter biased to count neutrons of energy greater than 10 Mev and placed at a distance of 160 cm from the neutron source. The hydrogen was contained in a pressure vessel 1 meter long at a pressure of 4000 psi. The number of moles of hydrogen in this vessel was known to ±0.1 percent. An identical evacuated cell was used to obtain the "sample-out" counting rate. The background produced by neutrons scattered from the room and surrounding objects was of the order of 0.5 percent, while the counting rates with the tritium gas target evacuated were of the order of 0.1 percent. The preliminary value of the total cross section is $\sigma_t=0.495\pm0.003$ barn at a neutron energy of 19.655 ± 0.035 Mev.

* Work performed under the auspices of the U. S. Atomic Energy Commission.

S5. Multiple Scattering of 2.5 Mev Positrons by 0.1 mil Gold Foil. L. GRODZINS, *Purdue University.*—An external beta ray spectrograph selects 2.5 ± 0.35-Mev positrons from a Ga^{68} source, and these are injected into the median plane of a 12-inch diameter cloud chamber illuminated over a $3\frac{1}{2}$-inch depth. A magnetic field bends them in an arc of 17 cm radius so that they strike a 0.1 mil gold foil in the chamber perpendicularly (within 15°). Projected scattering angles are measured with a reproducibility of about $\frac{1}{2}$°. The results of an examination at the first 1141 foil traversals are as follows:

Angle (degrees)	0–2	2–4	4–6	6–8	8–10	10–15	15–20	>20	Total
Experiment	437	251	197	116	60	58	6	16*	1141
Theory[1]	374	304	203	117	61	55†	15	12	1141

* In the previous examination of 10 430 foil traversals (see Phys. Rev. **94**, 758 (1954)) a search for large angle scatterings found 118 ± 11 scatterings >20° compared with the theoretical prediction of 111 for positrons and 201 for electrons of 2.5 Mev.
† Molière theory adjusted at angles >10° to take into account deviations from Rutherford scattering.
[1] G. Molière, Z. Naturforsch. **3A**, 78 (1948).

S6. Interaction of 4.1-Mev Neutrons with Nuclei.* M. WALT AND J. R. BEYSTER, *Los Alamos Scientific Laboratory.*—The differential cross sections for elastic scattering of 4.1-Mev neutrons from Be, C, Al, Ti, Fe, Zn, Zr, Cd, Sn, Ta, W, Au, Pb, and Bi have been measured using a geometry similar to that described previously.[1] Neutrons produced by the $H^3(p,n)He^3$ reaction were scattered by cylindrical samples and were detected with a biased scintillation counter. The detector, which was insensitive to gamma rays, was operated at three biases having neutron detection thresholds at about 2.0, 2.6, and 3.2 Mev. Inelastic collision cross sections were obtained by subtracting the integrals of the differential elastic cross

sections from the total cross sections. Listed below are the inelastic collision cross sections obtained with the highest bias.

Inelastic Collision Cross Sections

Element	σ_{in}	Element	σ_{in}	Element	σ_{in}
Be	0.57±0.1	Zn	1.7±0.2	W	2.4±0.3
C	0.08±0.1	Zr	1.8±0.2	Au	2.7±0.3
Al	0.7 ±0.2	Cd	2.1±0.2	Pb	1.9±0.3
Ti	1.2 ±0.2	Sn	2.1±0.2	Bi	2.2±0.3
Fe	1.55±0.2	Ta	2.7±0.2		

* Work performed under the auspices of the U. S. Atomic Energy Commission.

[1] M. Walt and H. H. Barschall, Phys. Rev. 93, 1062 (1954).

S7. Proton Scattering from N^{14}.* G. W. TAUTFEST, J. R. HAVILL, AND SYLVAN RUBIN, *Stanford Research Institute.*—The elastic scattering cross section of N^{14} for protons was measured at 152° (CM), from 1.3 to 1.9 Mev, using a thick target of melamine, and a high resolution magnetic spectrometer. Points were taken at energy intervals of about 20 kev. Complex resonance structure in the region between 1.5 and 1.8 Mev apparently corresponds to the three resonances at 1.55, 1.75, and 1.81 Mev in $N^{14}(p,\nu)O^{15}$ reported by Duncan and Perry.[1] The resonances are superimposed on a nonresonant yield approximately three times the Rutherford cross section. The cross sections at 1.43 Mev are 0.097 *b* for N^{14}, and 0.19 *b* for C^{12}, measured from the same profile curve. The carbon cross section agrees closely with that obtained by Jackson *et al.*[2] Further work is planned, using boron nitride targets.

* Supported by contract with Watertown Arsenal Laboratories.

[1] Duncan and Perry, Phys. Rev. 80, 136 (1950).
[2] Jackson, Galonsky, Eppling, Hill, Goldberg, and Cameron, Phys. Rev. 89, 365 (1953).

S8. A Fission Fast Counter Using the Gas Scintillation Principle. A. E. VILLAIRE AND L. F. WOUTERS, *University of California, Livermore.*—Fission fragments emitted from a uranium surface due to neutron bombardment, cause excitation events in a surrounding pure argon atmosphere. The ultraviolet radiation emitted by the decay of excited states is converted to blue light by a thin polystyrene film containing 3 percent tetraphenyl butadiene. The light pulse resulting from each fission event is detected by a 6292 photomultiplier tube, and is of such intensity that under average conditions the output pulse height is about 0.1 volt; the pulse width is 10^{-8} second or less. The pulse height ratio between fission pulses and the sea of background α pulses[1] is about 16:1. While the neutron detection efficiency is of the same order as for a proportional fission counter, the pulse resolution time is significantly shorter. The principal difficulty is the rapid poisoning of the argon gas, probably by the plastic converter; to circumvent this, our tests were conducted using continuous gas flow through the chamber. This work was performed under the auspices of the U. S. Atomic Energy Commission.

[1] C. Eggler and C. M. Huddleston, Phys. Rev. 95, 600(A) (1954).

S9. Elastic Scattering of 1.6-Mev Gamma Rays from Carbon. LUIS W. ALVAREZ, FRANK S. CRAWFORD, JR., AND M. LYNN STEVENSON, *University of California, Berkeley.*—Elastic scattering of 1.6-Mev gamma rays from carbon has been observed, at a scattering angle of 130°. Eighty curies of $Ba^{140}La^{140}$ provided about forty-five curies of 1.6-Mev gamma rays. A 15-kilogram ring-shaped carbon target located 47 inches from the source scattered gamma rays into a 4-by-4-inch sodium iodide counter. Uranium and lead absorbers shielded the crystal from the source. A ½-inch lead absorber surrounding the crystal eliminated pile-up from inelastic Compton scatters. An accurate 10^{-7} fraction of the radioactive source was placed at the average target position, and a 10-channel pulse-height analyzer was centered on the 1.6-Mev peak. Radiation scattered from the target showed a peak in the pulse-height spectrum having the shape and position corresponding to 1.6-Mev gamma rays. Lead absorbers attenuated the scattered radiation by the expected amount. The differential-scattering cross section was obtained by measuring the distance from source to target, the number of carbon atoms, the 10^{-7} dilution ratio, and the ratio of counting rates from scattered gamma rays and the 10^{-7} source. As a result, we obtain the classical Thomson differential cross section for carbon, 1.5×10^{-31} cm^2 ster^{-1}, with a 5-percent error due to counting statistics and a 25-percent error assigned to cover present uncertainties in systematic corrections. This work was performed under the auspices of the U. S. Atomic Energy Commission.

S10. A Millisecond Gamma Emitter from Protons on Ta. SHELDON D. SOFTKY, *University of California, Berkeley.*—A search for gamma emitters in the millisecond range of half life was conducted using the 32-Mev Berkeley proton linear accelerator. Foil targets of eighteen common elements were bombarded and the activity made in them followed between beam pulses with a gated scintillation counter. The only activity found of measurable yield was from Ta, and it exhibited a half life of 5.5±0.3 milliseconds. Using a gated nine-channel pulse-height analyzer with the NaI(Tl) crystal counter, the excitation curve of this activity was measured and its gamma spectrum deduced. Gammas of 0.35 Mev and 0.22 Mev are indicated by the pulse spectrum, and no β's are present commensurate with this half life. Comparison of the excitation curve for this activity with those of Ta^{180} (8 hr) and W^{179} (30 m) leads to the tentative assignment of this decay to W^{180m}. As far as can be determined, this is the first known isomer with half life in the millisecond range. This work was performed under the auspices of the U. S. Atomic Energy Commission.

S11. *L*-Conversion in Pure *E*2 Transitions.* F. BOEHM, P. MARMIER, AND J. W. M. DUMOND, *California Institute Technology.*—A number of pure *E*2 transitions at low energies were studied with the axial focusing β-ray spectrometer using a momentum resolution of 1.5 parts in 1000. Conversion coefficients for the *LI*, *LII*, and *LIII* shells were measured with high accuracy. The results obtained for transitions between 50 kev and 200 kev, and $Z=59$, 72, and 74 are given.

* Research work supported by contract with the U. S. Atomic Energy Commission and the Office of Ordnance Research (U. S. Army).

S12. Energy Levels of Hf^{177}.* P. MARMIER, F. BOEHM, AND J. W. M. DUMOND, *California Institute of Technology.*—The decay of 6.8 *d* Lu^{177} has been studied with the curved crystal γ-ray spectrometer and the axial focusing β-ray spectrometer. In addition to the lines at 113 kev, 208 kev, and 321 kev, two weak transitions were found at 72 kev and 250 kev. The decay scheme was established with the help of coincidence measurements. The levels of Hf^{177} have the following energies: 112.97 ±0.02 kev, 249.69±0.04 kev, and 321.33±0.04 kev. Multipole assignments are given for all transitions.

* Research work supported by contract with the U. S. Atomic Energy Commission and the Office of Ordnance Research (U. S. Army).

S13. Relative Stopping Powers for 20-Mev Protons.* C. P. SONETT† AND K. R. MACKENZIE, *University of California, Los Angeles.*—The stopping powers of Ni, Cu, Cb, Pd, Ag, Cd, In, Ta, Pt, Au, and Th relative to Al were measured using the 20.6 Mev external proton beam of the UCLA cyclotron. The measurements were made with sufficient precision so that a graph of ln Z *vs* stopping power per electron relative to aluminum showed some fluctuation from a linear relationship. For Cu and Ni the values differed by 2 percent from the values expected on the basis of a fit to a straight line through the mean of all values. The deviation for Th was 2.6 percent in the direction found by Kelley and Teasdale. Some suggestion is made that the difference between Cu and Ni could be due

to the differences in the electronic structures of the atoms and to the differences in the band structures of the metals.

* Supported by the joint program of the U. S. Atomic Energy Commission and the Office of Naval Research.
† Now at the Ramo-Wooldridge Corporation, Los Angeles, California.

S14. Gamma-Gamma Directional Correlation in the $Cl^{34} \rightarrow S^{34}$ Decay. HARRY E. HANDLER AND J. REGINALD RICHARDSON, *University of California, Los Angeles.**—The directional correlation between the 1.15- and 2.10-Mev gamma rays[1] which follow the decay of 33-minute Cl^{34} has been measured. Samples of Cl^{34} were made in the UCLA cyclotron by the (p,pn) reaction on NaCl. Sodium iodide scintillation counters with subsequent pulse-height discrimination were used. Preliminary analysis of the results of coincidence counting at five angles from 0° to 90° between the direction of emission of the two gamma rays using powdered crystalline sources is consistent with the assignments of spin 2 and even parity to both the first and second excited states of S^{34} and indicate that magnetic dipole radiation is favored over electric quadrupole radiation in the first transition. The correlation was unchanged when sources in water solution were used; this suggests that the interactions of the nuclei with external fields were small and did not attenuate the correlation when solid sources were employed.

* This work was assisted by the joint program of the Office of Naval Research and the U. S. Atomic Energy Commission.
[1] Harold K. Ticho, Phys. Rev. **84**, 847 (1951).

THURSDAY AFTERNOON AT 1:30

1 Le Conte Hall

(F. A. JENKINS, presiding)

Contributed Papers

T1. Scintillation Studies on Activated Alkali Halides. T. H. ANDERSON, *U. S. Naval Radiological Defense Laboratory.*—Values for the decay times of activated alkali halide scintillators determined by response to individual ionizing events are not precise because the energy available is too small to give statistically reliable results. To overcome this, crystalline specimens were irradiated with a very short pulse of many electrons, thereby increasing the light output several hundred times. The apparatus consisted of a 7 JP oscilloscope gun with 40 kv post acceleration. The beam was swept across a slit to give pulses of the order of 10^{-9} second. The scintillations were followed by a 6292 photomultiplier connected directly to a 517 Tectronix oscilloscope which was triggered together with the deflecting signal. No time jitter was observed. Measurements of the traces give decay times of 0.260 μsec for NaI(Tl) and 0.180 μsec for KI(Tl) at room temperature. A search for a lag in the onset of luminescence was made by alternately sweeping a fast organic scintillator and an inorganic crystal. Evidence of a time lag was found and two possible explanations for this delay are offered. Both energy transport mechanisms and trapping may occur.

T2. Microwave Dielectric Measurements on Single Fibers. J. J. WINDLE AND T. M. SHAW, *Western Utilization Research Branch, Agricultural Research Service.*—Microwave techniques, which have proved successful at wavelengths of 3.25 and 10.0 cm for the determination of the complex dielectric constant of fiber bundles,[1] have been extended to include a wavelength of 1.15 cm, where for the first time measurements on a single wool fiber have proved to be feasible. Such measurements make it possible to compare directly the results of electrical and mechanical measurements on the same single fiber. In addition, the single-fiber technique has provided a convenient, rapid, and nondestructive method for the determination of average mass of adjacent 1-cm sections of the fiber along its length. Variations as large as 2-fold in mass per unit of length are sometimes encountered within a single wool fiber. With single fibers preliminary measurements have been made of the complex dielectric constant and its variation with sorbed water at $\lambda = 1.15$ cm. The results appear to be in accord with the relationship proposed by us[2] to account for the dielectric properties observed for wool-water systems at $\lambda = 3.25$ cm and $\lambda = 10.0$ cm.

[1] T. M. Shaw and J. J. Windle, J. Appl. Phys. **21**, 956 (1950).
[2] J. J. Windle and T. M. Shaw, J. Chem. Phys. **22**, 1752 (1954).

T3. Changes in Photoelectric Probability Factor Resulting from Surface Contamination of Aluminum. R. L. PERRY AND J. J. BRADY, *Oregon State College.*—Measurements have been made on an aluminum cathode concentric sphere photocell using the 2537 A line of the mercury arc as a light source. The Fowler-DuBridge method was used to analyze the photocurrent *vs* retarding potential curves from which a value of the probability factor α was obtained. Starting with a freshly evaporated surface of aluminum, successive curves were obtained after the surface was contaminated with residual gas. To contaminate the surface a copper trap in the system was heated for a short time, resulting in an increase in pressure. All measurements were made with a pressure less than 4×10^{-7} mm. The contamination decreased the work function by about 10 percent while the corresponding change in α was an increase of about 3 percent.

T4. Vacuum Deposition of Magnetic Alloy Films.* M. S. BLOIS, JR., *Stanford University.*—Thin magnetic films have been prepared by vacuum evaporation in the thickness range, 1000 A to 50 000 A, and consisting of alloys in the iron-nickel and iron-cobalt systems. The magnetic properties—coercivity, saturation induction, and hysteresis loop form—have been observed, and the dependence of these properties upon the choice of magnetic materials and parameters of the evaporation process, has been studied. The change in alloy composition that takes place between the melting of the starting material and the final formation of the alloy film, has been studied for both the alloy systems above and will be compared with the behavior predicted on the basis of current theory. It has been found that a ferromagnetic film formed in the presence of a magnetic field has directional properties dependent upon this field. In particular, it has been possible to produce Permalloy films by evaporation with extremely square hysteresis loops. A general finding has been that these films have the properties characteristic of the bulk alloy, except for coercive force which is consistently higher for the films.

* This work was supported by the Office of Naval Research, and conducted at U. S. Naval Ordnance Laboratory, Corona, California.

T5. Absorption Bands of Rubidium in the Presence of Foreign Gases.* SHANG-YI CH'EN, ROBERT B. BENNETT, AND OLEG JEFIMENKO, *University of Oregon.*—The structureless absorption bands of rubidium caused by collisions with foreign gas molecules appearing in the neighborhood of certain mem-

bers of the principal series were investigated. When the temperature was 200°C or higher a band was observed at the short wavelength side of the resonance lines for all gases used. For H_2, He, Ne, N_2, and A a band was also observed at the short wavelength side of the second[1] and the third members of the series. For methane, ethane, propane, and butane a band appeared at the long wavelength side of each of the components of the first three doublets. The bands appearing near still higher members of the series were so close to the atomic lines that they were generally not resolved.

* Supported by the National Science Foundation.

[1] A part of the results for the second member of the Rb principal series had been given by Tsi-Ze Ny and Shang-Yi Ch'en, J. phys. et radium 9, 169 (1938).

T6. Phase Change on Reflection from Multilayer Films. F. A. JENKINS AND D. R. SPECK, *University of California, Berkeley.*—Two disadvantages of the use of multilayer films on Fabry-Perot interferometers are the restricted wavelength range of high reflection and the relatively large phase shift. The latter is ten to twenty times as great as that for silver, and might be thought to constitute a serious bar to precision wavelength measurements. If it can be calculated with sufficient accuracy to permit a unique assignment of order numbers, however, it can be determined and corrected for just as is done for metal films. We have photographed the fringes in the iron arc spectrum, and applied the method of exact fractions to the secondary wavelength standards, using 9-layer films of zinc sulfide and cryolite. By comparison with the theoretical phase shifts computed by the matrix method, agreement is found for one particular assignment of orders to 0.01 of an order. This result is in agreement with that found by other investigators in the infrared,[1] and shows that it is feasible to use such films for wavelength determinations. When one is working over a wavelength range of more than 1000 A, however, metal films would be preferable.

[1] Rank, Shearer, and Wiggins, Phys. Rev. 94, 575 (1954).

T7. Preliminary Report on the Quadrupole Moment of Niobium. D. R. SPECK AND F. A. JENKINS, *University of California, Berkeley.*—A study of the hyperfine structure in the spectrum of $Nb^{93}I$ has been undertaken in an attempt to measure the electric quadrupole moment of the niobium nucleus. Previous workers have concluded that to within the limits of accuracy of their experiment no quadrupole moment was detectable in niobium. However, the fact that this moment is different from zero has been established by recent nuclear resonance experiments on $KNbO_3$ in which the interaction of the nuclear electric quadrupole moment of niobium with the electric field gradient in the $KNbO_3$ molecule has been measured. In view of this latest result it was thought that a careful reinvestigation of the hyperfine structure in the niobium spectrum might be fruitful. Preliminary investigations on the line λ5271 ($^6F_{\frac{1}{2}}-{}^4D_{\frac{1}{2}}^0$) show within the probable error small deviations from the interval rule in the hyperfine structure of the $Hd^3\,5s^2\,{}^4F_{\frac{1}{2}}$ term. Fitting the observed intervals into the usual interaction formula yields the values $A=21.7\pm0.1$ mK for the magnetic splitting factor and $B=-0.0044\pm0.0027$ mK for the quadrupole coupling constant. Using this value for B and the h.f.s. formulas published by R. E. Trees, one obtains for the quadrupole moment $Q=-0.4\pm0.3\times10^{-24}$ cm². The error given is the standard deviation based on the internal consistency of the data. This value of Q is derived from measurements on only one line in the niobium spectrum.

T8. Penetration into Rarer Medium in Total Reflection of Microwaves. R. O. BRICK, J. J. BRADY, AND M. D. PEARSON, *Oregon State College.*—Two identical 45°−90°−45° prisms are mounted so that the distance between the two hypotenuse faces is adjustable. Microwaves in the 3-cm region are incident normal to one prism face. For a small separation between the prisms part of the power is transmitted through both and part is reflected at the first hypotenuse. Theory indicates that for high values of index of refraction, transmitted power polarized in the plane of incidence decreases more rapidly with prism spacing than power polarized perpendicular to the plane of incidence. For low values of index of refraction, n, the opposite is true. For a value of $n=1.732$ the decrease of transmitted power with distance is the same for both polarizations. The theory has been verified experimentally by using prisms of paraffin ($n=1.50$), sulfur ($n=1.90$), and salt ($n=2.43$).

T9. Cyclical Variations in the Effective Radiation Temperature of the Ozone Region. ARTHUR ADEL, *Arizona State College.*—Fluctuations both periodic and nonperiodic in ERTOR (Effective Radiation Temperature of the Ozone Region)[1] have been under systematic observation at Flagstaff, Arizona, since July, 1953. Of particular interest is the ERTOR oscillation, period ten weeks, which is superimposed upon the annual variation.

[1] Arthur Adel, in *The Atmospheres of the Earth and Planets*, edited by G. Kuiper (University of Chicago Press, Chicago, 1952), Chap. X. R. M. Goody, *The Physics of the Stratosphere* (Cambridge University Press, Cambridge, 1954), pp. 108–109.

THURSDAY AFTERNOON AT 1:30

3 Le Conte Hall

(W. A. WILDHACK, presiding)

Invited Paper

U1. Instrumentation Research at the National Bureau of Standards. W. A. WILDHACK, *National Bureau of Standards.* (30 min.)

Contributed Papers

U2. A Long-Wavelength X-Ray Reflection Microscope.* J. F. MCGEE, *Stanford University.*—The use of wavelengths of the order of ten angstroms (instead of the usual one or two) permits a larger field of view while enhancing the light-gathering power. The importance of surface irregularities becomes less, and materials of low atomic number become observable. A quantitative determination of the field aberrations of a system composed of two spherical mirrors was made by ray tracing, using an IBM Card-Programmed Calculator. Examination of the field *vs* resolution curves shows that the theoretical width of field is about 100 microns for a resolution of at least 1500A. Such a microscope was constructed in-

corporating two uncoated silica mirrors and an aperture stop so placed as to minimize image obliquity. The system was irradiated with aluminum K and continuous radiation from a tube with a focal spot intermediate in size between those of commercially available tubes and so-called "micro-focus" tubes. With dry helium replacing air in the optical path, photography of magnified images required exposures from five minutes to one-half hour.

* Supported by a grant-in-aid from the American Cancer Society upon recommendation of the Committee on Growth of the National Research Council.

U3. A Metal Vacuum Joint Suitable for Field Emitters.* HOWARD H. PATTEE, JR., *Stanford University.*—A demountable, all-metal, ultra-high vacuum joint, useful at pressures of 10^{-10} mm Hg, has been developed for a field-emission, point-focus x-ray tube. The joint consists of stainless-steel knife edges clamped into a copper gasket with special flanges, and it can be dismounted and reassembled in a few minutes. The entire joint can be baked out at 500°C. When the system is shut off at 10^{-10} mm Hg, no pressure rise is observed on a Bayard-Alpert ionization gauge in a week. The volume of the system is 0.2l, and the total length of seal is 10 cm. Field emitters or other electrodes can be introduced through these joints, and because the joint is slightly flexible, some adjustment of the electrodes inside the vacuum is possible. The continuous operation of field emitters under different conditions will be discussed.

* Supported by a grant-in-aid from the American Cancer Society upon recommendation of the Committee on Growth of the National Research Council.

U4. A High-Sensitivity Mass Spectrometer.* J. H. REYNOLDS, *University of California, Berkeley.*—A 4½-inch-radius, 60°-deflection, single-focusing, mass spectrometer, designed especially for isotope abundance measurements on small gas samples, has recently been completed. Emphasis in the design was placed on high sensitivity and low background. The envelope is of Pyrex and includes a total volume of about 2 liters. The analyzer tube is 20 mm Pyrex, internally silvered by chemical deposition where necessary; a section of this tube is bent and flattened so as to pass between the wedge-shaped poles of an electromagnet. Source and collector assemblies are compressed onto quartz (ion source) or Pyrex (collector) alignment rods by Inconel X springs, and terminate in stainless steel tubes which grip the inner surface of the glass analyzer tube. Errors in relative alignment of the metal and glass parts of the apparatus are compensated by electrostatic deflection. The ion source is of standard electron-bombardment design. The collector includes a 9-stage Allen-type electron multiplier preceded by a magnetically operated shutter, on which the beam can be collected for direct electrical measurement when desired. Spectrometer and sample system are both mounted on adjacent transite oven bases, above which permanent bake-out ovens are suspended. Identical mercury diffusion pumps and associated traps exhaust these systems through all-metal vacuum valves mounted in the bake-out region.

* This work has been supported by the Office of Naval Research.

U5. Performance Data for a High-Sensitivity Mass Spectrometer.* J. LIPSON AND J. H. REYNOLDS, *University of California, Berkeley.*—With 0.012-in. source slits and 0.024-in. collector slit, adjacent xenon peaks are flat-topped and resolved. Using 375°C bake-out and without rf heating of the ion source, operating pressures as low as 5×10^{-10} mm Hg have been achieved in 24 hours. Sensitivity measurements have seen made with argon and xenon samples of about 10^{-5} cc STP. Operating the spectrometer in the conventional way a "flow sensitivity," defined as electrons or ions out at the collector per atom in., is measured. Operating the machine with exhaust valve closed and the total sample admitted to the tube, a "static sensitivity," defined as electrons or ions to the collector per second per sample atom (and thus the inverse of the mean-life of sample atoms before excursions to the collector) is measured. For 5-ma source current and 320 volts per multiplier stage, we find as typical for xenon: multiplier gain 10^4, flow sensitivity 30 electrons per atom or 0.003 ion per atom, static sensitivity 3×10^{-2} electron per second per atom or 3×10^{-6} ion per second per atom, background noise equivalent to 1 ion per second or 3×10^5 sample atoms. This last figure represent the present detectability of the apparatus for xenon atoms. We find as typical for argon: multiplier gain 10^5, flow sensitivity 150 electrons per atom or 0.0015 ion per atom, static sensitivity 50 electrons per second per atom or 5×10^{-4} ion per second per atom, background at mass 36 (HCl) equivalent to 10^3 ions per second or 2×10^6 sample atoms.

* Work supported by the Office of Naval Research.

U6. Spin Echo Serial Storage Memory. A. G. ANDERSON, R. L. GARWIN, E. L. HAHN, J. W. HORTON, G. L. TUCKER, AND R. M. WALKER, *Watson Scientific Computing Laboratory (IBM).*—A series of short rf pulses applied to proton samples in liquids is stored, delayed and recovered in reverse or direct order by the spin echo method.[1,2] A maximum of the order of 1000 echo pulses has been obtained from a glycerine-water mixture. For the input, a pulse spacing of 20 μsec and pulse width of 7 μsec are typical parameters. Cycle repetition rate of the echo sequence is determined by the thermal relaxation time T_1 (~70 μsec for the glycerine-water mixture). For liquid samples with long relaxation times the upper limit on the number of observable echoes is determined, for a given number of protons, by the reduction of free precession coherence due to molecular self-diffusion. The application of a dc magnetic field H_c during storage and recovery times can be used (1) to eliminate fluctuation and attenuation of desired output echoes due to interaction between input pulses; (2) to eliminate mixtures of reverse and direct order echoes; (3) to permit any one of several serially stored groups of pulses to be immediately recalled; (4) to change the nuclear band width; and (5) to introduce information into the system.

[1] E. L. Hahn, Phys. Rev. **80**, 580 (1950).
[2] Initial research on such storage at Stanford has been done by S. Fernbach and W. Proctor.

U7. An Ultrasonic Technique for the Nondestructive Evaluation of Metal to Metal Adhesive Bonds. J. S. ARNOLD, *Stanford Research Institute.*—An ultrasonic technique has been developed for the non-destructive evaluation of structural adhesive bonds. A ferroelectric transducer is excited by a variable frequency driving current of constant amplitude, and the voltage developed across the transducer is displayed on an oscilloscope as a function of frequency. The voltage-frequency curve conveys information regarding the motional impedance of the system and hence the constraints that limit the vibration of the transducer. These constraints are imposed partly by the mechanical properties of the transducer and partly by the mechanical properties of the load (test specimen) to which it is coupled. The variation in the voltage-frequency curves that occur when the transducer is applied to satisfactory and defective test specimens can usually be correlated with the strength of the adhesive bonds, as indicated by subsequent destructive tests performed on the specimens. Block circuitry, typical oscilloscope patterns, and data on the correlation between destructive and non-destructive tests are presented.

U8. Aberrations and Fringing Effects in a Modified Siegbahn-Type Magnetic Spectrometer. S. A. BLUDMAN AND D. L. JUDD, *University of California, Berkeley.*—Obtaining high resolution with large aperture in a magnetic spectrometer with source and detector outside the field requires a study of nonlinear corrections and of fringing effects on entering and

leaving the magnetic field. We write the trajectory equations so as to exhibit terms linear in the radial and axial oscillations which fix the focus,[1] non-linear terms which produce aberrations, and effects of the same order due to fringing. These equations are integrated analytically through the region of cylindrical symmetry by an iterative process correct through second-order in axial and third-order in radial oscillations. The principal fringing effects are to impose boundary conditions on the radial and axial trajectory slopes and to introduce an extrapolated field boundary. Approximation of the fringing field by a decreasing exponential is justified theoretically and experimentally. For a point object, values of the second and third radial field derivatives are obtained which minimize the aberrations in the presence of fringing. Focal surfaces, image sizes, and resolution curves will be presented for several radial apertures. This work was performed under the auspices of the U. S. Atomic Energy Commission.

[1] D. L. Judd, Rev. Sci. Instr. 21, 213 (1950).

U9. High-Resolution Magnetic Spectrometer.* SYLVAN RUBIN AND D. C. SACHS, *Stanford Research Institute.*—A high-resolution point-focusing magnetic spectrometer has been constructed for the analysis of the momentum distribution of elastically scattered protons from the surface layers of solid targets.[1] With a radius of curvature of 12 in. and a maximum field of 7000 gauss, it will analyze protons up to an energy of 2 Mev, with a momentum resolution of approximately 1 part in 3000, at an aperture of 0.0025 steradian. The theoretical limit of attainable resolution due to second-order aberrations[2] has been approached by adjustment of the field shape by means of mechanical adjustments of the gap and pole shape. The 30-amp, 140-volt regulated motor-generator current supply is stable to 1 part in 10^4. The magnetic field is compared with a reference permanent magnet, by means of a null-balance flip coil, with a sensitivity of 1 part in 10^4. This spectrometer design is adaptable to higher energies and larger aperture, for high-resolution nuclear spectrometry.

* Supported by contract with Watertown Arsenal Laboratories.
[1] S. Rubin and V. K. Rasmussen, Phys. Rev. 78, 83 (1950).
[2] F. Shull and D. Dennison, Phys. Rev. 71, 681 (1947); 72, 256 (1947).

U10. A Charge-Exchange Accelerator. J. R. WOODYARD, *University of California, Berkeley.*—Following a suggestion of Alvarez[1] for an energy-doubling dc accelerator, a small machine has been constructed to produce one-Mev protons using a 500 kv dc source in order to test the method and to investigate design problems. A beam of protons at 30 kv is passed through a thin capture foil of aluminum or silicon monoxide with a thickness of about 10 micrograms per square cm. Approximately 20 percent of the incident protons capture two electrons and emerge as negative ions. Negative ion currents of 100 microamperes or more should be obtainable. The negative ions are accelerated by a high-voltage dc potential, are then passed through a stripping foil which changes them back to protons, and are finally accelerated again by the same potential. Both ion source and target are at ground potential. The 500-kv source is a 16-stage cascade rectifier voltage-multiplying circuit using 16 type 5825 rectifier tubes with rf filament heating. Initial performance data of the accelerator will be given.

[1] L. W. Alvarez, Rev. Sci. Instr. 22, 705 (1951).

U11. Multiple Scattering Microscope for "Constant Sagitta" Measurements. STEPHEN J. GOLDSACK* AND GERSON GOLDHABER, *University of California, Berkeley.*—A precision microscope has been built with several novel features, and in particular with an automatic device to select cells for measurement of the mass of charged particles with a variable cell length technique. The pre-selected cell scheme is generated by a punched tape which carries the information. Work has been done to callibrate the P_1 cell scheme of Biswas *et al.*[1]: the mean value of the scattering per cell, taken over 460 cells, is 1.08 ± 0.04 microns after a 1-percent correction for noise. The results form a convenient set of data for checking the sampling errors. When calculations are made using the arithmetic mean and a cut off at $4D$ the relative standard error is well represented by the empirical formula $0.8/(N)^{\frac{1}{2}}$, for N observations. This leads to a relative error on the mass $1.9/(N)^{\frac{1}{2}}$. Further work is proposed to calibrate alternative cell schemes. The results of measurements of the mass of K-particles with the microscope will be described. It is interesting to note that in measurements of mass by this technique, a fortunate cancellation of effects makes the dependence of the measurements on the water content of the emulsions negligibly small.

* Assisted by the joint program of the Office of Naval Research and the U. S. Atomic Energy Commission.
[1] Biswas, George, and Peters, Proc. Indian Acad. Sci. 38, 418 (1953).

U12. Four-Inch Diameter Liquid Hydrogen Bubble Chamber. D. PARAMENTIER, A. J. SCHWEMIN, L. W. ALVAREZ, F. S. CRAWFORD, JR., AND M. L. STEVENSON, *University of California, Berkeley.*—A chamber constructed of a cylindrical brass wall 4 in. in diameter and 3 in. deep with glass windows has been operated successfully for a limited number of expansions. The chamber is maintained at a constant temperature by means of a pressurized bath of liquid hydrogen that is in contact with the brass wall of the chamber. In the latent state, the chamber is restrained from boiling by maintaining $\sim$6 atmosphere of pressure on the liquid hydrogen. To activate the chamber, the liquid is super heated by reducing the pressure on the chamber to one atmosphere. The particle beams are then pulsed into the chamber and the tracks photographed with a triggered stroboscopic light. The chamber remains at one atmosphere for about ten milliseconds, after which time the chamber is again pressurized $\sim$6 atmospheres. The chamber is then ready for another expansion cycle. Photographs will be shown of various tracks and events obtained with this and other liquid hydrogen chambers developed here. This work was performed under the auspices of the U. S. Atomic Energy Commission.

THURSDAY AFTERNOON AT 1:30

2 Le Conte Hall

(K. K. DARROW, presiding)

Post-deadline papers, if any

SUPPLEMENTARY PROGRAMME

SP1. II. Recombination in an Argon Shock Front.* JOHN W. BOND, JR., *Los Alamos Scientific Laboratory.*—If a shock in argon is sufficiently strong, ionization takes place. Behind the shock front there is a luminous region in which thermal equilibrium exists. In order to compute the recombination coefficient for a plasma consisting of electrons, neutral atoms, and singly-ionized atoms, a method of detailed balancing was used. Three equilibrium reactions are of importance: ionizing reactions between argon atoms, those between argon atoms and electrons, and the photoelectric reaction. Since the ionizing cross sections are known, their inverses may be readily computed. Maxwellian distributions were assumed to exist for all the particles at all times; this is probably valid because of the high temperatures and densities behind the shock front. Kramer's classical theory of radiative recombination was considered but gave values too high by about 10^4. Thomson's theory of three-body recombination gives answers of the right order of magnitude, but its region of applicability is limited. The recombination coefficient was used in computing the thickness of the shock front, and, because of the short duration of the latter, excitation reactions were not included.

* To be given at the end of Session C if the Chairman rules that time permits.

THURSDAY EVENING AT 7:30

Men's Faculty Club

(A. C. HELMHOLZ, presiding)

Banquet of the American Physical Society

After-dinner speech by R. T. BIRGE

Author Index to Papers Presented at the Berkeley Meeting

Adel, Arthur—T9
Alburger, D. E. and A. W. Sunyar—P14
Allen, William A., Joe M. Mapes, Earle B. Mayfield—C6
Alperovitch, Edward A. and J. Malcolm Miller—G13
Alpert, D. H.—R2
Alvarez, Luis W., Frank S. Crawford, Jr., and M. Lynn Stevenson—S9
Anderson, A. B. C.—C3
Anderson, A. G., R. L. Garwin, E. L. Hahn, J. W. Horton, G. L. Tucker, and R. M. Walker—U6
Anderson, C. D.—B2
Anderson, John D., Robert W. Kenney, and Charles A. McDonald, Jr.—E3
Anderson, T. H.—T1
Armenteros, R., B. Gregory, P. Hendel, A. Lagarrigue, L. Leprince-Ringuet, F. Muller, and C. Peyrou—P7
Arnold, J. S.—U7
Arnold, W. H., J. Ballam, A. L. Hodson, R. Ronald Rau, George T. Reynolds, S. B. Treiman, and V. A. van Lint—P8
Asaro, F., F. Stephens, and I. Perlman—G4
Banas, E. M., B. A. Mrowca, and E. Guth—I7
Bandtel, K. C., W. J. Frank, L. Higgins, and B. J. Moyer—L14
Bailey, L. Evan—P3
Barber, W. C.—P9
Barnes, George—H2
Barut, A. O.—O14
Bennett, Arthur and Henry W. Wedaa—C5
Besdin, D. J. and Joseph H. Robinson III—O2
Blois, M. S., Jr.—T4
Bludman, S. A. and D. L. Judd—U8
Boehm, F., P. Marmier, and J. W. M. DuMond—S11
Bond, John W., Jr.—C4, SP1
Bowman, Harry R. and Lloyd G. Mann—P15
Bracewell, Ronald N.—R3
Brady, J. J., M. B. Larson, and T. A. O'Halloran—M8
Brick, R. O., J. J. Brady, and M. D. Pearson—T8
Brown, Frederick C.—H4
Brown, W. W.—P6
Burgess, John C.—D4
Chamberlain, Owen—K3
Ch'en, Shang-Yi, Robert B. Bennett, and Oleg Jefimenko—T5
Christy, R. F.—F1
Colladay, G. S. and S. Barshay—M1
Cork, Bruce—J3
Crasemann, Bernd and D. L. Manley—S1
Crowe, K. M., R. M. Friedman, and H. Motz—L3
Day, R. B., R. L. Mills, J. E. Perry, Jr., and F. Scherb—S4
Dixon, Dwight R. and Kenneth C. Bandtel—E4
Downs, B. W.—D8
Downs, B. W., D. G. Ravenhall, and D. R. Yennie—Q5
Dudziak, Walter, Ryokichi Sagane, and James Vedder—L11
Dyke, W. P., J. P. Barbour, J. K. Trolan, and E. E. Martin—H3
Evans, Marjorie W., Frank I. Given, and William E. Richeson, Jr.—C2
Fairhall, A. W.—P13
Feher, G. and R. A. Levy—I1
Fernbach, S., G. Culler, and N. Sherman—O10
Fleming, John R. and J. J. Lord—L2
Freda, A. R. and G. C. Kuczynski—M5
Friedman, Abraham S. and Irwin Oppenheim—D7
Fuller, Melvin Otis—P1
Fryer, Edward M. and Charles A. Fowler, Jr.—M2
Gardner, Andrew L.—H5
Garrett, C. G. B.—R1
Gasiorowicz, S., M. Newman, and R. Riddell, Jr.—D2
Gell-Mann, M.—B4
George, W., W. Barber, and D. Reagan—P12
Gilbert, F. C.—P4
Glass, R. A., R. J. Carr, J. W. Cobble, and G. T. Seaborg—G8
Gluckstern, Robert L.—P11
Goebel, Charles J.—O7

Goldhaber, Gerson, W. W. Chupp, S. J. Goldsack, J. Lannutti, and F. Webb—L1
Goldsack, Stephen J. and Gerson Goldhaber—U11
Green, G. K.—J2
Grodzins, L.—S5
Guth, Eugene—O11
Hahn, Beat and Robert Hofstadter—Q9
Hahn, E. L. and B. Herzog—I10
Handler, Harry E. and J. Reginald Richardson—S14
Harris, C. W. and E. Guth—O4
Heckrotte, Warren—E8
Heims, S. P., D. R. Yennie, and D. G. Ravenhall—Q6
Hofstadter, R.—Q1
Holder, B. E. and M. P. Klein—I5
Holland, D. H.—O6
Hollander, J. M., and M. I. Kalkstein—G3
Hubbard, Edward L. and Eugene J. Lauer—P10
Hudson, Gilbert G.—H9
Hummel, John P., F. Asaro, and I. Perlman—G6
Hutchison, C. A., Jr.—N3
Jankus, V. Z.—Q10
Jenkins, F. A. and D. R. Speck—T6
Johnson, M. H. and E. Teller—F4
Kaplan, Joseph—R4
Karplus, R. and M. A. Ruderman—F2
Kac, Mark—A2
Katz, Samuel—C7
Kerth, Leroy and Byron L. Youtz—E7
Kip, A. F.—N1
Klein, M. P. and B. E. Holder—I6
Kuczynski, G. C. and M. Doyama—M4
Lagarrigue, A.—B3
Lannutti, Joseph, Gerson Goldhaber, and Stephen J. Goldsack—E1
Levy, R. A.—I2
Lipson, J. and J. H. Reynolds—U5
Livingston, M. S.—J5
Lockary, T. E. and E. Guth—O12
Marmier, P., F. Boehm, and J. W. M. DuMond—S12
Mark, Hans, Clyde McClelland, and Clark Goodman—S3
Marshall, Leona—K1
Mathur, H. B. and E. K. Hyde—G9
Maunsell, C. D.—H7
McCarthy, Kathryn A. and Stanley S. Ballard—M12
McGee, J. F.—U2
McHale, J. L. and R. M. Thaler—O8
Miller, J. M.—G1
Minshall, Stanley—M13
Mitchell, A. H. and C. Kittel—M7
Montroll, Elliott—A3
Motz, H., K. M. Crowe, and R. M. Friedman—L4
Mullin, C. J. and E. Guth—Q2
Nervik, Walter E. and Glenn T. Seaborg—G7
Oppenheim, Irwin—D6
Pake, G. E.—N4
—— and R. H. Sands—I12
Panofsky, W. K. H.—J4
Parmentier, D., A. J. Schwemin, L. W. Alvarez, E. S. Crawford, Jr., and M. L. Stevenson—U12
Parzen, Philip—D5
Pattee, Howard H., Jr.—U3
Perlman, I. F. Stephens, and F. Asaro,—G11
Perry, R. L. and J. J. Brady—T3
Petroff, M. D., S. W. Mead, and W. O. Doggett—S2
Piccioni, O., D. Clark, R. Cool, G. Friedlander, and D. Kassner—P5
Portis, A. M. and D. Shaltiel—I3
Rasmussen, J. O. and H. Slätis—G10
Ravenhall, D. G. and D. R. Yennie—Q3
Rawitscher, George—O5
Reagan, D. D.—E2
Reilly, C. A., H. M. McConnell, and R. G. Meisenheimer—I4
Repp, Gordon W., Mark J. Jakobson, and R. Stephen White—L7
Reynolds, J. H.—U4
Richardson, J. R.—J1
Riddell, R., Jr., M. Neuman, and S. Gasiorowicz—D3
Rosenbluth, A. W. and M. N. Rosenbluth—F3
Rothstein, Jerome—M9
Rubin, Sylvan and D. C. Sachs—U9
Ruderman, M. A.—K7
Sagane, Ryokichi, Walter Dudziak, and James Vedder—L10
Salkovitz, E. I., J. Pasternak, and A. I. Schindler—M10
Sands, R. H.—I11
Saphir, G.—L9
Schiff, L. I.—Q8
Sells, R. L., C. W. Harris, and E. Guth—O3
Shaw, Harlan, David Cohen, Burton J. Moyer, and Charles Waddell—E5
Sherman, Dora F.—E9
Sherman, N., G. Culler, and S. Fernbach—O9
Shutt, R. P.—B1
Silver, M., R. S. Witte, and F. McCaffrey—M6
Simanton, J. R., R. A. Rightmire, A. L. Long, and T. P. Kohman—G2
Slichter, C. P.—N2
Smith, W. G. and J. M. Hollander—G12
Smythe, W. R. and R. M. Worlock—L13
Softky, Sheldon D.—S10
Sogo, P. B. and C. D. Jeffries—I8
Sonett, C. P. and K. R. MacKenzie—S13
Speck, D. R. and F. A. Jenkins—T7
Stauss, H. E. and G. Sandoz—M11
Stapp, Henry P.—K6
Stephens, F., J. Hummel, F. Asaro, and I. Perlman—G5
Stubbins, Warren Fenton—P2
Sutton, R. B.—K2
Suura, H.—Q7
Tautfest, G. W., J. R. Havill, and Sylvan Rubin—S7
Teem, J. M., W. Selove, and U. E. Kruse—E6
Tripp, R., C. Wiegand, T. Ypsilantis, O. Chamberlain, and E. Segrè—K4
Trolan, J. K., J. P. Barbour, E. E. Martin, and W. P. Dyke—H1
Twersky, V.—D1
Villaire, A. E. and L. F. Wouters—S8
Wagner, P. E.—H10
Walsh, J. L., A. G. Berger, J. V. Rogers, and W. D. Knight—I9
Walt, M. and J. R. Beyster—S6
Wang, Ming Chen and Eugene Guth—O13
Warren, Roger—H6
Wayland, Harold—C1
Westrum, Edgar F., Jr. and John J. McBride—M3
White, R. Stephen, Mark J. Jakobson, and Gordon W. Repp—L8
Wiener, Norbert—A1
Wilcox, L. and J. E. Drummond—H8
Wildhack, W. A.—U1
Wilson, Allan N.—L5
Windle, J. J. and T. M. Shaw—T2
Woodyard, J. R.—U10
Worlock, R. M. and W. R. Smythe—L12
Yennie, D. R., D. G. Ravenhall, and B. W. Downs—Q4
Yodh, Gaurang B.—L6
Ypsilantis, T., C. Wiegand, R. Tripp, E. Segrè, and O. Chamberlain—K5
Zernike, F.—O1

CONTENTS—*Continued*

Letters to the Editor:

Shell Theory for the Nuclei with Mass 19 . . . . . Martin G. Redlich 199

Spin and Lifetime of the 439-kev Excited State of Hg^{203} . . . . . Franz R. Metzger 200

Self-Energy Effects on Meson-Nucleon Scattering According to the Tamm-Dancoff Method . . . . . J. C. Taylor 201

Photoproduction of π^+ Mesons from Hydrogen near Threshold . . . . . J. E. Leiss, C. S. Robinson, and S. Penner 201

Nuclear Surface Energy and the Diffuseness of the Nuclear Surface . . . . W. J. Swiatecki 203

Average Nuclear Potentials and Densities . . . . . W. J. Swiatecki 204

Angular Distribution of Pions from θ^0 Decay . . . . . R. M. Sternheimer 205

Angular Correlation in Two-Photon Annihilation in Quartz . . . . . L. A. Page, M. Heinberg, J. Wallace, and T. Trout 206

Angular Distribution of Pickup Deuterons for 95-Mev Protons on Carbon, and Implications as to Internal Interactions in Carbon . . . . . W. Selove 208

Low-Energy Photoproduction of π^0 Mesons from Hydrogen: Total Cross Section . . . . . F. E. Mills and L. J. Koester, Jr. 210

Low-Energy Photoproduction of π^0 Mesons in Hydrogen: Differential Cross Sections at 135° . . . . . Louis J. Koester, Jr. 211

System of Even-Even Nuclei . . . . . Gertrude Scharff-Goldhaber and J. Weneser 212

First-Forbidden Nonunique Beta Spectra in Re^{186} . . . . . F. T. Porter, M. S. Freedman, T. B. Novey, and F. Wagner, Jr. 214

Possible Experiments to Determine the Transition Matrix for β-β Scattering . . . . . Reinhard Oehme 216

Electron Scattering from the Proton . . . . . Robert Hofstadter and Robert W. McAllister 217

Capture of Negative K Mesons . . . . . J. Hornbostel and E. O. Salant 218

Proceedings of the American Physical Society:

Minutes of the 1954 Thanksgiving Meeting Held at Chicago, Illinois, November 26–27, 1954 (Corresponding to *Bulletin of the American Physical Society*, Volume 29, No. 7) 220

Minutes of the 1954 Winter Meeting at the University of California, Berkeley, California, December 28–30, 1954 (Corresponding to *Bulletin of the American Physical Society*, Volume 29, No. 8) 254

CONTENTS

THE PHYSICAL REVIEW SECOND SERIES, VOLUME 98, NO. 1 APRIL

Isotope Shift in the X-Ray Spectra of Heavy Elements . . . . . M. S. Wertheim and G. [illegible] 1
Hyperfine Structure of He^{3+} and He^3 . . . . . A. M. Sessler and H. M. [illegible] 7
Gamma Rays of 100^{256} . . . . . Frank Asaro, Frank S. Stephens, Jr., S. G. Thompson, and I. Perlman 9
Alpha and Gamma Spectra of Cf^{246} . . . . . J. P. Hummel, Frank S. Stephens, Jr., Frank Asaro, A. Chetham-Strode, Jr., and I. Perlman 12
Theorem on Angular Correlation . . . . . S. Raboy and V. E. Krohn 24
Excitation Functions for Some Proton-Induced Reactions of Thorium . . . . . Howard A. Tewes 25
Elastic Scattering of 20.6-Mev Protons by Deuterons . . . David O. Caldwell and J. Reginald Richardson 29
Decay of the 3.5-min Metastable State of Sb^{122} . . . . . J. M. LaBlanc, J. M. Cork, and S. B. Burson 39
Excitation Function of $O^{16}(t,n)F^{18}$ . . . . . Nelson Jarmie 44
Half-Life of Rb^{81} . . . . . James B. Niday 45
Gamma Rays from the Deuteron Bombardment of Carbon-13 . . . . . R. J. Mackin, Jr., W. B. Mims, and W. R. Mills, Jr. 43
Redetermination of the Disintegration Constant of U^{238} . . . . . A. F. Kovarik and N. I. Adams, Jr. 46
$(n,2n)$ Cross Section of Na^{23} at 14.1 Mev . . . . . R. J. Prestwood 47
Angular Distributions and Yields of Neutrons from (p,n) Reactions . . . . . Bernard L. Cohen 49
Elastic Scattering of 9.76-Mev Protons by Helium . . . . John H. Williams and Stanley W. Rasmussen 56
Decay Of Y^{91} . . . . . R. Kahn and W. S. Lyon 59
Isotopic Spin Selection Rule for Electric Dipole Transitions . . . . . William M. MacDonald 60
Radioactivity of Co^{57} . . . . . Bernd Crasemann and D. L. Manley 65
Photodisintegration of the Deuteron . . . . . Y. Yamaguchi and Y. Yamaguchi 69
Reaction $D(t,\alpha)n$ at 1.5 Mev . . . . . A. Hemmendinger and H. V. Argo 70
Absolute Cross Section for the Reaction $C^{13}(\gamma,n)C^{12}$ . . . W. C. Barber, W. D. George, and D. D. Reagan 73
Correction to the Exponential Dependence of Neutron Transmissions . . . . . R. G. Thomas 77
Radiations of Mo^{99} and the Isomeric States of Nb^{99} . . . . . Hirdaya B. Mathur and Earl K. Hyde 79
Angular Distribution of Disintegration Products from the $O^{16}(d,p)O^{17}$, $Be^9(d,p)Be^{10}$ and $Be^9(d,t)Be^8$ Reactions . . . . . Mira K. Jurich 85
Spins and Parities of Excited States of Ce^{140} and Sr^{88} . . . . . G. R. Bishop and J. P. Perez Y. Jorba 89
Iridium-194 . . . . . C. E. Mandeville, Jagdish Varma, and Babulal Saraf 94
Measurement of the Scattering Constant in Nuclear Emulsion . . . . . Lyle W. Smith 100
Example of τ^+-Decay in Flight . . . . . J. R. Burwell, R. W. Huggett, and R. W. Thompson 101
Pion-Pair Production in a Nuclear Emulsion . . . . . Herman Yagoda 103
Latitude Effect of Cosmic Radiation at Low Altitudes . . . . . Martin A. Pomerantz 105
High-Energy Proton Spallation-Fission of Uranium . . R. L. Folger, P. C. Stevenson, and G. T. Seaborg 107
Production of Heavy Unstable Particles by 1.37-Bev Pions . . . . . W. B. Fowler, R. P. Shutt, A. M. Thorndike, and W. L. Whittemore 121
Recurrence Phenomenon in the 24-Hour Variation of Cosmic-Ray Intensity . . . . . R. P. Kane 130
Mass Spectrum of Shower Particles from Cosmic-Ray Interactions . . . . . A. Hussain and E. Pickup 135
Spin Polarization of the Deuteron . . . . . W. Lakin 139
Lower Limit for the Energy Derivative of the Scattering Phase Shift . . . . . Eugene P. Wigner 142
Scattering of Polarized Nucleon Beams . . . . . Reinhard Oehme 147
Mesonic Decay of an Ejected Triton . . . . . Herman Yagoda 153
Scattering of 192-Mev Electrons from the Deuteron . . . . . John A. McIntyre and Robert Hofstadter 159
Scintillation Counter Study of Energy Spectra of Cosmic-Ray Protons and Electrons at 11 200 Feet . . . . . C. N. Chou and Marcel Schein 162
Čerenkov Counter Flux Measurement of Cosmic-Ray Alphas at 41° . . . . . Nahmin Horwitz 165
Photodisintegration of Carbon-12 by 330-Mev Bremsstrahlung . . . . . Sheldon D. Softky 173
Relation between Multiple Coulomb Scattering and Residual Range in Nuclear Emulsion . . R. G. Glasser 174
Infrared Divergence in Bound State Problems . . . . . F. Rohrlich 181
Variational Principle for Scattering with Tensor Forces . . . . . S. I. Rubinow 183
Equivalent Two-Body Method for the Triton . . . . . Herman Feshbach and S. I. Rubinow 188
Variation Calculation of the Polarizability of the Deuteron . . . . . B. W. Downs 194
Derivation of the Feynman-Dyson Rules for Time-Independent Theory . . . . . Saul T. Epstein 196

(*continued on cover three*)
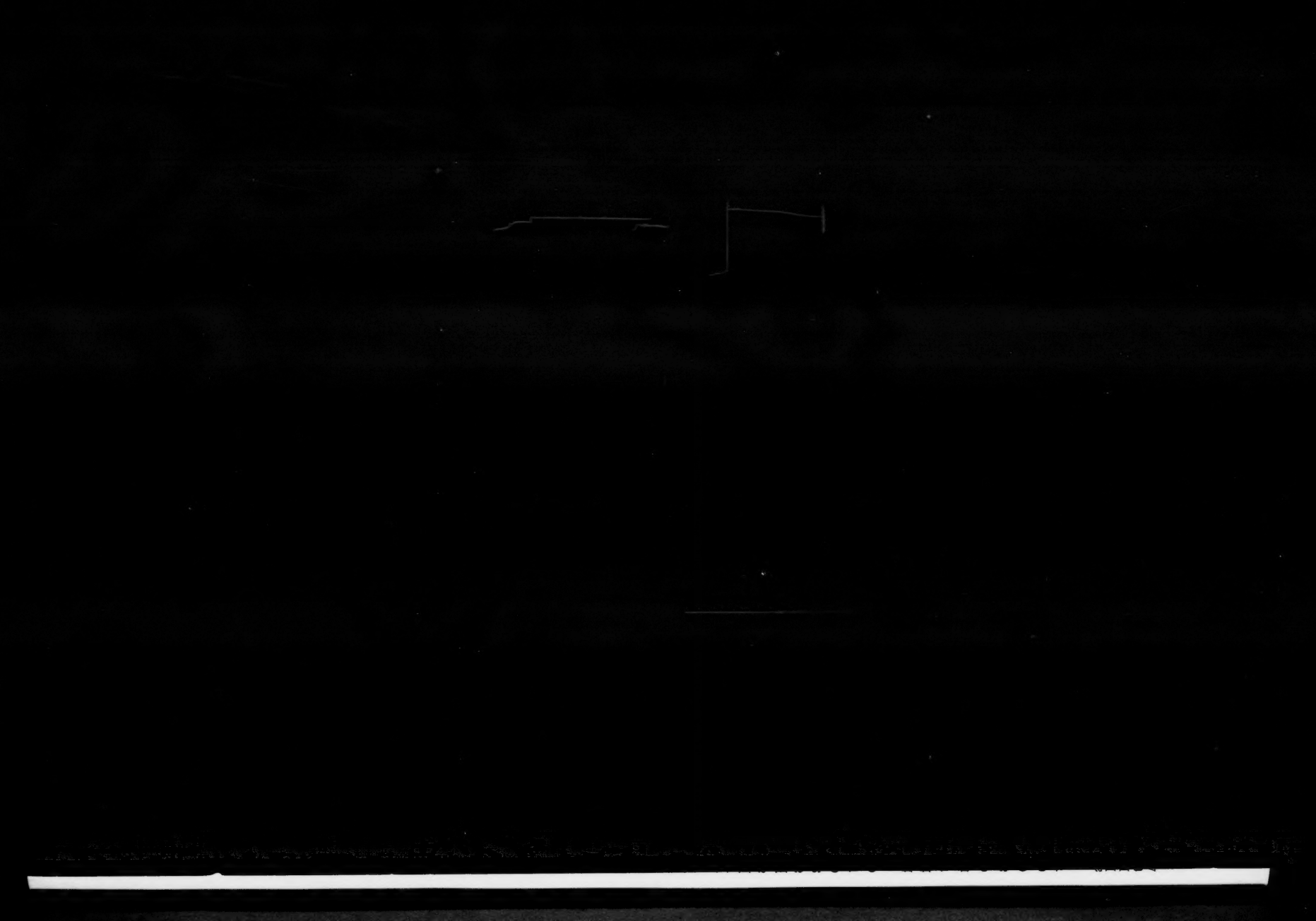
LANCASTER PRESS, INC., LANCASTER, PA.